PB86-122660

Fundamental Combustion Research Applied to Pollution Formation. Volume 1. FCR Program Overview and Gas-Phase Chemistry

Energy and Environmental Research Corp.
Irvine, CA

Prepared for

Environmental Protection Agency
Research Triangle Park, NC

Oct 85

U.S. Department of Commerce
National Technical Information Service
NTIS

PB86-122660

EPA/600/7-85/048
October 1985

FUNDAMENTAL COMBUSTION RESEARCH APPLIED TO POLLUTION FORMATION

Volume I

FCR Program Overview and Gas-Phase Chemistry

by

W. R. Seeker, M. P. Heap, T. J. Tyson
J. C. Kramlich and T. L. Corley

Energy and Environmental Research Corporation
18 Mason
Irvine, California 92718-2798

EPA Contract 68-02-2631

EPA Project Officer: J. E. Haebig
Air and Energy Engineering Research Laboratory
Office of Environmental Engineering and Technology
Research Triangle Park, North Carolina 27711

AIR AND ENERGY ENGINEERING RESEARCH LABORATORY
OFFICE OF RESEARCH AND DEVELOPMENT
U.S. ENVIRONMENTAL PROTECTION AGENCY
RESEARCH TRIANGLE PARK, NC 27711

REPRODUCED BY
NATIONAL TECHNICAL
INFORMATION SERVICE
U.S. DEPARTMENT OF COMMERCE
SPRINGFIELD, VA. 22161

TECHNICAL REPORT DATA

(Please read Instructions on the reverse before completing)

1. REPORT NO. EPA/600/7-85/048

2.

3. RECIPIENT'S ACCESSION NO. PB86 122660/AS

4. TITLE AND SUBTITLE Fundamental Combustion Research Applied to Pollution Formation; Volume I. FCR Program Overview and Gas-phase Chemistry

5. REPORT DATE October 1985

6. PERFORMING ORGANIZATION CODE

7. AUTHOR(S) W. R. Seeker, M. P. Heap, T. J. Tyson, J. C. Kramlich, and T. L. Corley

8. PERFORMING ORGANIZATION REPORT NO.

9. PERFORMING ORGANIZATION NAME AND ADDRESS
Energy and Environmental Research Corporation
18 Mason
Irvine, California 92714

10. PROGRAM ELEMENT NO.

11. CONTRACT/GRANT NO. 68-02-2631

12. SPONSORING AGENCY NAME AND ADDRESS
EPA, Office of Research and Development
Air and Energy Engineering Research Laboratory
Research Triangle Park, NC 27711

13. TYPE OF REPORT AND PERIOD COVERED Final; 1/77 - 9/80

14. SPONSORING AGENCY CODE EPA/600/13

15. SUPPLEMENTARY NOTES AEERL project officer is Jon E. Haebig, Mail Drop 65, 919/541-2432 (original project officer W. S. Lanier is no longer with the EPA).

16. ABSTRACT The report is the first in a series of four, documenting research performed under EPA's Fundamental Combustion Research (FCR) program. It is divided in two: Part A is a program overview and an introduction to the series; and Part B documents research performed in the gas-phase chemistry area. The primary focus of the FCR program is to better understand phenomena controlling formation of nitrogen oxides (NOx) from stationary combustion sources. A major effort was mounted to develop a set of elementary reactions describing NOx formation, particularly those involving fuel-bound nitrogen species. Since NOx formation is intimately coupled with the heat release process, it was essential that the assembled reaction set also accurately describe hydrocarbon oxidation. A methodology was employed whereby the kinetic set was systematically developed and evaluated. Development began with the simple hydrogen/air system and progressed in verified steps to methane/air. Each step involved comparison of prediction with available experimental data. Behavior at both short and long characteristic times was evaluated. There are many remaining uncertainties, particularly in the processing of nitrogenous intermediates, but the assembled reaction set may be used for engineering analysis of emerging NOx control strategies.

17. KEY WORDS AND DOCUMENT ANALYSIS

a. DESCRIPTORS		b. IDENTIFIERS/OPEN ENDED TERMS	c. COSATI Field/Group	
Pollution	Oxidation	Pollution Control	13B	
Combustion	Kinetics	Stationary Sources	12B	20K
Research		Fundamental Research	14F	
Gas Analysis		Gas-phase Chemistry	14B	
Nitrogen Oxides			07B	
Hydrocarbons			07C	

18. DISTRIBUTION STATEMENT Release to Public

19. SECURITY CLASS *(This Report)* Unclassified

20. SECURITY CLASS *(This page)* Unclassified

21. NO. OF PAGES 397

22. PRICE

EPA Form 2220-1 (9-73)

NOTICE

This document has been reviewed in accordance with U.S. Environmental Protection Agency policy and approved for publication. Mention of trade names or commercial products does not constitute endorsement or recommendation for use.

PREFACE

This report series presents the results of the first EPA Fundamental Combustion Research Applied to Pollution Formation program, under contract 68-02-2631. This program was divided into four program areas, each containing several subcontracts. The resulting final reports of the subcontracts in each program area are incorporated as chapters into a numbered bound EPA report volume as indicated in the following table. (For Program Area II there are three bound report volumes.)

EPA Report No.	Volume No.	Volume Title (" ") and Chapters
		Program Area I. Gas-Phase Chemistry
600/7-85-048	I	"FCR Program Overview and Gas Phase Chemistry" A. FCR Final Report Series Introduction B. Gas Phase Chemistry
		Program Area II. Physics and Chemistry of Two-Phase Systems
*	IIA	"Flame Combustion Processes" I. Volume Introduction II. Flame Combustion Processes III. The High Temperature Decomposition and Combustion of Pulverized Coal IV. The Detailed Measurement of Long Pulverized Coal Flames for the Characterization of Pollutant Formation V. Heavy Oil Spray Combustion in Shear Layers
*	IIB	"Devolatilization and Volatile Reactions" I. Method for Characterization of Coal During Thermal Decomposition II. The Volatility of Fuel Nitrogen Species III. Stirred Reactor Study of Pollutant Formation from Combusting Pulverized Coal Clouds IV. Pollutant Formation from Combustion of Fuel Oils in a Well-Mixed Combustor
*	IIC	"Heterogeneous NO Reduction: The Mechanism of NO Reduction on Solid Particles" I. Trials of Nitric Oxide and Ammonia II. Comparative Study of Coal and Char III. Trials on Fly Ashes
		Program Area III. Measurement Systems
*	III	"Measurement Systems" A. Spray Characterization B. The Application of Droplet-Sizing Interferometry and Holography to the Measurement of Spray Droplet Size C. Chemiluminescent Measurement of NO in Combustion Products D. Measurements of Fuel-Nitrogen Species in Flames
		Program Area IV. Engineering Analysis and Transport Phenomena
*	IV	"Engineering Analysis and Transport Phenomena" A. Development of a Coherent Flame Model for a Turbulent Chemically Reacting Flame B. Analytical Tool Development

---

* To be assigned

ABSTRACT

This report is the first in a four-volume series documenting research performed under EPA's Fundamental Combustion Research (FCR) program. Volume I is divided into two parts. Part A provides a program overview and an introduction to the report series. Part B documents research performed in the gas-phase chemistry area. The primary focus of the FCR program is to better understand phenomena controlling formation of nitrogen oxides from stationary combustion sources. A major effort was mounted to develop a set of elementary reactions describing NO formation, particularly those reactions involving fuel-bound nitrogen species. Since NO formation is intimately coupled with the heat release process, it was essential that the assembled reaction set also accurately describe hydrocarbon oxidation. A methodology was employed whereby the kinetic set was systematically developed and evaluated. Development began with the simple hydrogen/air system and progressed in verified steps to methane/air. Each step of the building process involved comparison of prediction with available experimental data. Behavior at both short and long characteristic times was evaluated. There are many remaining uncertainties, particularly in the processing of nitrogenous intermediates, but the assembled reaction set may be used for engineering analysis of emerging nitrogen oxide control strategies.

ACKNOWLEDGMENT

The EPA Project Officer who was responsible for this program is W. S. Lanier who is no longer with the Agency. The entire FCR program was initiated, structured, and managed through his efforts.

TABLE OF CONTENTS

		Page
A.	FCR Program and Final Report Series Introduction	A-i
A-1.	FCR Structure	A-1
A-2.	FCR Final Report Series	A-23
B.	Gas Phase Chemistry: Development and Verification of a Mechanism for NO Formation and Destruction in Hydrocarbon Flames	B-i
B-1.	Introduction	B-1-1
B-2.	Methodology of Kinetic Mechanism Development	B-2-1
B-3.	The CO-H_2-O_2 System	B-3-1
B-4.	The Hydrocarbon Reaction System	B-4-1
B-5.	Kinetic Models for Fuel-Nitrogen Reactions	B-5-1
B-6.	Summary and Conclusions	B-6-1
B-7.	References	B-7-1
APPENDIX I.	Gas Phase Processes Involved in the Control of Nitrogen Oxide Formation in Fossil Fuel Flames	B-I-i
APPENDIX II.	An Investigation of the Formation and Destruction of Nitrogenous Species During Hydrocarbon-Air Combustion	B-II-i

TABLE OF CONTENTS - SECTION A

Section A: FCR PROGRAM AND FINAL REPORT SERIES INTRODUCTION

Prepared by: W. R. Seeker, M. P. Heap, T. J. Tyson

Section . . . . . Page

1.0 FCR Structure A-1

- 1.1 Program Structure A-2
- 1.2 Gas-Phase Chemistry Program Area A-9
- 1.3 Physics and Chemistry of Two-Phase Systems A-12
- 1.4 Engineering Analysis and Transport Phenomena . . . A-18
- 1.5 Measurement Systems A-21

2.0 FCR FINAL REPORT SERIES A-23

LIST OF FIGURES-SECTION A

Figure Page

A-1 Solid/Liquid Fuel Processing in Turbulent Diffusion Flames . A-4

A-2 FCR-I Program Structure A-6

1.0 FCR STRUCTURE

The Fundamental Combustion Research applied to to Pollutant Control Program (FCR) had three major objectives. These are:

- To generate an understanding of combustor behavior necessary to aid the Combustion Research Branch (CRB) in development of control strategies to minimize NO_x emissions from stationary sources.
- To develop engineering models which would allow effective utilization of a large body of fundamental information in the development of new NO_x control techniques.
- To identify critical information necessary for low-NO_x combustor development and to generate it in a time frame which was consistent with the needs of the CRB technology development programs.

The overall goal of the CRB, and hence of the FCR program, is to provide the technology for the maximum control of NO_x emissions from stationary sources. The intent of FCR was to develop a focused program directed at the important issues of relevance to the CRB in order that the results could be applied in a relatively short time period. The program plan emphasized well-defined priority target areas, and the ensuing research effort was always guided towards engineering solutions to specific problems. There was a conscious effort to avoid projects which did not provide information critical to the needs of the CRB. Consequently, it was necessary to isolate the relevant issues, and the program was directed away from studies of the physics and chemistry of combustion which were not relevant to the goal of the CRB.

Fifty-six percent of the annual emission of nitrogen oxides from stationary sources in this country emanate from one general combustor category, boilers firing coal or oil. The dominant characteristics of the combustors can be characterized as follows:

- The flames are large, with energy release zones whose dimensions are on the order of tens of feet.
- The time mean motion is in steady state.
- The pressure is atmospheric.
- Radiation heat transfer has a dominant impact upon exchange from the heat release zone to the cold confining walls.
- Mass and thermal transport is turbulent.
- Fuel/air contacting occurs by diffusion and particle penetration.
- Fuels are injected as solids or liquids giving rise to two-phase transport and both homogeneous and heterogeneous reactions.
- The high fuel-bound nitrogen content of coal and residual fuel generally requires that NO_x emissions be minimized by the application of staged combustion.

Thus, the primary initial objective of the FCR program was to immediately establish a subcontractor-oriented program of fundamental investigations focused on the control of NO_x from large, confined, one-atmosphere turbulent diffusion flames burning heavy residual oil and pulverized coal.

1.1 Program Structure

The combustion of pulverized coal and oil in boilers is accomplished through the use of a burner of which there are many different designs. In fact, Combustion Engineering claim that they do not use burners, just fuel and air injectors and the whole boiler acts as the burner. For the purposes of this discussion, a burner will be considered as a device which allows fuel and air to be injected in such a way as to provide a stable flame whose characteristics are suited to a given combustion chamber. Pulverized coal is injected either through annular or axial nozzles with spreading devices. Liquid fuels are normally broken into droplets by atomizers of many different designs which produce a variety of fuel spray characteristics (spray angle, droplet size, drop velocity). The combustion air is supplied axially, either without tangential momentum or with tangential momentum which may vary across the burner throat. The burner throat might be composed of more than one annular passage. Depending upon the fuel and air injection parameters, two different types of flames can be readily distinguished, both of which are shown in Figure 1-1. The top half of the sketch shows a near-field dominated, burner-stabilized flame. These are relatively short, high-intensity flames typical of what is produced in wall-fired boilers with rapid fuel/air mixing. In a wall-fired unit there are generally multiple burners with each flame independently stabilized. The second class of flames is typified by those used in cement kilns or corner-fired boilers where the air is injected completely axially, producing a long, simple jet flame (see the bottom half sketch in Figure 1-1. In a corner-fired boiler these jet flames intersect on a firing circle and mix in the fireball which occupies a significant fraction of a combustion chamber. Regardless of the type of flame, the liquid droplets or pulverized coal particles exhibit the same phenomena as the potential chemical energy in the fuel is converted to thermal energy in the combustion products.

A simplified description of the phenomena occurring to solid particles and liquid droplets of fuels in turbulent diffusion flames is also illustrated in Figure 1-1. The fuels first decompose giving a vapor and a solid product. The vapor may be ejected from the solid as a single jet through a blowhole or may vaporize uniformly from the particle or droplet. This vapor will then either undergo pyrolysis producing soot particles, or undergo gas-phase oxidation. The solid remaining after devolatilization of coal is normally referred to as char. The char and soot may then undergo heterogeneous reaction which includes oxidation (burnout) and possible reaction with gaseous nitrogen species. Throughout this sequence of events, the fuel droplets/ particles and their products must be brought into contact with the oxidant and the high temperature combustion products in order to cause decomposition and subsequent reaction. This contacting is important on a macroscale because it dictates the major flame characteristics (i.e.,

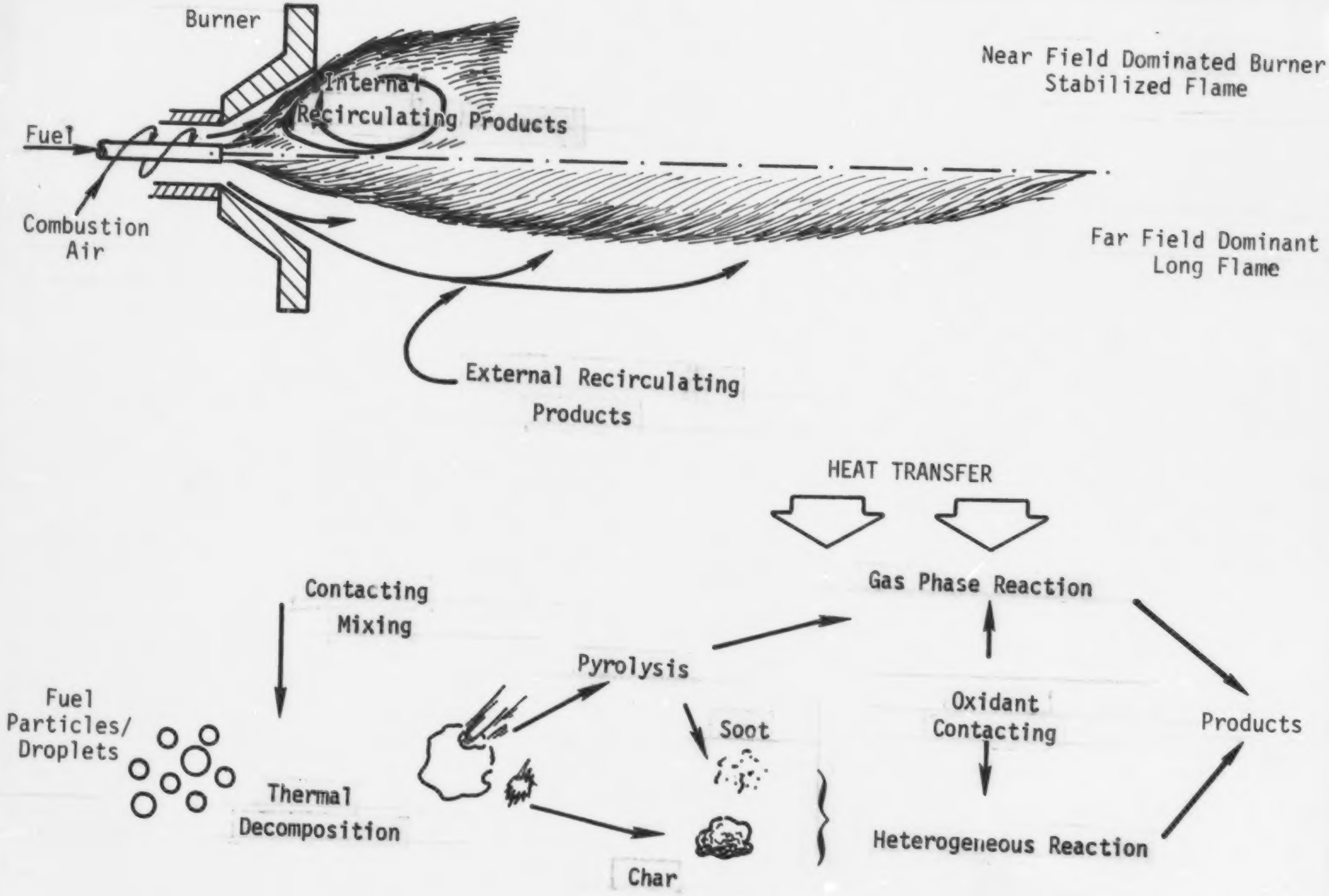
Burner
Internal Recirculating Products
Fuel
Combustion Air
Near Field Dominated Burner Stabilized Flame
Far Field Dominant Long Flame
External Recirculating Products
HEAT TRANSFER
Gas Phase Reaction
Contacting Mixing
Pyrolysis
Fuel Particles/ Droplets
Soot
Oxidant Contacting
Products
Thermal Decomposition
Char
Heterogeneous Reaction

Figure A-1. Solid Liquid Fuel Processing in Turbulent Diffusion Flames.

near-field dominated burner stabilized, or far-field dominated jet flame), and on a microscale because it ultimately dictates the production of pollutant species. FCR has been primarily concerned with the phenomena associated with the conversion of the nitrogen in the fuel droplets/particles to the ultimate nitrogen oxide released from the combustion chamber.

Based on the above series of phenomena which characterize coal and oil flames, the FCR program was divided into three program areas. These were concerned with: (1) transport processes in reacting systems, (2) gas-phase chemistry, and (3) the physics and chemistry of two-phase systems. Figure 1-2 presents an overall view of the program structure divided into three major program areas, specific program elements and support areas. This program structure was planned to lead to two major program outputs. These were:

- A description of the chemical limits of NO production in order to ascertain the lower bounds of both fuel and thermal NO production under a series of process constraints which were not limited in any way by fuel/air contacting.
- A description of fuel NO formation in turbulent diffusion flames for gas, liquid and pulverized coal systems.

This overall program was planned as a combined in-house and subcontract project effort. Energy and Environmental Research Corporation (EER), in conjunction with the EPA project officer, took responsibility for program planning, management and synthesis of the overall program, and subcontracted to various organizations separate projects included within the various program elements. Subcontracts accounted for 70 percent of the program and were used to ensure that FCR had the benefit of the best scientific talent available. Every effort was made to use subcontractors who had the necessary experience, and in many cases, equipment. The main synthesis role was accomplished by EER using the analytical tools developed in one of the program areas.

The reasoning behind the division of the total program into the three major program areas can most easily be described by consideration of the phenomena occurring to solid fuels in turbulent diffusion flames. A pulverized coal particle is heated, decomposes, and the fuel-bound nitrogen

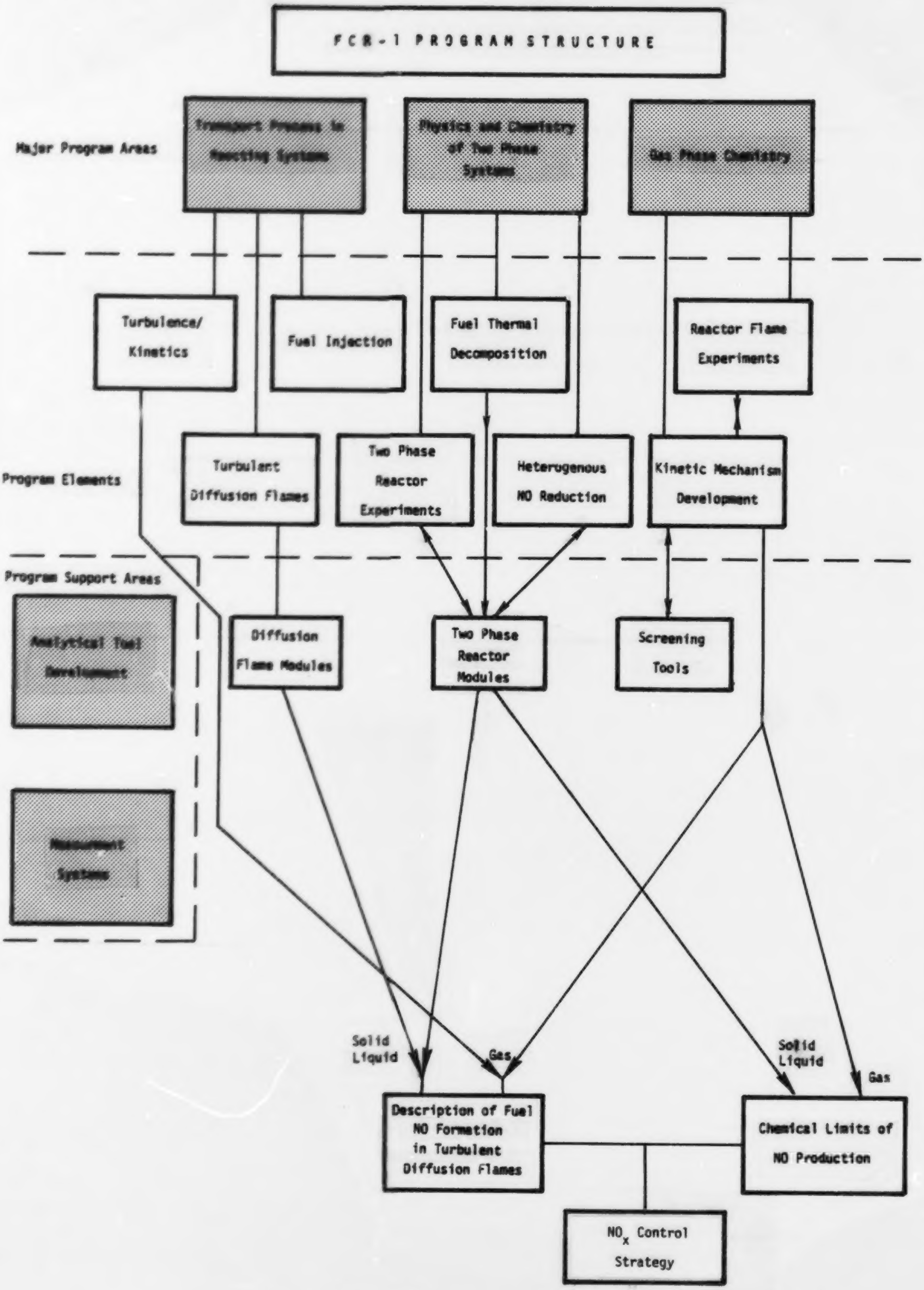
FCR-1 PROGRAM STRUCTURE
Major Program Areas
Transport Processes in Reacting Systems
Physics and Chemistry of Two Phase Systems
Gas Phase Chemistry
Turbulence/ Kinetics
Fuel Injection
Fuel Thermal Decomposition
Reactor Flame Experiments
Program Elements
Turbulent Diffusion Flames
Two Phase Reactor Experiments
Heterogenous NO Reduction
Kinetic Mechanism Development
Program Support Areas
Analytical Tool Development
Measurement Systems
Diffusion Flame Modules
Two Phase Reactor Modules
Screening Tools
Solid Liquid
Gas
Solid Liquid
Gas
Description of Fuel NO Formation in Turbulent Diffusion Flames
Chemical Limits of NO Production
NO$_x$ Control Strategy

Figure A-2. FCR-I Program Structure.

component is divided between that which stays with the solid (char) and that which is evolved with the volatile gases. The processes that lead to the division of fuel nitrogen are part of the physics and chemistry of two-phase systems, as are the subsequent reactions of the solid phase. Thus, two of the program elements in the two-phase program area were concerned with the thermal decomposition of the fuel and heterogeneous NO/char reactions. The fate of the volatiles depends upon the chemistry of nitrogenous species during combustion of the gas-phase pyrolysate (composed primarily of hydrocarbons). This whole area was treated in the gas-phase chemistry program area. The primary goal of the gas-phase chemistry program was to produce a description of the kinetic mechanisms adequate for predicting the fate of fuel nitrogen in gaseous mixtures which were likely to be found in pulverized coal and residual oil flames. Thus, the gas-phase chemistry area was divided into two program elements: one experimental, and one aimed at mechanism development using computer simulations. A considerable effort was expended in the development of two-phase reactor experiments. These provided coupled experiments in which both gas-phase chemistry and fuel decomposition were involved.

All of the above neglected the physics of turbulent transport. In flames, the particles must be mixed with high-temperature gases before they can decompose, and oxidant must be mixed with the volatile fuel fractions before they can react. These fuel/air contacting processes were treated in the program area defined as transport processes in reacting systems. Three projects were carried out in this major program area. These were concerned with turbulence kinetics coupling, fuel injection systems, and turbulent diffusion flames.

Although each of the projects in the various program areas were planned to provide information which was of value in itself and which was of direct use for data interpretation, the overall program flow was directed towards the development and verification of engineering tools. These tools could be used in the attainment of the two major goals which defined fuel NO formation in turbulent diffusion flames. It is not possible to show the overall interaction of the various program areas and program elements because of the additional complexity which would be added to Figure 1-2. However, it does demonstrate the importance placed upon the use of analytical tools to provide the program synthesis. Indeed, all the program elements can be considered as providing input to allow analytical tools to be developed, and the application of these tools then provides the ultimate output of the FCR program.

It was recognized from the outset that within the timeframe of FCR (three years) the development of a unified mathematical model for NO_x production in pulverized coal flames was unattainable. The major modeling effort in FCR concentrated upon the development of a framework of semiempirical modular models. Thus, a complex system could be approximately modeled using a collection of limit-case elements linked together by means of empirical knowledge of the exchange of heat and mass transfer between these elements. In its simplest application, these modular elements could be used to analyze the data generated in several of the program elements involving reactor experiments. The modules describing fuel decomposition could be applied to both reactors and turbulent diffusion flames. Recognizing how complex a pulverized-coal system is, the limit-case approach was deemed to be the most appropriate in analyzing fundamental data for application to real systems. In limit-case studies, certain phenomena are assumed to dominate the process while other phenomena become suppressed, thus allowing the implications of specific phenomenological behavior to be examined. Limit-case studies could be used to define the times and temperatures needed to reach a certain total fixed-nitrogen content in a fuel-rich combustion system, or in an attempt to define to what extent heterogeneous NO reduction took place in pulverized-coal flames.

Although FCR placed considerable emphasis on the provision of information which was necessary to provide near-term solutions, long-term research was not entirely neglected. FCR pioneered the use of holography and two-color pyrometry as tools to study the thermal decomposition and combustion of fuels. Activities in turbulence kinetics coupling are beginning to show considerable promise for the future. Effort was initiated to evaluate numerical techniques which could be used in the ultimate models of furnace performance. This combination of projects provided the CRB with a balanced, directed fundamental combustion research program.

Having established an overall program structure it was necessary to formulate individual research efforts directed toward meeting the overall program goals. The following subsections briefly describe the individual research projects which constituted the FCR effort in each of the three Major Program Areas.

1.2 Gas-Phase Chemistry Program Area

The projects initiated in FCR under this Program Area were:

- Kinetic Mechanism Development: J. C. Kramlich, W. R. Seeker and T. L. Corley, EER.
- The Modeling of Fuel Nitrogen Chemistry in Combustion: J. Levy and A. F. Sarofim, Massachusetts Institute of Technology.
- The Formation and Destruction of Nitrogeneous Species During Hydrocarbon/Air Combustion: D. W. Blair, Exxon Research & Engineering.
- Reactor Studies: W. Clark, EER.

Kinetic Mechanism Development: J. C. Kramlich, W. R. Seeker, and T. L. Corley, EER

This project was focused on the development of a kinetic mechanism which could give an adequate prediction of the conversion of fuel nitrogen compounds to NO in gaseous systems. The major objective was to provide a validated reaction model which could then be used as one component of more complex models describing the conversion of fuel nitrogen during the combustion of coal and liquid fuels.

The Modeling of Fuel-Nitrogen Chemistry in Combustion: The Influence of Hydrocarbons. J. M. Levy and A. F. Sarofim, MIT

There are uncertainties in the currently available mechanistic and kinetic data base suitable for modeling of fuel-nitrogen conversion in the presence of "simple" fuels; however, an attempt must be made to attack the problems of real fossil fuels. Real fuels introduce mechanistic complexities due to the presence of hydrocarbon species which do not decouple easily from solution of the fuel-nitrogen problem. This project was concerned with an assessment of these complexities and to the development of a methodology for dealing with them which would allow fuel nitrogen processing in real fuels to be modeled.

Having exhausted, as impractical or inapplicable, existing methods of treating hydrocarbons, a new quasi-global method was proposed with the following general form:

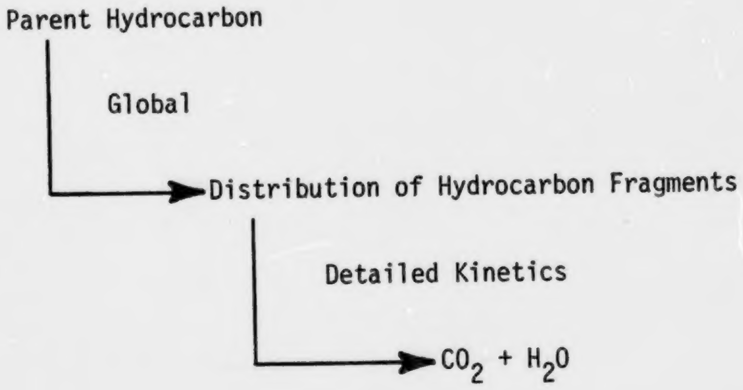

The method assumes: (1) that the initial degradation of the parent hydrocarbon in the preflame zone via pyrolysis and oxidative pyrolysis is very rapid; (2) that the initial decomposition products may be represented by a relatively small set of low molecular weight, stable, and/or unstable, hydrocarbon species; and, (3) that the decomposition mechanism can be justifiably represented by a global step.

The potential utility of this proposed method, referred to as the Quasi-Global Method Applied to Initial Reaction Extents (QUAGMIRE), lies in the following:

- The advantages of modeling free radical chemistry by detailed kinetics are retained, but the magnitude of the elementary reaction set required is vastly reduced.
- Unlike the quasi global approaches proposed by others, hydrocarbons are retained in the elementary reaction scheme.

QUAGMIRE is currently being used to model data generated in the post-flame region of flat flames doped with nitrogenous species. Initial results are encouraging and point to the need for more detailed measurement of the relevant free radicals in hydrocarbon flames in order to provide a basis for verifying the initial global step.

The Formation and Destruction of Nitrogenous Species During Hydrocarbon/Air Combustion: D.W. Blair, Exxon

Earlier work at Exxon has been funded by the CRB to develop two reactors for the investigation of NO formation: a strongly backmixed jet-stirred combustor (JSC) and an adiabatic laminar quasi-plug-flow combustor -- the multiburner (MB). This project was continued by FCR to utilize this expertise and equipment in several experiments:

- Extend the measurements to include nitrogen species other than NO.
- Investigate the impact of temperature on fuel NO formation.
- Initiate experiments on fuel nitrogen conversion with hydrocarbon fuels other than CH_4.

This information was necessary if a verified kinetic mechanism for fuel nitrogen oxidation was to be developed.

Reactor Studies: W. D. Clark, EER

A series of short reactor studies was carried out at EER to provide information to aid program planning and management. A high temperature plug-flow reactor was built originally to test model predictions which suggested that NO decayed relatively rapidly in the absence of hydrocarbons in fuel-rich systems. Experiments indicated that this decay did not take place, and that the divergence in prediction and experiment was due to improper assignment of the kinetic rate of the reaction $CO + NO + NCO + O$.

The reactor was modified to allow an investigation of heterogeneous effects (NO reduction and char nitrogen conversion) in a dispersed-phase system.

1.3 Physics and Chemistry of Two-Phase Systems

Eight individual research projects were performed under the FCR Program Area entitled "Physics and Chemistry of Two-Phase Systems." The primary thrust of these projects was to provide needed data on phenomena governing evolution, processing and fate of fuel-bound nitrogen during thermal decomposition of coal and heavy oil. These eight efforts include:

- The Characterization of Coals During Thermal Decomposition: J. P. Treihaut and D. J. Seery, United Technologies Research Center (UTRC).
- Volatility of Fuel Nitrogen: R. L. Gay, A. E. Axworthy, V. H. Payan and H. L. Recht, Rockwell International.
- The Physical and Chemical Effects Occurring During the Thermal Decomposition of Coal Particles: W. R. Seeker, G. S. Samuelsen, J. C. Kramlich and M. P. Heap, EER.
- Pollutant Formation from Combusting Pulverized-Coal Clouds: P. M. Goldberg, P. A. Cawley, J. T. Kelly, H. Tong and R. M. Kendall, Acurex.
- Detailed Measurements of Long, Pulverized-Coal Flames for the Characterization of Pollutant Formation: J. B. Michel and R. Payne, International Flame Research Foundation (IFRF).
- Mechanisms of Nitric Oxide Reduction on Solid Particles: G. G. de Soete, French Petroleum Institute (IFP).
- An Experimental Approach to the Study of Heavy Oil Spray Combustion in Shear Layers: A. Vranos, UTRC.
- Pollutant Formation During the Combustion of Residual Fuel Oils in Backmixed Reactors: M. J. Murphy, A. A. Putnam, A. Levy and J. R. Overley, Battelle/Columbus.

The first six of these studies concentrated on phenomena associated with nitrogen oxide formation and destruction in pulverized coal-fired systems. The last two efforts in the above listing addressed combustion phenomena in residual oil-fired systems. Brief abstracts from each of the eight efforts are presented below.

The Characterization of Coals During Thermal Decomposition. J. D. Freihuat and D. J. Seery, UTRC

United Technologies Research Center (UTRC) had developed an in-house capability to investigate coal inorganic structure and the products of thermal decomposition. A model was available which allowed the prediction of the time- and temperature-dependent evolution of the major products of pyrolysis from a knowledge of the coal's functional group distribution. The model assumes that large molecular fragments ("monomers") are released from the coal "polymer" with only minor alteration to form tar, while simultaneous cracking of the chemical component of the coal can, therefore, evolve as part of the tar or as an independent species. The model may be used to predict the amount of volatile fuel nitrogen evolved in pyrolysis which is essential if the formation of fuel nitrogen is to be accurately assessed.

A study was initiated to apply these concepts to the study of several coals which were being investigated in other programs. Particular attention was paid to the rate and forms of nitrogen evolution. Pyrolysis experiments were performed on Beulah, a North Dakota lignite, a Pittsburgh bituminous, Savage, a Montana lignite, and Rosa, a bituminous coal, between 400°C and 1800°C.

Volatility of Fuel Nitrogen. R. L. Gay, A. E. Axworthy, V. H. Payan, and H. L. Recht, Rockwell International

An experimental program measured fuel nitrogen volatility using a quartz two-stage pyrolysis reactor developed under a previous CRB program (EPA 68-02-1886). Solid and liquid fossil fuels were heated in helium in the first stage of the reactor at selected temperatures up to 1100°C. The volatile nitrogen compounds released were measured by converting them to HCN in the second stage of the reactor at 1100°C. The HCN was collected in dilute sodium carbonate solutions and measured calorimetrically.

Samples of twenty fossil fuels which were used on other CRB programs were supplied by EER. Petroleum-based fuel oils, synthetic oils from coal and shale, and coals were studied. All of the samples tested produced the greatest yields of volatile nitrogen compounds at a first-stage temperature of 1100°C. The maximum yields of volatile nitrogen from petroleum fuel oils were 35-48 percent of the nitrogen in the sample. The yield curves increased continuously from 300°C with a slight dip at 600-750°C. The maximum volatile nitrogen yields from shale oils were 70-79 percent, while the coal liquids yielded 50 percent. The nitrogen species in shale oils were very volatile at low temperatures, giving HCN yields of about 65 percent at a pyrolysis temperature of only 200°C.

The Physical and Chemical Effects Occurring During the Thermal Decomposition of Coal Particles. W. R. Seeker, G. S. Samuelsen, J. C. Kramlich, and M. P. Heap, EER

The events occurring during the thermal decomposition of coal particles in the initial stages of heat release in turbulent diffusion flames are of considerable significance to the designers of low-pollutant emission combustors. In pulverized-coal flames, the partition of fuel nitrogen between the volatile and char fractions, for example, will impact the production of fuel NO. Moreover, since the fate of fuel nitrogen in the volatiles is dictated by the environment in which they react, their conversion to NO or N_2 will depend upon the degree to which they mix with the bulk flow before reacting.

Earlier studies supported by FCR demonstrated that holography could be used to observe the behavior of coal particles during combustion. The approach taken in the present study was to observe particles under well-controlled conditions which simulated those encountered in real systems. This was accomplished by the construction of a reactor which allowed the particle to be injected into high-temperature gases whose temperature and composition could be varied. Diagnostics were designed to allow visualization of the particle/droplets during combustion, both by holography and high-speed photography. Two-color particle pyrometry was employed to measure particle temperatures, and solid and gaseous samples were extracted to investigate the variation of composition with time.

Pollutant Formation From Combusting Pulverized-Coal Clouds.

P. M. Goldberg, P. A. Cawley, J. T. Kelly, H. Tong, and
R. M. Kendall, Acurex

The objective of this experimental study was to provide information on the mechanisms of coal combustion and subsequent oxides of nitrogen formation under conditions similar to those found in the near-burner region of a high-intensity pulverized coal flame. A jet-stirred reactor system is utilized in this study to simulate this type of combustion environment. The conditions in the stirred combustor approximate those found in flames when a high degree of recirculation is present. In addition, a stirred reactor is capable of operating over a wide range of coal concentrations at high temperatures and residence times ranging from about 20 to 100 msec. The first goal of the program was to design a well-mixed coal reactor capable of operating over residence time range of 20 to 200 milliseconds. After completing the design and fabrication, noncombusting mixing studies were to be conducted to verify that a high level of gas-phase mixing exists in the reactor. Once gas-phase mixing performance was verified, subsequent experiments were to be directed at quantifying particle mixing behavior. Combustion experiments were to begin after the completion of this task.

The original experimental plan was modified somewhat during the course of this program. Instead of one reactor, two similar reactors were designed to cover the residence time ranges of about 20 to 50 and 50 to 100 msec, respectively, during combustion testing. The gas-phase mixing efficiency of the longer time scale reactor (SRII) was examined using a "cold" model reactor in conjunction with an He tracer method. Attempts have been made to quantify particle mixing in the SRII cold model by using a light attenuation technique. Experiments indicate that good mixing is achieved in SRII. However, the particle mixing study results indicate that the particle residence time might be longer than the gas residence time. The results also indicate that the particle residence time may vary significantly less than that of the gas.

Detailed Measurements of Long, Pulverized-Coal Flames for the Characterization of Pollutant Formation. J. B. Michel and R. Payne, IFRF

This program was initiated to provide experimental data which could be used both for model development and to provide a mechanistic understanding of nitrogen processing in flames of this type.

Six "long" coal flames were produced with the same burner under similar boundary conditions. The differences between these flames were mainly due to air and fuel input velocities and temperatures which have a direct effect on the mixing characteristics and the coal heating rates. A comprehensive set of flame data was generated. Despite the many difficulties encountered in making measurements in such flames, particularly for sampling in regions of high temperature and solid concentrations, the consistency between the various measurements is generally good. Indications are that globally, the combustion is controlled by mixing and that the influence of fuel kinetics is basically the same in all cases.

Mechanisms of Nitric Oxide Reduction on Solid Particles. G. T. de Soete, IFP

The scope of the work is to provide information on:

- The mechanism of heterogeneous NO reduction under typical flame and flue gas conditions.
- Determine the reaction rates of reactions controlling the disappearance of NO, the formation of intermediates, and their transformation to molecular nitrogen.

The study, performed on packed bed reactors was restricted to a general investigation of the heterogeneous NO reducing mechanisms.

An Experimental Approach to the Study of Heavy Oil Spray Combustion in Shear Layers. A Vranos, UTRC

This program was initiated during FCR and consisted of two phases: (1) design and fabrication of an apparatus, and (2) preliminary combustion experiments. A unique shear-layer mixing and combustion apparatus was developed which simulates high-shear diffusive combustion with heavy oil droplet injection as found in the near-field combustion zone of boilers and furnaces. The apparatus provides: (1) two-dimensional mixing and combustion of uniform streams of air and rich combustion products fed from opposite sides of a splitter plate; (2) uniform injection of a monodisperse heavy oil spray into the shear layer by means of a linear array of fuel injectors located beneath the combustor wall; (3) control of droplet path, residence time, and extent of vaporization; (4) control of hot- and cold-stream inlet properties, and (5) three-dimensional probing of the flow field.

The experimental phase of the program consisted of (1) verification of uniform properties of the hot and cold streams at the splitter plate trailing edge; (2) demonstration of high-injection velocities and uniform droplet size and penetration with No. 2, 5, and 6 oils in vibrating multicapillary injectors; (3) determination of stable flow regimes as a function of primary and secondary stream velocities; (4) flame stability and flashback studies; (5) high-speed cinematography of the shear layer with injection of No. 2 and No. 6 fuel oil, and (6) preliminary flame probing.

Pollutant Formation During the Combustion of Residual Fuel Oils in Backmixed Reactors.

M. J. Murphy, A. A. Putnam, Art Levy, and J. R. Overley, Battelle/Columbus

This program was included in FCR in an attempt to relate the production of NO_x from burning residual fuel oils to fuel-nitrogen in these fuels and to the combustion variables such as spray droplet size, fuel properties and time/temperature history. This objective was addressed through the use of a well-stirred reactor fired on fuel oil having the capability of variable residence time, stoichiometry, and droplet parameters (size and fuel composition). The program was organized into three tasks:

(1) Design, Construct, and Test a Reactor Model

(2) Construct and Test the Actual Reactor

(3) Demonstrate Reactor Operation and Data Acquisition

The performance of the well-stirred reactor design, task (1), was followed by extensive cold-flow testing, Criteria for well-mixedness were met satisfactorily with the selected design. Measurements of gas residence times were performed on the cold flow model using laser extinction techniques applied at the exhaust duct.

Technical problems associated with the prototype combustor have led to the design of the current combustor configuration. This combustor has eight fuel jets utilizing sonicore nozzles and eight air jets fired into a cylindrical chamber. The chamber dimensions were selected to allow a residence time range between 20 and 200 msec at a firing rate variable between 100,000 to 1.5×10^6 Btu/hr. Emissions data have been collected for natural gas burning over a stoichiometry range of 0.6 to 1.60 as a function of residence time. The combustor has been successfully fired for extended periods on a number 6 fuel oil to equivalence ratios greater than 2.0.

1.4 Engineering Analysis and Transport Phenomena

The research efforts pursued under this Major Program Area focused on development of mathematical models with the development efforts closely coupled to the numerous experimental studies. The majority of the modeling work was performed by EER and directed toward development of the overall modular model discussed earlier. One component of this Program Area was performed as a combined effort between the California Institute of Technology (CIT) and TRW. This modelling effort was an initial effort to address coupling between turbulence and chemical kinetic processes. Abstracts of these modeling studies are presented below.

Development of a Coherent Flame Model for Turbulent Chemically-Reacting Flame. F. W. Marble, and J. E. Broadwell, CIT/TRW

A coherent flame model was applied to a methane air turbulent diffusion flame with the objective of describing the production of nitric oxide. The example of a circular jet of methane discharging into a stationary air atmosphere was used to illustrate application of the model. In the model, the chemical reactions are assumed to take place in laminar flame elements which are lengthened by the turbulent fluid motion and shortened when adjacent flame segments consume intervening reactant. The rates with which methane and air are consumed and nitric oxide generated in the strained laminar flame are computed numerically in an independent calculation.

Analytical Tool Development. T. J. Tyson and C. J. Kau, EER

The major integration function in the FCR program was to be carried out through the use of mathematical models. The models were developed in close accord with the experimental investigations. These models include a description of the following phenomena:

- Particle thermal history, including the existence of particle super temperatures.
- Finite rate thermal decomposition.
- Heterogeneous chemical behavior.
- Finite-rate gas-phase chemistry.
- Fluid mechanics and ballistics of turbulent transport in two-phase systems.
- Complex flow fields associated with the near-field of highly swirl-stabilized combustors.
- The interaction between turbulent unmixedness and chemistry.

These modeling efforts have resulted in a hierarchy of analysis codes. Treatment of the fully-coupled finite-rate processes associated with: particle heatup, thermal decomposition, heterogeneous reactions, and gas-phase chemistry was emphasized. The codes can handle with ease and efficiency as many as 200 such coupled processes, although often such complexity is not warranted.

In the course of developing an understanding of the dominant mechanisms governing complex and poorly understood behavior, it is often necessary to start with a large coupled system and, through sensitivity analysis, reduce it in such a manner that it contains first-order phenomena only. A good example of a situation requiring such an approach is the development of an understanding of NO_x generation in p.c. flames. The complexities of HCN, NH_i, and C_2 chemistry, in conjunction with finite rate devolatilization, defies a simple intuitive understanding and requires complex analysis in order to generate such intuition.

The decomposition of coal is described assuming that the coal is composed of an arbitrary number of functional groups; the quantification and characterization of these is provided by utilization of independent experimental data. These functional groups are envisioned to decompose by one or more parallel paths with Arrhenius-like rate behavior. A given species may evolve from more than one functional group, and the functional groups can exchange between themselves with an equilibrium composition that is temperature dependent. This generalized model lends itself easily to the incorporation of observations from many different investigators.

The hierarchy of models developed during FCR allow a description of the following systems:

- Simple Reactor Models

These operational codes are routinely used for the analysis of well-stirred stoichiometric ratio (SR) and plug-flow (PF) reactors for both gas and coal. The SR module assumes either a perfectly stirred exponential distribution of particle residence times, or it will accept as input an arbitrary distribution obtained from experimental evidence, as will the PF module. The heat loss or heat-loss distribution can be specified as appropriate. The modules can be coupled, and the PF can receive additional combustion air and fuel in a staged fashion. These coupled reactors are ideally suited for simple modular modeling of combustion system performance (ignition stability, energy release distribution, heat transfer) and pollutant formation as a function of fuel, burner, and furnace characteristics.

- Simple Laboratory Diffusion Flames

These codes provide for the analysis of fundamental experiments on laminar one- and two-dimensional diffusion flames. In addition to simple coaxial flames, this code will describe behavior in opposed-jet flames. The mathematical solution for such a system proves to be self-similar with all properties independent of the radial coordinate with the exception of the radial velocity.

- Long Turbulent Diffusion Flames

This code represents the most ambitious, and perhaps the most satisfying, output of FCR. It is directly applicable to a large class of industrial furnaces. This operational code treats long, coaxial turbulent pulverized coal diffusion flames typified by tunnel furnace flames stabilized through convective blackflow along the wall as well as by radiation from the flame to the incoming particles.

1.5 Measurement Systems

As part of the FCR program four studies were conducted in the "measurement Systems" Program Support Areas. Two efforts were performed which focused on development/evaluation of laser based diagnostic tools for characterizing liquid droplet sprays. The third effort in this Program Support Area was designed to assess the accuracy of commercial chemiluminescent analyzers for measuring NO in combustion products. The final research project was directed toward establishment of a standarized method for using ion specific electrodes for HCN and NH_3 analysis.

Spray Characterization. W.R. Seeker and G.S. Samuelsen, EER

A program was established to help explain data obtained on a CRB-funded development program which showed the dependency of NO_x emission in fuel-oil combustion on atomizing nozzle type, and nozzle operating conditions. Toward this end, a cold chamber spray rig, patterned after the combustion system, was built for the purpose of characterizing nozzle spray behavior. As the initial step in the program, nonintrusive optical techniques are being applied and evaluated for (1) consistency of data measured, and (2) applicability to studying the spray behavior most likely important to NO_x emission. The optical techniques include diffraction, visibility, and holography.

The Application of Droplet-Sizing Interferometry and Holography to the Measurement of Spray Droplet Size. C.F. Hess, W.D. Bachale, SDL

Two optical techniques were used to characterize the droplet field produced by a sonicore nozzle under laboratory conditions. Droplet-sizing interferometry (DSI) and holography were used to obtain the size and velocity of fuel droplets in the presence of a surrounding air stream. The experiments were performed under cold conditions to provide data on droplet size and velocity correlations, size stratification, and droplet evaporation.

Due to the complex nature of the flow (two phases, small droplets, high number densities, recirculation, etc.) nonintrusive measuring methods must be used to avoid disturbing the flow. The methods must also have very high resolution since the droplets can be very small and move at high speeds. The techniques must be flexible enough to access the measuring volume from any direction since physical obstacles will be present in most combustion.

Chemiluminescent Measurement of Nitric Oxide in Combustion Products. B. A. Folsom and C. W. Courtney, EER

The response of commercially available chemiluminescent NO_x analysis to simulated combustion products containing NO was investigated. An accurate flow metering system was used to combine O_2, CO_2, CO, N_2, Ar, H_2O, CH_4, and H_2 into simulated combustion products modeling a wide range of fuels and excess air conditions. The simulated products were doped with known amounts of NO and then monitored by two commercial chemiluminescent NO_x analyzers.

Measurements of Fuel Nitrogen Species in Flames. D. W. Pershing, and R. M. Winter, University of Utah

There is currently no standardized approach for sampling and analyzing combustion gases to determine the gas phase concentration of HCN and NH_3. Ion specific electrodes are widely employed to analyze for these species but significantly different approaches to sample extraction and sample preparation are in use by various combustion researchers. Accordingly a study has been performed to evaluate the various approaches employed and to establish a standardized procedure for use under the FCR program.

2.0 FCR FINAL REPORT SERIES

The structure of the FCR final report series generally reflects the structure of the FCR program. Program final documentation is divided into four basic volumes plus a special report. Each volume documents work accomplished in an individual Program Area and is accompanied by a separate project summary. Thus, Volume I is devoted to work performed in the Gas-Phase Chemistry Program Area, Volume II addresses Physics and Chemistry of Two-Phase Systems, Volume III documents the FCR effort in Measurement Systems and Volume IV is concerned with Engineering Analysis and Transport Processes. In addition a special report has been issued as part of the FCR program to document the proceedings of an FCR Subcontractors Review Meeting.

As noted in the previous section the Program Area, Physics and Chemistry of Two-Phase Systems consisted of eight individual research projects. Accordingly Volume II has been subdivided into three components denoted as Volumes II a, b and c. The overall report series organization is defined below.

Volume I	A. FCR Program and Final Report Series Introduction B. Gas-Phase Chemistry
Volume II	Physics and Chemistry of Two-Phase Systems A. Flame Combustion Processes B. Devolatilization and Volatile Reactions C. Heterogeneous NO Reduction
Volume III	Measurements
Volume IV	Engineering Analysis and Transport Processes

Special Report--FCR Subcontractors Review Meeting

Because the FCR program is subcontract oriented, the individual subcontractor reports are incorporated directly into the appropriate volumes. Depending on the relative role that the subcontractor served in a program area, the subcontract reports are either used as a major section within the particular volume or as a supporting appendix to a major report. EER had direct responsibility for all reports on particular program elements which represented in-house work. In addition, EER, in conjunction with the EPA project officer, took responsibility for accumulating the reports, reviewing and getting the appropriate revisions made, integrating the individual reports into the final report series, and in many cases actually retyping and preparing the final manuscripts. It was not EER's intention to resolve all questions concerning the details of technical approach or data interpretation; on the contrary, such questions and differences of opinion generally result in exchanges of ideas and are advantageous to the overall program. For this reason, no strict format was established but rather the format of each volume was adapted to the character of the subject area and style of the individual author.

The remainder of this volume deals with the gas-phase chemistry program area. The overall effort consisted of an EER mechanism development, verification and application along with documentation from the support subcontracts at Massachusetts Institute of Technology and Exxon Research and Development.

B. GAS-PHASE CHEMISTRY

DEVELOPMENT AND VERIFICATION OF A MECHANISM FOR NO FORMATION AND DESTRUCTION IN HYDROCARBON FLAMES

by

J. C. Kramlich
W. R. Seeker
T. L. Corley

TABLE OF CONTENTS-SECTION B

Section — Page

1.0 INTRODUCTION B-1-1

2.0 METHODOLOGY OF KINETIC MECHANISM DEVELOPMENT B-2-1

3.0 THE CO-H_2-O_2 SYSTEM B-3-1
  3.1 The H_2-O_2 Reactions B-3-1
    3.1.1 Induction Period Phenomena B-3-4
    3.1.2 Flame Phenomena B-3-12
    3.1.3 Summary B-3-24
  3.2 The CO-H_2-O_2 Reactions B-3-28
    3.2.1 Shock Tube Data B-3-30
    3.2.2 Flame Phenomena B-3-41
    3.2.3 Summary B-3-56

4.0 THE HYDROCARBON REACTION SYSTEM B-4-1
  4.1 The CH_2O-O_2 Reaction B-4-1
  4.2 Hydrocarbon Reaction Mechanisms B-4-16
    4.2.1 Induction Phenomena During the Oxidation of CH_4 and C_2H_6 . . . . . B-4-17
    4.2.2 C_2H_2 and C_2H_4 Reaction Mechanisms B-4-54
    4.2.3 CH_4 Flame Phenomena B-4-60
    4.2.4 Summary B-4-70

5.0 KINETIC MODELS FOR FUEL NITROGEN REACTIONS B-5-1
  5.1 The NH_3- O_2, and NH_3-Inert Reactions B-5-4
  5.2 HCN Reactions B-5-28
  5.3 Fuel Nitrogen in Hydrocarbon Flames B-5-30

6.0 SUMMARY AND CONCLUSIONS B-6-1
  6.1 Mechanism Status B-6-1
  6.2 Further Efforts B-6-8

7.0 REFERENCES B-7-1

APPENDIX I. Gas-Phase Processes Involved in the Control of Nitrogen Oxide Formation in Fossil Fuel Flames--MIT . . B-I-1

APENDIX II. An Investigation of the Formation and Destruction of Nitrogenous Species During Hydrocarbon-Air Combustion--Exxon B-II-1

LIST OF FIGURES-SECTION B

Figure Page

2-1 Major Subelements in the Overall Mechanism B-2-3

3-1 Comparison Between Predictions and the Data of Slack (1977) for $H_2/O_2/N_2$ = 29.6/14.8/55.6, P-2 Atm B-3-6

3-2 Comparison of Induction Times From Skinner and Ringrose (1965) With Predictions: $H_2/O_2/Ar$ = 8/2/90 . . . . B-3-8

3-3 Exponential Growth Constants for $H_2/O_2/Ar$: Data From Jachimowski and Houghton (1970) B-3-11

3-4 Comparison of Model With Experiment for Ignition Delays of H_2-Air Mixtures B-3-13

3-5 Burning Velocity of H_2-Air Flames: T_o = 298°K, P_o = 1 Atm . B-3-16

3-6 Comparison With Modified Data for H_2-Air Burning Velocities B-3-19

3-7 Relation Between Burning Velocity and Peak H-Atom Concentration in H_2 Flames at Atmospheric Pressure: Data of Padley and Sugden (1959) Referred to V_o From Jahn (1934) . . B-3-21

3-8 Maximum Species Concentrations in H_2-Air Flames: T_o = 298°K, P_o = 1 Atm B-3-23

3-9 Prediction of Stable Species Profiles for an $H_2/O_2/N_2$ (18.83/4.6/76.57). Data of Dixon-Lewis et al., 1970 . . . . B-3-25

3-10 Predicted Temperature Profile for an $H_2/O_2/N_2$ = 18.83/4.6/76.57 Flat Flame (T_o = 336°K, P_o = 1 atm): Dixon-Lewis et al., 1970 . . . . B-3-26

3-11 Exponential Growth Constants for O-Atoms: $CO/H_2/O_2$ = 6/5/0.5 . . . . B-3-32

3-12 Exponential Growth Constants for Radicals: $CO/H_2/O_2/CO_2$ = 10.0/0.1046/0.503/4.99 . . . . B-3-34

3-13 Exponential Growth Constants for Radicals in Fuel-Lean CO Oxidation: $CO/H_2/O_2/CO_2$ = 6.01/0.1035/10.0/5.0 . . . . . . B-3-35

LIST OF FIGURES (Continued)

Figure		Page
3-14	Exponential Growth Constants for Radicals in CO Oxidation: $CO/H_2/O_2/CO_2$ = 0.11/0.21/10.0/5.0	B-3-36
3-15	Characteristic Time for CO_2 Production in CO Oxidation: $CO/H_2/O_2$ = 3.28/0.049/1.01	B-3-39
3-16	Time at Which CO_2 Concentration Reaches 13.3 x 10^{-9} Mole/cm^3: $CO/H_2/O_2$ = 3.28/0.049/1.01	B-3-40
3-17	Variation of Burning Velocity for CO-Air Flames With Stoichiometry for Fixed H_2O Concentrations (T_o = 298°K, P = 1 Atm): Data Are for "Dry" CO-Air From Günther and Janisch (1972)	B-3-43
3-18	Influence of HCO Chemistry on Predicted Burning Velocity of CO-Air Flames as a Function of Stoichiometry: 0.25 Percent H_2O, T_o = 298°K, P = 1 Atm	B-3-45
3-19	Effect of HCO Chemistry on H-Atoms: CO-Air + 0.25 Percent H_2O	B-3-46
3-20	Variation of Predicted Burning Velocity in a Stoichiometric CO-Air as a Function of Added H_2 and H_2O	B-3-48
3-21	Relative Contribution of Reaction 19 to the Maximum Rate of CO_2 Production	B-3-50
3-22	Predictions of CO-Air Burning Velocities as a Function of Hydrogen Content and Stoichiometry	B-3-52
3-23	Comparison of Predicted Stable Species Profiles With Data for a Low-Pressure, Fuel-Rich $CO/H_2/O_2/Ar$ = 5.8/27.6/12.7/53.9 Flat Flame: Data of Fenimore and Jones (1959), P_o = 60 Torr, T_o = 298°K, V_o = 59.7 cm/sec. Solid Lines Are Predictions	B-3-54
3-24	Comparison of Recombination of H-Atoms With Reported H_2 Profiles of Fenimore and Jones (1959): $CO/H_2/O_2/Ar$ = 5.8/27.6/12.7/53.9	B-3-55
3-25	Predicted and Measured Temperature Profiles in a Low Pressure, Fuel-Rich $CO/H_2/O_2/Ar$ = 5.8/27.6/12.7/53.9 Flat Flame: T_o = 298°K, P = 60 Torr, V_o = 59.7 cm/sec	B-3-57
4-1	CO_2 Induction Times for Fuel-Lean CH_2O Oxidation--$CH_2O/O_2/CO$ = 0.5/0.92/9.15	B-4-7

LIST OF FIGURES (Continued)

Figure Page

4-2 Times for CO_2 Concentration to Reach 7.47 x 10^{-8} Mole/ cm^3--$CH_2O/O_2/CO$ = 0.5/0.92/9.15 . . . . B-4-8

4-3 Linear Production Rate of CO_2 During Oxidation of CH_2O-$CH_2O/O_2/CO$ = 0.5/0.92/9.15 . . . . B-4-9

4-4 Correlation of CH_2O Induction Times. (Induction Times for Predictions Based on CO_2 Profiles) B-4-11

4-5 Correlation of Induction Times in CH_2O Oxidation--CH_2O/O_2 = 3.3/1.7. (Predictions of Induction Times Based Upon Maximum OH Concentration.) B-4-12

4-6 Correlation of CH_2O Induction Times at Lower Temperatures and Higher Reactant Concentrations B-4-14

4-7 Correlation of CH_4-O_2-Ar Induction Times B-4-27

4-8 Methane-Argon-Oxygen Ignition Correlation: Ar/O_2 = 4 . . . B-4-28

4-9 Correlation of CH_4-O_2-Ar Induction Times: Data of Skinner and Ruehrwein (1959) B-4-32

4-10 a & b CO_2 Production in CH_4 Oxidation [(a) Time to Reach (CO_2) = 8.3 x 10^{-9} Moles/cm^3, (b) Time to Reach (CO_2) = 2.49 x 10^{-8} Mole/cm^3] B-4-35

4-10c Comparison of When Absolute CO_2 = 4.15 x 10^{-8} Mole/cm^3 . . . B-4-36

4-11 Exponential Growth Constants for Radicals in CH_4 Oxidation--$CH_4/CO/O_2/CO_2$ = 0.0194/18.72/1.073/5.68 in Ar B-4-41

4-12 Exponential Growth Constants for Radicals in CH_4 Oxidation--$CH_4/CO/O_2$ = 0.0193/1.032/19.41 in Ar B-4-42

4-13 Exponential Growth Constants for Radicals in CH_4 Oxidation: $CH_4/CO/O_2$ = 0.205/1.056/19.54 in Ar B-4-43

4-14 Dependence of Predicted Induction Times on k_{43} B-4-46

4-15 Sensitivity of Induction Delay Times to k_{43} B-4-47

4-16 Ignition Delay Correlation for C_2H_6 Oxidation in Argon . . . B-4-49

4-17 Comparison of Predicted Induction Times With Correlation of Bowman (1970) B-4-50

LIST OF FIGURES (Concluded)

Figure | Page

4-18 Comparison of Time for CO_2 to Reach a Certain Level for $C_2H_6/N_2O/CO$ = 256 ppm/1.01/12.1 in Argon. [(a) Time to Reach (CO_2) = 2.49×10^{-8} Moles/cm^3] B-4-52

4-19 Stable Species Profiles for the Flat Flame of Peeters and Mahnen (1973) B-4-62

4-20 Flame Profiles of Biordi et al. (1975). Solid Lines Are Data; Dashed Are Model B-4-64

4-21 Profiles Through the Flame of Biordi et al. (1975) B-4-65

4-22 Profiles Through the Flame of Harvey and MacColl (1979). (Predictions Are for C_1 + C_2 Chemistry) B-4-66

4-23 Calculated Flame Profiles for the Data of Harvey and MacColl (1979). Dashed Lines Indicate C_1 Reaction Set; Solid Represents C_1 + C_2 Set B-4-67

4-24 Profiles of C_2 Species Through the Flat Flame of Harvey and MacColl (1979). Solid Lines Are Data; Dashed Lines Are Model B-4-68

5-1 Induction Time Correlation for Lean NH_3-O_2-Ar Mixture . . . B-5-16

5-2a Pyrolysis of NH_3: 6.1 Percent NH_3 + 5.8 Percent H_2 + Ar; 0.363 Atm; 2685°K B-5-21

5-2b Pyrolysis of NH_3: 6.2 Percent NH_3 in Ar, 0.309 Atm, 2511°K B-5-22

5-3 Stirred Reactor Species as a Function of Equivalence Ratio (Blair, 1980). Conditions Were CH_4-Air Combustion at 1900°K, and 3 msec Residence Time With 750 ppm Added NH_3 . . . . . . B-5-31

6-1 Simplified Mechanism for NO Production in Flames B-6-7

LIST OF TABLES-SECTION B

Table		Page
2-1	Experimental Data Considered	B-2-5
3-1	H_2-O_2 Reaction Mechanism	B-3-2
3-2	CO-H_2-O_2 Reaction Mechanism	B-3-29
4-1	CH_2O-O_2 Reaction Mechanism	B-4-5
4-2	CH_4 Oxidation--Reactions of C_1-Hydrocarbon Species	B-4-18
4-3	CH_4 Oxidation--Reactions Producing C_2-Hydrocarbon Species	B-4-20
4-4	C_2H_2 Oxidation Reactions	B-4-21
4-5	C_2H_6 Oxidation Reactions	B-4-22
4-6	C_2H_4 Oxidation Reactions	B-4-23
4-7	Reactions Between Hydrocarbon Species	B-4-24
4-8	Reactions Producing Polyacetylenes	B-4-25
4-9	Predicted Induction Times for C_1-Hydrocarbon and C_1- Plus C_2-Hydrocarbon Reaction Mechanisms at Atmospheric Pressure	B-4-29
4-10	Defining Equation for λ, the Exponential Growth Constant for O, OH, H, and CH_3	B-4-40
4-11	Reaction Mechanism for Ketene-CH_2CO	B-4-57
5-1	Reactions Describing NH_3 Oxidation	B-5-5
5-2	Reactions for N_2H_i Species	B-5-24
5-3	Reaction of NH_2 With NO According to Branch et al., 1979	B-5-27
5-4	HCN Reactions	B-5-29

1.0 INTRODUCTION

The value of staged combustion as a technique for minimizing the conversion of fuel nitrogen to NO has been recognized for several years. Development programs have demonstrated successfully that fuel-rich operation in an initial heat release zone of a coal or heavy oil-fired combustor reduces NO_x emissions. However, questions still remain:

- What is and why is there an optimum rich-zone stoichiometry?
- What is the relationship between time and temperature with regard to minimization of total fixed nitrogen species concentrations?
- Are there benefits to be gained from multistage operation (such as distributed air addition or reburning)?

A validated kinetic mechanism in conjunction with simple engineering models is a cost-effective method of providing an answer to these questions.

A primary goal of the FCR program is to understand the factors governing the fate of fuel nitrogen in combustion environments. Traditionally, fundamental research has focused on monovariant experiments to describe how a single parameter influences the NO_x formation process. In a practical boiler flame a wide variety of system parameters influence the processing of nitrogenous species and developing an understanding of how those parameters interact is an integral part of this FCR program goal. An objective of the FCR program is to formalize that understanding of the individual processes and their interaction in a computer model which could be used to predict boiler performance, optimize pollutant control and provide a design tool for parametric studies on performance.

The FCR model, as contemplated, consists of numerous subcomponents or modules describing different phenomena in the combustion process. From a chemical perspective of pulverized coal combustion the model will contain modules to describe:

- Solid fuel heating and devolatilization.

- Quasi-global oxidation of gaseous higher hydrocarbons to produce simple hydrocarbons.

- Detailed description of simple gas phase species oxidation or reduction.

- Char oxidation.

- Heterogeneous reaction of nitrogenous species with char.

Each of these elements can be separately developed and validated using the existing fundamental data base augmented by critical data produced under the FCR program. Simultaneous integration of the above submodels, coupled with a description of the fuel/air mixing processes is required to achieve a qualitative/quantitative prediction of the NO_X formation process. The core of such a modeling system is the component describing the set of elementary gas-phase kinetic reactions of simple hydrocarbon and nitrogenous species. The following sections describe the development, validation and limitations of the elementary gas-phase reaction core model.

Computational procedures to predict temporal variation of species concentration for chemically reacting flows have been available for many years. These computer codes require, as input, definition of the following critical parameters:

- Type of reactor environment; i.e., plug flow, stirred reactor, flat flame, etc.

- A list of chemical species to be considered and their thermodynamic properties.

- A list of elementary reactions among the considered species and a kinetic rate expression for each elementary reaction.

The FCR program effort has been directed toward the last two items above: defining a set of elementary kinetic reactions which describe the fate of fuel nitrogen species in combustion environments. Such a definition of the pertinent species, their interreactions and the kinetic rates for each reaction is generally referred to as a "kinetic set."

The impetus for developing the current FCR kinetic set was provided by the uncertainty associated with the general applicability of sets developed previously for other specific applications. These earlier sets, adapted from Engleman (1976) were successfully utilized for a number of applications associated with the fate of fuel nitrogen (Wilson et al 1974, Waldman et al 1974). However, confidence in any reaction set can only be established by using the set to predict the full range of experimental conditions and several limitations of this set were identified. At the same time, because of the increased interest in the fate of fuel nitrogen, a wealth of new experimental data and direct measurements of elementary reaction rates were available which were not incorporated into the original set.

In order to ensure that the kinetic set had the widest applicability possible, to update the set with new rate measurements and to correct deficiencies which were identified in existing literature sets, an applications-oriented development methodology was adopted. This methodology was designed to ensure that the various subsets within the full set were sufficiently tested for a wide range of conditions. This in turn assured that all elementary reactions were both sufficient and necessary for broad application before the subset was incorporated into the full set. The following section discusses this methodology. At the same time, parallel efforts were initiated at MIT and Exxon Research to aid in two areas which were identified early on as requiring additional input. These included higher hydrocarbon combustion and fuel-rich reactions. The MIT project was designed specifically to address the modeling of the fate of fuel nitrogen in the presence of higher hydrocarbons ($>C_2$) including the development of global modeling approaches. The Exxon program was to supply much needed experimental data on fuel nitrogen processing under rich conditions at various levels of mixing.

2.0 METHODOLOGY OF KINETIC MECHANISM DEVELOMENT

Assembling and testing a set of kinetic mechanisms meeting the requirements of the FCR program requires a concise development methodology. Efficient testing of the mechanism and preserving its internal consistency dictates the required steps. Not only must the nitrogen chemistry be described in detail, but the background combustion chemistry must be similarly modeled since the hydrocarbon and nitrogen chemistry are closely coupled. Also, the mechanism must be able to predict combustion behavior over conditions that range from cold reactants to adiabatic products. This implies that the methodology must provide for the testing of the mechanism against an equally wide range of conditions.

The literature contains a significant number of kinetic mechanisms describing hydrocarbon combustion with varying degrees of complexity. These mechanisms are usually assembled from published elementary rate data, and in many instances are used with only cursory verification. In the current study, a methodology was adopted to allow the assembly and validation of a kinetic mechanism which was capable of describing the fate of fuel nitrogen during simple hydrocarbon (CH_4, C_2H_2, C_2H_4 and C_2H_6) combustion.

The decision to restrict the gas phase kinetic model to combustion of these simple hydrocarbons is justifiable on a number of bases. First, these simple hydrocarbons are the major volatile products from thermal decomposition of both coal and heavy fuel oil (the thermal decomposition of such fuels will be accounted for in a separate module of the overall combustion model). Second, the oxidation of higher molecular weight hydrocarbons always proceeds through a sequence of reactions which eventually involve hydrocarbon fragments resembling these simpler structures (e.g., methyl radicals). Oxidation of higher hydrocarbons to form the simpler species will be treated via a quasi global reaction step rather than through definition of elementary reaction steps. Third, insufficient experimental data are available to verify a detailed kinetic reaction set for hydrocarbon fuels more complex than the $C_1$and C_2 species listed above. Fourth, the major coupling between hydrocarbon combustion and the nitrogeneous species involves the hydrocarbon-free-radicals (e.g., CH or CH_2) rather than the parent fuel molecule. Finally, this restriction reduces the complexity of developing the required kinetic set to manageable proportions.

The mechanism development methodology begins with a recognition that combustion of even the simple hydrocarbons may be divided into a sequence of subelements. This may be easily seen by examining the hydrocarbon oxidation process in reverse. Formation of water ultimately involves reaction of hydrogen and oxygen, while the formation of CO_2 proceeds through CO as an intermediate. Thus, the task of developing a complete kinetic set is simplified by proceeding in a building-block fashion. First, a kinetic subset is developed for the H_2/O_2 system. This subset is then used as a component in the slightly more complex reaction system involving carbon monoxide/hydrogen and oxygen as reactants. The model is then systematically complicated with addition of hydrocarbon species leading to a reaction set which describes combustion of methane including formaldehyde, acetylene, ethylene and ethane as potential reaction intermediates.

This building-block approach for assembling an elementary reaction set to describe nitric oxide formation and destruction during methane combustion is conveniently divided into three major elements (see Figure 2-1).

1. The hydrogen/oxygen and carbon monoxide/hydrogen/oxygen systems.

2. The hydrocarbon system with methane as the primary fuel and including formaldehyde, acetylene, ethylene and ethane as potential reaction intermediates.

3. The nitrogen subelement involving nitrogen/hydrogen and carbon/nitrogen species (i.e., ammonia and hydrogen cyanide).

When combined, these elements provide an overall mechanism which can both describe methane flame structure and pollutant formation.

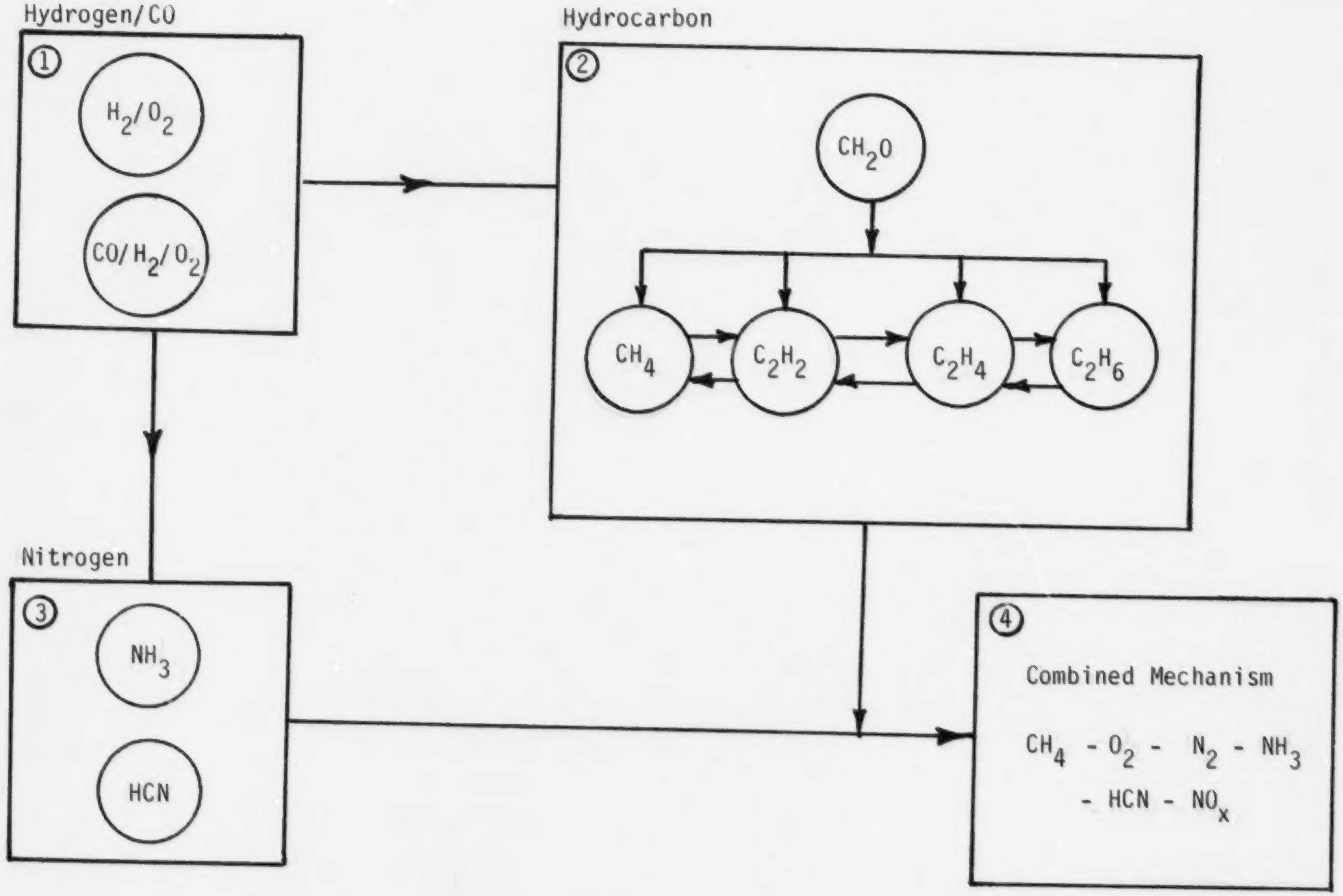
Hydrogen/CO
①
H_2/O_2
$CO/H_2/O_2$
Hydrocarbon
②
CH_2O
CH_4
C_2H_2
C_2H_4
C_2H_6
Nitrogen
③
NH_3
HCN
④
Combined Mechanism
$CH_4 - O_2 - N_2 - NH_3$
$- HCN - NO_x$

Figure 2-1. Major Subelements in the Overall Mechanism.

The mechanism development methodology is actually a system of rules and procedures which govern the testing of subelements (e.g., H_2/O_2 subelement) and define how the subelements will be combined into more complex elements (e.g., $H_2/CO/O_2$ subelement). There are three basic rules which were consistently used. First, each subelement must be thoroughly validated against a wide range of experimental data. Second, after validation, a subelement was assumed complete and could not be modified when used in the analysis of more complex systems unless it was shown that discrepancies in the new subelement could only be corrected by modifying the previously validated subelement. If modification was required, a third step was instituted wherein the modified subelement was again validated against relevant experimental data. This feedback loop ensured internal consistency of the final mechanism.

For each reaction subset the kinetic rates used in the mechanism were, wherever possible, obtained from critical evaluations. Where this could not be done, an attempt was made to select the most justifiable rate from those available. If rate data or temperature dependency were totally lacking, the values were estimated. The most critical component in the mechanism development methodology was validation of the reaction subsets against experimental data. In many experiments only a small fraction of the numerous possible reaction paths control the observed behavior. Thus, if such an experiment were used to test an entire mechanism, the results would be insensitive to the rates of the majority of the reactions. Conversely, such a simulation can be very useful if the reactions to be tested are those which control the experimental behavior.

Table 2-1 outlines the three types of experimental systems used for validating a reaction subset and defines the type of combustion phenomena which could be evaluated by comparison with predictions. The following discussion will focus on how each of these experimental system types is used in mechanism validation.

Table 2-1. Experimental Data Considered

Experimental Type	Reaction Set Tested
Shock Tube	
- Pyrolysis Data	Thermal Pyrolysis Reactions
- Induction/Ignition Times	Chain Initiation and Branching
- Exponential Growth Constants	Chain Branching
Flat Flames	
- Velocities	Global Reactant Consumption/ Energy Release
- Profiles	Details of Overall Chemistry
Stirred Reactor	
- Species	Overall or Global Chemistry

In general, three types of shock tube data are useful to the kinetic modeler. Pyrolysis data, where the subject compound and diluent are shock heated, tests the thermal pyrolysis reactions within the mechanism. The data usually take the form of species concentrations as a function of time. Using NH_3 as an example, the following reactions could be expected to dominate the observed behavior:

$$NH_i + M \rightarrow NH_{i-1} + H + M$$

$$NH_i + H \rightarrow NH_{i-1} + H_2 \qquad i = 1,2,3$$

$$NH + N \rightarrow N_2 + H$$

More commonly, shock tube data are obtained with fuel and oxidant comixed. Induction time measurements primarily test the chain initiation and chain branching steps of the mechanism. Examples of such steps for the H_2-O_2 system are:

$$H_2 + M \rightarrow H + H + M$$

$$O_2 + M \rightarrow O + O + M$$

$$H + O_2 \rightarrow OH + O$$

$$O + H_2 \rightarrow OH + H$$

The third type of shock tube data involve the time-dependent species profiles following the shock. These are usually expressed in terms of exponential growth constants for the radical species. Chain branching steps dominate the exponential growth period, which lasts only as long as a nonsignificant amount of the initial reactants have been consumed. Simulation of exponential growth constants provides a test whereby errors in individual chain branching reaction rates can, with careful interpretation, be discovered.

The two types of fundamental flame data used in simulations are the laminar-free flame speed and spatially-resolved profiles through the flame front. The laminar-free flame velocity is dependent on the rate of consumption of reactants. This, in turn, is governed by a number of interconnecting factors which may be best described as "global flame chemistry." While use of flame speed simulations for checking individual reaction rates is difficult, such a test does indicate the general utility of the mechanism.

Species and temperature profiles through the flame front provide a detailed test of most parts of the mechanism. The type of comparison is determined by the species measured by the investigator. As an example, the HO_2 peak early in the flame zone is caused by the upstream migration of H-atoms, which react with O_2 via

$$H + O_2 + M \rightarrow HO_2 + M.$$

The HO_2 is important in the early formation of flame radicals. The oxidation of CO to CO_2 via

$$CO + OH \rightarrow CO_2 + H$$

occurs in the flame zone and continues into the postflame gases. Radical and stable species measurements are often available throughout the flame zone. The use of flame data for mechanistic comparisons is usually limited only by the amount of the data collected by the investigator.

Stirred reactor species data provide a uniquely simple system for modeling. The customary probe measurements for stable species can be augmented by in situ radical measurements. Stirred reactor simulations are most useful for general combustion chemistry and global chemistry. However, no experimental stirred reactor is perfectly stirred--as is assumed in the model--so the modeler must be aware that experimental finite mixing effects rather than mechanistic errors may account for the difference between model and experiment.

This methodology thus utilizes measured reaction rates when they are available with a procedure of comparing predictions against a hierarchy of experimental data to verify all portions of the full kinetic set. In comparing predictions and experimental data, the deficiencies in the experimental system must be considered. For example, the perturbations associated with a molecular beam skimmer used for sampling in a flat flame can make the temporal information ambiguous; however, the data can often be reliably used for relative concentration levels and speciation. Thus, comparisons can only be made with those portions of the data which are reliable and not limited by the experimental techniques. This consideration can severely restrict the ability to verify some of the kinetic subsets.

After an element has successfully reproduced the shock tube and flame data selected for comparison, it is assumed to be complete and may be incorporated into more complex elements of the reaction model. As noted earlier, the development methodology requires that a validated subelement may not be modified when used in analysis of more complex elements. Modification is allowed only if it can be shown that discrepancies in the more complex system can only be corrected by changing features of the subelement. If this step is required, the modified subelement must be checked against the relevant data to determine if it still is able to predict the observations. This feedback loop ensures the internal consistency of the final kinetic mechanism.

The sections which follow describe the development of the kinetic set for each subset of reactions along with verification comparisons against experimental data. Each subset will be treated in individual sections.

3.0 THE CO-H_2-O_2 SYSTEM

3.1 The H_2-O_2 Reactions

The reactions and species which participate in the oxidation of hydrogen are well-established. However, the rate coefficients of many of the elementary steps are only very imperfectly known (Dixon-Lewis, 1979). This is particularly true if a wide temperature range, such as exists in the flame, is considered. In addition, reactions involving the hydroperoxyl radical and hydrogen peroxide, which are an essential part of the mechanism controlling certain characteristics of the slow reaction and explosion limit behavior under isothermal conditions, have been studied almost exclusively at isolated temperatures below 1000 K. A better definition of the temperature dependence of the rate parameters in the H_2 oxidation mechanism, as well as absolute values, will be achieved as more refined kinetic techniques are developed and applied to studies of the combustion of this simple fuel. We make these points to emphasize that even when a reaction mechanism is known, the rate coefficients used to define a model describing the course of the reaction may be time-dependent in the sense that additional experimental studies can require modifications in the expressions used to define the rate parameters as a function of temperature, and in certain cases as a function of composition.

The reaction mechanism proposed for H_2 oxidation is given in Table 3-1 and involves 18 simultaneous reactions with 8 species. At high temperatures, combustion of H_2 is dominated by the chain-branching steps:

$$H + O_2 = OH + O \qquad (6)$$

$$H_2 + O = OH + H \qquad (7)$$

$$OH + OH = H_2O + O \qquad (8)$$

$$H_2 + OH = H_2O + H \qquad (9)$$

Recombination reactions are important to establishing radical concentrations in postflame regions. The major paths occur via

$$H + H + M = H_2 + M \qquad (1)$$

Table 3-1. H_2-O_2 Reaction Mechanism

No.	Reaction	ΔH^0_r, 298 kcal/mole	A	b	E kcal/mole	Reference
1*	$H + H + M = H_2 + M$	-104.2	9. (17)	-1.	0	Baulch et al., 1972
2*	$H + OH + M = H_2O + M$	-119.4	2.2 (22)	-2.	0	Baulch et al., 1972
3	$O + O + M = O_2 + M$	-119.1	1. (18)	-1.	0	Benson et al., 1975
4	$H_2O_2 + M = OH + OH + M$	51.51	1.2 (17)	0	45.5	Baulch et al., 1972
5*	$H + O_2 + M = HO_2 + M$	-47.10	1.04 (15)	0	-1.0	This Study
6	$H + O_2 = OH + O$	16.95	4.5 (10)	1.0	14.805	Cohen and Westberg, 1979
7	$H_2 + O = OH + H$	2.035	1.8 (10)	1.0	8.90	Baulch et al., 1972
8	$OH + OH = H_2O + O$	-17.22	2.14 (9)	1.10	0	Rawlins and Gardiner, 1974
9	$OH + H_2 = H_2O + H$	-15.19	1.1 (9)	1.3	3.646	Cohen and Westberg, 1979
10	$H + HO_2 = OH + OH$	-38.12	2.5 (14)	0	1.9	Baulch et al., 1972
11	$H + HO_2 = O_2 + H_2$	-57.10	2.5 (13)	0	0.7	Baulch et al., 1972
12	$OH + HO_2 = H_2O + O_2$	-72.29	5. (13)	0	1.0	Lloyd, 1974
13	$O + HO_2 = OH + O_2$	-55.07	5. (13)	0	1.0	Lloyd, 1974
14	$H_2 + O_2 = OH + OH$	18.98	2.51 (12)	0	39.0	Ripley and Gardiner, 1966
15	$HO_2 + H_2 = H_2O_2 + H$	14.57	3.0 (11)	0	18.68	Lloyd, 1974
16	$HO_2 + HO_2 = H_2O_2 + O_2$	-42.53	2.0 (12)	0	0	Lloyd, 1974
17	$H + H_2O_2 = H_2O + OH$	-67.88	3.0 (14)	0	9.0	Kondratiev, 1972
18	$H_2O_2 + OH = H_2O + HO_2$	-29.76	1.0 (13)	0	1.0	Baulch et al., 1972

Forward rate coefficients are expressed as $k_i = AT^b \exp(-E/RT)$ in units of cm^3, mole, sec. Numbers in parentheses refer to powers-of-ten, i.e., 1. (07) = 1×10^7. M refers to total concentration.

*Chaperon efficiencies relative to N_2 = 1.0 are: #1 -- $H_2O:H_2:N_2$ = 5:1:1; #2 -- $H_2O:H_2:Ar:N_2$ = 5:1:1:0.38:1; #5 -- $H_2O:H_2:Ar:N_2$ = 15:2.5:0.72:1. If not specified, chaperon efficiencies are assumed to be identical for all species.

$H + OH + M = H_2O + M$ (2)

$H + O_2 + M = HO_2 + M$ (5)

The percentage of the total recombination of radicals caused by each of these reactions varies with flame temperature and stoichiometry. Formation of the hydroperoxyl radical, HO_2, increases in importance as a recombination process under fuel-lean conditions.

At lower temperatures, formation of HO_2 and its destruction have a major role in generating radicals due to the large activation energy of reaction 6 (Dixon-Lewis, 1979). A low activation energy process resulting in formation of the highly reactive OH radical at low temperatures is:

$H + O_2 + M = HO_2 + M$ (5)

$H + HO_2 = OH + OH$ (10)

As a result, additional reactions of HO_2 must be considered to correctly describe OH levels.

Production of hydrogen peroxide by one or both of the following steps is an important sink for HO_2:

$HO_2 + H_2 = H_2O_2 + H$ **(15)**

$HO_2 + HO_2 = H_2O_2 + O_2$ **(16)**

Although H_2O_2 is limited to a very small region at the start of the reaction zone in flames, its formation via reaction 15 is an important chain-propagating step during the induction period in shock tube studies. To extend the range of applicability of the reaction mechanism, it is, therefore, necessary to include reactions which describe the production and consumption of H_2O_2.

The sections below describe results of numerical simulations of various experimental studies relevant to the development and validation of a detailed reaction mechanism for the H_2-O_2 system. The phenomena examined, progress in complexity from ignition delay times to detailed species profiles in flames. Consistency of the predictions with the broad range of experimental conditions investigated provides strong support that the reaction mechanism presented in Table 3-1 can be used to accurately model combustion of hydrogen.

3.1.1 Induction Period Phenomena

Initial calculations with the reaction mechanism listed in Table 3-1 involved comparisons with induction times measured in shock tube studies of hydrogen oxidation. During the induction period, the concentrations of radicals (H, O, OH, and HO_2) grow exponentially via chain-branching and -propagating steps at essentially constant temperature and pressure. There is also a negligible depletion of reactants during this period. As the radical concentrations increase, reaction rates rise proportionally and the induction period ends when the reaction rates become sufficiently large to cause a rapid increase in temperature.

Below 1100 K, induction times are extremely sensitive to the rate coefficient for reaction 5. At these temperatures, this reaction can compete successfully with reaction 6 for molecular oxygen and decrease the rate at which other radicals grow during the induction period. A comparison of predicted and measured induction times, therefore, allows a determination of the rate coefficient for reaction 5 which is consistent with other rate coefficients used in the H_2 reaction mechanism. In addition, relative chaperon efficiencies for this recombination reaction can be determined by using data obtained with different diluents.

Simulations of data reported by Skinner and Ringrose (1965) and Slack (1977) were used as the first test of the mechanism. Skinner and Ringrose measured induction times for a fuel-rich mixture between 960 and 1080 K at 5 atmospheres pressure. The induction time was defined as the time between when the gas was first heated by the reflected shock wave and when the OH emission intensity reached its maximum value. Slack studied stoichiometric H_2-air mixtures in the temperature range 980 to 1176 K at 2 atmospheres pressure. The test mixtures were prepared by mixing H_2, O_2, and N_2 gases. Induction times were defined as the time between the reflected shock pressure rise and the maximum positive rate of change of the OH emission signal. These two experimental studies were used to determine

K_5 [the rate coefficient of reaction 5] and the relative chaperon efficiencies for N_2 and Ar.

In several investigations of oxidation reactions, electronically-excited H_2-O_2-Ar (8% H_2-2%O_2-90% Ar) OH and ground-state OH have been found to have completely different concentration-time histories (Bowman and Seery, 1968; Porter et al, 1967). Since the reaction mechanism includes only reactions of species in the ground-state, a major difficulty was defining an induction time for the numerical simulations which was consistent with experimental observations. Analysis of the initial calculations for these two sets of data indicated that the reactions could be separated into two distinct groups based on the time at which the reaction rate reached its maximum value. The first group of reactions reached maximum rates before the temperature had risen more than 1.0 percent. The second group of reactions reached maximum values after the temperature had risen several hundred degrees. It was decided that a calculated induction time based on the first group of reactions, for which there was negligible temperature rise and depletion of reactants, was more representative of the measurements. It is of interest to note that the times at which the first group of reactions reached maxima were within 1 μsec of each other. Alternative definitions which could be used for the simulations gave results which had the same temperature dependence but were 10 to 40 percent higher. It was assumed that H_2 oxidation occurred adiabatically in a plug flow reaction at the pressure and initial temperatures characteristic of each investigation.

The agreement with induction times shown in Figure 3-1 was obtained with the following rate coefficient:

$$k_5 = 1.04 \times 10^{15} \exp(1000/RT); \; M = N_2$$

The induction times were found to be relatively sensitive to the value of the preexponential factor for reaction 5. The following procedure was adopted to optimize the rate of this reaction. The activation energy and chaperon efficiencies--15, 2.5, and 1 for H_2O, H_2, and O_2, respectively, relative to N_2--matched the recommendations of Baulch et al (1972). The

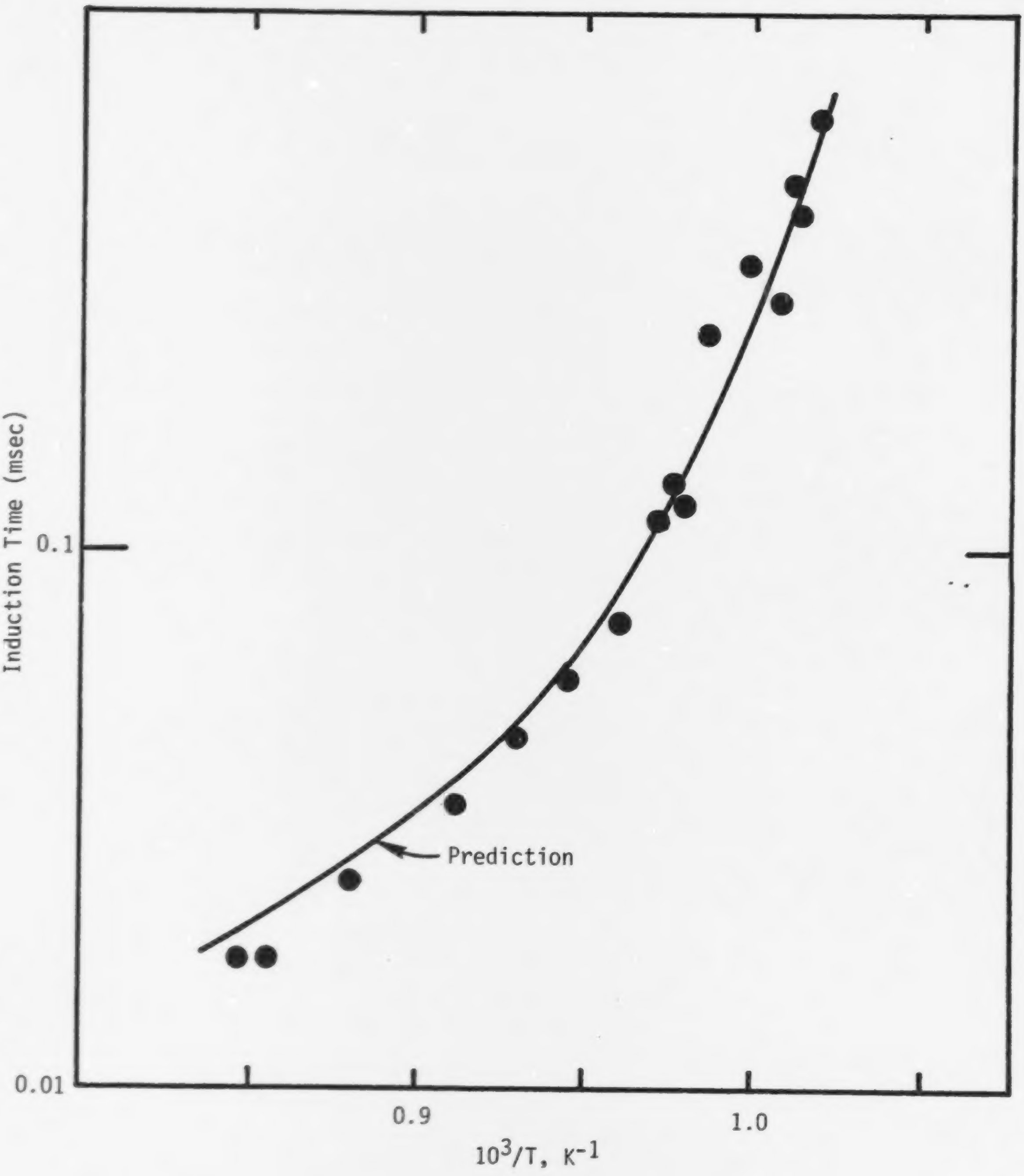

Figure 3-1. Comparison between predictions and the data of Slack (1977) for $H_2/O_2/N_2$ = 29.6/14.8/55.6, P = 2 atm.

Simulations of the data reported by Skinner and Ringrose (1965) were used to determine the chaperon efficiency of argon relative to nitrogen for reaction 5. The excellent agreement shown in Figure 3-2 was obtained for a chaperon efficiency of argon equal to 0.72 relative to nitrogen. This is in good agreement with the recommendations given by Baulch et al (1972)--$Ar:N_2$ = 0.75:1.0.

The contributions of other reactions to phenomena occurring during the induction period were also examined. The initial formation of radicals is due to reaction 14. Although decreasing k_{14} by a factor of two had no influence on the results, it was necessary to include this reaction to have any fuel consumption. For both systems investigated, reaction 16 was significant as a sink for HO_2 and in the production of H_2O_2:

$$HO_2 + HO_2 = H_2O_2 + O_2 \tag{16}$$

Reaction 10 was of equal importance for the removal of HO_2 in the stoichiometric H_2-air mixture and plays a lesser role in the fuel-rich mixture. This reaction plays a dual role as it also generates OH radicals and, therefore, promotes positive chain-branching:

$$H + HO_2 = OH + OH \tag{10}$$

The HO_2 radical is also converted to H_2O_2 via reaction 15, although the rate is slower than reactions 10 and 16. The destruction of H_2O_2 occurs mainly by thermal decomposition--reaction 4--and to a lesser extent by reaction 18:

$$H_2O_2 + M = OH + OH + M \tag{4}$$

$$H_2O_2 + OH = H_2O + HO_2 \tag{18}$$

Recombination reactions 1 to 3 were found to have no significant role during the induction period. These reactions were more important in the later stages of reaction after hydrogen, or oxygen, was largely depleted. Reactions 4 to 7, 9, 10, 16, and 18 are, therefore, the principal reactions which influence the induction period under these conditions of temperature, pressure, and reactant composition.

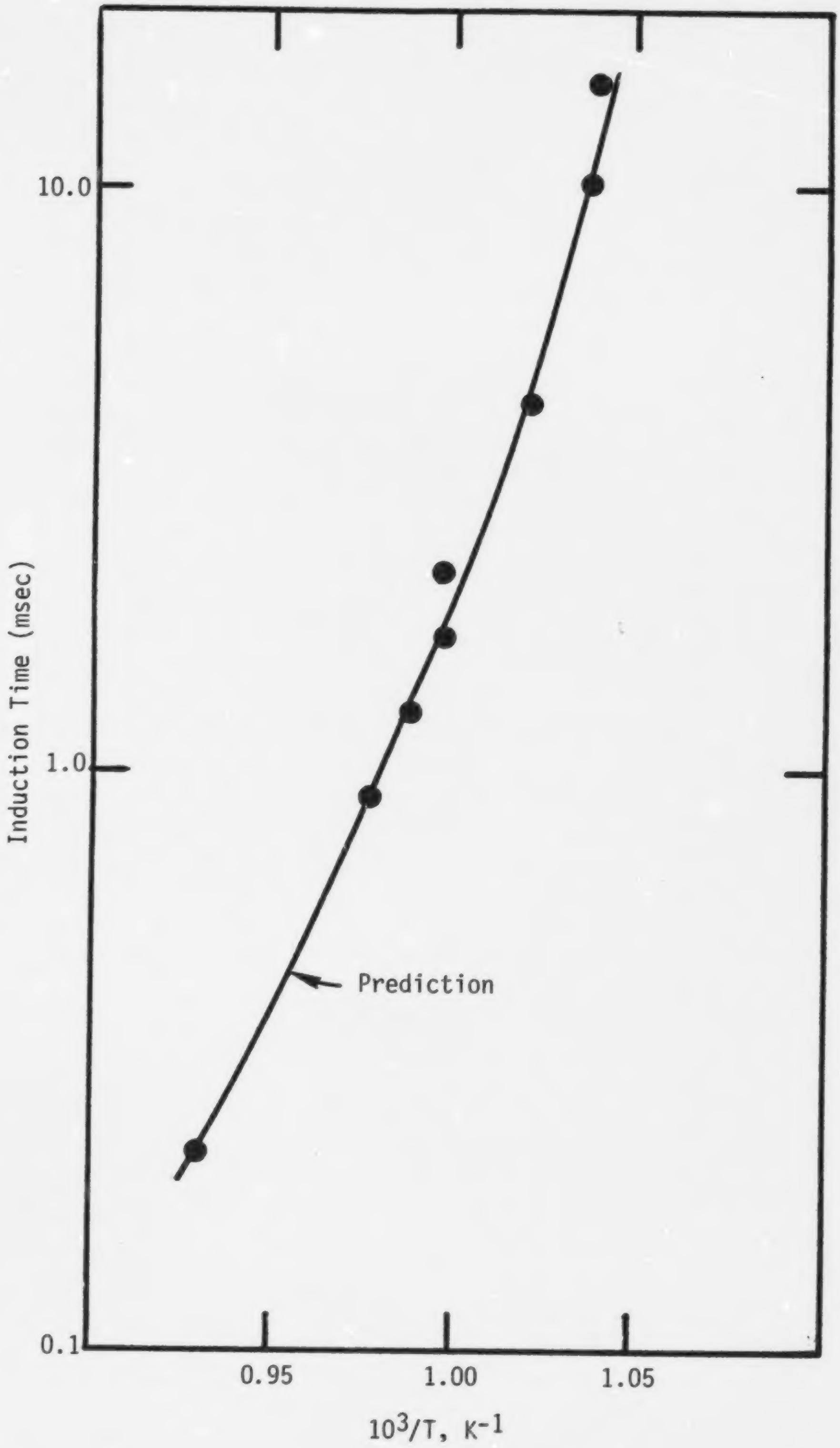

Figure 3-2. Comparison of induction times from Skinner and Ringrose (1965) with predictions: $H_2/O_2/Ar = 8/2/90$.

Since the data of Slack (1977) and Skinner and Ringrose (1965) were used to evaluate k_5 and the relative chaperon efficiencies of argon and nitrogen, the calculations described above are not a sufficient test of the reaction mechanism. Additional tests of the reaction mechanism used closed-form analytical solutions to the ignition kinetics of the hydrogen-oxygen system to examine the predictive capabilities of the mechanism at different conditions.

After a short induction time, it is assumed that radical concentrations grow exponentially under essentially isothermal conditions and with negligible depletion of reactants. It is further assumed that radical-radical reactions are not important because of their low concentrations. These assumptions are supported by the detailed kinetic simulations described above. With these constraints, the following reactions are assumed to dominate the production and destruction of radicals:

$$OH + H_2 = H_2O + H \qquad (9)$$

$$H + O_2 = OH + O \qquad (6)$$

$$O + H_2 = OH + H \qquad (7)$$

$$H + O_2 + M = HO_2 + M \qquad (5)$$

$$HO_2 + H_2 = H_2O_2 + H \qquad (15)$$

It is also assumed that the time dependence of each radical is given by:

$$C_i = A_i \exp(\lambda t), \; i = H, OH, O, HO_2$$

Analysis of the homogeneous, linear differential equations, which can be derived from the above simplified reaction scheme, yields an expression defining the exponential growth constant, λ:

$$\begin{aligned} \lambda^4 &+ \left[(k_9 + k_7 + k_{15})C_{H_2} + (k_6 + k_5\rho)C_{O_2}\right]\lambda^3 \\ &+ \Big[k_7k_9C_{H_2}^2 + (k_7 + k_9)k_5C_{H_2}C_{O_2}\rho \\ &+ \left(k_9CH_2 + k_6C_{O_2} + k_7C_{H_2}\right)k_{15}C_{H_2}\Big]\lambda^2 \\ &+ \left[(k_5\rho - 2k_6)C_{O_2} + k_{15}C_{H_2}\right]k_7k_9C_{H_2}^2\lambda \\ &- 2k_6k_7k_9k_{15}C_{H_2}^3C_{O_2} = 0 \end{aligned} \qquad (3\text{-}1)$$

If the initial hydrogen and oxygen concentrations, density (ρ), temperature and rate coefficients are specified, then this quartic equation may be solved for λ.

Jachimowski and Houghton (1970) monitored the growth of the OH radical in incident shock tube studies of H_2-O_2-Ar mixtures by ultraviolet absorption spectroscopy. Exponential growth constants for OH were reported in the temperature range of 1140 to 1900 K and for pressures between 0.25 and 0.75 atmospheres. The rate coefficients for reactions 5 to 7, 9 and 15 listed in Table 3-1 were used in conjunction with the experimental temperatures, densities, and reactant compositions to calculate λ from equation 3-1.

The comparisons with lean and rich mixtures shown in Figure 3-3 indicate reasonable agreement with the data, although the predictions (solid lines) have a slightly higher temperature dependence than experimentally observed. However, Jachimowski and Houghton (1970) assumed that the pressure and temperature during the induction period were the same as those calculated just behind the shock front for frozen chemistry conditions. Brabbs, Belles and Brokaw (1971) indicate that this assumption is not necessarily correct due to boundary-layer growth. Even with no heat release during the induction period caused by oxidation, the time-averaged temperature can be 1 - 3% higher than the initial value. Brabbs et al (1971) found that neglecting this correction results in rate constants, derived from exponential growth constant measurements, larger in absolute value (20 - 60%) and with lower dependencies on temperature. This is similar to the results shown in Figure 3-3 which suggests that the agreement between measurements and predicted behavior is much better than assessment of the calculations without the above considerations would indicate. A correction to the temperature scale for the observations on the order observed necessary by Brabbs et al (1971) would shift measured values for λ from 0.1 to 0.3 units to the left on the temperature scale and substantially improve the comparison between predicted and observed values for the exponential growth constant.

Brokaw (1965) derived equation 3-1 and showed that at atmospheric pressure a variety of reasonable assumptions about the initiation and termination of the induction period all lead to a simple relation between λ and

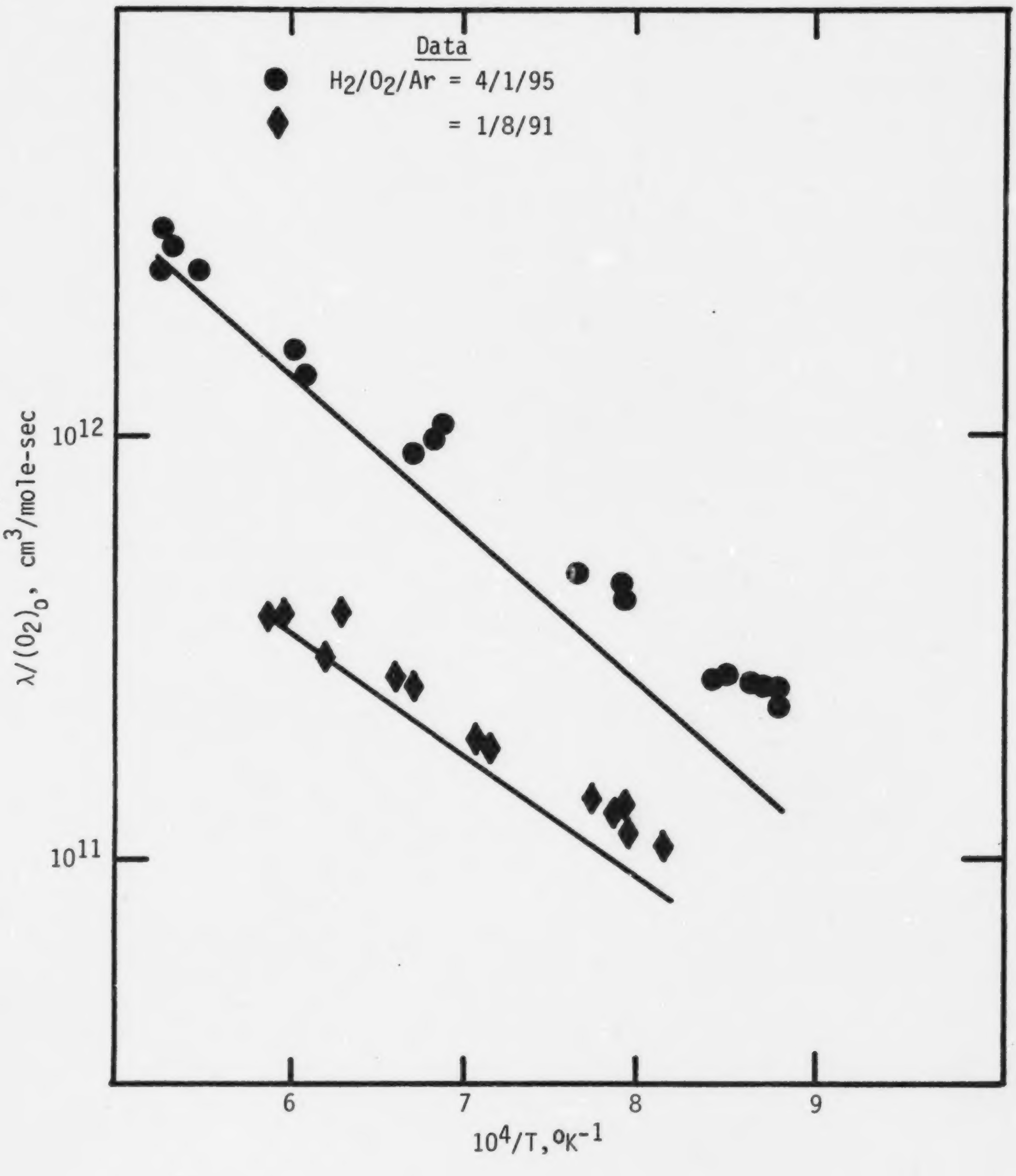

Figure 3-3. Exponential growth constants for $H_2/O_2/Ar$: Data from Jachimowski and Houghton (1970).

the induction time, τ:

$$\tau = B/\lambda \tag{3-2}$$

where B is a constant.

The region above the third explosion limit is characterized by long induction times with delays of several seconds observed between 833 and 873 K at atmospheric pressure. As a result, λ is small and it is not necessary to include the higher-order terms in equation 3-1 to obtain a good approximation of λ. Instead, the following expression is adequate for these conditions:

$$\lambda = 2k_6 k_{15} C_{H_2} / (k_5 \rho - 2k_6) \tag{3-3}$$

Equations 3-2 and 3-3 were, therefore, used with the relevant rate coefficients listed in Table 3-1 to predict induction times for hydrogen-air mixtures, as a function of initial H_2 concentration, at 867 K and atmospheric pressure. The calculations were compared with data reported by Anagnostou, Brokaw, and Butler (1956).

Figure 3-4 shows that the rate coefficients used for reactions 5 to 7, 9 and 15 reproduce the experimental trends and absolute values quite well. The value of B (27.5) was determined by matching the data at the leanest condition; i.e., 10 percent hydrogen, or a stoichiometric ratio of 3.78. Although a single data point was used to fix B, the fact that the experimental composition dependence of τ is well-predicted lends further support to the set of rate coefficients used. It should also be noted that the agreement obtained required the use of relative chaperon efficiencies for reaction 5 as given in Table 3-1. It was not possible to predict the dependence on initial reactant concentration if this rate coefficient was assumed to be independent of the relative concentrations of H_2, O_2, and N_2.

3.1.2 Flame Phenomena

The ability of the reaction mechanism given in Table 3-1 to accurately predict the growth of radicals, and therefore fuel consumption, under essentially isothermal conditions has been demonstrated in the previous section. A more stringent test of the capabilities of the mechanism is provided by comparing predicted and experimental phenomena which occur in simple flame

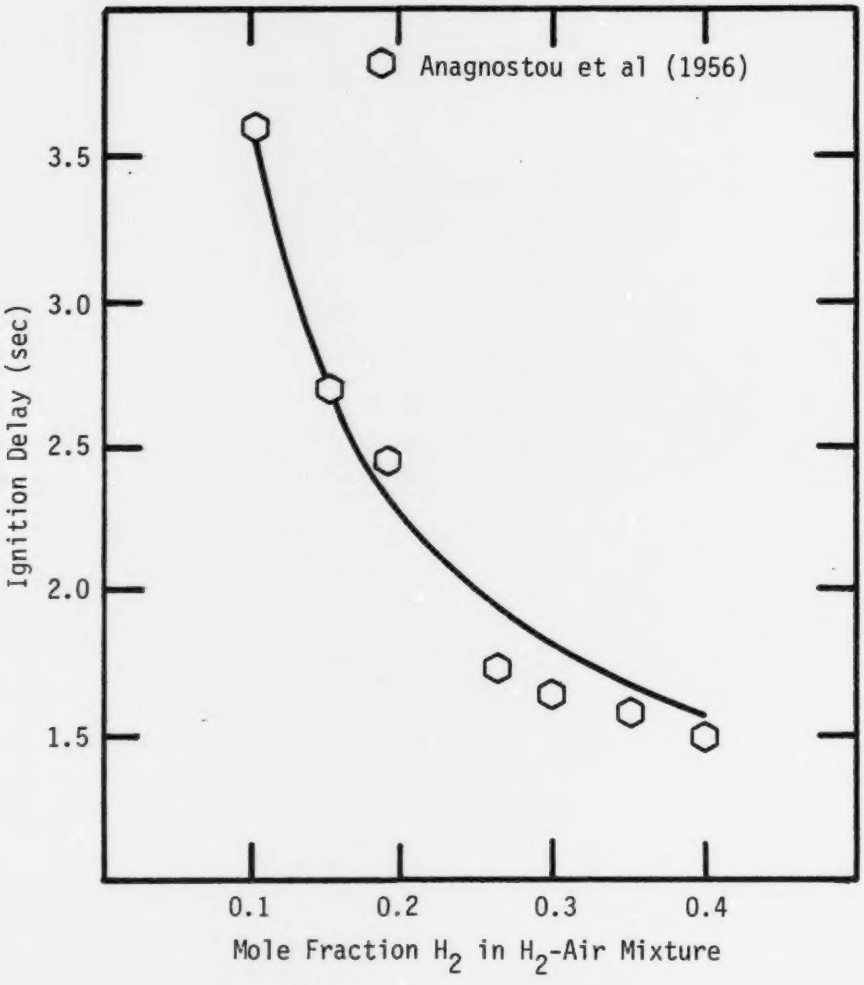

Figure 3-4. Comparison of model with experiment for ignition delays of H_2-air mixtures.

environments. Simulations of premixed, freely propagating, laminar H_2-air flames burning at atmospheric pressure were used in this sequence of calculations. Comparison with the observed burning velocity of an H_2-air flame, a phenomenon which is controlled by the rate of hydrogen or oxygen consumption, which, in turn, is determined by the production of radicals in the flame, provides a global check of the reaction mechanism. If calculated and measured species and temperature profiles are also in agreement, the accuracy of the reaction mechanism is definitely established.

The simulations were done using an implicit finite-difference approximation of the relevant time-dependent equations (see Volume IV, FCR Final Report). A simple bifurcation model was used to calculate the diffusion of stable and radical species relative to oxygen. This procedure circumvents the necessity of solving the Stefan-Maxwell equations, which strictly define the diffusion of species in a multicomponent mixture. Although calculations indicate that the results are not sensitive to changes of the bifurcation parameters by ±20 percent, computations are not yet completed which will quantify the differences between this simplified model and results which included the full Stefan-Maxwell formulation. Thermal diffusion is also neglected in the current calculations, although its inclusion at a later date involves minimal effort.

Two early sets of measurements of the burning velocities of hydrogen-air mixtures at atmospheric pressure were reported by Jahn (1934) and Scholte and Vaags (1959). Jahn divided the area of the Schlieren cone of the flame into volumetric flow rate of the gases entering it to determine burning velocity. Scholte and Vaags (1959) burned their flames as straight-sided cones on a constant velocity profile nozzle. In this study, the burning velocity was derived from $v = V \sin \alpha$, where V is the linear gas velocity, calculated from the total volumetric gas flow and the burner port area, and α is the measured cone half-angle. Both investigations found the maximum burning velocity occurred with about 42 percent H_2 in the premixed feed (SR = 0.58) with a value between 270 and 280 cm/sec.

More recent investigations of hydrogen-air burning velocities, again with the use of burner methods, employed the particle-tracking technique to directly measure the gas velocity, V, approaching the flame, and Schlieren photography to define the flame cone half-angle, α. By these means, Edmondson and Heap (1971) and Günther and Janisch (1972) found the burning velocity of a 50 percent hydrogen flame (SR = 0.42) to be 300 $\pm$5 cm/sec. This is significantly higher than the value reported by Scholte and Vaags (1959) and Jahn (1934)--250 $\pm$ 10 cm/sec. The more recent measurements, which have greater values than the earlier work for the entire range of hydrogen concentrations examined, are to be preferred since more refinements were incorporated into the measurement techniques.

Figure 3-5 shows the predicted (solid line) burning velocities for H_2-air mixtures between 25 and 70 percent hydrogen in the feed ($0.18 \leq SR \leq 1.25$). The calculations agree quite well with the data of Scholte and Vaags (1959) and Jahn (1934), but are significantly lower than the presumably more accurate and refined measurements of Günther and Janisch (1972) and Edmondson and Heap (1971). The theoretical curve accurately predicts the location of the maximum burning velocity (41 percent H_2, SR = 0.63), but the value is 25 percent lower than that reported by Günther and Janisch (1972). The occurrence of the maximum on the fuel-rich side is associated with the increase in OH and O-atom concentrations as stoichiometric conditions are approached and the increased contributions of reactions 12 and 13 to chain-breaking.

The sensitivity of the predicted burning velocities to variations of rate coefficients was investigated to determine whether the discrepancies indicated in Figure 3-5 were due to incorrect values, or temperature dependencies, used for the rate constants. Attention was focused on reactions involving HO_2 and the recombination reactions 1 and 2. The latter two reactions were included because the induction time studies did not provide a critical test of the rate coefficients used. Reactions 10 and 12 were included because experimental data recently reported by Hack et al (1978a, 1978b, 1978c, 1979) suggest that the values of the rate constants at low temperatures are low by up to a factor of two. These sensitivity studies were done at 41 percent hydrogen, which is the location of the maximum predicted burning velocity, 273 cm/sec).

Sensitivity of the maximum burning velocity to the recombination reactions, 1 and 2, was first examined. Dixon-Lewis (1979) suggests that a

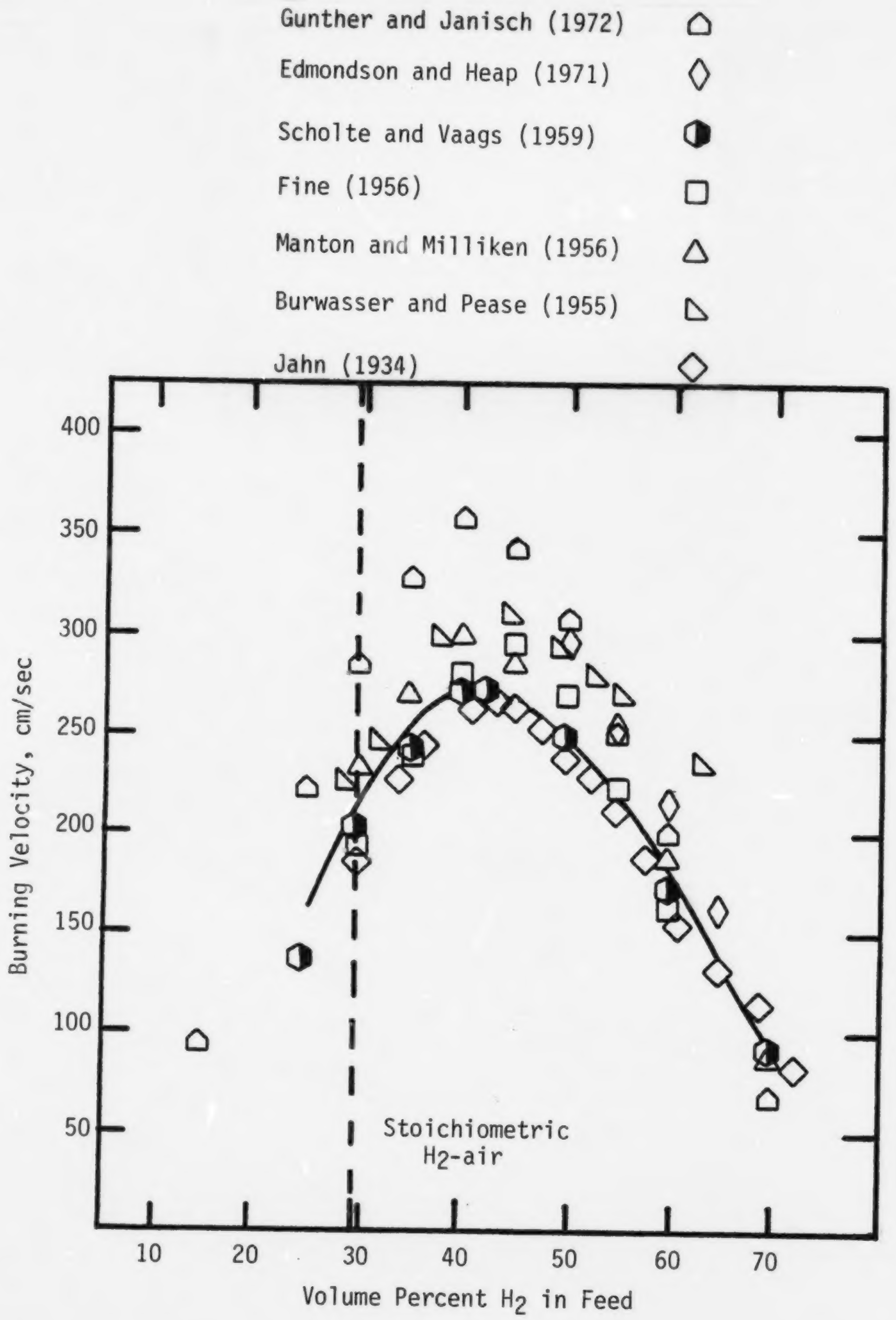

Figure 3-5. Burning velocity of H_2-air flames: T_o = 298°K, P_o = 1 atm.

slightly better value for k_2 with N_2 as the third body is

$$k_2 = 1.6 \times 10^{22} T^{-2.0} \quad .$$

Use of this rate coefficient with the relative chaperon efficiencies given in Table 3-1 increases the calculated burning velocity for the 41 percent H_2 flame to 282 cm/sec. This is not significant improvement with regard to the discrepancy observed between the measured maximum burning velocity of Günther and Janisch (1972) and that predicted.

Experimental studies of H-atom recombination indicate that not only are chaperon efficiencies not equal for many species but that the relative efficiencies vary with temperature (Walkankas and Kaufman, 1975). Dixon-Lewis (1979) recommends the following expressions which are consistent with the low-temperature data:

$$k_1(M = H_2) = 9.2 \times 10^{16} T^{-0.6}$$

$$k_1(M = H_2O) = 6.0\ 10^{19} T^{-1.25}$$

$$k_1(M = N_2, O_2) = 1.0 \times 10^{18} T^{-1}$$

The calculated burning velocity did not change when these rate coefficients were used instead of the expression given in Table 3-1 and chaperon efficiencies for species not specified in the above expressions were assumed to be identical to N_2 and O_2.

The last set of calculations involved changes in the preexponential factors of reactions 10 to 13 to reflect more recent experimental data at room temperature; the activation energies for these reactions were not changed. Since a reduction in k_2 was found to increase the predicted burning velocity by about 3 percent, the alternate rate coefficient suggested by Dixon-Lewis (1979) was included in the simulation to see whether the combined effect of these adjustments would significantly increase the predicted burning velocity. The resulting value--279 cm/sec--is about 1 percent lower than that obtained when only k_2 was modified.

The sensitivity analysis indicates that the lower-than-observed predicted burning velocities are not due to uncertainties of the rate parameters for reactions 1, 2, and 10 to 13. The possibility that other rate coefficients are incorrect cannot be precluded on the basis of these calculations. Consideration should be given to the important recombination process--reaction 5. If the chaperon efficiencies of various species have different temperature dependencies, as suggested for reaction 1, then the low temperature behavior of this reaction may not be accurately represented by the expression given in Table 3-1. Inaccuracies in the absolute values of the reverse of reaction 7 at low temperature are another possibility, as well as the temperature dependence assumed for reaction 8. It may also be that the simple bifurcation model is not adequate to describe diffusive processes of radicals in the H_2-air flame. Although questions regarding rate coefficients can be resolved via experimental techniques, the last point raised must await results of calculations in which the Stefan-Maxwell equations are included.

Dixon-Lewis (1979) has also calculated properties of H_2-air flame including burning velocities, with a reaction mechanism very similar to that used here. Predicted burning velocities were significantly lower than the more recent measurements of Edmondson and Heap (1971) and Günther and Janisch (1972) which are in agreement with our results. Dixon-Lewis suggested that since the important, rate-controlling process of radical production occurs in the hotter regions of flames, burning velocity measurements in flames which are not truly one-dimensional should be referenced to some position at the hot end of the flame. He derived a "correction" factor for the data of Edmondson and Heap (1971) and Günther and Janisch (1972) which used the position of maximum H-atom concentration, as determined from the simulations, for the new reference flame. Figure 3-6 shows that the reaction mechanism in Table 3-1 yields results in good agreement with the "corrected" measurements. Data reported by Andrews and Bradley (1973) using the single-kernel technique are also plotted in this figure. The values are based on the relation:

$$v^0 = \frac{\rho_b}{\rho^0} \frac{dr_b}{dt}$$

where r_b is the measured radius of the core of unburnt gas. Dixon-Lewis (1979) argues that the reduction procedure used by Andrews and Bradley is not meaningful and, therefore, the method can only yield lower limits to the burning velocity. Note that the arguments employed by Dixon-Lewis

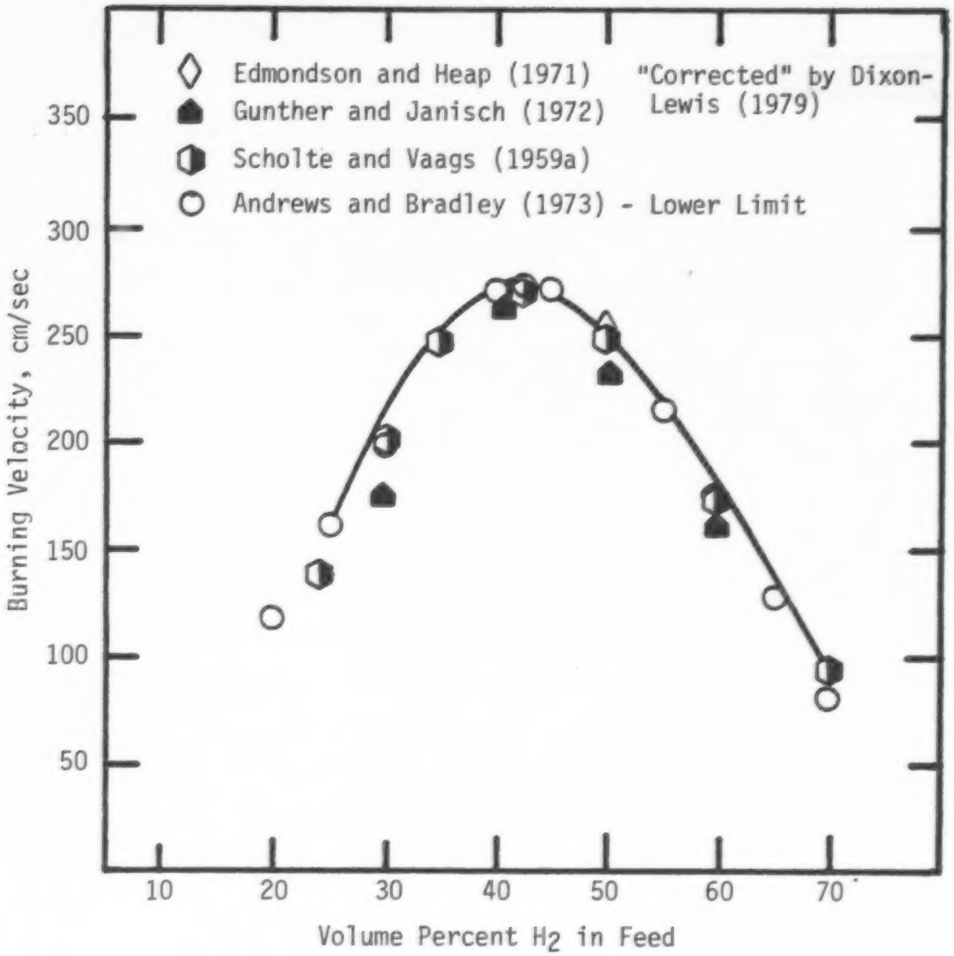

Figure 3-6. Comparison with modified data for H_2-air burning velocities.

(1979) result in "corrected" values for the more recent measurements which are consistent with the earlier data reported by Scholte and Vaags (1959a).

F3-7

Figure 3-7 illustrates the relation between burning velocity and peak H-atom concentration in atmospheric pressure H_2-air flames. Padley and Sugden (1959) measured H-atom concentrations in the recombination zone of a number of fuel-rich H_2-O_2-N_2 flames. These measurements were extrapolated back into the flames by use of partial equilibrium assumptions to estimate the maximum H-atom concentration and then plotted against the burning velocity measurements of Jahn (1934). Comparison with detailed kinetic calculations and the partial equilibrium assumptions suggest that this technique over-estimates the actual H-atom concentration by about 20 percent (Dixon-Lewis, 1979). This factor, in conjunction with uncertainty in the measured burning velocities, which are probably low, suggests that the predicted behavior, obtained with our reaction mechanism, is in agreement with the observations.

The results of the calculations shown in Figures 3-6 and 3-7 indicate that the reaction mechanism for H_2 oxidation predicts burning velocities and radical concentrations which are consistent with earlier studies of H_2-air flames. The calculated burning velocities also agree with the lower limits determined by Andrews and Bradley (1973). Although a correction procedure can be used which lowers the data of Edmondson and Heap (1971) and Günther and Janisch (1973) to values in agreement with predictions, the question of whether theory or experimental data is correct still exists. The issue is further clouded by data reported by Bertrand, Dussart, and Van Tiggelen (1979) which supports a value of the burning velocity for a stoichiometric H_2-air flame of about 225 cm/sec as compared to a predicted value of 211 cm/sec. Another question which arises in interpreting the numerical results is whether molecular nitrogen can be treated as an inert; i.e., can production of nitrogen oxides (NO, NO_2, and N_2O) be ignored? Grillo and Slack (1977) found that ignition delays in H_2-air mixtures were significantly reduced when NO or NO_2 was added to the feed. Below 950 K and at 2 atmospheres, the ignition delay was reduced by more than an order-of-magnitude when 5000 ppmV NO was added. At 0.27 atmosphere, a reduction of 30 percent, which was independent of NO mole percent (0.5 to 2.25 percent),

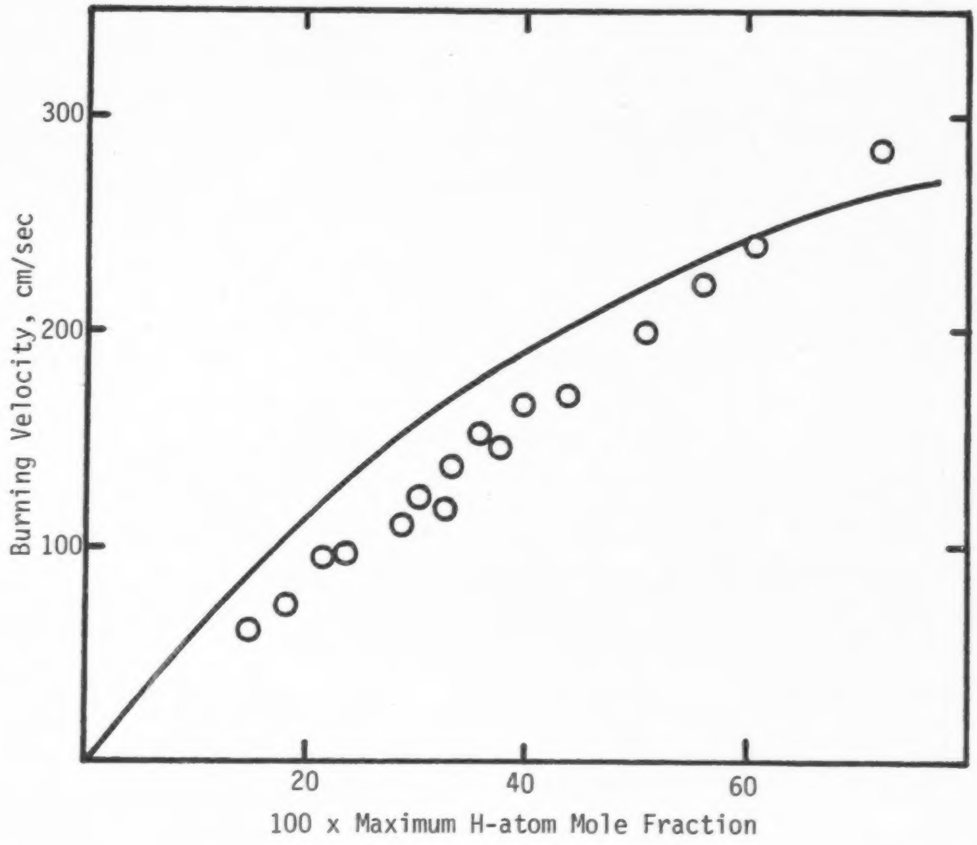

Figure 3-7. Relation between burning velocity and peak H-atom concentration in H_2 flames at atmospheric pressure: data of Padley and Sugden (1959) referred to V_0 from Jahn (1934).

was observed between 900 and 1400 K. At 1000 K and atmospheric pressure, reductions in the measured ignition delays ranged from 40 percent at 0.5 percent NO to 47 percent at 2.25 percent NO. The effect was attributed to the fast, homogeneous, gas-phase, catalytic chain:

$HO_2 + NO = OH + NO_2$

$H + NO_2 = OH + NO$

which converted the hydroxyl formed via recombination (reaction 5) to the chain-branching OH radical.

The occurrence of the sensitization of temperatures between 800 and 1400 K, which is a critical temperature range for flame propagation reactions, suggests that the sequence of reactions recycling NO, which is globally equivalent to reaction 10, could play a significant role in predicting H_2-air flame phenomena. Adiabatic temperatures for the freely propagating, laminar, flat flames simulated are greater than 1800 K even at a stoichiometric ratio of 0.40. This information, as well as consideration of the peak species concentrations shown in Figure 3-8 indicates that significant concentrations of NO can be formed under conditions where the burning velocity is maximum (SR = 0.63). An increase of predicted burning velocities would depend on the concentrations of NO in the flame and the subsequent diffusion of NO into cooler regions in the flame zone. Further calculations are obviously required to evaluate the importance of NO, NO_2, and N_2O reactions to simulations of flame phenomena.

Although there is a discrepancy between predicted and measured burning velocities, the calculations do provide insight into the mechanism of flame propagation. In all cases examined, the release of energy extends over the entire temperature range in the flame, but occurs primarily by the low activation energy sequence initiated by recombination of H-atoms with molecular oxygen (reaction 5) and followed by reactions of HO_2 with H, OH, or O-atoms (reactions 10 to 13). Hydrogen atoms are regenerated by reaction of OH, which is produced in reactions 10 and 13 with H_2 via reaction 9 and/or by reaction of O-atoms with H_2 (reaction 7) depending upon the stoichiometry. These heat release cycles, which occur in the cooler regions of the flame, are effectively chain propagating or chain-terminating. The radicals responsible, H, O, and OH, are produced by the chain-branching cycle,

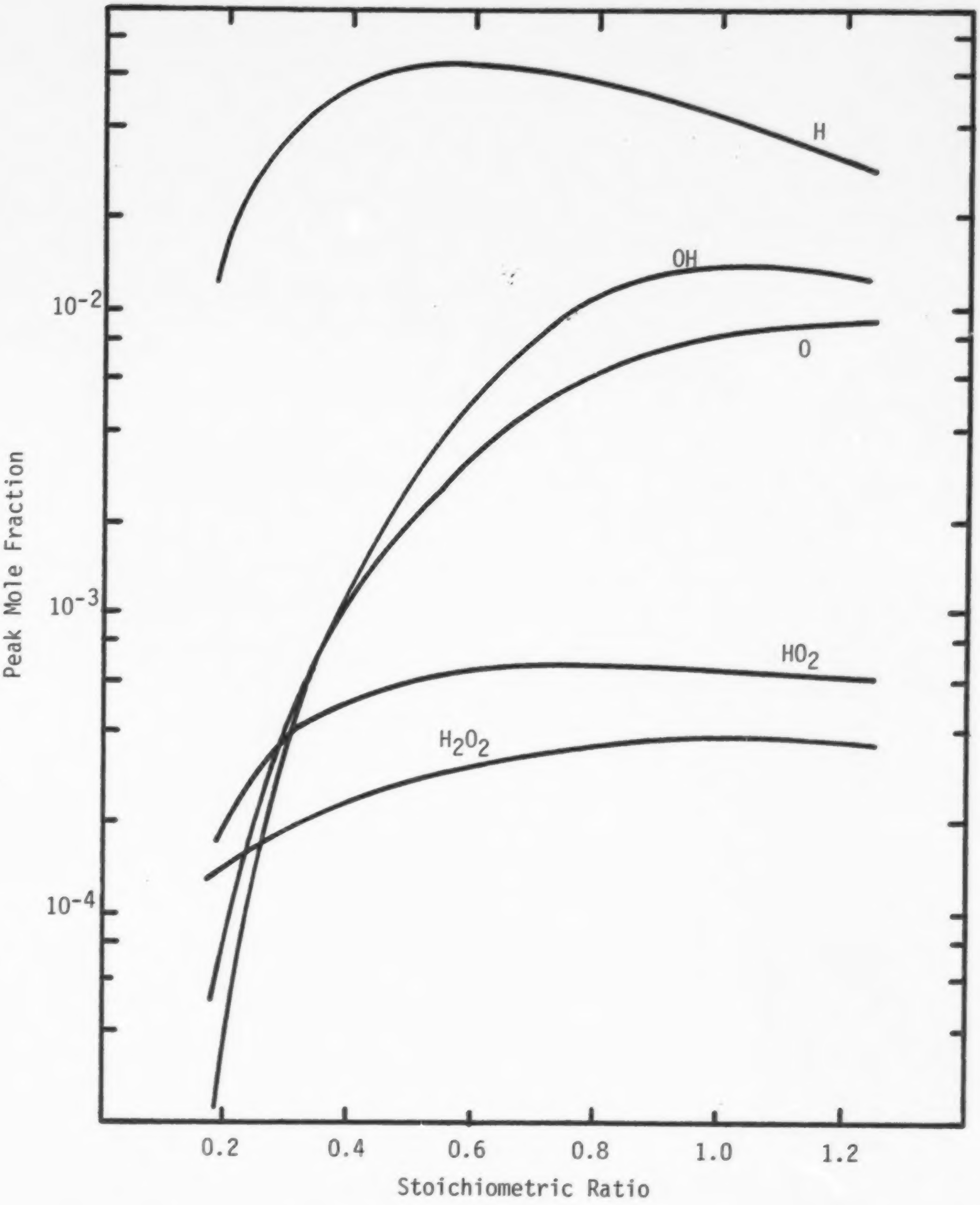

Figure 3-8. Maximum species concentrations in H_2-air flames: T_o = 298 K, P_o = 1 atm.

reactions 6, 7, and 9, in the hotter regions of the flame, and diffuse upstream to react with molecular oxygen via the cycle started by reaction 5. The recombination steps, reactions 1 and 2, are dominant only for conditions where O_2 is at low levels, such as the recombination zones of fuel-rich flames.

The H_2 oxidation reaction mechanism was also tested against data reported by Dixon-Lewis, Sutton, and Williams (1970) for a low-temperature, fuel-rich H_2-O_2-N_2 flame. Mass spectrometry was used to measure H_2, O_2, and H_2O, and a coated thermocouple was used to measure temperature as a function of distance above the burner. The authors indicate that special procedures, which were not described, were required to reduce the mass spectrometer meeasurements to mole fractions in order to minimize errors introduced by the sampling technique. It was assumed that the flame could be described as a freely propagating, laminar, flat flame with the initial conditions $T^o = 336$ K and P = 1.0 atm.

Figure 3-9 compares the predicted profiles with the measurements; the comparison of temperature profiles is shown in Figure 3-10. The lower decay rate predicted for hydrogen is probably due to lack of thermal diffusion in the computer model (Warnata, 1979). Although the calculated profile for H_2O is higher than the measurements in the lower temperature region of the flame, it is certainly reasonable when the scatter of the data is considered. The excellent agreement with the temperature data reinforces the contention that the reaction mechanism accurately models this flame. The predicted burning velocity is 9.1 cm/sec ($T < 336$ K, $P = 12$ atm), which is lower than that determined experimentally using the particle tracking method, 10.5 ±0.2 cm/sec (T = 336 K, P = 1 atm). However, if the arguments postulated by Dixon-Lewis (1979) are applicable to this flame, then the experimental value is an upper limit. It is concluded that the reaction mechanism is in agreement with the experimental observations.

3.1.3 Summary

The reaction mechanism describing oxidation of hydrogen has been demonstrated to accurately predict induction period and flame phenomena. Comparisons with shock tube data for H_2-O_2-Ar and H_2-air mixtures near 1000 K established a rate coefficient for reaction 5 consistent with the other

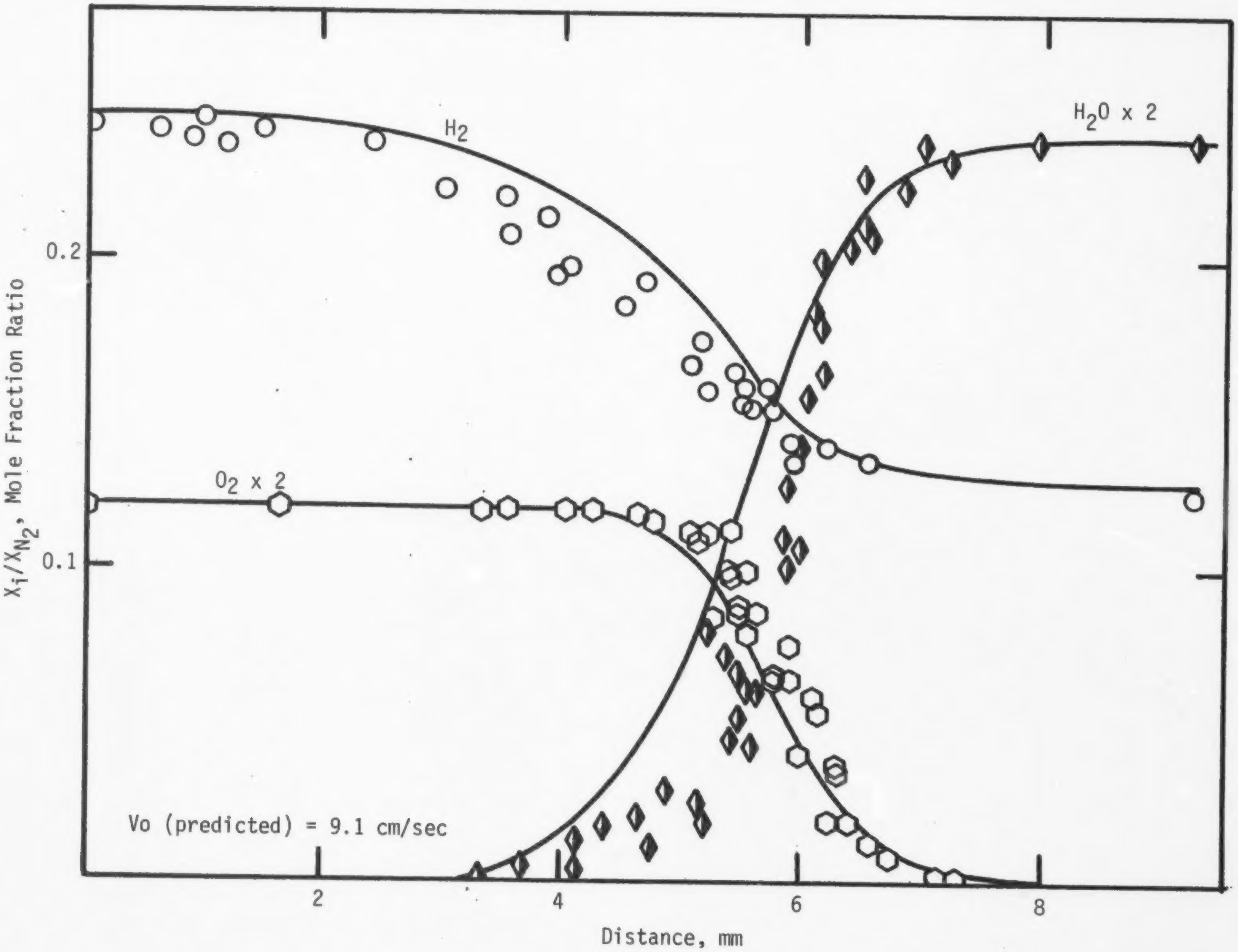

Figure 3-9. Prediction of stable species profiles for a $H_2/O_2/N_2$ (18.83/4.6/76.57). Data of Dixon-Lewis et al., 1970.

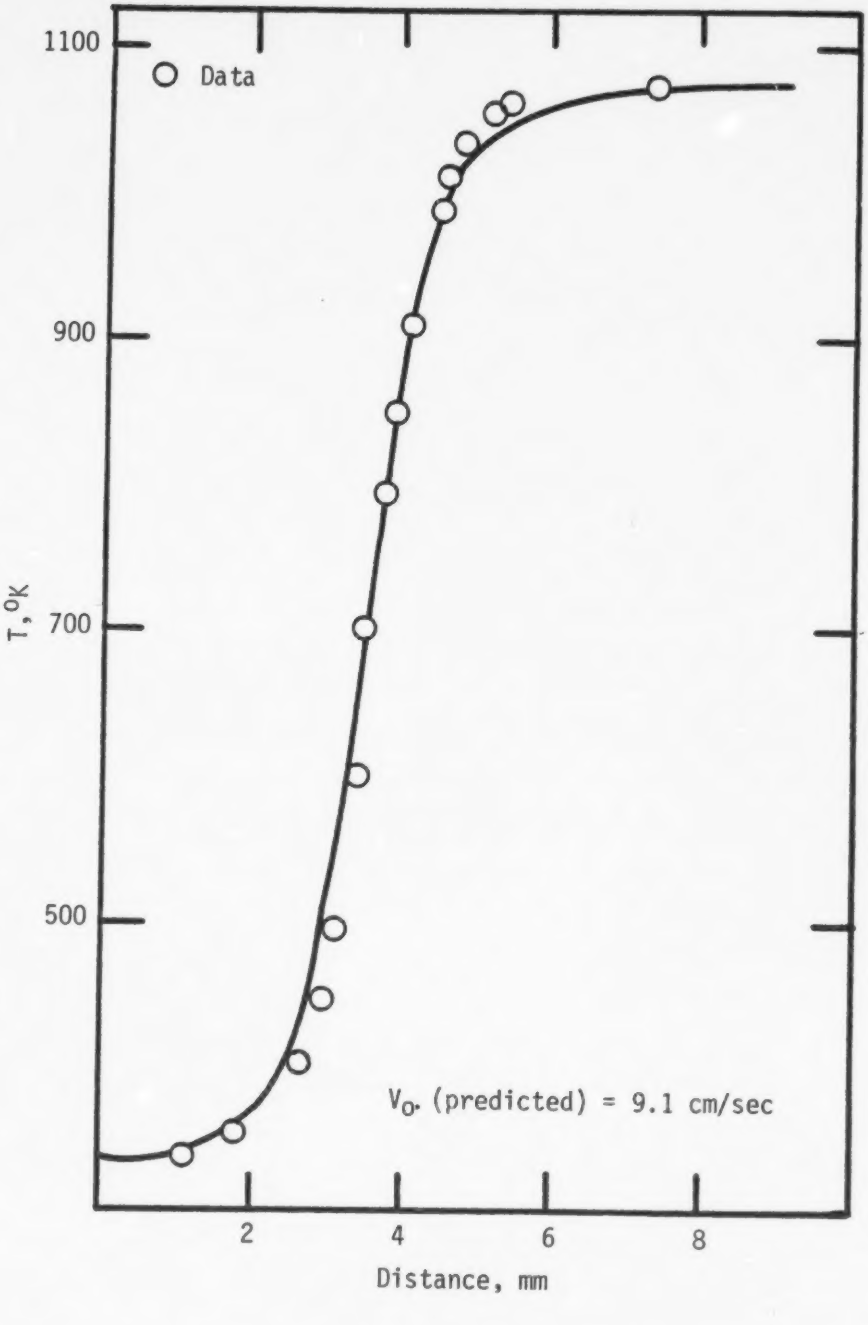

Figure 3-10. Predicted temperature profile for a $H_2/O_2/N_2$ = 18.83/4.6/76.57 flat flame (T_o = 336 K, P_o = 1 atm): Dixon-Lewis et al. 1970.

rate coefficients used. Relative chaperon efficiencies of argon and nitrogen were also established--Ar:N_2 = 0.72:1.0. Additional calculations for H_2-O_2-Ar mixtures indicated that the mechanism reproduced exponential growth constants for the OH radical during the induction period for temperatures between 1100 and 1900 K for both lean and rich mixtures.

Predicted burning velocities for atmospheric pressure, freely propagating, laminar H_2-air flames were consistent with earlier data reported in the literature. However, the calculated values were significantly lower than the more recent data reported by Günther and Janisch (1972) and Edmondson and Heap (1971), although the values do agree with the lower limits established by Andrews and Bradley (1973). A sensitivity analysis of the simulations indicated that changes in recombination reaction rate coefficient (reactions 1 and 2), and modifications of rate coefficients for reactions of HO_2 with H, O, and OH radicals (reactions 10 to 13) would not appreciably increase the predicted values. The issue was further clouded since the reaction mechanism was shown capable of predicting the relation between burning velocity and peak H-atom concentration reported by Padley and Sugden (1959). Modification of the measured burning velocities reported by Günther and Janisch (1972) and Edmondson and Heap (1971) as suggested by Dixon-Lewis yields values consistent with the predictions.

The reaction mechanism has also been shown capable of predicting stable species profiles and the temperature profile for a low-temperature, fuel-rich, H_2-O_2-N_2 flat flame. The predicted H_2 profile was less steep than that observed because thermal diffusion was not included in the flame model. The congruence of predicted and measured temperature profiles indicates that heat release is accurately reproduced by the reaction mechanism.

Analysis of the results for the flat flame simulations demonstrated that production of HO_2 and its subsequent destruction at low temperature constituted the dominant heat release cycle. The radicals which participate in this cycle are generated in the hotter regions of the flame by chain-branching mechanisms, then diffuse upstream to react with molecular oxygen via reaction 5 and HO_2 via reactions 10 to 13. The hydroperoxyl radical is, therefore, an important species in determining the structure of hydrogen flames, as well as induction phenomena for hydrogen-oxygen mixtures.

The H_2-O_2 reaction mechanism is now believed to be sufficiently accurate to form the basis of subsequent fuel oxidation mechanisms. However, additional experimental data pertaining to the absolute values and temperature dependencies of reactions 5 and 10 to 13 are desirable in light of the questions concerning burning velocities. In particular, the temperature dependence of reaction 5 as a function of various third-bodies should be investigated. Additional calculations are necessary to determine the impact of reactions involving NO, NO_2, and N_2O on the structure of H_2-O_2-N_2 flames. It is also recommended that the computer model be modified to include multicomponent diffusion as defined by the Stefan-Maxwell equations. A series of calculations with this added complexity would quantify any error associated with using the simple bifurcation model.

3.2 The CO-H_2-O_2 Reactions

The importance of CO oxidation in the latter stage of hydrocarbon combustion processes establishes the need for an accurate reaction mechanism which can describe the conversion of CO to CO_2. Since the initial, relatively rapid, transformation of hydrocarbon fuels to intermediate combustion products yields H_2 and H_2O in addition to CO, simulations designed to verify the correctness of the CO reaction mechanism emphasized comparison with experimental investigations in which the oxidation of CO in the presence of H_2 or H_2O was studied. Comparisons of predictions with data from shock tubes (induction times and species profiles, burning velocity, and flat flame species profiles) provided the criterion for establishing the adequacy of the reaction mechanism.

Table 3-2 lists the reactions which, in addition to reactions 1 to 18 define the mechanism describing CO oxidation. Carbon monoxide is converted to CO_2 primarily by

$$CO + OH = CO_2 + H \tag{21}$$

because the spin-hindered, recombination process

$$CO + O + M = CO_2 + M \tag{22}$$

is much slower under typical combustion conditions. Reaction of CO with molecular oxygen (reaction 23) is a minor process, although its importance increases at high temperatures and as the concentration of hydrogen-

Table 3-2. CO-H_2-O_2 Reaction Mechanism

No.	Reaction	ΔH_r^0, 298 kcal/mole	A	b	E kcal/mole	Reference
19*	$CO + O + M = CO_2 + M$	-127.2	3.8 (24)	-3.	6.17	Est. This Study
20*	$HCO + M = H + CO + M$	16.68	1.55 (14)	0	14.675	Schecker and Jost, 1969
21	$CO + OH = CO_2 + H$	-25.03	1.51 (7)	1.3	-0.765	Baulch and Drysdale, 1974
22	$CO + HO_2 = CO_2 + OH$	-63.14	1.0 (11)	0	10.	Lloyd, 1974
23	$CO + O_2 = CO_2 + O$	-8.078	6.90 (7)	1.0	34.81	Est. This Study
24	$HCO + H = CO + H_2$	-87.52	2.0 (14)	0	0	Niki et al., 1969
25	$HCO + O = CO + OH$	-85.48	5.5 (12)	0.5	0	Est. This Study
26	$HCO + O = CO_2 + H$	-110.5	5.5 (12)	0.5	0	Est. This Study
27	$HCO + OH = CO + H_2O$	-102.7	3. (10)	1.0	0	Engleman, 1976
28	$HCO + O_2 = CO + HO_2$	-30.42	5. (11)	0.5	0.834	Est. This Study

Forward rate coefficients are expressed as $k_j = AT^b \exp(-E/RT)$ in units of cm^3, mole, sec. Numbers in parentheses refer to powers-of-ten, i.e., 1.(17) = 1×10^{17}. M refers to total concentration.

*All chaperon efficiencies (for Reactions 19 and 20) are assumed equal. In addition, CO, CO_2, and HCO are assumed to have the same chaperon efficiency as N_2 for Reactions 1 and 2 in Table 1-2. For Reaction 5, the relative chaperon efficiencies are: $CO_2:CO:HCO:N_2 = 3.75:1:1:1$.

containing compounds decreases. This reaction also contributes to the initial production of radicals in the high-temperature, shock tube oxidation of CO. Reaction 23 is included in the mechanism for completeness, since it represents a minor path for CO_2 production above 1000 K.

The production of the formyl radical (HCO) via reaction 20 and its consumption via reactions 24 to 28 are considered because of the potential impact on low-temperature flame phenomena (Gardiner, 1978). The argument is essentially that reaction 20 may compete with the important step of HO_2 formation via reaction 5 and alter the rate at which other radicals, especially OH, are produced at low temperatures. In addition, the destruction of HCO is a chain-breaking process which could also influence the flame structure. Cherian et al (1981) have independently arrived at the conclusion that HCO chemistry is necessary to describe fuel-rich CO/H_2 or CO/H_2O combustion.

3.2.1 Shock Tube Data

Monitoring the initial stages of CO oxidation in shock tubes can provide information pertinent to the growth of radicals as a function of temperature, pressure, and stoichiometry. Brabbs, Belles, and Brokaw (1971) investigated the reaction of CO-H_2-O_2-CO_2-Ar mixtures behind incident shock waves between 1083 and 1900 K. Optical techniques were used to record the intensity of the CO flame band emission (which is proportional to the product of CO and O-atom concentrations) as a function of time behind the shock wave. Since very little CO was consumed, the light intensity monitors the growth of oxygen atoms during the reaction. The authors report exponential growth constants for atomic oxygen derived from semilogarithmic plots of the emission intensity versus time for different mixtures and temperatures.

The exponential growth data of O-atoms was used to derive rate coefficients for reactions 6, 7, 8, and 21. Brabbs et al (1971) assumed that, after a short initiation phase, the production of radicals during the oxidation of carbon monoxide was controlled by a small number of reactions:

$$H + O_2 + M = HO_2 + M \qquad (5)$$

$$H + O_2 = OH + O \qquad (6)$$

$$O + H_2 = OH + H \tag{7}$$

$$OH + H_2 = H_2O + H \tag{8}$$

$$CO + OH = CO_2 + H \tag{21}$$

Analysis of this subset of reactions in a manner similar to that used to develop equation 3-1 yields a cubic equation, the roots of which define the exponential growth constant, λ;

$$\begin{aligned}
&\lambda^3 + \left[k_9C_{H_2} + k_6C_{O_2} + k_7C_{H_2} + k_5C_{O_2} + k_{21}C_{CO}\right]\lambda^2 \\
&\quad + \left[\left(k_9C_{H_2} + k_{21}C_{CO}\right)\left(k_7C_{H_2} + k_5C_{O_2}\rho\right) + k_7k_5C_{H_2}C_{O_2}\rho\right]\lambda \\
&\quad - k_7C_{H_2}\left(k_9C_{H_2} + k_{21}C_{CO}\right)\left(2k_6C_{O_2} - k_5C_{O_2}\rho\right) = 0
\end{aligned} \tag{3-4}$$

For realistic conditions, equation 3-4 has one positive, real root, which should correspond to the data. This equation provides an alternate means of evaluating the rate coefficients used in the present analysis.

Detailed kinetic simulations of a fuel-rich CO-H_2-O_2-Ar mixture studied by Brabbs et al (1971) were used as the initial test for the carbon monoxide reaction mechanism. Adiabatic combustion was assumed at the initial temperatures and pressures reported by the authors. The values do not correspond to conditions immediately behind the incident shock wave, but refer to mean values for the period during which λ was measured. The average values were obtained by calculating the changes in temperature, density, and residence time caused by boundary-layer growth (Brabbs et al, 1971). Calculations performed in this study for this particular fuel-rich mixture used the rate coefficients listed in Table 3-1 for reactions 5 to 7, 9, and 21 in conjunction with equation 3-4 to determine values for λ.

Figure 3-11 compares the predicted values for λ, as a function of temperature, with measurements. Computed values of λ were determined by a simple least-squares analysis of the semilogarithmic plot of the product of CO and O-atom concentrations versus time. Identical results were obtained when only the O-atom profiles were used, since the carbon monoxide concentration was essentially constant during the time period which exhibited exponential growth of radicals. Agreement with the data is satisfactory,

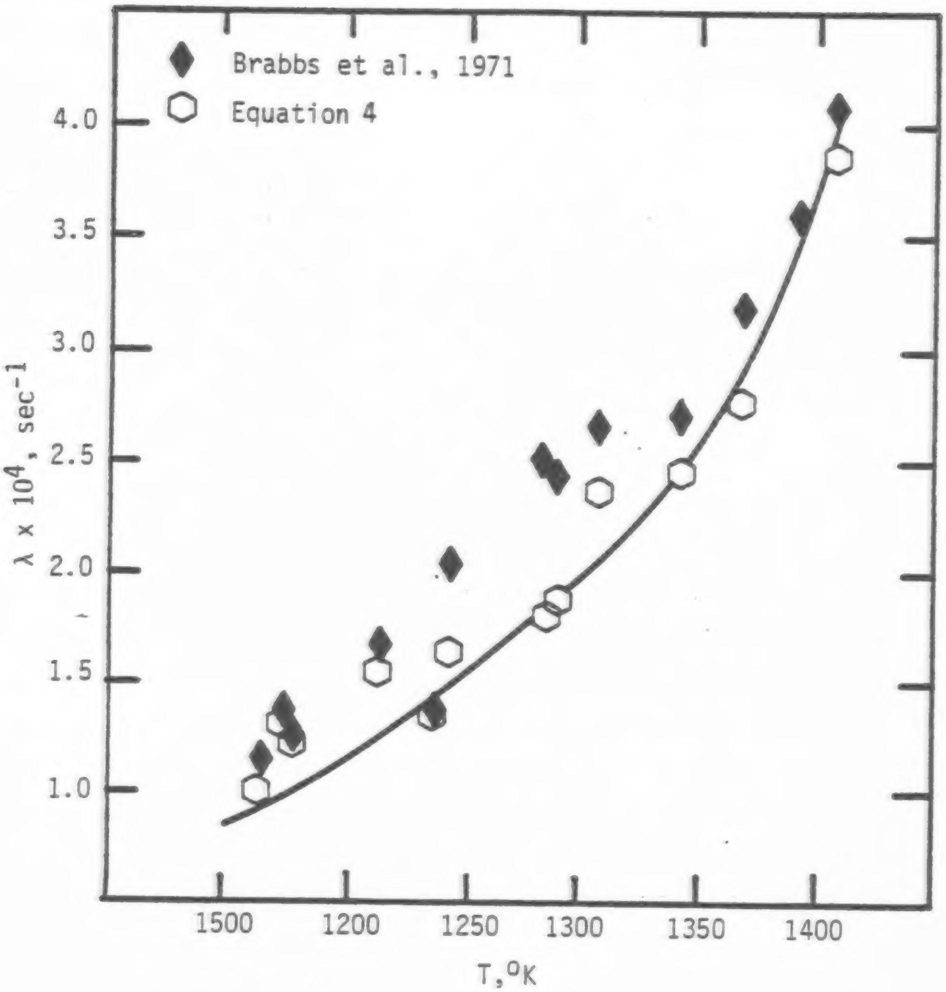

Figure 3-11. Exponential growth constants for O-atoms: $CO/H_2/O_2 = 6/5/0.5$.

which indicates that radical growth for this fuel-rich mixture is correctly modeled by the reaction mechanism.

Exponential growth constants determined by solution of equation 3-4, with the appropriate rate coefficients taken from Table 3-2, are also shown in Figure 3-11. Results are essentially identical to the values obtained with detailed kinetic simulations. This finding confirms the assumption that the growth of radicals in this fuel-rich mixture is contolled by reactions 5 to 7, 9, and 21. It also suggests that comparison with other data reported by Brabbs et al (1971) for different initial mixture compositions can be made simply by solution of equation 3-4 with the appropriate concentrations, temperatures, and densities specified.

Figures 3-12 to 3-14 show that this computationally simpler approach yields values for λ which are consistent with the majority of measurements. The agreement of the predictions with data for the fuel-rich mixture (SR = 0.10) in Figure 3-12 and the fuel-lean mixture (SR = 3.27) shown in Figure 3-13 is much better than with the data for the ultra-lean mixture (SR = 62.5) presented in Figure 3-14. Although the calculations for this very lean mixture appear to yield exponential growth constants which are higher than observed, additional analysis of the data as described below, indicates that the predictions are lower in absolute value and temperature dependence than experimentally determined. Part of this discrepancy may be due to the increased importance of reaction 23, which was necessarily neglected in the development of equation 3-4, to the initial production of atomic oxygen. Brokaw (1967) indicates that exclusion of this reaction results in an under-estimation of radical growth. Another possible explanation for the less satisfactory agreement achieved for this mixture is that one of the assumptions required to derive equation 3-4 is no longer applicable. In particular, the high ratio of O_2 to both CO and H_2 are constant during the exponential growth period for radicals. Detailed simulations of this oxidation data are necessary to completely explain the disparities.

Part of the scatter in the data points and predicted values seen in Figures 3-11 to 3-14 is due to the changes in pressure behind the incident shock waves as temperature varies. This increased the difficulty of

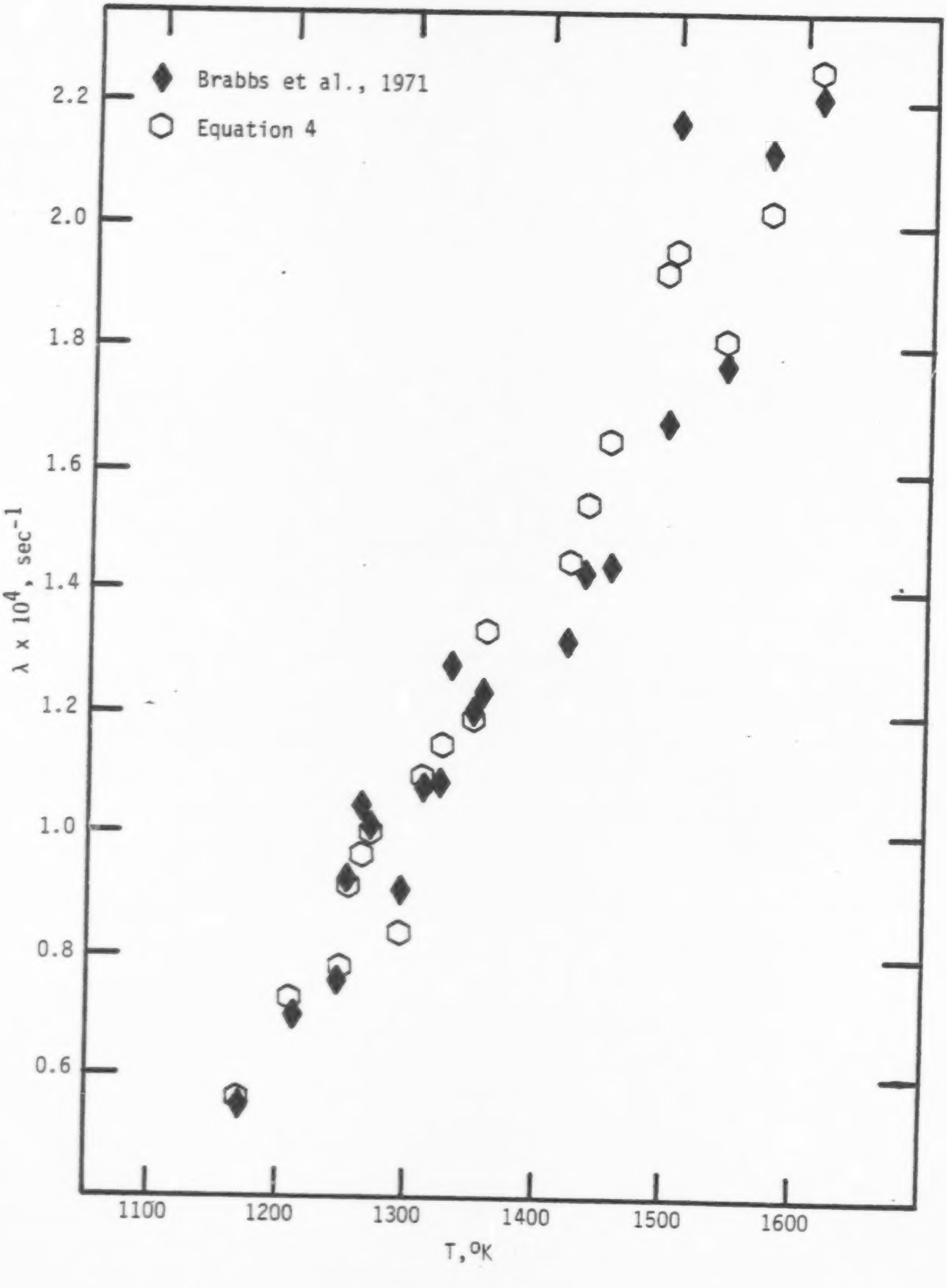

Figure 3-12. Exponential growth constants for radicals: $CO/H_2/O_2/CO_2$ = 10.0/0.1046/0.503/4.99.

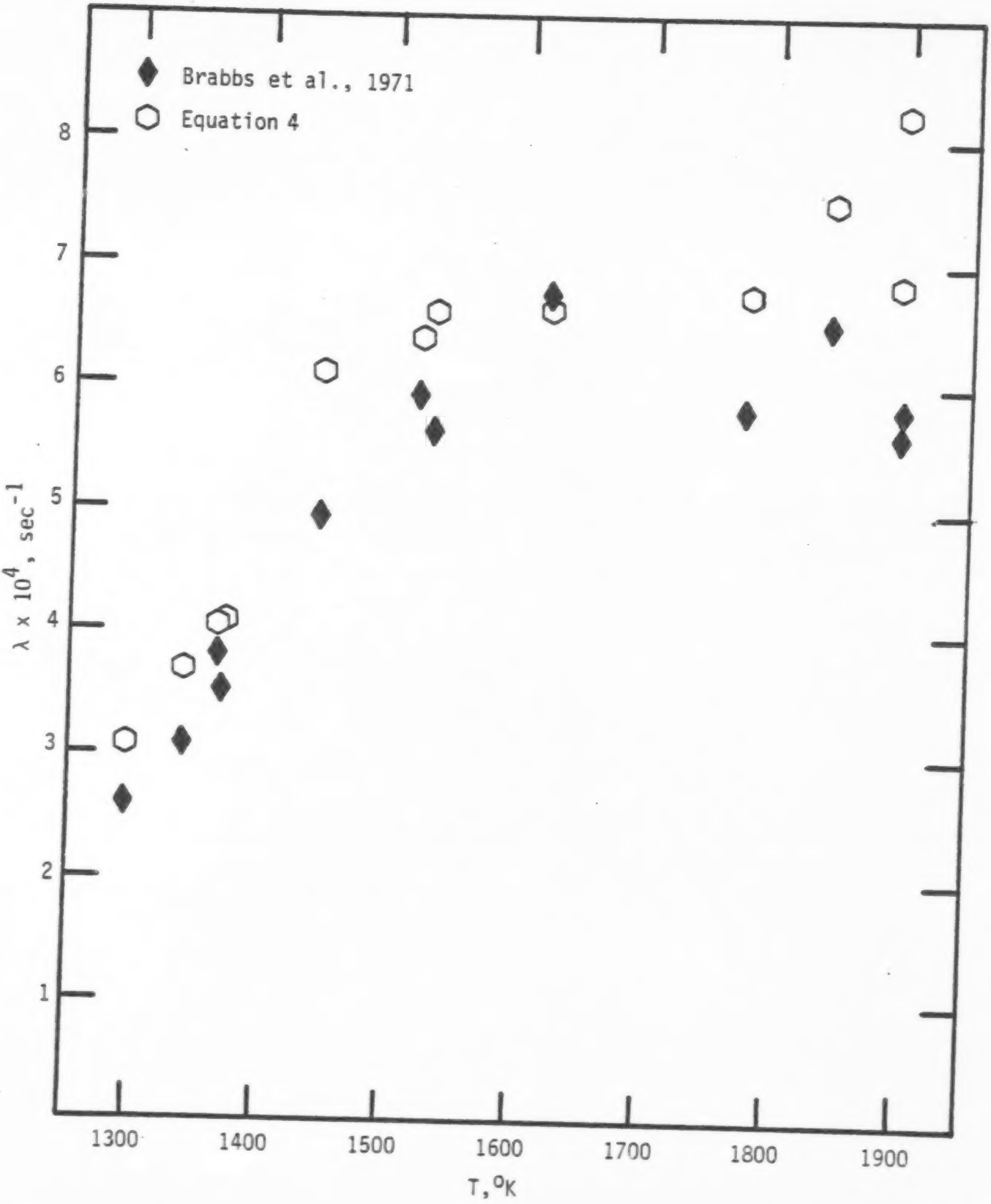

Figure 3-13. Exponential growth constants for radicals in fuel-lean CO oxidation: $CO/H_2/O_2/CO_2$ = 6.01/0.1035/10.0/5.0.

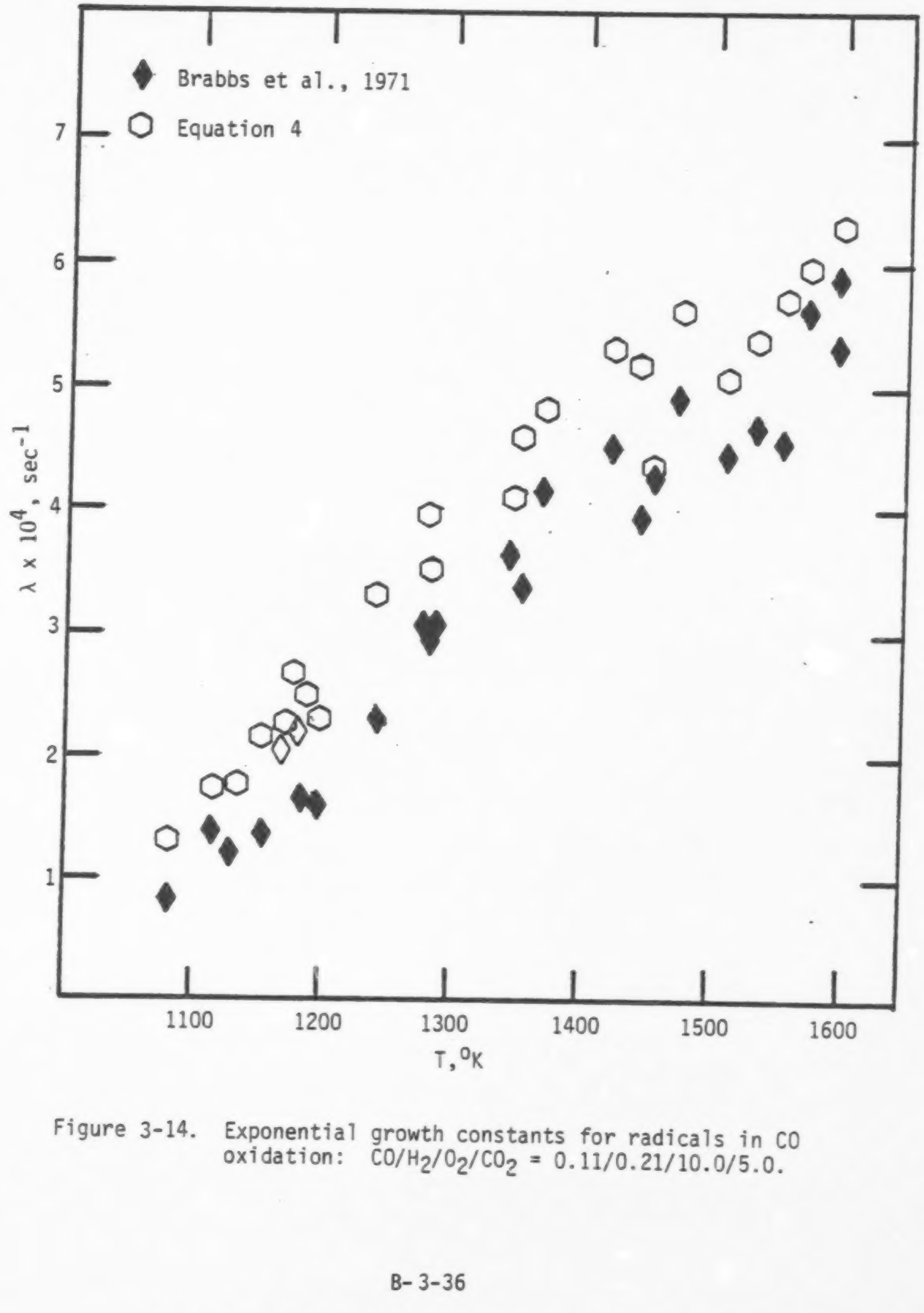

Figure 3-14. Exponential growth constants for radicals in CO oxidation: $CO/H_2/O_2/CO_2$ = 0.11/0.21/10.0/5.0.

adequately comparing the calculated values for λ with the measurements, especially with regard to the temperature dependence. Additional evaluation of the reaction mechanism involved normalization of λ by dividing the corresponding density as the first step. Least-squares analysis of both computed and experimental values for λ/ρ, which assumed a single Arrhenius temperature dependence, indicated that the regression equations for the predictions were identical to those derived from the measurements at the 95 percent confidence level except for the results shown in Figure 3-14. This analysis confirms in a more condensed fashion the conclusion which can be derived from visual inspection of the relevant figures; i.e., the $CO\text{-}H_2\text{-}O_2$ reaction mechanism accurately reproduces the exponential growth of radicals, which occurs in the initial stages of oxidation, between 1080 and 1900 K for a broad range of mixture compositions.

Another required capability for the reaction mechanism is that it correctly models the rate at which carbon monoxide is converted to carbon dioxide. Dean, Steiner, and Wang (1978) studied the oxidation of CO behind reflected shock waves at temperatures above 2000 K. Infrared emission from CO_2 was monitored for fuel-rich $CO\text{-}H_2\text{-}O_2\text{-}Ar$ mixtures and the time-resolved data were transformed to concentration profiles via calibration factors determined by these investigators from a series of $CO_2\text{-}Ar$ shock tube studies. Data reported included an induction time for CO_2 production, τ, which was defined by the intercept with the time-axis of the line which passed through the section of the CO_2 profile exhibiting linear growth. Later points on the measured profile were characterized in terms of the time at which a particular CO_2 concentration was reached. The times reported by Dean et al (1978) for these data were measured with respect to the time at which the reflected shock wave reached the midpoint of the observation window, t_{mp}. The authors indicate that this time is about 5 μsec after the reflected shock can first be detected.

Calculations were done which simulated the combustion of a fuel-rich $CO\text{-}H_2\text{-}O_2\text{-}Ar$ mixture under adiabatic conditions for initial temperatures and pressures reported by Dean et al (1978). Results of the computations indicated that the temperature profiles were essentially isothermal because of the low reactant concentrations used. Since the experimental data were measured relative to t_{mp}, 5 μsec were subtracted from the predicted times to obtain a time-scale consistent with that used by the investigators.

Predicted CO_2 induction times are compared with the measurements in Figure 3-15. The times at which the CO_2 concentration reached 13.3×10^{-9} mole/cm^3 are compared with the observed values in Figure 3-16. Calculated induction times are in excellent agreement with the data, which indicates that the oxidation of CO at short times is well-described. However, the significantly longer times predicted for the CO_2 concentration to reach a particular level indicates that the rate of CO oxidation is too slow at longer times, at least in this temperature range (2050 to 2810 K).

The oxidation of carbon monoxide above 2000 K is dominated by reactions 2, 6, 8, and 21 (Brokaw, 1967). The disparity between computed and measured values seen in Figure 3-16 suggests that at least one of the rate coefficients for these reactions is incorrect in this temperature range. A simple and straightforward analysis of this subset of the reaction mechanism, assuming steady-state conditions for H- and O-atoms, approximately constant CO concentrations, and that the recombination reaction may be neglected, yields the following relation between time and CO_2:

$$t - \tau = \frac{\ln\left[2\left(C_{CO_2} - C^0_{CO_2}\right)/C^0_{OH}\right]}{2k_{21}C_{CO}} \tag{3-5}$$

where superscript 0 denotes values at the induction time. It is, therefore, reasonable to conclude that the longer predicted times for CO_2 to reach a particular level are due to uncertainties in k_{21} above 2000 K.

The rate coefficient listed in Table 3-2 for reaction 21 is an alternative expression reported by Baulch and Drysdale (1974) which is in good agreement with their preferred relation for k_{21} up to 2000 K:

$$k'_{21} = 6.76 \times 10^{10} \times 10(3.94 \times 10^{-4}\ T)$$

Equation 3-5 indicates that if the overprediction of the characteristic time to reach a specified CO_2 concentration, t_c, is due to an incorrect rate

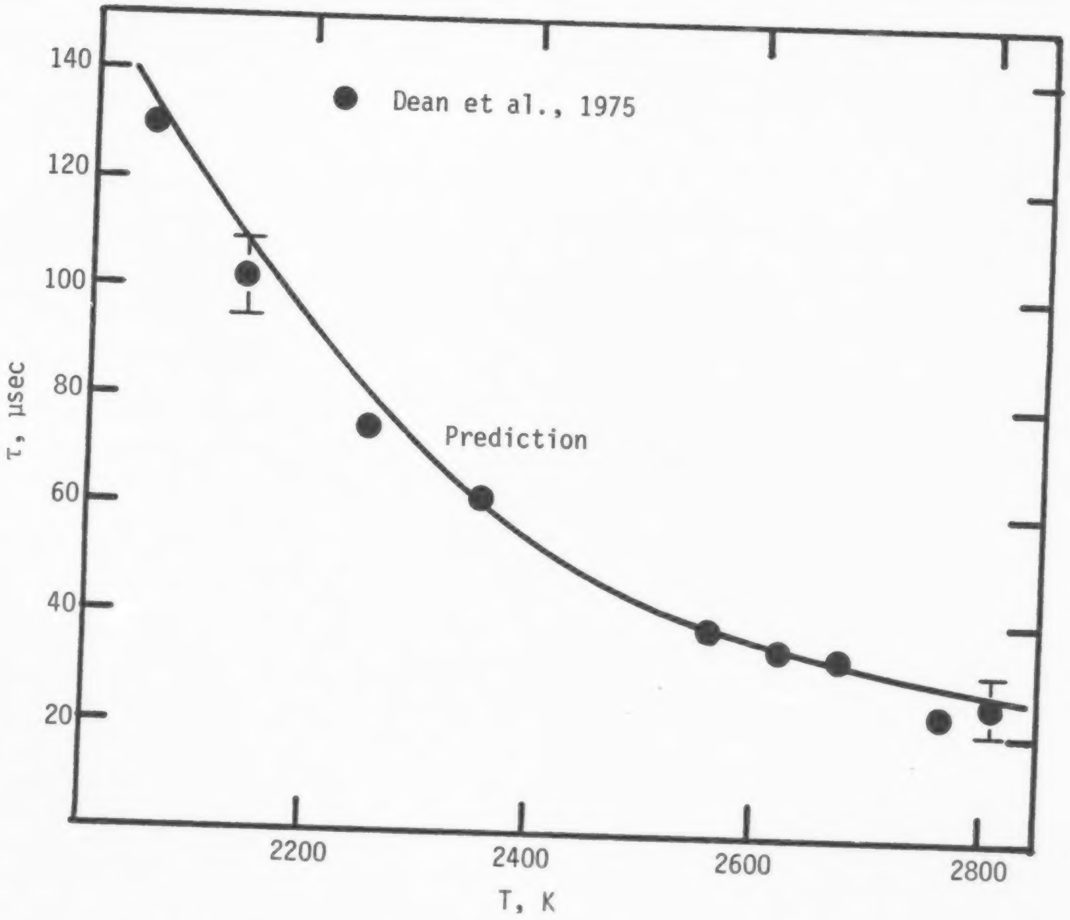

Figure 3-15. Characteristic time for CO_2 production in CO oxidation: $CO/H_2/O_2 = 3.28/0.049/1.01$.

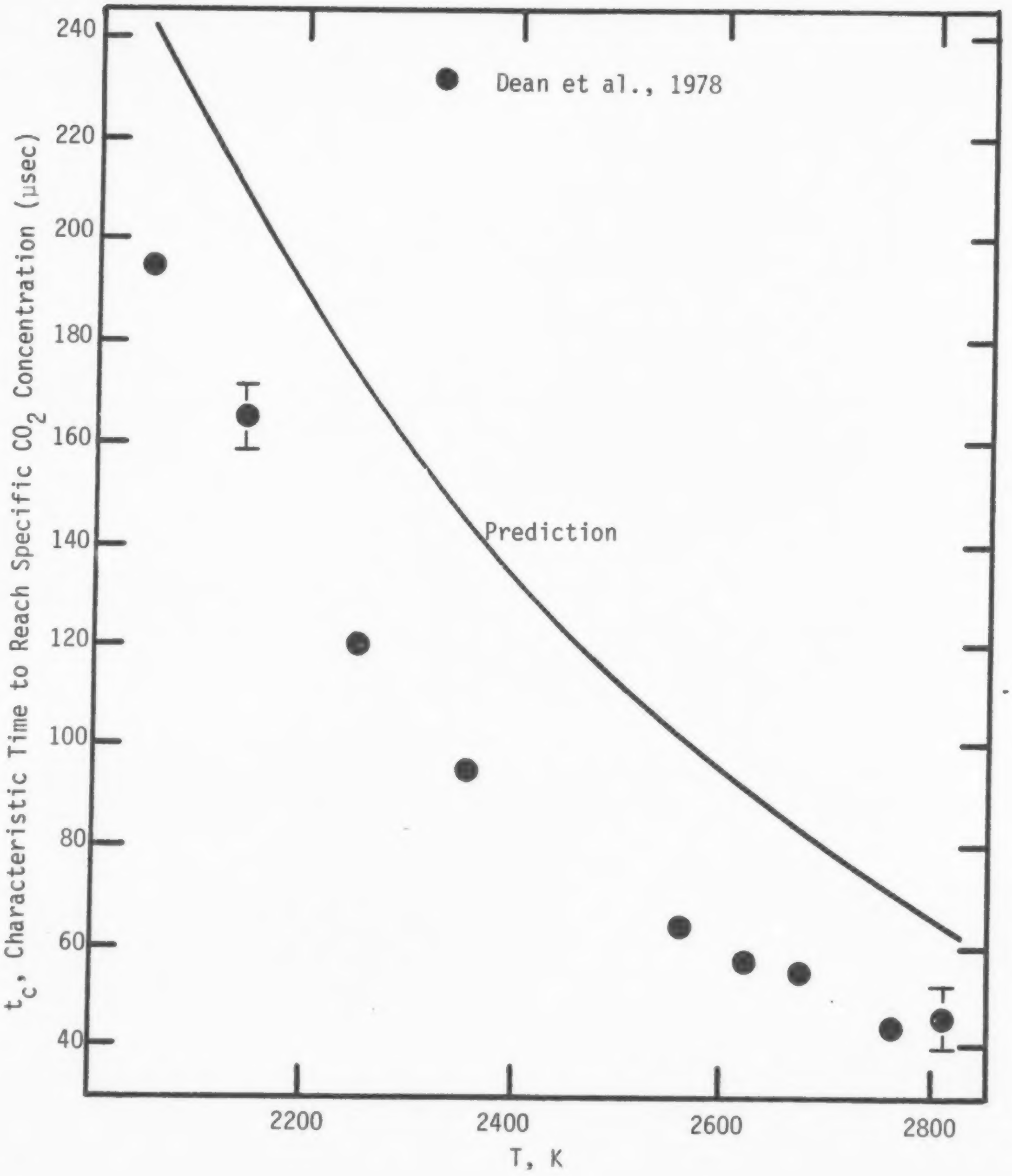

Figure 3-16. Time at which CO_2 concentration reaches 13.3 x 10^{-9} mole/cm^3: $CO/H_2/O_2$ = 3.28/0.049/1.01.

coefficient for reaction 21, the temperature dependence of the error is given by:

$$\frac{(t - \tau)}{(t' - \tau)} = \frac{k_{21}}{k'_{21}} \quad (3\text{-}6)$$

Analysis of the data and the predicted values for t_c yields the following ratio:

$$\frac{t_{c,\ \text{measured}}}{t_{c,\ \text{predicted}}} = 0.3808 \exp(1512 \pm 850)/T \quad (3\text{-}7)$$

Calculations at selected temperatures indicate that equation 3-7 is consistent with the ratio defined in equation 3-6, k_{21}/k'_{21}. It is, therefore, concluded that the slower predicted CO_2 production is due entirely to known inaccuracies of k_{21} above 2000 K. The uncertainties associated with k_{21} will not be significant at temperatures below 2000 K which are more typical of practical combustion systems. However, to extend the range of conditions over which the reaction mechanism can be accurately used, the recommended value, k'_{21}, should be used. Since the computer models presently used accept rate coefficients only in the form given in Table 3-2, no alterations in this rate coefficient can be made until modifications to the computer code are made.

3.2.2 Flame Phenomena

The series of calculations discussed in the previous section demonstrated the accuracy of the reaction mechanism for temperatures between 1080 and about 2000 K for a broad range of mixtures. The CO-H_2-O_2 oxidation mechanism was further tested by comparing predicted and experimental values of burning velocities and species profiles in flame environments. Since flame structure is heavily influenced by reactions occurring at temperatures above and below 1000 K, the calculations served as a test of the low-temperature oxidation mechanism which was not validated in the shock tube studies. Again, a simple bifurcation model was assumed for diffusion of stable and labile species, and thermal diffusion was neglected. The simulations only included premixed flames with H_2 or H_2O present in the feed mixture.

For most of the burning velocity data reported in the literature, the hydrogen and water content of the initial mixture has not been specified with sufficient precision to be used for quantitative comparison with predictions. This is particularly true for experimental studies in which only the specification "dry" is given. The issue is further complicated because trace organic impurities containing hydrogen can also alter the rate of CO oxidation. Scholte and Vaags (1959b) studied the effect of H_2, H_2O, CH_4, and C_3H_8 on measured burning velocities of CO-air flames. They found a linear relation between burning velocity and the "effective amount of H_2" in the total gas mixture up to about 2.5 percent by volume of additive; as the hydrogen content increased, so did the burning velocity. In addition, Dean and Kistiakowsky (1971) indicate that ppmV levels of organic impurities significantly increase the rate of CO oxidation in high-temperature shock tube studies. As a result of these factors, the calculated burning velocities for CO-air flames, to which H_2 or H_2O is added, are compared with measurements from studies which included the systematic variation of the H_2 or H_2O level in the feed.

Figure 3-17 illustrates the effect of increasing H_2O concentration in the premixed feed on predicted burning velocities of freely propagating, laminar CO-air flat flames. The trends are consistent with data reported by Scholte and Vaags (1959b) and the more recent literature of Günther and Janisch (1972). The calculations suggest that the data reported by Günther and Janisch (1972) for a "dry" CO-air mixture actually refers to a mixture with about 2500 ppmV H_2O in the feed, or, in light of the data reported by Scholte and Vaags (1959), an organic compound impurity equivalent to 2500 ppmV hydrogen. Quantitative comparisons with data reported in these two studies are difficult due to the unknown quantity of water, or other hydrogen-containing impurities, in the feed for the studies conducted by Günther and Janisch (1972), and because there was a suspected hydrogen impurity in the carbon monoxide used by Scholte and Vaags (1959b). The maximum burning velocity computed for the "wet" CO-air mixtures is located at 45 percent CO (SR = 0.51) which is leaner than the measurements of Scholte and Vaags (1959) would indicate. However, the predicted burning velocity of the 50 percent CO mixture with 1 percent H_2O in the feed is in good agreement with values reported by Gilbert (1957)--31 ± 2 cm/sec.

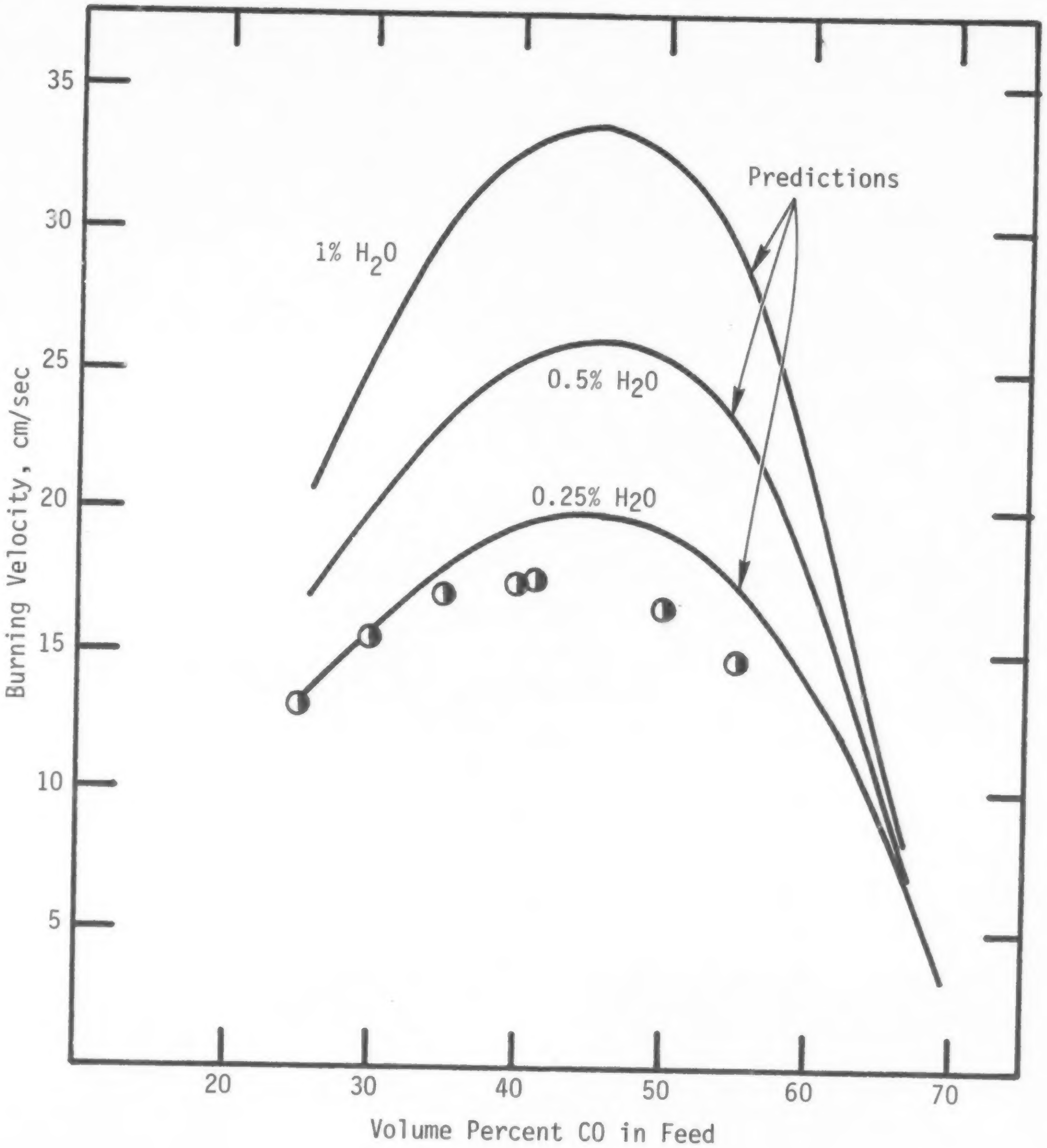

Figure 3-17. Variation of burning velocity for CO-air flames with stoichiometry for fixed H_2O concentrations (T_o = 298 K, P = 1 atm): Data are for "dry" CO-air from Gunther and Janisch (1972).

Additional calculations were done with the lowest H_2O concentration to examine the importance of reactions forming and destroying the formyl radical. Figure 3-18 demonstrates that omission of reactions 20 and 24 to 26 dramatically increases the predicted burning velocity for feed mixtures containing more than 50 percent CO; i.e., for stoichiometric ratios less than 0.5. At the richest condition examined, 70 percent CO or SR = 0.18, the burning velocity increases from 2.9 cm/sec to 10.3 cm/sec when the HCO reactions are neglected. The difference introduced by excluding these reactions is only 2 percent at 50 percent CO in the premixed feed. For less than 40 percent CO in the inlet mixture, the predictions are essentially the same.

In order to understand the effect introduced by inclusion of reactions for a trace species (the maximum predicted HCO concentration was less than 5 ppmV in all of the simulations), it is necessary to consider the processes which define the flame structure. When a hydrogen-containing compound is added to a CO flame, the hydrogen-oxygen reaction dominates radical production and the major path for oxidation of CO to CO_2 occurs by reaction of CO with the hydroxyl radical. Labile species are generated in the hotter regions of the flame and diffuse upstream to react via the HO_2 cycle at low temperatures. Hydroxyl radicals generated by reactions 10 and 13 may then react with CO via reaction 21. Analysis of the reaction rates and the net production rates of species for the 70 percent CO flame agreed with this description of the flame structure whether or not HCO reactions were included. For the simulation of this flame when HCO chemistry was omitted, CO consumption occurred between 410 and 1385 K (the adiabatic equilibrium flame temperature is 1400 K). The maximum rate of CO oxidation occurred at 1175 K. This position in the flame was also the location of maximum O-atom production. The peak OH production rate was located about 0.1 mm upstream, and that of H-atoms about 0.1 mm downstream of the position of maximum O-atom production. Formation of H-atoms was confined to the hotter regions of this flame between 1110 and 1370 K.

Examination of the reaction rates and net production rates of species for this fuel-rich flame when HCO chemistry was included identified the reason for the lower predicted burning velocity. Formation of and destruction of the formyl radical in the hotter regions of the flame depleted the O, OH, and H radicals. The differences caused are illustrated in Figure 3-19

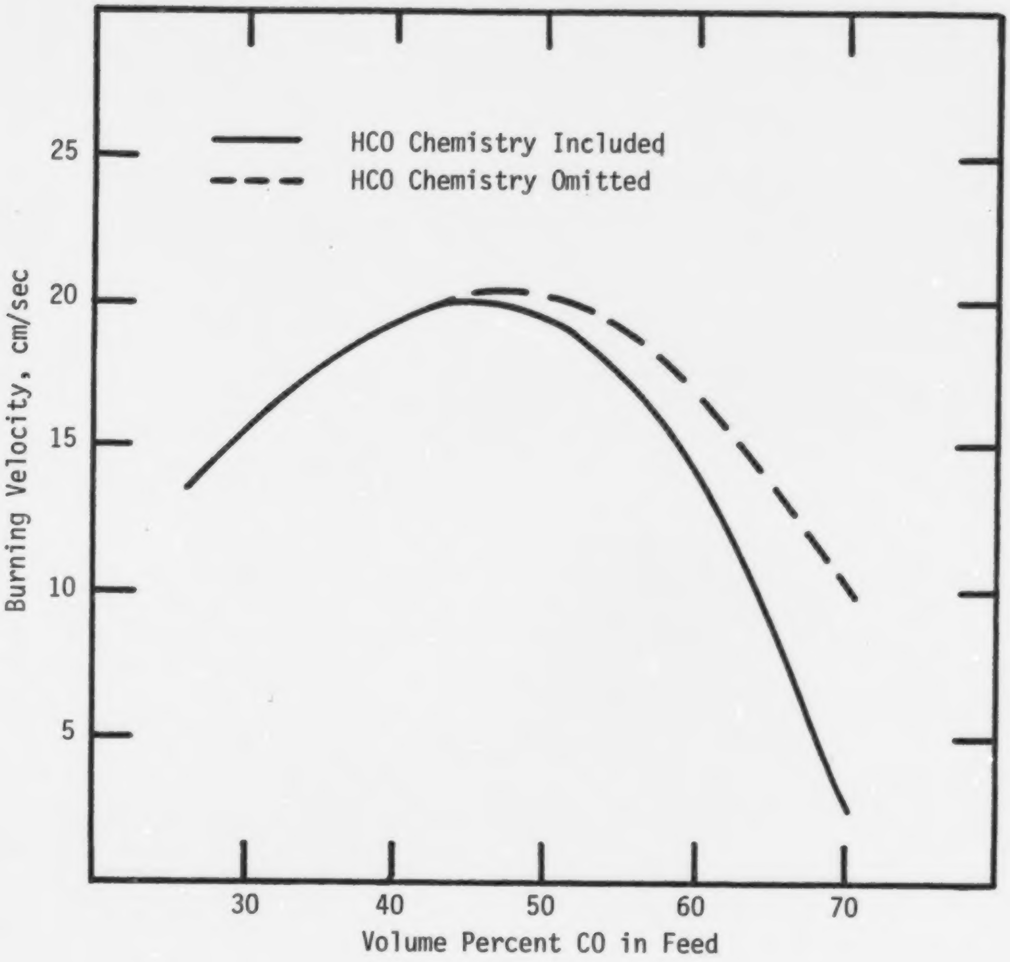

Figure 3-18. Influence of HCO chemistry on predicted burning velocity of CO-air flames as a function of stoichiometry: 0.25 percent H_2O, T_o = 298 K, P = 1 atm.

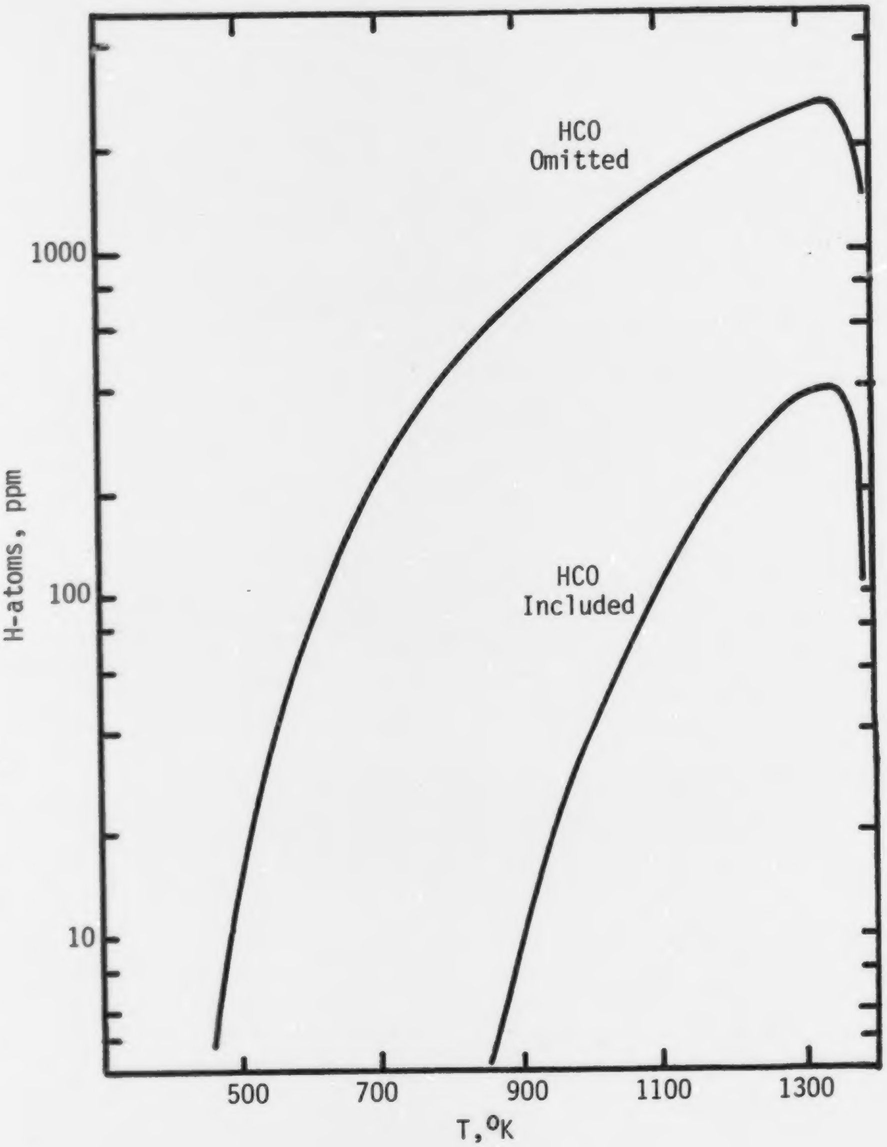

Figure 3-19. Effect of HCO chemistry on H-atoms: CO-air + 0.25 percent H_2O.

for H-atoms. Due to the lower concentrations of these species, diffusive fluxes into the low-temperature region of the flame were reduced, which decreased concentrations of H, OH, and O-atoms in this region of the flame. As a result, production of radicals via the HO_2 cycle was greatly reduced. The chain-breaking and chain-terminating reactions of the HCO radical (reactions 24 to 28), which occur at higher temperatures in the flame, decrease radical concentrations throughout the flame and, therefore, yield a lower rate of CO oxidation and a lower burning velocity.

The consumption of CO for this simulation occurred predominately between 700 and 1390 K. The maximum rate of CO oxidation, the maximum net production rate of O-atoms, and the maximum production of H-atoms were located at the same flame position corresponding to a temperature of 1249 K. The peak rate of OH formation was 0.13 mm upstream of this location at a temperature of 843 K. In addition, the net production of H-atoms was confined to a high-temperature region between 1240 and 1380 K.

The influence of added H_2O or H_2 on predicted burning velocity for a stoichiometric CO-air mixture was also examined. For both additive studies, a particular dopant concentration was specified in the feed and the CO-to-air ratio was maintained constant. This means that the overall stoichiometric ratio decreased with addition of hydrogen since additional air to oxidize this dopant fuel species was not added. The results shown in Figure 3-20 indicate that H_2 and H_2O have similar, but not identical, catalytic effects on the burning velocity below about 1 percent by volume of the reactants. At higher dopant concentrations, the greater effect of H_2 is due to the increasing dominance of the hydrogen-oxygen reaction mechanism as the "fuel" becomes more characteristic of a hydrogen-air supported flame. The maximum burning velocity for H_2O addition, which occurs at about 10 percent by volume H_2O, is a result of the balance between increased energy release due to more rapid oxidation of CO and the thermal quenching effect of water which lowers the peak flame temperature.

Yumlu (1967) reported measurements of the burning velocity of stoichiometric CO-air flames containing various concentrations of H_2O. At 1.4 percent H_2O in the feed, he found the burning velocity to be 31 cm/sec and at 2 percent H_2O the burning velocity increased to 35 cm/sec. Other

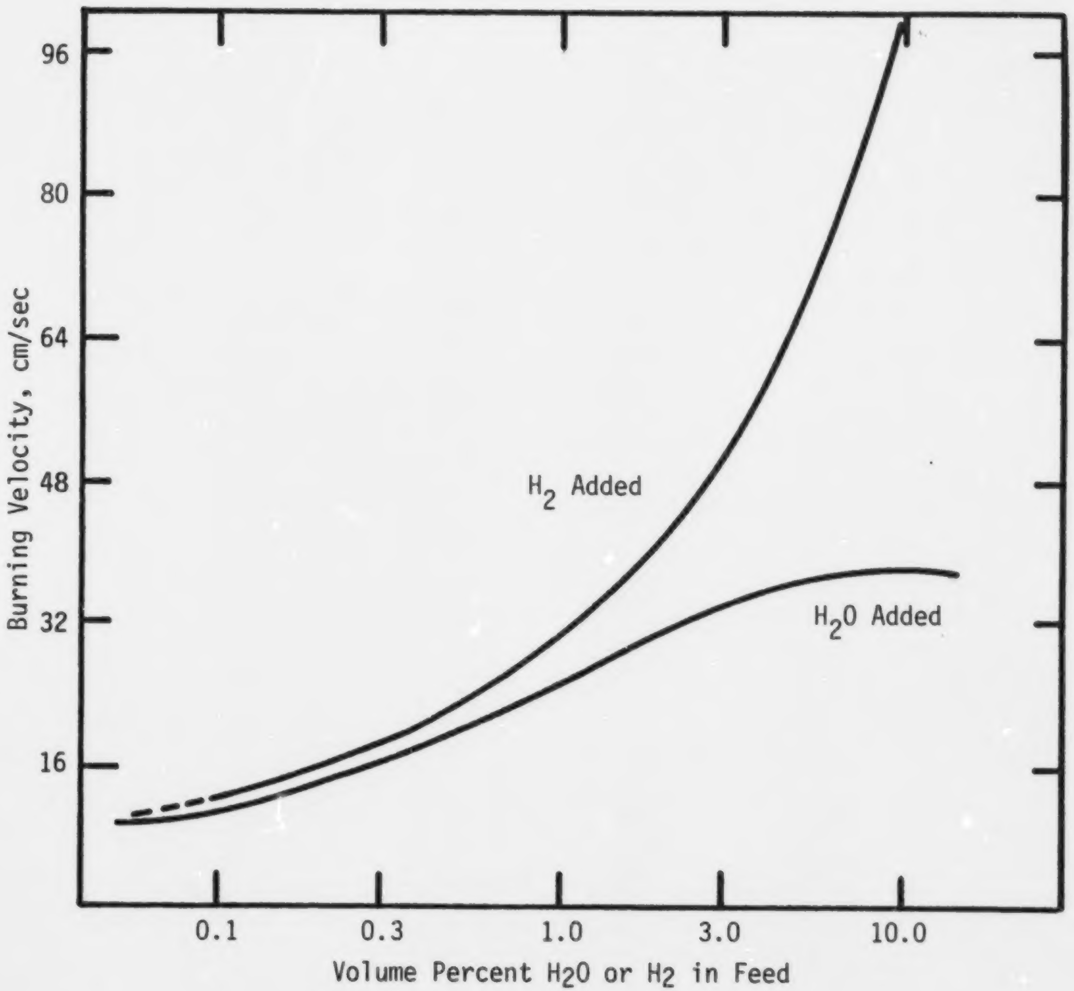

Figure 3-20. Variation of predicted burning velocity in a stoichiometric CO-air as a function of added H_2 and H_2O.

measurements for water vapor contents up to about 11 percent by volume were also higher than the reaction mechanism predicted. However, the data are suspect because the burner technique used experimentally is known to yield burning velocities which are a function of burner diameter (Heap, 1980). In addition, extrapolation to adiabatic conditions on a plot of burning velocity versus measured heat loss to the burner is not necessarily correct. More importantly, Yumlu (1967) reported a value for the burning velocity of a dry (0 percent H_2), stoichiometric CO-air mixture of 18 cm/sec. Experimental studies of stoichiometric CO-O_2 flames, which have higher burning velocities than CO-air flames, indicate that burning velocities between 10 and 26 cm/sec occur for H_2 feed concentrations between 60 and 500 ppmV (Wires, Watermeier, and Strehlow, 1959). These investigators also reported that the burning velocity was less than 3 cm/sec for less than 10 ppmV H_2 in the feed. This information strongly suggests that the data reported by Yumlu (1967) are influenced by trace impurities of hydrogen-containing species. The calculations indicate that about 3000 ppmV of H_2 or H_2O are required to yield a burning velocity near 20 cm/sec. A much lower organic impurity level could also produce a value near 20 cm/sec (Scholte and Vaags, 1959b).

Another factor which should be considered in the comparison between experimental and predicted burning velocities is whether reactions have been excluded which are important to establishing radical concentrations. The high temperatures associated with the flame simulations shown in Figure 3-20 (2156 to 2382 K) suggest that formation of nitrogen oxides, which was neglected, could play a role in defining the flame structure. Further calculations should be done to quantify what effect, if any, nitrogen oxide reactions have on predicted properties of CO-air flames.

Although the uncertainty with regard to experimental CO-air flame data precludes a conclusive quantitative comparison with predictions, the simulations do provide information pertaining to the relative importance of CO_2-producing reaction paths. Figure 3-21 shows the relative contribution of reaction 19 to the maximum rate of CO_2 production in stoichiometric CO-air flames to which H_2O is added. The recombination of atomic oxygen with carbon monoxide accounts for greater than 20 percent of the peak CO_2

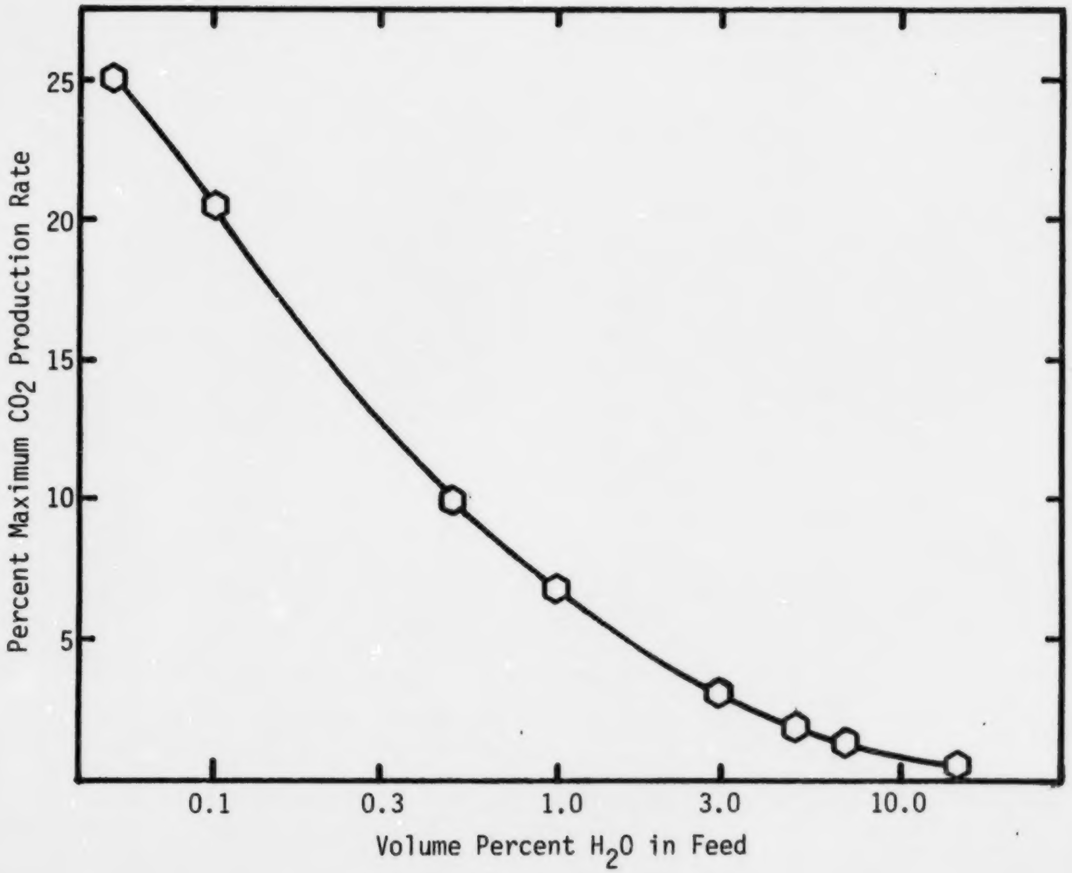

Figure 3-21. Relative contribution of reaction 19 to the maximum rate of CO_2 production.

production below 1000 ppmV H_2O in the feed. A similar analysis of the flames yielding the predictions shown in Figure 3-17 indicates that the contribution of reaction 19 varies from 12 percent for lean conditions to 16.5 percent at a stoichiometric ratio of 0.18 (70 percent CO). The major points to be made are that the recombination of O-atoms and CO to produce CO_2 is a significant step for all stoichiometries and that even with only 500 ppmV H_2O in the feed mixture the dominant production of CO_2 occurs via reaction of CO with hydroxyl radicals. Reaction of oxygen atoms with the formyl radical contributed less than 5.5 percent to the maximum production rate of CO_2 for all stoichiometries and H_2O concentrations investigated.

The calculations for CO-air burning velocities are summarized in Figure 3-22 in a manner suggested by Friedman and Cyphers (1956). A single curve is not found because of the differences in flame temperature as stoichiometry varies. The predictions are consistent with the data reported by Friedman and Cyphers (1956), although the comparison is limited to simulations with postflame temperatures near 2000 K. In addition, a correlation of burning velocity versus temperature reported by these authors is identical to that obtained from analysis of the calculations, if experimental uncertainty is considered:

$$v^2_{0,\mathrm{exp't}} = 3.8 \times 10^6 \left(Y^0_{CO}\right)\left(Y^0_{H_2O}\right)^{1/2}\left(P/P_{atmos}\right)^{-0.24} \exp\left(-11130/T_{ad}\right)$$

$$v^2_{0,\mathrm{calc}} = 2.35 \times 10^6 \left(Y^0_{CO}\right)\left(Y_{H_2O}\right)^{1/2}\left(\exp -10790/T_{ad}\right)$$

The semiquantitative agreement indicated lends further support that the reaction mechanism is accurate.

The ability of the CO-H_2-O_2 reaction mechanism to predict species and temperature profiles in flame environments is a more stringent, and conclusive test in that it can accurately describe combustion of carbon monoxide. Fenimore and Jones (1959) reported measurements of CO, H_2, O_2, CO_2, and H_2O concentrations normalized by argon and temperature as a function of distance in a low-pressure, burner-stabilized, fuel-rich CO-H_2-O_2-Ar flat flame. The stable species were measured by mass spectrometry. Gas samples were withdrawn from the flame into a sample flask which was maintained at about 2 torr to reduce the possibility of further reaction. The contents of the

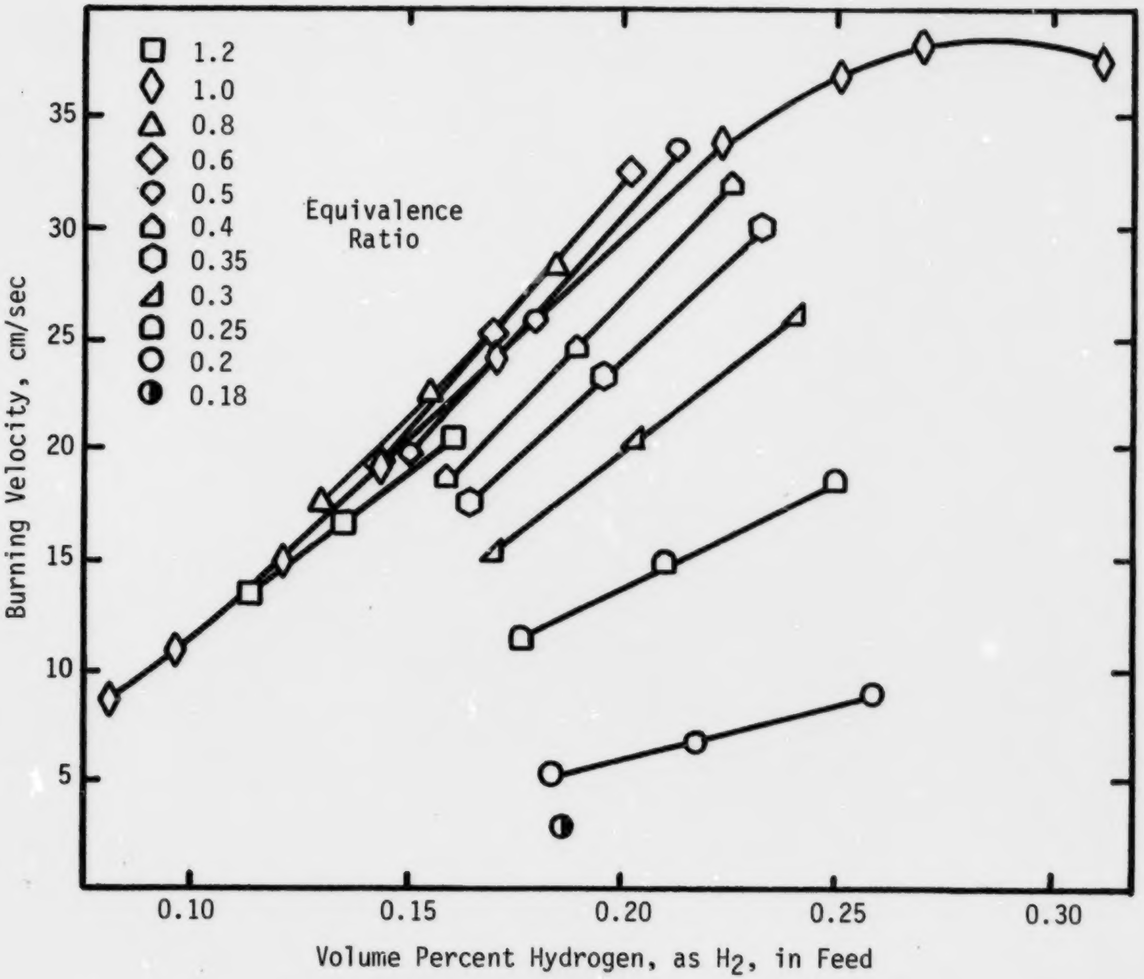

Figure 3-22. Predictions of CO-Air Burning Velocities as a Function of Hydrogen Content and Stoichiometry.

flask were then introduced into the mass spectrometer. Temperatures were measured with a 0.0012 cm diameter, quartz-coated, Pt/Pt-Rh thermocouple.

In order to mathematically simulate this flame, it was necessary to use different lower boundary conditions than employed for other simulations. Zero-order boundary conditions for species and velocity cannot be imposed because the flame is stabilized by heat transfer to the burner. Instead, it is necessary to specify initial reactant concentrations and gas velocity at minus infinity and permit the computer model to calculate species concentrations and velocity at the burner surface which are consistent with an assumption that the temperature at the burner is maintained at 298 K. The experimental cold gas velocity of 59.7 cm/sec at 298 K and 60 torr was used for the minus infinity value. Catalytic recombination of radicals at the burner surface was neglected because relevant data were not available. It should be noted that these assumptions are the simplest which could be employed in the simulation and do not reflect actual limitations of the flame model.

The predicted species profiles are compared with the measurements in Figure 3-23. It can be seen that the calculated H_2 levels are significantly lower than the data beyond 4.0 mm. Predicted CO_2 concentrations are also lower than observed in the later stages of the flame. However, both H_2O and CO profiles determined by the reaction mechanism agree with the data in this part of the flame. The predicted O_2 profile agrees with the measurements in the early stages of oxidation and is higher than observed at greater distances from the burner surface.

Part of the disparity between predicted and measured species profiles may be due to the sampling technique and the accuracy of the measurements. Fenimore and Jones (1959) assumed that the low pressure maintained in the sample flask would reduce or eliminate the possibility of further reactions in the gas sample. Figure 3-24 indicates that if all H-atoms at a particular flame position recombine to form molecular hydrogen, the agreement between measured and "predicted" H_2 profiles is excellent. This suggests that the gas volume withdrawn from the flame was still reactive at the temperature and pressure of the sample flask.

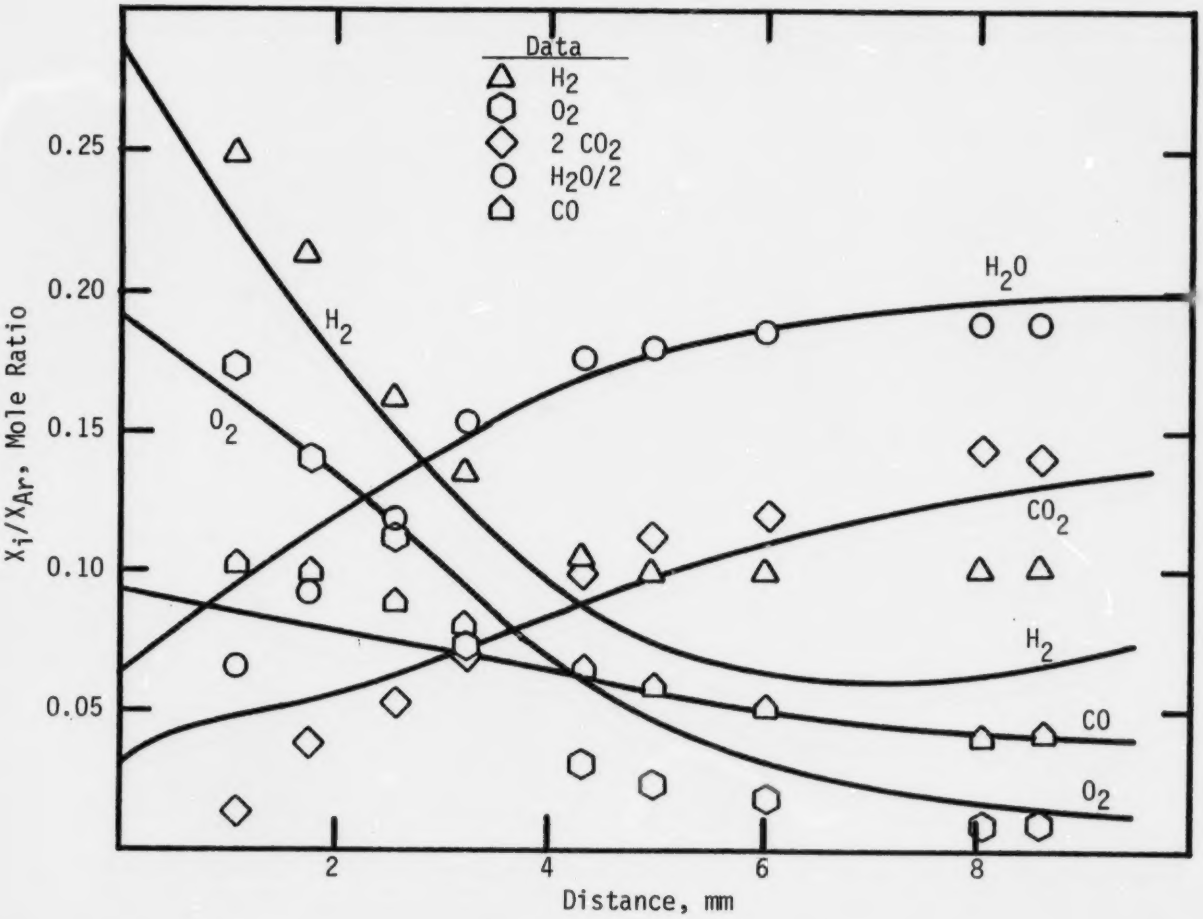

Figure 3-23. Comparison of predicted stable species profiles with data for a low pressure, fuel-rich $CO/H_2/O_2/Ar = 5.8/27.6/12.7/53.9$ flat flame: Data of Fenimore and Jones (1959), P_o = 60 torr, T_o = 298 K, V_o = 59.7 cm/sec. Solid Lines Are Predictions.

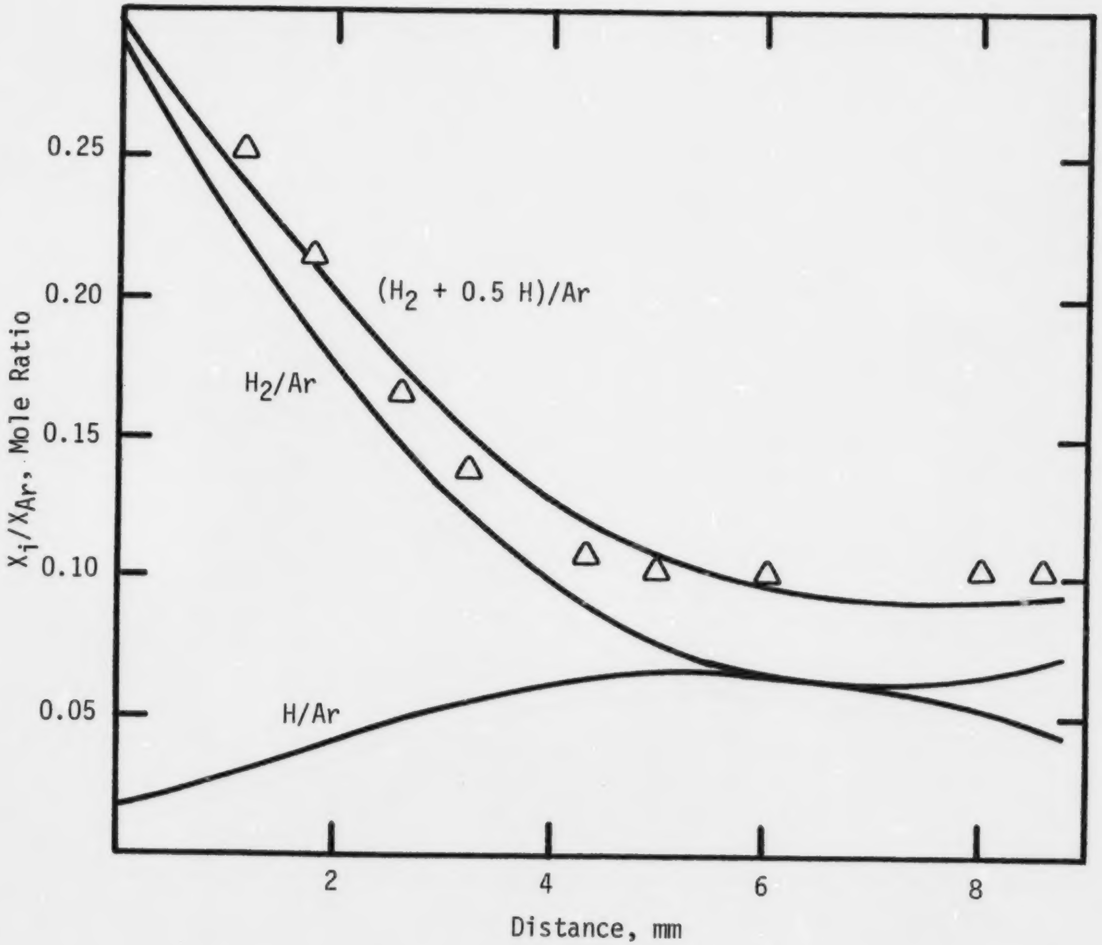

Figure 3-24. Comparison of recombination of H-atoms with reported H_2 profiles of Fenimore and Jones (1959): $CO/H_2/O_2/Ar$ = 5.8/27.6/12.7/53.9.

In the latter stages of the flame, where diffusive fluxes are negligible, it is possible to calculate an element mass balance from the data. Comparing the values obtained with the feed conditions is a means of estimating the accuracy of the measurements. The following ratios for grams of C, H, and O in the far field to grams of C, H, and O in the feed were determined: $R_C = 1.06$; $R_H = 0.939$; $R_O = 1.00$. These results, coupled with the simple calculation shown in Figure 3-24, indicate that the predicted profiles agree with the data within the error limits of the measurements.

Figure 3-25 compares the predicted and measured temperature profiles for this fuel-rich flame. Kaskan (1959) has compared temperature measurements made with a silica-coated Pt/Pt-10 percent Rh thermocouple to the OH rotational temperature determined by absorption spectroscopy. Kaskan observed differences of 100 degrees between the two techniques (thermocouple measurements were higher) for CO flames with radical concentrations similar to those predicted for this low-pressure flame. The higher temperatures obtained with the coated thermocouple were due to recombination of radicals on the surface of the thermocouple. Although this information was obtained for different flames, it suggests that the predicted temperature profile is in reasonable agreement with this measurement.

Fenimore and Jones (1959) also reported an estimate of the H-atom concentration 2.5 mm above the burner surface. The value was dependent upon the rate constant for a particular reaction and the measured temperature of the flame position. Their estimated H-atom concentration was 2.3×10^{-8} mole/cm^3, which is increased to 3.2×10^{-8} mole/cm^3 if more recent rate data are used. The predicted value at 2.5 mm is 2.90×10^{-8} mole/cm^3. This is excellent agreement if the uncertainty in experimental temperature at this location and the assumptions required to derive the H-atom concentration are considered.

3.2.3 Summary

Comparisons with shock tube data for lean and rich $CO-H_2-O_2-CO_2-Ar$ mixtures have demonstrated that the reaction mechanism accurately predicts the exponential growth constants for radicals between 1080 and 1900 K. Calculations at temperatures above 2000 K for a fuel-rich $CO-H_2-O_2-Ar$ mixture

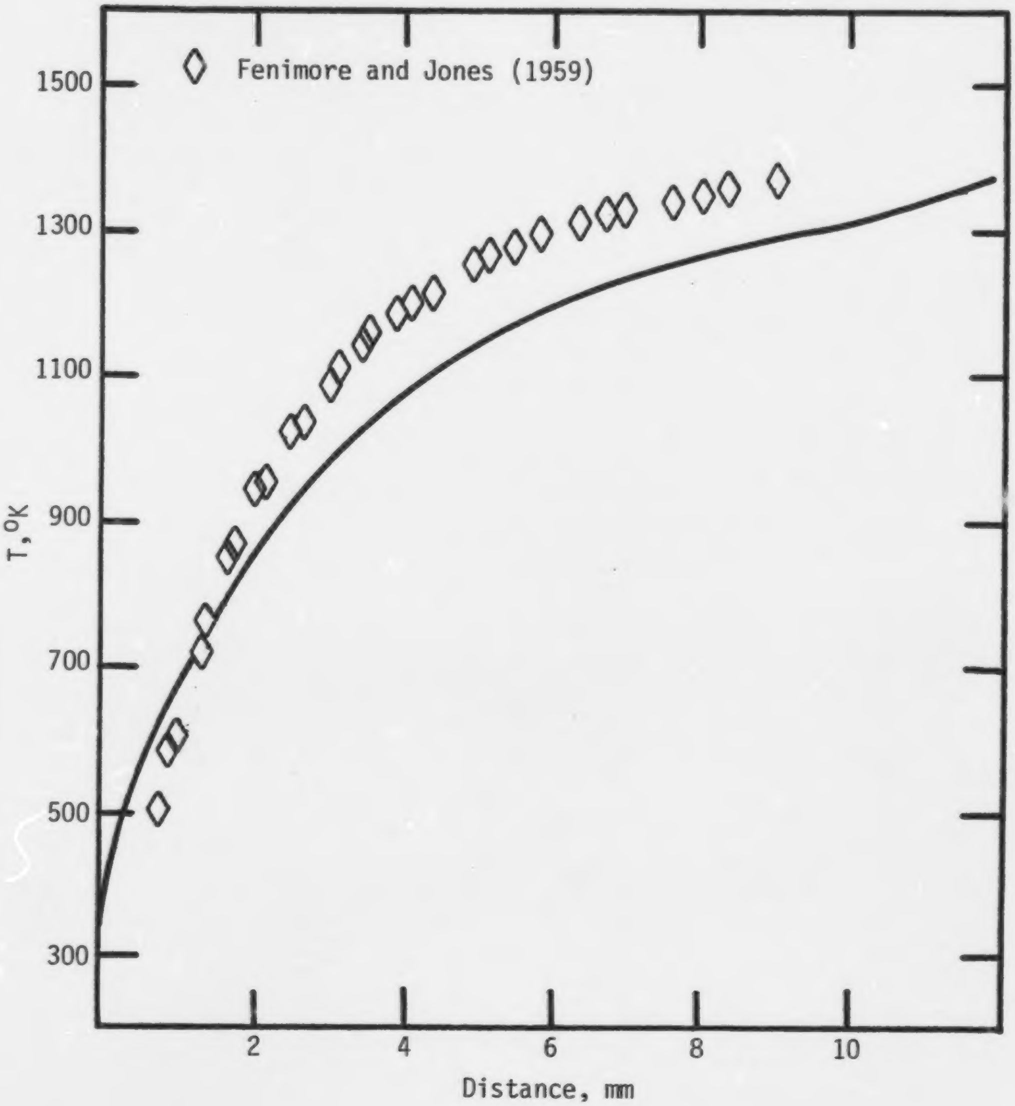

Figure 3-25. Predicted and measured temperature profiles in a low pressure, fuel-rich $CO/H_2/O_2/Ar$ = 5.8/27.6/12.7/53.9 flat flame: T_o = 298 K, P = 60 torr, V_o = 59.7 cm/sec.

indicated that, although the early production of CO_2 could be predicted, known inaccuracies in the rate coefficient for reaction 21 listed in Table 3-1 resulted in slower rates of CO oxidation than observed at later times.

Simulations of atmospheric pressure, freely propagating, laminar $CO-H_2O$-air and $CO-H_2$-air flat flames indicated that the reaction mechanism could yield values for burning velocities which were consistent with experimental trends. Quantitative comparisons with measurements were not possible, in our opinion, due to uncertainties regarding the experimental technique, or the concentration of hydrogen-containing compounds in the initial gas mixtures. The calculations indicate that burning velocity data reported for "dry" CO-air mixtures by Günther and Janisch (1972), Scholte and Vaags (1959b), and Yumlu (1967) are consistent with predicted values with less than 5000 ppmV H_2 or H_2O in the reactants. The experimental work of Scholte and Vaags (1959b) and the analysis of CO oxidation data described by Dean and Kistiakowsky (1971) suggest that substantially lower organic impurities present in the reactants could be responsible for the higher burning velocities for CO-air flames reported in the literature. Another possible contribution to the disparity between predicted and measured burning velocities is the exclusion of reactions producing nitrogen oxides (NO, NO_2, and N_2O) in the mechanism. The high temperatures associated with the CO-air flames simulated ($T > 2000$ K for $SR \geq 0.35$) suggests that formation of NO is kinetically feasible over a broad range of stoichiometries. Additional calculations are recommended to determine whether NO and NO_2 formation can significantly affect the predicted global rates of CO oxidation by accelerating production of the OH radical through the homogeneous, catalytic mechanism described in Section 3.1.2.

An important result of the simulations is the demonstration that formation and destruction of the HCO radical has a significant impact on flame structure and burning velocity of "wet", fuel-rich CO-air flames. Reactions involving HCO reduced free radical concentrations in the hotter regions of the flame. The low-temperature HO_2 cycle, which is important for fuel oxidation, depends on diffusion of labile species upstream. Thus, reduction of radical concentrations in the high-temperature region lowers the concentrations of these reactive species in the low-temperature region of the flame. This in turn decreases the rates of reactions participating in the HO_2 cycle and reduces the rate of CO consumption. Omission of the HCO reactions increased the burning velocity of a 70 percent CO (SR = 0.18) flame with 2500 ppmV H_2O in the feed, by a factor of 3.5. Predictions without these reactions were only 2 percent higher at SR = 0.42 than the values calculated with these reactions included. It is of interest to note in this development of an accurate reaction mechanism, that a species for which the calculated concentration was always less than 5 ppmV played a dominant role in establishing the flame characteristics. This reemphasizes the approach used in the present validation process which precludes elimination of species and reaction paths simply on the basis that the absolute concentration of the species is much lower than other species included in the mechanism.

The reaction mechanism was also shown to reproduce stable species and temperature profiles for a low-pressure, burner-stabilized, fuel-rich $CO-H_2-O_2-Ar$ flat flame within the accuracy of the measurements. Comparison of measured and predicted H_2 profiles suggested that experimentally the recombination of H-atoms to form molecular hydrogen occurred before the gas samples were analyzed. The differences between measured and predicted temperatures, in conjunction with data reported by Kaskan (1959), suggested that at the high radical concentrations existing in the flame catalytic recombination of radicals on the thermocouple surface was significant, even though a quartz-coated thermocouple was used to reduce this process. Reasonable agreement with a single H-atom concentration reported by Fenimore and Jones (1959) was also predicted.

The calculations with the $CO-H_2-O_2$ reaction definitely indicate that it is sufficiently accurate at temperatures between 1000 and 2000 K to be used as a subset of hydrocarbon oxidation mechanisms. However, additional computations are required to assess its capabilities in predicting flame structure. It is recommended that further simulations of flames in which species concentrations were measured, such as the data reported by Vandooren, Peeters and Van Tiggelen (1975) for a low-pressure, $CO-H_2-O$ flame, be made. If the reaction mechanism can predict the observations in detailed flame structure investigations, the results of the burning velocity calculations would gain support. It is also suggested that at least some of the burning velocity calculations be repeated with NO, NO_2, and N_2O reactions included to determine the impact of these trace species on predictions. And lastly, the preferred expression for k_{21} recommended by Baulch and Drysdale (1974) should be used in a series of calculations to determine whether significantly different flame characteristics than obtained with the value of k_{21} listed in Table 3-1 result.

4.0 THE HYDROCARBON REACTION SYSTEM

4.1 The CH_2O-O_2 Reaction

Formaldehyde is well-known to be an intermediate in the oxidation of hydrocarbons, especially methane (Jachimowski, 1977; Bowman, 1975; Peeters and Mahnen, 1973; Fristrom, 1963). It is, therefore, of interest to examine the kinetics of CH_2O oxidation and pyrolysis in the absence of other hydrocarbon species. Establishing a reaction mechanism which accurately describes the consumption of CH_2O over a broad range of temperatures and stoichiometries removes a major uncertainty in other hydrocarbon combustion mechanisms. Attention can then be focused on the elementary steps which control formaldehyde production during the oxidation of simple hydrocarbon fuels, such as methane, acetylene, ethylene, and ethane.

In contrast with the other hydrocarbon species considered in the present development of gas phase reaction mechanisms, there have been relatively few high-temperature studies of formaldehyde oxidation or pyrolysis. The first shock tube study of both pyrolysis and oxidation of CH_2O was done by Gay et al (1965). Time-of-flight mass spectrometry and ionization measurement techniques were used to monitor the reaction of CH_2O and CH_2O-O_2 mixtures, which were diluted with neon, between 1400 and 2100 K. An exponential decay, after an induction period which decreased with rising temperature, was observed for thermal decomposition of CH_2O. In addition to the major products, CO and H_2, the formation of the CH_3O radical, or its isomer, was detected. Gay et al (1965) indicate that the mass to charge (m/e) peak height for the CH_3O radical rises to as much as 5 percent of the m/e peak height for CH_2O in the initial stages of the reaction, and then is more or less in a steady state throughout the reaction. The oxidation studies conducted by these investigators suggested that decomposition of CH_2O was greatly accelerated by the presence of oxygen. At the higher temperatures, the major combustion products--H_2, H_2O, and CO--appeared to arise at almost the same time, while at lower temperatures the formation of CO and H_2 significantly preceded that of H_2O.

A more significant finding of this pioneering work was derived from investigations of the pyrolysis of equimolar mixtures of CH_2O and CD_2O (deuterated formaldehyde). In these tests, molecular hydrogen was formed in a statistically random isotopic distribution from the beginning of the reaction. This observation, as well as the presence of an induction period, led Gay et al. (1965) to conclude that a radical, rather than molecular, mechanism must be postulated to explain thermal decomposition of formaldehyde. This information is consistent with the low-temperature pyrolysis data of Klein, Scheer, and Schoen (1956) which indicated that pyrolysis of CH_2O occurred predominately by a chain mechanism.

Pyrolysis of formaldehyde was also studied by Schecker and Jost (1969) with argon as the diluent between 1400 and 2300°K. Initial CH_2O concentrations were varied from 200 ppmV to 1 percent and infrared absorption spectroscopy was used to follow the decay of CH_2O behind the shock wave. An induction period before exponential decay of CH_2O was observed regardless of the initial reactant level. This information, in conjunction with the observation that the activation energy of the apparent rate constant decreased from 55 kcal/mole for initial levels of CH_2O between 200 and 500 ppmV to 34.4 kcal/mole for reactant concentrations near 1 percent, led these investigators to conclude that, even at the lowest concentration of CH_2O used, participation of secondary reactions was of major importance in determining the measured decomposition rate.

The most recent study of CH_2O pyrolysis is, apparently, that reported by Dean et al (1979). The major contribution of these authors, since the data obtained were consistent with the earlier experiments, was to use computer modeling to demonstrate that the simple chain mechanism proposed by Gay et al (1965):

$$CH_2O + M = HCO + H + M \qquad (29)$$

$$CH_2O + H = HCO + H_2 \qquad (30)$$

$$HCO + M = H + CO + M \qquad (20)$$

$$H + HCO = H_2 + CO \qquad (24)$$

could quantitatively reproduce the concentration and temperature dependencies of the observed formaldehyde decay. The mechanism could also reproduce the data reported by Schecker and Jost (1969) for much higher total densities. Dean et al (1979) indicate that the previous attempts to interpret CH_2O pyrolysis data via this simple reaction mechanism failed because the mechanistic analysis via steady-state assumptions for H-atoms and HCO was incorrect, and not because of deficiencies in the mechanism.

Another point of interest addressed by Dean et al (1979) deals with the possibility of a molecular dissociation path for formaldehyde:

$$CH_2O + M = CO + H_2 + M \qquad (29')$$

The question arises as a result of the interpretation of low pressure, CH_4 -O_2 flat flame data reported by Peeters and Mahnen (1973). These authors maintained that reaction (29') is the rate-limiting step in CH_4combustion and is necessary to explain the H_2 produced in the low temperature region ($T > 1400$ K) of the flame they studied. However, this conclusion is questionable because Peeters and Mahnen (1973) explicitly limited the species and reactions considered in the analysis and because the rate constant derived for reaction (29') yields decomposition rates of CH_2O which are 3 to 4 orders of magnitude higher than any of the measurements in shock tube investigations. Dean et al (1979) concluded that reaction (29') does not play a significant role in the high temperature pyrolysis of CH_2O. Virtually identical results were predicted whether reaction 29' was included with the same rate constant as for reaction 29 or $k_{29'}$ was set equal to zero. This indicates that the chain mechanism dominates after radicals are generated by reaction 29.

Other than the initial studies of Gay et al (1965), there are apparently only two experimental investigations of CH_2O oxidation in shock tubes. Dean, Johnson, and Steiner (1980) examined CH_2O oxidation between 1600 and 3000 K and used O_2 or N_2O as the oxidant. Formaldehyde decay was followed by infrared emission; oxygen atom production was measured via flame-band emission; and CO_2 was measured via infrared emission in mixtures with added CO. The most significant conclusion of these authors was that the rate constant for reaction of OH with CH_2O was at least an order of magnitude lower than values reported in the literature. It was also concluded that the rate coefficient for reaction 31 exhibited non-Arrhenius behavior.

The other shock-initiated investigation of CH_2O oxidation is that reported by Drummond (1971). A correlation of induction times, which were defined by the interval between the reflected shock passing the observation windows and the commencement of OH absorption, was reported for temperatures between 1166 and 1509 K. Since the measured induction times were independent of the initial oxygen concentration and inversely proportional to the CH_2O concentration, Drummond suggested that the dissociation of CH_2O or a reaction between CH_2O and an intermediate was the rate-limiting step in this temperature range, which controlled the oxidation process.

The current numerical studies primarily use the data reported by Dean et al (1980) as a test of the mechanism describing CH_2O oxidation. This mechanism consists of the reactions listed in Table 4-1 and those listed in Table 3-1. Additional simulations of shock tube data were included in the validation process to determine whether the reaction mechanism could reproduce the observations reported by Gay et al (1965) and Drummond (1971). Detailed kinetic simulations of the pyrolysis of CH_2O-diluent mixtures were not considered.

As mentioned above, Dean et al (1980) monitored infrared emission of CO_2 behind reflected shock waves to gain insight into the processes controlling CH_2O oxidation. The time-dependent emission traces were converted to concentration profiles via calibration factors determined by these investigators. The CO_2 profile was characterized, as a function of temperature, by three variables: (1) τ, the time relative to t_{mp} when the tangent to the CO_2-time plot intercepted the time-axis; (2) tc, the time relative to t_{mp} when the CO_2 concentration reached 7.47×10^{-8} mole/cm^3; and (3) S_{CO_2}, the slope of the initial region of the CO_2 profile after the induction time, t_i. The reference time, t_{mp}, was the time at which the shock passes the midpoint of the observation window and was typically 5 μsec after the reflected shock was first visible to the detector.

Table 4-1. CH_2O-O_2 Reaction Mechanism

No.	Reaction	$\Delta H^0_{r,298}$ kcal/mole	A	b	E kcal/mole	Reference
29*	$CH_2O + M = HCO + H + M$	87.05	3.31 (16)	0	81.02	Dean et al., 1979
30	$HCO + HCO = CH_2O + CO$	-70.37	4.0 (13)	0	0	Reilly et al., 1978
31	$CH_2O + H = HCO + H_2$	-17.15	2.5 (10)	1.0	3.20	Est. This Study
32	$CH_2O + OH = HCO + H_2O$	-32.34	5.0 (9)	1.0	1.65	Est. This Study
33	$CH_2O + O = HCO + OH$	-15.12	1.3 (10)	1.0	2.05	Est. This Study
34	$CH_2O + HO_2 = HCO + H_2O_2$	-2.58	1.0 (12)	0	8.0	Lloyd, 1974

*Expression derived for argon as the dominant third-body. It is assumed that all chaperon efficiencies are the same as Ar.

Simulations were done for an intial reactant composition of 0.5 percent CH_2O, 0.92 percent O_2, and 9.15 percent CO in argon. Adiabatic combustion at the temperatures and pressures reported by Dean et al (1980) was assumed, although the predicted temperature profiles indicate nearly isothermal conditions throughout the reaction. In addition, 5 μsec were subtracted from calculated values of τ and tc to yield a time-scale consistent with the experimental data.

Results of these calculations are compared with the measured values in Figures 4-1 to 4-3. The predicted values for τ and tc are in excellent agreement with the data between 1670 and 2160 K. The calculated production rate of CO_2 is also in good agreement with the observed values between 1605 and 2160 K. The slightly lower value predicted for S_{CO_2} at 2160 K may reflect an increased uncertainty of the experimental values at higher temperatures. The inadequacies previously noted for k_{21} above 2000 K could also be used to explain the disparity. The reason for the discrepancies between predicted and observed values for τ and tc at 1605 K is discussed below in this section.

The CH_2O oxidation mechanism was next used to predict induction times which could be compared with the data reported by Gay et al (1965) and Drummond (1971). The major reason for these additional calculations was to determine whether the reaction mechanism was consistent with phenomena relevant to shock-initiated combustion of CH_2O over a broader range of temperature and initial reactant concentrations than examined by Dean et al (1980). The results of the simulations were compared with induction time correlations reported by Gay et al (1965) and Drummond (1971).

The measured H_2O profile was used by Gay et al (1965) to define an induction time for CH_2O oxidation. The data were correlated by:

$$\tau(O_2)_o = \left(3.98^{+2.33}_{-1.47}\right) \times 10^{-15} \exp[(22900 \pm 1700)/RT]$$

with units of seconds, moles, and cm^{-3}. To facilitate comparison with one of the correlations reported by Drummond (1971), data for one of the mixtures studied by Gay et al (1965)--$CH_2O/O_2/Ne$ = 3.3/1.7/95--were modified by multiplying by the ratio: $(CH_2O)_o/(O_2)_o$. The resulting values are

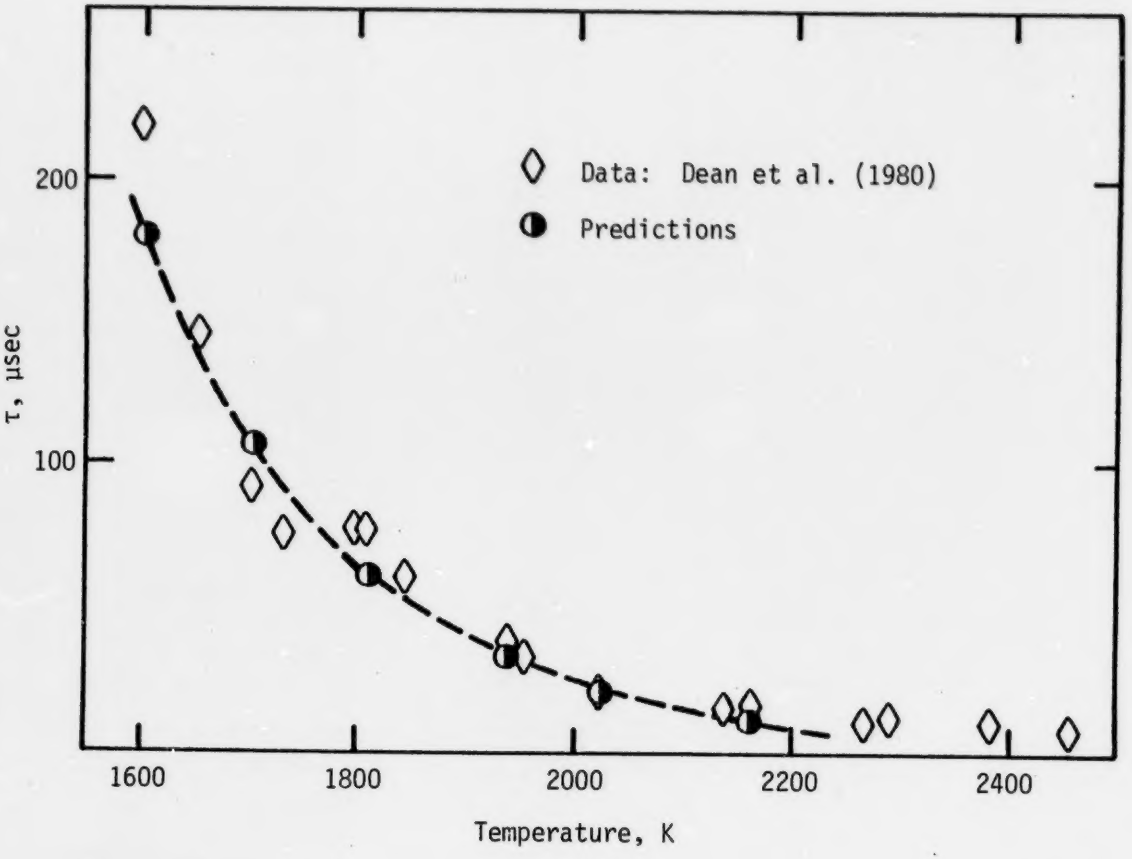

Figure 4-1. CO_2 induction times for fuel-lean CH_2O oxidation - $CH_2O/O_2/CO$ = 0.5/0.92/9.15.

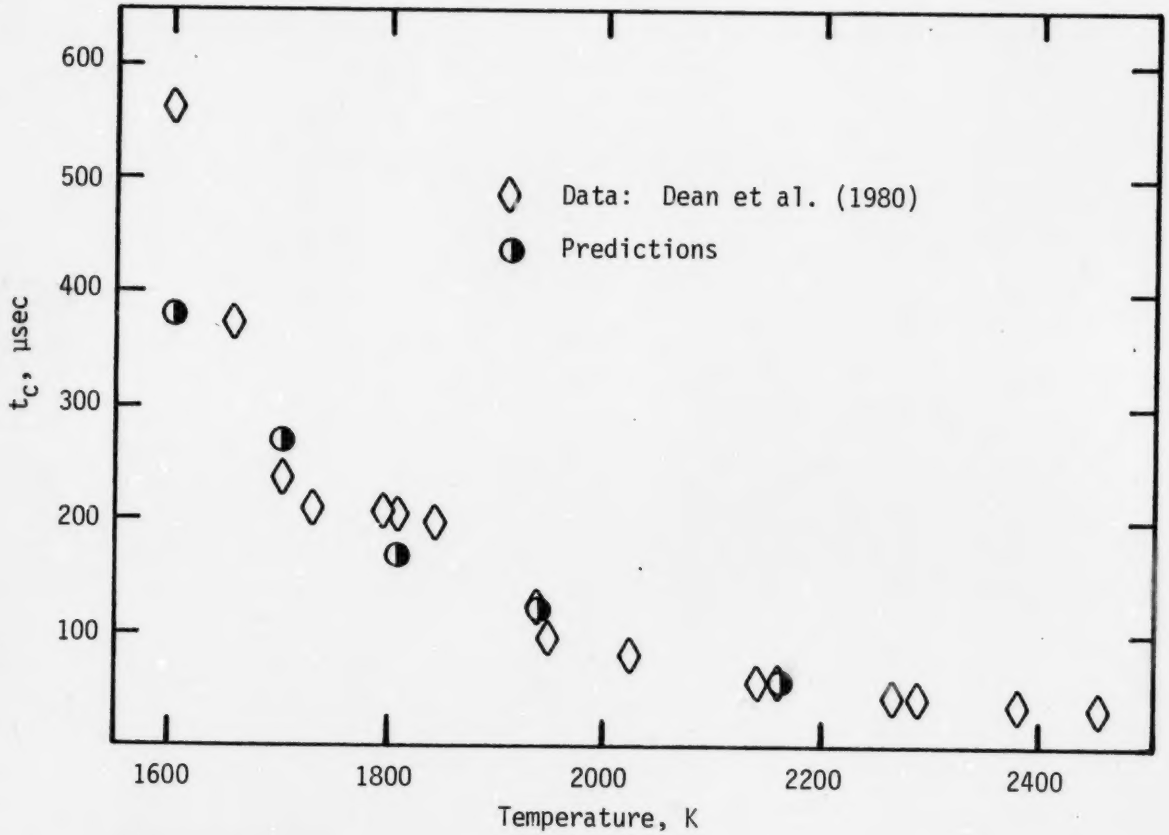

Figure 4-2. Times for CO_2 concentration to reach 7.47 x 10^{-8} mole/cm^3 - $CH_2O/O_2/CO$ = 0.5/0.92/9.15.

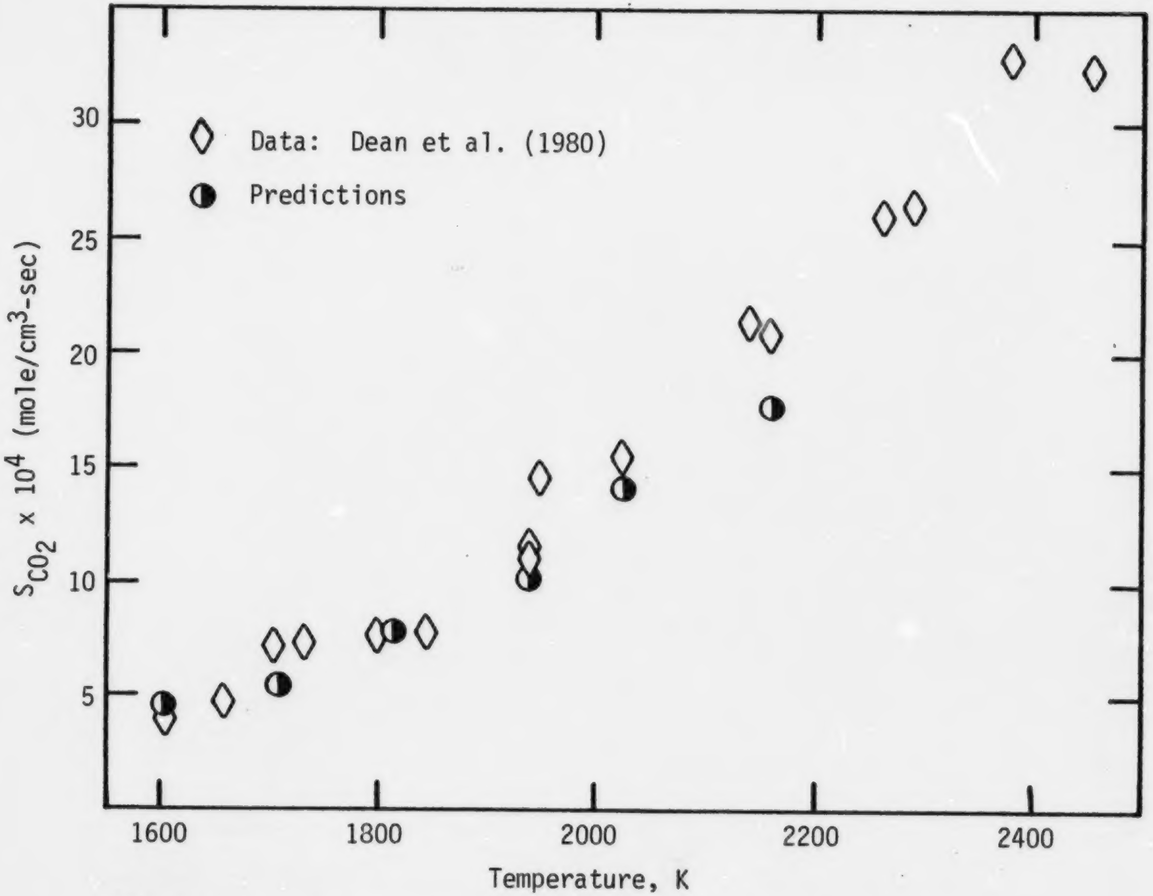

Figure 4-3. Linear production rate of CO_2 during oxidation of CH_2O-$CH_2O/O_2/CO$ = 0.5/0.92/9.15.

compared in Figure 4-4 with induction times reported by Dean et al (1980) based on the CO_2 profile, and with predicted values obtained from the reactant mixture corresponding to that used by Dean et al (1980). Although the data of Gay et al (1965), which were selected for this plot, are slightly higher than the induction times based on CO_2 profiles, the agreement is quite reasonable. If the definition of induction time for the predictions is based on the time at which the OH radical concentration reaches its maximum, better quantitative agreement with the data of Gay et al (1965) is achieved, as shown in Figure 4-5.

The calculated induction times based on the CO_2 profile are well represented by a single line between 1300 and 2160 K. A least-squares analysis of the predicted values yields:

$$\tau\left(CH_2O\right)_o = 4.525 \times 10^{-16} \exp(30710/RT)$$

with units of seconds, moles, and cm^3. This equation is in reasonable agreement with the induction correlation reported by Drummond (1971), although he found a higher temperature dependence:

$$\tau\left(CH_2O\right)_o = \left(5.50^{+1.58}_{-1.23}\right) \times 10^{-16} \exp[(33000 \pm 700)]$$

Again, the units are seconds, moles, and cm^3.

Simulations of CH_2O oxidation at lower temperatures and higher reactant concentrations were performed in order to determine whether the higher temperature dependence reported by Drummond (1971) for the induction time correlation was due to a change in the dominant reactions controlling CH_2O oxidation. Since Drummond defined the induction period as the interval between the reflected shock passing the observation window and the commencement of absorption by OH, it is difficult to assign *a priori* a definition for predicted induction times consistent with the experimental definition without information describing the sensitivity of the measurement approach. The CO_2 profile and the time at which 10 percent of the initial CH_2O was consumed were, therefore, used to check against the absolute values and the measured temperature dependence.

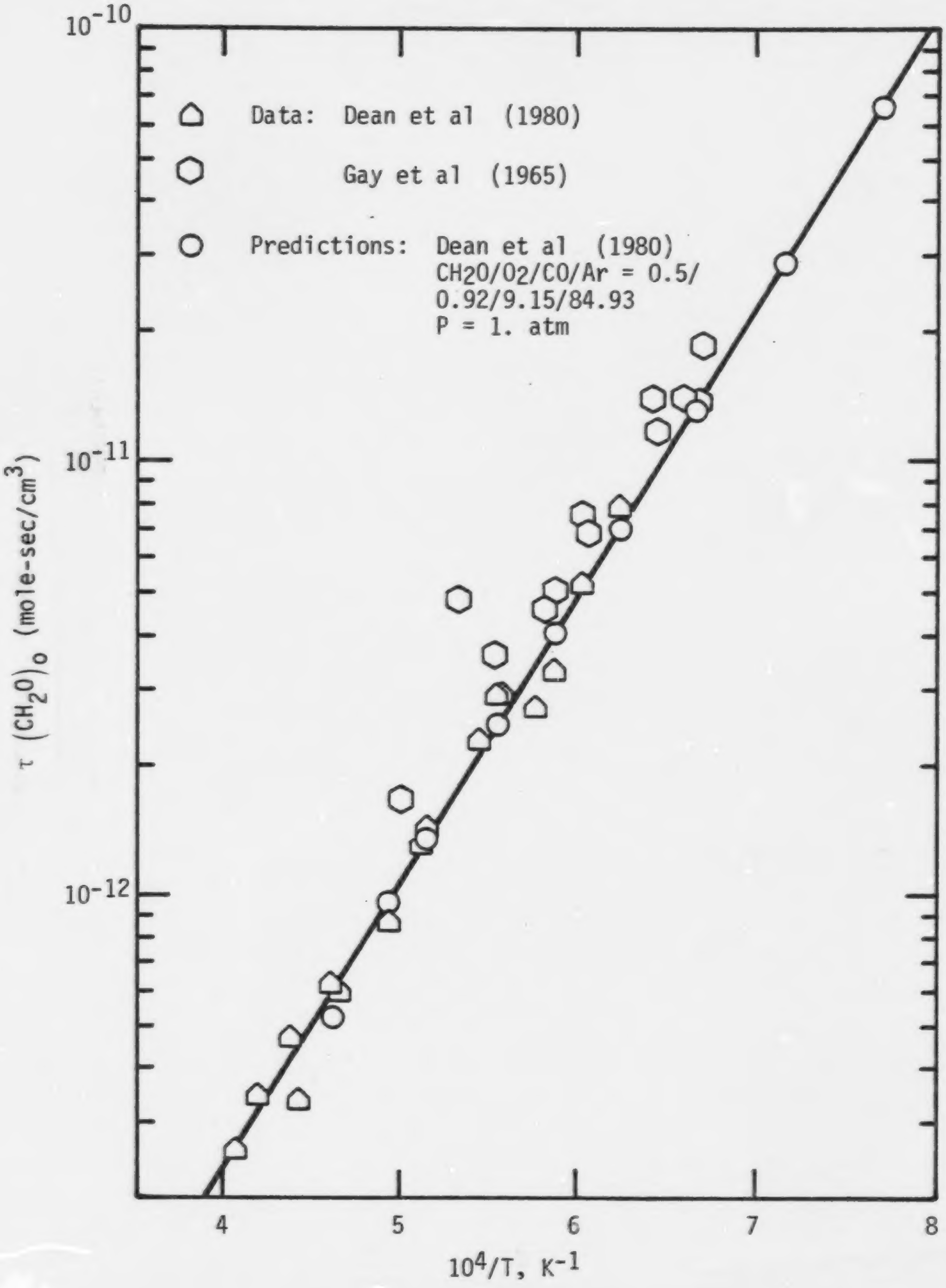

Figure 4-4. Correlation of CH_2O induction times. (Induction times for predictions based on CO_2 profiles).

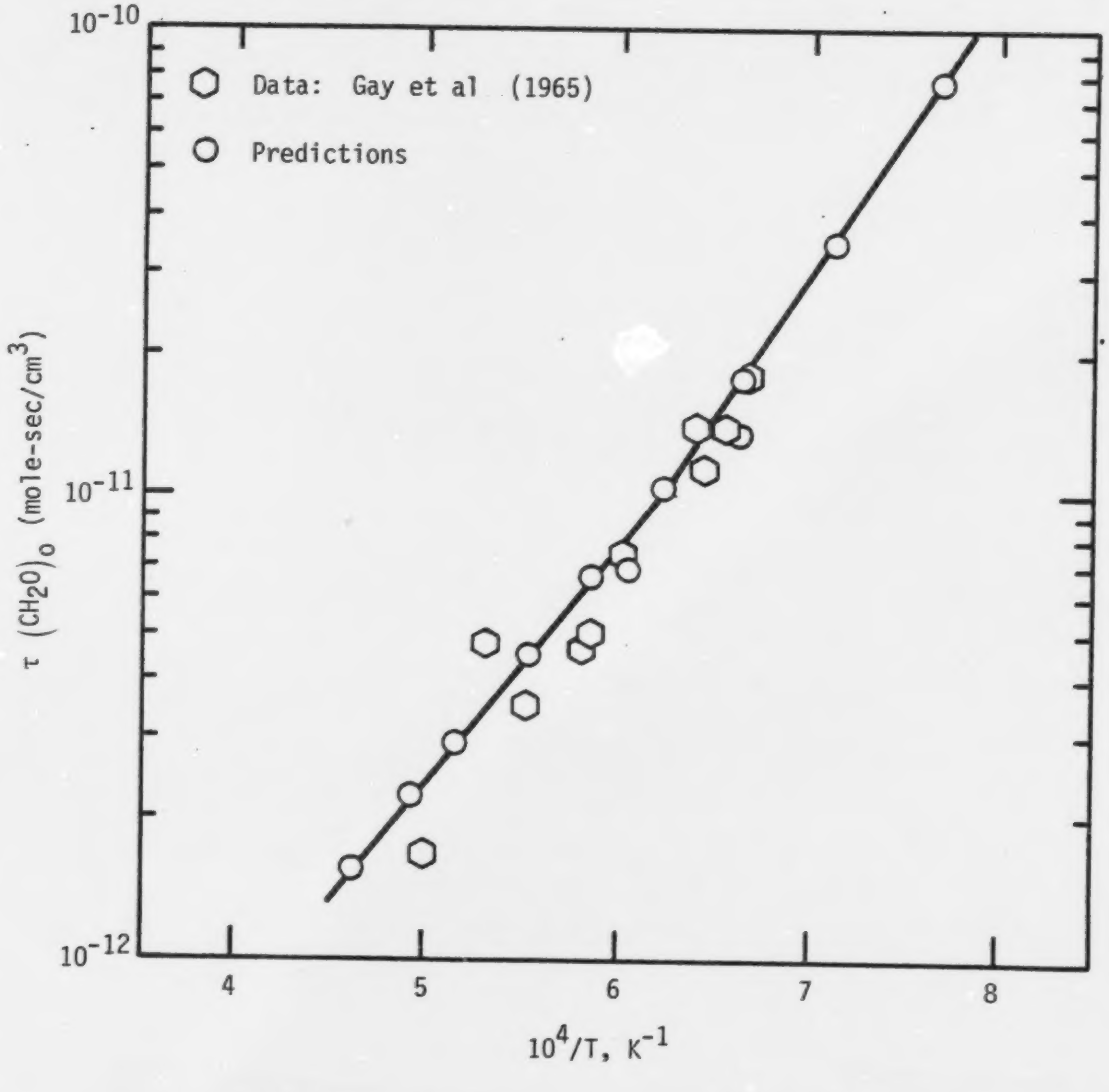

Figure 4-5. Correlation of induction times in CH_2O oxidation-- CH_2O/O_2 = 3.3/1.7. (Predictions of induction times based upon maximum OH concentration).

FH-6

Figure 4-6 compares predicted values based on the time for 10 percent CH_2O consumption with the data of Drummond (1971), which was correlated in this case by:

$$\tau\ (CH_2O)_o\ P = \left(5.13^{+1.33}_{-1.05}\right) \times 10^{-15} \exp\left[(29300 \pm 600)/RT\right]$$

where the units are seconds, moles, cm^{-3}, and atmospheres. Although the absolute values calculated are lower, the temperature dependence appears to be consistent with that observed between 1250 and 1509 K. Induction times based on the CO_2 profiles were about 50 percent longer than those based on the consumption of CH_2O; the temperature dependence for both cases was essentially the same. It should be noted that a better test of the reaction mechanism against the data shown in Figure 4-6 would involve simulations which used the experimental postshock pressure and temperature for each point.

After the completion of the numerical studies described above, additional sets of low temperature data for reactions 32 and 33 were found in the literature. Atkinson and Pitts (1978) measured the rate of reaction 32 between 299 and 426 K. Least-squares analysis of their data gave the following temperature dependence for the rate of this reaction:

$$k'_{32} = 7.53 \times 10^{12} \exp[-(175 \pm 300)/RT]$$

The faster rate for reaction 32, which would result from using this rate coefficient instead of the expression given in Table 4-1, would increase the values for τ predicted for the data of Dean et al (1980). This is due to the increased competition for OH and its depletion by CH_2O which decreases the rate of CO_2 production via reaction 21. Preliminary analysis suggests that the changes in τ scale with the square root of the ratio k'_{32}/k_{32}. The use of this alternate rate coefficient, which we recommend, may improve the agreement with the data reported by Drummond (1971).

Morrison and Heicklen (1980) studied reaction 32 at room temperature. These authors suggest that there are two reaction channels for this elementary step:

$$CH_2O + OH = H_2O + HCO \qquad (32a)$$

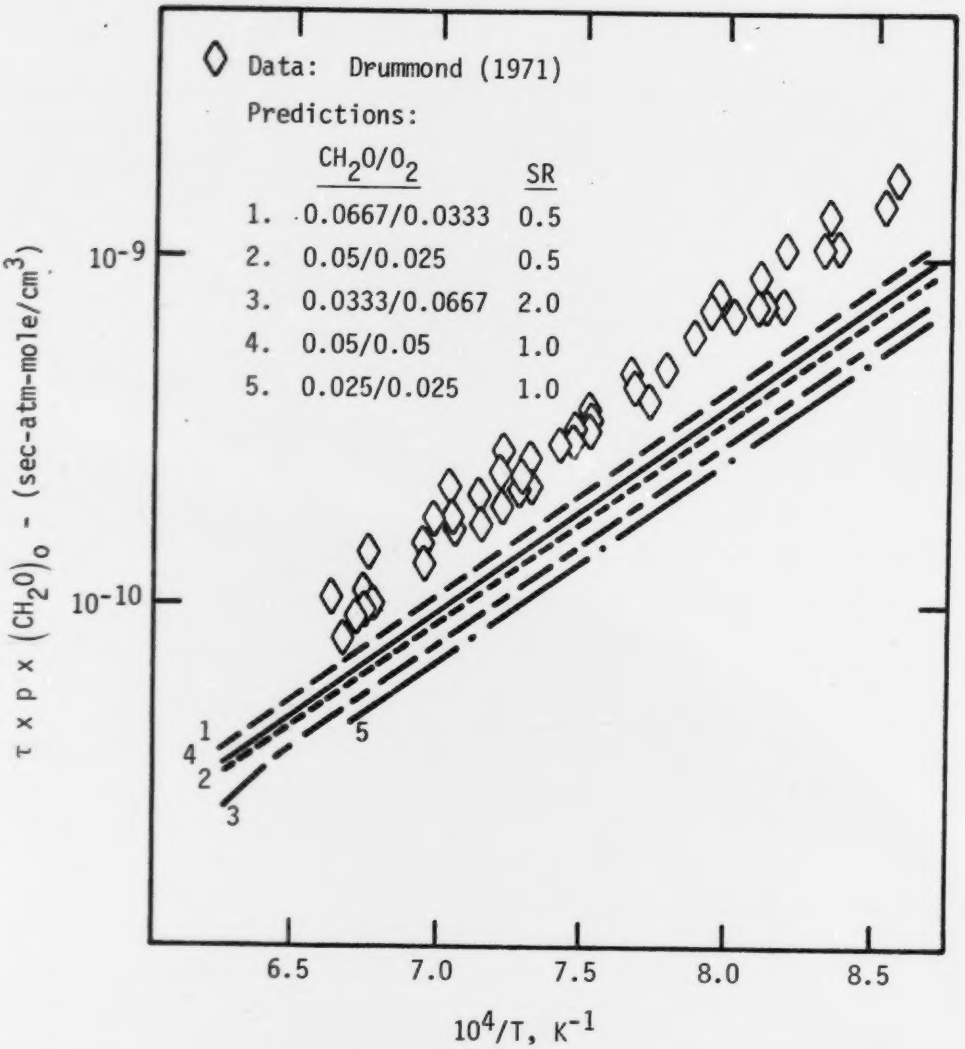

Figure 4-6. Correlation of CH_2O induction times at lower temperatures and higher reactant concentrations.

$CH_2O + OH = H_2O + HCO^*$ (32b)

where HCO* is a vibrationally excited radical with sufficient energy to decompose spontaneously. An upper limit for the branching ratio at room temperature was derived: $k_{32b}/k_{32a} = 0.49^{+0.16}_{-0.13}$. If the branching ratio reported by these investigators has a weak dependence on temperature, inclusion of reaction 32b could have a major impact on the rate at which radicals grow during CH_2O oxidation. However, until additional measurements are reported for higher temperature, this reaction channel cannot be included in the reaction mechanism.

The rate of reaction 33 has been measured between 296 and 433 K by Chang and Barker (1979). Although the observed temperature dependence of the reaction is in agreement with the rate coefficient listed in Table 4-1, the authors concluded that two reaction channels were operative:

$CH_2O + O = HCO + OH$ (33a)

$CH_2O + O = HCO_2 + H$ (33b)

with subsequent decomposition of the HCO_2 radical. The results suggest that the activation energy for the addition reaction is virtually the same as that of the simple abstraction reaction. In addition, the contribution of reaction 33b to the total rate of reaction 33 is about 30 percent between 298 and 497 K based on the CO_2 yields measured. Inclusion of the second reaction channel would change the rate of radical growth, as well as the rate of CO_2 production, during the oxidation of CH_2O. However, the availability of thermochemical data for the HCO_2 species will ultimately determine whether reaction 33b can be considered in the reaction mechanism.

We believe that the reaction mechanism describing CH_2O oxidation is sufficiently accurate if the rate coefficient for reaction 32 reported by Atkinson and Pitts (1978) is incorporated into the hydrocarbon reaction mechanisms described in the following sections. Additional calculations to quantify the impact of k'_{32} on the predictions, especially between 1100 and 1600 K, are recommended. Simulations are also recommended to determine whether the multiple reaction channels reported for reactions 32 and 33 have a significant effect on shock-initiated CH_2O oxidation. Further testing is also required on flame speed and species profiles when such data becomes available.

4.2 Hydrocarbon Reaction Mechanisms

Development of detailed kinetic mechanisms, which can accurately describe oxidation and pyrolysis of simple hydrocarbon species--CH_4, C_2H_2, C_2H_4, and C_2H_6--is necessary, at least as a first step, to understand the phenomena which control conversion of fuel nitrogen compounds to nitric oxides and molecular nitrogen in hydrocarbon flame environments. In addition to predicting concentrations of stable intermediates, products, and the important free radicals H, O, and OH, which occur during the oxidation of these organic fuels, the reaction mechanisms must be able to reproduce the transient behavior of hydrocarbon radicals, which when present play a dominant role in fuel nitrogen chemistry. This particular task is more difficult than the work described in the previous sections not only because of the larger number of species and elementary reactions which may participate and, therefore, must be considered, but also because it is not possible to completely validate each hydrocarbon reaction mechanism independently of the other hydrocarbon mechanisms included in the present analysis. This last point is substantiated by numerous studies of hydrocarbon combustion which show that C_2H_2, C_2H_4, and C_2H_6 are present during the fuel-rich combustion of CH_4 mixtures (Glick, 1959; Skinner and Ruehrwein, 1959; Fenimore and Jones, 1961; Dove and Moulton, 1965, Crossley et al , 1972; D'Alessio et al , 1977; Harvey and MacColl, 1979) and are also present during stoichiometric and fuel-lean CH_4 combustion (Dryer and Glassman, 1973; Peeters and Mahnen, 1973; Harvey and MacColl, 1979). It has also been shown that CH_4, C_2H_2, and C_2H_4 are produced in stoichiometric and fuel-lean ethane oxidation (Fristrom, Avery, and Grunfelder, 1959; Burcat et al , 1972), that CH_4, C_2H_4, and C_2H_6 are present in fuel-rich C_2H_2 oxidation (Shaub and Bauer, 1978) and that CH_4 and C_2H_2 are present during fuel-lean combustion of ethylene (Fristrom, Avery, and Grunfelder, 1959; Gay et al , 1967)

The increased number of possible reaction channels, especially for the C_2-hydrocarbons, and the paucity of data for many of the elementary reactions over a broad temperature range further complicate the process by which each reaction mechanism must be validated.

Detailed kinetic simulations and/or simplified closed-form expressions of phenomena relevant to shock tube investigations of CH_4 and C_2H_6 oxidation, which are discussed in the material below, have been used to examine subsets of the pertinent reaction mechanisms to determine whether these particular elements of the reaction sets are sufficiently accurate to be treated as known quantities in subsequent work. Since calculations designed to test the acetylene and ethylene reaction mechanisms are still in the initial phases, discussion of these mechanisms focuses on the elementary reaction steps included, the rate coefficients used, and whether additional species and reaction paths are necessary to describe oxidation and pyrolysis of these C_2-hydrocarbons.

4.2.1 Induction Phenomena During the Oxidation of CH_4 and C_2H_6

The complete set of reactions and the associated rate coefficients, which were initially considered, consists of the elementary steps listed in Table 3-1 and 4-1 describing H_2, CO, and CH_2O oxidation, and those listed in Tables 4-2 through 4-7 which describe the oxidation and pyrolysis of CH_4, C_2H_2, C_2H_4, and C_2H_6. Production of polyacetylenes via the reactions given in Table 4-8 was not included in the detailed kinetic simulations because of the uncertainty which exists for thermochemical and kinetic rate data, and because the increased number of species would have required extensive modifications to the computer code which was used. However, it is anticipated on the basis of experimental observations that reactions of this type will be necessary to model, at least, fuel-rich C_2H_2 and C_2H_4 combustion and, in light of the data reported by D'Alessio et al (1977), as well as others, may be required to simulate fuel-rich CH_4 oxidation.

The initial tests of the CH_4 and C_2H_6 reaction mechanisms involved comparisons between predicted and observed induction delay times, which were determined in shock tube investigations of these hydrocarbon species. Two series of calculations were included in the analysis of the CH_4 reaction mechanism. The first set of computations used only the reactions listed in Table 4-2 to describe CH_4 oxidation; the second set of simulations included the reactions listed in Tables 4-3 through 4-7, in addition to those given

Table 4-2. CH_4 Oxidation--Reactions of C_1-Hydrocarbon Species

No.	Reaction	ΔH_r^0, 298 kcal/mole	A	b	E kcal/mole	Reference
35	$CH_4 + M = CH_3 + H + M$	104.8	1.26 (17)	0.0	88.4	Hartig, Troe & Wagner, 1971
36	$CH_4 + OH = CH_3 + H_2O$	-14.58	1.55 (6)	2.13	2.45	Ernst, Wagner & Zellner, 1978
37	$CH_4 + O = CH_3 + OH$	2.648	1.17 (7)	2.08	7.63	Roth and Just, 1977
38	$CH_4 + H = CH_3 + H_2$	0.613	1.41 (7)	2.0	8.84	Shaw, 1978
39	$CH_4 + O_2 = CH_3 + HO_2$	57.72	8.51 (6)	2.0	51.97	Shaw, 1978
40	$CH_4 + HO_2 = CH_3 + H_2O_2$	15.18	2.0 (13)	0.0	18.0	Skinner et al., 1972
41	$CH_3 + O = CH_2O + H$	-68.23	9.0 (13)	0.0	2.0	Roth and Just, 1977
42	$CH_3 + OH = CH_2 + H_2O$	-9.76	6.3 (10)	0.7	2.0	Engleman, 1976
43	$CH_3 + O_2 = CH_3O + O$	27.74	6.0 (9)	1.0	28.0	Est. This Study
44	$CH_3O + M = CH_2O + H + M$	23.15	5.0 (13)	0.0	21.0	Brabbs and Belles, 1975
45	$CH_3O + H = CH_2O + H_2$	-81.05	1.0 (14)	0.0	0.0	Engleman, 1976
46	$CH_3O + OH = CH_2O + H_2O$	-96.24	3.0 (13)	0.0	0.0	Engleman, 1976
47	$CH_3O + O = CH_2O + OH$	-79.02	1.0 (14)	0.0	0.0	Engleman, 1976
48	$CH_2 + O_2 = CH_2O + O$	-58.74	7.7 (9)	1.0	0.54	Est. This Study
49	$CH_2 + O = HCO + H$	-90.81	6.5 (13)	0.0	0.0	Vinchier & Debruyn, 1979
50	$CH_2 + OH = CH + H_2O$	-17.64	5.0 (11)	0.5	6.0	Engleman, 1976
51	$CH_2 + OH = CH_3 + O$	-7.46	5.0 (11)	0.5	6.0	Engleman, 1976
52	$CH_2 + OH = CH_2O + H$	-75.69	1.0 (13)	0.0	5.0	Engleman, 1976
53	$CH_2 + H_2 = CH_3 + H$	-5.43	1.0 (11)	0.5	5.73	Est. This Study
54	$CH + H_2 = CH_2 + H$	2.45	1.2 (13)	0.0	0.0	Butler et al., 1979
55	$CH + O = CO + H$	-175.9	5.0 (11)	0.5	0.0	Engleman, 1976

(continued)

Table 4-2 (Concluded)

No.	Reaction	ΔH^0_r, 298 kcal/mole	A	b	E kcal/mole	Reference
56	$CH + OH = HCO + H$	-90.39	5.0 (11)	0.5	5.62	Engleman, 1976
57	$CH + O_2 = HCO + O$	-73.44	2.0 (13)	0.0	0.0	Messing, Sadowski & Filseth, 1979
58	$CH + CO_2 = HCO + CO$	-159.4	1.0 (10)	0.5	6.0	Engleman, 1976
59	$CH + CH_4 = CH_2 + CH_3$	3.06	2.5 (11)	0.7	6.0	Engleman, 1976
60	$CH_2 + CH_2 = CH_3 + CH$	-7.88	5.0 (11)	0.5	6.0	Engleman, 1976
61	$CH_2 + CH_4 = CH_3 + CH_3$	-4.82	1.26 (12)	0.7	20.0	Engleman, 1976

Forward rate coefficients are expressed as $k_i = AT^b \exp(-E/RT)$ in units of cm^3, mole, sec. Numbers in parentheses refer to powers-of-ten, i.e., 1. (17) = 1×10^{17}. M refers to total concentration. All species are assumed to have the same chaperon efficiency for Reactions 35 and 44. For Reaction 5, the relative chaperon efficiency of CH_4 to H_2 is 3.75:1.

Table 4-3. CH_4 Oxidation--Reactions Producing C_2-Hydrocarbon Species

No.	Reaction	ΔH^0_r, 298 kcal/mole	A	b	E kcal/mole	Reference
62	$CH_2 + CH_3 = C_2H_4 + H$	-62.50	6.0 (13)	0.0	0.0	Carr, 1972
63	$CH + CH_4 = C_2H_4 + H$	-59.46	1.5 (12)	0.0	0.0	Brann et al., 1967
64	$CH_2 + CH_2 = C_2H_2 + H_2$	-130.5	3.2 (13)	0.0	0.0	Laufer and Bass, 1974
65	$CH_4 + CH_3 = C_2H_6 + H$	14.91	8.0 (13)	0.0	40.0	Tabayaski & Bauer, 1979
66	$CH_4 + CH_3 = C_2H_5 + H_2$	10.56	1.0 (13)	0.0	23.0	Tabayaski & Bauer, 1979
67	$CH_3 + CH_3 = C_2H_6$	-89.91	2.4 (13)	0.0	0.0	Lifshitz & Frenklach, 1975

Forward rate coefficients expressed as $k_i = AT^b \exp(-E/RT)$ in units of cm^3, mole, sec.

Table 4-4. C_2H_2 Oxidation Reactions

No.	Reaction	ΔH^0_r, 298 kcal/mole	A	b	E kcal/mole	Reference
68	$C_2H_2 + M = C_2H + H + M$	128.7	4.17 (16)	0.0	107.0	Just and Franck, 1979
69	$C_2H_2 + O = CH_2 + CO$	-47.82	6.73 (13)	0.0	4.0	Vandooren & Van Tiggelen, 1977
70	$C_2H_2 + O = C_2H + OH$	26.50	3.2 (15)	-0.6	17.0	Browne et al., 1969
71	$C_2H_2 + OH = C_2H + H_2O$	9.28	1.4 (13)	0.0	7.0	Fenimore & Jones, 1964
72	$C_2H_2 + OH = CH_3 + CO$	-55.28	5.5 (13)	0.0	13.7	Vandooren & Van Tiggelen, 1977
73	$C_2H_2 + H = C_2H + H_2$	24.47	7.76	3.2	0.50	Tanzawa & Gardiner, 1979
74	$C_2H_2 + O_2 = HCO + HCO$	-36.19	4.0 (12)	0.0	28.0	Gardiner & Walker, 1968
75	$C_2H + O_2 = HCO + CO$	-148.2	1.0 (13)	0.0	0.0	Browne et al., 1969
76	$C_2H + O = CH + CO$	-74.74	5.0 (13)	0.0	0.0	Browne et al., 1969
77	$C_2H + OH = CO + CH_2$	-74.32	6.0 (12)	0.0	0.0	Shaviv and Barnun, 1975

Forward rate coefficients expressed as $k_i = AT^b \exp(-E/RT)$ in units of cm^3, mole, sec. M refers to total concentration. All species are assumed to have the same chaperon efficiency for Reaction 68.

Table 4-5. C_2H_6 Oxidation Reactions

No.	Reaction	ΔH^0_r, 298 kcal/mole	A	b	E kcal/mole	Reference
78	$C_2H_6 + H = C_2H_5 + H_2$	-4.35	5.37 (2)	3.5	5.2	Clark and Dove, 1973
79	$C_2H_6 + OH = C_2H_5 + H_2O$	-19.54	6.31 (13)	0.0	2.45	Westbrook et al., 1977
80	$C_2H_6 + O = C_2H_5 + OH$	-2.32	2.5 (13)	0.0	6.36	Herron and Huie, 1973
81	$H + C_2H_4 = C_2H_5$	-37.16	1.0 (13)	0.0	1.5	Allara & Edelson, 1975
82	$C_2H_5 + H = C_2H_4 + H_2$	-67.04	1.86 (12)	0.0	0.0	Camilleri, Marshall & Purnell, 1974
83	$C_2H_5 + H = CH_3 + CH_3$	-9.94	3.72 (13)	0.0	0.0	Camilleri, Marshall & Purnell, 1974
84	$C_2H_5 + O_2 = C_2H_4 + HO_2$	-9.94	1.0 (12)	0.0	5.0	Cooke and Williams, 1971

Forward rate coefficients expressed as $k_i = AT^b \exp(-E/RT)$ in units of cm^3, mole, sec.

Table 4-6. C_2H_4 Oxidation Reactions

No.	Reaction	ΔH^0_r, 298 kcal/mole	A	b	E kcal/mole	Reference
85	$C_2H_4 + M = C_2H_2 + H_2 + M$	41.65	2.6 (17)	0.0	79.29	Just, Roth & Damm, 1977
86	$C_2H_4 + M = C_2H_3 + H + M$	105.7	3.8 (17)	0.0	98.17	Just, Roth & Damm, 1977
87	$C_2H_4 + O = CH_2 + CH_2O$	-5.70	8.06 (6)	2.0	0.307	Est. This Study
88	$C_2H_4 + O = CH_3 + HCO$	-28.28	5.93 (10)	0.74	0.56	Est. This Study
89	$C_2H_4 + H = C_2H_3 + H_2$	1.53	1.1 (14)	0.0	8.5	Jackimoswki, 1977
90	$C_2H_4 + OH = CH_3 + CH_2O$	-13.16	4.5 (12)	0.0	0.22	Smith & Zellner, 1973
91	$C_2H_4 + OH = C_2H_3 + H_2O$	-13.66	1.0 (14)	0.0	3.5	Baldwin, Simmons & Walker, 1966
92	$C_2H_3 + M = C_2H_2 + H + M$	40.12	7.94 (14)	0.0	31.5	Benson & Haugen, 1967
93	$C_2H_3 + H = C_2H_2 + H_2$	-64.08	1.0 (13)	0.0	0.0	Olson and Gardiner, 1978

Forward rate coefficients expressed as $k_i = AT^b \exp(-E/RT)$ in units of cm^3, mole, sec. M refers to total concentration. Chaperon efficiencies for Reactions 85 and 86 are assumed to be the same for all species

Table 4-7. Reactions Between Hydrocarbon Species

No.	Reaction	ΔH^0_r, 298 kcal/mole	A	b	E kcal/mole	Reference
94	$C_2H_2 + CH = C_2H + CH_2$	26.92	1.08 (12)	0.5	26.92	Est. This Study
95	$C_2H_2 + CH_2 = CH_3 + C_2H$	19.04	1.05 (12)	0.5	19.04	Est. This Study
96	$C_2H_4 + CH_2 = C_2H_3 + CH_3$	-3.90	1.09 (13)	0.0	12.4	Carr, 1972
97	$C_2H_4 + CH_3 = C_2H_3 + CH_4$	0.915	5.0 (12)	0.0	13.0	Tabayashi & Bauer, 1979
98	$C_2H_6 + CH_2 = C_2H_5 + CH_3$	-9.78	1.22 (13)	0.0	15.7	Carr, 1972
99	$C_2H_6 + CH_3 = C_2H_5 + CH_4$	-5.3	0.55	4.0	8.28	Clark & Dove, 1973
100	$C_2H_5 + CH_3 = CH_4 + C_2H_4$	-67.66	2.55 (11)	0.0	0.0	Allara & Edelson, 1975
101	$C_2H_5 + C_2H_5 = C_2H_6 + C_2H_4$	-62.69	5.0 (10)	0.0	0.0	Allara & Edelson, 1975
102	$C_2H_5 + C_2H_3 = C_2H_4 + C_2H_4$	-68.57	3.16 (17)	0.0	35.6	Benson & Haugen, 1967

Forward rate coefficients expressed as $k_i = AT^b \exp(-E/RT)$ in units of cm^3, mole, sec.

Table 4-8. Reactions Producing Polyacetylenes

No.	Reaction	ΔH^0_r, 298 kcal/mole	A	b	kcal/mole	Reference
103	$C_2H_2 + C_2H_2 = C_4H_3 + H$	46.72	1.0 (13)	0.0	45.89	Tanzawa & Gardiner, 1979
104	$C_2H_2 + C_2H = C_4H_2 + H$	-19.95	1.87 (13)	0.0	0.0	Laufer & Bass, 1979
105	$C_4H_3 + M = C_4H_2 + H + M$	62.00	1.0 (16)	0.0	59.75	Tanzawa & Gardiner, 1979
106	$C_4H_2 + M = C_4H + H + M$	95.40	3.5 (17)	0.0	80.07	Tanzawa & Gardiner, 1979
107	$C_2H_2 + C_4H = C_6H_2 + H$	13.11	4.0 (13)	0.0	0.0	Tanzawa & Gardiner, 1979
108	$C_4H_2 + C_2H = C_6H_2 + H$	-20.16	4.0 (13)	0.0	0.0	Tanzawa & Gardiner, 1979
109	$C_6H_2 + M = C_6H + H + M$	95.40	5.0 (16)	0.0	80.07	Tanzawa & Gardiner, 1979
110	$C_6H_2 + C_2H = C_8H_2 + H$	-21.46	1.0 (12)	0.0	0.0	Tanzawa & Gardiner, 1979
111	$C_6H + C_2H_2 = C_8H_2 + H$	11.81	1.0 (12)	0.0	0.0	Tanzawa & Gardiner, 1979
112	$C_4H_2 + C_4H = C_8H_2 + H$	11.60	1.0 (12)	0.0	0.0	Tanzawa & Gardiner, 1979
113	$C_8H_2 + M = C_8H + H + M$	114.6	5.0 (16)	0.0	80.07	Tanzawa & Gardiner, 1979

Thermochemical data for C_4H, C_4H_2, C_4H_3, C_6H, C_6H_2, C_8H, and C_8H_2 were taken from Duff and Bauer (1962). Forward rate coefficients expressed as $k_i = AT^b \exp(-E/RT)$ in units of cm^3, mole, sec. M refers to total concentration.

in Table 4-2, to determine the effects, if any, that production and consumption of C_2-hydrocarbon species had on the predicted induction delay times for CH_4 oxidation. The reactions in Tables 4-2 through 4-7 were also used in the simulations of C_2H_6 oxidation. As mentioned above, the reactions and associated rate coefficients required to describe H_2, CO, and CH_2O oxidation were taken from Table 3-1 and 4-1.

The induction delay data which were selected for comparison with computed results were reported by Skinner and Ruehrwein (1959), Seery and Bowman (1970), Tsuboi and Wagner (1975), and Grillo and Slack (1976). Since several experimental criteria, which were not easily related to the model, were used to define the measured induction delay times, a somewhat arbitrary definition for this parameter was used in the simulations--the time at which 10 percent of the initial CH_4 was consumed. The capabilities of the reaction mechanism were evaluated on the basis of how well it could reproduce the induction delay correlations reported by the investigators. These correlations included density dependence which should reduce the necessity to use the exact postshock pressures covered by each experiment. However, it will be shown that none of the correlations were developed over a broad enough range of densities to completely account for the influence of density on all sets of data. The approach taken in these simulations was to use a limited range of densities and use the correlations to extrapolate to higher densities. Future work should include verification simulations at the exact higher densities of the experimental data if these conditions are of importance for a particular application. For the simulations reported here, adiabatic combustion of the reactants was assumed to occur at a starting pressure of one atmosphere for temperatures between 1400 and 2200 K for all of the detailed kinetic simulations. The ratios of CH_4, O_2, and argon in the initial mixture were $CH_4 + O_2 : Ar = 10/90$.

Computed induction delay correlations for CH_4 oxidation are compared with the experimental observations in Figure 4-7 and 4-8. The predicted induction times, which are given in Table 4-9 for the C_1-hydrocarbon and C_1- and C_2-hydrocarbon reaction mechanisms as a function of temperature and

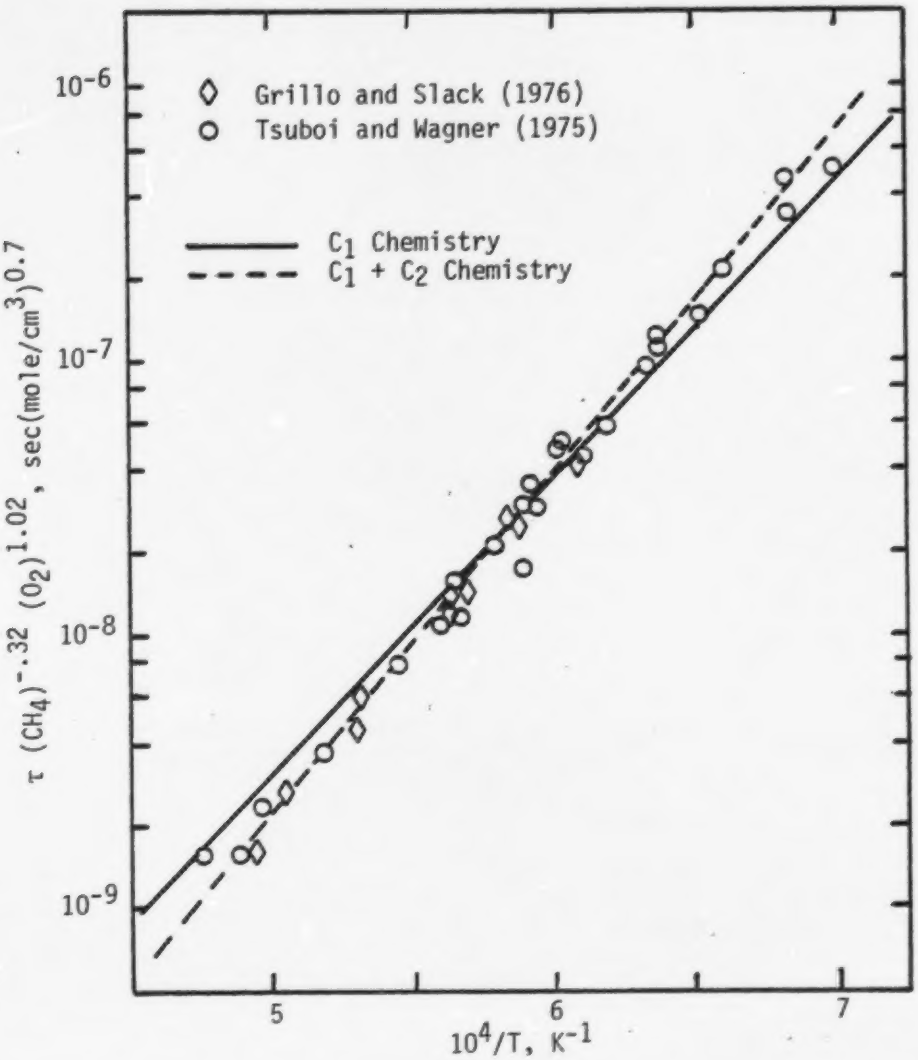

Figure 4-7. Correlation of CH_4-O_2-Ar induction times.

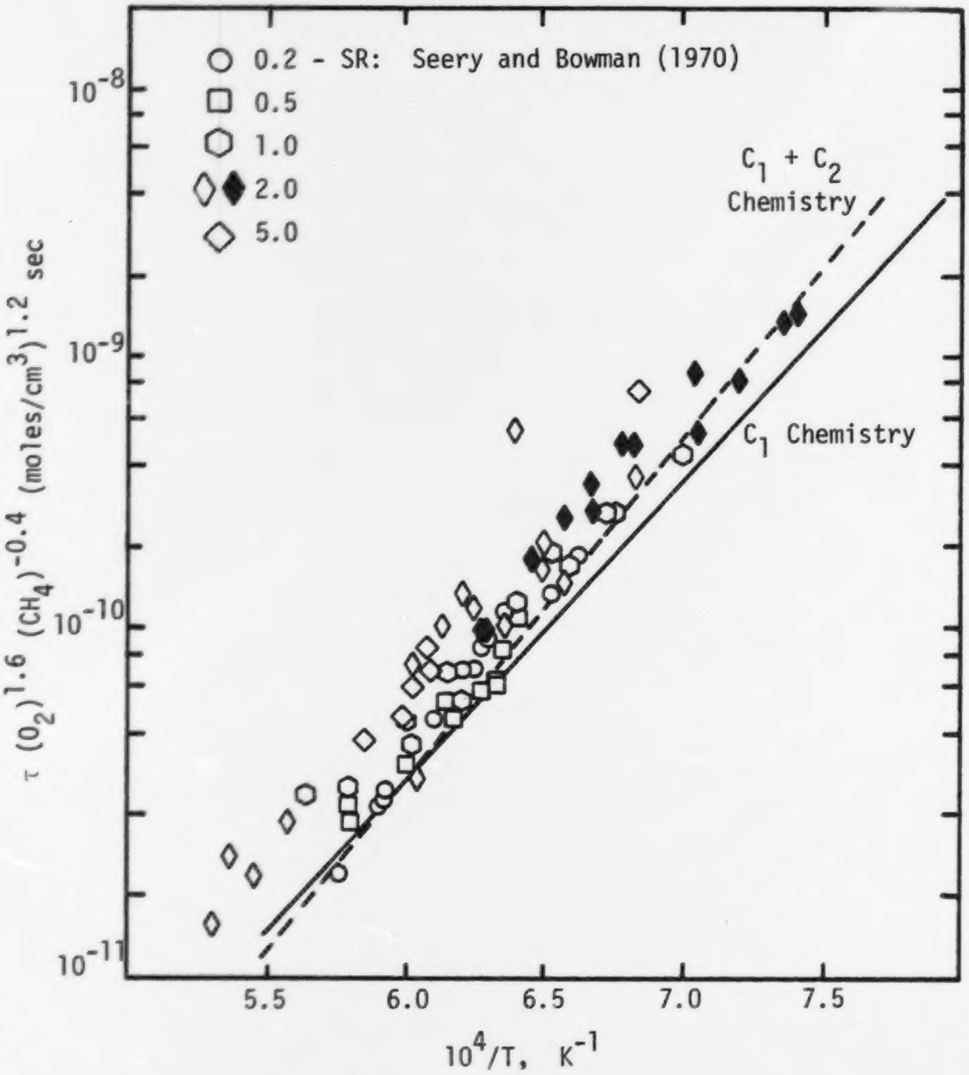

Figure 4-8. Methane-argon-oxygen ignition correlation: $Ar/O_2 = 4$.

Table 4-9. Predicted Induction Times for C_1-Hydrocarbon and C_1- Plus C_2-Hydrocarbon Reaction Mechanisms at Atmospheric Pressure

T (K)	t_i = μsec							
	SR = 0.5		SR = 0.75		SR = 1.0		SR = 1.25	
	C_1	C_1+C_2	C_1	C_1+C_2	C_1	C_1+C_2	C_1	C_1+C_2
2200	25.	18.9	22.0	18.0	21.3	17.6	20.3	17.4
2000	110.	69.5	97.5	65.5	89.0	64.5	83.0	62.5
1800	---	293.	425.	270.	385.	260.	355.	252.
1600	2440.	1910.	2000.	1710.	1740.	1590.	1580.	1500.
1400	14000.	25000.	11100.	22000.	9500.	20300.	8600.	19100.

Note: Reactant concentrations for a given stoichiometric ratio are:

SR:	0.5	0.75	1.0	1.25
CH_4/O_2:	0.05/0.05	0.04/0.06	0.0333/0.0667	0.0286/0.0714

stoichiometry, were reduced to the straight lines shown in the figures via least-squares analysis to yield the expressions:

$$\tau \left(CH_4\right)^{-0.32}\left(O_2\right)^{1.02} = \beta, \left(\text{mole/cm}^3\right)^{0.7} \text{ sec}$$

$$C_1 \text{ mechanism : } \beta = 1.344 \times 10^{-14} \exp(49170/RT)$$

$$C_1 + C_2 \text{ mechanism : } \beta = 1.661 \times 10^{-15} \exp(56190/RT)$$

$$\tau \left(CH_4\right)^{-0.40}\left(O_2\right)^{1.6} = \beta, \left(\text{mole/cm}^3\right)^{1.2} \text{ sec}$$

$$C_1 \text{ mechanism : } \beta = 5{,}525 \times 10^{-18} \exp(50870/RT)$$

$$C_1 + C_2 \text{ mechanisms : } \beta = 6.860 \times 10^{-19} \exp(57910/RT)$$

Inspection of the results shown in Figure 4-7 indicates good agreement between predictions and measurements with regard to both absolute values and the temperature dependence of the correlation function. It is also seen that inclusion of reaction paths which produce and consume C_2-hydrocarbon species improves the agreement. This point is more apparent if the expressions for β derived from the data are considered:

$$\beta \text{ (Tsuboi and Wagner, 1975)} = 2.5 \times 10^{-15} \exp\ (53600/RT) \left(\text{mole/cm}^3\right)^{0.7} \text{ sec}$$

$$\beta \text{ (Grillo and Slack, 1976)} = 1.27 \times 10^{-15} \exp(57180/RT \left(\text{mole/cm}^3\right)^{0.7} \text{ sec}$$

The fact that the temperature dependence of β is higher in the Grillo and Slack (1976) data than that reported by Tsuboi and Wagner (1975) is consistent with the findings of these authors, which indicate that the apparent activation energy for β increases as the total density decreases. It should be noted that although Tsuboi and Wagner varied the stoichiometric ratio from 0.5 to 5.0 the CH_4 concentration was always less than or equal to 2 percent of the reactants. The data reported by Grillo and Slack (1976) were also for initial CH_4 concentrations of 2 percent or less and were taken at only two stoichiometric ratios: 0.5 and 1.0. Thus, these correlations were developed for low concentrations of reactants and not necessarily extrapolatable to higher concentrations.

The agreement between computed and experimental values for the induction delay correlation demonstrated in Figures 4-8 and 4-9 is still satisfactory, even though the reactant concentrations used by Seery and Bowman (1970) and Skinner and Ruehrwein (1959) were significantly higher than those used in the simulations. Again, if reactions describing C_2-hydrocarbon species production and oxidation are included in the CH_4 oxidation mechanisms, there is less disparity between calculated and measured values. The major discrepancies are seen in the comparisons with the data reported by Skinner and Ruehrwein (1959) for stoichiometric ratios below 0.333, and for the undiluted CH_4-O_2 mixture when the C_2-hydrocarbon reaction mechanism is added to the reaction model. Since Skinner and Ruehrwein measured C_2H_2, C_2H_4, and C_2H_6 in the quenched products of various reaction mixtures, the disagreement may be due to the differences between experimental reactant concentrations and those used for the simulations. Additional calculations, which use the reactant concentrations, pressures, and temperatures reported, are necessary to explain the disagreement with the data of Skinner and Ruehrwein (1959) and, in order to be complete, the data of Seery and Bowman (1970) should also be examined at the exact experimental conditions used.

The results shown in Figure 4-7 to 4-9 definitely indicate that the CH_4 reaction mechanism can reproduce induction delay data over a broad range of reactant concentrations and temperatures. The calculations also show that reactions of C_2-hydrocarbon species are necessary to accurately model the temperature and stoichiometry dependencies of the induction delay times for CH_4 oxidation. The quantitative changes listed in Table 4-9 demonstrate that below 1600 K production of C_2-hydrocarbons retards the rate at which CH_4 is oxidized, while at the higher temperatures examined formation of higher hydrocarbons accelerates the rate at which CH_4 is consumed. Analysis of the results indicates that this behavior is due to the effect which C_2H_6 production has on the growth of radicals, and the higher rates of oxidation, compared to that of CH_4, for C_2H_6, C_2H_4, and C_2H_2. At low temperatures, recombination of methyl radicals via reaction 67 competes effectively with reaction 43, which is a major chain-branching step in the

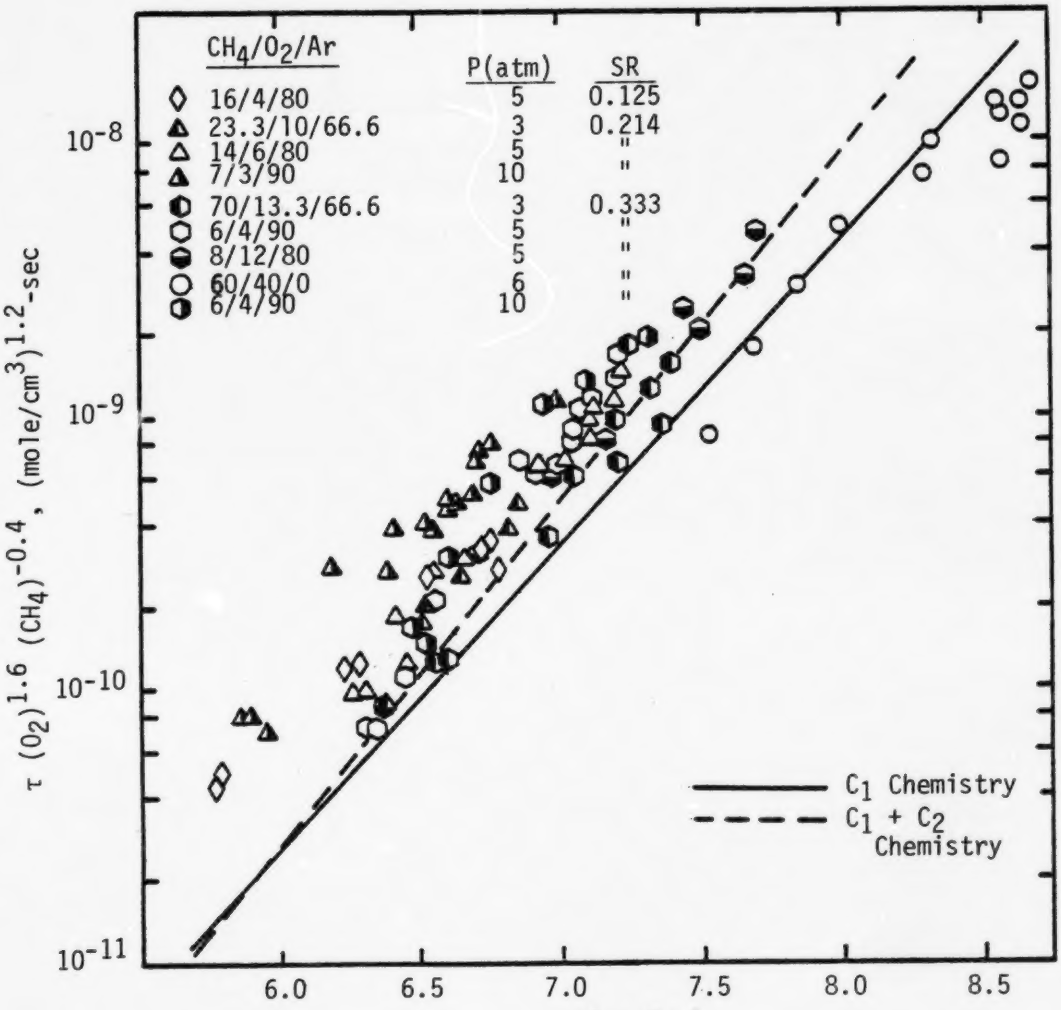

Figure 4-9. Correlation of CH_4-O_2-Ar induction times: data of Skinner and Ruehrwein (1959).

induction period, and reduces the rate at which H, O, and OH grow:

$$CH_3 + O_2 = CH_3O + O \qquad (43)$$

$$CH_3O + M = CH_2O + H + M \qquad (44)$$

$$CH_3 + CH_3 = C_2H_6 \qquad (67)$$

The ratio of the rates of reaction 67 and 43 establishes the relative concentrations of CH_3 and O_2 necessary for the recombination process to be more significant as a sink for methyl radicals; that is, at 1400 K : $(CH_3) \geq 1.49 \times 10^{-5}(O_2)$; at 1600 K : $(CH_3) \geq 6.0 \times 10^{-5}(O_2)$; at 1800 K : $(CH_3) \geq 1.79 \times 10^{-4}(O_2)$; and at 2000 K : $(CH_3) \geq 4.36 \times 10^{-4}(O_2)$. The lower radical production rates due to recombination reactions obviously lengthen the predicted induction delay times as compared to those calculated with only the reactions in Table 4-2.

At the higher temperatures, C_2H_6 formation via reaction 43 is still a major consumption path for methyl radicals. However, the rate at which H-atoms are produced via decomposition of CH_4 increases by a factor of 46 when the temperature is increased from 1400 to 1600 K. The production of O and OH is also greater since the rate coefficient of reaction 6 doubles with a temperature change from 1400 to 1600 K and the production of H-atoms has increased substantially. Reaction of C_2H_6 with these free radicals is more significant and produced the C_2H_5 radical which rapidly decomposes to produce C_2H_4 and H-atoms:

$$C_2H_6 + H = C_2H_5 + H_2 \qquad (78)$$

$$C_2H_6 + O = C_2H_5 + OH \qquad (79)$$

$$C_2H_6 + OH = C_2H_5 + H_2O \qquad (80)$$

$$C_2H_5 = C_2H_4 + H \qquad (81)$$

The more rapid production of H-atoms via this reaction sequence has a positive effect on radical growth because H reacts with O_2 to yield O-atoms and the OH radical. Oxidation of C_2H_4 produced via reaction 81 or reaction 82 also has a positive impact on the growth of free radicals because species formed via reactions 87 to 91--CH_2O, HCO, C_2H_3--decompose rapidly to again yield atomic hydrogen, O, and OH. The acceleration may be illustrated by considering reactions 87, 29, and 20, for which two hydrogen atoms are produced for each oxygen atom consumed.

$$C_2H_4 + O = CH_2 + CH_2O \tag{87}$$

$$CH_2O + M = HCO + H + M \tag{29}$$

$$\underline{HCO + M = H + CO + M} \tag{20}$$

$$C_2H_4 + O = CO + CH_2 + 2H$$

The reaction mechanism for CH_4 oxidation, which on the basis of the induction delay calculations must include reactions describing the formation and destruction of C_2-hydrocarbon species (i.e., the reactions listed in Tables 4-2 through 4-7), was next used to simulate the data reported by Dean and Johnson (1980) for the high-temperature oxidation of methane with N_2O as the oxidant. These authors monitored atomic oxygen and CO_2 production behind reflected shock waves via optical techniques in the temperature range of 1875 to 2840 K for an initial reactant mixture of 1 percent N_2O, 12.12 percent CO, and 503 ppmV CH_4 in argon. Three parameters were used to characterize the CO_2 profiles: $t_{0.5}$, which indicates the time that $(CO_2) = 8.3 \times 10^{-9}$ mole/cm^3; $t_{1.5}$, which is the time that $(CO_2) = 2.49 \times 10^{-8}$ mole/cm^3; and $t_{2.5}$, which is the time that $(CO_2) = 4.15 \times 10^{-8}$ mole/cm^3. These times are relative to the time at which the shock passes the observation window midpoint. This is typically about 5 μsec after the reflected shock is first visible at the detector.

The results of the detailed kinetic calculations, which used the reactions listed in Tables 4-2 to 4-7 to describe CH_4 oxidation, and reactions for N_2O, NO, and NO_2 discussed in Section 5.1, are shown in Figures 4-10a through 4-10c. Adiabatic combustion at the initial temperatures and post-shock densities reported by Dean and Johnson (1980) was assumed. Consideration of the predicted values in Figures 4-10a and 4-10b indicates that the mechanism accurately reproduces the early production of CO_2 from 1875 to 2715 K. However, the results shown in Figure 4-10 indicate that the model yields long characteristic times for CO_2 production which are consistently greater than measured, although the trend determined experimentally

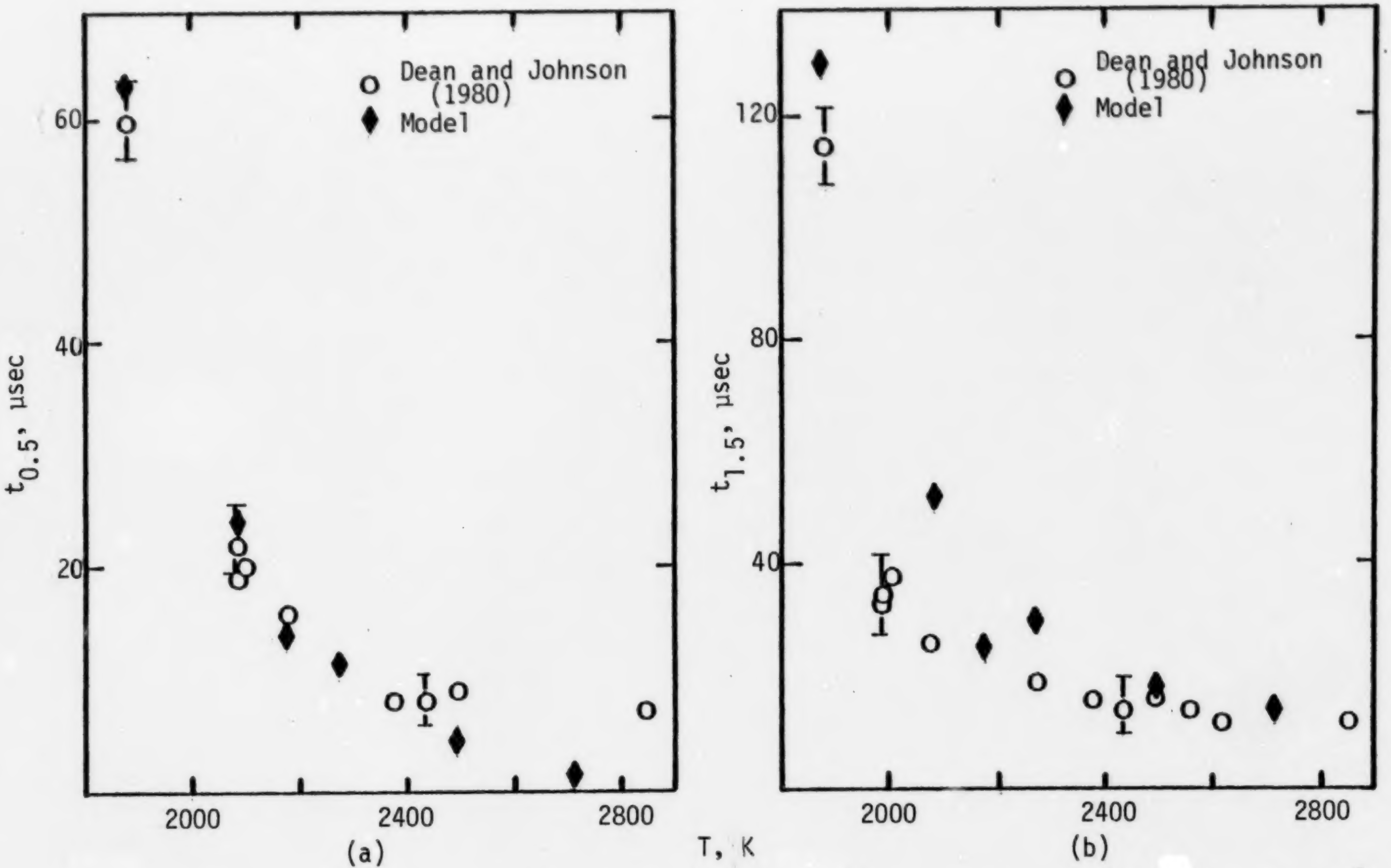

Figure 4-10 a and b. CO_2 production in CH_4 oxidation [(a) time to reach $(CO_2) = 8.3 \times 10^{-9}$ moles/cm^3, (b) time to reach $(CO_2) = 2.49 \times 10^{-8}$ mole/cm^3].

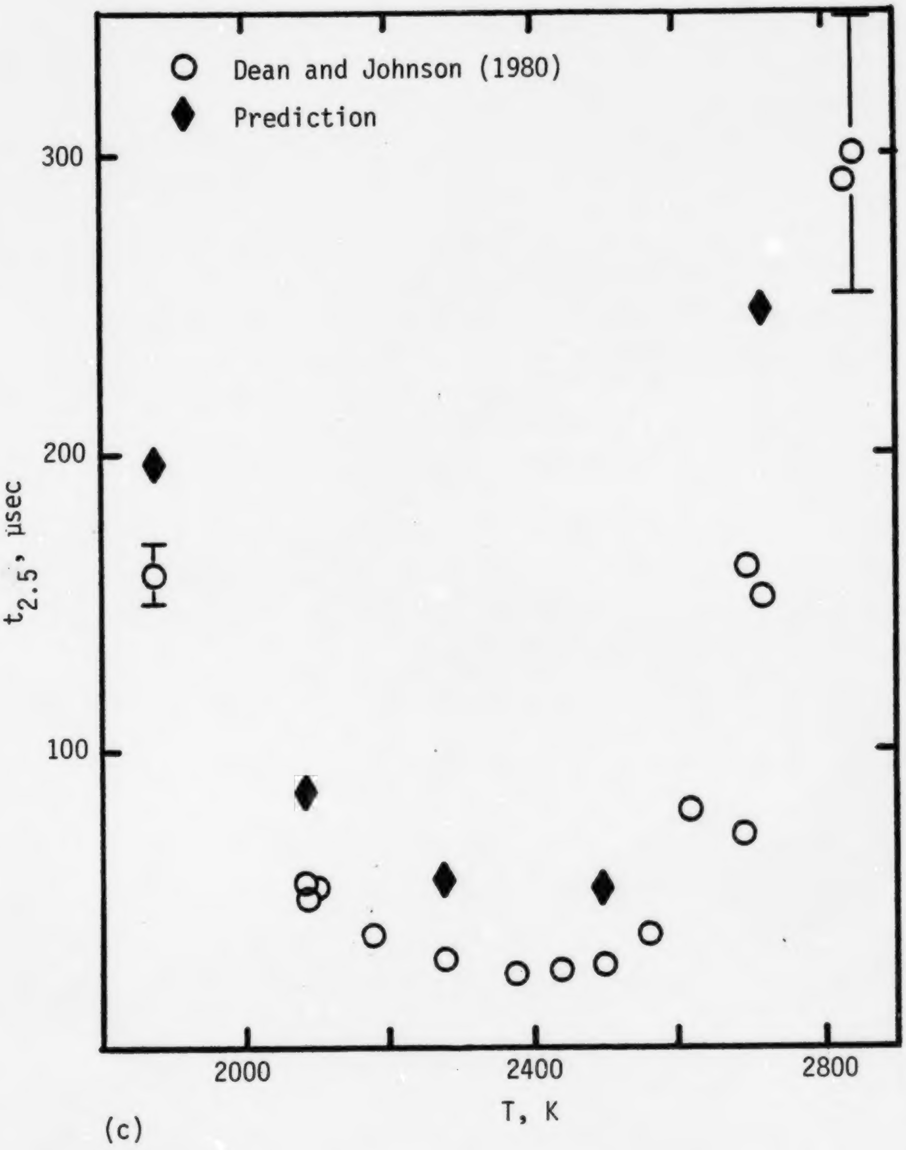

Figure 4-10c. Comparison of when absolute CO_2 = 4.15×10^{-8} mole/cm^3.

with regard to a minimum in $t_{2.5}$ is reproduced. It should be noted that the rate coefficient for reaction 21 has already been shown to be inaccurate above 2000 K. If a correction factor to the predicted values defined by equation (4) is used, the discrepancy is removed.

Analysis of the simulations indicated that the results were most sensitive to the rate coefficient used for:

$$CH_4 + O = CH_3 + OH \qquad (37)$$

The excellent agreement between predicted and measured values for the characteristic times of CO_2 production confirms the absolute values and temperature dependence of k_{37} calculated in this temperature range from the expression listed in Table 4-2. It is of interest to note that the rate constant for reaction 37 used in the CH_4 mechanism is also consistent with the low temperature data for this reaction reported by Klemm et al. (1980):

$$k'_{32}(474\text{-}1176\ K) = (1.51 \pm 0.21) \times 10^{14} \exp[-(10870 \pm 190)/RT]$$

$$k'_{32}(T_m = 815\ K) = 1.06 \times 10^4 \exp(-11000/RT)$$

Comparison with the rate measurements of Felder and Fontijn (1979) indicates that k_{32} yields values which are in excellent accord with these data between 525 and 1250 K. Therefore, k_{32} will be treated as a well-defined quantity in all subsequent work.

The results presented thus far indicate the necessity of including reactions describing C_2-hydrocarbon production and destruction during CH_4 oxidation to accurately reproduce observed induction delay times. However, at the low initial CH_4 concentration used in the studies of Dean and Johnson (1980), these additional reactions had no significant impact on the results, which suggests that under certain conditions, i.e., very low CH_4 concentration and high temperature, a simpler oxidation model for methane may be used. This assumption was implicit in the experimental studies and analysis of CH_4 oxidation reported by Brabbs and Brokaw (1975), who measured the exponential growth of CO flame band emission behind incident shock waves, and derived rate coefficients for elementary reactions derived from a simplified description of radical growth in CH_4 oxidation. The most important conclusion from their data analysis was that reaction 43 must occur to reproduce the exponential growth of atomic oxygen observed.

A subset of the reactions given in Table 4-2 was used to determine whether the rate coefficients assigned for certain elementary processes, which are different than those used or derived by Brabbs and Brokaw (1975), were consistent with the data reported for the exponential growth constants of radicals. The reactions used to derive the quartic equation defining the exponential growth of radicals, λ, were:

$$CH_4 + O = CH_3 + OH \qquad (37)$$

$$CH_4 + H = CH_3 + H_2 \qquad (38)$$

$$CH_4 + OH = CH_3 + H_2O \qquad (36)$$

$$CH_3 + O_2 = CH_3O + O \qquad (43)$$

$$CH_3O + M = CH_2O + H + M \qquad (44)$$

$$H + O_2 = OH + O \qquad (6)$$

$$H + O_2 + M = HO_2 + M \qquad (5)$$

$$CO + OH = CO_2 + H \qquad (21)$$

$$CO + O + M = CO_2 + M \qquad (19)$$

$$CH_3O + O_2 = CH_2O + HO_2 \qquad (114)$$

$$CH_3O + CO = CH_3 + CO_2 \qquad (115)$$

The rate coefficients k_{114}, which is that reported by Cox et al (1980) in their critical evaluation of the rate data, and k_{115}, which is taken as that that for the isoelectronic reaction of CO with HO_2, are given by:

$$k_{114} = 7.59 \times 10^{10} \exp(-2687/RT)$$

$$k_{115} = 1 \times 10^{11} \exp(-10000/RT)$$

Analysis of this subset of reactions in a manner similar to that used to develop equation 1 yields the quartic equation in Table 4-10, if the further assumption that CH_3O is in steady state with CH_3 is made. Since a general solution for quartic equations is available, it is a simple exercise to calculate λ at the temperatures, pressures, and reactant concentrations studied by Brabbs and Brokaw (1975).

The results, which are compared with the measurements in Figures 4-11 through 4-13, suggest that it is necessary to alter the rate coefficient for reaction 43 to predict λ's which agree in absolute value and temperature dependence with the measurements. The best fit was obtained for:

$$k'_{43} = 4 \times 10^{13} \exp(-29000/RT)$$

Although this is consistent with the values reported by Brabbs and Brokaw (1975), the results shown in Figures 4-11 and 4-12 argue that such a change is still not consistent with the data at temperatures below about 1350 K and at the lower initial CH_4 concentrations.

The discrepancies indicated by this simplified analysis of the data may, in part, be due to neglect of reactions which have a major effect on radical growth, during CH_4 oxidation, or the assumption of near constant CH_4 concentration during the time when radicals grow exponentially. If the explanation lies with the limited reaction set used, the most likely candidate for an additional reaction, which could have a significant impact on λ, is the recombination of methyl radicals to produce C_2H_6. This argument is quite reasonable, since Westbrook et al (1977) found that C_2H_6 and C_2H_4 production and destruction were important processes necessary to describe oxidation of CH_4 between 1000 and 1350 K even when the initial CH_4-to-O_2 ratio was about 0.02. For ethane production via reaction 67 to be of importance, the following condition, at least as a first-order approximation, should be true:

$$(CH_3) \geq k_{43}(O_2)/k_{1.67}$$

Calculations at the conditions studied by Brabbs and Brokaw (1975) shown in Figure 4-11 indicate that the methyl radical concentration need only be 0.3 ppmV when the temperature is 1200 K for the above equality to hold; at 1546 K the concentration must increase to 4 ppmV for the rate of reaction 67

Table 4-10. Defining Equation for λ, the Exponential Growth Constant for O, OH, H, and CH_3

$$
\begin{aligned}
&\lambda^4 + (\nu_1 + \nu_2 + \nu_3 + \nu_4 + \nu_5 + \nu_6 + \nu_7 + \beta\nu_8)\lambda^3 \\
&\quad + \big[(\nu_4 + \nu_5 + \beta\nu_8)(\nu_1 + \nu_2 + \nu_3 + \nu_7) + \nu_7(\nu_1 + \nu_2 + \nu_6) + \nu_6(\nu_3 + \nu_4 + \nu_5) \\
&\quad + \nu_1\nu_2 + \nu_4\nu_8 + (\beta - \alpha)\nu_6\nu_8 + (\beta - 1)\nu_5\nu_8\big]\lambda^2 \\
&\quad + \{(\nu_1 + \nu_2)(\beta\nu_4\nu_8 + \nu_4\nu_7 + \nu_5\nu_7) + \nu_3\nu_4(\nu_2 + \nu_6 + \beta\nu_8) + \nu_3\nu_5(\nu_2 + \nu_6 - \nu_1) \\
&\quad + \nu_6\nu_7(\nu_4 + \nu_5) + \nu_7\nu_8(\beta\nu_2 + \beta\nu_4 - \nu_5) - \alpha\nu_5\nu_8(\nu_1 + \nu_6) + \beta\nu_2\nu_3\nu_8 \\
&\quad + (\beta - \alpha)\big[\nu_1\nu_7\nu_8 + \nu_6\nu_8(\nu_3 + \nu_4 + \nu_7)\big] \\
&\quad + \nu_5\nu_8(\beta - 1)(\nu_1 + \nu_2 + \nu_3 + \nu_6 + \nu_7)\} \\
&\quad + \{\nu_2\nu_7\nu_8(\beta\nu_4 - \nu_5) + \nu_3\nu_8\big[\beta\nu_2\nu_4 - (1 + \alpha)\nu_5\nu_6\big] - \nu_5\nu_8\big[(1 + 3\alpha)\nu_1\nu_7 \\
&\quad + (1 + \alpha)\nu_6\nu_7 + (\beta + \alpha)\nu_1\nu_3\big] + (\beta - \alpha)\nu_4\nu_8(\nu_1\nu_7 + \nu_3\nu_6 + \nu_6\nu_7) \\
&\quad + (\beta - 1)\nu_5\nu_8(\nu_1\nu_7 + \nu_2\nu_3 + \nu_2\nu_7 + \nu_3\nu_6 + \nu_6\nu_7)\} = 0 \qquad (4.1)
\end{aligned}
$$

where

$$\alpha = \left(1 + \frac{k_{114}\,Y_{O_2}}{k_{44}}\;\frac{k_{115}Y_{CO}}{k_{44}}\right)^{-1}$$

$$\beta = \left(1 + \frac{k_{114}\,Y_{O_2}}{k_{44}}\right)\alpha$$

and

$\nu_1 = k_6(O_2)$ $\quad\nu_2 = k_5(O_2)$ $\quad\nu_3 = k_{21}(CO)$

$\nu_4 = k_{19}(CO)(M)$ $\quad\nu_5 = k_{37}(CH_4)$ $\quad\nu_6 = k_{38}(CH_4)$

$\nu_7 = k_{36}(CH_4)$ $\quad\nu_8 = k_{43}(O_2)$

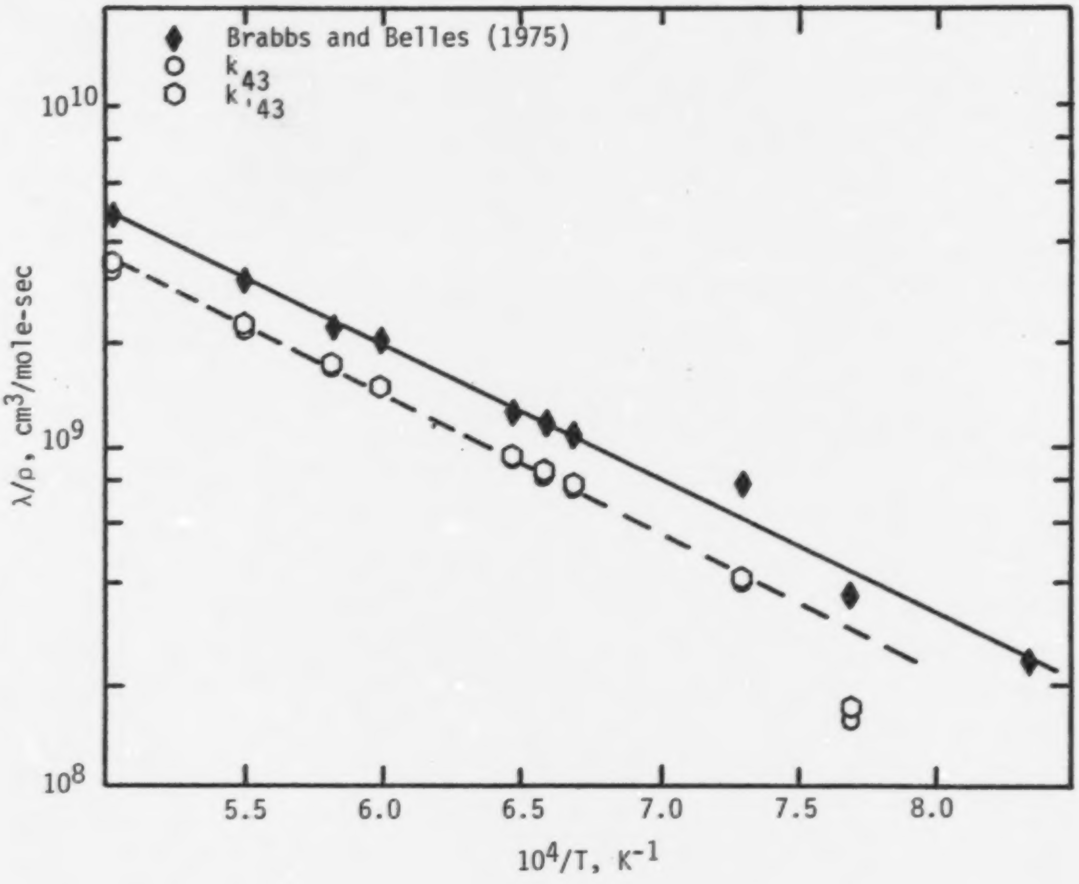

Figure 4-11. Exponential growth constants for radicals in CH_4 oxidation - $CH_4/CO/O_2/CO_2$ = 0.0194/18.72/1.073/5.68 in Ar.

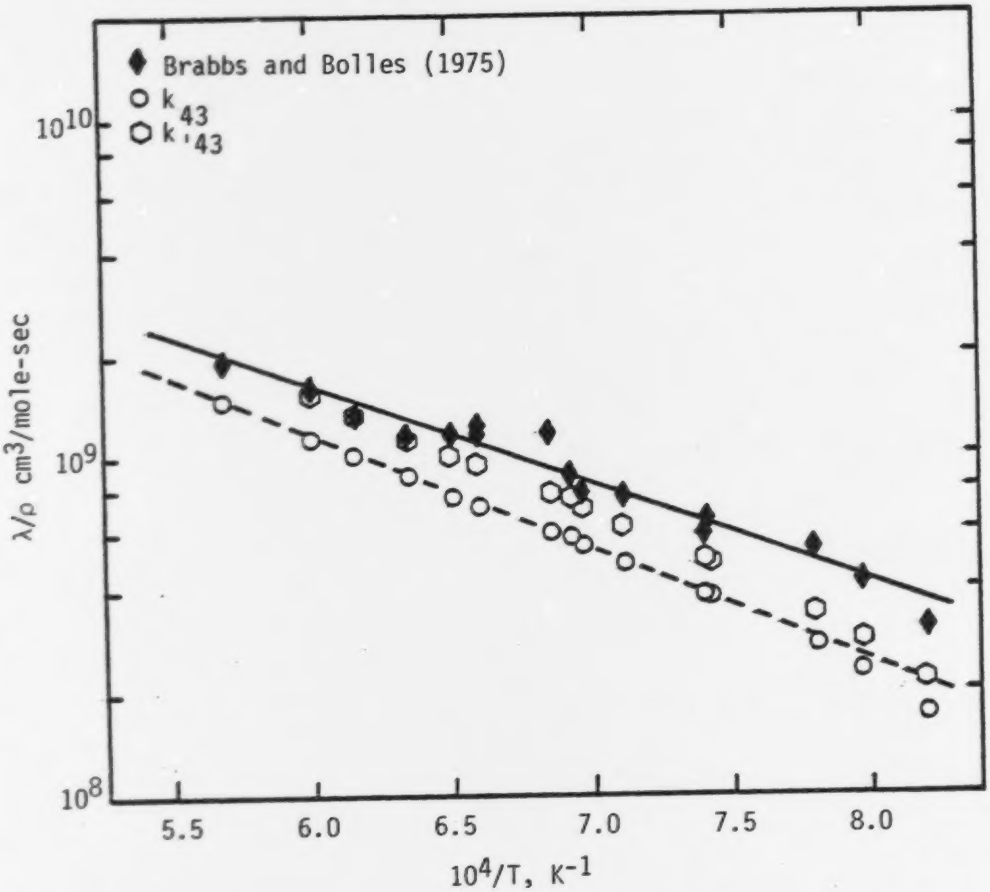

Figure 4-12. Exponential growth constants for radicals in CH_4 oxidation - $CH_4/CO/O_2$ = 0.0193/1.032/19.41 in Ar.

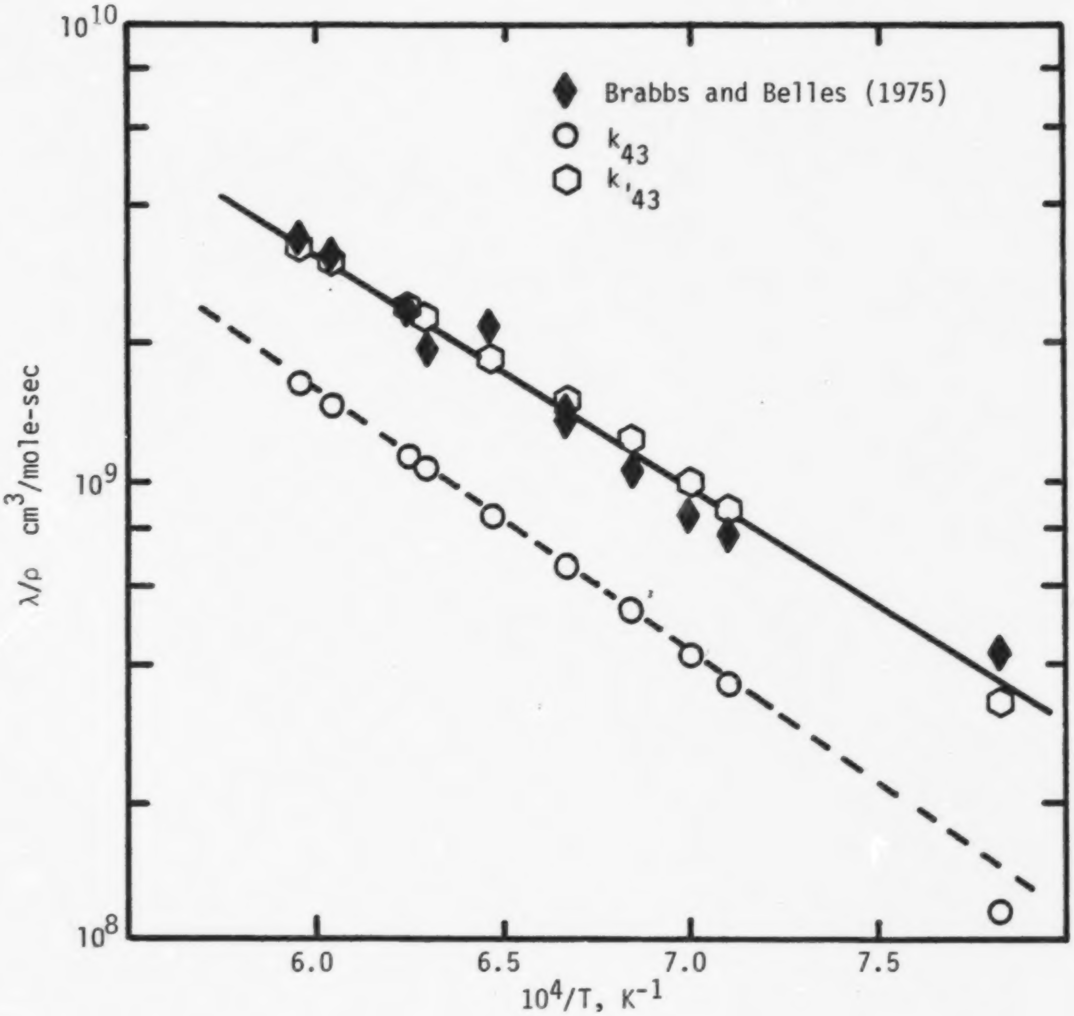

Figure 4-13. Exponential growth constants for radicals in CH_4 oxidation: $CH_4/CO/O_2$ = 0.205/1.056/19.54 in Ar.

to be equal to that of reaction 43. This certainly suggests the possibility that it is necessary to consider C_2-hydrocarbon reactions to explain the experimental observations. Since production of C_2H_6 is due to recombination of methyl radicals, the analysis described above would no longer be valid, which implies that the relative importance of C_2-hydrocarbon species under these experimental conditions can only be assessed via detailed kinetic simulations.

Additional insight with regard to the sensitivity of the results presented earlier to the value assigned to k_{43} may be gained by considering another subset of reactions which dominate during the induction period of CH_4 oxidation:

$$H + O_2 = OH + O \qquad (6)$$

$$CH_4 + M = CH_3 + H + M \qquad (35)$$

$$O + CH_4 = CH_3 + OH \qquad (37)$$

$$OH + CH_4 = CH_3 + H_2O \qquad (36)$$

$$CH_3 + O_2 = CH_3O + O \qquad (43)$$

$$CH_3O + M = CH_2O + H + M \qquad (44)$$

If it is assumed that O, OH, H, and CH_3O are in quasi-steady state, in the sense that the rates of consumption and production are very nearly equal, although the concentrations of these species change, which is confirmed by numerical calculations, then it is possible to derive the following expressions for the rates at which CH_3 and CH_4 change:

$$\frac{dCH_3}{dt} = 4k_{35}(CH_4)(M) + 4k_{43}(CH_3)(O_2)$$

$$\frac{dCH_4}{dt} = -4k_{35}(CH_4)(M) - 5k_{43}(CH_3)(O_2)$$

It should be noted that the development of these differential equations follows the analysis reported by Creighton (1977), although the equation he reports for CH_4 is incorrect, since he apparently ignores the decomposition of CH_4 as a term in the differential equation for methane.

Simultaneous solution of these two equations yields the following expression for methane concentrations as a function of time:

$$\frac{(CH_4)}{(CH_4)^o} = \exp(2\left[k_{43}(O_2) - k_{35}(M)\right] t)* \left[\cosh(2at) - \frac{k_{43}(O_2) + k_{35}(M)\sinh(2at)}{a}\right] \tag{4.2}$$

where

$$a = \left[k_{35}^2\,(M)^2 - 3k_{43}k_{35}\,(M)(O_2) + k_{43}^2\,(O_2)^2\right]^{1/2}$$

Equation 4.2 was used to calculate induction delay times as defined before; i.e., when 10 percent of the initial CH_4 was consumed, for several values of k_{43}.

Figure 4-14 shows the results of these computations compared to data reported by Tsuboi and Wagner (1975). It is obvious that increasing the rate coefficient for reaction 43, which occurs if k'_{43} is used instead of k_{43}, yields values for the induction delay times which are about a factor of 2 lower than observed. The use of k_{43} gives induction times which are essentially identical to those measured. Figure 4-15, which compares the predicted induction times with data reported by Seery and Bowman (1970), again indicates that k_{43} produces results which are more consistent with measurements than k'_{43}. It should also be noted that the data reported by Grillo and Slack (1976) for stoichiometric mixtures is accurately reproduced if k_{43} is used in conjunction with equation 4.2.

This set of computations confirms the value of k_{43} listed in Table 4-2 and used in the detailed kinetic simulations of CH_4 oxidation. In addition, the fact that using k'_{43} yields values for induction delay times which are lower than observed, provides further support to the argument described above. That is, the disparities between predicted and measured exponential growth constants, obtained via equation 4.1 arising from an incomplete description of the elementary processes which occur, and not from an

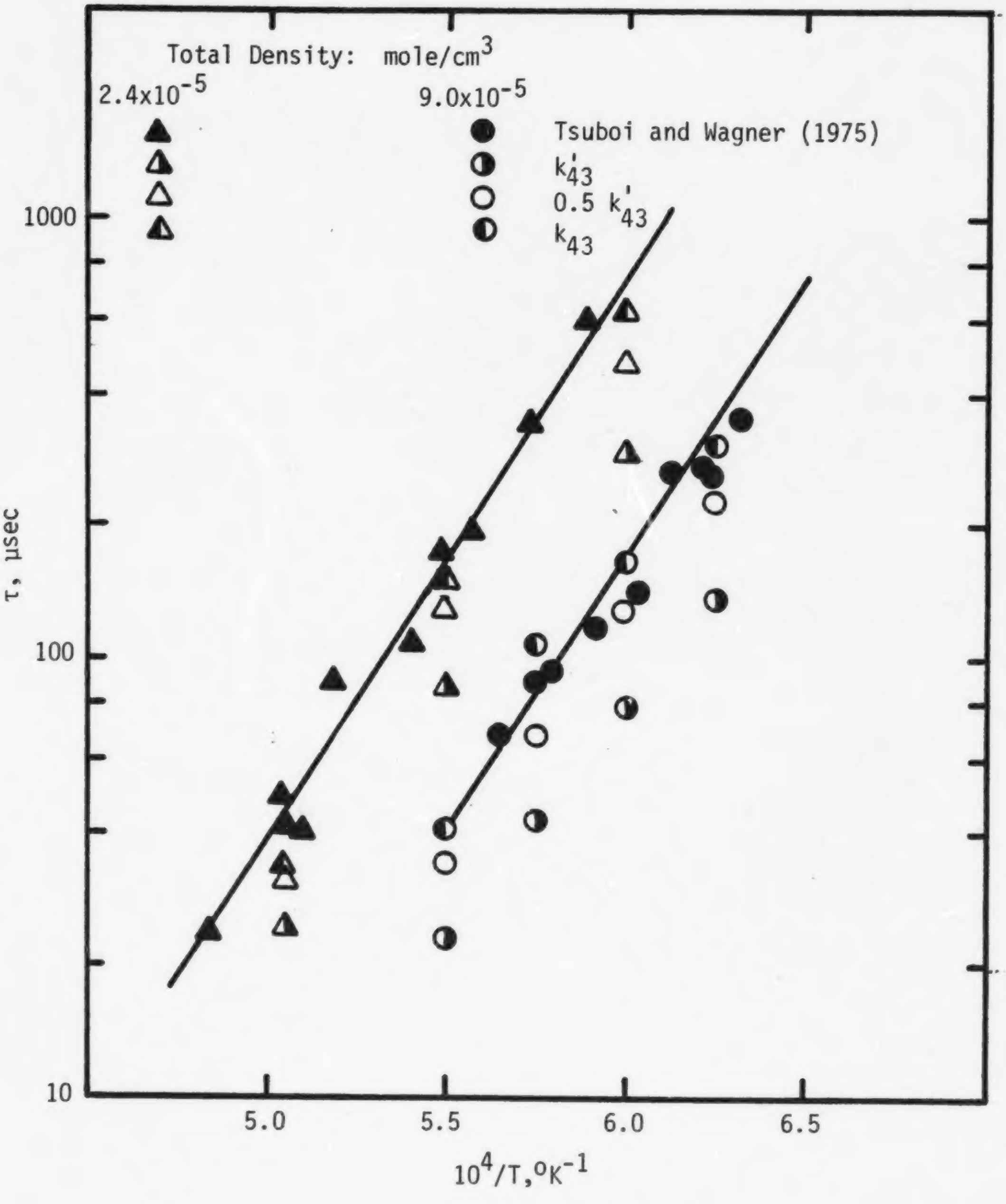

Figure 4-14. Dependence of predicted induction times on k_{43}.

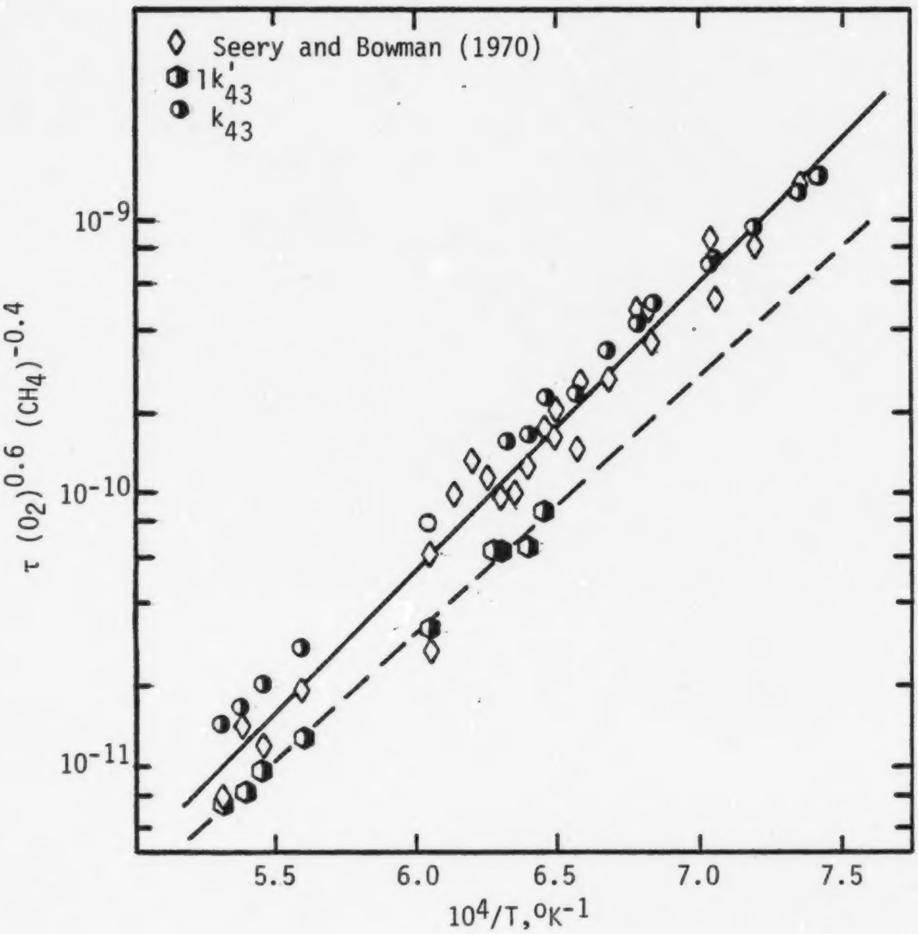

Figure 4-15. Sensitivity of induction delay times to k_{43}.

incorrect value for k_{43}. It should be noted that although equation 4-2 can yield induction delay times in agreement with measurements for the conditions pertaining to the data in Figures 4-14 and 4-15, it cannot be successfully used for other systems of interest, such as higher initial CH_4 concentrations, higher total densities, and fuel-rich CH_4/O_2 mixtures.

The calculations discussed thus far indicate that the CH_4 reaction mechanism is consistent with data reported for shock-initiated oxidation of CH_4, and that including the formation of C_2-hydrocarbon species is necessary to accurately model the dependence of induction period phenomena on temperature and reactant concentration. Although the improved temperature dependence of induction times is due to formation and destruction of C_2H_6, which strongly suggests that at least part of the C_2H_6 reaction is correct, additional simulations of shock-initiated C_2H_6 oxidation were done to confirm the accuracy of the reaction mechanism for C_2H_6. Adiabatic combustion of the reactants was assumed for initial temperatures between 1200 and 1600 K at atmospheric pressure. The ethane concentration was always 2 percent of the mixture and the oxygen concentration was varied from 3.5 to 8.75 percent to examine different stoichiometries. Calculated values for induction times were again based on the time at which 10 percent of the fuel was consumed.

Predicted induction times were compared with one of the correlations reported by Cooke and Williams (1975) and with the correlation suggested by Bowman (1970) for stoichiometric and fuel-lean oxidation of ethane. Figures 4-16 and 4-17 demonstrate that the agreement is quite good and suggest that the reactions listed in Tables 4-2 through 4-7 correctly describe the induction period. However, this set of calculations is not sufficient to confirm the accuracy of the reaction mechanism over a broader range of reactant concentrations, pressures, and temperatures. It is considered necessary to include additional detailed kinetic simulations of the data reported by Cooke and Williams (1975), Bowman (1970), and that reported by Burcat et al (1972), which was obtained at higher total densities, to complete this phase of the model validation.

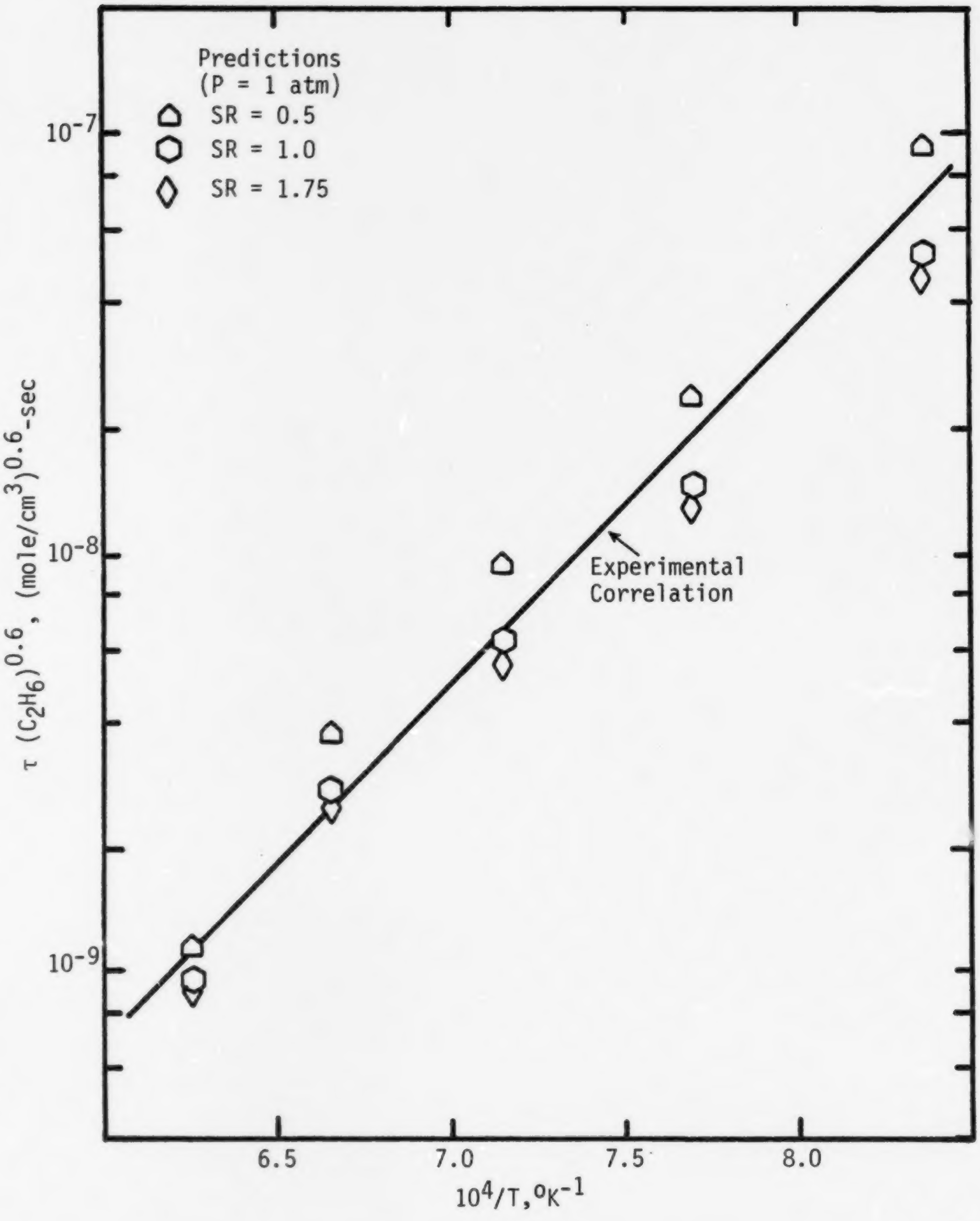

Figure 4-16. Ignition delay correlation for C_2H_6 oxidation in argon.

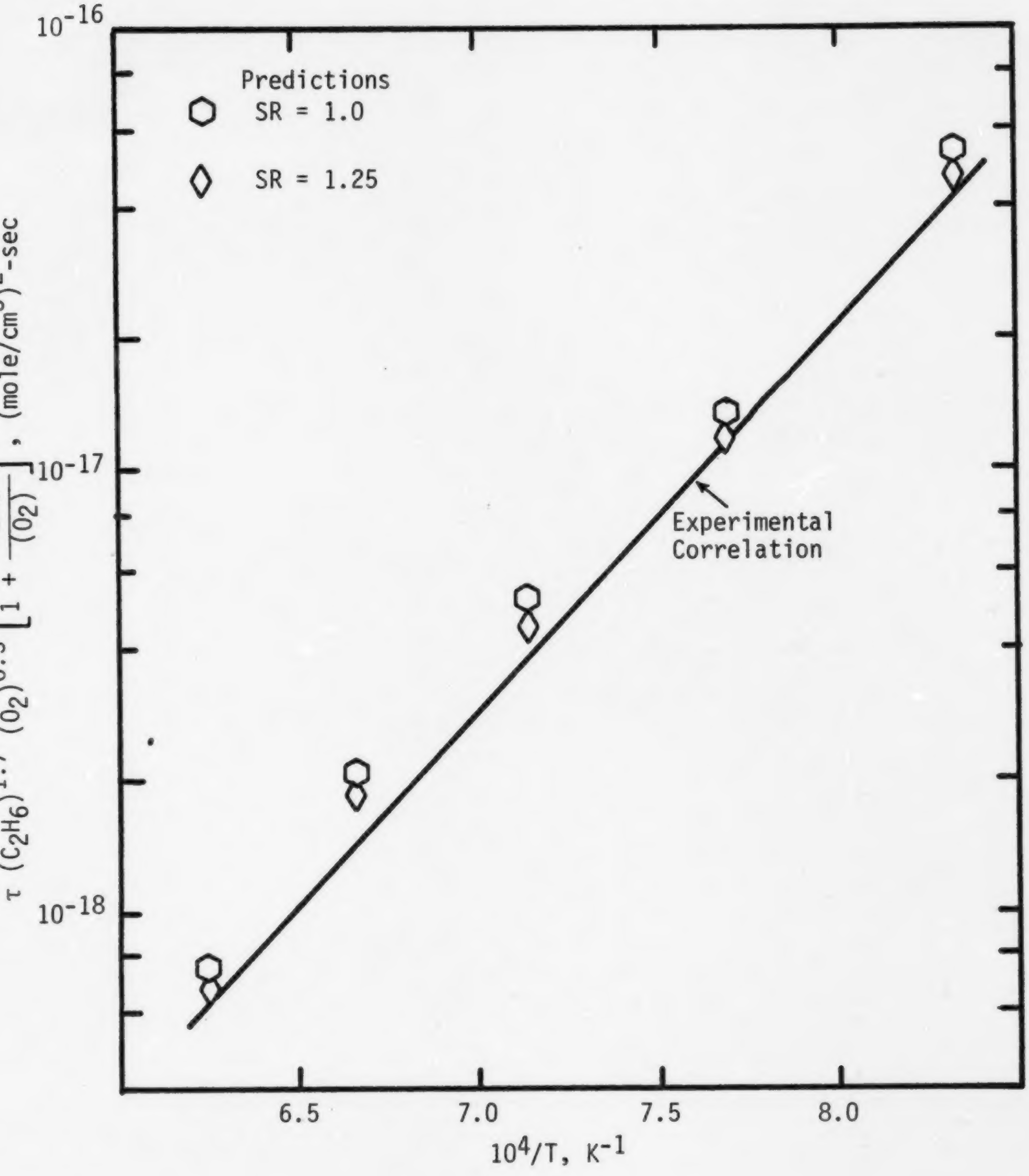

Figure 4-17. Comparison of predicted induction times with correlation of Bowman (1970).

These simulations did establish that the dominant paths for ethane consumption are:

$$C_2H_6 + H = C_2H_5 + H_2 \tag{78}$$

$$C_2H_6 + OH = C_2H_5 + H_2O \tag{79}$$

$$C_2H_6 + O = C_2H_5 + OH \tag{80}$$

Reaction 99 is also of some importance by accelerating the rate of fuel consumption during the transition period between the initiation and chain-branching phases of the induction period of ethane oxidation:

$$C_2H_6 + CH_3 = C_2H_5 + CH_4 \tag{99}$$

This reaction has a more significant role for fuel-rich mixtures, since the rate of H, O, and OH production decreases at the lower oxygen concentrations. The ethyl radical produced in reactions 78 to 80 and 99 rapidly decomposes via the reverse of reaction 81 to yield C_2H_4 and atomic hydrogen:

$$C_2H_5 = C_2H_4 + H \tag{81}$$

The H-atom thus formed provides chain propagation via reaction 78 and chain-branching via reaction 6.

The ethane reaction mechanism was also used to simulate data reported by Dean and Johnson (1980) for temperatures greater than 2000 K and for a reactant mixture of $C_2H_6/N_2O/CO$ (156 ppmV/1.01/12.10) diluted in argon. Production of CO_2 was monitored via infrared emission and characterized by the time at which the CO_2 concentration reached a particular level. Results are compared with the measurements in Figures 4-18a and 4-18b and indicate that the reaction mechanism is accurate at short times. The discrepancies seen in Figure 4-18b are again due to the known error in k_{21} at temperatures above 2000 K; a first-order correction at the lowest temperature, which is derived from equation 3.7, reduces the predicted $t_{1.5}$ to 42.5 μsec, which is in excellent agreement with the data, 43 μsec.

As a result of the high temperatures, the predicted values for $t_{0.5}$ and $t_{1.5}$ are insensitive to the rate coefficient for C_2H_6 decomposition.

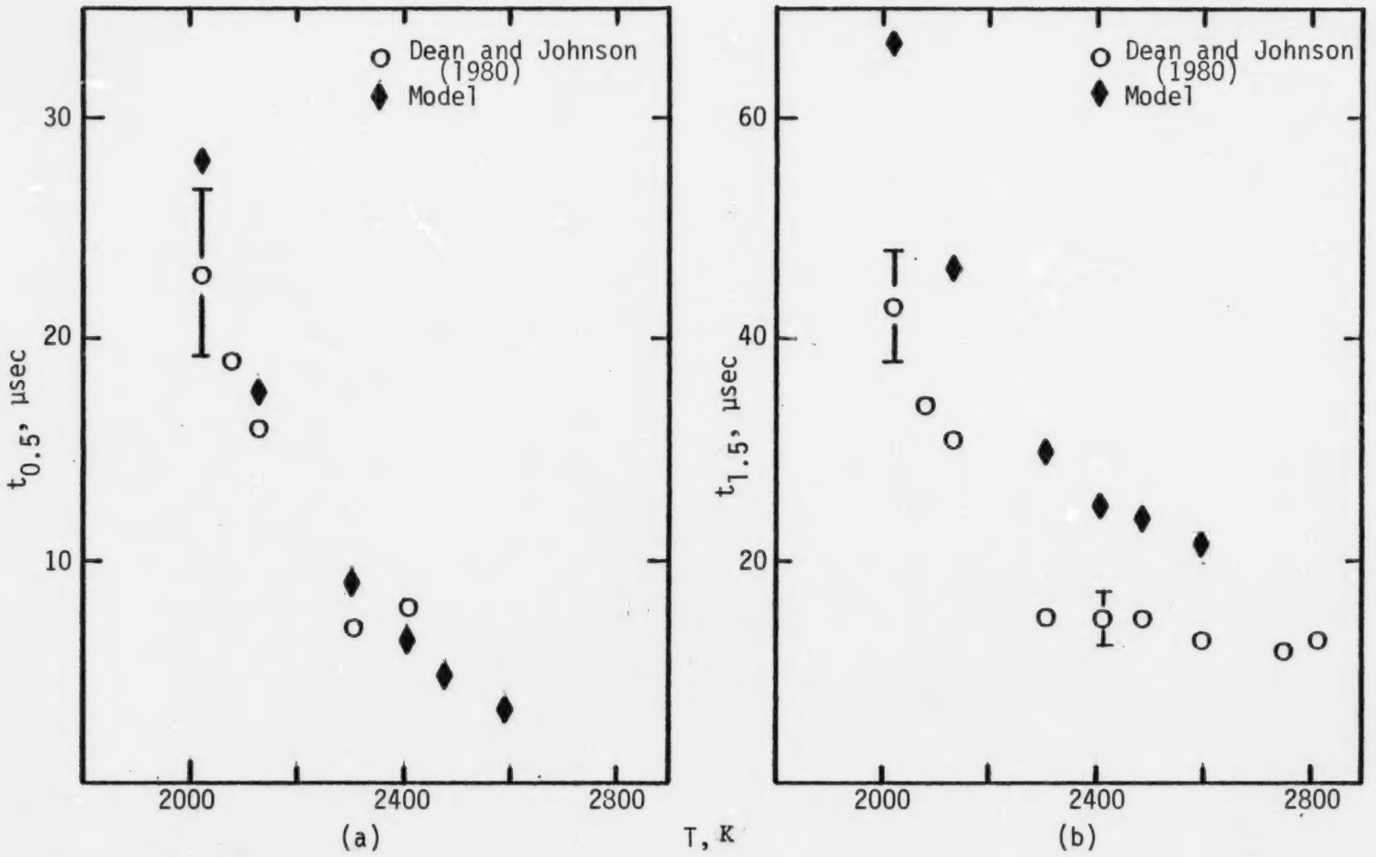

Figure 4-18. Comparison of time for CO_2 to reach a certain level for $C_2H_6/N_2O/CO$ = 256 ppm/ 1.01/12.1 in argon. [(a) Time to reach $(CO_2) = 8.3 \times 10^{-9}$ moles/cm^3, (b) time to reach $(CO_2) = 2.49 \times 10^{-8}$ moles/cm^3].

Surprisingly, the calculations indicate that varying k_{41} by a factor of 2 has a relatively small effect on the results. A maximum change of 20 percent in $t_{0.5}$ (T = 2020 K) and a change of about 5 percent to 10 percent for $t_{1.5}$ results when k_{41} is halved. These simulations suggest that the rate of CH_2O formation via reaction 41 is correct in this temperature range and, furthermore, confirm the CH_2O oxidation mechanism since CO_2 production is controlled by the rate of CH_2O destruction.

In summary, the calculations have explicitly demonstrated the necessity of including reactions which describe production and destruction of C_2-hydrocarbon species with regard to accurately predicting induction delay times in shock-initiated CH_4 oxidation. The results also suggest that formation and subsequent consumption of these higher hydrocarbons are required to correctly model the exponential growth of radicals during the induction period of CH_4 oxidation at temperatures below 1400 K even though the initial CH_4 concentration is below 2000 ppmV. The rate of CO_2 production at temperatures above 1850 K, which is computed with the reaction mechanism, is in excellent agreement with observations and verifies the rate coefficient used for reaction 37. Simulations of ethane oxidation in shock tube systems confirms the rate coefficients used, at least for stoichiometric and fuel-lean oxidation, with regard to the temperature and concentration dependence of induction delay times. The rate at which ethane is converted to CO_2 at temperatures above 2000 K is in agreement with measurements as well.

Additional detailed kinetic simulations of shock-initiated CH_4 and C_2H_6 oxidation are suggested in order to completely verify the proposed reaction mechanisms. These would include computations which use the exact reactant concentrations, temperatures, and pressures studied by Skinner and Ruehrwein (1959), Seery and Bowman (1970), and Tsuboi and Wagner (1975) for CH_4 oxidation. The predictive capabilities of the model should also be tested against the data reported by Bowman (1975), who reports maximum O-atom concentrations, the time at which the maximum O-atom level is reached, and the concentrations of OH and H_2O at this time, for stoichiometric and fuel-rich CH_4 oxidation. A more extensive investigation of

C_2H_6 oxidation should include simulations of the data reported by Burcat et al (1972), fuel-rich data reported by Bowman (1970), and data reported by Glick (1959), which gives the production distribution of C_2H_2, C_2H_4, and CO after a particular reaction time for $C_2H_6/H_2O/Ar$ mixtures for temperatures between 1100 and 2200 K. Simulations of data reported by Crossley et al (1972) on the effect of trace quantities of C_2H_6 on CH_4 induction delay times should also be examined to determine whether the sensitization observed can be reproduced by the reactions listed in Tables 4-1 through 4-6. The success of these computations will enhance the confidence in the reaction mechanism when simulations of flame data are done. However, the mechanism is felt to be sufficiently validated to move to the next step in the development methodology.

4.2.2 C_2H_2 and C_2H_4 Reaction Mechanisms

Preliminary calculations with the reaction mechanisms for C_2H_2 and C_2H_4 utilized data reported by Gay et al (1967), Homer and Kistiakowsky (1967a, 1967b), and Drummond (1968) on the shock-initiated oxidation of these species. The predicted temperature dependence of the induction delay period for ethylene was much greater than Drummond observed. Simulations of the systems studied by Homer and Kistiakowsky (1967a, 1967b) indicated that the exponential growth of CO and CO_2 was incorrectly predicted. As a consequence, the mechanisms for C_2H_2 and C_2H_4 oxidation and pyrolysis were reexamined to determine whether rate coefficients were consistent with values reported in the literature, and if additional reaction paths and species should be considered in the mechanism.

The error associated with the computed temperature dependence of induction delay times for C_2H_4 oxidation is apparently due to an incorrect value for the rate coefficient of reaction 102:

$$C_2H_5 + C_2H_3 = C_2H_4 + C_2H_4 \qquad (102)$$

The expression listed in Table 4-7 would yield a reverse rate coefficient with an activation energy near 100 kcal/mole, which is exactly the temperature dependence computed for induction times. The rate coefficient for reaction 102 is also inconsistent with data reported by Pratt and Rogers

(1979), which indicates a value of 1.2×10^{12} for k_{102} near 1000 K. If the preexponential factor for k_{102} is assumed to be 1×10^{14}, which is more reasonable, then a value for the activation energy can be derived from the value for k_{102} reported by Pratt and Rogers (1979), which is probably an upper limit--E = 8.8 kcal/mole. Additional calculations are necessary to determine whether the predicted induction time behavior of C_2H_4 is significantly improved by using either the approximate rate constant, i.e., $k_{102} = 1 \times 10^{14}$ exp(-8800/RT), or the value reported by Pratt and Rogers (1979) with the assumption that it is independent of temperature.

Additional analysis of the reactions listed in Table 4-6 indicates that the products assigned to reaction 87 are incorrect. The products of CH_2 and CH_2O were assumed on the basis of the arguments given by Westenberg and de Haas (1969). However, the recent studies of Kanofsky, Lucas, and Gutman (1973), Pruss, Slagle, and Gutman (1974), and Blumenberg, Hoyermann, and Sievert (1977) indicate that the major reaction channel is:

$$C_2H_4 + O = CH_3 + HCO$$

A minor path is the production of ketene and hydrogen:

$$C_2H_4 + O = H_2 + CH_2CO$$

Since k_{87} is consistent with the measurements of Westenberg and de Haas (1969) and the more recent data of Singleton and Cvetanovic (1976), it is recommended that k_{87} still be used but with reaction products of CH_3 and HCO. Reaction 88 in Table 4-6 should then be eliminated, although it may be of interest to replace this reaction with the secondary reaction channel for the reaction of O-atoms and C_2H_4:

$$C_2H_4 + O = H_2 + CH_2CO \qquad (88')$$

An estimate for $k_{88'}$ may be derived from the results of Peeters and Mahnen (1973), if it is assumed that the rate coefficient reported refers to reaction 88'. This is reasonable since it does extrapolate to room temperature in fair agreement with data for reaction 88', and from the value reported by Pruss et al. (1974):

$$k_{88'} = 1.74 \times 10^{13} \exp(-3950/RT)$$

If $k_{88'}$ is reasonably correct, it is simple to show that reaction 88' contributes a maximum of about 26 percent to the total rate of reaction between ethylene and atomic oxygen at about 900 K. The contribution is roughly 18 percent at 2000 K. This suggests the necessity of expanding the C_2H_4 oxidation mechanism to include reactions which describe the destruction of ketene since it is unreasonable to exclude a reaction path which may contribute 20 percent to the rate of reaction of C_2H_4 and O. A preliminary reaction mechanism is shown in Table 4-11.

Examination of the reaction mechanism describing C_2H_2 oxidation (Table 4-4) suggested that the discrepancies noted for the simulations of shock-initiated oxidation of this species were due to incorrect rate coefficients and/or incorrect products specified for a particular reaction. In particular, the value for k_{73} recommended by Tanzawa and Gardiner (1979) is inconsistent with the endoergicity of the reaction at temperatures lower than they studied. Recent studies of acetylene pyrolysis (Frank and Just, 1980) yield an expression for k_{73} which is a factor of two greater than that of Tanzawa and Gardiner at 1600 K and a factor of 4.4 greater at 2000 K,

$$k_{73'} = 7.7 \times 10^{14} \exp(-26000/RT) \ .$$

However, Frank and Just (1980) indicate that predictions of their data are relatively insensitive to the absolute value of $k_{73'}$. A combination of low temperature measurements of the reverse of reaction 73 (Lange and Wagner, 1975; Laufer and Bass, 1979) with the high temperature data via equilibrium data may yield a better estimate for this important reaction. At present it can only be suggested that $k_{73'}$ be used in a series of calculations to determine whether it will yield better agreement with shock-initiated C_2H_2 oxidation measurements.

The C_2H_2 reaction mechanism presently used considers only two channels for the reaction of C_2H_2 and O-atoms:

$$C_2H_2 + O = CH_2 + CO \qquad (69)$$

$$C_2H_2 + O = C_2H + OH \qquad (70)$$

Table 4-11. Reaction Mechanism for Ketene-CH_2CO

No.	Reaction	ΔH^0_r, 298 kcal/mole	A	b	E kcal/mole	Reference
116	$CH_2CO + M = CH_2 + CO + M$	71.0	3.6 (15)	0	59.3	Wagner & Zabel, 1971
117	$CH_2CO + H = CH_3 + CO$	32.8	3.6 (12)	0	2.34	Slemr & Warneck, 1975
118	$CH_2CO + O = CH_2O + CO$	-101.	5.3 (11)	0	0	Carr et al., 1968
119	$CH_2CO + OH = CH_2O + HCO$	-15.0	2.8 (13)	0	0	Vandooren & Van Tiggelen, 1977

Kanofsky et al (1974), Blumenberg et al (1977), and Homann, Warnatz, and Wellmann (1977) indicate that another reaction channel occurs at room temperature:

$$C_2H_2 + O = HC_2O + H \tag{69'}$$

However, there is considerable uncertainty with regard to the contribution of reaction 69' to the total reaction of C_2H_2 and O-atoms. Kanofsky et al (1974) cite data which indicates that reaction 69' is responsible for 50 to 75 percent of the total reaction, and Blumenberg et al (1977) report that only 3 percent of the total reaction is due to reaction 69' between 300 and 600 K. Inclusion of reaction 69' in the reaction mechanism for acetylene may improve the ability of the model to predict the rate of CO and CO_2 production, since the likely products of reaction for HC_2O with H, O, and OH radicals are readily oxidized to CO and/or CO_2. Further work is necessary to clarify the potential role of reaction 69'.

Experimental data reported by Kanofsky et al (1974) and Vandooren and Van Tiggelen (1979) indicate that the reaction of C_2H_2 and OH produces ketene:

$$C_2H_2 + OH = CH_2CO + H \tag{72'}$$

Both investigations are in agreement with each other since Kanofsky et al observed only the occurrence of reaction 72' at room temperature and the relative rates of $k_{72'}$ reported by Vandooren and Van Tiggelen at 300 K indicate only the ketene-producing path should be observable:

$$k_{72'} = 3.2 \times 10^{11} \exp(-200/RT)$$

It would appear necessary to include this additional reaction path since even at 2000 K reaction 72' contributes 15 percent of the total reaction of C_2H_2 and OH.

Recent work at MIT (see Appendix A) also indicates that the reactions of methyl radical and OH are of importance. Estimates by Levy (Appendix A) based upon the fuel-rich acetylene decay data of Bittner (1981) indicate that reaction 73' should have a rate coefficient of:

$$k'_{73} = 2 \times 10^{12} \text{ cm}^3/\text{mole sec}$$

Also, since the data indicated that reaction with OH does not feed significantly into the CH_i manifold, the following reaction was recommended:

$$CH_2CO + OH \rightarrow CH_2O + CHO \qquad k = 1 \times 10^{13}\ cm^3/mole\ sec.$$

The predictions with fuel-rich hydrocarbon decay have been found to be improved by the reaction

$$CH_3 + OH \rightarrow CH_2O + H + H$$

although thermochemical considerations argue against the viability of this process at the proposed rate.

Other possible inadequacies of the C_2H_2 and C_2H_4 reaction mechanisms concern the oxidation of the C_2H_3 radical, the formation of acetylene via reaction 64, and reactions which produce polyacetylenes (Table 4-8). At present, the reaction mechanism considers only two paths for the destruction of the vinyl radicals:

$$C_2H_3 + M = C_2H_2 + H + M \qquad (92)$$

$$C_2H_3 + H = C_2H_2 + H_2 \qquad (93)$$

Homann et al (1977) indicate that the rate of reaction of C_2H_3 with O-atoms is about a factor of 30 greater than k_{93} at room temperature, i.e., about 4×10^{13} cm^3/mole-sec. The authors suggested that the reaction which was most consistent with their results was:

$$C_2H_3 + O = HCO + CH_2$$

Inclusion of this reaction would certainly affect the rate at which radicals grow during ethylene oxidation.

Formation of C_2H_2 via reaction 64 assumes that H_2 is also produced. Recent data reported by Russell and Rowland (1979), who studied the photolysis of $^{14}CH_2CO$ and CH_2CO, indicate that this reaction actually yields H-atoms and C_2H_3:

$$CH_2 + CH_2 = C_2H_3 + H \qquad (64')$$

Although reaction 64 was unimportant in the calculations described previously, an incorrect assignment of reaction products may have a more significant effect in other systems modeled, such as the flame data of Harvey and MacColl (1979). The rate of C_2H_2 formation and the influence of this reaction on radical concentrations changes if H-atoms and C_2H_3 are assumed as products. It is recommended that reaction 64' replace 64, although the rate coefficient should remain the same.

The reaction mechanism for polyacetylene production has uncertainties due to limited measurements of the rate coefficients and because of the poorly defined thermodynamic data for the species involved. Tanzawa and Gardiner (1980) and Frank and Just (1980) have examined many of the reactions and report rate data which should improve this portion of the C_2H_2 reaction mechanism. In addition, basic thermodynamic data, i.e., heat of formation, are given for the species involved. The reactions in Table 4-8 should be modified to reflect these data.

4.2.3 CH_4 Flame Phenomena

The modeling of flame phenomena is a relatively stringent test of the capabilities of a kinetic mechanism. The strong coupling between reaction rates and energy release/temperature serve to identify mechanistic errors which are overlooked in the more global, usually nearly isothermal shock tube comparisons. The advantages of flame comparisons are somewhat offset by the increased complexity of the model. In flame simulations, not only is the adequacy of the kinetic mechanism tested, but also that of the flame diffusion model and the assumed flame boundary conditions.

Two categories of data are available from flame studies: laminar flame velocity and flame profiles (temperature and species). The flame velocity is a global measure of fuel and oxidant consumption. This, in turn, is determined by radical production rates and diffusion. Measurement of concentration and temperature profiles through the flame front provide a detailed test for the mechanism. In particular, errors in the portions of the mechanism which deal with minor species will be revealed. While these errors may not impact global comparisons, there may be a significant effect on nitrogen processing.

Peeters and Mahnen (1973) studied fuel-lean and stoichiometric CH_4-O_2 flames at 40 torr. Profiles for stable species and a number of radical intermediates were reported for the fuel-lean flame. The initial reactants were 9.5 percent CH_4 and 90.5 percent O_2; these entered the flame at a cold flow velocity of 67 cm/sec.

These data were simulated as a freely-propagating laminar flat flame. Two calculations were performed: including and excluding the reactions involving C_2 species. The predicted burning velocities are listed below:

Case	Velocity (cm/sec)
Data	67
Model without C_2	49
Model with C_2	42

For real flames, the actual cold reactant velocity must be either less than the free flame velocity (i.e., burner stabilized) or equal to the free velocity. A greater cold reactant velocity will result in flame blow off unless some other stabilizing mechanism occurs. Whether the disagreement between the model and data is due to experimental difficulties or model inadequacies cannot be currently ascertained.

Profiles through the flame front are compared with the model results for stable species in Figure 4-19. In general, the results show encouraging agreement. Two points should be noted. First, the rate-limiting step leading to CO from the hydrocarbon pool appears to be too slow. This is also indicated in the discussion of the other flames that follows. Second, the rate of oxidation of CO to CO_2 is too slow at higher temperatures. This is consistent with the non-Arrhenius behavior of the reaction CO + OH at elevated temperatures, as previously discussed.

Biordi et al (1975) studied a stoichiometric (10.3 percent CH_4 - 21.6 percent O_2 - 68.1 percent Ar) flame at 32 torr and an initial velocity of 80 cm/sec. Molecular beam mass spectroscopy was again used to determine stable and labile species concentrations. Simulation of this experiment yielded a free-flame velocity of 76.2 cm/sec, agreeing very well with the experimental value.

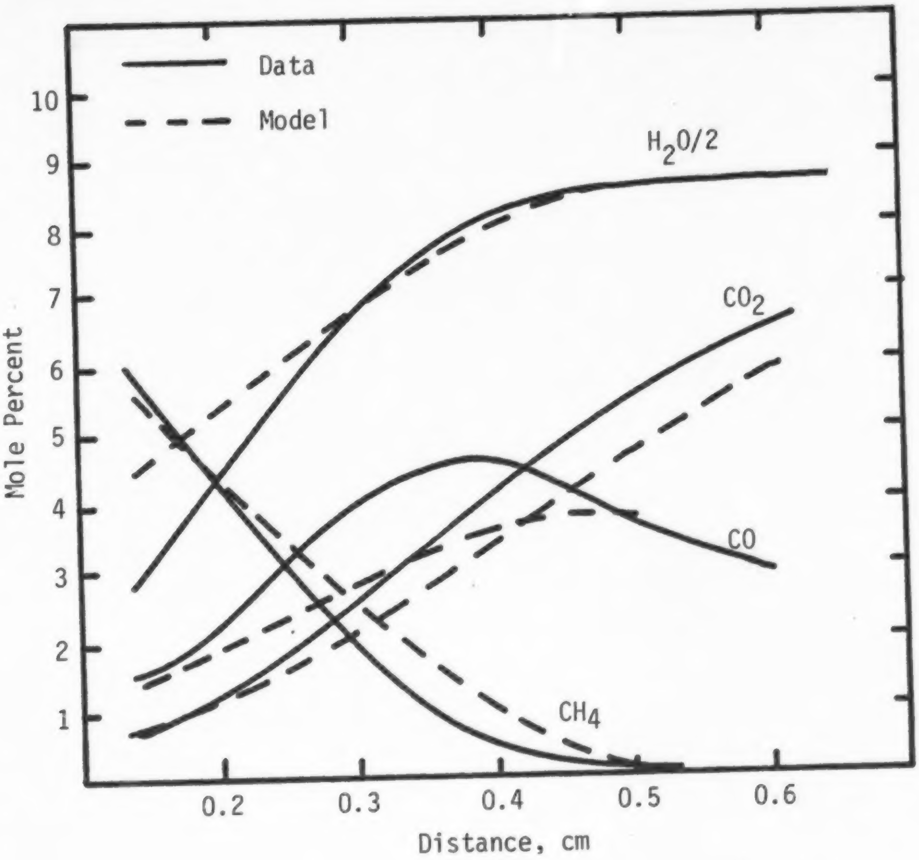

Figure 4-19. Stable species profiles for the flat flame of Peeters and Mahnen (1973).

The stable species profiles of Biordi et al (1975) agree quite well with the model predictions. Figure 4-20 illustrates the comparison. As in the Peeters simulation, the principal deviation appears to be due to an underprediction of the oxidation rate of CO to CO_2. Figure 4-21 shows the less satisfactory comparison between data and model for a number of radical species. While the model OH profile shows fair agreement with the data, both O and OH are ca. 50 percent below the data. Again, the results indicate that pyrolysis is occurring too slowly in the model. The products of pyrolysis (O, H, H_2) are underpredicted while the single pyrolysis reactant shown, CH_4, is overpredicted.

The third set of flame data simulated was that of Harvey and MacColl (1979). Temperature and concentration profiles were presented for a stoichiometric methane-oxygen flame diluted with 43 percent argon. The cold gas velocity was 119 cm/sec and the flame pressure was 20 torr. The sampling and mass spectroscopy analysis system follows closely the work of Biordi et al (1975). This work is of particular value because the authors report profiles for C_2H_2 and C_2H_4, presenting an opportunity to check the C_2 mechanism.

The steepness of the temperature profile in the vicinity of the burner face suggests that the flame is attached (i.e., stabilized by heat loss to the burner face). The model was run in the free-flame mode which resulted in a free-flame velocity greater than the observed 119 cm/sec. These observations both indicate an attached flame and, thus, the flame was modeled in this manner. The burner face temperature was assumed to be 300 K.

Results for the species CH_3, CH_2, and CH_2O are shown in Figure 4-22. Again, all hydrocarbon pyrolysis intermediates are overpredicted. The calculation was repeated with the C_2 chemistry section removed. In Figure 4-23 the accuracy of the prediction is shown to be reduced by this step. The obvious interpretation here is that the C_2 steps provide an additional, though secondary, pathway for the removal of hydrocarbon fragments.

Ethylene and acetylene comparisons are shown in Figure 4-24. Although C_2H_4 shows fair agreement, C_2H_2 is overpredicted by a factor of eight. If these data are correct and the discrepancy is real, it would still be impossible to assess whether the mechanistic errors would affect nitrogen proces-

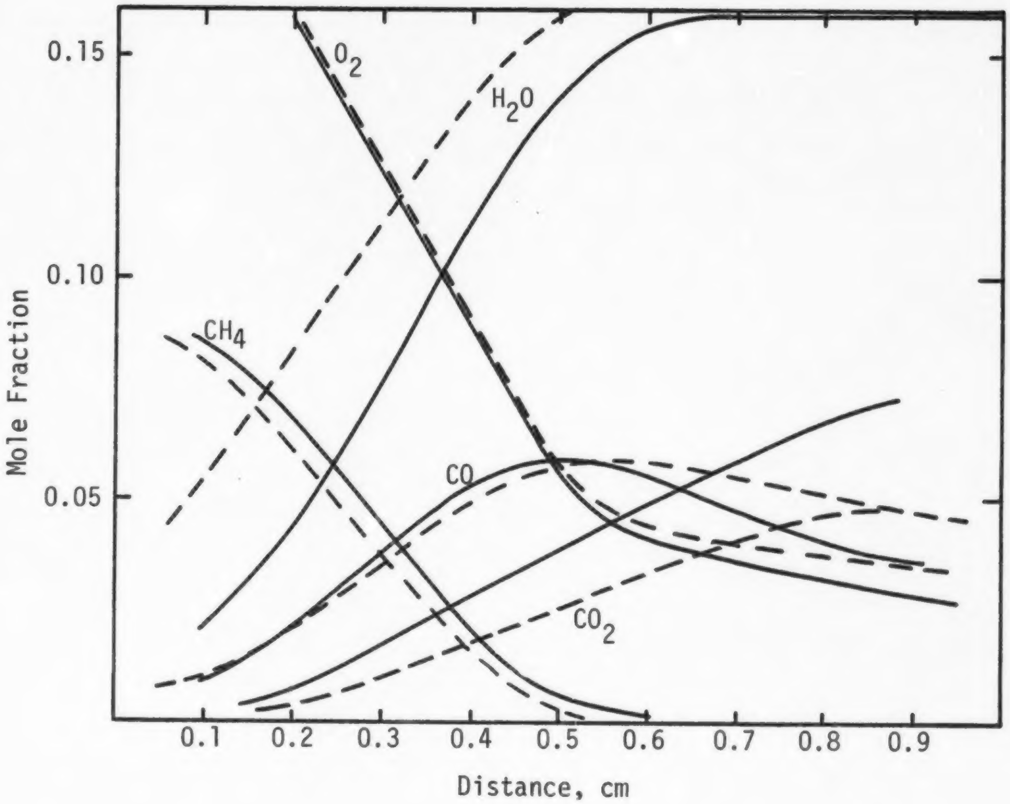

Figure 4-20. Flame profiles of Biordi et al (1975). Solid lines are data; dashed are model.

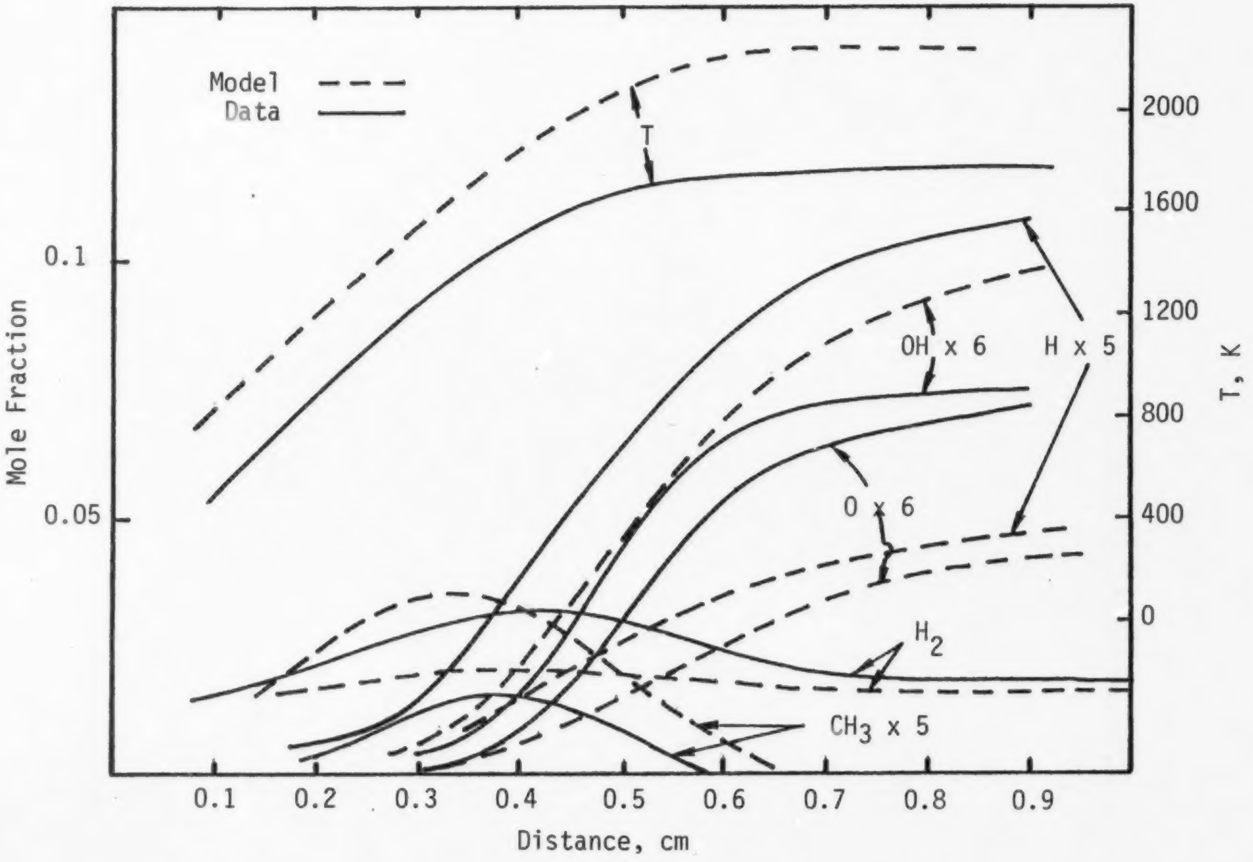

Figure 4-21. Profiles through the flame of Biordi et al (1975).

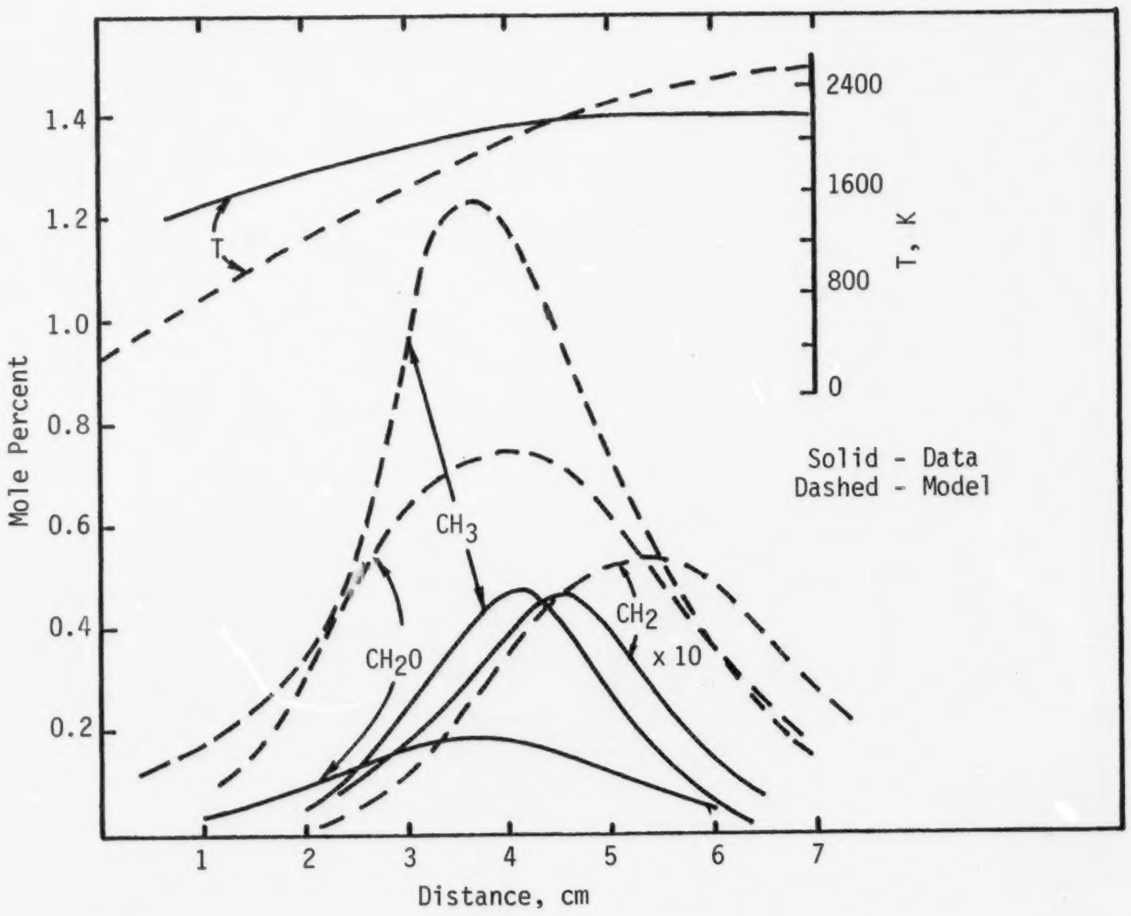

Figure 4-22. Profiles through the flame of Harvey and MacColl (1979). (Predictions are for $C_1 + C_2$ Chemistry).

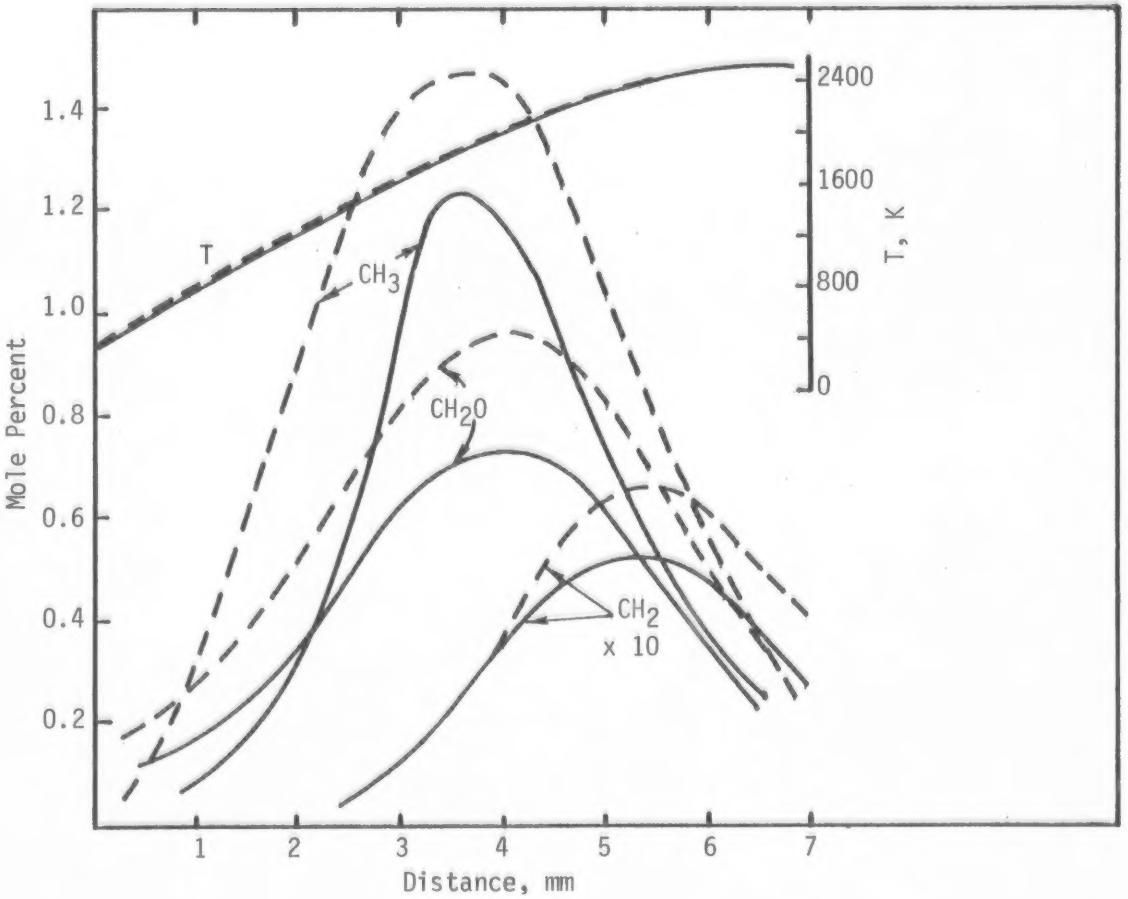

Figure 4-23. Calculated flame profiles for the data of Harvey and MacColl (1979). Dashed lines indicate C_1 reaction set; solid represents $C_1 + C_2$ set.

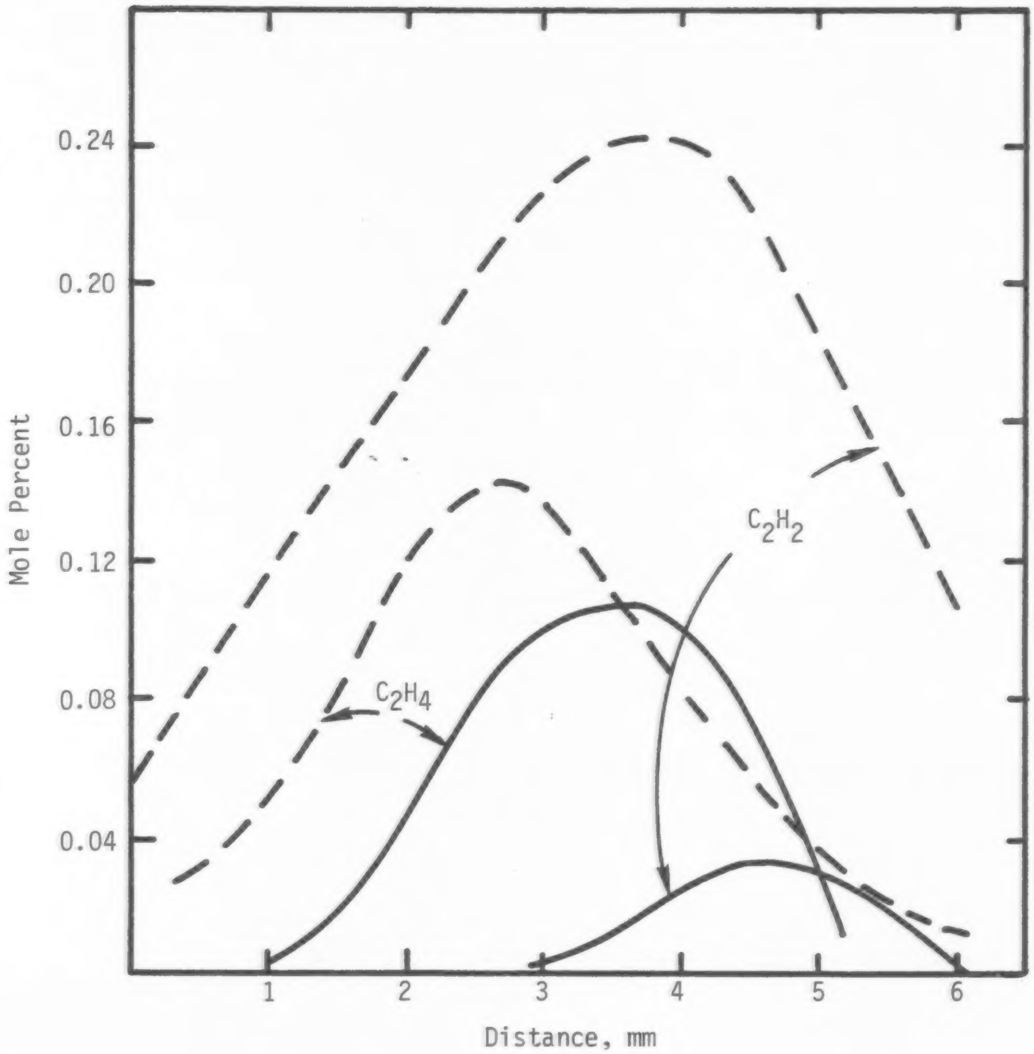

Figure 4-24. Profiles of C_2 species through the flat flame of Harvey and MacColl (1979). Solid lines are data; dashed lines are model.

sing. In any case, the C_2 chemistry must be substantially correct before flames containing C_2-hydrocarbons are studied.

The assumption of a 300 K burner face temperature is open to question. An additional calculation was performed to determine the sensitivity of the model profiles to this temperature. The results indicated a strong sensitivity, which unfortunately adds an additional uncontrolled parameter to the flat flame model.

Some general observations on modeling of flame data are appropriate to conclude this section. Our experience in modeling flame results has led us to recognize two basic categories of problems. The first concerns the correctness of the reported measurements, and the second, the adequacy of our modeling of the flames.

Among the problems in obtaining flame measurements are problems in flame stabilization and geometry. Frequently the mechanism of stabilization is not apparent from the reference. Also, the expansion ratio of the flame is often not available. Of considerably greater importance are the problems associated with obtaining and interpreting mass spectrometer measurements. The bulky sampling cones are known to distort the flame front. Recent investigations have indicated that the distortion is caused principally by the physical bulk of the sampling cone preventing upstream diffusion of flame radicals in its immediate vicinity (Zabielski et al , 1981). Such distortions may be particularly severe when making radical measurements since radicals respond much more rapidly to changes in the flame environment than stable species.

Another experimental problem is the difficulty in unambiguously interpreting the mass spectra resulting from these complicated flames. Frequently, intricate arguments or further experiments with deuterated fuel are necessary to quantify the spectra.

Lastly, the application of the model to experiments is, in many cases, uncertain. This is particularly true for burner stabilized flames, as was previously discussed. The conclusion to be drawn from this discussion is that although flame data are helpful in verifying mechanisms, concentration profile comparisons must not be regarded as final until all sources of error, both numerical and experimental, are evaluated.

4.2.4 Summary

Simulations have demonstrated that the CH_4 reaction mechanism, which is defined by the reactions in Tables 3-1 through 4-7, is capable of accurately reproducing induction delay times observed in shock-initiated CH_4 oxidation studies over a broad range of temperature, reactant concentrations, and total densities. The same set of reactions reproduces induction delay times for C_2H_6 oxidation, although it is necessary to consider data over a greater range of conditions to completely validate the reactions and associated rate coefficients which dominate during the induction period. Examination of the oxidation reactions for C_2H_2 and C_2H_4 indicates that several rate coefficients should be modified, and that additional species are necessary for the mechanism to be consistent with fundamental studies of C_2H_2 and C_2H_4 oxidation. Additional simulations of shock-initiated oxidation of acetylene and ethylene are required to examine the effects of the changes in rate coefficients on predictions and the impact of additional species, such as CH_2CO, on the simulated combustion of C_2H_2 and C_2H_4

Flame simulations have been only moderately successful in reproducing data. Free-flame velocities and stable species profiles have, in general, been accurately reproduced. However, radical and C_2 profiles have not agreed with experiment. Further studies are indicated for investigating the cause of these discrepancies.

5.0 KINETIC MODELS FOR FUEL NITROGEN REACTIONS

The development of a detailed kinetic mechanism which accurately describes the oxidation of chemically-bound nitrogen present in fossil fuels to nitric oxides, or reduction of these species to molecular nitrogen, is beyond our present capabilities. Although it has been established that much of the nitrogen in heavy oils is in the form of heterocyclic organic compounds, and indications are that the same is true for nitrogen in coals (Axworthy et al , 1976), the identity and distribution of the chemical types of nitrogen are not well-established, particularly for coals. The uncertainty with regard to the identity of nitrogenous compounds which are present in fossil fuels, and the lack of data in the literature for reaction paths and appropriate rate coefficients (necessary as inputs to a model) for oxidation and/or pyrolysis of complex nitrogenous species, forced us to introduce simplifications in the kinetic model, and restrict the development of detailed reaction sets to those relevant to oxidation and pyrolysis of HCN and NH_3, and to the reduction of NO in hydrocarbon flame environments.

Data from inert and oxidative pyrolysis studies of model fuel nitrogen compounds, pyrolysis studies of coals and heavy oils, and fundamental studies in flames of nitric oxide formation from nitrogenous species added to a simple hydrocarbon flame indicate that N_2, HCN, NH_3, NO, NO_2, and N_2O are the primary stable nitrogen intermediates and products. Axworthy et al. (1976) investigated the pyrolysis of pyridine, quinoline, pyrrole, and benzonitrile at temperatures between 1123 and 1373 K to determine the major nitrogen-containing species formed. The results show that the nitrogen present in the model compound is, in large part, converted to HCN with small amounts forming NH_3. At 1373 K, HCN accounted for 100 percent of the nitrogen in pyridine, 82 percent of the nitrogen in benzonitrile, and about 55 percent of that initially present in quinoline. The distribution of species identified in the oxidative pyrolysis of pyridine and benzonitrile were qualitatively similar to that obtained under inert conditions although quantitative measurements were not made. Extrapolation of the results, which for pyridine, pyrrole, and quinoline could be represented as first-order processes, to temperatures of interest, i.e., 1800 K, yields the following half-lives for pyridine, pyrrole, and quinoline: 60 μsec, 200 μsec, and .84 msec, respectively. The result for pyridine is in fair agreement with the high-temperature, shock tube data of Proctor and Laurendeau (1975), which indicates a half-life of 15 to 30 μsec at 1800 K.

In oxidative pyrolysis experiments (Axworthy, 1980) of pyridine and benzonitrile, large amounts of HCN, NH_3, and CO were formed at low temperatures (750 C) similar to inert pyrolysis. At high temperatures, the major oxidative products were found to be CO_2, N_2, N_2O, and NO. These two-stage experiments indicated that the observed products at higher temperatures were formed in secondary reactions of NH_3, HCN, and volatile tars formed in the primary reaction process.

Axworthy et al (1976, 1980) also examined pyrolysis of six No. 6 fuel oils, one crude oil, and two coals under inert conditions at 1123 and 1373 K. Although a significant amount of the nitrogen present in the fuel oils was converted to HCN at 1373 K (23 to 50 percent), conversion was not quantitative as found for pyridine. It was not possible for the authors to give an accurate determination of the NH_3 content in the pyrolysis gases, but an upper limit of 15 to 30 percent of the initial nitrogen is indicated. Data for the two coals studied indicate conversion to HCN of about 30 percent at 1373 K and slightly higher upper limits for the amount of NH_3 produced than observed for the fuel oils. It should be noted that HCN and NH_3 have also been observed in the pyrolysis gases of coals studied by Blair, Wendt, and Bartok (1977), who observed that the relative yields of HCN and NH_3 were dependent upon pyrolysis temperature and coal type.

Various investigators have examined the fate of simple fuel nitrogen compounds (NH_3, NO, methylamine, pyridine, and methacrylonitrile) in fuel-rich hydrocarbon flames. Morley (1976) found near quantitative conversion of NO, NH_3, CH_3CN, and pyridine to HCN in the reaction zones of fuel-rich hydrocarbon flames with postflame temperatures above 2000 K. Fenimore (1976) found that fuel nitrogen introduced as pyridine and not yet converted to NO or N_2 existed in large part as HCN just downstream of the primary reaction zone. Similar conclusions are indicated for fuel-rich hydrocarbon flames to which NH_3 was added. In addition, Fenimore (1976) reports data for fuel-rich methane flames doped with N_2O which show that HCN is the dominant nitrogenous species downstream of the flame zone. The studies of Haynes, Iverach, and Kirov (1975), and Haynes (1977a, 1977b) further confirm the rapid conversion of a substantial portion of the initial fuel nitrogen compound to HCN within the flame zone. However, it should be noted that with the possible exception of the data reported by Morley (1976) the initial distribution of nitrogenous species was dependent upon the parent fuel nitrogen species (see DeSoete, 1975, for additional discussion of this point). In all of the studies cited, ammonia or other amine species, were observed to grow as HCN decayed.

These studies thus indicate that HCN is the principal nitrogen intermediate in the oxidation and pyrolysis of nitrogen containing fuels whether they are model compounds, heavy fuel oils, or coals. It is not rigorously correct to consider only the intermediate species HCN, NH_3, and NO as the only fuel nitrogen species, but there is support that these are rate controlling; i.e., the time constants of conversion of the parent nitrogen species to these intermediates is much faster than the conversion of the intermediates to NO and N_2 products. As a first step, therefore, the detailed analyses will be limited to these simple nitrogen compounds.

In certain cases, such as when the fuel nitrogen compound is pyridine, it will be assumed that conversion to HCN is quantitative and instantaneous. However, as the data for quinoline decomposition, and to a lesser extent that for pyrrole indicate, the assumption of very short times for conversion to HCN may not be justified for more complex fuel nitrogen compounds. An approach similar to that suggested earlier for semiglobal modeling of oxidation of complex hydrocarbon species may be useful, although at present there are insufficient data on pyrolysis of fuel nitrogen compounds to include such an approach in the model under development. Finally, reactions pertinent to the oxidation and pyrolysis of ammonia are obviously required since it is formed under fuel-rich conditions and the ultimate NO emissions from a combustion system will depend on the rate at which NH_3 is converted to NO and N_2. A detailed understanding of NH_3 reactions is also necessary with regard to the homogeneous removal of NO in postcombustion processes achieved via addition of NH_3.

The sections which follow describe the detailed kinetic mechanisms developed for NH_3 and HCN oxidation and/or pyrolysis. As before, the capabilities of the reaction sets were determined by comparisons with studies reported in the literature which investigated the reaction of these species under well-defined experimental conditions amenable to analysis. Since ammonia is an intermediate occurring in the oxidation of HCN, results for this species are discussed first to determine the extent to which an element of the HCN reaction mechanism is known. Discussion of the HCN mechanism is limited to the feasibility of the reactions included because data which could be used to verify the accuracy of this model were only recently reported (Fenimore, 1979) and because of the limitations identified for the NH_3 oxidation mechanism.

5.1 The NH_3- O_2 and NH_3-Inert Reactions

The oxidation of ammonia has been fairly extensively studied in shock tube investigations (Roose, Hanson, and Kruger, 1980 and 1977; Duxbury and Pratt, 1975 and 1973; Dove and Nip, 1974; Drummond, 1972; Soloukhin, 1971; Bull, 1968; Bradley, Butlin, and Lewis, 1968; Miyama, 1968; Drummond and Hiscock, 1967; Miyama and Endoh, 1967; and Takayama and Miyama, 1965), and in laminer, premixed flat flames (Seery and Zabielski, 1977; Fisher, 1977; Kaskan and Hughes, 1973; MacLean and Wagner, 1967; and Fenimore and Jones, 1961). Pyrolysis of NH_3 has also been studied in shock tubes (Yumura et al , 1980; Roose et al , 1979; Dove and Nip, 1979; Bradley, Butlin, and Lewis, 1967; and Michel and Wagner, 1965). Low temperature oxidation data for NH_3 have been reported by Lyon, Hardy, and Benn (1979), and Lyon and Benn (1979). Unfortunately, there is remarkably little agreement among these investigators with regard to the elementary processes which control production of NO and, more importantly, N_2 during the oxidation of ammonia. However, the data reported do permit an analysis of the accuracy of the NH_3 reaction mechanism, which consists of the steps listed in Tables 3-1 and 5-1, to be made.

Takayama and Miyama (1965), who were the first to study the high temperature oxidation of ammonia, monitored emission from NH, NH_2, and NO, and ultraviolet absorption by OH and NH behind reflected shock waves to characterize

Table 5-1. Reactions Describing NH_3 Oxidation

No.	Reaction	ΔH^0_r, 298 kcal/mole	A	b	E kcal/mole	Reference
120	$NH_3 + M = NH_2 + H + M$	108.6	2.52 (16)	0.	93.8	Roose, Hanson & Kruger, 1979
121	$NH_3 + M = NH + H + M$	95.47	2.52 (14)	0.	93.8	Roose, Hanson & Kruger, 1979
122	$NH + H + M = NH_2 + M$	-90.80	2. (16)	-0.5	0.	Est. This Study
123	$N + H + M = NH + M$	-80.90	3. (16)	-0.5	0.	Est. This Study
124	$N_2 + M = N + N + M$	226.0	3.7 (21)	-1.6	225.0	Baulch et al., 1973
125	$NO + O + M = NO_2 + M$	-73.23	1.0 (21)	-1.86	0.	Michael, Payne & Whytock, 1976
126	$N_2O + M = N_2 + O + M$	39.95	1.42 (14)	0.	51.28	Monat, Hanson & Kruger, 1977
127	$H + NO + M = HNO + M$	-49.88	2.2 (17)	-0.5	0.	Dixon-Lewis & Williams, 1977
128	$NH_3 + H = NH_2 + H_2$	4.37	3.63 (10)	0.75	13.79	Est. This Study
129	$NH_3 + OH = NH_2 + H_2O$	-10.82	8.5 (9)	0.75	1.10	Est. This Study
130	$NH_3 + O = NH_2 + OH$	6.40	5.5 (9)	0.75	5.03	Est. This Study
131	$NH_3 + HO_2 = NH_2 + H_2O_2$	18.94	1.0 (12)	0.	24.3	Est. This Study
132	$NH_2 + O = HNO + OH$	-71.77	1.0 (11)	0.5	0.	Est. This Study
133	$NH_2 + O = NH + OH$	-11.37	1.0 (11)	0.5	1.	Est. This Study
134	$NH_2 + OH = NH + H_2O$	-28.59	6.3 (11)	0.5	0.	Est. This Study
135	$NH_2 + HO_2 = NH_3 + O_2$	-61.47	2.0 (10)	0.5	2.59	Est. This Study
136	$NH_2 + HO_2 = NH + H_2O_2$	1.17	1.0 (14)	0.	1.20	Est. This Study

(continued)

Table 5-1 (continued)

No.	Reaction	ΔH^0_{r}, 298 kcal/mole	A	b	E kcal/mole	Reference
137	$NH_2 + HNO = NH_3 + NO$	-58.69	5.0 (11)	0.5	2.74	Est. This Study
138	$NH_2 + O_2 = HNO + OH$	-12.21	5.0 (6)	0.75	6.08	Est. This Study
139	$NH_2 + H = NH + H_2$	-13.40	5.0 (11)	0.5	7.57	Est. This Study
140	$NH + HO_2 = HNO + OH$	-55.91	6.3 (11)	0.5	0.	Est. This Study
141	$NH + O_2 = HNO + O$	-0.84	5. (11)	0.5	4.37	Est. This Study
142	$NH + OH = N + H_2O$	-38.49	5. (11)	0.5	4.45	Est. This Study
143	$NH + OH = HNO + H$	-17.79	5. (11)	0.5	5.62	Est. This Study
144	$NH + O = NO + H$	-70.08	6.31 (11)	0.5	0.	Benson et al., 1975
145	$NH + O = N + OH$	-21.27	6.31 (11)	0.5	8.0	Benson et al., 1975
146	$NH + H = N + H_2$	-23.30	6.31 (11)	0.5	8.0	Benson et al., 1975
147	$N + OH = NO + H$	-48.81	6.31 (11)	0.5	0.	Benson et al., 1975
148	$N + O_2 = NO + O$	-31.86	6.4 (9)	1.0	6.26	Baulch et al., 1973
149	$NH_2 + NH_2 = NH_3 + NH$	-17.77	1.2 (11)	0.5	5.64	Est. This Study
150	$NH + NH = N_2 + H_2$	-168.4	3.6 (11)	0.55	1.9	Mayer, Schieler & Johnston, 1967
151	$N + NH_3 = NH + NH_2$	27.67	1.0 (11)	0.5	31.64	Est. This Study
152	$N + NH_2 = NH + NH$	9.90	2. (11)	0.5	22.16	Est. This Study
153	$N + NH = N_2 + H$	-145.1	6.31 (11)	0.5	0.	Benson et al., 1975
154	$NO + HO_2 = NO_2 + OH$	-9.18	3. (11)	0.5	0.	Est. This Study
155	$H + NO_2 = NO + OH$	-28.94	2.9 (14)	0.	0.80	Clyne & Monkhouse, 1977

(continued)

Table 5-1 (continued)

No.	Reaction	ΔH^0_r, 298 kcal/mole	A	b	E kcal/mole	Reference
156	$NO_2 + O = NO + O_2$	-45.89	1. (13)	0.	0.60	Baulch et al., 1973
157	$NO_2 + N = N_2O + O$	-41.74	3. (11)	0.5	0.	Est. This Study
158	$N_2O + O = N_2 + O_2$	-79.17	6.23 (13)	0.	24.54	Monat, Hanson & Kruger, 1979
159	$N_2O + O = NO + NO$	-36.01	3.06 (13)	0.	21.80	Monat, Hanson & Kruger, 1979
160	$H + N_2O = N_2 + OH$	-62.22	2.27 (10)	1.0	12.44	Est. This Study
161	$N_2O + NO = N_2 + NO_2$	-33.28	2. (14)	0.	50.	Fisburne & Edse, 1964
162	$H + HNO = H_2 + NO$	-54.32	1. (13)	0.	2.5	Schofield, 1967
163	$HNO + OH = H_2O + NO$	-69.51	1. (12)	0.5	2.74	Est. This Study
164	$HNO + O = OH + NO$	-52.29	5. (11)	0.5	2.74	Est. This Study
165	$N + NO = N_2 + O$	-75.02	3.1 (13)	0.	0.334	Baulch, Drysdale & Horne, 1969
166	$NH + N_2O = N_2 + HNO$	-80.01	2. (10)	1.	12.0	Est. This Study
167	$NH + NO = N_2O + H$	-34.07	5.4 (16)	-1.4	0.	Est. This Study
168	$NH_2 + NO = N_2O + H_2$	-47.74	5. (8)	0.5	0.	Roose, Hanson & Kruger, 1977
169	$NH_2 + NO = N_2 + H_2O$	-125.1	2.37 (17)	-1.85	0.	Est. This Study
170	$NH_2 + NO = N_2 + H + OH$	-5.49	1.38 (17)	-1.85	0.	Est. This Study

Rate coefficients expressed as $k_f = AT^b \exp(-E/RT)$ in units of cm^3, mole and sec. M refers to total density and numbers in parentheses to powers-of-ten. For Reactions 120, 121, and 126, rate constants are for M = Ar; third-body for Reaction 124 is N_2. For Reaction 125, rate constant is for M = Ar; Michael et al., (1976) report:

$$k_{125}\ (M = N_2) = 1.38 \times 10^{21}\ T^{-1.82}$$

Initial calculations assume relative chaperon efficiencies for other species identical. Technique described by Tunder et al. (1967) used for entries designated "Est." Note that ΔH^0_f, 298 (NH) = 84.2 kcal/mole (Piper, 1979).

the induction period for stoichiometric and lean NH_3-O_2-Ar mixtures at temperatures between 1550 and 2300 K. An induction period for the appearance of OH absorption was measured and correlated with temperature via:

$$\tau\ (O_2) = 5.1 \times 10^{14} \exp[(42500 \pm 1500)/RT],\ \text{mole-sec/cm}^3$$

According to the authors, absorptions of OH and NH appeared at the same time; emissions of NO and NH appeared and reached their maxima at essentially the same time, while the emission of NH_2 reached its maximum at slightly shorter times than NO and NH. The absorption of NH reached its maximum earlier than that of OH and decayed within tens of microseconds. On the basis of this information and the observed experimental "activation energy" for the induction delay correlation, the authors concluded that the main steps governing the induction period were:

$$NH_2 + O_2 = NH + HO_2 \qquad \Delta H^0_{r,298} = 43.7 \text{ kcal/mole}$$

$$NH + O_2 = NO + OH \qquad \Delta H^0_{r,298} = 53.13 \text{ kcal/mole}$$

$$NH_3 + OH = NH_2 + H_2O \qquad \Delta H^0_{r,298} = 10.82 \text{ kcal/mole}$$

However, the analysis described by Takayama and Miyama (1965) could not explain the observations that NH absorption reached its maximum before that of OH and that NH decayed within tens of microseconds, while OH remained at maximum concentration for times on the order of milliseconds. In addition, Bradley (1967) indicates that the analysis employed is incorrect if an intermediate such as HNO, which was suggested by Husain and Norrish (1965), is involved. It should also be noted that the results presented previously for CH_4 oxidation indicate that the temperature dependence of an induction delay correlation does not necessarily have a one-to-one correspondence with a particular elementary reaction.

Drummond and Hiscock (1967) used reflected shock waves to initiate reactions in mixtures of NH_3 with O_2, H_2O, and NO which were diluted with argon. Absorption spectroscopy was used to identify species which were formed during the oxidation of ammonia. Although this study was limited to one mixture of NH_3-O_2-Ar, NH_3-N_2O-Ar, and NH_3-NO-Ar, the information is useful in terms of developing a kinetic mechanism for ammonia oxidation. Between 1640 and 2060 K, the authors observed for the NH_3-O_2 system that NH and OH had identical induction periods and that OH reached a maximum value which was constant for several hundred microseconds while after reaching a maximum, NH decayed in a short time. Both of these observations are consistent with the data of Takayama and Miyama (1965). The data for the NH_3-N_2O-Ar and NH_3-NO-Ar mixtures indicate a greater temperature dependence for the induction delay correlation based on NH and OH absorption than observed for the NH_3-O_2-Ar mixtures--56 kcal/mole versus 42.5 kcal/mole. The data for the three mixtures indicate that induction periods decrease in the order $O_2 > N_2O > NO$. The authors suggest that the rapid decay of NH observed in all three mixtures is due to:

$$NH + NO = N_2 + OH$$

Infrared emission techniques were used by Bull (1968) to monitor OH, H_2O, NH_3, NO, N_2O, and NO_2 in reflected shock studies of stoichiometric and lean NH_3-O_2-Ar mixtures at temperatures between 1500 and 2300 K. Finite induction periods were observed for all species with the indication that the occurrence of OH, NO, NO_2, and N_2O during the course of NH_3 oxidation followed the same induction time. Although absolute concentrations of the species monitored were not made, the similarity in induction delay times can be used to determine whether the reaction mechanism is accurate with regard to the time scales involved for formation of OH, NO, NO_2, and N_2O. Bull (1968) reports that the various induction delay times could be correlated via:

$$\tau\ (O_2) = 5.1 \times 10^{13} \exp[(30500 \pm 4800)/RT] \text{ mole-sec/cm}^3$$

or, if data reported by other investigators were included in the correlation, via:

$$\tau\ (O_2) = 1.9 \times 10^{14} \exp[(37700 \pm 2600)/RT] \text{ mole-sec/cm}^3$$

The simultaneous appearance of NO and OH was explained on the basis of the following reactions:

$$NH_2 + O_2 = HNO + OH$$

$$HNO + M = H + NO + M$$

A reasonable explanation for the occurrence of N_2O during the induction period was not obtained.

Bradley et al (1968) examined oxidation of NH_3-O_2-Ar mixtures behind incident shock waves at temperatures between 2000 and 3000 K. A major contribution was the extension of the oxidation studies to substoichiometric NH_3-O_2 ratios (NH_3:O_2 varied from 6:1 to 2:5). Although these authors found that absorption of NO and OH had identical induction periods, they did not observe an induction time for NH absorption, which is in contradiction to the data cited above. The NH radical was observed to rise steadily followed by a similar decrease at about the time that OH absorption appeared; the concentration-time dependence of NH was fitted best by a parabolic rate law. Bradley et al (1968) contend that the conclusions of Takayama and Miyama (1965) with regard to an induction period for NH are incorrect due to the difficulty of interpreting the traces obtained for NH emission and absorption. Bradley et al. conclude that the formation of NH during the induction period is due to pyrolysis reactions of NH_3 and is independent of the oxidation mechanism. With regard to the oxidation of NH_3, these authors conclude that NH_2 must react with O_2 to give OH either directly or indirectly, i.e.:

$$NH_2 + O_2 = HNO + OH$$

$$HNO + M = H + NO + M$$

This is consistent with the conclusion reached by Bull (1968).

Drummond (1972) investigated the oxidation of lean NH_3-O_2-Ar mixtures ($1.3 \leq SR \leq 4.0$) behind incident and reflected waves at temperatures between 1570 and 2460 K and for three pressure regions: 0.2 to 0.3, 3.3 to 5.3, and 27.2 to 44.4 atmospheres. Induction periods measured from absorption due to NH were in agreement with those obtained from absorption of OH. Nitric oxide was also observed during the induction period. Drummond maintains that the mechanism proposed by Takayama and Miyama (1965), with inclusion of additional reactions describing the formation and destruction of the HO_2 radical, provides the most plausible explanation for his data. He cites the similarity of the endothermicity for the reaction of NH_2 with O_2 to yield NH and HO_2 with his measured temperature dependence of the induction delay correlations (about 50 kcal/mole) as supporting evidence for this mechanism.

The studies of Duxbury and Pratt (1973, 1975) on shock-initiated oxidation of NH_3-O_2-Ar (1900 to 3200 K) and NH_3-NO-Ar (1450 to 3250 K) mixtures provide additional data which support the values for induction periods and the temperature dependence of this parameter observed by Drummond (1972) and Drummond and Hiscock (1967). Duxbury and Pratt (1973) concluded that NH_i species enhance removal of NO; NO is more readily removed in the NH_3-O_2 system. The later study of Duxbury and Pratt focused on the NH_3-NO-Ar system and showed that for fuel-lean mixtures NH_3 is completely removed after a short induction period and that the NO level after this period was given approximately by $(NO)_0 - (NH_3)_0$. It was also noted that peak NH concentrations were about a factor of two lower than observed earlier (Duxbury and Pratt, 1973) for the NH_3-O_2 system with the same initial atom balance. The major conclusion was that the Zeldovich mechanism could not account for the profiles measured in the NH_3-NO system and, therefore, that a reaction of NH_2 and NH with NO was required. Dove (1975) suggests that the products of the reaction of NH with NO are N_2O and H-atoms based on his studies of the NH_3-NO system at temperatures between 2600 and 2900 K. The work of Roose et al. (1977) also confirms the presence of N_2O as an intermediate in high temperature oxidation of NH_3-NO-Ar mixtures.

Studies of NH_3 oxidation in laminar flat flames provide qualitative and quantitative information with regard to the elementary processes which occur as NH_3 is converted to molecular nitrogen and various nitrogen oxides. Fenimore and Jones (1961) added NH_3 to fuel-rich and fuel-lean H_2-O_2 (or N_2O)-Ar flames and measured the resulting stable species profiles. They indicate that the NH_2 radical is partially equilibrated with NH_3 in the reaction zone and that NO is formed rapidly from NH_3 with a subsequent rapid removal via reaction with the NH_2 radical. The authors also observed that under fuel-lean conditions the NO concentration rose smoothly through the reaction zone and did not decay in the postflame gases. Under fuel-rich conditions, NH_3 continued to decay in the postflame gases although oxygen and the transient NO had become inappreciable. In addition, N_2O was observed as a transient during the oxidation of NH_3, which decayed to zero in the reaction zone. Nitrous oxide was formed more readily under fuel-lean conditions, i.e., when NO was greatest in the postflame gases, and decreased in importance at richer conditions--4.8 percent of the initial NH_3 was converted to N_2O for the leanest NH_3-H_2-O_2-Ar flame (SR = 2.7), which represents about 10 percent of the total nitrogen oxides; and 2.7 percent of the initial NH_3 was converted to N_2O for the richest flame data reported (SR = 0.83), or about 25 percent of the total nitrogen oxides.

The major conclusions of Fenimore and Jones (1961) were that NO is formed and destroyed rapidly during the NH_3 oxidation via two processes:

$$NH_3 + O \rightarrow \ldots \rightarrow NO +$$

$$NH_2 + NO \rightarrow \ldots \rightarrow N_2 +$$

Since the authors maintain that NH_2 and NH_3 are partially equilibrated in the flame, it is possible that the first global step actually consists of:

$$NH_2 + O \;=\; HNO + H$$

$$HNO + H,O,OH \;=\; NO + H_2,OH,H_2O$$

With regard to the second global step, although the reaction of NH_2 and NO to produce N_2 is well-established, at least at low temperatures, extrapolation of the best data for the rate coefficient (Hack et al., 1979) indicates that the value reported by Fenimore and Jones--6 $\pm$ 1 x 10^{13} cm^3/mole-sec at 1700 to 1900 K--is about one order-of-magnitude high. This discrepancy may be in part due to the sampling procedure used in which gas samples were taken into a sample bottle maintained at 1 mm Hg pressure or less, and then analyzed in a mass spectrometer. Gehring et al (1973) and Hack et al. (1979) measured the rate coefficient for reaction of NH_2 with NO at 1 mm Hg total pressure and 298°K. The data reported suggest half-lifes for NO on the order of milliseconds. Depending on the time between introduction of the gas samples into the sample bottle and analysis by the mass spectrometer, a substantial portion of the NO which was actually present in the flame gases could have reacted with the result that Fenimore and Jones (1961) overestimated the rate coefficient for this reaction.

MacLean and Wagner (1967) report profiles for NO, H_2O, N_2, NH_3, H_2, and N_2O obtained by mass spectrometry in three low pressure NH_3-O_2 flat flames (SR = 2.0, 1.0, 0.72). Optical spectrophotometric techniques gave OH radical concentrations, NH absorption profiles, and emission profiles of excited NH_2, NO, NH, and OH. Nitric oxide did not decay significantly in the post-flame gases of lean and stoichiometric flames, although a substantial decay occurred in the rich flame. In agreement with the data of Fenimore and Jones (1961), N_2O reached its maximum in the reaction zone and then disappeared completely; the trends with regard to the fraction of the initial NH_3 converted to N_2O, and the fraction of total nitrogen oxides which was N_2O as a function of stoichiometry, were also in agreement with the earlier work. The maximum N_2O concentration always occurred at the same location in the flame as the maximum rate of NO formation.

Unfortunately, the authors did not present a quantitative analysis of their data in terms of elementary reaction steps which would account for the products observed and the rates at which the species were formed. Inspection of the data reported suggests that the maximum NH concentration occurred at the same height in the flame as the maximum rate of N_2O formation, and for the lean and stoichiometric flames at the same location as the peak rate of N_2 formation. The peak NH concentration occurred before the maximum rate of OH growth in the stoichiometric and lean flames, but under rich conditions the positions were apparently the same. It was also observed that the location of the peak emission from NO relative to the maximum NH absorption shifted from a lower height in the flame under lean conditions to a slightly greater height at stoichiometric and fuel-rich conditions. This information suggests, in part, that N_2O is formed by a reaction of NH with NO which may occur as Dove (1975) postulated:

$$NH + NO = N_2O + H$$

MacLean and Wagner (1967) indicate that their data support the reaction of OH with NH_3 as the key reaction in the oxidation mechanism. However, the data reported did not provide information with regard to the relative importance of reactions of ammonia with O and H. The authors comment that the mechanism for NH_3 oxidation is complicated by the concurrent pyrolysis of all excess ammonia in the fuel-rich flames studied.

Kaskan and Hughes (1973) and Fisher (1977) report data for the decay of NO, NH_3, NH_2, NH, and OH in the post-flame gases of NH_3-O_2 and NH_3-O_2-N_2 flames burning at atmospheric pressure. Concentrations of species were determined by absorption spectroscopy. The data show that in this region of the flames NH_2, NH, and NH_3 are maintained in partial equilibrium via reactions with OH and H-atoms. This behavior was observed for both rich and lean mixtures. In addition, Kaskan and Hughes indicate that the decay of NO observed in their lean flame, which contrary to the authors, is consistent with the data of MacLean and Wagner (1967) although larger, is consistent with a reaction of NO with NH or NH_2. A similar mechanism was proposed by Fisher to explain the leveling off of the NH_i concentrations he observed for fuel-rich flames. However, the amount of NO required to account for the behavior of NH_i species was inconsistent with his data since NO could not be measured with his optical system and the levels required would have been observable. It should be noted that according to Piper (1979), the concentrations of OH obtained in these studies are overestimated by 50 percent, which also affects NH and NH_2 concentrations reported because of the manner in which these species levels were determined. This will have a direct impact on the arguments developed by Kaskan and Hughes (1973) concerning the rate constants for reaction of NO with NH and NH_2. An additional error for relative NH_i concentrations is also introduced in these two studies because the value used for the heat of formation for the NH radical is too high (Piper, 1979).

The final sets of data which were considered are those reported by Lyon, Hardy, and Benn (1978) and Lyon and Benn (1979) for the NH_3-O_2-He and NH_3-NO-O_2-He systems, respectively, at temperatures between 1145 and 1350°K. Lyon et al observed a relatively rapid production of NO during the induction period of the NH_3-O_2 system, which is consistent with shock tube data. It was also observed that some critical amount of H_2, produced during this period, was necessary before the start of the chain reaction. Nitric oxide was a minor product regardless of the amount of NH_3 which was oxidized. Both studies showed that the presence of NO in the reactants greatly accelerated the rate at which NH_3 was oxidized. In addition, Lyon and Benn (1979) indicate that as the NH_3 concentration approached that of O_2, the extent of NO reduction occurring during a given reaction time decreased from a near-quantitative removal of NO to little or no reduction. A mechanism was discussed which qualitatively explained the observed behavior. The main feature is that the increased rate of NH_3 consumption is due to an increased production of free radicals which, in what obviously must be considered a global process, was represented as:

$$NH_2 + NO \rightarrow N_2 + H + OH \tag{5.1}$$

$$NH_2 + NO \rightarrow N_2 + H_2O \tag{5.2}$$

For a self-sustaining chain reaction to occur, Lyon and Benn (1979) indicate that between 25 and 50 percent of the total reaction of NH_2 with NO must occur via equation 5.1. It is of interest that the synergistic effect of oxidants reported by these investigators was also observed by Armitage and Gray (1965), who found that burning velocities were higher and flammability limits wider when NH_3 was oxidized with mixtures of N_2O and NO than was observed at the same NH_3-to-oxygen ratio when only N_2O or NO was used as the oxidant.

The ammonia oxidation reaction mechanism (Table 5.1) was used in an initial series of calculations to determine to what extent the model was capable of reproducing phenomena observed in the shock-initiated combustion of NH_3-O_2-Ar mixtures. Since Drummond (1972) found little variation in the induction period correlation for pressures between 0.2 and 45 atmospheres with fuel-lean mixtures, it was considered reasonable to use atmospheric pressure for all simulations. In addition, the initial reactant concentrations were chosen to be representative of his mixtures ($NH_3/O_2/Ar$ = 2/2/96) and temperatures were varied between 1500 and 1950°K. Adiabatic combustion of the gases was assumed to occur. The calculated induction delay times were again based on the time at which 10 percent of the initial NH_3 was consumed. Results within 5 percent of these values were obtained by extrapolating the tangent to the point of maximum NH_3 destruction back to the time axis.

The results of these calculations are compared with data reported by Drummond (1972), Bull (1968), and Takayama and Miyama (1967) in Figure 5-1.

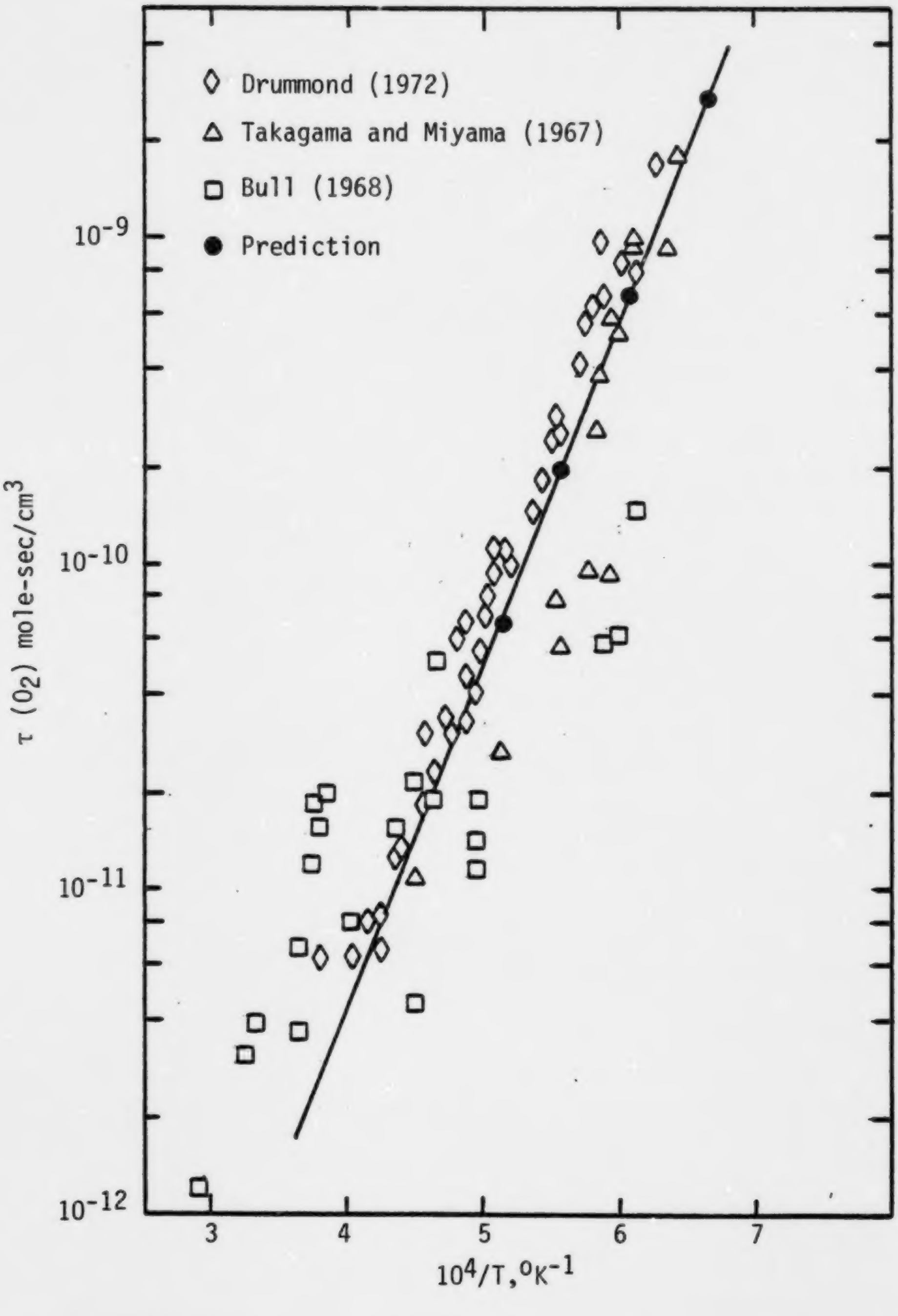

Figure 5-1. Induction time correlation for lean NH_3-O_2-Ar mixture.

Excellent agreement is observed both with regard to absolute values and the temperature dependence of the correlation, which for the simulations is given by:

$$\tau\ (O_2) = 3.20 \times 10^{-16} \exp(47550/RT),\ \text{mole-sec/cm}^3$$

This prediction is in excellent accord with the results of Drummond (1972). The scatter in data reported by Bull (1968) and Takayama and Miyama (1967) explains the lower "activation energies" which they derived for the induction delay correlation.

A detailed examination of the production rates of various radicals during the intermediate phase of the induction period shows that the dominant reaction paths are:

$NH_3 + OH = NH_2 + H_2O$ (129)

$NH_2 + O_2 = NHO + OH$ (138)

$HNO + M = H + NO + M$ (127)

$H + O_2 = OH + O$ (6)

Reactions 138 and the reverse of 127 provide a path which rapidly yields both H and OH. Atomic hydrogen then reacts with O_2 via reaction 6 to produce O and OH. The NH_2 radical is regenerated via reaction 129 which is the major consumption path for NH_3 in this phase of the induction period. It should be noted that it was impossible to obtain induction delay times in agreement with the data if the products of reaction 138 were assumed to be NH and HO_2.

As the concentration of radicals grows, the rate at which NH_3 is oxidized increases and radical-radical reactions start to contribute significantly to the overall production of reactive species via:

$NH_2 + O = HNO + H$ (132)

$NH_2 + O = NH + OH$ (133)

$NH_2 + OH = NH + H_2O$ (134)

$NH + O_2 = HNO + O$ (141)

The HNO produced in reactions 132 and 141, in part decomposes via the reverse of reaction 127 and reacts with H, O, and OH to yield NO, H_2, OH, and H_2O (reactions 162 through 164). The reactions of NH_2 with NO (reactions 168 through 170) have a relatively minor impact on the predicted induction delay time. If the total rate of reaction yields N_2 and H_2O as products, or if it is assumed that N_2, H, and OH are the only products, the calculated induction delays vary by about 10 percent in absolute value at each temperature.

The reaction mechanism quantitatively describes the experimental measurements of induction periods in fuel-lean, dilute NH_3-O_2-Ar mixtures, as a function of temperature. The observations that NO and OH are both present during this time interval and that these species have essentially identical induction periods are accounted for by reaction 138 followed by the reverse of 127, or in the later phase of the induction period, by reactions 138, 132, and 141 followed by 127 and 162 through 164. Of course, other reactions contribute to NO formation in the last stage of the induction period--reactions 144, 147, and 148. Nitrous oxide production in the early phase of the induction period is the result of reaction 168. Formation of H_2O is accelerated as the NH concentration increases since the rate coefficient for reaction 167 is about five orders-of-magnitude larger than k_{168} in the temperature interval 1000 to 2500 K. These results confirm the analysis of the NH_3 oxidation mechanism reported by Bradley et al (1968) and Husain and Norrish (1963), i.e., that oxidation occurs via a degenerative, chain-branching mechanism.

The reaction mechanism was next tested against data reported by Miyama and Endoh (1967) on shock-initiated combustion of NH_3-air mixtures in the temperature range 1400 to 2100 K, and for stoichiometric ratios between 0.25 and 4.0; i.e., 6.5 to 52.5 percent NH_3 in reactants. These data were examined to determine whether the reaction mechanism was still accurate at higher NH_3 concentrations more typical of the flame studies which were to be included in the validation of the reaction mechanism. Miyama and Endoh (1967) correlated the induction delay times as:

$$\tau\,(O_2) = (3.55^{+1.95}_{-1.26}) \times 10^{-18} \exp[(59480 \pm 1370)/RT], \quad \text{mole-sec/cm}^3$$

This expression yields significantly shorter induction times above 1400 K than the correlation of the results for the NH_3-O_2-Ar mixtures, and longer induction delays at lower temperatures. The reaction mechanism failed to reproduce the majority of the data since no significant oxidation of NH_3 occurred even after reaction times which were a factor of five longer than the expected induction period for mixtures with initial NH_3 concentrations greater than 10 percent of the reactants.

Consideration of the dominant reaction paths for radical formation at low NH_3 concentration indicates that the major sink for H-atoms was reaction 6 which produces O and OH. Reaction with OH radicals was the most significant path for consumption of NH_3. However, at higher NH_3 concentrations reaction 128 may compete effectively with reaction 6 for H-atoms and, therefore, decrease the rate of radical growth:

$$NH_3 + H = NH_2 + H_2 \tag{128}$$

$$H + O_2 = OH + O \tag{6}$$

If this were the case, then the calculations would suggest that k_{128} is too high. However, recent data reported by Demissy and Lesclaux (1980) and Yumura et al (1980) indicate that k_{128} is actually low and is better represented for temperatures between 350 and 3000°K by:

$$k_{128} = 4.89 \times 10^{10}\ T^{0.75}\ \exp(-11925/RT), \quad cm^3/mole\text{-}sec$$

Another possibility is that the rate of NH_3 decomposition (reaction 120) is too slow as a result of assuming that the chaperon efficiencies of NH_3 and N_2 are the same as argon. Unfortunately, there is apparently no information in the literature which addresses this point directly, although data reported by Lozovskii et al (1979) and Khe, Soulignae, and Lesclaux (1977) for the recombination of NH_2 to yield hydrazine show relative chaperon efficiencies for NH_3:N_2:Ar to 10:2.5:1. If similar values are applicable to NH_3 decomposition, then the rate constant and equal chaperon efficiencies used underestimate the initial decomposition rate of NH_3 by a factor of 3.4 at 11.5 percent NH_3 in the reactants, and by a factor of 4.2 at 22.5 percent

NH_3 in the reactants. This is speculative until data become available for NH_3 decomposition in various bath gases.

By analogy with the CH_4 system at high initial concentrations, it is reasonable to suggest that reaction between NH_i radicals and reactions of fuel radicals with NH_3 may be more important at the conditions used by Miyama and Endoh (1967). If it can be shown that a subset of the NH_3 reaction mechanism accurately describes pyrolysis of NH_3, then the discrepancy observed must be due to one or more reactions of NH_3, NH_2, NH, and N-atoms with oxygen-containing species. This question was addressed by comparing predictions with data reported by Dove and Nip (1979) for the high temperature pyrolysis of NH_3 and NH_3-H_2 mixtures diluted with krypton.

These authors used mass spectrometry to measure NH_3, NH_2, NH, and N_2 profiles behind reflected shock waves at temperatures between 2500 K. Measurements of the time-dependent NH_3 and N_2 concentrations used argon as an internal standard in the mass spectrometer. It was assumed that the sensitivity of the mass spectrometer to NH_2 and NH was identical to the sensitivity to NH_3, which probably results in underestimation of the concentrations of these radicals. (Dove and Nip estimate a factor of 2 for NH and a factor of 5 for NH_2.) Due to the uncertainties in the values reported for these species, comparisons with N_2 profiles were used to assess the NH_3 pyrolysis mechanism.

The results of the simulation, which assumed adiabatic conditions at the initial temperature and pressure given by Dove and Nip (1979), are shown in Figures 5-2a and 5-2b. Argon is the diluent for the detailed kinetic calculations, which is justified on the basis that the rate constant reported by these investigators for reaction 120, if compared to the data of Roose et al (1979) and Yumura et al (1980), indicates identical chaperon efficiencies for argon and krypton. It is immediately apparent that the reaction subset describing NH_3 pyrolysis is inadequate. Molecular nitrogen is produced less rapidly than observed and the final values are a factor of 2 to 5 lower than measured. If it is assumed that the analysis of Dove and Nip (1979) is correct, which shows that a major path for N_2 production is via

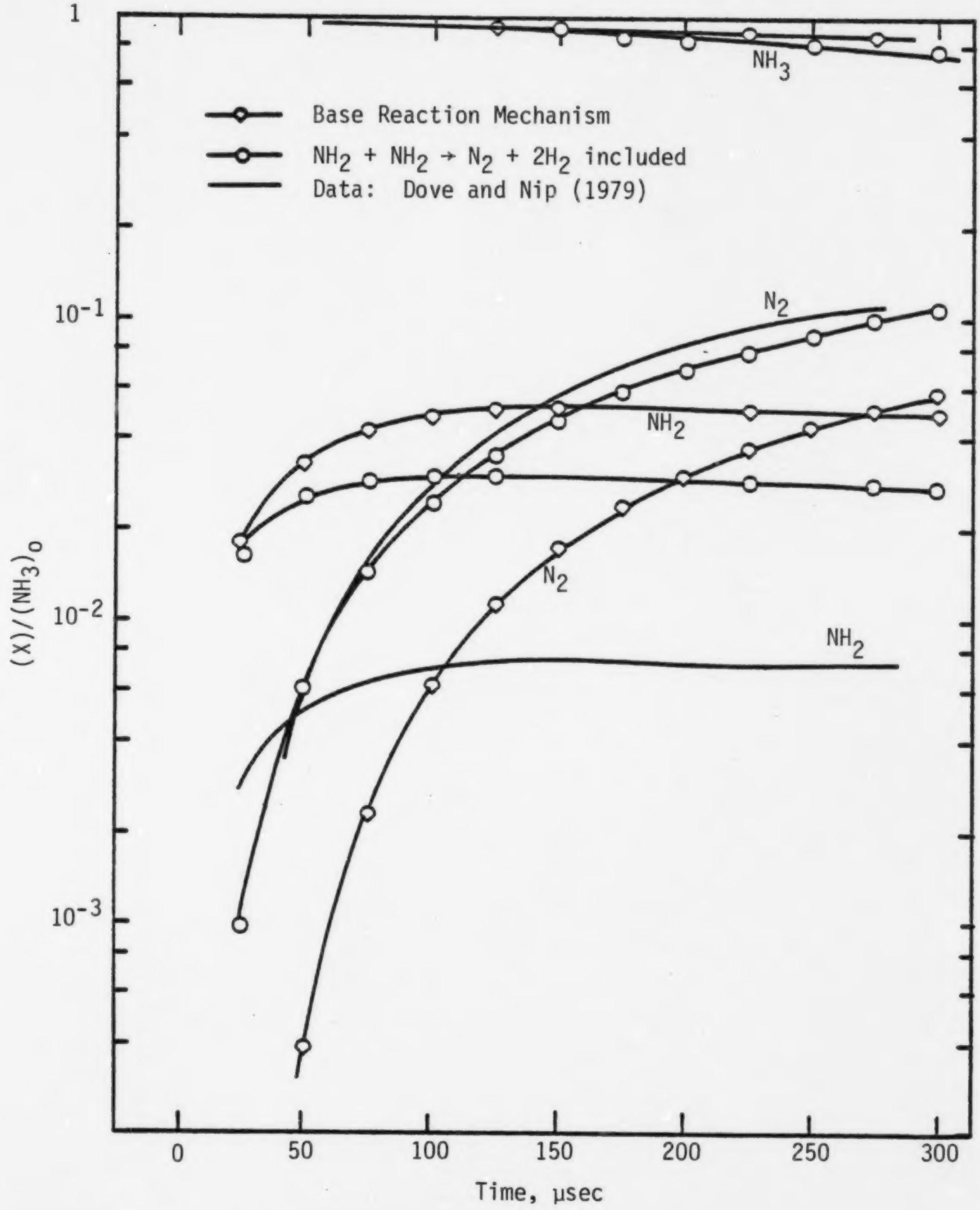

Figure 5-2a. Pyrolysis of NH_3: 6.1 percent NH_3 + 5.8 percent H_2 + Ar; 0.363 atm; 2685°K.

103

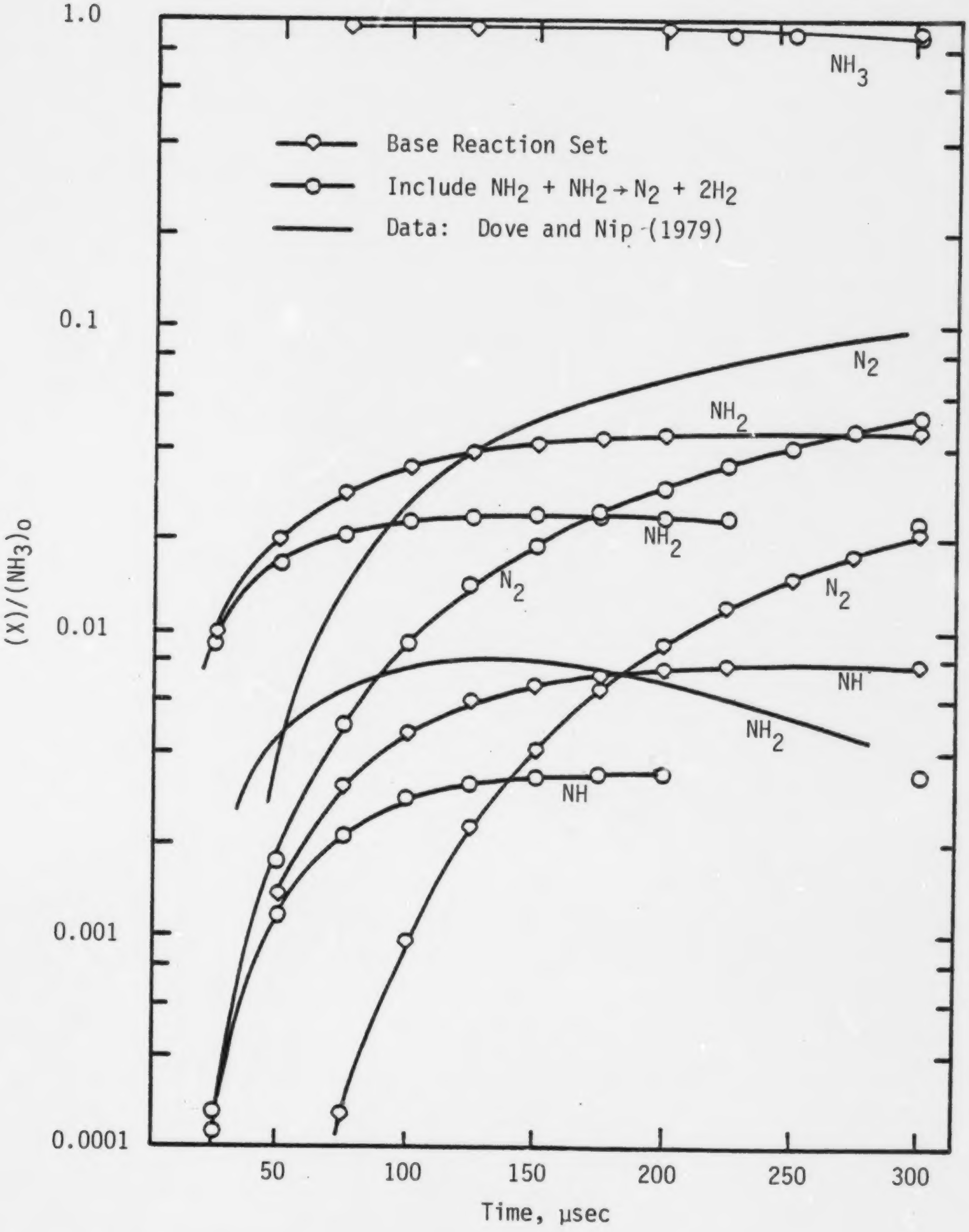

Figure 5-2b. Pyrolysis of NH_3: 6.2 Percent NH_3 in Ar, 0.309 atm, 2511°K.

reaction of NH_2 with itself or with NH_3, then a substantial improvement may be achieved by introducing the global step (Dove and Nip, 1979):

$$NH_2 + NH_2 \rightarrow N_2 + 2H_2$$

$$k = 4 \times 10^{13} \exp(-12000/RT)$$

For this rate constant (Michel, 1965), the products of reaction should be N_2H_2 and H_2; it is assumed that diimide decomposes rapidly to produce nitrogen and hydrogen. Inclusion of this global process also improves the qualitative agreement with NH and NH_2 profiles (see Figure 5.2).

These results suggest that part of the difficulty associated with simulating the data of Miyama and Endoh (1967) is caused by inaccuracies in the reaction mechanism with regard to pyrolysis of NH_3. Apparently there is a rapid sequence of reaction steps producing N_2, which is not included in the mechanism given in Table 5.1. The experimental observation that this path is initiated by reaction of NH_2 with NH_2 or NH_3, and the improvement obtained when the global step was added to the mechanism suggest that additional species (N_2H_i) are required. A preliminary mechanism describing the production and destruction of N_2H, N_2H_2, N_2H_3, and N_2H_4 is given in Table 5-2. Additional calculations are necessary to test the impact of these reaction paths on the oxidation of NH_3 at high initial concentrations. By analogy with CH_4, it might also be expected that these reactions will be important at low NH_3 concentrations for low-temperature oxidation. It should be noted that a preliminary simulation of fuel-rich NH_3 flame data reported by Fenimore and Jones (1961) required the inclusion of the global step above to have a stable flame.

The final question which needs to be addressed in this discussion is the reduction of NO to molecular nitrogen by reaction with NH and NH_2 radicals, which are:

$$NH + NO = N_2O + H \qquad (167)$$

$$NH_2 + NO = N_2O + H_2 \qquad (168)$$

Table 5-2. Reactions for N_2H_i Species

No.	Reaction	ΔH^0_r, 298 kcal/mole	A	b	E kcal/mole	Reference
171	$NH_2 + NH_2 = N_2H_4$	-68.1	1.5 (13)	0.	0.	Khe et al., 1977
172	$NH + NH_2 = N_2H_3$	-81.6	7. (13)	0.	0.	Pagsbert et al., 1979
173	$H + N_2H_4 = N_2H_3 + H_2$	-26.9	1.3 (13)	0.	2.5	Gehring et al., 1971
174	$N_2H_3 + H = NH_2 + NH_2$	-9.2	1.6 (12)	0.	0.	Gehring et al., 1971
175	$N_2H_3 + H = N_2H_2 + H_2$	-50.2	1. (11)	0.	0.	Est. This Study
176	$H + N_2H_4 = NH_2 + NH_3$	-40.5	1. (13)	0.	7.0	Eberstein & Glassman, 1965
177	$NH_2 + N_2H_4 = N_2H_3 + NH_3$	-31.3	2. (13)	0.	2.5	Est. This Study
178	$NH_2 + N_2H_3 = N_2H_2 + NH_3$	-54.5	2. (12)	0.	0.	Peterson, 1974
179	$NH_2 + NH_2 = N_2H_2 + H_2$	-41.0	3.98 (13)	0.	12.	Michel, 1965
180	$N_2H_2 + M = N_2H + H + M$	82.2	4. (15)	0.	80.	Michel & Wagner, 1965
181	$N_2H_3 + M = N_2H_2 + H + M$	54.0	1. (14)	0.	54.	Est. This Study
182	$N_2H_4 + O = N_2H_2 + H_2O$	-90.3	6.3 (13)	0.	1.2	Cehring et al., 1973
183	$N_2H_4 + OH = N_2H_3 + H_2O$	-42.1	3.7 (13)	0.	0.	Harris, Atkinson & Pitts, 1979

Forward rate constants expressed as $k_i = AT^b \exp(-E/RT)$ in units of cm^3, mole, sec. $k_{1.171}$ is for N_2 as third body; relative chaperon efficiencies for NH_3:N_2:Ar are 4:1:0.4. $k_{1.172}$ is for Ar as dominant third body. Reactions for N_2H radical are given in Table 1-17. Heats of formation for N_2H_4, N_2H_3, N_2H_2 and N_2H were 22.9, 48.1, 50., and 80.1 kcal/mole, respectively (Dove and Nip, 1979).

$NH_2 + NO = N_2 + H_2O$ (169)

$NH_2 + NO = N_2 + H + OH$ (170)

Reaction products for reactions 169 and 170 were based on the arguments given by Lyon and Benn (1979), which indicated that it was necessary to produce radicals via the reaction of NH_2 and NO, but that in part, the step must be chain-terminating. The temperature dependence of these reactions was based on the data of Hack et al (1979) with the total rate of NO removal and the branching ratio ($k_{170}/k_{169} + k_{170}) = 0.368$) adjusted to match data reported by Lyon (1975). These two reactions should be interpreted as global steps which are strictly applicable only in a narrow temperature range. Reaction 168 was included in the mechanism since Roose et al (1977) found it necessary to explain the early formation of N_2O in the high temperature oxidation of NH_3 by NO. Reaction 167 was considered because of the observations in shock tube and flame studies of NH_3 oxidation cited earlier. The rate coefficient was based on room temperature data (see Hanson et al , 1976, and references therein) with a temperature dependence based on that observed for the isoelectronic reaction of CH_2 with NO (Vinckier and Debruyn, 1979). A comparison with the value for k_{167} reported by Kaskan and Hughes (1973), which was high by a factor of 2.25 due to an error in OH and, subsequently, NH concentration, at 2010°K, indicates good agreement (1.07×10^{12} cm^3/mole-sec versus 1.28×10^{12} cm^3/mole-sec calculated from k_{167} given in Table 5-1) after correction of the NH concentration.

The nonelementary nature of reactions 169 and 170 and perhaps 168 is disturbing since it is not known *a priori* whether the rate constants assigned will correctly describe the global processes of chain-branching and chain-termination at temperatures other than those used to set the preexponential factors. In fact, preliminary simulations of data reported by Duxbury and Pratt (1975) for shock-initiated oxidation of NH_3-NO-Ar mixtures indicate that the rate coefficients for reactions 169 and 170 will not reproduce the temperature dependence nor absolute values of the measured induction delay times. An alternative mechanism involving elementary steps has been suggested by Branch, Miller, and Kee (1979) which accounts for the observations of Lyon et al (1979) with regard to chain-branching and chain-termination. The most important feature of their model is the reaction sequence:

$$NH_2 + NO = N_2H + OH \qquad (184)$$

$$N_2H + NO = N_2 + HNO \qquad (195)$$

$$HNO + M = H + NO + M \qquad (127)$$

This is obviously equivalent to the overall step reaction 130. Chain-termination to produce H_2O and N_2 is accounted for by a rapid reaction of OH with N_2H. The mechanism is reproduced by Table 5-3.

The arguments used by Branch et al (1979) center on the negative temperature coefficient for reaction of NH_2 with NO observed by Hack et al (1979) and the necessity to provide a logical explanation for the enhanced radical growth when NO is added to NH_3-O_2-diluent mixtures. Branch et al (1979) note that the negative temperature dependence results from the fact that long-range attractive forces between the reactants are inhibited from forming an intermediate complex at high collision energies, and that it is essential that the formation of products has no significant net energy barrier. The authors argue that the potential energy drop in going from reactants to the complex, which is estimated to be at least 20 kcal/mole, may cancel out the energy barrier to formation of the products from the complex which results in no net energy barrier.

A straightforward analysis of the Branch et al (1979) mechanism which assumes quasi-steady-state conditions for N_2H, HN_2O, and HNO, shows that the rate of N_2 formation is governed only by the concentration of NH_2 and NO and the rate coefficient used for reaction 184 for temperatures between 1000 and 1700 K. The only additional assumption necessary is that the sum of the concentrations of H, O, and OH be greater than 100 ppmV and that the concentration of NO be less than 5 percent by volume. The rates of N_2O and H_2O formation are changed to an extent which can only be quantified by detailed calculations. The validity of the alternate mechanism and the associated rate coefficients for a broad range of conditions--high temperature shock tube data for NH_3-NO, NH_3-O_2, NH_3-N_2O, and NH_3-air mixtures; fuel-rich and

Table 5-3. Reaction of NH_2 With NO According to Branch et al., 1979

No.	Reaction	A	b	E kcal/mole
184	$NH_2 + NO = N_2H + OH$	3.7 (17)	-1.85	0.
185	$NH_2 + NO = HN_2O + H$	2.0 (11)	0.	10.
186	$HN_2O + H = N_2O + H_2$	2.0 (13)	0.	0.
187	$HN_2O + O = N_2O + OH$	2.0 (13)	0.	0.
188	$HN_2O + OH = N_2O + H_2O$	2.0 (13)	0.	0.
189	$HN_2O + OH = N_2H + H_2O$	1.0 (13)	0.	0.
190	$HN_2O + H = N_2H + OH$	1.0 (13)	0.	0.
191	$HN_1O + O = N_1H + O$	1.0 (13)	0.	0.
192	$HNO + NO = HN_2O + O$	2.0 (12)	0.	27.
193	$HN_2O + NO = HNO + N_2O$	2.0 (12)	0.	15.
194	$N_2H + NO = N_2 + HNO$	6.0 (12)	0.	3.5
195	$H_2N + H = N_2 + H_2$	3.7 (13)	0.	3.0
196	$N_2H + O = N_2 + OH$	1.0 (13)	0.	0.
197	$N_2H + OH = N_2 + H_2O$	1.5 (13)	0.	0.
198	$N_2H + O = N_2O + H$	5.0 (13)	0.	13.

Forward rate coefficients as $k_i = AT^b \exp(-E/RT)$ in units of cm^3, mole and sec. Thermochemistry of species not specified.

fuel-lean flame data, etc.--must be checked via detailed kinetic calculations which is hindered to a certain degree by the lack of accurate thermochemical data for the additional species considered.

In summary, the NH_3 oxidation reaction mechanism has been shown to accurately reproduce induction delay times for dilute, fuel-lean NH_3-O_2-Ar mixtures for temperatures between 1500 and 2500 K. Simulations of shock-initiated combustion of NH_3-air data, and subsequent studies of ammonia pyrolysis, suggest that the NH_3 pyrolysis reaction mechanism is incomplete. Additional reaction paths which produce and destroy N_2H_i species appear to be required to explain in detail the behavior of NH_3 oxidation at high initial reactant concentrations. It is further suggested that in order to extend the region of applicability for the NH_3 reaction mechanism, the alternate reaction mechanism describing the reduction of NO to molecular nitrogen via reaction with NH_2 proposed by Branch et al (1979) be extensively tested to determine whether a significant improvement in the predicted behavior of NH_3-oxidant combustion systems is obtained. Additional simulations are obviously necessary to investigate the impact of the above modifications on the ability to accurately model the oxidation and pyrolysis of NH_3. A primary goal will be to determine whether increased complexity of the reaction model is necessary for combustion systems in which NH_3 is a trace and not a major species.

5.2 HCN Reactions

At the present time the HCN reaction mechanism shown in Table 5-4 has not been extensively tested. A few simulations, reported in the following section, have been performed utilizing the entire mechanism for hydrocarbon combustion with fuel nitrogen. Thus, a major task for completion of this study is the verification of the HCN set. The discussion in Section 5.0 indicates how important these HCN steps are to the overall fuel nitrogen chemistry since fuel nitrogen from complex organic molecules is pyrolyzed principally into HCN in the early stages of combustion. The testing of the proposed HCN mechanism has been delayed due to the unavailability of suitable data for simulation. These data have recently appeared (Fenimore, 1979) so the verification process can begin.

Table 5-4. HCN Reactions

No.	Reaction	$\Delta H^0_{r,298}$ kcal/mole	A	b	E kcal/mole
199	$HCN + M = CN + H + M$	123.8	5.7 (16)	0.	117.
200	$HCN + O = H + NCO$	-1.76	1.3 (11)	.5	6.81
201	$HCN + O = CH + NO$	71.72	1. (14)	0.	72.
202	$HCN + OH = CN + H_2O$	4.41	2. (11)	.5	5.
203	$HCN + OH = HNCO + H$	5.62	2. (10)	.5	5.62
204	$HCN + N = CH + N_2$	-3.3	2.5 (11)	0.	16.
205	$CN + O = CO + N$	-76.96	6.3 (11)	.5	0.
206	$CN + OH = NCO + H$	-23.39	6.2 (13)	0.	0.
207	$CN + OH = HCN + O$	-21.63	3.2 (12)	0.	3.
208	$CN + O_2 = NCO + O$	-6.44	3.2 (13)	0.	1.
209	$CN + H_2 = HCN + H$	-19.6	6.2 (12)	0.	5.3
210	$CN + CO_2 = NCO + CO$	1.64	4. (11)	.5	7.
211	$CN + NH_2 = HCN + NH$	-33.	5. (10)	.7	2.
212	$CN + NH_3 = HCN + NH_2$	-15.23	7. (10)	.7	2.
213	$NCO + O = NO + CO$	-102.39	5. (11)	.5	6.86
214	$NCO + H = NH + CO$	-32.32	5. (11)	.5	6.86
215	$NCO + H_2 = HNCO + H$	-101.98	3. (10)	.5	5.7
216	$NCO + NH_2 = NH + HNCO$	-23.6	1. (11)	.5	5.
217	$HNCO + OH = NCO + H_2O$	-4.99	1. (11)	.5	6.29
218	$HNCO + H = NH_2 + CO$	-8.72	5. (11)	.5	4.83
219	$CH_4 + CN = CH_3 + HCN$	-18.98	3.2 (11)	.7	5.
220	$CH_3 + CN = CH_2 + HCN$	-14.17	1. (11)	.7	3.
221	$CH_2 + NO = CH_2O + N$	-26.88	1.6 (12)	0.	7.
222	$CH_2 + N_2 = HCN + NH$	24.15	1. (14)	0.	60.
223	$CH + N = CN + H$	-98.9	6.3 (11)	.5	0.
224	$CHO + N = CH + NO$	41.58	1. (14)	0.	48.6
225	$CHO + N = HCN + O$	-30.14	1. (14)	0.	0.

Rate coefficients expressed as $k_f = AT^b \exp(-E/RT)$ in units of cm^3, mole and sec. M refers to total density and numbers in parentheses to powers-of-ten.

5.3 Fuel Nitrogen in Hydrocarbon Flames

The final test of the gas-phase mechanism was its ability to reproduce data from nitrogen-seeded hydrocarbon flames. The literature does not contain a large number of these data (a notable exception is de Soete (1975) who reports flat-flame species profiles for various hydrocarbon fuels seeded with NH_3, HCN, and C_2N_2). For this reason it was necessary to independently generate such a data base. The work at Exxon (Appendix B of this volume) was designed to generate some of the required data.

The objective of this brief set of simulations was to see how closely the full mechanism predicted actual data. These simulations lie outside the normal development methodology because the nitrogen subsets used have not been verified (i.e., the NH_3 subset has not yet yielded completely satisfactory shock tube and flame results, and the HCN subset has not been tested in its present form).

A series of five stirred reactor simulations were obtained for the following conditions: T = 1900 K, τ = 3 msec, NH_3 input = 750 ppm, and fuel/air equivalence ratio = 0.80, 0.97, 1.20, 1.40, and 1.80. The 1.4 and 1.8 equivalence ratio cases were rerun with the C_2 chemistry set included.

The results of the comparison are shown in Figure 5-3a for stable species and 5-3b for nitrogenous species. The quality of the stable species prediction is in general excellent. However, O_2 is underpredicted at fuel-rich conditions. Surprisingly, including the C_2 chemistry steps markedly improves the O_2 prediction. The agreement between model and data indicates that the general combustion is effectively predicted by the mechanism.

The results for the nitrogenous species, Figure 4.3b, do not show good agreement. However, some aspects are well-predicted. The behavior of NO at lean conditions and the behavior of the sum of fixed nitrogen (ΣXN) (particularly the location of minimum ΣXN and its absolute value) are well-correlated by the model. The details of the speciation are poorly predicted at very fuel-rich conditions, particularly in the region of "hydrocarbon breakthrough."

These results indicate that the NH_3 and HCN reaction sets require further work, as noted in previous sections, before they can be incorporated into the full reaction set.

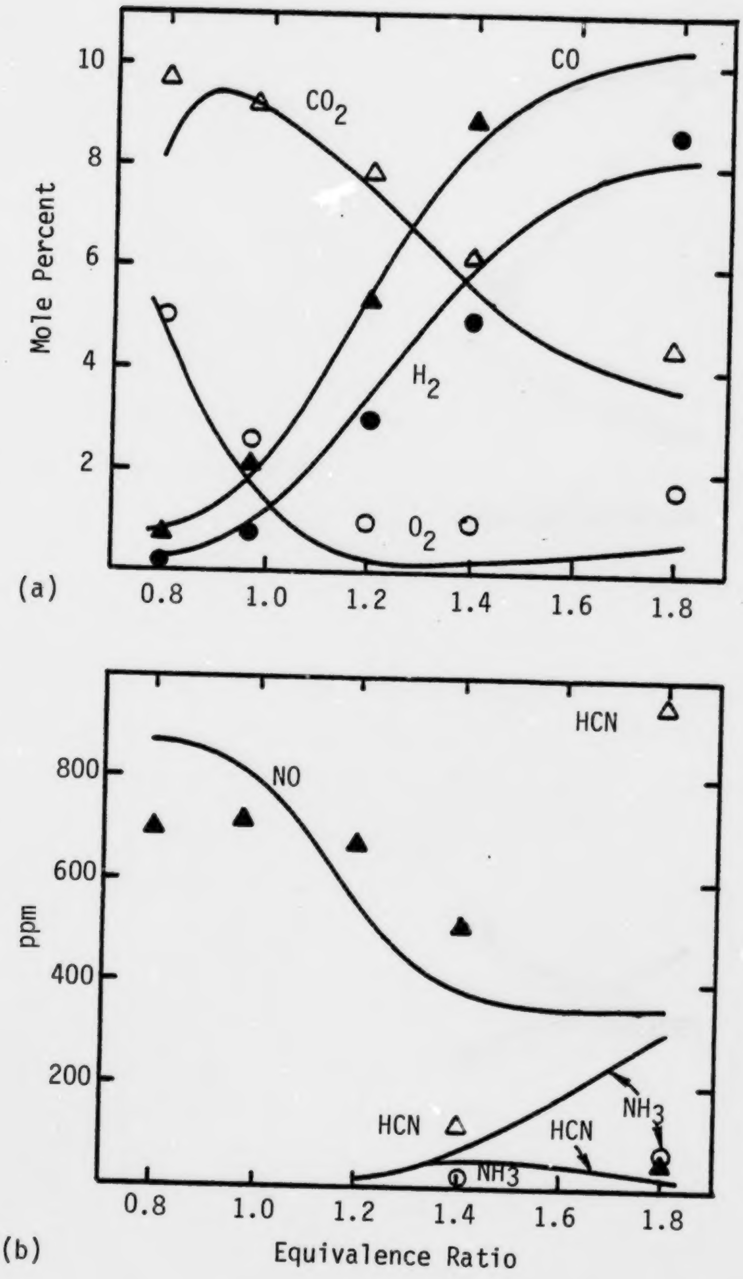

Figure 5-3. Stirred reactor species as a function of equivalence ratio (Blair, 1980). Conditions were CH_4-air combustion at 1900 K, and 3 msec residence time with 750 ppm added NH_3.

6.0 SUMMARY AND CONCLUSIONS

This report reviews the progress on the development of an elementary gas-phase mechanism for describing combustion reactions of hydrocarbons--through C_2 structure--and the fate of fuel nitrogen (including the compounds HCN, NH_3, NO and respective intermediates). Because of the active research in this area, this development is of necessity an evolutionary process. As rate data are updated particularly for hot, rich conditions and as new reaction pathways are discovered, they must be incorporated into the mechanism. However, the incorporation process must follow a methodology which stipulates that the additions are both necessary and consistent with the verified mechanism. The evolutionary nature of the mechanism is also caused by the continuing generation of experimental data for verification. Key parts of the mechanism have not been verified due exclusively to the lack of high quality experimental data at conditions of interest for modeling fuel nitrogen conversion in hydrocarbon flames. As such become available, it should be carefully modeled with the reaction set to determine the limitations of the set and identify those areas which require further work.

6.1 Mechanism Status

The mechanism identified at this point in time is composed of the subsets listed in the following tables:

H_2-O_2 Reactions--Table 3-1

CO-H_2-O_2 Reactions--Table 3-2

CH_2O-O_2 Reactions--Table 4-1

C_1 Hydrocarbon Reactions--Table 4-2

C_2 Hydrocarbon Reactions--Table 4-3

C_2H_2-O_2 Reactions--Table 4-4

C_2H_6-O_2 Reactions--Table 4-5

C_2H_4-O_2 Reactions--Table 4-6

Reactions Between Hydrocarbon Species--Table 4-7

Reactions Between Polyacetylene--Table 4-8

Ketene (CH_2CO) Reactions--Table 4-11

Reactions Describing NH_3 Oxidation--Table 5-1

Reactions for N_2H_i Species--Table 5-2

HCN Reactions--Table 5-4

Each of the subsets have been compiled and tested, but not all sets have been completely verified by the development methodology. The status of each subset is summarized in the following sections.

The Hydrogen/Oxygen System

The hydrogen/oxygen system has been studied by many workers, most notable of which include Dixon-Lewis at Leeds University (Dixon-Lewis, 1979). The reaction mechanism proposed for hydrogen oxidation has been demonstrated to accurately predict both induction periods and flame phenomena. Comparisons with shock tube data for hydrogen/oxygen/argon and hydrogen/air mixtures near 1000 K established a rate coefficient for the reaction $H + O_2 + M = HO_2 + M$, which was consistent with the other rate coefficients in the mechanism. Although the calculated burning velocities were significantly lower than the most recent data reported by Gunther and Janisch (1972) and Edmondson and Heap (1971), they are in agreement with Dixon-Lewis' correction to account for variations in conical flames from true one-dimensionality. The reaction mechanism has also been shown capable of predicting stable species profiles and temperature profiles for a low temperature, fuel-rich H_2-O_2-N_2 flat flame. The predicted H_2 profile was less steep than that observed, and this could be attributed to the fact that thermal diffusion was not included in the flame model. However, the congruence of predicted and measured at temperature profiles indicates that the mechanism accurately predicts heat release rates.

Analysis of the results for the flat flame simulations showed that production of HO_2 and its subsequent destruction at low temperature constituted the dominant heat-release cycle. The radicals which participate in this cycle are generated in the hotter region of the flame by chain-branching mechanisms. They then diffuse upstream to react with molecular oxygen. The hydroperoxal radical is, therefore, an important species in determining the structure of hydrogen flames, as well as induction phenomena for hydrogen/oxygen mixtures.

The Carbon Monoxide/Hydrogen/Oxygen Set

Shock tube simulations indicated that at temperatures above 2000 K the rate coefficients used for the reaction $CO + OH = CO_2 + H$ are too low. Simulation with the mechanism yield two main results. First, the HCO radical must be included to accurately reproduce the flame speed of fuel-rich CO/air flames. This result is surprising since very small concentrations of HCO are calculated by the mechanism. Second, quantitative comparisons with measured flame speeds are not possible due to uncertainties regarding experimental techniques, or the concentration of hydrogen-containing compounds in the initial gas mixtures. The calculations indicate that the burning velocity data reported for dry CO mixtures by Gunther and Janisch (1972) are consistent with predicted values with less than 500 ppm volume hydrogen or hydrocarbon in the reactants. It is also possible that the disparity between predicted and measured burning velocity is due to the exclusion of reactions producing nitrogen oxide in the mechanism.

The Hydrocarbon Set

Formaldehyde is well-known intermediate in the oxidation of hydrocarbons, especially methane. Therefore, it is of interest to examine the kinetics of CH_2O oxidation and pyrolysis in the absence of other hydrocarbon species. Establishing a reaction mechanism which accurately describes the consumption of CH_2O over a broad range of temperatures and stoichiometries removes a major uncertainty in other hydrocarbon combustion mechanisms. Attention can then be focused on the elementary steps which control formaldehyde production during the oxidation of a simple hydrocarbon fuel such as methane, acetylene, ethylene, and ethane. The formaldehyde, methane, and C_2 chemistry subelements of the overall mechanism were tested extensively against shock tube data to establish the need and the conditions necessary to augment the C_1 set with C_2 chemistry.

The current state of the mechanism is best described by reference to attempts to simulate methane flame phenomena. The modeling of flame phenomena is a relatively stringent test of the capabilities of a kinetic mechanism. The powerful coupling between reaction rates and energy release/temperature serve to identify mechanistic errors which may be overlooked in more global comparisons. Advantages of flame comparisons are somewhat offset by the increased complexity of the simulation, since not only the adequacy of the kinetic mechanism is tested, but also the flame physics. However, attempts to match detailed temperature and species profiles through the flame front provide a detailed test of the mechanism. In particular, errors in the portion of the mechanism which deal with minor species will be revealed. While these errors may not impact global comparisons, they may have a significant impact on the formation of pollutants in flames. In general, the results show encouraging agreement. However, two points should be noted:

- The rate-limiting step leading to CO formation from the hydrocarbon pool appears to be too slow.
- The rate of oxidation of CO to CO_2 is too slow at higher temperatures. This is consistent with a known Arrhenius behavior of the reaction CO + OH at elevated temperatures.

Biordi et al (1975) studied a stoichiometric (10.3 percent methane, 21.6 percent oxygen and 68.1 percent argon) flame at 32 torr with an initial velocity of 80 cm/sec. Simulation of this experiment yielded a free-flame velocity of 76.2 cm/sec, agreeing very well with the experimental value. Comparisons of stable species calculated with the current mechanism with those measured by Borgdi et al indicates that the principal deviation is an under-prediction of the oxidation rate of CO to CO_2. The comparison between measurement and prediction for the radical species is less satisfactory. While the model OH profile shows fair agreement with the data, both O and OH are approximately 50 percent below the data. Again, the results indicate that pyrolysis is occurring too slowly in the model.

The data of Harvey and McColl (1979) provide a third opportunity to compare the mechanism with experiment. Temperature and concentration profiles were obtained for a stoichiometric methane/oxygen flame diluted with 43 percent argon. The cold gas velocity was 119 cm/sec and the flame pressure was 20 torr. The steepness of the measured temperature profile in the vicinity of the burner suggests that the flame is attached (i.e., stabilized by heat loss to the burner face). Thus, the comparisons were made assuming an attached flame and the burner face temperature was assumed to be 300 K. A free-flame model resulted in a flame velocity much greater than the observed 119 cm/sec. Results with species CH_3, CH_2, and CH_2O indicate that hydrocarbon pyrolysis intermediates are over-predicted. The calculation was repeated with the C_2 chemistry subset removed. The accuracy of this prediction is reduced by this step, indicating that the C_2 steps provide additional, though secondary, pathways for the removal of hydrocarbon fragments. Comparison of measured and predicted ethylene and acetylene profiles indicated fair agreement with measurements of C_2H_4, but C_2H_2 is overpredicted by a factor of eight.

In summary, simulations have demonstrated that the methane reaction mechanism is capable of accurately reproducing ignition delay times observed in shock-initiated CH_4 oxidation studies over a broad range of temperature, reactant concentrations, and total densities. The same reaction set reproduces induction delay times for C_2H_6 oxidation, although it is necessary to consider data over a greater range of conditions to completely validate the reactions and associated rate coefficients which dominate during the induction period. Examination of the oxidation reactions for C_2H_2 and C_2H_4 indicates that several rate coefficients should be modified, and that additional species are necessary for the mechanism to be consistent with fundamental studies of C_2H_2 and C_2H_4 oxidation. Flame simulations have only been moderately successful in reproducing data. Free-flame velocities and stable species profiles have, in general been accurately reproduced. However, computed radical and C_2 profiles are not in agreement with experiment.

The Nitrogen Subelement

The primary oxide of nitrogen formed during combustion is nitric oxide, NO. However, nitrogen dioxide, NO_2, has also been found when rapid flame quenching occurs at high oxygen levels (e.g., gas turbines or partially aerated range burners). Recently nitrous oxide, N_2O, has also been observed in flame systems. (Kramlich, 1982), although normally associated with fuels containing large quantities of bound nitrogen. Recent work also suggests that N_2O is an intermediary in the formation of N_2 in fuel-rich ammonia mixtures.

Figure 6-1 summarizes the mechanism whereby NO is formed in combustion systems. The litetature differentiates between thermal and fuel NO mechanisms. Thermal NO is that nitrogen oxide produced from molecular nitrogen, whereas fuel NO is formed because the fuel contains significant quantities of bound nitrogen. Molecular nitrogen can form NO via two different paths. The first is referred to as thermal NO because the rate of production is very strongly dependant upon temperature. The primary reaction path involves the production of nitrogen atoms by the reaction $N_2 + O = NO + N$ followed by $N + O_2 = NO + O$. This reaction mechanism is usually referred to as the Zeldovich mechanism and dominates NO production under fuel-lean conditions. Under fuel-rich conditions nitrogen can be broken down by hydrocarbon radicals such as CH, producing CN species which then are converted to NH_i species, ultimately increasing the N pool. Under fuel-rich conditions N_2 production is favored. It should also be noted that hydrocarbon radicals can react with NO producing CN species. The existence of fuel nitrogen which can be considered as NH_3, HCN, or NO in a combustion system increases the nitrogen pool, thus, tending to promote NO formation. Various investigators have examined the fate of simple nitrogen compunds (NH_3, NO, methylamine, pyridine and methacrylonitrile) in hydrocarbon flames. Morley (1976) found near quantitative conversion of NO, NH_3, CH_3N and pyridine to HCN in the reaction zone of fuel-rich hydrocarbon flames with postflame temperatures above 2000 K. Fenimore reports data for fuel-rich methane flames doped with N_2O which show that HCN is the dominant nitrogenous species downstream from the flame zone. The study of Haynes, Iverach and Kirov (1975) and Haynes (1977a, 1977b) further confirm the rapid conversion of a substantial portion of the initial fuel nitrogen compound to HCN within the flame zone. However, it should be noted that with the possible exception of the data reported by Morley (1976)

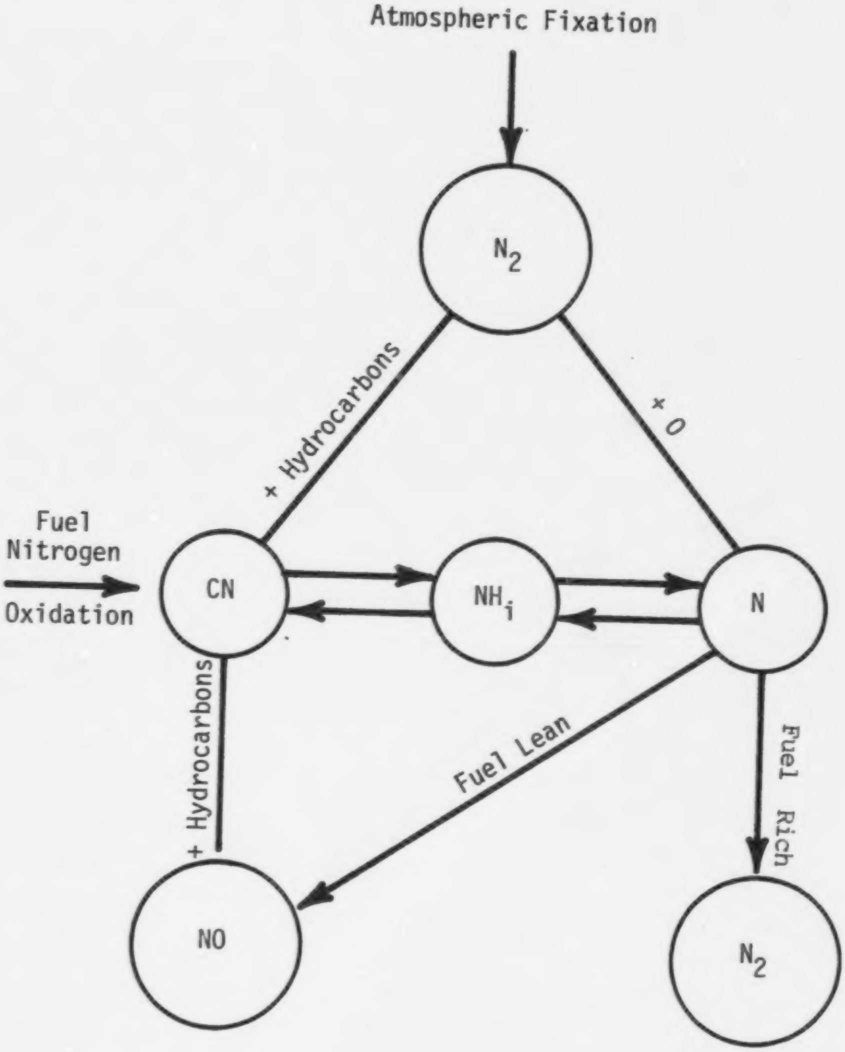
Atmospheric Fixation
N2
+ Hydrocarbons
+ O
Fuel Nitrogen
Oxidation
CN
NHi
N
+ Hydrocarbons
Fuel Lean
Fuel Rich
NO
N2

Figure 6-1. Simplified Mechanism for NO Production in Flames.

the initial distribution of nitrogenous species was dependant upon the parent fuel nitrogen compound (see de Soete, 1975). In all of the studies cited, ammonia or other amine species were observed to grow as HCN decayed. Thus, if the formation of NO in methane flames is to be adequately modeled, then the nitrogen subelement should also include reactions relevant to ammonia and HCN oxidation.

The results of shock tube simulations (both inert pyrolysis and oxidation) indicate that the proposed NH_3 oxidation set as compiled is incomplete. While the set is capable of predicting qualitative trends, the quantitative experimental results are not reproduced. Reactions involving species such as N_2H_i were ignored due to lack of rate and thermal chemistry data, and the lack of these mechanistic steps is probably the cause of the mechanisms' inability to simulate experimental data. At the present time the HCN reaction mechanism has not been adequately tested.

Recognizing that the reaction mechanism has not been completely tested, a brief set of simulations were carried out to determine how well the mechanism was capable of simulating data obtained by Blair et al (1980)* for a methane-fired stirred reactor seeded with ammonia. A series of five stirred reactor simulations were obtained for the following conditions: T = 900K, t = 3 msec, NH_3 = 750 ppm, and fuel/air equivalence ratio = 0.8, 0.97, 1.20, 1.40, and 1.80. The 1.4 and 1.8 equivalence ratio cases were rerun with the C_2 chemistry included. The stable species production is, in general, excellent; however, O_2 is underpredicted at fuel rich conditions. Including the C_2 chemistry markedly improves the O_2 prediction. The results for the nitrogenous species do not show good agreement. However, some aspects are well-predicted. The behavior of NO at lean conditions and the behavior of the sum of the fixed nitrogen species are well-correlated by the model. The details of the speciation are poorly predicted at fuel-rich conditions, particularly in the presence of hydrocarbons.

6.2 FURTHER EFFORTS

A study is underway currently to improve the mechanism described in the previous section. It has been determined that the H_2/O_2, CO/H_2O_2 and CH_2O portions of the mechanism require no further work at this time. This conclusion does not infer that these portions cannot be changed, but that rather the remaining questions concerning these steps are of low priority. Several questions still exist concerning the C_1 hydrocarbon combustion mechanism. Ignition delay characteristics for CH_4/oxidant/diluent mixtures have been well-predicted. However, species flame profiles have not been reproduced, particularly for flame radicals. The cause of this discrepancy cannot be confidently attributed to either the mechanism or the experimental data. Seery and Zabielski (1981) indicate that the use of molecular beam sampling cones can cause severe distortion in flat flames. Further modifications are also necessary for the C_2 chemistry set. In particular, ketene, which is known to be an intermediate in acetylene combustion, will be added to the mechanism. The modified C_2 mechanism will then be checked against shock tube ignition delays.

Further NH_3 mechanism tests are planned to address some of the outstanding questions concerning NH_3 processing under rich or pyrolysis conditions. These will be directed at the behavior of NH_3 oxidant mixtures, rather than at thermal pyrolisis of NH_3. Planned work involves simulation of shock tube profiles and one or more of the available flame studies.

The current HCN mechanism has not been extensively verified. It was decided initially to check and justify the current reactions and rates, bringing in updated and high-temperature values wherever possible. Since the reaction $HCN + CN = C_2N_2 + H$ has been found to be rapid in recent Stanford shoch tube work, effort will be made to include cyanogen in the mechanism. The full mechanism, including hydrocarbons and nitrogen chemistry, will finally be tested against flow reactor data being generated at Exxon and elsewhere. These data avoid the sampling distortions associated with flame data, and are considerably easier to model.

7.0 REFERENCES

Allara, D. L., and D. Edelson. A Computational Modeling Study of the Low-Temperature Pyrolysis of n-Alkanes; Mechanisms of Propane, n-Butane, and n-Pentane Pyrolyses. Int. J. Chem. Kinet., 1975. 7, 479.

Anagnostou, E., R. S. Brokaw, and J. N. Butler. Effect of Concentration on Ignition Delays for Various Fuel-Oxygen-Nitrogen Mixtures at Elevated Temperatures. NACA TN 3887, 1956.

Andrews, G. E., and D. Bradley. Determination of Burning Velocity by Double Ignition in a Closed Vessel. Comb. Flame, 1973. 20, 77.

Armitage, J. W., and P. Gray. Flame Speeds and Flammability Limits in the Combustion of Ammonia: Ternary Mixtures with Hydrogen, Nitric Oxide, Nitrous Oxide or Oxygen. Comb. Flame, 1965. 9, 173.

Atkinson, R., and J. N. Pitts, Jr. Kinetics of the Reactions of the OH Radical with HCHO and CH_3CHO Over the Temperature Range 299-426°K. J. Chem. Phys., 1978. 68, 3581.

Axworthy, A.E., G. R. Schneider, M. D. Shuman, and V. H. Dayan. Chemistry of Fuel Nitrogen Conversion to Nitrogen Oxides in Combustion. EPA-600/2-76-039, 1976.

Axworthy, A. E., D. R. Kahn, V. H. Dayan, and D. O. Wollery. Fuel Decomposition and Flame Reactions in Conversion of Fuel Nitrogen to NO_x. EPA Final Report. Contract 68-02-1886, 1980.

Baldwin, R. R., R. F. Simmons, and R. W. Walker. Inhibition of the Hydrogen + Oxygen Reaction by Ethylene. Trans. Faraday Soc., 1966. 62, 248b.

Baulch, D.L., and D. D. Drysdale. An Evaluation of the Rate Data for the Reaction $CO + OH \rightarrow CO_2 + H$. Comb. Flame, 1974. 23, 215.

Baulch, D. L., D. D. Drysdale, and D. G. Horne. Critical Evaluation of Rate Data for Homogeneous Gas Phase Reactions of Interest in High Temperature Systems. The University, Leeds, Department of Physical Chemistry, 1969. Rept. 5.

Baulch, D. L., D. D. Drysdale, D. E. Horne, and A. C. Lloyd. Evaluated Kinetic Data for High Temperature Reactions, Vols. 1 and 2. CRC Press, Cleveland, Ohio, 1973.

Benson, S. W., D. M. Golden, R. W. Lawrence, R. Shaw, and R. W. Woolfolk. Estimating the Kinetics of Combustion: Including Reactions Involving Oxides of Nitrogen and Sulfur. EPA-600/1-75-019, 1975.

Benson, S. W., and G. R. Haugen. Mechanisms for Some High-Temperature Gas-Phase Reactions of Ethylene, Acetylene, and Butadiene. J. Phys. Chem., 1967. 71, 1735.

Bertrand, C., B. Dussart, and P. J. Van Tiggelen. Use of Electric Fields to Measure Burning Velocity. In: Proceedings of the Seventeenth Symposium (International) on Combustion, The Combustion Institute, 1979. p. 967.

Biordi, J. C., C. P. Lazzara, and J. F. Papp. Flame Structure Studies of CF_3Br-Inhibited Methane Flames. II. Kinetics and Mechanisms. In: Proceedings of the Fifteenth Symposium (International) on Combustion, The Combustion Institute, 1975. p. 917.

Blair, D. W., J. O. L. Wendt, and W. Bartok. Evolution of Nitrogen and Other Species During Controlled Pyrolysis of Coal. In: Proceedings of the Sixteenth Symposium (International) on Combustion, The Combustion Institute, 1977. p. 475.

Blumenberg, B., K. Hoyermann, and R. Sievert. Primary Products in the Reactions of Oxygen Atoms with Simple and Substituted Hydrocarbons. In: Proceedings of the Sixteenth Symposium (International) on Combustion, The Combustion Institute, 1977. p. 841.

Bowman, C. T. An Experimental and Analytical Investigation of the High-Temperature Oxidation Mechanisms of Hydrocarbon Fuels. Comb. Sci. Tech., 1970. 2, 161.

Bowman, C. T. Nonequilibrium Radical Concentrations in Shock-Initiated Methane Oxidation. In: Proceedings of the Fifteenth Symposium (International) on Combustion, The Combustion Institute, 1975. p. 869.

Bowman, C. T., and D. J. Seery. Chemiluminescence in High-Temperature Oxidation of Methane. Comb. Flame, 1968. 12, 611.

Burwasser, H., and R. N. Pease. Burning Velocities of Hydrogen-Air Flames. J. Am. Chem. Soc., 1955. 77, 5806.

Brabbs, T. A., F. E. Belles, and R. S. Brokaw. Shock Tube Measurements of Specific Reaction Rates in the Branch-Chain H_2-CO-O_2 System. In: Proceedings of the Thirteenth Symposium (International) on Combustion, The Combustion Institute, 1971. p. 129.

Brabbs, T. A., and R. S. Brokaw. Shock Tube Measurements of Specific Reaction Rates in the Branched-Chain CH_4-CO-O_2 System. In: Proceedings of the Fifteenth Symposium (International) on Combustion, The Combustion Institute, 1975. p. 893.

Bradley, J. N. Induction Times and Exponential Growth Rates in Branching-Chain Reactions. Trans. Faraday Soc., 1967. 63, 2945.

Bradley, J. N., R. N. Butlin, and D. Lewis. Shock Wave Studies in Nitrogen + Hydrogen Systems. Part 4. Thermal Decomposition of Ammonia. Trans. Faraday Soc., 1967. 63, 2962.

Bradley, J. N., R. N. Butlin, and D. Lewis. Oxidation of Ammonia in Shock Waves. Trans. Faraday Soc., 1968. 64, 71.

Branch, M. C., J. A. Miller, and R. J. Kee. Chemical Kinetics of the $NH_3/NO/O_2$ System. Paper No. 79-38. Western States Section, The Combustion Institute, Berkeley, California, 1979.

Braun, W., J. R. McNesby, and A. M. Bass. Flash Photolysis of Methane in the Vacuum Ultraviolet. II. Absolute Rate Constants for Reactions of CH with Methane, Hydrogen, and Nitrogen. J. Chem. Phys., 1967. 46, 2071.

Brokaw, R. S. Ignition Kinetics of the Carbon Monoxide-Oxygen Reaction. In: Proceedings of the Eleventh Symposium (International) on Combustion, The Combustion Institute, 1967. p. 1063.

Brokaw, R. S. Analytic Solutions to the Ignition Kinetics of the Hydrogen-Oxygen Reaction. In: Proceedings of the Tenth Symposium (International) on Combustion, The Combustion Institute, 1965. p. 269.

Browne, W. G., R. P. Porter, J. D. Verlin, and A. H. Clark. A Study of Acetylene-Oxygen Flames. In: Proceedings of the Twelfth Symposium (International) on Combustion, The Combustion Institute, 1969. p. 1035.

Bull, D. C. A Shock Tube Study of the Oxidation of Ammonia. Comb. Flame, 1968. 12, 603.

Burcat, A., R. W. Crossley, J. Soheller, and G. B. Skinner. Shock Tube Investigation of Ignition in Ethane-Oxygen-Argon Mixtures. Comb. Flame, 1972. 18, 115.

Butler, J. E., L. P. Goss, M. C. Lin, and J. W. Hudgens. Production, Detection and Reactions of the CH Radical. Chem. Phys. Letters, 1979. 63, 104.

Camilleri, P., R. M. Marshall, and J. H. Purnell. Reaction of Hydrogen Atoms with Ethane. JCS Faraday I, 1974. 70, 1434.

Carr, R. W., Jr. Predictions of the Rates of Hydrogen Abstraction by $CH_2(^3B_1)$ by the Bond-Energy Bond-Order Method. J. Phys. Chem., 1972. 76, 1581.

Carr, R. W., Jr., I. D. Gay, G. P. Glass, and H. Niki. Reaction of Ketene with Atomic Hydrogen and Oxygen. J. Chem. Phys., 1968. 49, 846.

Chang, J. S., and J. R. Barker. Reaction Rate and Products for the Reaction $O(^3P) + CH_2O$. J. Phys. Chem., 1979. 83, 3059.

Cherian, M. A., P. Rhodes, R. J. Simpson, and G. Dixon-Lewis. Kinetic Modeling of the Oxidation of Carbon Monoxide in Flames. In: Proceedings of the Eighteenth Symposium (International) on Combustion, The Combustion Institute, 1981. (To be published)

Clark, T. C., and J. E. Dove. Examination of Possible Non-Arrhenius Behavior in the Reactions $H + C_2H_6 \rightarrow H_2 + C_2H_5$, $H + CH_4 \rightarrow H_2 + CH_3$, $CH_3 + C_2H_6 \rightarrow CH_4 + C_2H_5$. Can. J. Chem., 1973. 51, 2147.

Clyne, M. A. A., and P. E. Monkhouse. Atomic Resonance Fluorescence for Rate Constants of Rapid Bimolecular Reactions. Part 5. Hydrogen Atom Reactions; $H + NO_2$ and $H + O_3$. JCS Faraday II, 1977. 73,298.

Cohen, N., and K. Westberg. Private communication. 1979.

Cooke, D. F., and A. Williams. Shock Tube Studies of the Ignition and Combustion of Ethane and Slightly Rich Methane Mixtures with Oxygen. In: Proceedings of the Thirteenth Symposium (International) on Combustion, The Combustion Institute, 1971. p. 757.

Cooke, D. F., and A. Williams. Shock Tube Studies of Methane and Ethane Oxidation. Comb. Flame, 1975. 24, 245.

Cox, R. A., R. G. Dernent, S. V. Kearsey, L. Batt, and G. Patrick. Photolysis of Methyl Nitrite: Kinetics of the Reaction of the Methoxy Radical with O . J. Photochem., 1980. 13, 149.

Creighton, J. R. Some General Principles Obtained from Numerical Studies of Methane Combustion. J. Phys. Chem., 1977. 81, 2520.

Crossley, E. A. Dorko, K. Scheller, and A. Burcat. The Effect of Higher Alkanes on the Ignition of Methane-Oxygen-Argon Mixtures in Shock Waves. Comb. Flame, 1972. 19, 373.

D'Alessio, A., F. Dilorenzo, A. Borghere, F. Beretta, and S. Masi. Study of the Soot Nucleation Zone of Rich Methane-Oxygen Flames. In: Proceedings of the Sixteenth Symposium (International) on Combustion, The Combustion Institute, 1977. p. 695.

Demissy, M., and R. Lesclaux. Kinetics of Hydrogen Abstraction by NH_2 Radicals from Alkanes in the Gas Phase. A Flash Photolysis-Laser Resonance Absorption Study. J. An. Chem. Soc., 1980. 102, 2987.

Dean, A. M., B. L. Craig, R. L. Johnson, M. C. Schultz, and E. E. Wang. Shock Tube Studies of Formaldehyde Pyrolysis. In: Proceedings of the Seventeenth Symposium (International) on Combustion, The Combustion Institute, 1979. p. 577.

Dean, A. M., and R. L. Johnson. Shock Tube Studies of the $N_2O/CH_4/CO/Ar$ and $N_2O/C_2H_6/CO/Ar$ systems. Comb. Flame, 1980. 37, 109.

Dean, A. M., R. L. Johnson, and D. C. Steiner. Shock Tube Studies of Formaldehyde Oxidation. Comb. Flame, 1980. 37, 41.

Dean, A. M., and G. B. Kistiakowsky. Oxidation of Carbon Monoxide/Methane Mixtures in Shock Waves. J. Chem. Phys., 1971. 54, 1718.

Dean, A. M., D. C. Steiner, and E. E. Wang. A Shock Tube Study of the $H_2/O_2/CO/Ar$ and $H_2/N_2O/CO/Ar$ Systems: Measurement of the Role Constant for $H + N_2O = N_2 + OH$. Comb. Flame, 1978. 32, 73.

De Soete, G. La Formation des Oxyde D'Azote Dans La Zone d'Oxydation des Flammes d'Hydrocarbures. Final Report No. 23306. Institut Francais due Petrole, Ruiell Malmaison, France, 1975.

Dixon-Lewis, G. Kinetic Mechanism, Structure and Properties of Premixed Flames in Hydrogen-Oxygen-Nitrogen Mixtures. Phil. Trans. Roy. Soc. Lond., 1979. 292A, 45.

Dixon-Lewis, G., M. M. Sutton, and A. Williams. Flame Structure and Flame Reaction Kinetics. IV. Experimental Investigations of a Fuel-Rich Hydrogen + Oxygen + Nitrogen Flame at Atmospheric Pressure. Proc. Roy. Soc. Lond. A., 1970. 317, 227.

Dove, J. E. In: Proceedings of the Fifteenth Symposium (International) on Combustion, The Combustion Institute, 1975. p. 855.

Dove, J. E., and D. McL. Moulton. Shock Wave Studies by Mass Spectrometry. III. Description of Apparatus; Data on the Oxidation of Acetylene and of Methane. Proc. Roy. Soc., 1965. A283, 216.

Dove, J. E., and W. S. Nip. Shock Tube Studies of the Reactions of Hydrogen Atoms. I. The Reaction $H + NH_3 \rightarrow H_2 + NH_2$. Can. J. Chem., 1974. 52, 1171.

Dove, J. E., and W. S. Nip. A Shock Tube Study of Ammonia Pyrolysis. Can. J. Chem., 1979. 57, 689.

Drummond, L. J. Shock-Initiated Exothermic Reactions. V. The Oxidation of Ethylene. Anst. J. Chem., 1968. 21, 2641.

Drummond, L. J. Shock Initiated Oxidation of Formaldehyde. Comb. Sci. Tech., 1971. 3, 47.

Drummond, L. J. High Temperature Oxidation of Ammonia. Comb. Sci. Tech., 1972. 5, 175.

Drummond, L. J., and S. W. Hiscock. Shock-Initiated Exothermic Reactions. II. The Oxidation of Ammonia. Aust. J. Chem., 1967. 20, 825.

Dryer, F. L., and I. Glassman. High Temperature Oxidation of CO and CH_4. In: Proceedings of the Fourteenth Symposium (International) on Combustion, The Combustion Institute, 1973. p. 987.

Duff, R. W., and S. H. Bauer. Equilibrium Composition of the C/H System at Elevated Temperatures. J. Chem. Phys., 1962. 36, 1754.

Duxbury, J., and N. H. Pratt. A Shock Tube Investigation of the Fuel Nitrogen-Nitric Oxide Problem. In: Proceedings of the Combustion Intitute European Symposium, The Combustion Institute (British Section), 1973. p. 433.

Duxbury, J., and N. H. Pratt. A Shock Tube Study of NO Kinetics in the Presence of H_2 and Fuel-N. In: Proceedings of the Fifteenth Symposium (International) on Combustion, The Combustion Institute, 1975. p. 843.

Eberstein, I. J., and I. Glassman. The Gas-Phase Decomposition of Hydrazine and Its Methyl Derivatives. In: Proceedings of the Tenth Symposium (International) on Combustion, The Combustion Institute, 1965. p. 365.

Edmondson, H., and M. P. Heap. The Burning Velocity of Hydrogen-Air Flames. Comb. Flame, 1971. 16, 161.

Engleman, V. S. Survey and Evaluation of Kinetic Data on Reactions in Methane/Air Combustion. EPA-600/1-76-003, 1976.

Ernst, J., H. Gg. Wagner, and R. Zellner. A Combined Flash Photolysis/Shock Tube Study of the Absolute Rate Constants for Reactions of the Hydroxyl Radical with CH_4 and CH_3H Around 1300 K. Ber. Bunsenges. Phys. Chem., 1978. 82, 409.

Felder, W., and A. Fontijn. High Temperature Photochemistry, A New Technique for Rate Coefficient Measurements Over Wide Temperature Ranges: Initial Measurements on the O + CH_4 Reaction From 525-1250 K. Chem. Phys. Letters, 1979. 67, 53.

Fenimore, C. P. Reactions of Fuel Nitrogen in Rich Flame Gases. Comb. Flame, 1976. 26, 249.

Fenimore, C. P. Studies of Fuel Nitrogen Species in Rich Flame Gases. In: Proceedings of the Seventeenth Symposium (International) on Combustion, The Combustion Intitute, 1979. p. 661.

Fenimore C. P., and G. W. Jones. Rate of Reaction in Hydrogen, Nitrous Oxide and in Some Other Flames. J. Phys. Chem., 1959. 63, 1154.

Fenimore, C. P., and G. W. Jones. Oxidation of Ammonia in Flames. J. Phys. Chem., 1961. 65, 298.

Fenimore, C. P., and G. W. Jones. Formation of Carbon Monoxide in Methane Flames by Reaction of Oxygen Atoms with Methyl Radicals. J. Phys. Chem., 1961. 65, 1532.

Fenimore, C. P., and G. W. Jones. Rate of Destruction of Acetylene in Flame Gases. J. Chem. Phys., 1964. 41, 1887.

Fine, B. Stability Limits and Burning Velocities of Laminar Hydrogen-Air Flames at Reduced Pressure. NACA TN 3833, 1956.

Fishburne, E. S., and R. Edse. Shock Tube Study of Nitrous Oxide Decomposition. J. Chem. Phys., 1964. 41, 1297.

Fisher, C. J. A Study of Rich Ammonia/Oxygen/Nitrogen Flames. Comb. Flame, 1977. 30, 143.

Frank, P., and Th. Just. High Temperature Thermal Decomposition of Acetylene and Diacetylene at Low Relative Concentrations. Comb. Flame 1980. 38. 231.

Friedman, R., and J. A. Cyphers. On the Burning Rate of Carbon Monoxide. J. Chem. Phys., 1956. 25, 448.

Fristrom, R. M. Radical Concentrations and Reactions in a Methane-Oxygen Flame. In: Proceedings of the Ninth Symposium (International) on Combustion, The Combustion Institute, 1963. p. 560.

Fristrom, R. M., W. H. Avery, and C. Grunfelder. Reactions of Simple Hydrocarbons in Flame Fronts - Microstructure of C_2 Hydrocarbon - Oxygen Flames. In: Proceedings of the Seventh Symposium (International) on Combustion, The Combustion Institute, 1959. p. 304.

Gardiner, W. C. Private Communication, 1978.

Gardiner, W. C., Jr., and B. F. Walker. Source of Schlieren Signals from Acetylene Combustion Shock Waves. J. Chem. Phys., 1968. 48, 5279.

Gay, I. D., G. P. Glass, R. D. Kern, and B. G. Kistiakowsky. Ethylene-Oxygen Reaction in Shock Waves. J. Chem. Phys., 1967. 47, 313.

Gay, I. D., G. P. Glass, G. B. Kistiakowsky, and H. Niki. Pyrolysis and Oxidation of Formaldehyde in Shock Waves. J. Chem. Phys., 1965. 43, 4017.

Gehring, M., K. Hoyermann, H. Schacke, and J. Wolfrum. Direct Studies of Some Elementary Steps for the Formation and Destruction of Nitrix Oxide in the H-N-O System. In: Proceedings of the Fourteenth Symposium (International) on Combustion, The Combustion Institute, 1973. p. 99.

Gehring, M., K. Hoyermann, H. Gg. Wagner, and J. Wolfrum. Die Reaktion von atomarem Wasserstoff mit Hydrazin. Ber. Dunsenges. Phys. Chem, 1971. 75, 1287.

Gilbert, M. Influence of Pressure on Flame Speed. In: Proceedings of the Sixth Symposium (International) on Combustion, The Combustion Institute, 1957. p. 74.

Glick, H. S. Shock Tube Studies of Reaction Kinetics of Aliphatic Hydrocarbons. In: Proceedings of the Seventh Symposium (International) on Combustion, The Combustion Institute, 1959. p. 98.

Grillo, A., and M. W. Slack. Shock Tube Study of Ignition Delay Times in Methane-Oxygen-Nitrogen-Argon Mixtures. Comb. Flame, 1976. 27, 377.

Günther, R., and G. Janisch. Measurements of Burning Velocity in a Flat Flame Front. Comb. Flame, 1972. 19, 49.

Hack, W., H. Schacke, M. Schröter, and H. Gg. Wagner. Reaction Rates of NH_2-Radicals with NO, NO_2, C_2H_2, C_2H_4 and Other Hydrocarbons. In: Proceedings of the Seventeenth Symposium (International) on Combustion, The Combustion Intitute, 1979. p. 505.

Hansen, I., K. Höinghaus, C. Zetzsch, and F. Stuhl. Detection of NH($X^3\Sigma^-$) by Resonance Fluorescence in the Pulsed Vacuum UV Photolysis of NH_3 and Its Application to Reactions of NH Radicals. Chem. Phys. Letters, 1976. 46, 370.

Harris, G. W., R. Atkinson, and J. N. Pitts, Jr. Kinetics of the Reactions of the OH Radical with Hydrazine and Methylhydrazine. J. Phys. Chem., 1979. 83, 2557.

Hartig, R., J. Troe, and H. Gg. Wagner. Thermal Decomposition of Methane Behind Reflected Shock Waves. In: Proceedings of the Thirteenth Symposium (International) on Combustion, The Combustion Intitute, 1971. p. 147.

Harvey, R., and A. MacColl. The Formation of C_2 Hydrocarbons Within Methane-Oxygen Flames. In: Proceedings of the Seventeenth Symposium (International) on Combustion, The Combustion Institute, 1979. p. 857.

Haynes, B. S. Reactions of Ammonia and Nitrix Oxide in the Burnt Gases of Fuel-Rich Hydrocarbon-Air Flames. Comb. Flame, 1977a. 28, 81.

Haynes, B. S. The Oxidation of Hydrogen Cyanide in Fuel-Rich Flames. Comb. Flame, 1977b. 28, 113.

Haynes, B. S., D. Iverach, and N. Y. Kirov. The Behavior of Nitrogen Species in Fuel-Rich Hydrocarbon Flames. In: Proceedings of the Fifteenth Symposium (International) on Combustion, The Combustion Institute, 1975. p. 1103.

Heap, M. P. Private Communication, 1980.

Herron, J. T., and R. E. Huie. Rate Constants for the Reactions of Atomic Oxygen with Organic Compounds in the Gas Phase. J. Phys. Chem., 1973. Ref. Data 2, 467.

Homann, K. H., J. Warnatz, and C. Wellmann. The Formation of Higher Hydrocarbons in the Reaction of O-Atoms with Acetylene. In: Proceedings of the Sixteenth Symposium (International) on Combustion, The Combustion Institute, 1077. p. 853.

Homer, J. B., and G. B. Kistiakowsky. Acetylene-Oxygen Reaction in Shock Waves. Origin of CO_2. J. Chem. Phys., 1967a. 46, 4213.

Homer, J. B., and G. B. Kistiakowsky. Oxidation and Pyrolysis of Ethylene on Shock Waves. J. Chem. Phys., 1967b. 47, 5290.

Husain, D., and R. G. W. Norrish. The Explosive Oxidation of Ammonia and Hydrazine Studied by Kinetic Spectroscopy. Proc. Roy. Soc., 1963. A 273, 145.

Jachimowski, C. J. An Experimental and Analytical Study of Acetylene and Ethylene Oxidation Behind Shock Waves. Comb. Flame, 1977. 29, 55.

Jachimowski, C. J., and W. M. Houghton. Shock Tube Study of the Induction-Period Kinetics of the Hydrogen-Oxygen Reaction. Comb. Flame, 1970. 15, 125.

Jahn, G. Der Zundvergang in Gasgemischen. Oldenbourg : Berlin, 1934.

Just, Th., P. Roth, and R. Damm. Production of Hydrogen Atoms During the Thermal Dissociation of Ethylene Between 1700 and 2200 K. In: Proceedings of the Sixteenth Symposium (International) on Combustion, The Combustion Institute, 1977. p. 961.

Kanofsky, J. P., D. Lucas, and D. Gutman. Direct Identification of Free-Radical Products of O-Atom Beams. In: Proceedings of the Fourteenth Symposium (International) on Combustion, The Combustion Institute, 1973. p. 285.

Kanofsky, J. R., D. Lucas, F. Pruss, and D. Gutman. Direct Identification of the Reactive Channels in the Reactions of Oxygen Atoms and Hydroxyl Radicals with Acetylene and Methylacetylene. J. Phys. Chem, 1974. 78, 311.

Kaskan, W. E. Excess Radical Concentrations and the Disappearance of Carbon Monoxide in Flame Gases from Some Lean Mixtures. Comb. Flame, 1959. 3, 49.

Kaskan, W. E., and D. E. Hughes. Mechanism of Decay of Ammonia in Flame Gases from an NH_3/O_2 Flame. Comb. Flame, 1973. 20, 381.

Khe, P. V., J. C. Soulignae, and R. Lesclaux. Pressure and Temperature Dependence of NH_2 Recombination Rate Constant. J. Phys. Chem, 1977. 81, 210.

Klein, R., M. D. Scheer, and L. J. Schoen. The Pyrolysis of Formaldehyde. J. Am. Chem. Soc., 1959. 78, 50.

Klemm, R. B., T. Tanzawa, E. G. Skolnik, and J. V. Michael. A Resonance Fluorescence Kinetic Study of the $O(^3P) + CH_4$ Reaction Over the Temperature Range 474°K to 1156°K. In: Proceedings of the Eighteenth Symposium (International) on Combustion, The Combustion Institute, University of Waterloo, Canada, 1980. Paper No. 75.

Kondrotiev, V. N. Rate Constants for Gas Phase Reactions. 1972. NBS Pub. COM-72-10014.

Kramlich, J. C., R. N. Nihart, S. L. Chen, D. W. Pershing, and M. P. Heap. "Behavior of N_2O in Staged Pulverized Coal Combustion." Combustion Flame, In press, 1982.

Lange, W., and H. Gg. Wagner. Massenspektrometrische Untersuchungen über Erzeugung und Reaktionen von C_2H-Radikalen. Ber. Bunsanges. Phys. Chem., 1975. 79, 165.

Laufer, A. H., and A. M. Bass. Rate Constants for Reactions of Methylene with Carbon Monoxide, Oxygen, Nitric Oxide, and Acetylene. J. Phys. Chem., 1974. 78, 1344.

Laufer, A. H., and A. M. Bass. Photochemistry of Acetylene. Biomolecular Rate Constant for the Formation of Butadiyne and Reactions of Ethynyl Radicals. J. Phys. Chem., 1979. 83, 310.

Lifshitz, A., and M. Frenklach. Mechanism of the High Temperature Decomposition of Propane. J. Phys. Chem., 1975. 79, 686.

Lozovskii, V. A., V. A. Nadtochenko, O. M. Sarkisov, and S. G. Cheskis. Study of NH_2 Recombination by Intraresonator Laser Spectroscopy. English Translation of Kinet. Katal., 1979. 20, 918.

Lyon R. K., and D. Benn. Kinetics of the NO-NH_3-O_2 Reaction. In: Proceedings of the Seventeenth Symposium (International) on Combustion, The Combustion Institute, 1979. p. 601.

Lyon, R. K., J. E. Hardy, and D. J. Benn. A Flow Reactor Study of the Ammonia-Oxygen Reaction. Western States Section, The Combustion Institute, Laguna Beach, CA, October 1978. Paper 78-51.

MacLean, D. I., and H. Gg. Wagner. The Microstructure of the Reaction Zones of Ammonia-Oxygen and Hydrazine Decomposition Flames. In: Proceedings of the Eleventh Symposium (International) on Combustion, The Combustion Institute, 1967. p. 871.

Manton, J., and B. B. Milliken. In: Proceedings of the Gas Dynamics Symposium on Aerothermochemistry, 1956. Northwestern Univ. Press. p. 151.

Mayer, S. W., L. Schieler, and H. S. Johnston. Computation of High-Temperature Rate Constants for Bimolecular Reactions of Combustion Products. In: Proceedings of the Eleventh Symposium (International) on Combustion, The Combustion Institute, 1967. p. 837.

Messing, I., C. M. Sadowski, and S. V. Filseth. Absolute Rate Constant for the Reaction of CH with O_2. Chem. Phys., 1979. Letters 66, 95.

Michael, J. V., W. A. Payne, and D. A. Whytock. Absolute Rate Constants for $O + NO + M\ (=He, Ne, Ar, Kr) \rightarrow NO_2 + M$ from 217-500 K. J. Chem. Phys., 1976. 65, 4830.

Michel, K. W. In: Proceedings of the Tenth Symposium (International) on Combustion, The Combustion Institute, 1965. p. 351.

Michel, K. W., and H. Gg. Wagner. The Pyrolysis and Oxidation of Hydrazine Behind Shock Waves. In: Proceedings of the Tenth Symposium (International) on Combustion, The Combustion Institute, 1965. p. 353.

Miyama, H. Ignition of Ammonia-Oxygen Mixtures by Shock Waves. J. Chem. Phys., 1968. 48, 1421.

Miyama, H., and R. Endoh. Ignition of Ammonia-Air Mixtures by Reflected Shock Waves. Comb. Flame, 1967. 11, 359.

Monat, J. P., R. J. Hanson, and C. H. Kruger. Kinetics of Nitroux Oxide Decomposition. Comb. Sci. Tech., 1977. 16, 21.

Monat, J. P., R. K. Hanson, and C. H. Kruger. Shock Tube Determination of the Rate Coefficient for the Reaction $N + O \rightarrow NO + N$. In: Proceedings of the Seventeenth Symposium (International) on Combustion, The Combustion Institute, 1979. p. 543.

Morley, C. The Formation and Destruction of Hydrogen Cyanide from Atmospheric and Fuel Nitrogen in Rich Atmospheric-Pressure Flames. Comb. Flame, 1976. 27, 189.

Morrison, B. M., Jr., and J. Heicklen. The Reactions of HO with CH_2O and of HCO with NO_2. J. Photochem., 1980. 13, 189.

Olson, D. B., and W. C. Gardiner, Jr. Combustion of Methane in Fuel-Rich Mixtures. Comb. Flame, 1978. 32, 151.

Padley, P. J. and T. M. Sugden. Chemiluminescence and Radical Recombination in Hydrogen Flames. In: Proceedings of the Seventh Symposium (International) on Combustion, The Combustion Institute, 1959. p. 235.

Pagsberg, P. B., J. Eriksen, and H. C. Christensen. Pulse Radiolysis of Gaseous Ammonia-Oxygen Mixtures. J. Phys. Chem., 1979. 83, 582.

Peeters, J., and G. Mahnen. Reaction Mechanisms and Rate Constants of Elementary Steps in Methane-Oxygen Flames. In: Proceedings of the Fourteenth Symposium (International) on Combustion, The Combustion Institute, 1973. p. 133.

Peterson, D. B. The Radication Chemistry of Gaseous Ammonia. National Bureau of Standards, Office of Standard Reference Data, 1974. Report NSRDS-NBS 44.

Piper, L. G. On the Heat of Formation of NH. J. Chem. Phys., 1979. 70, 3417.

Porter, R. P., A. H. Clark, W. D. Kaskan, and W. E. Browne. A Study of Hydrocarbon Flames. In: Proceedings of the Eleventh Symposium (International) on Combustion, The Combustion Institute, 1967. p. 907.

Pratt, G., and D. Rogers. Wall-less Reactor Studies. Part I. Ethane Pyrolysis. JCS Faraday I, 1979. 75, 1089.

Proctor, C. L., II, and N. M. Laurendeau. A Shock Tube Study of the Inert Pyrolysis of Pyridine. Western States Section, The Combustion Institute, Laguna Beach, CA, 1978. Paper 78-55.

Pruss, F. J., Jr., I. R. Slagle, and D. Gutman. Determination of Branching Ratios for the Reaction of Oxygen Atoms with Ethylene. J. Phys. Chem., 1974. 78, 663.

Reilly, J. P., J. H. Clark, C. B. Moore, and G. C. Pimentel. HCO Production, Vibrational Relaxation, Chemical Kinetics, and Spectroscopy Following Laser Photolysis of Formaldehyde. J. Chem. Phys., 1978. 69, 4381.

Roose, T. R., R. K. Hanson, and C. H. Kruger. Decomposition of NO in the Presence of NH_3. Paper presented at the 11th International Shock Tube Symposium, Seattle, Washington, 1977.

Roose T. R., R. K. Hanson, and C. H. Kruger. Thermal Decomposition of NH_3 in Shock Waves. Paper presented at the 12th International Shock Tube Symposium, Jerusalem, Israel, 1979.

Roose, T. R., R. K. Hanson, and C. H. Kruger. A Shock Tube Study of the Decomposition of NO in the Presence of NH_3. In: Proceedings of the Eighteenth Symposium (International) on Combustion, The Combustion Institute, Waterloo, Canada, 1980. Paper 88.

Roth, P., and Th. Just. Atomabsorptionsmessungen zur Kinetik der Reaktion $CH_4 + O \rightarrow CH_3 + OH$ in Temperaturbereich $1500 \leq T \leq 2250$ K. Ber. Bunsenges. Physc. Chem., 1977. 81, 572.

Russell, R. L., and F. S. Rowland. Mechanism of Product Formation During the Photolysis of Ketene. J. Phys. Chem., 1979. 83, 2073.

Schecker, H. G., and W. Jost. Zum Homogenen Thermischen Zerfall von Formaldehyd. Ber. Bunsenges Phys. Chem., 1969. 73, 521.

Schofield, K. An Evaluation of Kinetic Rate Data for Reactions of Neutrals of Atmospheric Interest. Planet. Space. Sci., 1967. 15, 643, 1336.

Scholte, T. G., and P. B. Vaags. The Burning Velocity of Hydrogen-Air Mixtures and Mixtures of Some Hydrocarbons with Air. Comb. Flame, 1959a. 3, 495.

Scholte, T. G., and P. B. Vaags. The Influence of Small Quanitites of Hydrogen and Hydrogen Compounds on the Burning Velocity of Carbon Monoxide-Air Flames. Comb. Flame, 1956b. 3, 503.

Seery, D. J., and C. T. Bowman. An Experimental and Analytical Study of Methane Oxidation Behind Shock Waves. Comb. Flame, 1970. 14, 37.

Seery, D. J., and M. F. Zabielski. Mass Spectrometer Probing of a CO-NH_3-O_2 Flame. Comb. Flame, 1977. 28, 93.

Seery, J. J. and M. F. Zabielski. "Molecular Beam Sampling--Mass Spectrometer Study of H_2-O_2-NO Flames." The Eighteenth Symposium (International) on Combustion. The Combustion Institute, Pittsburgh, PA, 1981. p. 397.

Shaub, W. M., and S. H. Bauer. The Reduction of Nitric Oxide During the Combustion of Hydrocarbons: Methodology for a Rational Mechanism. Comb. Flame, 1978. 32, 35.

Shaviv, A., and A. Barnun. The Oxidation of Hydrocarbons by Water Vapor Behind High-Temperature Shock Waves. Int. J. Chem. Kinet., 1975. 7, 661.

Shaw, R. Semi-Empirical Extrapolation and Estimation of Rate Constants for Abstraction of H from Methane by H, O, HO, and O_2. J. Phys. Chem. Ref. Data, 1978. 7, 1179.

Singleton, D. L., and R. J. Cvetanovic. Temperature Dependence of the Reactions of Oxygen Atoms with Olefins. J. Am. Chem. Soc., 1976. 98, 6812.

Skinner, G. B., A. Lifshitz, K. Scheller, and A. Burcat. Kinetics of Methane Oxidation. J. Chem. Phys., 1972. 56, 3853.

Skinner, G. B., and R. A. Ruehrwein. Shock Tube Studies on the Pyrolysis and Oxidation of Methane. J. Phys. Chem., 1959. 63, 1736.

Skinner, G. B., and G. H. Ringrose. Ignition Delays of a Hydrogen-Oxygen-Argon Mixture at Relatively Low Temperatures. J. Chem. Phys., 1965. 42, 2190.

Slack, M. W. Rate Coefficient for $H + O_2 + M = HO_2 + M$ Evaluated from Shock Tube Measurements of Induction Times. Comb. Flame, 1977. 28, 241.

Slack, M. W., and A. R. Grillo. Kinetics of Hydrogen-Oxygen and Methane-Oxygen Ignition Sensitized by NO or NO_2. In: Proceedings of the 11th International Symposium on Shock Tube and Waves, University of Washington Press, 1977. p. 408.

Slemr, F., and P. Warneck. Reactions of Atomic Hydrogen with Ketene and Acetaldehyde. Ber. Bunsenges. Phys. Chem., 1975. 75, 152.

Smith, I. W. M., and R. Zellner. Rate Measurements of Reactions of the OH Radical with H_2, CO, C_2H_4 and C_2H_2 Between 210 K and 460 K. In: Proceedings of the Combustion Institute European Symposium, The Combustion Institute (British Section), 1973. p. 24.

Soloukhin, R. I. High-Temperature Oxidation of Ammonia, Carbon Monoxide, and Methane by Nitrous Oxide in Shock Waves. In: Proceedings of the Thirteenth Symposium (International) on Combustion, The Combustion Institute, 1971. p. 121.

Tabayaski, K., and S. H. Bauer. The Early Stages of Pyrolysis and Oxidation of Methane. Comb. Flame, 1979. 34, 63.

Takayama, T., and H. Miyama. Kinetic Studies of Ammonia Oxidation in Shock Waves. I. The Reaction Mechanism for the Induction Period. Bull. Chem. Soc. Japan, 1965. 38, 1670.

Takayama, T., and H. Miyama. A Shock-Tube Study of the Ammonia-Oxygen Reaction. In: Proceedings of the Eleventh Symposium (International) on Combustion, The Combustion Institute, 1967. p. 845.

Tanzawa, T., and W. C. Gardiner, Jr. Thermal Decomposition of Acetylene. In: Proceedings of the Seventeenth Symposium (International) on Combustion, The Combustion Institute, 1979. p. 563.

Tanzawa, T., and W. C. Gardiner, Jr. Reaction Mechanism of the Homogeneous Thermal Decomposition of Acetylene. J. Phys. Chem., 1980. 84, 236.

Tsuboi, T., and H. Gg. Wagner. Homogeneous Thermal Oxidation of Methane in Reflected Shock Waves. In: Proceedings of the Fifteenth Symposium (International) on Combustion, The Combustion Institute, 1975. p. 833.

Vandooren, J., J. Peeters, and P. J. Van Tiggelen. Rate Constant of the Elementary Reaction of Carbon Monoxide with Hydroxyl Radical. In: Proceedings of the Fifteenth Symposium (International) on Combustion, The Combustion Institute, 1975. p. 745.

Vandooren, J., and P. J. Van Tiggelen. Reaction Mechanisms of Combustion in Low Pressure Acetylene-Oxygen Flames. In: Proceedings of the Sixteenth Symposium (International) on Combustion, The Combustion Institute, 1977. p. 1133.

Vinckier, C., and W. Debruyn. Temperature Dependence of the Reactions of Methylene with Oxygen Atoms, Oxygen, and Nitric Oxide. J. Phys. Chem., 1979. 83, 2057.

Wagner, H. Gg., and F. Zabel. Zum Ehermischen Zerfall von Keten in der Gasphase. Ber. Bunsenges. Phys. Chem., 1971. 71, 114.

Waldman, C. H., R. P. Wilson, Jr., and K. L. Maloney. "Kinetic Mechanism of Methane/Air Combustion with Pollutant Formation." EPA 650/2-74-045, June 1974.

Waldman, C. H., R. P. Wilson, Jr., and V. S. Engleman. "Analysis of the Kinetic Mechanism of Methane Air Combustion with Pollutant Formation. Western States Section/Combustion Institute, Paper 74/2.

Walkauskas, L. P., and F. Kaufman. Gas Phase Hydrogen Atom Recombination. In: Proceedings of the Fifteenth Symposium (International) on Combustion, The Combustion Institute, 1975. p. 691.

Warnatz, J. Calculation of the Structure of Laminar Flat Flames II: Flame Velocity and Structure of Freely Propagating Hydrogen-Oxygen and Hydrogen-Air Flames. Ber. Bunsenges. Phys. Chem., 1978. 82, 643.

Westbrook, C. K., J. Creighton, and C. Lund. A Numerical Model of Chemical Kinetics of Combustion in a Turbulent Flow Reactor. J. Phys. Chem., 1977. 81, 2542.

Westenberg, A. A., and N. deHaas. Absolute Measurements of the O + C_2H_4 Rate Coefficients. In: Proceedings of the Twelfth Symposium (International) on Combustion, The Combustion Institute, 1969. p. 289.

Yumura, M., T. Asaba, Y. Matsumoto, and H. Matsui. Thermal Decomposition of Ammonia in Shock Waves. Int. J. Chem. Kinet., 1980. 12, 439.

Zabielski, M. F., L. G. Dodge, M. B. Colket, and D. J. Seery. The Optical and Probe Measurement of NO: A Comparative Study. In: Proceedings of the Eighteenth Symposium (International) on Combustion, The Combustion Institute, 1981. To be published.

APPENDIX I

GAS PHASE PROCESSES INVOLVED IN THE CONTROL OF NITROGEN OXIDE FORMATION IN FOSSIL FUEL FLAMES

By

J. M. Levy
M.I.T. Energy Laboratory
Cambridge, Massachusetts 02139

ABSTRACT

Optimization of a control strategy for NO_x emissions from fossil fuel combustion requires an understanding of the mechanistic chemistry of fuel-nitrogen conversion. Computational capabilities are demonstrated to be quite accurate in the presence of simple fuels, but break down somewhat in the presence of hydrocarbons. A quasi-global method for computing fuel-nitrogen conversion in a higher hydrocarbon environment is described, and the current status of modeling bound nitrogen profiles in a C_1/C_2 environment is presented.

TABLE OF CONTENTS

Section Page

1.0 INTRODUCTION B-I-1

2.0 THE FUEL-NITROGEN MECHANISM B-I-4

3.0 THE HYDROCARBON PROBLEM B-I-11

4.0 METHODOLOGY FOR DEALING WITH HIGHER HYDROCARBONS B-I-13

- 4.1 Detailed Kinetics B-I-13
- 4.2 The Global and Semi-Global Methods B-I-13
- 4.3 The Quasi-Global Method B-I-14
- 4.4 Development of a New Quasi-Global Method: QUAGMIRE . B-I-17

5.0 MODELING OF FUEL-NITROGEN CONVERSION IN A HYDROCARBON ENVIRONMENT B-I-19

6.0 SUMMARY B-I-28

REFERENCES B-I-29

LIST OF FIGURES

Figure		Page
1a	Post-Flame Zone of a $C_2H_4/O_2/N_2$ Flame Doped with 700 ppm NH_3 ($\phi = 1.52$, T = 2010 K) Modeled with the Reaction Set of Table I. Data from Haynes (23)	B-I-5
1b	Post-Flame Zone of a $C_2H_4/O_2/N_2$ Flame Doped with 700 ppm NH_3 ($\phi = 1.52$, T = 2010 K) Modeled with the Reaction Set of Table I. Data from Haynes (23)	B-I-6
1c	Post-Flame Zone of a $C_2H_4/O_2/N_2$ Flame Doped with 700 ppm NH_3 ($\phi = 1.52$, T = 2010 K) Modeled with the Reaction Set of Table I. Data from Haynes (23)	B-I-7
2a	Post-Flame Zone of a C_2H_4/Air Flame Doped with 500 ppm NO ($\phi = 1.66$, T = 2000 K) Modeled with the hydrocarbon-Free Reaction Set of Table I. Data from Haynes (23). .	B-I-9
2b	Post-Flame Zone of a C_2H_4/Air Flame Doped with 500 ppm NO ($\phi = 1.66$, T = 2000 K) Modeled with the Hydrocarbon-Free Reaction Set of Table I. Data from Haynes (23). .	B-I-10
3	Species Mole Fractions as Function or Residence Time (τ_{SR}) in an adiabatic stirred-reactor. CH_4/air Flame Doped with 1% NH_3, $\phi = 1.33$	B-I-16
4a	Post-Flame Zone of a C_2H_4/Air Flame Doped with 500 ppm NO ($\phi = 1.66$, T = 2000 K) Including Hydrocarbon "Breakthrough," Modeled with Gardiner's Reaction Set (32) Altered to Include a Ketene Intermediate, Supplemented by the Reactions of Tables I-III. Data from Haynes (23)	B-I-25
4b	Post-Flame Zone of a C_2H_4/Air flame Doped with 500 ppm NO ($\phi = 1.66$, T = 2000 K) Including Hydrocarbon "Breakthrough," Modeled with Gardiner's Reaction Set (32) Altered to Include a Ketene Intermediate, Supplemented by the Reactions of Tables I-III. Data from Haynes (23)	B-I-26

LIST OF TABLES

Table		Page
I	Simplified Fuel-Nitrogen Reaction Mechanism	B-I-20
II	Reactions Involving CH to be Appended to the Olson and Gardiner Mechanism	B-I-23
III	Hydrocarbon Fragment/Fuel-Nitrogen Interactions	B-I-24

1.0 INTRODUCTION

With the depletion of natural gas and petroleum reserves (which are lacking or low in nitrogen content and, hence, relatively low in the emission of NO_x formed from the nitrogen bound in the fuel) and the increasing substitution of coal, coal-derived liquids, residual fuel-oils, and shale oils (which are high in nitrogen content), NO_x emissions which are already unacceptably high in several urban areas, are bound to increase unless an abatement strategy is developed and implemented. Insofar as the mechanism by which fuel-bound nitrogen is converted to NO_x is complex, and insofar as early attempts (1,2) to reduce NO_x emissions by empirical adjustment of combustion parameters (e.g., temperature, fuel/air ratio, degree of mixedness, etc.) utilizing conventional combustors have achieved only a fraction of their full potential, a more fundamental elucidation of the NO_x formation mechanism has become essential in order to achieve the desired engineering goal of modifying the combustion process in such a way as to favor the conversion of fuel-bound nitrogen to the desired (combustion) end product, N_2, rather than to the undesired product, NO.

It is well understood that for any condensed phase fuel, combustion may proceed through parallel homogeneous and heterogeneous processes wherein the fuel is initially heated and undergoes devolatilization followed by rapid homogeneous gas phase oxidation of ~~the~~ volatile species and, if a devolatilized residue remains, slower heterogeneous burnout of the char. This is apparently the case for the combustion of pulverized coal and residual fuel oils. Distillate oils, however, may well burn entirely in the gas phase as a diffusion flame surrounding a shrinking, evaporating droplet. Certain fuels, of course, are gaseous from the outset.

Of primary interest here is the chemistry of volatile fuel-nitrogen conversion. Traditional gaseous fuels (natural gas) contain little or no bound nitrogen, although it is projected that the products of coal gasification which undergo a high temperature desulfurization may well contain significant quantities of ammonia. In addition, light distillate oils which for coal and shale-derived fuels may have nitrogen contents in excess of 1% by weight burn entirely in the volatile phase.

For fuels which leave a devolatilized residue, the relative significance of gas phase (versus heterogeneous) processes on NO_x formation is less obvious.

The distribution of nitrogenous species between volatiles and char has recently been studied (3,4,5,6,7) for pulverized coal combustion for temperatures ranging from 1250 to 1750 K. The results (for a Montana Lignite) demonstrate that at higher temperatures under fuel lean conditions, as much as 80% of the NO_x formed may originate in the volatile phase. This reflects the fact that at high enough temperatures, nearly all of the nitrogen in coal can be driven into the gas phase (3). Indeed, even under conditions (1750^o K) where 70% or more of the fuel nitrogen is volatilized during the course of the experiments (5), for equivalence ratios above about 1.5, over 50% of the NO_x originates from the char! These results reflect the long established facts that increases in fuel nitrogen concentration (8) and equivalence ratio (8,9,10) in the gas phase all tend to lower the conversion efficiency to NO_x. The strategy for controlling NO_x emission, therefore, is to drive as much fuel nitrogen as possible into the gas phase in a primary fuel rich zone (7,8,9,10,11) where the reaction kinetics can be "engineered" to minimize conversion to NO_x, as opposed to the alternative of allowing the nitrogen to remain in the char where subsequently it will be partially converted tc NO_x in the fuel lean secondary combustion zone (12). Clearly, optimizing this reaction engineering (minimizing NO_x emissions) is best achieved through a true understanding of the gas phase reaction mechanism. Insofar as the residence times in typical combustors are too short to acheieve chemical equilibrium in the burnt gases, it is necessary to consider the time dependent flow of nitrogenous species through the many sequential and competing reaction pathways leading to NO_x and N_2 formation, in order to develop a methodology for maximizing or minimizing certain product yields, i.e., bcth the elementary reaction pathways and reaction rates must be considered.

Unfortunately, trace emissions from rich stationary source combustors are the product of several, lumped chemical/physical processes, and even if the problems of coupling finite-rate chemistry with complex flow-fields are neglected for the moment, the necessity of computing NO_x levels to within the ppm range places rather stringent requirements on the mechanistic accuracy of whatever model is invoked.

Despite residual uncertainties in the currently available mechanistic and kinetic data base, adequate if imperfect, modeling of fuel-nitrogen conversion in the presence of "simple" fuels can now be achieved (11, 13,14). Unfortunately, however, real combustion systems, i.e., real fossil fuels, present incremental mechanistic complexities which do not decouple easily from solution of the fuel-nitrogen problem. It is to an assessment of these complexities and to the development of a methodology for dealing with them that this paper is addressed.

2.0 THE FUEL-NITROGEN MECHANISM

A large literature has appeared recently directed towards the experimental elucidation of the mechanistic details of fuel-nitrogen conversion under flame conditions (8,15). Synthesis of these observations into a master reaction set has been the subject of other studies reported elsewhere (16,17,18). Validation and refinement of the reaction set, based upon efforts to model independent data under as broad a range of conditions as possible, is an ongoing effort (11,13).

Initial attempts (18) by this author to construct a comprehensive fuel nitrogen mechanism utilized the method of Engleman (19) in which all species expected to be present are permitted to inter-react via elementary reactions. Rate constants were selected from tabulated estimates (made, generally, by the method of Johnston (20)). The method, however, suffers from the limitation of often necessitating the use of an impractically large reaction set (especially when combined with hydrocarbon mechanisms--see below) and, additionally, is limited in its accuracy by the capability to select, a priori, all species, including intermediates which are present. Recent suggestions by Branch et al (21) of mechanistic refinements to the NO/NH_3 reaction set underline this limitation. Current efforts have, therefore, tended back towards the use of a much smaller, conceptually clearer, fuel nitrogen reaction set.

To this end, equal success has been achieved in modeling the post-flame zones of several nitrogen-doped hydrocarbon flames using the "minimum subset" of fuel nitrogen reactions shown in Table I, as with the larger master set. It is cautioned, however, that the full range of applicability of this minimum subset is not yet established. Thus, for example, though significant contribution to the destruction of NO by reaction with NH_2 is precluded in modeling post-flame data in the range of 2000 K, recent indications (22) of the very strong inverse temperature coefficient of the effective $NO + NH_2$ rate constant suggest that mechanistic addition may still prove appropriate at lower temperatures.

An example of the modeling success achievable is indicated in Figure 1, showing the data of Haynes (23) in the post-flame gases of a rich ($\phi = 1.52$), atmospheric pressure, ethylene/oxygen/nitrogen flame doped with 700 ppm of ammonia. In view of Haynes' rather flat temperature profile (22 degree variation over 9.6 msec) and the arbitrariness of any assumed rate of heat loss,

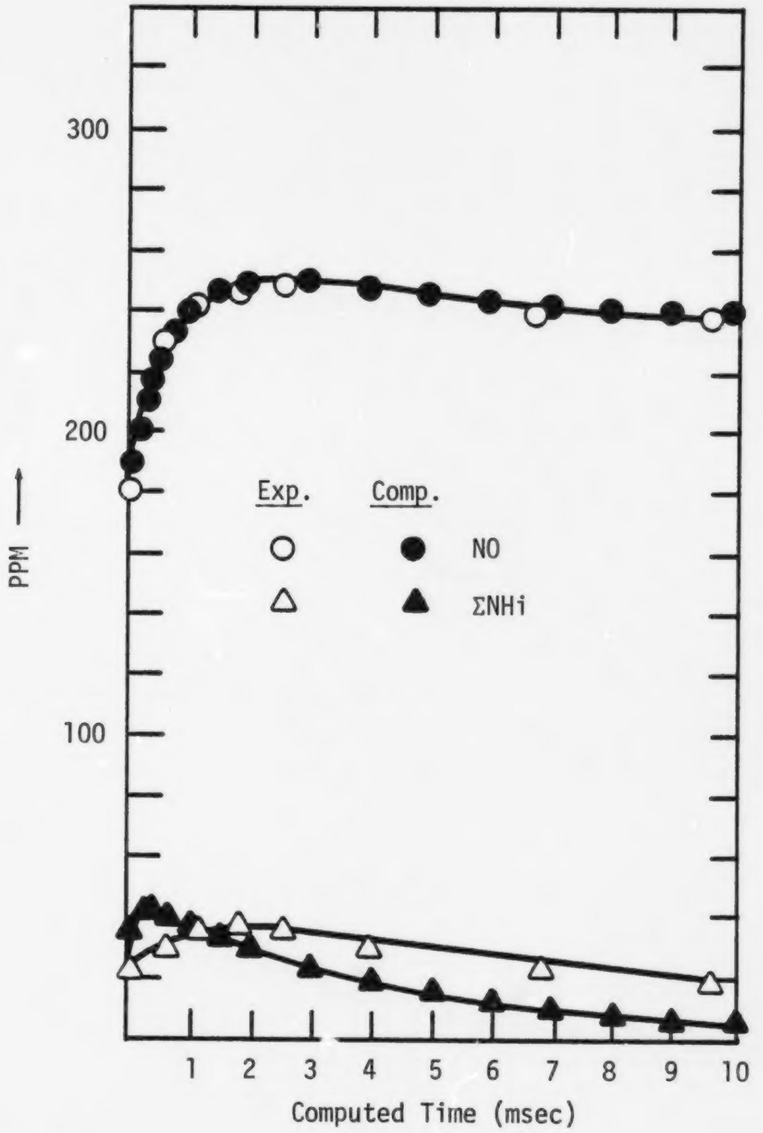

Figure 1a. Post-flame zone of a $C_2H_4/O_2/N_2$ flame doped with 700 PPM NH_3 ($\phi = 1.52$, $T = 2010$ K) modeled with the Reaction set of Table I. Data from Haynes (23).

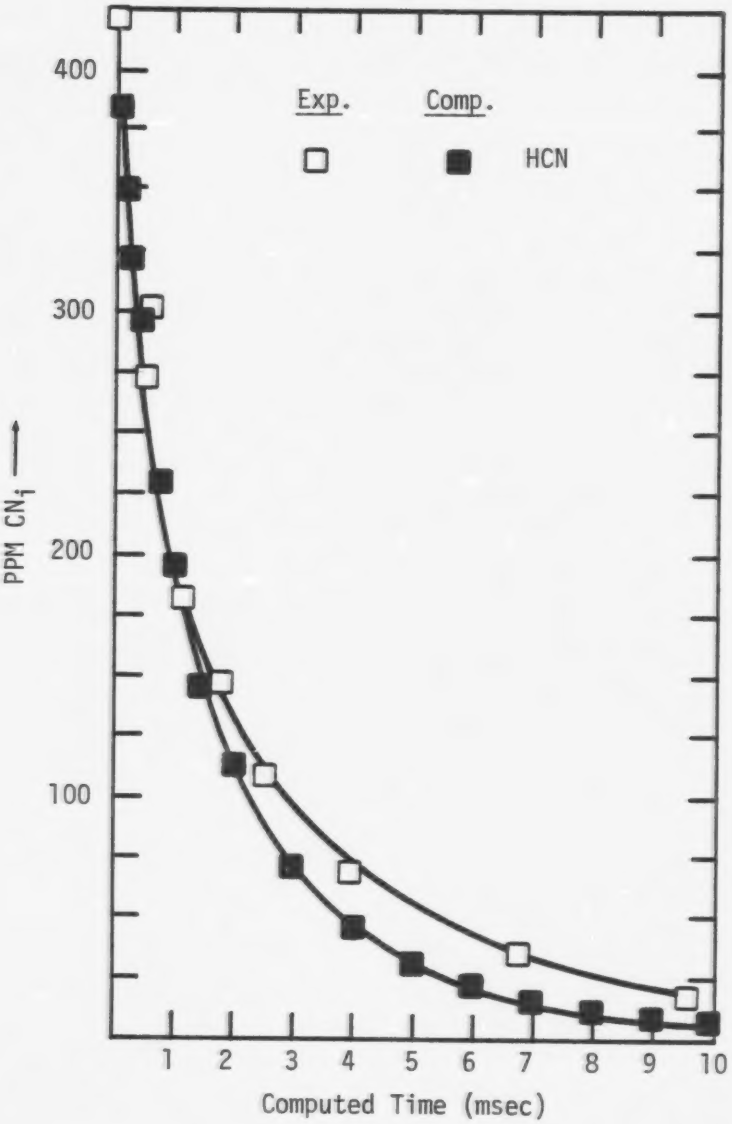

Figure 1b. Post-flame zone of a $C_2H_4/O_2/N_2$ flame doped with 700 PPM NH_3 (ϕ = 1.52, T = 2010 K) modeled with the Reaction set of Table I. Data from Haynes (23).

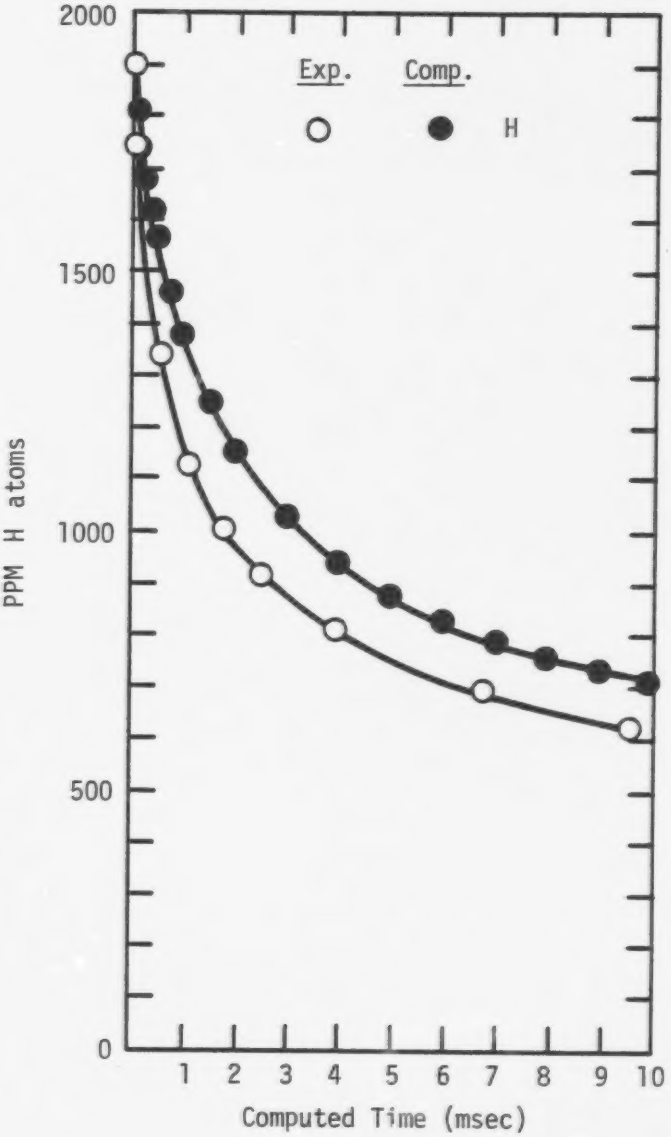

Figure 1c. Post-flame zone of a $C_2H_4/O_2/N_2$ flame doped with 700 PPM NH_3 ($\phi = 1.52$, T = 2010 K) modeled with the Reaction set of Table I. Data from Haynes (23).

modeling was performed isothermally at an average temperature of 2010 K. Calculations were in plug-flow, initialized assuming partial equilibration of the radical pool, and were performed on an IBM 360/65 using a computer code written at MIT for the integration of the stiff rate equations. Essential to the discussion to follow is the observation that no hydrocarbon species were observed in the post-flame zone of this flame.

Contrasting with the results of Figure 1 are those shown in Figure 2 for Haynes' richer ethylene/air flame ($\phi = 1.66$) doped with 500 ppm NO. The major distinction in this flame is the "breakthrough" of hydrocarbons (roughly 0.2% of the total flow) into the post-flame zone. The results of Figure 2 were generated by ignoring the hydrocarbons. Although the fits to the concentration profiles are not really bad, better success in fitting the HCN and NO profiles has been achieved (see below) through consideration of the pertinent hydrocarbon chemistry. (Ammonia profiles remain systematically in error.) It should be clearly noted, also, that the influence of hydrocarbons upon fuel-nitrogen chemistry is potentially much greater in the highly backmixed environment of a practical combustor than may be suggested by Figure 2. This is demonstrated by a series of computations performed (using a detailed hydrocarbon mechanism) on a methane/air system doped with 1% ammonia. In these calculations, a well-stirred reactor (WSR) section of varying residence time fed a plug-flow reactor (PFR) section, also of varying residence time, such that the total residence time remained approximately constant. Bound nitrogen concentrations are shown in Figure 3 for an adiabatic calculation at a fuel/air equivalence ratio of 1.33, and demonstrate nicely that for a fixed total reaction time, HCN exit concentrations (the major product of fuel-nitrogen/hydrocarbon interactions) are increased with increased stirred reactor residence time. This conclusion follows logically, of course, from the recognition that strong backmixing necessarily increases the possibility for reaction between hydrocarbon and nitrogenous fragments.

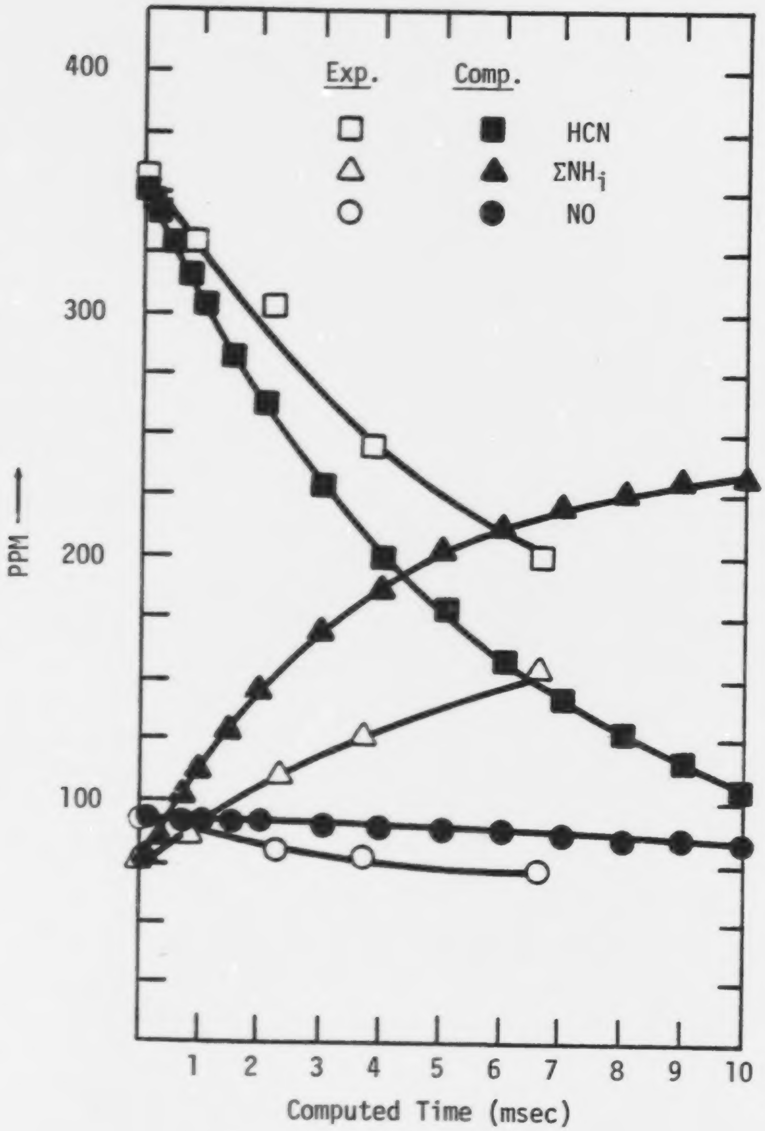

Figure 2a. Post-flame zone of a C_2H_4/air flame doped with 500 PPM NO (ϕ = 1.66, T = 2000 K) modeled with the hydrocarbon-free reaction set of Table I. Data from Haynes (23).

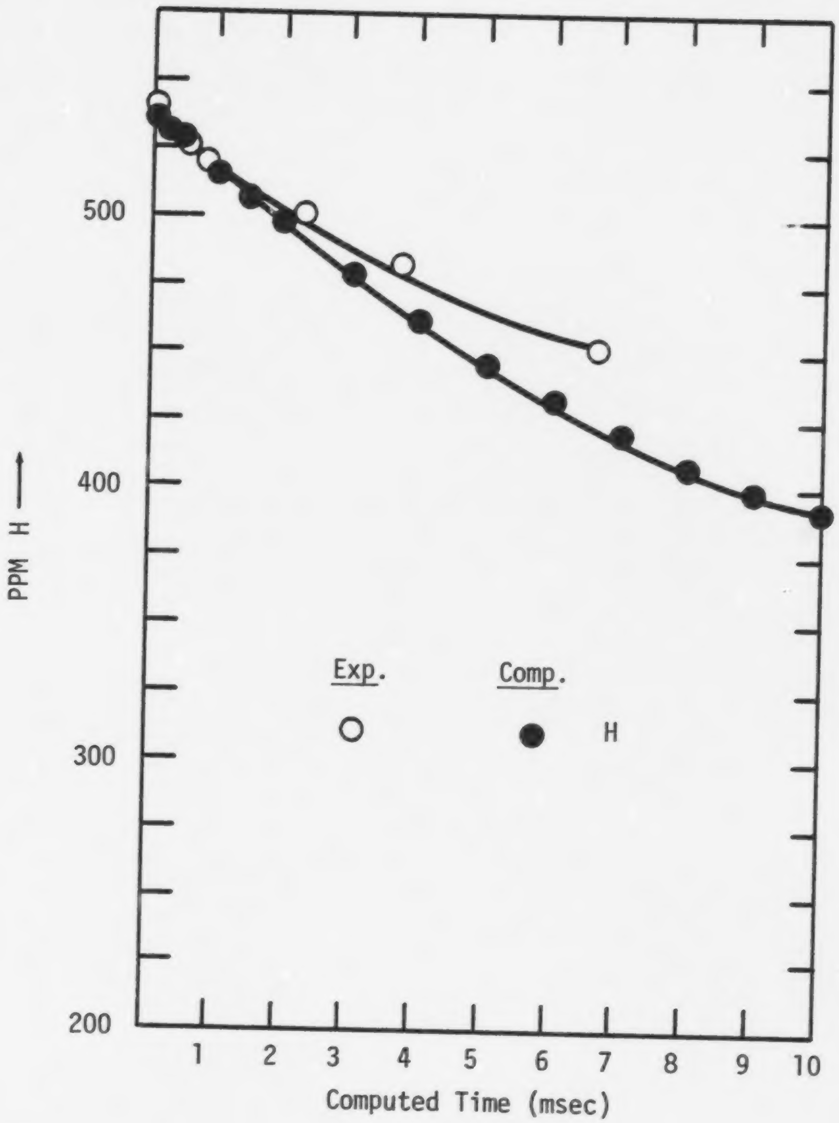

Figure 2b. Post-flame zone of a C_2H_4/air flame doped with 500 PPM NO ($\phi = 1.66$, $\bar{T} = 2000$ K) modeled with the hydrocarbon-free reaction set of Table I. Data from Haynes (23).

3.0 THE HYDROCARBON PROBLEM

The results of Figure 2 serve in miniature to demonstrate that additional mechanistic complexities arise in the computation of fuel-nitrogen chemistry when hydrocarbons are present. Indeed, predictive modeling of bound-nitrogen emissions in a real-fuel, fuel-rich environment can be seen to be dependent when the capability to model hydrocarbon decay kinetics for the following reasons:

1. Interactions of fuel-nitrogen and hydrocarbon fragments may be quite significant, especially in recycling NO back to HCN. Omission of this class of reactions is consistent with the enhanced NO profile and diminished HCN profile calculated in Figure 2. Also,
2. the radical pool (H, O, OH) which drives the fuel-nitrogen chemistry is determined primarily by the hydrocarbon chemistry which dominates the system at early times.

Insofar as fuel-rich operation contributes to NO_x abatement strategies, it seems necessary to model hydrocarbon burnout if ppm-level accuracy is to be demanded of a fuel-nitrogen mechanism. Unfortunately, however, aside from having only the most phenomenological knowledge of the specifics of the interactive reactions between hydrocarbons and nitrogenous species, even modeling the combustion of methane--the simplest of hydrocarbons--currently comes close to straining the state-of-the-art. In addition, the validity of generalizing conclusions applicable to design considerations of real fuel systems based upon computations using methane as a model hydrocarbon fuel is still not, a priori, clear. Indeed, methane is an atypical fuel in that

1. its H/C ratio of 4 greatly exceeds the H/C ratios of fuels of interest (H/C might equal 1.3, for example, for a coal-derived liquid),
2. its combustion details might simulate paraffin-type species, but many fuels of practical nature are highly aromatic in character, and
3. even as a paraffin, methane may be atypical in that methyl recombinations may be of unusual significance in its combustion mechanism.

Two questions of significance have, therefore, been identified:

1. To what extent can the results of NO_x modeling in the presence of methane be taken as representative of fuels of practical interest? And, in order to answer that question,

2. How can the combustion kinetics of higher hydrocarbons, more representative of fuels of practical interest, be modeled for the purpose of predicting fuel-nitrogen conversion to NO_x?

4.0 METHODOLOGY FOR DEALING WITH HIGHER HYDROCARBONS

4.1 Detailed Kinetics

In this method, all species of significance and all essential elementary reactions of each species are identified, resulting in an extensive set of coupled rate equations which describe the kinetic behavior of the system. This, of course, is the most correct way to characterize the system. The method suffers, however, from the limitations that:

a. for higher hydrocarbons, even straight chain paraffins, neither a complete set of species nor, certainly, of reactions is known, i.e., with few exceptions, the detailed combustion mechanisms are simply not available.

b. Theoretical synthesis of combustion mechanisms for higher hydrocarbons (as performed for CH_4, for example, by the method of Engleman (19,24)) is impractical because the magnitude of the problem grows exponentially (25) with the number of carbon atoms, resulting in reaction sets impractically large for computational studies, and because, in any event, virtually none of the elementary reaction rate constants are known. Additionally,

c. even if such an approach were viable, the time and cost necessary to screen such reaction sets down to reasonable sizes, as well as the current dearth of experimental data necessary for model validation would render the method impractical.

Detailed kinetics are therefore rejected as a viable method of modeling the combustion chemistry of fuels of practical interest.

4.2 The Global and Semi-Global Methods

In this method, hydrocarbon burnout is modeled by a single "global" (or overall) relation of the form

$$CnHm + (n + \frac{m}{4})\, O_2 \rightarrow nCO_2 + \frac{m}{2}\, H_2O$$

for which a rate expression must be empirically determined. Even as a first estimate, this method really has little basis in theory, and has been shown to be applicable only where a single major heat release step is involved, thereby excluding its applicability to hydrocarbon oxidation. In any event, the method completely overlooks elementary reaction kinetics and intermediate radical formation and is of no utility in computing NO_x levels.

Hydrocarbon oxidation can be conceived of occurring, however, in two overlapping heat release steps: a rapid oxidation of the hydrocarbon to carbon monoxide and hydrogen (or water), followed by subsequent oxidation of the CO (and H_2). It is possible, therefore, to develop a semi-global method utilizing two (or more) sequential global steps and one (or more) stable intermediate species to describe the overall combustion process. Thus, for example

$$C_nH_m + (\frac{n}{2} + \frac{m}{4})\ O_2 \rightarrow nCO + (m/2)H_2O$$

followed by

$$CO + 1/2\ O_2 \rightarrow CO_2$$

This method has been used with some success (26) for the relatively simple case of methane oxidation, but again, in any case, suffers from the limitation of completely neglecting intermediate, radical species essential to prediction of trace NO formation levels.

A conceptually similar, but somewhat more detailed, semi-global method has been under development by Dryer (27) for application to hydrocarbon burnout. In this method, paraffin oxidation has been separable into three global steps of the form

$$\text{Alkane} \rightarrow \text{Alkene} \rightarrow CO \rightarrow CO_2$$

Although this may be regarded as a significant improvement over two-step semi-global modeling for purposes of modeling heat release, it offers little practical improvement for purposes of modeling NO levels. Additionally, empirical rate expressions characterizing each global step are currently available only for paraffins up to butane. No rates are yet available for aromatic systems.

4.3 The Quasi-Global Method

In this method, the simple global step

$$C_nH_m + \frac{n}{2}\ O_2 \rightarrow nCO + \frac{m}{2}\ H_2$$

is followed by an elementary reaction mechanism (which is well known) for the $H_2/CO/O_2$ system. Because the time scale for CO burnout is long compared with the global conversion of the parent hydrocarbon to CO, a certain amount of modeling success may be achieved by assuming the global step to occur at an infinite rate--especially if attention is focused primarily upon post-flame reactions--although, following the work of Edelman and Fortune (28), a finite rate expression for the global step may also be used to enhance modeling accuracy. Utilization of detailed kinetics for the CO/H_2 oxidation admits free radical chemistry to the mechanism, thus opening the door to computations coupling the detailed kinetics of fuel-nitrogen conversion with hydrocarbon burnout.

Several serious limitations to this method, however, must be noted:

a. Although a degree of "elementary" reaction chemistry is preserved in modeling the CO/H_2 oxidation step via detailed kinetics, the actual temporal history of the free radical pool may be seriously miscalculated. Thus, attempts to model thermal-NO_x formation (29) in a methane flame by means of the quasi-global method have proven inadequate largely due to errors in the computed oxygen atom levels.

b. The nature of the global step is such as to remove all consideration of hydrocarbons from the model. However, as suggested by Figure 3 above, "recycling" of NO to form HCN in fuel-rich systems via reactions with hydrocarbons (e.g., $CH + NO \rightarrow HCN + O$) is a limiting factor in bound nitrogen decay in the presence of hydrocarbons, and must be considered in developing staging strategies to eliminate bound nitrogen from the combustor exhaust stream. Omission of all hydrocarbons from consideration is tantamount to neglect of many of the processes which require modeling.

c. Distinction among different hydrocarbon fuels is not readily apparent in any other manner other than purely stoichiometric in the quasi-global model, although differences in molar enthalpies of fuels should lead to somewhat different computed time/temperature histories. Of course, the degree to which mechanistic chemistry differences (rather than temperature differences) distinguish NO_x emission levels from the combustion of different hydrocarbons is currently unclear (no

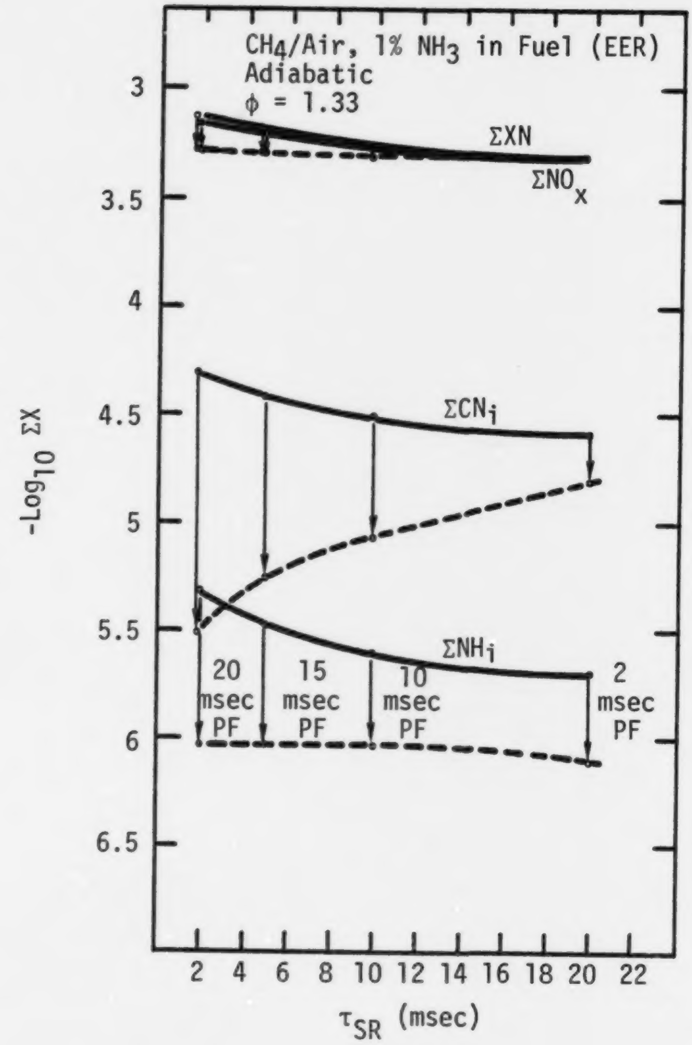

Figure 3. Species mole fractions as function of residence time (τ_{SR}) in an adiabatic stirred-reactor. CH_4/air flame doped with 1% NH_3, ϕ = 1.33. The vertical lines denote the effects of varying times in plug-flow following the stirred-reactor section, the plug-flow residence times being (from left to right) 20 msec, 15 msec, 10 msec, and 2 msec. The dashed lines denote species concentrations for combined stirred-reactor and plug-flow sections. Thus, ΣCN_i = 4.88 x 10^{-10} for τ_{SR} = 2 msec, but falls to 3.08 x 10^{-6} after an additional 20 msec in plug-flow (total reaction time = 22 msec), whereas ΣCN_i = 2.51 x 10^{-5} for τ_{SR} = 20 msec, but falls to 1.51 x 10^{-5} after an additional 2 msec in plug-flow.

definitive experimental data are currently available), and the hope is that mechanistic differences (for example, the distribution of intermediate hydrocarbon fragments) will prove to have only a second order influence upon NO_x levels. However, construction of a computational model which a priori neglects such considerations does seem less desirable than one which permits them.

It is concluded, therefore, that the quasi-global method, as currently utilized, is, if not inapplicable to the modeling of NO_x emissions from higher hydrocarbons, at least undesirable as a method with adequate predictive capabilities.

4.4 Development of a New Quasi-Global Method: QUAGMIRE

Having exhausted, as impractical or inapplicable, all existing methods of treating hydrocarbons of which we are aware, we have proposed a new quasi-global method of the following, general form:

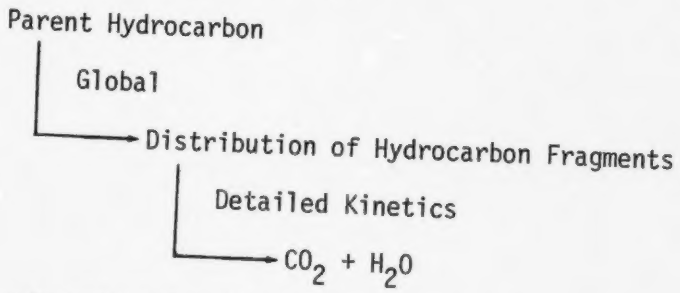

The basis underlying this hypothesized method rests upon the assumptions that the initial degradation of the parent hydrocarbon in the preflame zone via pyrolysis and oxidative pyrolysis routes is very rapid; that the initial decomposition products may be represented by a relatively small set of low molecular weight, stable and/or unstable hydrocarbon species; and, of course, that the decomposition mechanism can be justifiably represented by a global step.

The potential utility of the method lies in the following:

a. The advantages of modeling free radical chemistry by detailed kinetics are retained, but the magnitude of the elementary reaction set required is vastly reduced. Again, this reflects the exponential-like growth in reaction set magnitude with number of carbon atoms in the parent species. If only hydrocarbon fragments with relatively few carbon atoms are present following the global step, then the magnitude of the reaction set--given by the union of the combustion reaction sets of the fragment species--will be small relative to the (hypothetical) reaction set of the parent hydrocarbon.

b. Whereas, even if the magnitude of the problem could be handled computationally, the detailed combustion mechanism of the parent hydrocarbon is generally unknown, detailed combustion mechanisms of many of the hydrocarbon fragments, which may be assumed to predominate at flame conditions, are known or are in varying stages of development.

c. Unlike the quasi-global method of Edelman and Fortune, hydrocarbons are retained in the elementary reaction scheme.

d. To the extent that an initial global step is applicable according to the method of Edelman and Fortune, the approximation should be more accurate here. This reflects a reduction in the mechanistic size of the global step, or, more significantly, a reduction in the magnitude of the reaction time or extent encompassed by the global step. That is, whereas the method of Edelman and Fortune takes a giant global step nearly to the postflame zone (where hydrocarbons have disappeared and CO has formed), it is arguable that the global step proposed here is completed in the preflame zone or early into the primary reaction zone (30), which is where much of the essential fuel-nitrogen chemistry occurs! Thus, the global step may be regarded as faster on a time scale pertinent to fuel-nitrogen conversion. The probability of miscalculating the concentration/time history of the radical pool, for purposes of modeling NO_x emissions, is concurrently reduced.

In distinction to the quasi-global method of Edelman and Fortune, the technique proposed here may be referred to as the Quasi-Global Method applied to Initial Reaction Extents (QUAGMIRE). Details of QUAGMIRE, including justification of its computational applicability and discussion of associated research questions are presented elsewhere (31).

5.0 MODELING OF FUEL-NITROGEN CONVERSION IN A HYDROCARBON ENVIRONMENT

It can be shown (31) that the detailed kinetic mechanisms of combustion of the C_1 and C_2 species under fuel-rich conditions are the basic building blocks of QUAGMIRE. Recent developments in this area have been rapid and substantial, and have laid an adequate foundation upon which it is possible to develop QUAGMIRE. Olson and Gardiner (32) have published a methane mechanism which includes chemistry through the C_4 species, although the formaldehyde reaction rates should, probably, be updated by Dean's (33) more recent shock tube measurements. Through extensive modeling of shock tube data, Gardiner (34) has concluded that his is the best existing methane mechanism, although Gardiner (35) has also identified inadequacies in it in modeling C_2 chemistry. Levy (31), however, has rectified at least one of the residual C_2 problems in Gardiner's mechanism by demonstrating that the products of hydroxyl attack upon acetylene do not feed strongly into the CH_i set, but are better modeled as running through a ketene intermediate to formaldehyde. Accordingly, in an attempt to model Haynes' rich, fuel-nitrogen doped ethylene/air post-flame hydrocarbon decay data (Figure 2), Gardiner's modified reaction set was combined with the minimum subset fuel-nitrogen mechanism of Table I, a small subset of CH-generating reactions borrowed from the Engleman (24) methane reaction set compilation shown in Table II (Gardiner's set does not include CH), and a small set of postulated hydrocarbon/fuel-nitrogen interactions, shown in Table III, of which all but one are gleaned from Engleman's compilation (24), the remaining dominant (global) reaction of CH_3 with NO being taken from Haynes' (17,23) analysis. The resulting reaction mechanism of 102 reactions in 36 species is integrated to yield the results shown in Figure 4, which demonstrate nicely the desired hydrocarbon decay data, as well as coupled fuel-nitrogen profiles improved over those of Figure 2.

The prognosis for establishment of an adequate C_2 modeling capability in the near future does, therefore, look quite bright, although the reader should not be misled into believing that either C_1 or C_2 mechanisms can yet be considered to be adequately characterized. Thus, free radical profiles computed for the hydrocarbon "breakthrough" case fall far below the measured values. This demonstrates a residual problem with Gardiner's C_1/C_2 mechanism, and indicates the need for further developments of the elementary hydrocarbon mechanisms. It should be noted that excessive radical destruction is also predicted for this

Table I. Simplified Fuel-Nitrogen Reaction Mechanism*
Rate Constant, $k_f = AT^n \exp(-E/RT)$

	REACTION	A (cm^3/mole-sec)	n	E (cal/mole)	REFERENCE
1	$HCN + OH \rightarrow CN + H_2O$	2.00×10^{11}	0.60	5000.	b
2	$CN + H_2 \rightarrow HCN + H$	3.16×10^{12}	0	5000.	c
3	$CN + OH \rightarrow NCO + H$	5.60×10^{13}	0	0.	d
4	$HCN + OH \rightarrow HNCO + H$	4.00×10^{11}	0	0.	e
5	$NCO + H_2 \rightarrow HNCO + H$	3.20×10^{11}	0	0.	a
6	$NCO + H \rightarrow NH + CO$	3.00×10^{14}	0	0.	a
7	$HNCO + H \rightarrow NH_2 + CO$	1.00×10^{13}	0	0.	a
8	$NH_3 + H \rightarrow NH_2 + H_2$	5.00×10^{11}	0.50	2000.	f
9	$NH_3 + OH \rightarrow NH_2 + H_2O$	1.39×10^{11}	0	1600.	m,n,o
10	$NH_2 + H \rightarrow NH + H_2$	3.50×10^{10}	0.79	4460.	g
11	$NH_2 + OH \rightarrow NH + H_2O$	3.00×10^{10}	0.68	1300.	f
12	$NH + H \rightarrow N + H_2$	1.00×10^{12}	0.68	1900.	f
13	$NH + OH \rightarrow N + H_2O$	5.00×10^{11}	0.50	2000.	f
14	$NO + H \rightarrow N + OH$	1.34×10^{14}	0	49200.	h
15	$N + NO \rightarrow N_2 + O$	3.10×10^{13}	0	344.	i
16	$NH + NO \rightarrow N_2O + H$	9.00×10^{9}	0.75	0.	j
17	$N_2O + H \rightarrow N_2 + OH$	7.60×10^{13}	0	15101.	k
18	$N_2O + M \rightarrow N_2 + O + M$	1.42×10^{14}	0	51280.	l
19	$NH + NH \rightarrow N + NH_2$	3.60×10^{11}	0.55	1900.	f
20	$N + NH_3 \rightarrow NH_2 + NH_2$	2.10×10^{11}	0.50	23160.	f
21	$NH + N \rightarrow N_2 + H$	6.30×10^{11}	0.50	0.	q,r
22	$NH_2 + NH_2 \rightarrow NH + NH_3$	1.70×10^{11}	0.63	3600.	f,p

*For a discussion of reactions 1 - 18 see Reference (a).

References - Table I

a. Foster, D. E., J. B. Heywood, J. C. Keck, J. P. Longwell, A. F. Sarofim, and B. R. Taylor, "Control of NO_x Emissions from Combustion of Fuels Derived from Shale and Coal," Summary Technical Progress Report, October 23, 1978. Prepared for the Department of Energy under Contract EX-76-A-01-2295, The Energy Laboratory, MIT.

b. Tunder, R., S. Mayer, E. Cook, and L. Schieler, Aerospace Report No. TR-1001 (9210-02)-1, AD 813 485, Aerospace Corp., Thermochemistry Research Dept., 1967.

c. Benson, S. W., D. M. Golden, and R. Shaw, "Estimating the Kinetics of Combustion," EPA Report EPA-600/2-75-019, 1975.

d. Haynes, B.S., "The Formation and Behavior of Nitrogen Species in Fuel-Rich Hydrocarbon Flames," Ph.D. Thesis, The University of New South Wales, 1975.

e. Estimate, this work.

f. Bahn, G. S., "Reaction Rate Compilation for the N-O-H System," Gordon and Breach, 1968.

g. Mayer, S. W., L. Schieler, and H. S. Johnston, "Computations of High-Temperature Rate Constants for Bimolecular Reactions of Combustion Products," Eleventh Symposium (International) on Combustion, The Combustion Institute, Pittsburgh, PA, 1967.

h. Flower, W. L., R. K. Hanson, and C. H. Kruger, "Kinetics of the Reaction of Nitric Oxide with Hydrogen," Fifteenth Symposium (International) on Combustion, The Combustion Institute, p. 823, 1974.

i. Baulch, D. L., D. D. Drysdale, and A. C. Lloyd, "Critical Evaluation of Rate Data for Homogeneous Gas-Phase Reactions of Interest in High Temperature Systems," Volume 4, The University of Leeds, England, 1969.

j. Roose, T. R., R. K. Hanson, and C. H. Druger, "Decomposition of NO in the Presence of NH_2," presented at the 11th Annual International Shock Tube Symposium, Seattle, Washington, 1974.

k. Baulch, D. L., et al., Evaluated Kinetic Data for High Temperature Reactions, Volume 2, CRC Press, 1973.

l. Monat, J. P., R. K. Hanson, and C. H. Kruger, "Kinetics of Nitrous Oxide Decomposition," Combustion Science and Technology, 16, 21-28, 1977.

m. Dove, J. E., and S. N. Wing, "Shock Tube Studies of the Reactions of Hydrogen Atoms: I - The Reaction of $H + NH_3 \rightarrow H_2 + NH_2$," Can. J. Chem., 52, 1171, 1974.

n. Zellner, R., and I. W. Smith, "Rate Constants for the Reactions of OH with NH_3 and HNO_3," Chemical Physics Letters, 26 (1), 1974.

o. Perry, R. A., R. Atkinson, and J. N. Pitts, Jr., "Rate Constants for the Reactions of $OH + H_2S \rightarrow H_2O + SH$ and $OH + NH_3 \rightarrow H_2O + NH_2$ Over the Temperature Range 297-427^{o}K," The Journal of Chemical Physics, 64 (8), 3237, 1976.

p. Mayer, S. W., and L. Schieler, Aerospace Corp. Report TR-66 (8210-02)-3, June, 1966.

q. Engleman, V. S., "Survey and Evaluation of Kinetic Data on Reactions in Methane/Air Combustion," EPA Report EPA-600/2-76-003, 1976.

r. Benson, S. W., D. M. Golden, R. W. Lawrence, and R. Shaw, Quarterly Progress Report No. 2, EPA Grant No. R-800798, February, 1973.

Table II. Reactions Involving CH to be Appended to the Olson and Gardiner Mechanism

$$k_f = AT^N \exp(-E/RT)$$

REACTION		A(cm^3/mole-sec)	n	E(Cal/mole)
1	$CH_2 + H = CH + H_2$	3.16×10^{11}	0.70	5,000
2	$CH_2 + OH = CH + H_2O$	5.00×10^{11}	0.50	6,000
3	$CH + CO_2 = CHO + CO$	1.00×10^{10}	0.50	6,000
4	$CH + OH + CHO + H$	5.00×10^{11}	0.50	10,000
5	$CH + O_2 = CHO + O$	5.00×10^{11}	0.50	6,000
6	$CH + O = CO + H$	5.00×10^{11}	0.50	0

All rates from Engleman, V.S., "Survey and Evaluation of Kinetic Data on Reactions in Methane/Air Combustion," EPA Report EPA-600/2-76-003, 1976.

Table III. Hydrocarbon Fragment/Fuel-Nitrogen Interactions

$k_f = AT^N \exp(-E/RT)$

	REACTION	A(cm^3/mole-sec)	N	E (Cal/mole)	REFERENCE
1	$CH_4 + CN = CH_3 + HCN$	3.16×10^{11}	0.70	5,000	a
2	$CH_2 + N_2 = HCN + NH$	1.00×10^{14}	0	60,000	b
3	$CH_2 + NO = CH_2O + N$	1.60×10^{12}	0	7,000	a
4	$CHO + N = CH + NO$	1.00×10^{14}	0	48,600	c
5	$CHO + N = HCN + O$	1.00×10^{14}	0	0	a
6	$CHO + N = CO + NH$	2.00×10^{11}	0.50	2,000	a
7	$HCN + N = CH + N_2$	2.50×10^{11}	0	16,000	b
8	$HCN + O = CH + NO$	1.00×10^{14}	0	72,000	b
9	$CN + NH = CH + N_2$	1.00×10^{14}	0	40,000	b
10	$CH_3 + NO = \ldots = HCN + H_2O$	2.20×10^{11}	0	0	d

References

a. Engleman, V.S., "Survey and Evaluation of Kinetic Data on Reactions in Methane/Air Combustion," EPA Report, EPA-600/2-76-003, 1976.

b. Benson, S. W., D. M. Golden, R. W. Lawrence, R. Shaw, and R. W. Woolfolk, "Estimating the Kinetics of Combustion: Including Oxides of Nitrogen and Sulfur," EPA Report, EPA-600/2-75-019, 1976, and estimates based thereon.

c. Estimate based upon Engleman; Reference (a) above.

d. Haynes, B. S., "Kinetics of Nitrogen Oxide Formation in Combustion," in Progress in Astronautics and Aeronautics, Volume 62, Alternative Hydrocarbon Fuels: Combustion and Chemical Kinetics (C. T. Bowman and J. Birkeland, Eds.), American Institute of Aeronautics and Astronautics, 1978.

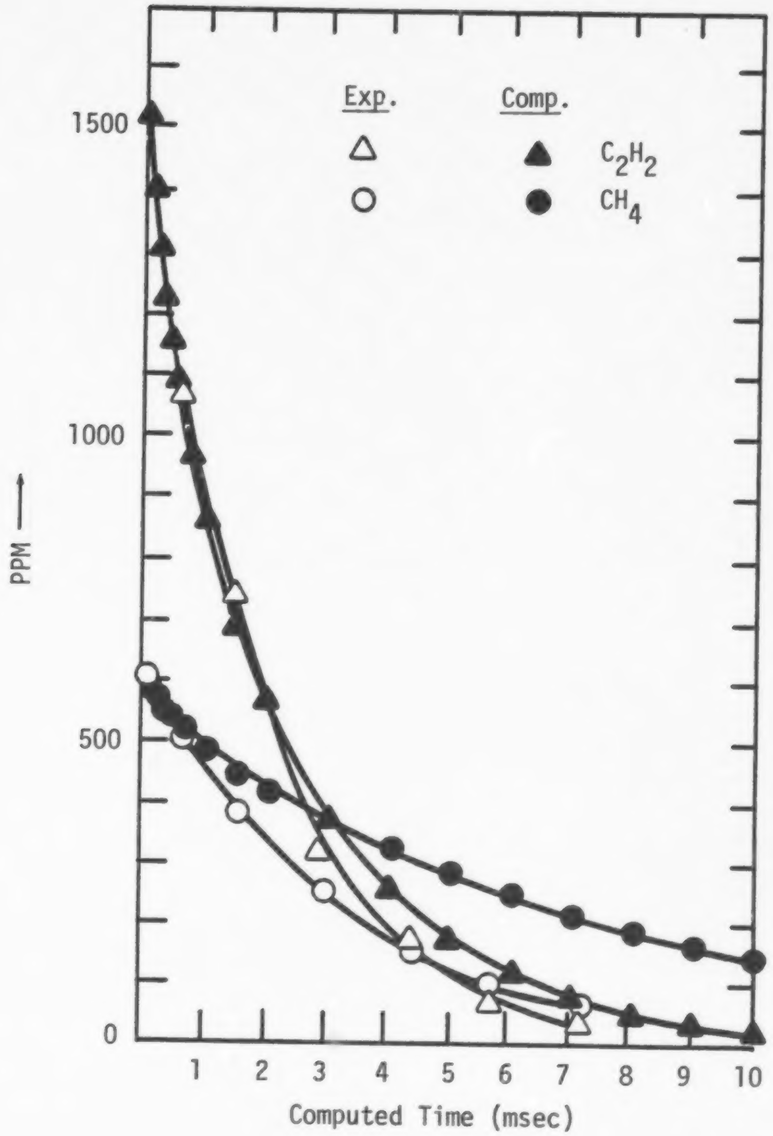

Figure 4a. Post-flame zone of a C_2H_4/air flame doped with 500 PPM NO (ϕ = 1.66, $\bar{T}$ = 2000 K) including hydrocarbon "breakthrough," modeled with Gardiner's reaction set (32) altered to include a ketene intermediate, supplemented by the reactions of Tables I-III. Data from Haynes (23).

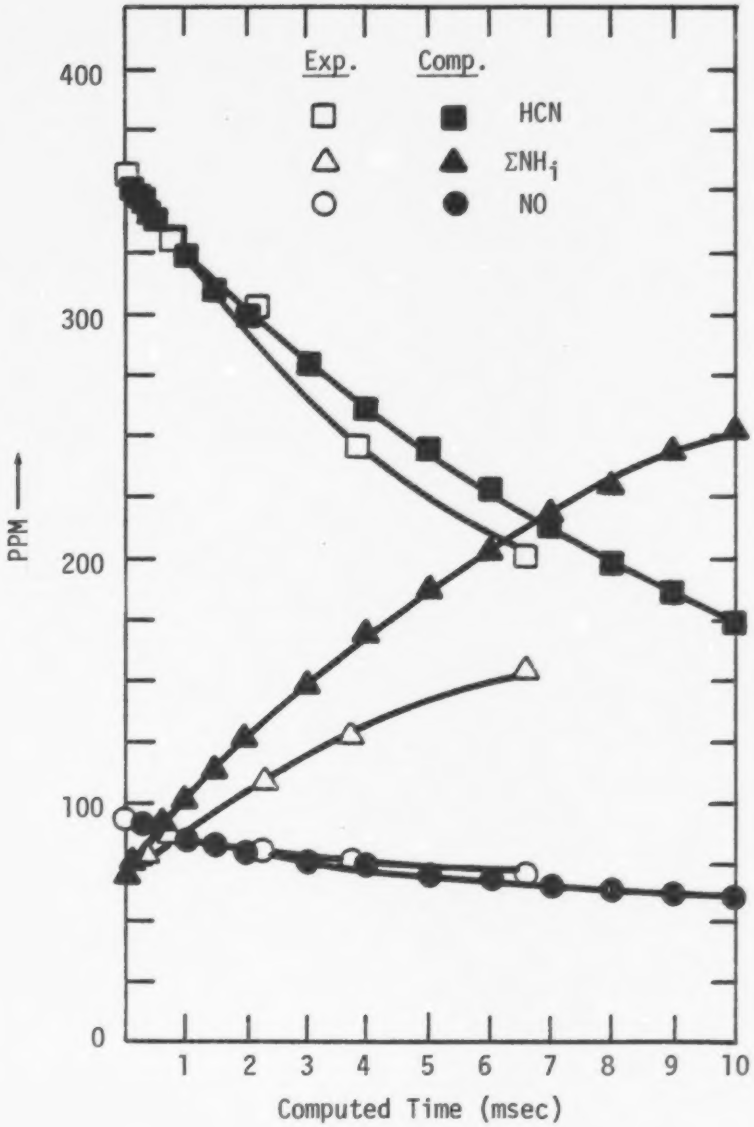

Figure 4b. Post-flame zone of a C_2H_4/air flame doped with 500 PPM NO ($\phi = 1.66$, $\bar{T}$ - 2000 K) including hydrocarbon "breakthrough," modeled with Gardiner's reaction set (32) altered to include a ketene intermediate, supplemented by the reactions of Tables I-III. Data from Haynes (23).

system (36) by the newly published mechanism of Westbrook (37). In this regard, it is vital that additional data, similar to those of Haynes (23), be obtained for validation or refinement, under post-flame conditions pertinent to practical fuel-nitrogen chemistry, of the mechanistic hydrocarbon chemistry developments which are generally derived from shock tube studies.

6.0 SUMMARY

Capabilities to model fuel-nitrogen conversion in the absence of hydrocarbons under aerodynamically clean conditions have been demonstrated, although the mechanistic chemistry of the amines still requires refinement. Modeling capabilities under conditions of hydrocarbon "breakthrough," however, are limited by the necessity to model higher hydrocarbon oxidation. This problem, however, may be reduced in computational magnitude through a quasi-global method which limits necessary hydrocarbon mechanisms to C_1 and C_2 species. Although not yet fully developed, available C_1 and C_2 mechanisms are improving. Additional experimental data are required, however, for refinement and validation of C_1 and C_2 reaction sets; elucidation of hydrocarbon fragment distributions in the post-flame zone as a function of parent higher hydrocarbon, equivalence ratio and temperature; and provision of a data base for the modeling of the coupled chemistry of fuel-nitrogen conversion in a higher hydrocarbon environment.

REFERENCES

1a. Turner, D. W., and C. W. Siegmund, "Staged Combustion and Flue Gas Recycle: Potential for Minimizing NO_x from Fuel Oil Combustion," American Flames Research Committee Flame Days, Chicago, September, 1972.

1b. Turner, D. W., R. L. Andrews, and C. W. Siegmund, "Influence of Combustion Modifications and Fuel Nitrogen Content on Nitrogen Oxide Emissions from Fuel Oil Combustion," AIChE Symposium Series 68, 55, 1972.

1c. Siegmund, C. W., and D. W. Turner, "NO_x Emissions from Industrial Boilers: Potential Control Methods," J. Eng. Power, p. 1-6, January, 1974.

2a. Bartok, W., A. R. Crawford, and G. J. Piegari, "Systematic Field Study of NO_x Emission Control Methods for Utility Boilers," Esso Research and Engineering Co., Report No. GRU. 4GNOS. 71 to the Office of Air Programs, Research Triangle Park, North Carolina, December, 1971.

2b. Martin, G. B., and E. E. Berkau, "An Investigation of the Conversion of Various Fuel-Nitrogen Compounds to Nitrogen Oxides in Oil Combustion," AIChE Symposium Series 68, 126, 45, 1972.

2c. Heap, M. P., T. M. Lowes, R. Walmsley, and H. Bartelds, "Burner Design Principles for Minimum NO_x Emissions," Proceedings of the Coal Combustion Seminar, Research Triangle Park, North Carolina, EPA Report No. EPA 650/2-73-021, September, 1973.

3. Pohl, J. H., "Fate of Fuel Nitrogen," Sc.D. Thesis, M.I.T., 1976.

4. Pohl, J. H., and A. F. Sarofim, "Devolatilization and Oxidation of Coal Nitrogen," Sixteenth Symposium (International) on Combustion, The Combustion Institute, p. 491, Pittsburgh, 1977.

5. Song, Y. H., "Fate of Fuel Nitrogen During Pulverized Coal Combustion," Sc.D. Thesis, M.I.T., 1978.

6. Song, Y. H., J. M. Beér, and A. F. Sarofim, "Fate of Fuel Nitrogen During Pyrolysis and Oxidation," Second Annual Symposium on Stationary Source Combustion, New Orleans, Louisiana, 1977.

7. Levy, J. M., J. H. Pohl, A. F. Sarofim, and Y. H. Song, "Combustion Research on the Fate of Fuel-Nitrogen Under Conditions of Pulverized Coal Combustion," EPA Report No. EPA-600/7-78-165, August, 1978.

8. Fenimore, C. P., "Formation of Nitric Oxide from Fuel Nitrogen in Ethylene Flames," Comb. and Flame, 19, 289, 1972.

9a. DeSoete, G. G., "Le Mecanisme de Formation D'Oxyde Azotique a Partir D'Ammoniac et D'Amines Dan Les Flammes D'Hydrocarbures," Revue de L'Institute Francais Du Petrole, 28, 95, 1973.

9b. DeSoete, G. G., and A. Queraud, "Formation D'Oxyde D'Azote Dans Les Flammes: Formation D'Oxyde D'Azote A Partir De L'Azote Du Combustible. C-Addition de NO Dans Les Melanges Inflammables," Report No. I.F.P. No. 21. 681, Institute Francais Du Petrole, Rueil Malmaison, France, 1973.

10. Sarofim, A. F., G. C. Williams, M. Modell, and S. M. Slater, "Conversion of Fuel Nitrogen to Nitric Oxide in Premixed and Diffusion Flames," AIChE Symposium Series 148, Volume 7, 51, 1975.

11. Levy, J. M., J. P. Longwell, A. F. Sarofim, T. L. Corley, M. P. Heap, and T. J. Tyson, "NO_x Abatement in Fossil Fuel Combustion: Chemical Kinetic Considerations," Proceedings of the Third Symposium on Stationary Source Combustion, Volume IV, EPA-600/7-79-050, p. 3, March, 1979.

12. Pershing, D. W., and J. O. L. Wendt, "Pulverized Coal Combustion: The Influence of Flame Temperature and Coal Combustion on Thermal and Fuel NO_x," Sixteenth Symposium (International) on Combustion, The Combustion Institute, p. 389, Pittsburgh, 1977.

13. Corley, T. L., "Development of a Kinetic Mechanism to Describe the Fate of Fuel Nitrogen in Gaseous Systems," Fifth E.P.A. Fundamental Combustion Research Workshop, Newport Beach, California, January, 1980.

14. Heap, M. P., T. J. Tyson, J. E. Cichanwicz, R. Gersham, C. J. Kau, G. B. Martin, and W. S. Lanier, "Environmental Aspects of Low BTU Gas Combustion," Sixteenth Symposium (International) on Combustion, The Combustion Institute, p. 535, 1977.

15a. Fenimore, C. P., "Reactions of Fuel-Nitrogen in Rich Flame Gases," Comb. and Flame, 26, 249, 1976.

15b. Morley, C., "The Formation and Destruction of Hydrogen Cyanide from Atmospheric and Fuel-Nitrogen in Rich, Atmospheric-Pressure Flames," Comb. and Flame, 27, 189, 1976.

15c. Haynes, B. S., "Reactions of Ammonia and Nitric Oxide in the Burnt Gases of Fuel-Rich Hydrocarbon-Air Flames," Comb. and Flame, 28, 81, 1977.

15d. Haynes, B. S., "The Oxidation of Hydrogen Cyanide in Fuel-Rich Flames," Comb. and Flame, 28, 113, 1977.

16. Sarofim, A. F., J. H. Pohl, and B. R. Taylor, "Strategies for Controlling Nitrogen Oxide Emissions During Combustion of Nitrogen Bearing Fuels," AIChE 69th Annual Meeting, Chicago, 1976.

17. Haynes, B. S., "Kinetics of Nitrogen Oxide Formation in Combustion," in Progress in Astronautics and Aeronautics, Volume 62 (C. T. Bowman and J. Birkeland, Eds.), Alternative Hydrocarbon Fuels: Combustion and Chemical Kinetics, American Institute of Aeronautics and Astronautics, 1978.

18. Levy, J. M., J. P. Longwell, and A. F. Sarofim, "Conversion of Fuel-Nitrogen to Nitrogen Oxides in Fossil Fuel Combustion: Mechanistic Considerations," Report to Energy and Environmental Research Corp. by the MIT Energy Laboratory, EPA FCR Program, 1978.

19. Engleman, V. S., "Detailed Approach to Kinetic Mechanisms in Complex Systems," J. Phys. Chem., 81, 2320, 1977.

20a. Mayer, S. W., L. Schieler, and H. S. Johnston, "Computation of High-Temperature Rate Constants for Bimolecular Reactions of Combustion Products," Eleventh Symposium (International) on Combustion, The Combustion Institute, p. 837, Pittsburgh, 1966.

20b. Tunder, R., S. Mayer, E. Cook, and L. Schieler, Aerospace Corporation Report TR-1001 (9210-02)-1, 1967.

21. Branch, M. C., J. A. Miller, and R. J. Kee, "Chemical Kinetics of the $NH_3/NO/O_2$ System," 1979 Fall (Western States Section) Combustion Meeting, The Combustion Institute, WSS Paper No. 79-38, Berkeley, California, October, 1979.

22a. Hack, W., H. Schacke, M. Schröter, and H. G. Wagner, "Reaction Rates of NH_2 Radicals with NO, NO_2, C_2H_2, C_2H_4 and Other Hydrocarbons," Seventeenth Symposium (International) on Combustion, The Combustion Institute, p. 505, 1979.

22b. Silver, J. A., C. M. Gozewski, and C. E. Kolb, "Chemical Kinetics of the NH_3/NO Reaction System Under Combustion Exhaust Flow Conditions," to be presented at the Eighteenth Symposium (International) on Combustion, Waterloo, Ontario, August, 1980.

23. Haynes, B. S., "The Formation and Behavior of Nitrogen Species in Fuel Rich Hydrocarbon Flames," Ph.D. Thesis, University of New South Wales, Sydney, Australia, 1975.

24. Engleman, V. S., "Survey and Evaluation of Kinetic Data on Reactions in Methane/Air Combustion," EPA Report, EPA-600/2-76-003, 1976.

25. Cohen, R. C., "The High Temperature Oxidation and Pyrolysis of Ethane," Ph.D. Thesis, Princeton University, Department of Aerospace and Mechanical Sciences, 1972.

26a. Dryer, F. L., "High Temperature Oxidation of Carbon Monoxide and Methane in a Turbulent Flow Reactor," Ph.D. Thesis, Princeton University, Department of Aerospace and Mechanical Sciences, 1972.

26b. Dryer, F. L., and I. Glassman, "High Temperature Oxidation of CO and CH_4," Fourteenth Symposium (International) on Combustion, The Combustion Institute, Pittsburgh, PA, p. 987, 1973.

27. Dryer, F. L., and I. Glassman, "Combustion Chemistry of Chain Hydrocarbons," in Progress in Astronautics and Aeronautics, Volume 62 (Bowman, C. T. and J. Birkeland, Eds.), Alternative Hydrocarbon Fuels: Combustion and Chemical Kinetics, American Institute of Aeronautics and Astronautics, 1978.

28. Edelman, R. B., and O. F. Fortune, "A Quasi-Global Chemical Kinetic Model for the Finite Rate Combustion of Hydrocarbon Fuels with Application to Turbulent Burning and Mixing in Hypersonic Engines and Nozzle," AIAA Paper No. 69-86, 1969.

29. Bowman, C. T., and A. S. Kesten, "Kinetic Modeling of Nitric Oxide Formation in Combustion Processes," presented at the Fall Meeting, Western States Section of the Combustion Institute, Paper No. 71-28, Irvine, California, October, 1971.

30. Millikan, R. C., "Non-Equilibrium Soot Formation in Premixed Flames," J. Phys. Chem. 66, 794, 1962.

31. Levy, J. M., "Modeling of Fuel-Nitrogen Chemistry in Combustion: The Influence of Hydrocarbons," Fifth E.P.A. Fundamental Combustion Research Workshop, Newport Beach, California, January, 1980.

32. Olson, D. B., and W. C. Gardiner, Jr., "Combustion of Methane in Fuel-Rich Mixtures," Comb. and Flame 32, 151, 1978.

33a. Dean, A. M., B. L. Craig, R. L. Johnson, M. C. Schultz, and E. E. Wang, "Shock Tube Studies of Formaldehyde Pyrolysis," Seventeenth Symposium (International) on Combustion, The Combustion Institute, p. 577, 1979.

33b. Dean, A. M., R. L. Johnson, and D. C. Steiner, "Shock Tube Studies of Formaldehyde Oxidation," in press, 1979.

34. Olson, D. B., and W. C. Gardiner, Jr., "An Evaluation of Methane Combustion Mechanisms," J. Phys. Chem. 81, 2514, 1977.

35. White, J. N., and W. C. Gardiner, Jr., "An Evaluation of Methane Combustion Mechanisms: 2 - Comparison of Model Predictions with Experimental Data from Shock-Initiated Combustion of C_2H_2, C_2H_4, and C_2H_6," J. Phys. Chem. 83, 562, 1979.

36. Levy, J. M., unpublished results.

37. Westbrook, C. K., "An Analytical Study of the Shock Tube Ignition of Mixtures of Methane and Ethane," Comb. Sci. and Technology 20, 5, 1979.

APPENDIX II

AN INVESTIGATION OF THE FORMATION AND DESTRUCTION OF NITROGENOUS SPECIES DURING HYDROCARBON-AIR COMBUSTION

by

David W. Blair
Exxon Research and Engineering Company
Contract Research Division
P.O. Box 45
Linden, New Jersey 07036

ABSTRACT

The purpose of this work was to provide reliable experimental information on the conversion of nitrogenous species in the combustion of hydrocarbon fuels (both with and without fuel nitrogen) with air. This information is to be used to provide critical insights into computer models of NO_x formation and critical tests of those models. Experiments were run at constant temperature at a quasi-plug flow combustor (laminar flow) and in a strongly backmixed (jet-stirred) combustor. Temperatures ranged from 1800 to 2000 K and equivalence ratios ranged from 0.7 to 1.8. Fuels were methane, ethylene, or propane and fuel nitrogen was represented by ammonia or a mixture of ammonia and nitric oxide. Significant differences in nitrogen conversion were observed between the two combustors with the plug flow reactor (residence time 30 ms) being the more sensitive to fuel and fuel nitrogen species and the backmixed reactor (residence time 3 ms) being the more copious emitter of fixed nitrogen products both with and without fuel nitrogen. It was concluded that these differences stemmed much more from differences in combustion environment than from differences in residence time between the two combustors.

TABLE OF CONTENTS

Section		Page
ES	EXECUTIVE SUMMARY	B-II-1
I	INTRODUCTION	B-II-16
II	APPARATUS AND METHOD	B-II-19
	II-1. The Multiburner	B-II-19
	II-2. The Jet-Stirred Combustor (JSC)	B-II-22
	II-3. Data Reduction	B-II-30
	II-4. Gases Used in the Experiments	B-II-33
III	RESULTS	B-II-34
	III-1. Results from Multiburner	B-II-34
	III-2. Results from the Jet-Stirred Combustor	B-II-59
	III-3. Comparison of Results Obtained in the Multiburner and the Jet-Stirred Combustor	B-II-75
IV	CONCLUSIONS	B-II-89
V	SUGGESTED WORK	B-II-91
VI	ACKNOWLEDGMENTS	B-II-92
VII	REFERENCES	B-II-93
APPENDIX A	COMPARISON OF RESULTS FROM THE PRESENT JET-STIRRED COMBUSTOR WITH THOSE FROM PREVIOUS JSC's	B-II-94
APPENDIX B	RADIAL UNIFORMITY IN THE MULTIBURNER	B-II-103

LIST OF FIGURES

Figure		Page
ES1	Schematic Diagram of the Jet-Stirred Combustor.	B-II-13
ES2	Gas Analysis.	B-II-14
ES3	Schematic Diagram of the Multiburner.	B-II-15
II-1.1	Schematic Diagram of the Multiburner.	B-II-20
II-2.1	Schematic Diagram of the Jet-Stirred Reactor.	B-II-23
II-2.2	Overall View of the Jet-Stirred Reactor Test System . . .	B-II-25
II-2.3	Sample Probe.	B-II-26
II-2.4	Sample Conditioning System.	B-II-27
II-2.5	Gas Analysis System	B-II-29

LIST OF TABLES

Table		Page
ES1	Thermal Fixed Nitrogen from Methane Flames at 1900 K Flame Temperature.	B-II-5
ES2	Ratio of Thermal Fixed Nitrogen from Methane Flames at 1900 K to Equilibrium Values.	B-II-6
ES3	Total Thermal Fixed Nitrogen from Methane Flames in the Multiburner.	B-II-7
ES4	Comparative Effect of Fuel Species on Thermal Fixed Nitrogen Produced in Flames at 1900 K and 1.4 Equivalence Ratio.	B-II-8
ES5	Comparative Effect of Temperature on Fuel Nitrogen (200 ppm NH_3) Conversion in Methane Flames	B-II-9
ES6	The Influence of Fuel and FN Species (210 ppm FN) on Conversion in the Multiburner at 1900 K.	B-II-10
ES7	Comparative Effect of Fuel Nitrogen Species (200 ppm) on Conversion in Methane Flames at 1900 K.	B-II-11
ES8	Comparative Effect of Fuel Species on the Conversion of Fuel Nitrogen (200 ppm NH_3) in Flames at 1900 K . . .	B-II-12
III-1.1	Combinations of Independent Variables Run in the Multiburner Experiments.	B-II-40
III-1.2	Experimental Results from $CH_4/O_2/N_2$ Flames in the Multiburner With 1800 K Flame Temperature.	B-II-42
III-1.3	Experimental Results from $CH_4/O_2/N_2$ Flames in the Multiburner With 1900 K Flame Temperature.	B-II-43
III-1.4	Experimental Results from $CH_4/O_2/N_2$ Flames in the Multiburner With 2000 K Flame Temperature.	B-II-44
III-1.5	Experimental Results from $C_2H_4/O_2/N_2$ Flames in the Multiburner.	B-II-45
III-1.6	Experimental Results from $C_3H_8/O_2/N_2$ Flames in the Multiburner.	B-II-46
III-1.7	Effect of Equivalence Ratio on Fixed Nitrogen Produced in Hydrocarbon/O_2/N_2 Flames at 1900 K Without Fuel Nitrogen in the Multiburner.	B-II-47
III-1.8	Effect of Equivalence Ratio and Temperature on Fixed Nitrogen Produced in Methane/O_2/N_2 Flames Without Fuel Nitrogen in the Multiburner.	B-II-48

LIST OF TABLES (Continued)

Table Page

III-1.9 Effect of Equivalence Ratio, Temperature, and Concentration of Fuel Nitrogen (NH_3) on Conversion of Fuel Nitrogen in $CH_4/O_2/N_2$ Flames. B-II-49

III-1.10 Effect of Equivalence Ratio and Fuel Nitrogen Species (NH_3 or $NO + NH_3$) on Conversion of Fuel Nitrogen in $CH_4/O_2/N_2$ Flames at 1900 K B-II-51

III-1.11 Effect of Equivalence Ratio and Fuel Nitrogen Species (NH_3 or $NO + NH_3$) on Conversion of Fuel Nitrogen in $CH_4/O_2/N_2$ Flames at 1900 K B-II-52

III-1.12 Effect of Equivalence Ratio and Fuel Nitrogen Species (NH_3 or $NH_3 + NO$) on Conversion of Fuel Nitrogen in $C_2H_4/O_2/N_2$ Flames at 1900 K. B-II-53

III-1.13 Effect of Equivalence Ratio and Fuel Nitrogen Species (NH_3 or $NH_3 + NO$) on Conversion of Fuel Nitrogen in $C_2H_4/O_2/N_2$ Flames at 1900 K. B-II-55

III-1.14 Effect of Equivalence Ratio and Fuel Nitrogen Concentration (NH_3) on Conversion of Fuel Nitrogen in $C_3H_8/O_2/N_2$ Flames at 1900 K. B-II-56

III-1.15 Effect of Equivalence Ratio, Fuel Nitrogen Concentration and Species, and Fuel Species on Nitrogen Conversion in Hydrocarbon/O_2/N_2 Flames at 1900 K B-II-57

III-2.1 Combinations of Variables Run in the Jet-Stirred Combustor Experiments. B-II-62

III-2.2 Results from All Experiments Run in the Jet-Stirred Combustor. B-II-71

III-2.3 Effect of Equivalence Ratio on Fixed Nitrogen Produced in the Jet-Stirred Combustor With Hydrocarbon/O_2/N_2 Flames at 1900 K Without Fuel Nitrogen B-II-64

III-2.4 Effect of Equivalence Ratio, Temperature, and Concentration of Fuel Nitrogen (NH_3) on Conversion of Fuel Nitrogen in $CH_4/O_2/N_2$ Flames in the Jet-Stirred Combustor. B-II-65

III-2.5 Effect of Equivalence Ratio and Fuel Nitrogen Species (NH_3 or $NO + NH_3$) on Conversion of Fuel Nitrogen in $CH_4/O_2/N_2$ Flames at 1900 K in the Jet-Stirred Combustor. B-II-67

LIST OF TABLES (Continued)

Table		Page
III-2.6	Effect of Equivalence Ratio, Concentration, and Fuel Species on Conversion of Fuel Nitrogen in the Jet-Stirred Combustor.	B-II-68
III-3.1	Comparison of Thermally Fixed Nitrogen in the Multiburner and the Jet-Stirred Combustor for Hydrocarbon/O_2/N_2 Flames at 1900 K	B-II-81
III-3.2	Comparison of the Effects of Temperature and Fuel Nitrogen (NH_3) Concentration on Fuel Nitrogen Conversion in Methane Flames in the Multiburner and the Jet-Stirred Combustor.	B-II-82
III-3.3	Fuel Nitrogen (NH_3) Conversions Averaged Over All Input Concentrations in the Two Combustors	B-II-87
III-3.4	Effects of Equivalence Ratio, Fuel Nitrogen Concentration, and Fuel Nitrogen Species on Fuel Nitrogen Conversion Compared for the Multiburner and the Jet-Stirred Reactor at Nominal 1900 K for the CH_4/O_2/N_2 System	B-II-88

SECTION ES

EXECUTIVE SUMMARY

This is the final report on a program that was designed to provide accurate quantitative experimental information on critical aspects of the formation and destruction of nitrogenous chemical species during hydrocarbon/air combustion.

A primary purpose of this work is to provide reliable experimental information that can be used to provide both critical insights into computer models of NO_x formation and critical tests of these models. Thus, the results should provide both a guide and a challenge to modelers. Responding to this purpose, results were obtained for a very wide range of experimental conditions to aid users in testing the generality of various kinetic models. To achieve this end, experiments were run in two significantly different laboratory combustors over a wide range of independent thermochemical variables.

The first was a very strongly backmixed reactor--the jet-stirred combustor (JSC). It is shown schematically in Figure ES1. In this combustor premixed gaseous reactants are injected through numerous small ports in a hemispherical injector into a hemispherical ceramic reaction volume of two inch diameter. Exhaust products issue from this reactor through numerous radial exhaust ports. The average residence time within the reactor is 3 ms. The injection jets are sonic. They vigorously stir the mixture within the reactor to maintain highly turbulent, near homogeneous conditions. These jets have a mixing time within the reactor of the order of 30 μs. Under these conditions, even "preflame" reactions occur in the presence of products from all stages of the combustion reaction mechanism. There is no physical separation of the process into preflame, intermediate, and final combustion zones. Samples of products from this reaction are withdrawn from the reactor through cooled quench-probes and analyzed for stable chemical species by standard means (Figure ES2).

The second combustor was an adiabatic, laminar, quasi-plug flow combustor--the multiburner (MB). It is shown schematically in Figure ES3. In this combustor a radially uniform laminar stream of premixed gaseous reactants flows upward through a porous stainless steel flat flame burner into a zirconia tube. A laminar flat flame is stabilized adjacent to the upper face of the burner and postflame products flow upward through the cylindrical combustor tube. This tube is held at the pre-calculated adiabatic flame temperature by an electrically heated furnace which surrounds it. Because many important reactions involving nitrogenous species proceed at rates much less than those of predominant combustion reactions, nitrogen conversion occurs in the post-flame gases throughout the combustion tube. Samples of product were withdrawn through a cooled quench probe from a point 2 cm (30 ms residence time) above the burner face. These samples were analyzed by standard methods (Figure ES2).

In each of the combustors experiments were run at constant flame temperature (maintained by adjusting the N_2/O_2 ratio in the combustion "air") over a range of equivalence ratios from 0.7 to 1.8, with either CH_4, C_2H_4, or C_3H_8 as fuels, and with "fuel" nitrogen represented either by NH_3 or by a 1/1 ratio mixture of NH_3 + NO. "Fuel" nitrogen concentrations in the reactants ranged from 0 to 1000 ppm and flame temperatures of 1800, 1900, and 2000 K were investigated.

Table ES1 compares results of experiments without fuel nitrogen (the resulting fixed nitrogen in the products is "thermal" nitrogen) in the two combustors with 1900 K flame temperature and CH_4 as the fuel. From this table it is observed that:

- The JSC is a more prolific producer of total fixed nitrogen (TFN) at all equivalence ratios (ϕ) than is the MB.
- For $\phi<1.2$ the MB produces more NH_3 and HCN than does the JSC.
- For $\phi>1.2$ the JSC produces more HCN than does the MB.
- TFN maximizes around $\phi = 1.2$ in the MB but it increases monotonically with ϕ in the JSC.
- For $\phi<1.8$ the major product species is NO while for $\phi = 1.8$ it is HCN.

These observations raise the question whether the differences in performance of the two combustors results primarily from differences in reaction time (3 ms in the JSC vs 30 ms in the MB) of from differing chemical environment in the two combustors (backmixed vs plug flow). Because longer times should produce more thermal NO and TFN, it is concluded that combustion environment is the critical factor.

Table ES2 presents the results of Table ES1 as fractions of equilibrium values. It can be immediately observed that:

- Equivalence ratio 1.2 separates the regions where (lower ϕ) TFN and NO are present in less than equilibrium quantities and (higher ϕ) where they are present in greater than equilibrium quantities.
- NH_3 and HCN are present in greater than equilibrium quantities at all equivalence ratios but the ratio for NH_3 decreases monotonically with ϕ while that for HCN appears to maximize around $\phi = 1.0$.
- For $\phi<1.2$ the MB is further from equilibrium than the JSC while for $\phi>1.2$ the converse is true.

Table ES3 shows the effect of flame temperature on the production of thermal TFN in methane flames in the MB. It can be understood in terms of the equilibrium ratios of Table ES2.

- Below $\phi = 1.2$ (where TFN is present in subequilibrium quantities) increasing temperature increases TFN (drives the system towards equilibrium, as would be expected).

- Above $\phi = 1.2$ (where TFN is present in superequilibrium quantities) increasing temperature decreases TFN (drives the system towards equilibrium, as would be expected).

Table ES4 shows the effect of fuel species on thermal TFN at 1900 K and equivalence ratio 1.4. It shows that:

- All nitrogen species and, thus, TFN show more fuel sensitivity for the MB than for the JSC.

- TFN, NH_3, and HCN decrease monotonically with carbon number in the MB but except for HCN (which increases monotonically) they appear to be highest with C_2H_4 in the JSC.

- The trends of NO with carbon number are similar in the two combustors but more is produced in the JSC.

It is reasonable to speculate that these observations reflect differing combustion environments in the two combustors. In the MB a significant period (O|1 ms|) exists for preflame reactions to occur. During this period initial fuel breakdown products are almost the only radical species present. While they influence subsequent reaction paths, they carry much of the identity of their parent fuel species with them. In the JSC this preflame reaction period is very much shorter. Reaction occurs in the presence of radicals that result predominantly from later reaction steps and these radicals carry much less of the identity of the fuel species with them. Based upon these considerations one would expect backmixed systems to be more independent of fuel molecular structure than are plug flow systems.

Table ES5 shows the effect of temperature on fuel nitrogen (200 ppm NH_3) conversion in CH_4 flames in the two combustors. As was the case with thermal nitrogen, TFN and NO are at subequilibrium at $\phi = 1.0$ and at superequilibrium at $\phi > 1.0$. Thus, for $\phi = 1.0$ increasing temperature increases TFN and NO (drives the system towards equilibrium) but for $\phi > 1.0$ the situation is less clear. In the JSC at $\phi > 1.0$ both TFN and NO decrease with increasing temperature (move towards equilibrium) but this is not always true of the MB, nor does increasing temperature generally move HCN and NH_3 towards equilibrium for either burner at any ϕ. Kinetics are clearly controlling these results. The following additional observations may be drawn from this table:

- Conversion of fuel nitrogen to TFN and NO appears to be more sensitive to temperature in the MB than in the JSC and while it tends to increase with temperature in the MB it tends to decrease in the JSC.

- Conversion to NH_3 and HCN differs considerably between the MB and the JSC.

Table ES6 shows the effect of fuel species and fuel nitrogen species on conversion to TFN in the multiburner at $\phi = 1.4$ and a flame temperature of 1900 K. With CH_4 as the fuel, conversion to TFN greatly increases as fuel NO is substituted for some of the fuel NH_3 but that large sensitivity disappears when C_2H_4 is the fuel. Conversion of fuel NH_3 to TFN is rather insensitive to fuel species.

Table ES7 compares the effect of fuel nitrogen species on conversion to TFN in the two combustors with 1900 K CH_4 flames. The multiburner shows more sensitivity to this substitution at all ϕ than does the JSC. Also, the substitution of NO for NH_3 as fuel nitrogen increases conversion to TFN in the MB and decreases it in the JSC. Also for $\phi = 1.4$ or 1.8 this substitution causes TFN to move further from equilibrium in the MB and towards equilibrium (or leaves it unchanged) in the JSC (at $\phi = 1.0$ it causes the JSC to move away from equilibrium). While shorter residence times might be expected to increase sensitivity to fuel nitrogen species that is not the case between these two combustors. This further strengthens the hypothesis that the differences in results obtained from them stem from differences in combustion environment, not from differences in residence time.

Table ES8 compares the effect of fuel species on conversion of fuel nitrogen (NH_3) in the two combustors. With all fuels, conversion in the JSC exceeds that in the MB. The MB shows a considerable fuel effect at $\phi = 1.0$ while the JSC does not. Neither combustor shows much effect of fuel species at $\phi = 1.4$.

The following conclusions are drawn from this work:

- With both equivalence ratio and flame temperature held constant, specific hydrocarbon chemistry influences both thermal nitrogen fixation and fuel nitrogen conversion.
- Fuel chemistry is more important in the multiburner than it is in the jet-stirred combustor. The contributions of combustion environment to this difference appear to exceed those of reaction time.
- While the conversion of fuel nitrogen is dependent upon fuel nitrogen species, the dependency in the MB considerably exceeds that in the JSC. This argues that differences in combustion environment between the two combustors is important.
- Because production of fixed nitrogen products differs significantly between the MB and the JSC, when choosing between these combustors as models of given practical combustors the choice should be based upon which one best approaches conditions that will exist in the given combustor.

While there is a need for considerable additional work in this area (extending range of variables, verifying results, expanding range and areas of overlap between the several independent variables) this project has terminated at ER&E Co. and further work on it is not contemplated there at this time.

Table ES1

THERMAL FIXED NITROGEN FROM METHANE FLAMES AT 1900 K FLAME TEMPERATURE

ϕ	DEVICE	FIXED NITROGEN IN COMBUSTION GAS ppm			
		TFN	NH_3	HCN	NO
0.8	MB	18	7.2	1.8	9.2
0.8	JSC	41	1.6	1.5	38
1.0	MB	39	14	2.4	23
0.97	JSC	60	1.0	1.0	58
1.2	MB	53	4.8	17	31
1.4	MB	42	2.4	6.8	33
1.4	JSC	80	3.0	15	62
1.8	MB	35	2.2	27	5.7
1.8	JSC	133	1.4	121	11

Table ES2

RATIO OF THERMAL FIXED NITROGEN FROM METHANE FLAMES AT 1900 K TO EQUILIBRIUM VALUES

ϕ	DEVICE	TFN	NH_3	HCN	NO
0.8	MB	0.0071	2.1E5	5.3E4	0.0036
0.8	JSC	0.016	4.8E4	4.5E4	0.015
1.0	MB	0.088	2.6E4	4.0E6	0.052
0.97	JSC	0.072	1.9E3	1.7E6	0.12
1.2	MB	3.1	46	1.0E4	1.8
1.4	MB	5.7	7.4	7.3E2	4.7
1.4	JSC	11	9.2	1.6E3	8.8
1.8	MB	9.7	2.3	5.2E2	1.4
1.8	JSC	37	1.5	2.3E3	2.8

Table ES3

TOTAL THERMAL FIXED NITROGEN FROM METHANE FLAMES IN THE MULTIBURNER

ϕ	TFN, ppm			RATIO TO EQUILIBRIUM		
	1800	1900	2000 K	1800	1900	2000 K
0.8	--	18	98	--	0.0071	0.030
1.0	39	39	70	0.19	0.088	0.10
1.2	47	53	48*	15	3.1	1.8
1.4	64	42	43**	39	5.7	3.5
1.8	38	35	22	23	9.7	4.0

* $\phi = 1.25$

** ϕ 1.44

Table ES4

COMPARATIVE EFFECT OF FUEL SPECIES ON THERMAL FIXED NITROGEN PRODUCED IN FLAMES AT 1900 K AND 1.4 EQUIVALENCE RATIO

DEVICE	FUEL	FIXED NITROGEN OUTPUT, ppm			
		TFN	NH_3	HCN	NO
MB	CH_4	42	2.4	6.8	33
JSR	CH_4	80	3.0	15	62
MB	C_2H_4	38	2.0	2.0	34
JSR	C_2H_4	96	6.2	17	73
MB	C_3H_8	24	0.94	1.3	22
JSR	C_3H_8	89	3.7	26	59

Table ES5

COMPARATIVE EFFECT OF TEMPERATURE ON FUEL NITROGEN (200 ppm NH_3) CONVERSION IN METHANE FLAMES

ϕ	DEVICE	TFN, PERCENT*		NH_3, PERCENT*		HCN, PERCENT*		NO, PERCENT*	
		1800	1900	1800	1900	1800	1900	1800	1900
1.0	MB	52 (0.49)	66 (0.32)	0.38 (3.1E3)	0.43 (-)	0.61 (1.9E7)	0.43 (-)	51 (0.49)	65 (0.32)
1.0	JSC		86 (0.19)		3.1 (-)		3.5 (-)		80 (0.18)
1.2	MB	43 (28)	175 (32)	0.52 (7.6)	69 (1.3E3)	4.9 (5.8E3)	1.1 (1.3E3)	38 (25)	105 (19)
1.2	JSC	127 (84)	100 (19)	0.64 (10)	2.1 (41)	1.5 (1.7E3)	2.9 (3.4E3)	125 (87)	95 (18)
1.4	MB	96 (112)	94 (38)	0.38 (1.8)	6.1 (37)	79 (1.6E4)	0.66 (134)	17 (26)	87 (38)
1.4	JSC	109 (128)	107 (44)	1.7 (8.1)	4.9 (29)	3.7 (743)	29 (5.8E3)	103 (162)	73 (32)

* Values in parentheses are ratios to equilibrium concentration. Where only dashes are present the value is very large.

Table ES6

THE INFLUENCE OF FUEL AND FN SPECIES (210 ppm FN) ON CONVERSION IN THE MULTIBURNER AT 1900 K

ϕ	FN	PERCENT AS TFN		
		CH_4	C_2H_4	C_3H_8
1.4	NH_3	94	85	88
1.4	NH_3/NO	146	73	--
RATIO W/WO NO		1.6	0.86	--

Table ES7

COMPARATIVE EFFECT OF FUEL NITROGEN SPECIES (200 ppm) ON CONVERSION IN METHANE FLAMES AT 1900 K

ϕ	DEVICE	TFN AS PERCENT OF FN* NH_3	 NH_3 + NO	RATIO W/WO NO
0.97	JSC	86 (0.19)	55 (0.12)	0.64
1.4	MB	94 (38)	146 (59)	1.6
1.4	JSC	107 (44)	109 (45)	1.0
1.8	MB	77 (44)	97 (55)	1.3
1.8	JSC	145 (83)	119 (68)	0.82

* Values in parentheses are ratios to equilibrium concentrations.

Table ES8

COMPARATIVE EFFECT OF FUEL SPECIES ON THE CONVERSION OF FUEL NITROGEN (200 ppm NH_3) IN FLAMES AT 1900 K

ϕ	DEVICE	PERCENT AS TFN		
		CH_4	C_2H_4	C_3H_8
1.0	MB	66	--	14
0.97	JSC	86	101	98
RATIO JSC/MB		1.3	--	7.0
1.4	MB	94	85	88
1.4	JSC	107	107	114
RATIO JSC/MB		1.1	1.3	1.3

Figure ES1

Schematic Diagram of the Jet Stirred Combustor

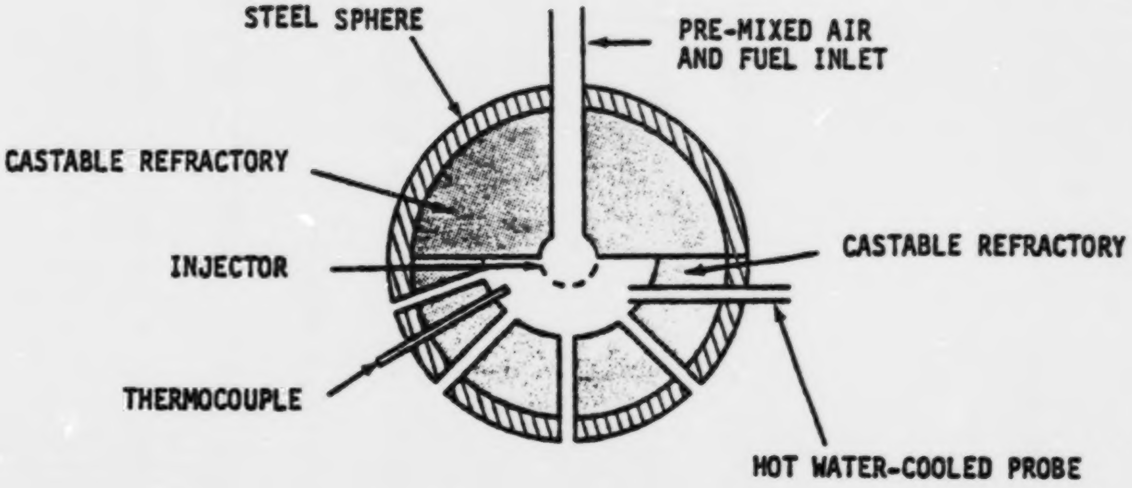
STEEL SPHERE
PRE-MIXED AIR AND FUEL INLET
CASTABLE REFRACTORY
INJECTOR
CASTABLE REFRACTORY
THERMOCOUPLE
HOT WATER-COOLED PROBE

Figure ES2

Gas Analysis

CO_2 BY NON-DISPERSIVE IR (LIRA MODEL 303, MB, OR BECKMAN MODEL 864, JSC)

CO BY NON-DISPERSIVE IR (LIRA MODEL 303, MB, OR BECKMAN MODEL 864, JSC)

O_2 BY POLAROGRAPHY (BECKMAN MODEL 702)

H_2 BY CHROMATOGRAPHY (CARLE MODEL GC 8700)

UHC BY FID AS METHANE (BECKMAN MODEL 400, MB, OR BECKMAN MODEL 402, JSC)

NO BY CHEMILUMINESCENCE (THERMO ELECTRON MODEL 10A)

HCN BY SCRUBBING IN 0.5 M NaOH FOLLOWED BY ION-SPECIFIC ELECTRODE ANALYSIS

NH_3 BY SCRUBBING IN 0.2% H_2SO_4 FOLLOWED BY ION-SPECIFIC ELECTRODE ANALYSIS

Figure ES3

Schematic Diagram of the Multiburner

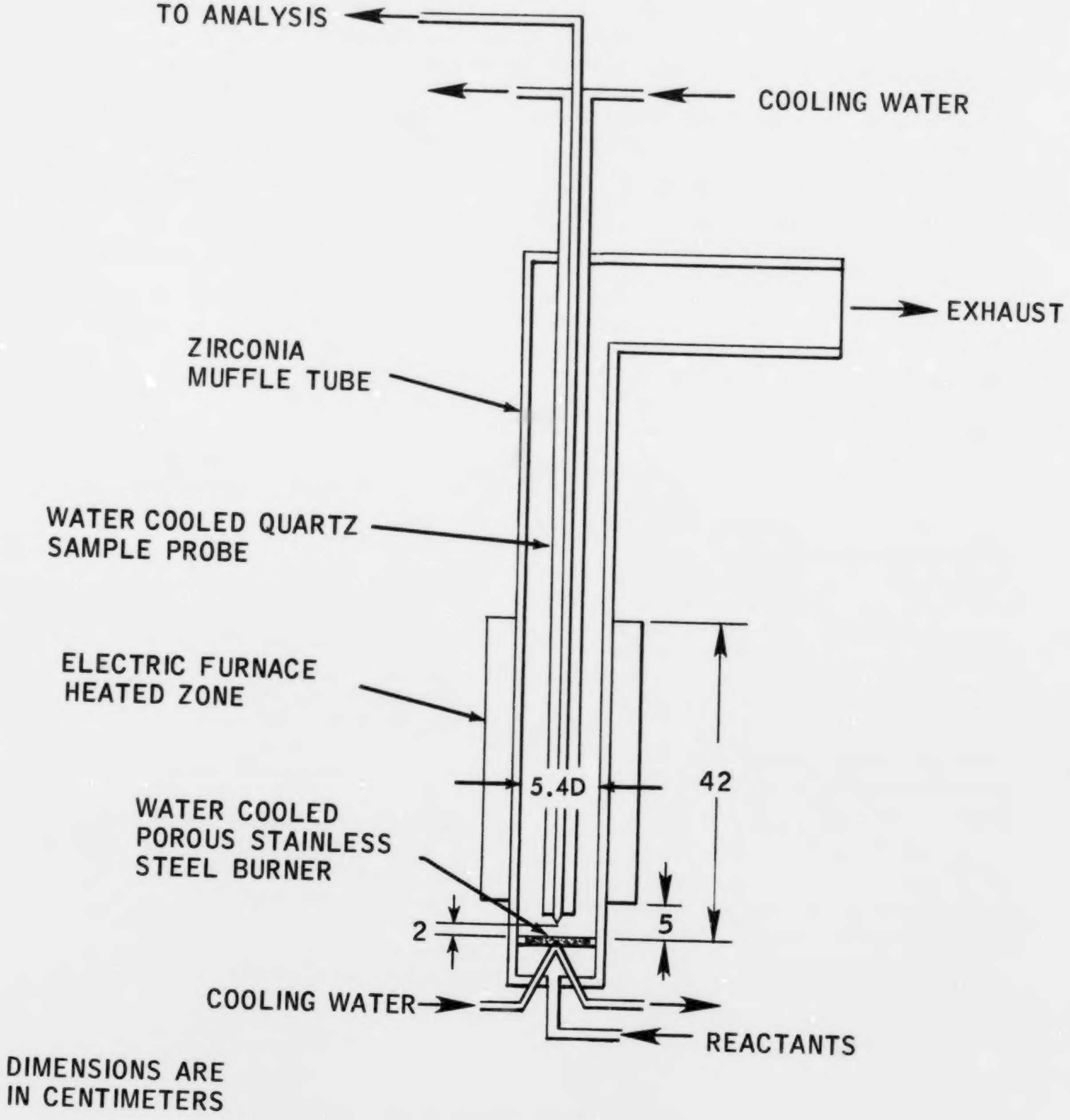
TO ANALYSIS
COOLING WATER
EXHAUST
ZIRCONIA MUFFLE TUBE
WATER COOLED QUARTZ SAMPLE PROBE
ELECTRIC FURNACE HEATED ZONE
5.4D
42
WATER COOLED POROUS STAINLESS STEEL BURNER
2
5
COOLING WATER
REACTANTS
DIMENSIONS ARE IN CENTIMETERS

I. INTRODUCTION

The purpose of this program is to advance the understanding of the conversion of fuel nitrogen to NO_x in hydrocarbon combustion systems. The specific objective was stated at the outset of the work as follows:

> "A quantitative understanding of the formation and destruction of nitrogenous species in hydrocarbon flames is necessary for the development of a modular model describing pollutant formation in stationary combustors. In the intermediate time period it is also needed in the search for the lower bounds on fuel nitrogen conversion to NO_x in gaseous systems given a certain set of design constraints. The objective of this procurement is the provision of reliable detailed information on the fate of nitrogenous species under combustion conditions using idealized reactor systems with well-defined fluid mechanics. The experimental information generated in this procurement will be used by EER* and MIT** in conjunction with the contractor to advance the state-of-the-art of kinetic modeling of fuel NO_x formation." (2)

Succinctly put, the object of the program was to study fuel nitrogen conversion in gaseous combustion systems wherein the fluid mechanics were such that they did not intolerably confound the chemical kinetics of the conversion.

In pursuing this objective, two extreme types of combustors (as regards their fluid mechanical details) were employed. The first was a strongly backmixed hemispherical reactor wherein mixing was designed to be sufficiently vigorous to produce near-homogeneous reaction conditions, i.e., to ensure that mixing times were short relative to the important chemical reaction times. This reactor is referred to as the jet-stirred combustor (JSC). To the extent that it achieved homogeneity, the reaction system within it can be described kinetically without attention to its fluid mechanical details. A typical residence time in the JSC was of the order of 3 ms. The second combustor, referred to as the multiburner (MB), was the antithesis of the first. It was an adiabatic quasi-plug flow tubular reactor. It was adiabatic because it was housed within a furnace which heated the tube wall to the flame temperature and held it there thermostatically, and it was quasi-plug flow because the flow within the tube was laminar. Plug flow implies turbulent flow and cross-sectional homogeneity at any axial station; thus, it is a truly one-dimensional (and consequently simple) system. The existence of laminar flow upsets this simplicity in that radial inhomogeneity appears, the system becomes two-dimensional, and consequent radial transport may become important. Observations which cite only axial position as a variable should be restricted to a single designated streamline. In this work a single on-axis axial position was used and it provided residence times of the order of 30 ms. Again, in plug flow systems the fluid mechanical situation is chosen so as to render its details unimportant; this is achieved to only a slightly lesser degree in a well-chosen quasi-plug flow reactor.

---

* Energy and Environmental Research Corporation, Santa Ana, CA.

** Massachusetts Institute of Technology, Cambridge, MA.

The details of the two reactors will be discussed in the section on apparatus. The significant difference between them is that in the JSC reactions occur simultaneously in the presence of a near-homogeneous mixture of reactants, intermediates, and final products at a single temperature, while in the MB reactions occur sequentially along the tube with intermixing of reactants, intermediates, and products occurring only through molecular diffusion and in the presence, near the flame front, of large axial temperature gradients. An adequate kinetic model must be able to describe the conversions in both reactors. Accordingly, a common set of experiments was designed for them. With premixed gaseous reactants the effects of equivalence ratio (0.7 to 1.8), temperature (1800-2000 K), fuel species (CH_4, C_2H_4, and C_3H_8), fuel nitrogen species (NH_3 and NH_3 + NO), and fuel nitrogen concentration (0 to 1000 ppm) on fuel nitrogen conversion were studied in each combustor.

Fuel nitrogen was converted not only to NO but also to N_2, NH_3, and HCN. Accordingly, the output species NO, NH_3, and HCN were measured and reported separately, while their sum was reported as total fixed nitrogen (TFN). Other effluent species that were measured were CO, CO_2, O_2, H_2, NO_2 (in some cases), and unburned hydrocarbons (UHC) reported as methane equivalent.

The results of this work are presented in tabular form. The reasons for this are twofold. Their primary use is to be in mathematical modeling; therefore, they must be available in tabular form. Also only very limited numbers of experimental points are available over the range of any given independent variable, and existing chemical literature demonstrates that fitting intrinsically non-linear curves to limited data leads almost inevitably to a counterproductive application of artistic license. The tabulations are, however, arranged into several subsets, each of which is chosen to illustrate the influence of specific independent variables. While this leads to a proliferation of tables, it has the virtue that an able observer can readily glean the message from each subset unencumbered with prejudices other than his own.

One conclusion is readily reached from the results. It is that for even the relatively simple and (superficially) similar hydrocarbon fuels used in this study, fuel effects can be significant in the production of effluent fixed nitrogen, either from "fuel" nitrogen or from molecular nitrogen in the combustion air. The effect is sensitive to mixing conditions. This conclusion holds even when other pertinent variables such as temperature, pressure, and equivalence ratio are held constant. The most likely source of these differences lies in the early pyrolysis and oxidative breakdown of the original fuel molecule. To the extent that this is true, it poses a formidable challenge for kinetic modelers. These early breakdown processes are complex and they involve numerous poorly understood steps for which quantitative kinetic data are usually unavailable. To the extent that these results facilitate and encourage progress in this area, they will represent effort well-spent.

During the course of this project there was a change of principal investigators. The original principal investigator, Dr. A. L. Myerson, left the project towards its very end and was replaced by the author of this report. Dr. Myerson's contributions included planning all of the experiments and overseeing all of the work on the jet-stirred combustor and the initial work on the multiburner. This author had responsibility for overseeing most of the final work on the MB, reducing the data to the forms presented herein, and writing the final report. Dr. Myerson's major contribution to this project is hereby acknowledged with great appreciation.

II. APPARATUS AND METHOD

This section describes the combustors used in this work together with their associated gas-analysis instruments, the gases used as reactants, and the manner of data reduction.

II-1. The Multiburner*

The multiburner is an electrically-heated, vertical muffle-tube furnace. The muffle tube is made of dense zirconia, 5.40 cm. I.D. x 60.6 cm long. The heated zone is 35.6 cm long. Premixed reactants were fed to the bottom of the muffle tube through a 4 cm diameter porous plug flat flame burner that was welded in a water-cooled mounting assembly. The face of the burner was located 5 cm below the heated zone. Gas samples were withdrawn through a water-cooled quartz probe with a 1 mm dia. tip that was axially located 2 cm above the burner face. This was the length of the reaction zone. Figure II-1.1 shows a schematic diagram of the multiburner.

Premixed gases were fed to the burner. They were metered separately by rotameter and then joined in a section of 1/4 in. stainless steel tubing which led to the burner. The separate gases were fuel (CH_4, C_2H_4, or C_3H_8), air, N_2, 50% O_2/50% N_2, and dopant (NH_3 or 50% NH_3/50% NO) in N_2.

Total flowrates into the burner were held close to 0.5 scfm (236 scc/s). Experiments were run at specified adiabatic flame temperatures which were set independently of equivalence ratio or fuel type by varying the oxygen/nitrogen ratio in the combustion "air". This ratio was varied by mixing metered streams of laboratory air, 50/50 ratio O_2/N_2 gas, and/or pure N_2. Required ratios were precalculated using crossplots of calculations made using the NASA Chemical Equilibrium code (1). Actual attained equivalence ratios were then checked with the code using recorded laboratory flowrates.

Reaction times were calculated as residence times between the burner face (approximate location of flame front) and the sampling point (2 cm distance). The method was:

$$\tau = \text{residence time} = \frac{\text{length}}{\text{velocity}} = \frac{L}{v}$$

$$v = \frac{\text{volume flowrate}}{\text{area}} = \frac{\dot{V}}{A}$$

$$\dot{V} = \dot{V}_{\text{input}} \left[\frac{\text{moles product}}{\text{moles input}} \right] \left[\frac{T_{\text{product}}}{T_{\text{input gas}}} \right]$$

---

* This is the same combustor, with some modifications, that was used by Engleman (7,8).

Figure II-1.1

Schematic Diagram of the Multiburner

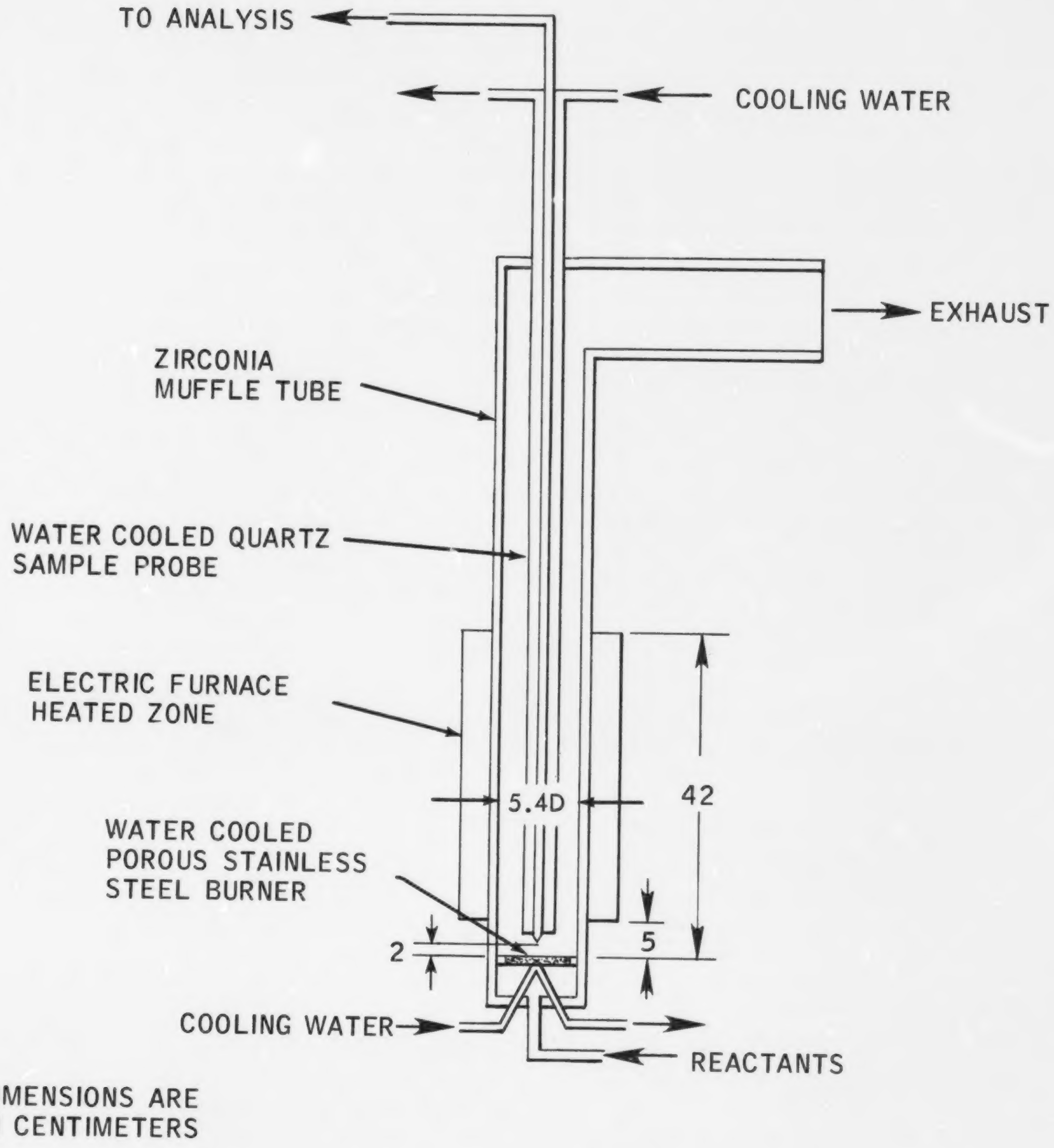
TO ANALYSIS
COOLING WATER
EXHAUST
ZIRCONIA MUFFLE TUBE
WATER COOLED QUARTZ SAMPLE PROBE
ELECTRIC FURNACE HEATED ZONE
5.4D
42
WATER COOLED POROUS STAINLESS STEEL BURNER
2
5
COOLING WATER
REACTANTS
DIMENSIONS ARE IN CENTIMETERS

$$\frac{\text{moles product}}{\text{moles input}} = \frac{\text{mole fraction AR input}}{\text{mole fraction AR products}} = \frac{XAR_{in.}}{XAR_{prod.}}$$

$$\dot{V} = \dot{V}_{input}\left[\frac{XAR_{in.}}{XAR_{prod.}}\right]\left[\frac{T_{prod.}}{T_{in.}}\right]$$

$XAR_{prod.}$ is taken as the calculated equilibrium value.

In the calculation the following values were used:

$T_{in.}$ = 299 K

$T_{prod.}$ = calculated adiabatic flame temp.

Tube dia. = 5.4 cm

L = 2 cm

$\dot{V}_{in.}$ = total input volume in scfm

$XAR_{in.} = \frac{\dot{V}AR_{in.}}{\dot{V}_{in.}}$, both experimental values where $\dot{V}AR_{in.}$ = 0.00934 $\dot{V}air_{in.}$

Expressing τ in milliseconds this gave:

$$\tau = 29016\left[\frac{XAR_{prod.}}{\dot{V}AR_{in.}}\right]\left[\frac{1}{T_{prod.}}\right]$$

The electrical furnace was set to maintain the muffle-tube wall temperature equal to the adiabatic flame temperature. This eliminated radial thermal gradients but the necessity of operating the tube at the adiabatic flame temperature gave a problem of short life for flames of 2000 K and above.

The flow in the tube was laminar and expected to change from near uniform flow at the porous burner face to parabolic flow at the tube outlet (taking 0.5 scfm input of air and a temperature of 2000 K at one atmosphere pressure gives a Reynold's number of 106).

Standard on-line analysis systems were used, with appropriate filters, moisture knockouts, and heated lines to measure O_2, CO_2, CO, NO and unburned hydrocarbons (UHC) as methane equivalent. They were:

CO and CO_2 - Non-dispersive IR (Lira model 303)

O_2 - Polarographic (Beckman model 702)

UHC - FID as methane (Beckman model 400)

NO and NO_2 - Chemiluminescence (Thermo Electron model 10A)

Three remaining products were measured by batch methods. They were:

H_2 - Chromatography (Carle Model GC 8700)

HCN - Scrub known volume of product gas in 0.5 M NaOH followed by ion-specific electrode analysis (Orion model 90-01 reference electrode, model 94-06A CN^- electrode, and model 801A Ionalyzer)

NH_3 - Scrub known volume of product gas in 0.2% H_2SO_4 followed by ion-specific electrode analysis (Orion model 95-10-00 gas-sensing electrode and model 801A Ionalyzer)

It was expected that under these experimental conditions, radial transport in the reactor tube would be negligible. This was checked and confirmed by taking radial profiles in the tube. The results of these tests are presented in Appendix B.

II-2. The Jet-Stirred Combustor (JSC)

The jet-stirred combustor that was used in this work was a modification of the Longwell-Weiss reactor with hemispherical geometry.** JSC's have been used extensively in fluid mechanic and combustion modeling because their combustion rates are limited more by chemical kinetic rates than by transport rates. An advantage of the JSC is that its strong backmixing provides a simulation of the recirculating characteristics of many combustor primary zones. A more important advantage of the stirred combustor to this program is that it is near homogeneous* in species concentration and temperature; thus, each operating condition is characterized by a single set of temperature and concentration parameters. This greatly simplifies the tasks of obtaining and interpretating data.

The JSC (Figure II-2.1) consists of an outer shell of castable refractory shaped as two halves of a sphere, 15.2 cm in diameter. It is fabricated from Castable 141A, a product of Combustion Engineering Refractories. The upper hemisphere is solid with the exception of a hole through which the reactant supply tube passes to the injector. The lower portion contains a hemispherical reactor cavity 5.08 cm diameter. Twenty-five 3.2 mm diameter radial exhaust ports connect the cavity to the atmosphere. Combustion experiments are conducted at atmospheric pressure. Residence times range up to 4 ms. Thermocouples are used to

---

* Nearness to homogeneous as used here implies that mixing rates are so fast that, for a given packet of gas, departures from average conditions are eliminated at a rate that is fast relative to the chemical kinetic rates that are being studied.

** The same modification used by Blazowski (9).

Figure II-2.1

Schematic Diagram of the Jet Stirred Combustor

The small ports in the injector are 0.5 mm diameter. If the input jets are traveling at the sonic velocity (34000 cm/s for cold jets) and break up in about 20 jet diameters, their mixing time is of the order of 30 μs.

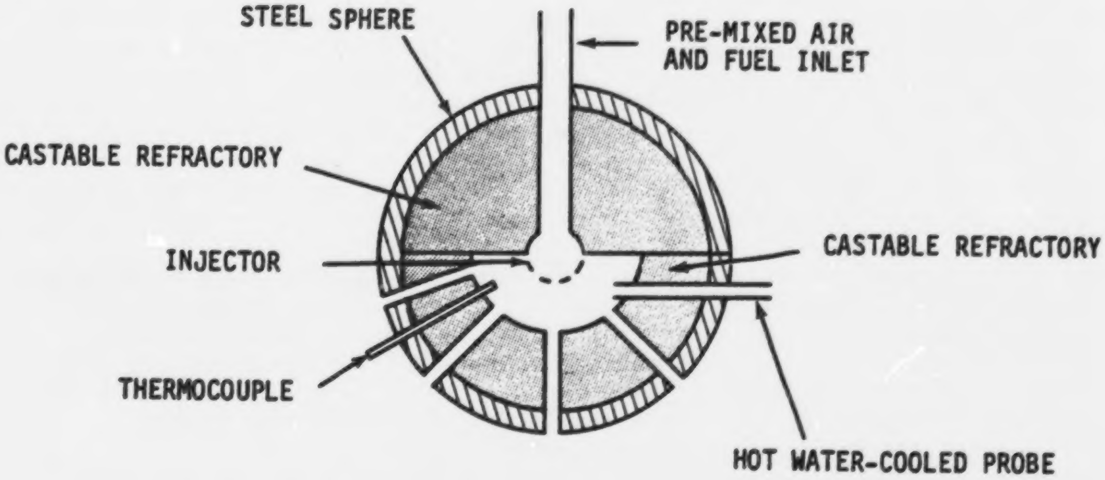
STEEL SPHERE
PRE-MIXED AIR AND FUEL INLET
CASTABLE REFRACTORY
INJECTOR
CASTABLE REFRACTORY
THERMOCOUPLE
HOT WATER-COOLED PROBE

measure the temperature within the reactor. Because of vigorous flow conditions within the reactor, the gas temperature is quite close to the wall temperature and the radiation error should be neglibible.

Fuel, air, nitrogen, oxygen, and NH_3 or NO doped nitrogen are metered separately through calibrated rotameters, preheated to the desired inlet temperature and then mixed before entering the combustor. The reactants can be heated up to 350°C in an aluminum block heater. Separate coils for fuel and "air" are embedded in the solid aluminum block which is wrapped with electrical resistance heaters.*

The temperature of the fuel/"air" stream is measured immediately before injection. This measurement actuates a digital controller which provides power to the block heater to maintain injector inlet temperature within ±10°C of the set point. The fuel-air mixture enters the reaction zone through a hemispherical Inconel injector of 1.27 cm diameter which contains forty radial injection holes of 0.5 mm diameter. Reactants enter the reaction zone as small sonic jets which stir the reactor contents and produce a mixture of essentially uniform temperature and composition in a characteristic time which is very short compared with the average residence time. An overall view of the fuel and air system as well as the JSC is shown in Figure II-2.2.

A probe is inserted through one of the exhaust ports to extract a sample. This sampling probe (Figure II-2.3) is hot-water cooled and sample transfer is through electrically heated sample lines to prevent condensation of water or unburned hydrocarbons within the probe and sample lines (high concentrations of these constituents are expected at mixture ratios of interest in this study). All sample conditioning (pumping, filtering, and valving) is accomplished within a Blue-M Model OV-18A oven maintained at 150°C. Valves in the system are rated for operation at temperatures up to at least 175°C, and their design characteristics are such that lubricated valve components are isolated from the gas path. The sample pump is a high temperature metal bellows type (Model MD-158 HT) driven by a 1/4 horsepower motor external to the oven. The sample conditioning system is shown in Figure II-2.4.

Gas analysis is accomplished with conventional process instrumentation. A filter within the oven removes particulates from gases passing to instrumentation. A first gas stream leaving the oven is transferred through hot (~150°C), electrically-heated lines to a Beckman Model 402 analyzer for total hydrocarbon (THC) measurement. This instrument has a dynamic range of hydrocarbon concentrations from parts-per-million through tens of mole percent. It was calibrated with a mixture containing CH_4 and all reported THC results are "as methane". A second sample-gas stream leaving the oven was chilled to eliminate condensable water (to a dew point of about 10°C) and hydrocarbons prior to introduction into NDIR analyzers for CO and CO_2 measurements. These were both Beckman Model 864 instruments with maximum CO range of 10 mole

---

* Quotation marks around "air" signify that the "air" used in these experiments was a mixture of laboratory air, nitrogen, and oxygen. Such "air" was used to provide a variable nitrogen/oxygen ratio to provide for independent control of equivalence ratio and flame temperature.

Figure II-2.2

Overall View of Jet-Stirred Reactor Test System

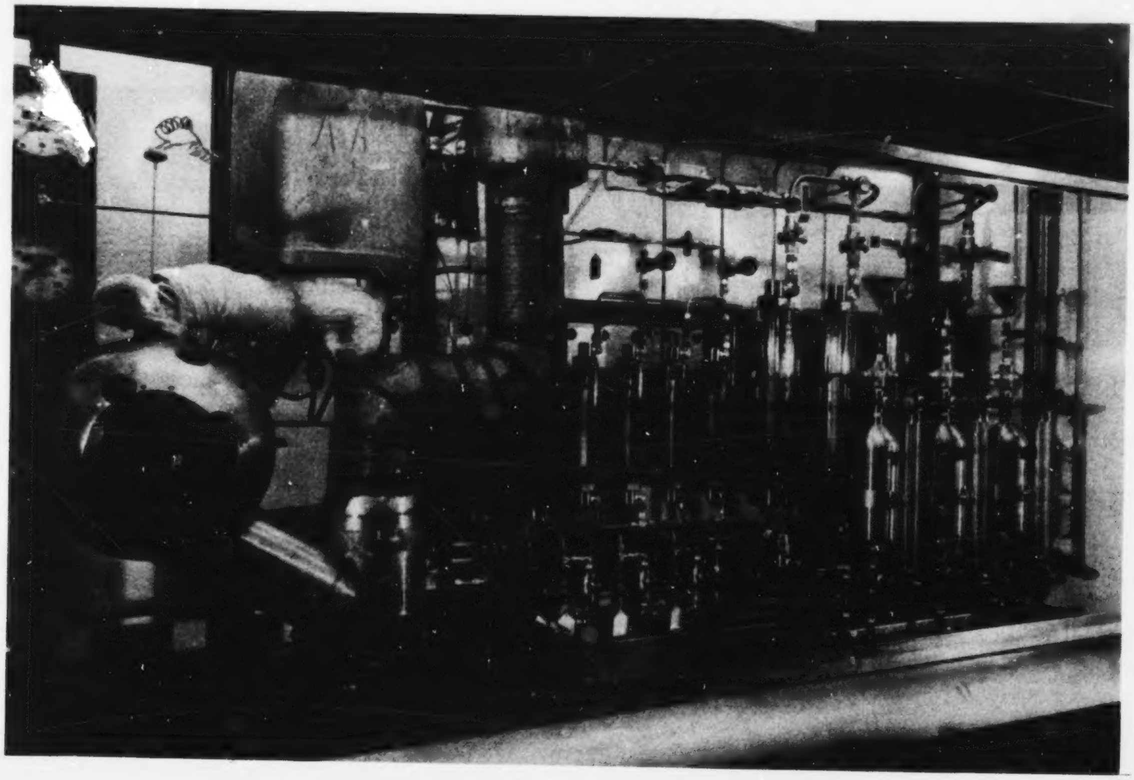

Figure II-2.3

Sample Probe

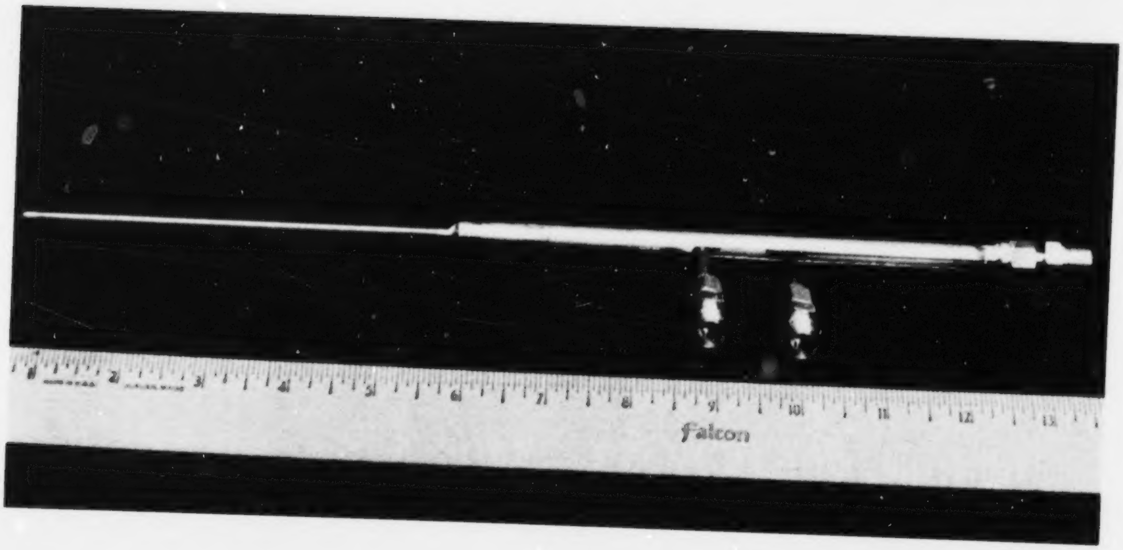

Figure II-2.4

Sample Conditioning System

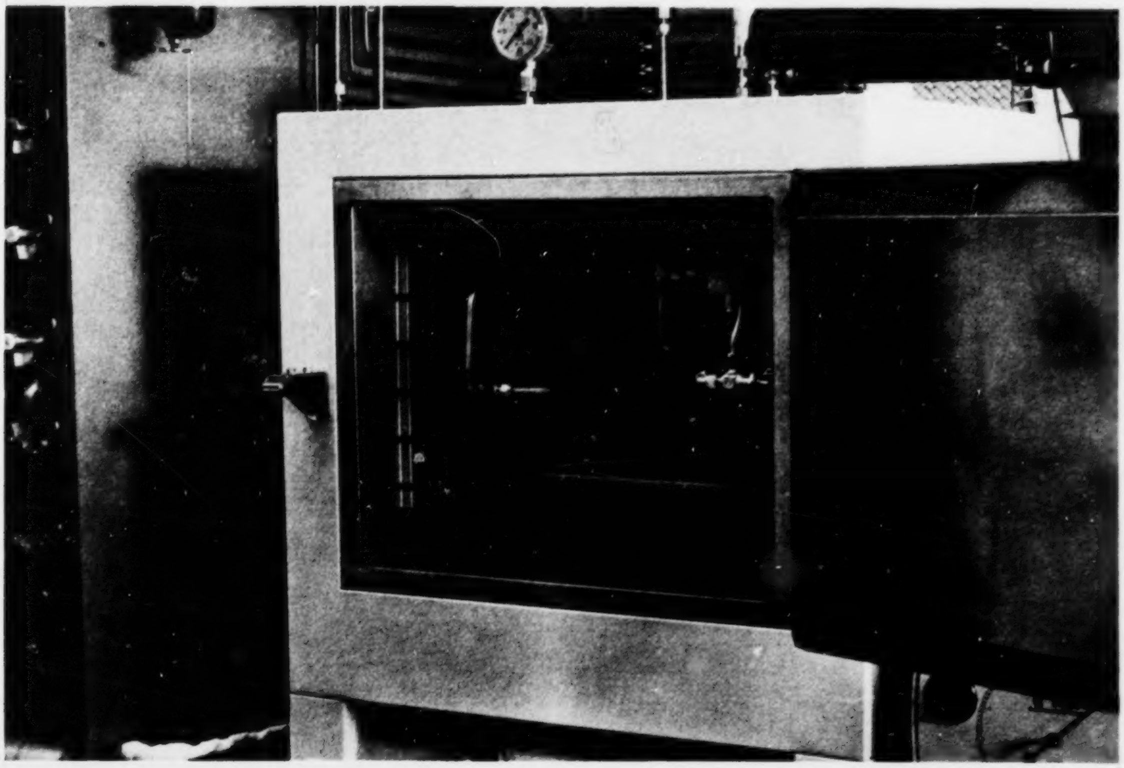

percent and maximum CO_2 range of 20 mole percent. Oxygen was analyzed with a Beckman model 778 Process Oxygen Analyzer and hydrogen with a Carle Instruments, Inc. model GC 8700 Basic Gas Chromatograph with N_2 carrier gas. An overall view of the gas analysis system is shown in Figure II-2.5.

Analyses for HCN and NH_3 were performed by scrubbing sample gas streams in solutions of 0.5 M NaOH or 0.1% H_2SO_4, respectively and then analyzing the solutions with appropriate Orion ion-specific electrodes. These analyses were performed by using a 3-way switching valve to direct the sample train away from the on-line instrument train to the appropriate scrubber. Gas volumes through the scrubbers were measured with a wet test meter.

With the JSC it was not possible to prespecify all flows to give predetermined values of temperature, equivalence ratio, and residence time as was the case in the (adiabatic) multiburner. Heat losses in the JSC significantly affected the temperature and precluded this. Thus, it was necessary, for a given inlet temperature, to adjust the N_2/O_2 ratio of the combustion "air" (by using separate metering and control systems for atmospheric air, N_2, and O_2) to achieve the desired measured reactor temperature while holding equivalence ratio and total flow (i.e., residence time) constant. While rather time-consuming, this was done successfully.

Residence times in the JSC were calculated as follows:

The JSC is a 2 in. dia. hemisphere.

The injector is a 0.5 in. dia. sphere with its lower hemisphere located within the JSC.

Free combustor volume, V_R, $= \left[0.5\right]\left[\frac{4}{3}\pi\right]\left[(1.0)^3-(0.25)^3\right]$

$$V_R = 2.06 \text{ cu. in.} = 0.00119 \text{ cu. ft.}$$

$$\tau = \frac{V_R}{\dot{V}}$$

where $\dot{V}$ ≡ flowrate through combustor at combustion conditions

If $\dot{V}_T$ ≡ total volume flowrate into the injector

Then

$$\frac{\dot{V}}{\dot{V}_T} = \left(\frac{\text{moles out}}{\text{moles in}}\right)\left(\frac{Tc}{Tin}\right)$$

where T_c ≡ combustion temperature

T_{in} ≡ input temperature

Figure II-2.5

Gas Analysis System

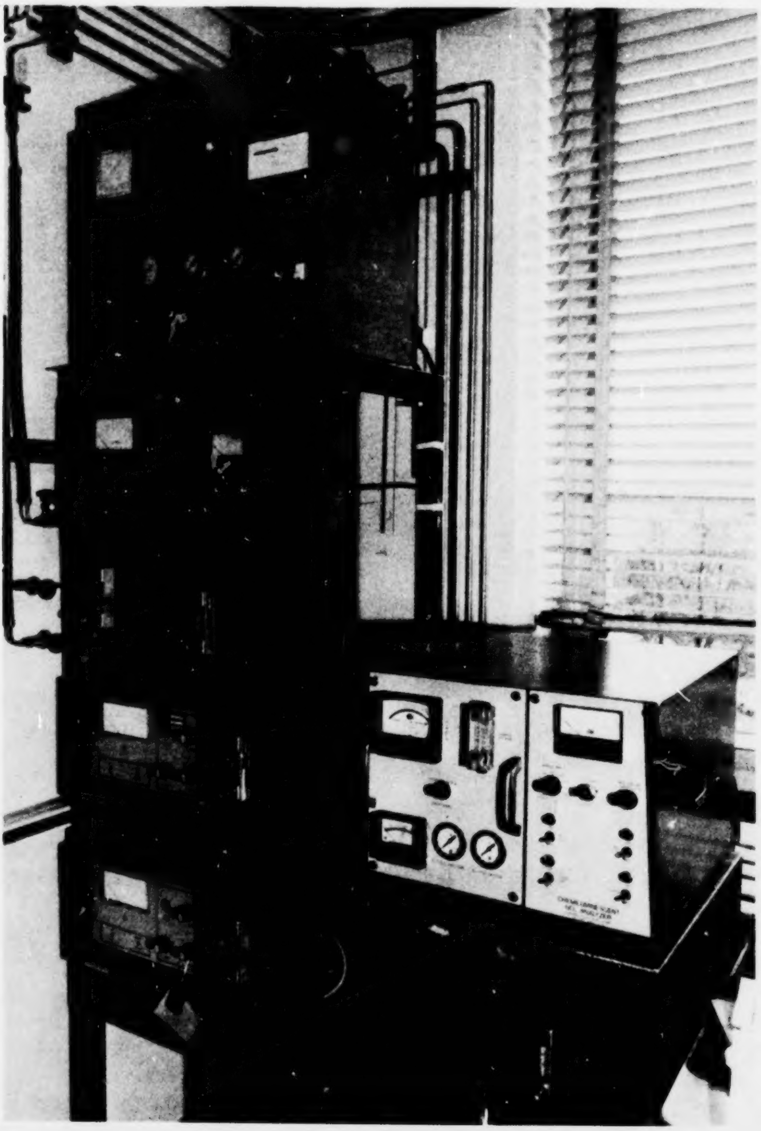

Reproduced from
best available copy.

But if XAR is the mole fraction of argon in gas then

$$\frac{\text{moles out}}{\text{moles in}} = \frac{\text{XARin}}{\text{XARout}}$$

and

$$\frac{\dot{V}}{\dot{V}_T} = \left(\frac{\text{XARin}}{\text{XARout}}\right)\left(\frac{\text{Tc}}{\text{Tin}}\right)$$

$$= \left(\frac{\dot{V}\text{ARin}}{\dot{V}_T}\right)\left(\frac{1}{\text{XARout}}\right)\left(\frac{\text{Tc}}{\text{Tin}}\right)$$

$$\dot{V} = \left(\frac{\dot{V}\text{ARin}}{\text{XARout}}\right)\left(\frac{\text{Tc}}{\text{Tin}}\right)$$

$$\tau = \left(\frac{V_R}{\dot{V}\text{ARin}}\right)\left(\text{XARout}\right)\left(\frac{\text{Tin}}{\text{Tc}}\right)$$

Expressing τ in ms, V_R in cu. ft., and VARin in cu. ft./min. this becomes

$$\tau = 71.58 \left(\frac{\text{XARout}}{\dot{V}\text{arin}}\right)\left(\frac{\text{Tin}}{\text{Tc}}\right)$$

$\dot{V}$ARin was taken as 0.00934 times the volume flowrate of laboratory air into the injector and XARout was calculated (ref. 1) as the equilibrium argon mole fraction in the product gas.

Experiments were run to compare the performance of the present JSC with that of the one that was used by Engleman (ref. 4). The results of these tests, which showed satisfactory agreement, are presented in Appendix A.

II-3. Data Reduction

Data were reported by the on-line instruments as ppm in the product gas as received. This gas was received after most of the combustion water had been precipitated at room temperature. Thus, it was at near one hundred percent relative humidity. The water represented as humidity was a very small fraction of the water produced by combustion, and for purposes of calculation this gas was considered to be dry with all of the combustion water removed.

A similar situation existed with the gas that was scrubbed for NH_3 and HCN. The sample lines were heated and condensation prevented until the gas passed into the appropriate scrubber. The effluent gas leaving the scrubber (near 100% RH) was then metered in a wet-test meter. The NH_3 or HCN removed in the scrubber was referred to this metered volume to calculate ppm in the "dry" (combustion water removed) gas.

In those cases where fuel nitrogen was added to the combustor it was desired to report various nitrogen species (NO, NH_3, HCN) and their sum (TFN ≡ total fixed nitrogen) as percent yields from the input fuel nitrogen. To do this it was necessary to correct ppm in the product gas to account for both the change in number of moles of total gas during combustion and the removal of water from the product gas. This was done by using equilibrium calculations based upon the actual species input flowrates, correcting for calculated equilibrium combustion water, and using equilibrium input and output argon mole fractions to correct for the change in moles of gas during combustion.

The analysis was as follows:

Define the following quantities:

FNin ≡ total moles of fixed nitrogen input in reactant gas

FNout ≡ moles of given fixed nitrogen species (or total fixed nitrogen) in product gas

Vin ≡ volume of reactant (input) gas

Vair ≡ volume of air in reactant gas

Vout total ≡ volume of wet product gas

Vout ≡ volume of product gas (dry)

Vout(H2O) ≡ volume of water in product gas

XH2O ≡ mole fraction of water in product gas

XARin ≡ mole fraction of argon in reactants

XARout ≡ calculated mole fraction of argon in wet (total) product gas

$$\frac{\mathrm{FNout}}{\mathrm{FNin}} = \left[\frac{\frac{\mathrm{FNout}}{\mathrm{Vout}}}{\frac{\mathrm{FNin}}{\mathrm{Vin}}}\right]\left[\frac{\mathrm{Vout}}{\mathrm{Vin}}\right]$$

$$= \left[\frac{\mathrm{PPM\ FNout}}{\mathrm{PPM\ FNin}}\right]\left[\frac{\mathrm{Vout}}{\mathrm{Vin}}\right]$$

But since the moles of argon remain constant during combustion:

$$\frac{\text{XARout}}{\text{XARin}} = \frac{\dfrac{\text{moles AR}}{\text{Vout total}}}{\dfrac{\text{moles AR}}{\text{Vin}}} = \frac{\text{Vin}}{\text{Vout total}}$$

$$\frac{\text{Vout total}}{\text{Vin}} = \frac{\text{XARin}}{\text{XARout}}$$

$$\text{Vout} = \text{Vout total} \left[1 - \text{XH2O}\right]$$

$$\frac{\text{Vout}}{\text{Vin}} = \frac{\text{XARin}}{\text{XARout}} \left[1 - \text{XH2O}\right]$$

The mole fraction of argon in air was taken to be 0.00934. Thus,

$$\text{XARin} = \frac{0.00934\ \text{Vair}}{\text{Vin}}$$

$$\frac{\text{FNout}}{\text{FNin}} = \left[\frac{\text{PPM FNout}}{\text{PPM FNin}}\right] \left[\frac{0.00934\ \text{Vair}}{\text{Vin}}\right] \left[\frac{1-\text{XH2O}}{\text{XARout}}\right]$$

$$= \left[\frac{\text{PPM FNout}}{\text{PPM FNin}}\right] \text{Fcorr}$$

where

$$\text{Fcorr} = \left[\frac{0.00934\ \text{Vair}}{\text{Vin}}\right] \left[\frac{1-\text{XH2O}}{\text{XARout}}\right]$$

Here, again, Vair/Vin is the ratio of input air to total input (reactant) gas, XARout is the calculated equilibrium mole fraction of argon in the wet product gas (based upon input volume of argon as 0.00934 of input air volume), and XH2O is the calculated mole fraction of water in the wet product gas. PPM FNout is measured (NO, NH_3, HCN or their sum as TFN) in the dry product gas and PPM FNin is calculated directly from the volume flowrates of the several input gases.

II-4. Gases Used in the Experiments

The various gases that were used in this work (with the exception of the laboratory air supply) were obtained from Scientific Gas Products, Inc. of South Plainfield, New Jersey. The ethylene was polymer grade (99.9% minimum purity), the methane was ultrahigh purity grade (99.9% minimum purity), and the propane was instrument grade (99.5% minimum purity).

Fuel nitrogen was added either as ammonia in nitrogen or as nitric oxide in nitrogen. In these mixtures all components were ultrahigh purity grade and the mixtures were analyzed and certified.

III. RESULTS

In this section results from experiments in the multiburner and jet-stirred combustor are reported and compared. They include temperature, equivalence ratio, fuel type, fuel nitrogen concentration, and fuel nitrogen species as independent variables.

III-1. Results from Multiburner

In the multiburner work, five independent variables were investigated. They were fuel species (CH_4, C_2H_4, C_3H_8), equivalence ratio (0.7-2.0), temperature (1800-2000 K), fuel nitrogen species (NH_3 or NH_3 + NO), and fuel nitrogen concentration (0 to 1040 ppm in reactants). A complete set of all combinations of these variables was not run. To run such a set would have consumed far more time than was available to this work. The combinations that were run are shown in Table III-1.1. Most of the temperature and equivalence ratios in Table III-1.1 are nominal values; exact values appear in Tables III-1.2-.6. Values of NH_3 and NH_3/NO concentrations in Table III-1.1 which appear in the same row denote separate distinct runs. Areas of overlap of experimental conditions among the three fuels are apparent in the table. Temperature overlap occurs only at 1900 K except for zero additive runs at equivalence ratio 1.4 at 1800 K. Fuel nitrogen type overlap (NH_3 + NO) occurs only for CH_4 and C_2H_4. In general, there is more extensive overlap between runs with CH_4 and C_2H_4 than between either of those fuels and C_3H_8.

Detailed results and experimental conditions of all multiburner runs are given in Tables III-1.2 through 1.6. The column headings of these tables require some explanation. "Set T" is the nominal furnace (and flame) temperature of the run in degrees Kelvin, i.e., the desired temperature. "Actual temperature" is the furnace temperature that was achieved and indicated by the furnace temperature gauge. "Set ϕ" is the nominal equivalence ratio, i.e., the desired equivalence ratio. "Computed ϕ" and "computed T" are the values of equivalence ratio and adiabatic flame temperature that were calculated for the actual reactant flows by the program of reference 1. "Additives, vppm" are the concentrations of NH_3 or NO in the reactant gas reported as volumetric parts per million. "Collected, vppm in Dry Gas" is the measured value of the indicated species in the dry combustion products (100 percent relative humidity at room temperature) reported as vppm. TFN, total fixed nitrogen, refers to the sum of NH_3, HCN, and NO. "Collected, Percent of N added" refers to gram atoms of nitrogen collected as the given species reported as percent of gram atoms of fuel nitrogen input. (Columns headed NH_3, HCN, NO, TFN give percent of nitrogen for total values of those species collected. With "Fuel" included in those headings the values report percent of fuel nitrogen exclusive of nitrogen found in those species under identical combustion conditions with no fuel nitrogen in the reactants, i.e., exclusive of "thermal" nitrogen.) "Collected in Dry Exhaust Gas" reports volumetric fractions of indicated species measured in the dry (100% RH at room temperature) combustion products either as percent or vppm. τ is the calculated residence time in ms.

The information in these comprehensive tables has been extracted and placed in more restricted tables to facilitate investigation of the influence of particular independent variables. These are Tables III-1.7 through 1.15.

Table III-1.7 shows the performance (in producing fixed nitrogen products) of the three fuels at 1900 K as a function of equivalence ratio without fuel nitrogen in the reactants. All product fixed nitrogen is "thermal nitrogen". Methane shows a maximum in TFN at equivalence ratio 1.2. This coincides with its maximum in HCN. Its NH_3 maximum is at 1.0 while its NO maximum at 1.4 appears to be part of a broad maximum that extends from 1.2. The two runs available for C_2H_4 are insufficient to establish maxima, but their relative magnitudes for each fixed nitrogen product do not agree with the trends for CH_4. The three available runs for C_3H_8 show strong monotonic increases in TFN and NO from $\phi = 1.0$ to 1.8 with a somewhat similar trend indicated for HCN from 1.4 to 1.8 and no significant trend for NH_3.

The general observation may be drawn from these data that:

1. At 1900 K hydrocarbon fuel species plays an important part in thermal nitrogen fixation both in magnitude and in trend with changing equivalence ratio for residence times of the order of 30 ms.

Table III-1.8 shows results on thermal nitrogen fixed in CH_4 flames with both equivalence ratio and temperature as independent variables. Total fixed nitrogen shows maxima in ϕ at T = 1800 and 1900 K with the maximum shifting to lower ϕ with higher T. At T = 2000 K there is no maximum; TFN increases monotonically with decreasing ϕ. Both HCN and NH_3 are present in unexpectedly high amounts at the lower ϕ, especially at 2000 K. The sensitivity of NO to ϕ is much less at constant temperature (here) than in the usual adiabatic flame temperature case. At 2000 K both HCN and NH_3 are present in amounts comparable to NO at the lower ϕ's.

The behavior of TFN at 2000 K is dominated by NH_3 and HCN. In fact, the trend of NO with changing ϕ is contrary to that of TFN, NH_3 and HCN (except from $\phi = 1.4$ to 1.8 for HCN). At 2000 K NO production increases with ϕ from 0.8 to 1.2, shows a broad maximum from 1.2 to 1.4 and then decreases. Conversely, HCN production shows a broad minimum from $\phi = 1.2$ to 1.4 while NH_3 decreases with increasing ϕ over the entire range with the possible exception of the range from 1.4 to 1.8. This trend in NO production also holds true at 1900 and 1800 K and even the magnitudes show little change from 1900 to 2000 K. However, for the other species and for TFN both trends and magnitudes change at the lower temperatures. At 1900 K HCN displays a maximum rather than a minimum over the range of ϕ. NH_3 trends appear similar to the 2000 K case over the range of ϕ except at the lowest value, but the magnitudes are reduced. The result is that at 1900 K TFN shows a maximum at $\phi = 1.2$. At the lowest temperature, 1800 K, NO shows a maximum $\phi = 1.4$, NH_3 shows a near monotonic increase with ϕ as does HCN (except in the range 0.7 to 1.0 for both HCN and NH_3) and TFN shows a broad maximum from $\phi = 1.4$ to 1.6.

The following general observations may be drawn from these data.

2. At 1800 and 1900 K, thermal TFN produced from methane combustion shows maxima in the range $\phi = 1.2$ to 1.6. Magnitudes of TFN are similar at the two temperatures. At these two temperatures, NO is the dominant component of TFN and it shows maxima over the same range of ϕ while stationary values are not apparent for NH_3 over the range of ϕ from 0.8 to 1.8. From $\phi = 0.7$ to 1.8 HCN displays a possible shallow minimum at 1800 K and a maximum ($\phi = 1.2$) at 1900 K.

3. At 2000 K thermal TFN increases monotonically with decreasing ϕ. Depending upon the given value of ϕ, either NH_3, HCN, or NO may be the most abundant species. The trend in TFN with changing ϕ is the result of a combination of a broad maximum in NO, a similarly broad minimum in HCN and a monotonic inverse relationship of NH_3 with ϕ.

4. Inasmuch as TFN behavior at all three temperatures reflects important contributions from NH_3 and HCN, these data may not be explained in terms of Zeldovich kinetics. They are pertinent to the phenomena of "prompt" NO_x formation, and they probably reflect nitrogen fixation by hydrocarbon radicals.

Table III-1.9 examines fuel nitrogen (NH_3) conversion in methane flames at 1800, 1900 and 2000 K over the range of ϕ from 0.8 to 1.8. Output fixed nitrogen species (NH_3, HCN, NO) are expressed as nitrogen atom percents of input species (NH_3). Input NH_3 is expressed as molar ppm of total reactants ($CH_4 + N_2 + O_2 + NH_3$).

Because of the quantity of information that it contains, analysis of this table is rather complex. Its data extends over a very wide range of flame conditions and, thus, single dominant themes are not apparent.

At the lowest temperature, 1800 K, TFN remains remarkably constant at the highest ϕ's. Although the input fuel nitrogen was NH_3, this was not an important output species at this temperature. For ϕ from 0.8 to 1.2 the dominant product is NO while for greater ϕ it is HCN. Output TFN can exceed 100% (indicating substantial N_2 fixation) at $\phi = 1.8$ as the result of large HCN production. In fact (see Table III-1.2) under these conditions output Fuel TFN can exceed 100 percent. This indicates the fixation of additional N_2 from the combustion air (over and above "thermal" fixation) caused by the addition of fuel nitrogen as ammonia. The presence of fuel nitrogen has obviously enhanced the fixation of molecular nitrogen at $\phi = 1.8$, $T = 1800$ K. This effect is absent at 1900 K. It is evident that HCN production is favored by high ϕ and low temperature. For $T = 1900$ K, it is not a quantitatively important species for any ϕ. At 1900 and 2000 K NO is the dominant output species with NH_3 of secondary importance, with NO production at 1900 being remarkably insensitive to ϕ. (At $\phi = 0.8$ and input NH_3 equal to 379 ppm, the very low TFN reflects an unreasonably low NO which must be regarded with great suspicion unless later verified.)

Some general observations may be immediately extracted from this data.

5. Fuel NH_3 conversion to NO decreases monotonically but slowly with increasing ϕ at 1800 [illegible] but stays almost constant over all ϕ at the higher temperatures.

6. Low temperatures and high ϕ favor conversion of fuel NH_3 to HCN.

7. Under conditions of highest HCN production, substantial enhanced fixation of N_2 occurs, and "Fuel" TFN exceeds 100 percent in some cases.

8. At all conditions except around $\phi = 1.2$ almost all fuel NH_3 is converted to other nitrogenous species.

9. On a percentage basis, conversion of fuel NH_3 to TFN out is rather insensitive to input fuel nitrogen concentration.

Table III-1.10 examines the influence of input fuel nitrogen concentration and species (NH_3 or NH_3 + NO) on fixed nitrogen emitted from methane flames at various equivalence ratios. Here the data subset is less extensive and more specifically directed than in the previous tables.

Input fuel nitrogen is either pure NH_3 or NH_3 plus NO in 1/1 ratio. Results are reported both as percent of input fuel nitrogen and as molar ppm in the dry (100% RH at room temperature) combustion products.

At equivalence ratio 0.8 no fuel NO was used. However, the addition of fuel NH_3 reduced the output NH_3 value below the pure thermal value (1.9 ppm or 1.1 ppm from 7.2 ppm). This effect increased with increasing fuel NH_3 concentration. It is also apparent at $\phi = 1.0$ but the effect is reversed at $\phi = 1.2$. It is seen in the HCN output at $\phi =$ 1.0-1.8. It is very strong for HCN output at $\phi = 1.8$ for input concentrations of 199 and 398 ppm NH_3 but is reversed at 994 ppm input. At $\phi = 0.8$ and 199 ppm input, NO output increased strongly over the thermal value. The result at 379 ppm input is the doubtful result discussed in the previous section on Table III-1.9.

At equivalence ratio 1.4 results with fuel NO addition first appear. Comparing 324 ppm pure NH_3 input with 170 ppm NH_3 + 169 ppm NO input (total 339 ppm), a striking change is noted. TFN increases from 83% to 206% as NO is added. Not only is conversion changed but increased fixation of N_2 (above that observed without fuel nitrogen present) becomes evident (indicated by "Fuel" TFN exceeding 100 percent). This increase is largely NH_3 (107 percent) with some contribution from NO (15 percent). These effects are diminished at $\phi = 1.8$. At all equivalence ratios NO is the overwhelming output species (except for NH_3 at $\phi = 1.4$ and 339 ppm N_{Total}) for either input species. At $\phi = 1.8$ additional fixation of N_2 over the case without input fuel nitrogen is no longer present.

Again, some general observations emerge from this examination.

10. Output fixed nitrogen is affected by the partial substitution of fuel NH_3 with fuel NO in the multiburner. The effect is strong at $\phi = 1.4$ and considerably diminished at $\phi = 1.8$. Data are not available for other equivalence ratios.

11. At $\phi = 1.4$ fixation of N_2 increases as fuel NH_3 is replaced with fuel NO even though fuel nitrogen quantities are far too small to discernibly change flame stoichiometry.

Table III-1.11 is a regrouping of data in Table III-1.10 to more clearly illustrate the effects of input fuel nitrogen species. Direct comparisons of input species effects at given equivalence ratios and total input nitrogen concentrations are shown in adjacent rows. Observations 10 and 11 are clearly reinforced by these comparisons.

Table III-1.12 is an examination of results with ethylene flames. It shows effects of equivalence ratio, fuel nitrogen species, and fuel nitrogen concentration on output fixed nitrogen. As was the case with CH_4 flames, at $\phi = 1.2$ the addition of fuel NH_3 increased output NH_3 but with ethylene it had little effect upon HCN (although addition of NH_3 + NO slightly decreased HCN). At $\phi = 1.4$ this effect reversed and behaved as with CH_4 flames.

Unfortunately, flows for $\phi = 1.8$ were improperly set and instead of being run at $\phi = 1.8$, T = 1900 K a series of runs were made at $\phi = 2.06$, T = 1772 K (adiabatic flame temperature, the multiburner tube was held near 1900 K). However, these data also show output NH_3 decreasing below the purely thermal value as fuel NH_3 or NO is added but with output HCN and NO both increasing strongly.

Table III-1.13 is a rearrangement of the data of Table III-1.12 to facilitate comparisons of the influences of input nitrogen species. Its data should be compared directly with those of Table III-1.11. Ethylene flames show no significant effect of changing input fuel nitrogen species from NH_3 to NH_3 + NO.* The important observation to be made is:

12. Unlike methane flames, the fixed nitrogen output from ethylene flames is largely independent of the input fuel nitrogen species (NH_3 or NH_3 + NO) for 1900 K flame temperature.

As in the case of CH_4 flames, at 1900 K and $\phi = 1.2$ or 1.4 the dominant output fixed nitrogen species is NO.

Unfortunately, NO additions were not made on propane flames and these observations cannot be extended to that fuel.

Table III-1.14 shows effects of equivalence ratio and fuel nitrogen concentration (NH_3 only) on nitrogen fixation in propane flames at 1900 K. The effect of input NH_3 reducing output NH_3 and HCN below purely thermal values that was noted for the other two fuels is absent from these data. The predominant output species is NO with both NH_3 and HCN outputs being much less at both equivalence ratios. At $\phi = 1.0$ percent TFN production as a function of input concentration shows a maximum while it monotonically decreases with input concentration at $\phi = 1.4$.

Finally, Table III-1.15 shows direct comparisons of fuel, fuel nitrogen species and concentration, and equivalence ratio effects on fixed nitrogen production in flames at 1900 K. Several observations can immediately be drawn from this table.

---

* That is at 1900 K. For the inadvertent points at 1772 K a large effect is evident.

13. In general, the ability to thermally fix N_2 as NH_3, HCN, or NO (and thus TFN) is inversely related to carbon number with the possible exception of ethylene relative to methane at $\phi = 1.4$ and with NO production by propane at $\phi = 1.8$. At $\phi = 1.4$ the abilities of methane and ethylene to thermally produce NO appear to be equal but greater HCN production with methane relative to that with ethylene preserves the above trend for TFN. At $\phi = 1.8$ propane produces more NO but less NH_3 and HCN than does methane.

14. Methane is more effective in converting fuel-fixed nitrogen to output fixed nitrogen (with the possible exception of output HCN) than are propane or ethylene which are about equal in effectiveness. (Conversely by implication the two higher hydrocarbons are more effective in converting fuel nitrogen to molecular nitrogen than is methane.)

15. Conversion of fuel-fixed nitrogen to output fixed nitrogen is species sensitive for methane but not for ethylene. Data are not available for propane.

16. Of the three fuels, only methane appears capable of converting over 100 percent of fuel nitrogen to output fixed nitrogen.

Table III-1.1

Combinations of Independent Variables Run in Multiburner Experiments

Fuel	T,K	Equivalence Ratio	Fuel Nitrogen Type and Concentration, ppm	
			NH_3	NH_3/NO
CH_4	1800	0.7, 1.0, 1.2, 1.4, 1.6, 1.8	0	0/0
CH_4	1800	0.8	208, 416, 787	0/0
CH_4	1800	1.0, 1.2, 1.8	208, 416, 1040	0/0
CH_4	1800	1.4	208, 416, 745	0/0
CH_4	1900	0.8, 1.0, 1.2, 1.4, 1.8	0	0/0
CH_4	1900	0.8	199, 379	0/0
CH_4	1900	1.0	199, 398	0/0
CH_4	1900	1.2	199, 398, 820	0/0
CH_4	1900	1.4	199, 324	170/169
CH_4	1900	1.8	199, 398, 994	104/104, 208/208, 520/520
CH_4	2000	0.8, 1.0, 1.2, 1.4, 1.8	0	0/0
CH_4	2000	1.0	208, 416, 935	0/0
CH_4	1946 1898 1769	0.8	200 385 867	0/0

(Continued)

Table III-1.1 (Continued)

Fuel	T,K	Equivalence Ratio	Fuel Nitrogen Type and Concentration, ppm	
			NH_3	NH_3/NO
C_2H_4	1772	2.06	0, 208, 416, 467	104/104, 208/208, 234/234
C_2H_4	1800	1.4	0	0/0
C_2H_4	1900	0.8	208, 416	0/0
C_2H_4	1900	1.2, 1.4	0	0/0
C_2H_4	1900	1.2	208, 416, 1040	208/208, 416/416, 520/520
C_2H_4	1900	1.4	208, 416, 1040	104/104, 208/208, 520/520
C_3H_8	1800	1.4	0	0/0
C_3H_8	1900	1.0, 1.4, 1.8	0	0/0
C_3H_8	1900	1.0	208, 418, 1040	0/0
C_3H_8	1900	1.4	208, 416, 608	0/0

Table III-1.2

Experimental Results from $CH_4/O_2/N_2$ Flames in the Multiburner with 1800 K Flame Temperature

Set	Actual	Set	Computed	Computed	Additives, VPPM		Collected, VPPM in Dry Gas				Collected, Percent of N Added				Collected, Percent of N Added				Collected in Dry Exhaust Gas					τ
T,K	T,K	φ	φ	T,K	NH_3	NO	NH_3	HCN	NO	TFN	NH_3	HCN	NO	TFN	Fuel NH_3	Fuel HCN	Fuel NO	Fuel TFN	CO_2 %	CO %	O_2 %	H_2 %	HC VPPM	ms
1800	1800	0.7	0.700	1795	0	0	8.6	6.4	17	32	----	-----	----	---	-----	------	-----	----	8.8	0.6	4.5	-----	7	32.4
1800	1798	1.0	1.00	1802	0	0	5.1	2.0	32	39	----	-----	----	---	-----	------	-----	----	6.6	2.5	0.1	1.8	10	32.2
1800	1808	1.2	1.20	1806	0	0	4.9	2.1	40	47	----	-----	----	---	-----	------	-----	----	6.3	4.5	0.12	3.7	150	31.3
1800	1809	1.4	1.40	1791	0	0	8.4	9.5	46	64	----	-----	----	---	-----	------	-----	----	5.3	8.5	0.10	6.4	305	30.4
1800	1796	1.6	1.60	1803	0	0	8.2	15	43	66	----	-----	----	---	-----	------	-----	----	5.1	11	0.08	8.7	535	29.2
1800	1797	1.8	1.80	1800	0	0	9.2	19	9.7	38	----	-----	----	---	-----	------	-----	----	2.7	7.1	1.0	6.5	2150	27.9
1800	1810	0.8	0.800	1792	208	0	1.3	1.2	125	128	0.55	0.49	52	53	-----	------	-----	----	7.8	0.0	3.6	0.10	8	32.4
1800	1809	0.8	0.800	1792	416	0	1.0	1.2	260	262	0.21	0.25	54	54	-----	------	-----	----	7.7	0.0	3.6	0.03	6	32.4
1800	1811	0.8	0.800	1792	787	0	1.0	1.3	510	512	0.11	0.14	56	56	-----	------	-----	----	7.8	0.0	3.0	0.06	6	32.4
1800	1813	1.0	1.00	1802	208	0	0.91	1.5	123	125	0.38	0.61	51	52	-1.7	-0.22	38	36	6.5	0.85	1.8	0.94	4	32.2
1800	1810	1.0	1.00	1802	416	0	0.87	1.9	235	238	0.18	0.39	49	50	-0.88	-0.03	42	42	6.4	1.1	1.7	1.2	4	32.2
1800	1810	1.0	1.00	1802	1040	0	1.3	2.2	350	354	0.11	0.19	29	29	-0.32	0.02	27	26	6.3	1.1	1.7	1.2	3	32.2
1800	1810	1.2	1.20	1806	208	0	1.2	12	90	103	0.52	4.9	38	43	-1.5	4.0	21	24	5.4	2.8	1.7	3.3	23	31.2
1800	1808	1.2	1.20	1806	416	0	1.1	24	175	200	0.22	5.0	37	42	-0.80	4.5	29	32	6.0	3.0	1.7	3.6	26	31.2
1800	1811	1.2	1.20	1806	1040	0	1.0	63	320	384	0.41	5.3	27	33	0.41	5.1	24	29	6.0	3.0	1.9	3.4	22	31.2
1800	1816	1.4	1.40	1791	208	0	0.88	182	38	221	0.38	79	17	96	-3.3	75	-3.5	68	5.2	5.0	1.8	6.0	1800	30.4
1800	1814	1.4	1.40	1791	416	0	1.0	345	48	394	0.23	75	10	85	-1.6	73	0.43	72	5.2	5.0	1.8	5.9	2400	30.4
1800	1814	1.4	1.40	1791	745	0	1.5	394	82	478	0.18	48	10	58	-0.84	47	4.4	50	5.2	5.0	1.8	5.9	2100	30.4
1800	1799	1.8	1.80	1798	208	0	8.5	205	7.0	221	4.0	96	3.3	103	-0.33	88	-1.3	86	5.2	9.4	2.2	11	12000	28.0
1800	1798	1.8	1.80	1798	416	0	1.1	514	14	529	0.25	121	3.3	125	-1.9	117	1.0	116	5.6	8.5	1.9	11	12000	28.0
1800	1797	1.8	1.80	1798	1040	0	19	1132	20	1171	1.8	107	1.8	111	0.90	105	0.92	107	5.3	9.4	2.0	11	19500	28.0

Table III-1.3

Experimental Results from $CH_4/O_2/N_2$ Flames in the Multiburner with 1900 K Flame Temperature

Set T,K	Actual T,K	Set ϕ	Computed ϕ	Computed T,K	Additives, VPPM		Collected, VPPM in Dry Gas				Collected, Percent of N Added				Collected, Percent of N Added				Collected in Dry Exhaust Gas					τ ms
					NH_3	NO	NH_3	HCN	NO	TFN	NH_3	HCN	NO	TFN	Fuel NH_3	Fuel HCN	Fuel NO	Fuel TFN	CO_2 %	CO %	O_2 %	H_2 %	HC VPPM	
1900	1906	0.8	0.800	1896	0	0	7.2	1.8	9.2	18	------	-----	------	------	------	-----	----	----	7.9	0.0	1.5	-----	40	30.6
1900	1891	1.0	0.999	1901	0	0	14	2.4	23	39	------	-----	------	------	------	-----	----	----	7.6	1.4	2.2	<.01	50	30.5
1900	1900	1.2	1.20	1900	0	0	4.8	17	31	53	------	-----	------	------	------	-----	----	----	6.8	4.2	2.0	3.9	620	29.6
1900	1905	1.4	1.38	1908	0	0	2.4	6.8	33	42	------	-----	------	------	------	-----	----	----	6.3	7.1	1.5	6.4	525	28.6
1900	1912	1.8	1.80	1899	0	0	2.2	27	5.7	35	------	-----	------	------	------	-----	----	-----	5.6	13	1.0	12	1100	26.1
1900	1896	0.8	0.800	1896	199	0	1.9	1.3	125	128	0.80	0.57	54	55	-2.3	-0.22	50	47	8.5	0.0	3.1	-----	21	30.6
1900	1902	0.8	0.800	1896	379	0	1.1	1.7	0.65	3.5	0.23	0.45	0.15	0.83	-1.4	-0.04	-1.9	-3.4	8.5	0.0	3.0	-----	26	30.6
1900	1894	1.0	0.999	1901	199	0	1.2	1.2	150	152	0.43	0.43	65	66	-5.7	-0.52	55	49	7.8	0.7	0.15	0.53	6	30.5
1900	1903	1.0	0.999	1901	398	0	1.0	1.1	280	282	0.22	0.22	60	61	-2.9	-0.28	55	52	7.8	0.5	0.18	0.38	4	30.5
1900	1903	1.2	1.20	1900	199	0	158	2.5	240	401	69	1.1	105	175	67	-6.5	91	152	6.5	2.8	1.4	2.8	25	29.6
1900	1909	1.2	1.20	1900	398	0	78	0.66	255	334	17	0.14	56	73	16	-3.6	49	61	6.3	3.2	1.6	3.3	28	29.6
1900	1909	1.2	1.20	1900	820	0	18	0.71	620	639	2.0	0.08	66	68	1.4	-1.8	62	62	7.1	3.0	1.4	3.0	24	29.6
1900	1912	1.4	1.38	1908	199	0	14	1.5	195	211	6.1	0.66	87	94	5.1	-2.4	72	75	6.5	5.0	1.6	5.9	27	28.6
1900	1913	1.4	1.38	1908	324	0	9.1	1.9	290	301	2.5	0.51	80	83	1.9	-1.4	71	71	6.5	5.0	1.6	5.9	22	28.6
1900	1909	1.8	1.80	1898	199	0	10	6.9	140	157	5.0	3.4	69	77	4.0	-9.8	66	60	5.8	11	1.6	11	17	26.1
1900	1911	1.8	1.80	1898	398	0	17	5.0	200	222	4.2	1.2	49	54	3.7	-5.4	48	46	5.8	11	1.6	11	34	26.1
1900	1911	1.8	1.80	1898	994	0	5.1	127	195	327	0.50	12	19	32	0.28	9.8	19	29	5.3	12	1.5	14	150	26.1
* 1900	1892	1.0	0.587	1895	99	104	6.7	23	245	275	2.8	9.7	103	116	------	-----	----	-----	7.6	0.2	1.5	<.01	4	30.6
* 1900	1895	1.0	0.639	1897	199	208	2.9	1.5	485	489	0.61	0.32	102	103	------	-----	----	-----	7.8	0.3	1.4	<.01	4	30.6
* 1900	1895	1.0	0.871	1905	520	520	5.6	1.4	765	772	0.46	0.12	63	64	------	-----	----	-----	7.8	0.4	1.3	<.01	11	30.5
* 1900	1896	1.4	1.29	2060	104	104	1.9	10	340	352	0.79	4.1	141	146	------	-----	----	-----	6.9	4.2	1.2	4.4	7	26.8
1900	1895	1.4	1.38	1908	170	169	418	2.5	360	781	110	0.66	95	206	109	-1.1	86	194	6.9	4.4	1.3	4.6	4	28.6
1900	1895	1.8	1.80	1898	104	104	2.0	20	185	207	0.95	9.2	87	97	-0.08	-3.4	84	81	6.0	11	1.2	12	39	26.1
1900	1900	1.8	1.80	1898	208	208	7.8	26	230	264	1.8	6.0	54	62	1.3	-0.33	53	53	5.8	11	1.3	10	71	26.1
1900	1898	1.8	1.80	1898	520	520	2.1	51	305	358	0.19	4.8	29	34	-0.01	2.3	28	30	5.8	11	1.3	10	150	26.1

* Note large difference between target conditions and set conditions included within box.

Table III-1.4

Experimental Results from $CH_4/O_2/N_2$ Flames in the Multiburner with 2000 K Flame Temperature

Set T,K	Actual T,K	Set ϕ	Computed ϕ	Computed T,K	Additives, VPPM		Collected, VPPM in Dry Gas				Collected, Percent of N Added				Collected, Percent of N Added				Collected in Dry Exhaust Gas					τ
					NH_3	NO	NH_3	HCN	NO	TFN	NH_3	HCN	NO	TFN	Fuel NH_3	Fuel HCN	Fuel NO	Fuel TFN	CO_2 %	CO %	O_2 %	H_2 %	HC VPPM	ms
2000	1995	0.8	0.799	1996	0	0	59	29	9.8	98	----	----	--	--	----	----	----	----	7.7	0.0	6.0	<0.05	29	29.1
2000	1991	1.0	1.00	1998	0	0	19	25	26	70	----	----	--	--	----	----	----	----	8.2	0.8	3.0	0.74	24	29.0
2000	1997	1.2	1.25	1959	0	0	16	2.2	30	48	----	----	--	--	----	----	----	----	5.8	3.3	2.7	3.6	19	28.3
2000	2004	1.4	1.44	1969	0	0	11	2.2	30	43	----	----	--	--	----	----	----	----	6.9	3.3	2.4	4.3	16	27.2
2000	2008	1.8	1.80	2004	0	0	11	9.2	2	22	----	----	--	--	----	----	----	----	5.2	12	2.3	12	15000	24.4
2000	2005	0.8	0.799	1946	200	0	7.7	2.7	135	145	3.3	1.1	58	62	----	----	----	----	7.6	<0.1	5.8	<0.05	20	27.6
2000	2010	0.8	0.799	1898	385	0	1.0	1.7	250	253	0.23	0.38	56	56	----	----	----	----	7.0	0.0	5.8	<0.05	22	28.3
2000	2010	0.8	0.799	1769	867	0	10	1.4	600	611	1.0	0.14	60	62	----	----	----	----	6.9	<0.1	4.7	<0.05	24	27.3
2000	2008	1.0	1.00	1998	208	0	4.7	1.4	150	156	1.9	0.56	61	64	-5.7	-9.4	51	35	6.9	0.8	2.4	0.72	32	29.0
2000	2009	1.0	1.00	1998	416	0	5.7	1.3	280	287	1.2	0.26	57	59	-2.6	-4.7	52	44	7.0	0.9	2.4	0.79	31	29.0
2000	2008	1.0	1.00	1998	935	0	5.3	2.1	560	567	0.48	0.19	51	51	-1.2	-2.0	48	45	7.0	1.1	2.4	0.88	24	29.0

Table III-1.5

Experimental Results from $C_2H_4/O_2/N_2$ Flames in the Multiburner

Set	Actual	Set	Computed	Computed	Additives, VPPM		Collected, VPPM in Dry Gas				Collected, Percent of N Added				Collected, Percent of N Added				Collected in Dry Exhaust Gas					τ
T,K	T,K	φ	φ	T,K	NH_3	NO	NH_3	HCN	NO	TFN	NH_3	HCN	NO	TFN	Fuel NH_3	Fuel HCN	Fuel NO	Fuel TFN	CO_2 %	CO %	O_2 %	H_2 %	HC VPPM	ms
1900	1906	1.2	1.20	1880	0	0	1.1	2.6	8.6	12	----	------	----	---	------	-------	----	---	8.3	0.0	2.5	<0.001	14	30.1
1900	1906	1.4	1.40	1902	0	0	2.0	2.0	34	38	----	------	----	---	------	-------	----	---	8.8	----	1.3	1.1	125	28.8
1900	1906	1.8	2.06	1772	0	0	55	1.2	2.2	58	----	------	----	---	------	-------	----	---	4.3	----	1.1	9.1	3900	27.4
1900	1906	0.8	0.800	1900	208	0	1.7	2.0	125	129	0.73	0.88	55	57	------	-------	----	---	6.0	0.0	8.0	<0.01	29	30.5
1900	1907	0.8	0.800	1900	416	0	1.7	1.8	230	234	0.37	0.39	51	51	------	-------	----	---	5.8	0.0	8.0	<0.05	10	30.5
1900	1899	1.4	1.40	1902	208	0	1.1	0.97	183	185	0.49	0.45	84	85	-0.43	-0.45	69	68	9.2	0.6	1.5	0.23	11	28.8
1900	1888	1.4	1.40	1902	416	0	0.94	0.92	280	282	0.22	0.21	64	65	-0.24	-0.24	57	56	9.0	0.7	1.5	0.30	12	28.8
1900	1894	1.4	1.40	1902	1040	0	0.97	0.96	600	602	0.089	0.088	55	55	-0.095	-0.091	52	52	8.8	0.8	1.5	0.36	13	28.8
1900	1892	1.8	2.06	1772	208	0	1.2	19	110	130	0.62	10	58	69	-28	9.6	57	39	5.8	8.5	1.4	6.3	29	27.4
1900	1888	1.8	2.06	1772	416	0	1.6	61	145	208	0.43	16	38	55	-14	16	38	39	5.4	9.4	1.4	6.5	91	27.4
1900	1887	1.8	2.06	1772	467	0	1.3	110	135	246	0.30	26	32	58	-13	26	31	44	5.4	8.5	1.4	6.1	340	27.4
1900	1898	1.4	1.40	1902	104	104	1.2	1.4	155	158	0.56	0.63	71	73	-0.36	-0.27	56	55	8.2	1.6	1.3	0.69	130	28.8
1900	1898	1.4	1.40	1954	208	208	2.6	1.7	270	274	0.59	0.39	62	63	0.13	-0.058	54	54	8.8	1.4	1.5	0.50	220	29.1
1900	1898	1.4	1.40	1902	520	520	1.8	1.2	650	653	0.16	0.11	60	60	-0.019	-0.065	57	57	8.5	1.4	1.5	0.59	17	28.8
1900	1898	1.8	2.06	1772	104	104	2.0	243	28	273	1.1	128	15	144	-28	128	14	114	4.4	9.4	1.3	6.9	7200	27.4
1900	1898	1.8	2.06	1772	208	208	1.3	373	36	410	0.33	99	9.5	108	-14	98	8.9	93	4.5	9.4	1.4	6.5	11000	27.4
1900	1898	1.8	2.06	1772	234	234	3.1	402	38	443	0.73	94	8.9	104	-12	94	8.4	90	4.5	11	1.0	6.7	9400	27.4
1900	1895	1.2	1.20	1880	208	0	6.6	2.8	185	194	2.9	1.3	83	87	2.5	0.10	79	82	7.6	0.0	2.8	<0.001	59	30.1
1900	1895	1.2	1.20	1880	416	0	2.1	4.1	260	266	0.46	0.91	58	60	0.22	0.33	56	57	7.6	0.0	2.6	<0.001	29	30.1
1900	1895	1.2	1.20	1880	1040	0	3.4	1.0	625	629	0.31	0.093	56	56	0.21	-0.14	55	55	7.8	0.0	2.5	<0.001	20	30.1
1900	1895	1.2	1.20	1880	208	208	1.9	1.6	300	304	0.42	0.36	67	68	0.18	-0.22	65	65	7.8	0.0	2.5	<0.001	16	30.1
1900	1895	1.2	1.20	1880	416	416	1.3	1.4	520	523	0.14	0.15	58	59	0.022	-0.13	57	57	7.6	0.0	2.3	<0.001	16	30.1
1900	1895	1.2	1.20	1880	520	520	1.8	1.4	680	683	0.16	0.13	61	61	0.063	-0.10	60	60	7.6	0.0	2.3	<0.001	16	30.1
1800	1800	1.4	1.40	1802	0	0	1.1	2.1	3.9	7.1	----	------	--	---	-------	------	----	---	6.9	0.0	3.8	<0.001	11	30.6

Table III-1.6

Experimental Results from $C_3H_8/O_2/N_2$ Flames in the Multiburner

Set T,K	Actual T,K	Set ϕ	Computed ϕ	Computed T,K	Additives, VPPM		Collected, VPPM in Dry Gas				Collected, Percent of N Added				Collected, Percent of N Added				Collected in Dry Exhaust Gas					τ
					NH_3	NO	NH_3	HCN	NO	TFN	NH_3	HCN	NO	TFN	Fuel NH_3	Fuel HCN	Fuel NO	Fuel TFN	CO_2 %	CO %	O_2 %	H_2 %	HC VPPM	ms
1800	1795	1.4	1.40	1796	0.0	0.0	1.1	1.5	19	22	--	--	--	--	--	--	--	--	10	<0.1	1.6	<0.05	7	29.1
1900	1905	1.0	1.00	1897	0.0	0.0	0.98	1.4	2.2	4.6	--	--	--	--	--	--	--	--	5.4	<0.1	5.5	<0.01	120	29.7
1900	1910	1.4	1.40	1899	0.0	0.0	0.94	1.3	22	24	--	--	--	--	--	--	--	--	11	<0.1	1.6	<0.01	10	27.3
1900	1908	1.8	1.80	1906	0.0	0.0	1.4	12	45	58	--	--	--	--	--	--	--	--	8.0	10	1.1	6.4	130	24.2
1900	1906	1.0	1.00	1897	208	0.0	1.4	2.3	28	32	0.61	1.0	12	14	0.18	0.41	11	12	3.8	0.4	7.5	<0.01	3400	29.7
1900	1906	1.0	1.00	1897	418	0.0	2.8	1.0	225	229	0.61	0.22	50	51	0.39	-0.073	49	49	5.2	0.0	7.5	<0.05	38	29.7
1900	1888	1.0	1.00	1897	1040	0.0	25	1.3	420	446	2.2	0.11	37	39	2.1	-0.0053	37	39	5.3	0.0	7.5	<0.01	28	29.7
1900	1906	1.4	1.40	1899	208	0.0	0.99	0.98	185	187	0.46	0.46	87	88	0.023	-0.13	77	77	13	0.4	0.9	0.19	28	27.3
1900	1903	1.4	1.40	1899	416	0.0	3.1	1.4	300	305	0.72	0.34	70	71	0.50	0.040	65	66	11	7.7	0.9	1.3	22	27.3
1900	1903	1.4	1.40	1899	608	0.0	1.2	1.1	410	412	0.20	0.17	66	66	0.047	-0.031	62	62	11	7.9	0.8	1.3	23	27.3

Table III-1.7

Effect of Equivalence Ratio on Fixed Nitrogen Produced in Hydrocarbon/O_2/N_2 Flames at 1900 K Without Fuel Nitrogen in the Multiburner

ϕ	TFN in Dry Gas, PPM			NH_3 in Dry Gas, PPM			HCN in Dry Gas, PPM			NO in Dry Gas, PPM			Residence Time, ms		
	CH_4	C_2H_4	C_3H_8	CH_4	C_2H_4	C_3H_8	CH_4	C_2H_4	C_3H_8	CH_4	C_2H_4	C_3H_8	CH_4	C_2H_4	C_3H_8
0.8	18	--	--	7.2	--	--	1.8	--	--	9.2	--	--	31	--	--
1.0	39	--	4.6	14	--	0.98	2.4	--	1.4	23	--	2.2	31	--	30
1.2	53	12	--	4.8	1.1	--	17	2.6	--	31	8.6	--	30	30	--
1.4	42	38	24	2.4	2.0	0.94	6.8	2.0	1.3	33	34	22	29	29	27
1.8	35	--	58	2.2	--	1.4	27	--	12	5.7	--	45	26	--	24

Table III-1.8

Effect of Equivalence Ratio and Temperature on Fixed Nitrogen Produced in Methane/O_2/N_2 Flames Without Fuel Nitrogen in the Multiburner

	TFN in Dry Gas, PPM			NH_3 in Dry Gas, PPM			HCN in Dry Gas, PPM			NO in Dry Gas, PPM			Residence Time, ms		
ϕ	1800 K	1900 K	2000 K	1800 K	1900 K	2000 K	1800 K	1900 K	2000 K	1800 K	1900 K	2000 K	1800 K	1900 K	2000 K
0.7	32	--	--	8.6	--	--	6.4	--	--	17	--	--	32	--	--
0.8	--	18	98	--	7.2	59	--	1.8	29	--	9.2	9.8	--	31	29
1.0	39	39	70	5.1	14	19	2.0	2.4	25	32	23	26	32	31	29
1.2	47	53	48*	4.9	4.8	16	2.1	17	2.2	40	31	30	31	30	28
1.4	64	42	43**	8.4	2.4	11	9.5	6.8	2.2	46	33	30	30	29	27
1.6	66	--	--	8.2	--	--	15	--	--	43	--	--	29	--	--
1.8	38	35	22	9.2	2.2	11	19	27	9.2	9.7	5.7	2	28	26	24

* $\phi = 1.25$

** ϕ 1.44

Table III-1.9

Effect of Equivalence Ratio, Temperature, and Concentration of Fuel Nitrogen (NH_3) on Conversion of Fuel Nitrogen in $CH_4/O_2/N_2$ Flames

ϕ	Input NH_3 PPM	Percent of Input Fuel Nitrogen as TFN Out 1800 K	1900 K	2000 K	Percent of Input Fuel Nitrogen as NH_3 Out 1800 K	1900 K	2000 K	Percent of Input Fuel Nitrogen as HCN Out 1800 K	1900 K	2000 K	Percent of Input Fuel Nitrogen as NO Out 1800 K	1900 K	2000 K	Residence Time, ms 1800 K	1900 K	2000 K
0.8	200			62			3.3			1.1			58			
	208	53			0.55			0.49			52			32	31	29
	199		55			0.80			0.57			54				
	385			56			0.23			0.38			56			
	416	54			0.21			0.25			54					
	379		0.83			0.23			0.45			0.15				
	787	56			0.11			0.14			56					
	867			62			1.0			0.14			60			
1.0	208	52		64	0.38		1.9	0.61		0.56	51		61			
	199		66			0.43			0.43			65		32	31	28
	416	50		59	0.18		1.2	0.39		0.26	49		57			
	398		61			0.22			0.22			60				
	1040	29			0.11			0.19			29					
	935			51			0.48			0.19			51			
1.2	208	43			0.52			4.9			38					
	199		175			69			1.1			105		31	30	
	416	42			0.22			5.0			37					
	398		73			17			0.14			56				
	1040	33			0.41			5.3			27					
	820		68			2.0			0.08			66				

(Continued)

Table III-1.9 (Continued)

ϕ	Input NH_3 PPM	Percent of Input Fuel Nitrogen as TFN Out			Percent of Input Fuel Nitrogen as NH_3 Out			Percent of Input Fuel Nitrogen as HCN Out			Percent of Input Fuel Nitrogen as NO Out			Residence Time, ms		
		1800 K	1900 K	2000 K	1800 K	1900 K	2000 K	1800 K	1900 K	2000 K	1800 K	1900 K	2000 K	1800 K	1900 K	2000 K
1.4	208	96			0.38			79			17					
	199		94			6.1			0.66			87		30	29	
	416	85			0.23			75			10					
	324		83			2.5			0.51			80				
	745	58			0.18			48			10					
1.8	208	103			4.0			96			3.3					
	199		77			5.0			3.4			69		28	26	
	416	125			0.25			121			3.3					
	398		54			4.2			1.2			49				
	1040	111			1.8			107			1.8					
	994		32			0.50			12			19				

Table III-1.10

Effect of Equivalence Ratio and Fuel Nitrogen Species (NH_3 or NO + NH_3) on Conversion of Fuel Nitrogen in $CH_4/O_2/N_2$ Flames at 1900 K

	Input Fuel N, PPM			Percent of Input FN Out As				Collected in Exhaust Gas, VPPM				Percent of Input FN Out As			
ϕ	NH_3	NO_3	N_{Total}	TFN	NH_3	HCN	NO	TFN	NH_3	HCN	NO	Fuel TFN	Fuel NH_3	Fuel HCN	Fuel NO
0.8	0	0	0	--	--	--	--	18	7.2	1.8	9.2	--	--	--	--
0.8	199	0	199	55	0.80	0.57	54	128	1.9	1.3	125	47	-2.3	-0.22	50
0.8	379	0	379	0.83	0.23	0.45	0.15	3.5	1.1	1.7	0.65	-3.4	-1.4	-0.04	-1.9
1.0	0	0	0	--	--	--	--	39	14	2.4	23	--	--	--	--
1.0	199	0	199	66	0.43	0.43	65	152	1.2	1.2	150	49	-5.7	-0.52	55
1.0	398	0	398	61	0.22	0.22	60	282	1.0	1.1	280	52	-2.9	-0.28	55
1.2	0	0	0	--	--	--	--	53	4.8	17	31	--	--	--	--
1.2	199	0	199	175	69	1.1	105	401	158	2.5	240	152	67	-6.5	91
1.2	398	0	398	73	17	0.14	56	334	78	0.66	255	61	16	-3.6	49
1.2	820	0	820	68	2.0	0.08	66	639	18	0.71	620	62	1.4	-1.8	62
1.4	0	0	0	--	--	--	--	42	2.4	6.8	33	--	--	--	--
1.4	199	0	199	94	6.1	0.66	87	211	14	1.5	195	75	5.1	-2.4	72
1.4	324	0	324	83	2.5	0.51	80	301	9.1	1.9	290	71	1.9	-1.4	71
1.4	170	169	339	206	110	0.66	95	781	418	2.5	360	194	109	-1.1	86
1.8	0	0	0	--	--	--	--	35	2.2	27	5.7	--	--	--	--
1.8	199	0	199	77	5.0	3.4	69	157	10	6.9	140	60	4.0	-9.8	66
1.8	398	0	398	54	4.2	1.2	49	222	17	5.0	200	46	3.7	-5.4	48
1.8	994	0	994	32	0.50	12	19	327	5.1	127	195	29	0.28	9.8	19
1.8	104	104	208	97	0.95	9.2	87	207	2.0	20	185	81	-0.08	-3.4	84
1.8	208	208	416	62	1.8	6.0	54	264	7.8	26	230	53	1.3	-0.33	53
1.8	520	520	1040	34	0.19	4.8	29	358	2.1	51	305	30	-0.01	2.3	28

Table III-1.11

Effect of Equivalence Ratio and Fuel Nitrogen Species (NH_3 or NO + NH_3) on Conversion of Fuel Nitrogen in $CH_4/O_2/N_2$ Flames at 1900 K

	Input Fuel N, PPM			Percent of Input FN Out As				Percent of Input FN Out As			
ϕ	NH_3	NO	N_{Total}	TFN	NH_3	HCN	NO	Fuel TFN	Fuel NH_3	Fuel HCN	Fuel NO
1.4	324	0	324	83	2.5	0.51	80	71	1.9	-1.4	71
1.4	170	169	339	206	110	0.66	95	194	109	-1.1	86
1.8	199	0	199	77	5.0	3.4	69	60	4.0	-9.8	66
1.8	104	104	208	97	0.95	9.2	87	81	-0.08	-3.4	84
1.8	398	0	398	54	4.2	1.2	49	46	3.7	-5.4	48
1.8	208	208	416	62	1.8	6.0	54	53	1.3	-0.33	53
1.8	994	0	994	32	0.50	12	19	29	0.28	9.8	19
1.8	520	520	1040	34	0.19	4.8	29	30	-0.01	2.3	28

Table III-1.12

Effect of Equivalence Ratio and Fuel Nitrogen Species (NH_3 or NH_3 + NO) on Conversion of Fuel Nitrogen in $C_2H_4/O_2/N_2$ Flames at 1900 K

	Input Fuel N, PPM			Percent of Input FN Out As				Collected in Exhaust Gas, VPPM			
ϕ	NH_3	NO	N_{Total}	TFN	NH_3	HCN	NO	TFN	NH_3	HCN	NO
0.8	208	0	208	57	0.73	0.88	55	129	1.7	2.0	125
0.8	416	0	416	52	0.37	0.39	51	234	1.7	1.8	230
1.2	0	0	0	--	--	--	--	12	1.1	2.6	8.6
1.2	208	0	208	87	2.9	1.3	83	194	6.6	2.8	185
1.2	416	0	416	60	0.46	0.91	58	266	2.1	4.1	260
1.2	1040	0	1040	56	0.31	0.093	56	629	3.4	1.0	625
1.4	0	0	0	--	--	--	--	38	2.0	2.0	34
1.4	208	0	208	85	0.49	0.45	84	185	1.1	0.97	183
1.4	416	0	416	65	0.22	0.21	64	282	0.94	0.92	280
1.4	1040	0	1040	55	0.089	0.088	55	602	0.97	0.96	600
1.2	208	208	416	68	0.42	0.36	67	304	1.9	1.6	300
1.2	416	416	832	59	0.14	0.15	58	523	1.3	1.4	520
1.2	520	520	1040	61	0.16	0.13	61	683	1.8	1.4	680
1.4	104	104	208	73	0.56	0.63	71	158	1.2	1.4	155
1.4	208	208	416	63	0.59	0.39	62	274	2.6	1.7	270
1.4	520	520	1040	60	0.16	0.11	60	653	1.8	1.2	650

(Continued)

Table III-1.12 (Continued)

ϕ	Input Fuel N, PPM			Percent of Input FN Out As				Collected in Exhaust Gas, VPPM			
	NH_3	NO	N_{Total}	TFN	NH_3	HCN	NO	TFN	NH_3	HCN	NO
2.06*	0	0	0	--	--	--	--	58	55	1.2	2.2
2.06*	208	0	208	69	0.62	10	58	130	1.2	19	110
2.06*	416	0	416	55	0.43	16	38	208	1.6	61	145
2.06*	467	0	467	58	0.30	26	32	246	1.3	110	135
2.06*	104	104	208	144	1.1	128	15	273	2.0	243	28
2.06*	208	208	416	108	0.33	99	9.5	410	1.3	373	36
2.06*	234	234	468	104	0.73	94	8.9	443	3.1	402	38

* Flame temperature of these runs was 1772 K

Table III-1.13

Effect of Equivalence Ratio and Fuel Nitrogen Species (NH_3 or NH_3 + NO) on Conversion of Fuel Nitrogen in $C_2H_4/O_2/N_2$ Flames at 1900 K

ϕ	Input Fuel N, PPM			Percent of Input FN As			
	NH_3	NO	N_{Total}	TFN	NH_3	HCN	NO
1.2	416	0	416	60	0.46	0.91	58
1.2	208	208	416	68	0.42	0.36	67
1.2	1040	0	1040	56	0.31	0.093	56
1.2	520	520	1040	61	0.16	0.13	61
1.4	208	0	208	85	0.49	0.45	84
1.4	104	104	208	73	0.56	0.63	71
1.4	416	0	416	65	0.22	0.21	64
1.4	208	208	416	63	0.59	0.39	62
1.4	1040	0	1040	55	0.089	0.088	55
1.4	520	520	1040	60	0.16	0.11	60
2.06*	208	0	208	69	0.62	10	58
2.06*	104	104	208	144	1.1	128	15
2.06*	416	0	416	55	0.43	16	38
2.06*	208	208	416	108	0.33	99	9.5
2.06*	467	0	467	58	0.30	26	32
2.06*	234	234	468	104	0.73	94	8.9

* Flame temperature of these runs was 1772 K.

Table III-1.14

Effect of Equivalence Ratio and Fuel Nitrogen Concentration (NH_3) on Conversion of Fuel Nitrogen in $C_3H_8/O_2/N_2$ Flames at 1900 K

		Percent of Input FN Out As				Nitrogen Species in Combustion Gas, PPM			
ϕ	NH_3 In PPM	TFN	NH_3	HCN	NO	TFN	NH_3	HCN	NO
1.0	0	--	--	--	--	4.6	0.98	1.4	2.2
1.0	208	14	0.61	1.0	12	32	1.4	2.3	28
1.0	418	51	0.61	0.22	50	229	2.8	1.0	225
1.0	1040	39	2.2	0.11	37	446	25	1.3	420
1.4	0	--	--	--	--	22	1.1	1.5	19
1.4	208	88	0.46	0.46	87	187	0.99	0.98	185
1.4	416	71	0.72	0.34	70	305	3.1	1.4	300
1.4	608	66	0.20	0.17	66	412	1.2	1.1	410

Table III-1.15

Effect of Equivalence Ratio, Fuel Nitrogen Concentration and Species, and Fuel Species on Nitrogen Conversion in Hydrocarbon/O_2/N_2 Flames at 1900 K

ϕ	Fuel	Input Fuel N, PPM			Percent of Input FN Out As				Nitrogen Species in Dry Combustion Gas, PPM				Yield Ratio Relative to Methane Fuel			
		NH_3	NO	N_{Total}	TFN	NH_3	HCN	NO	TFN	NH_3	HCN	NO	TFN	NH_3	HCN	NO
1.0	CH_4	0	0	0	--	--	--	--	39	14	2.4	23	1	1	1	1
1.0	C_3H_8	0	0	0	--	--	--	--	4.6	0.98	1.4	2.2	0.12	0.070	0.58	0.096
1.0	CH_4	199	0	199	66	0.43	0.43	65	152	1.2	1.2	150	1	1	1	1
1.0	C_3H_8	208	0	208	14	0.61	1.0	12	32	1.4	2.3	28	0.21	1.4	2.3	0.18
1.0	CH_4	398	0	398	61	0.22	0.22	60	282	1.0	1.1	280	1	1	1	1
1.0	C_3H_8	418	0	418	51	0.61	0.22	50	229	2.8	1.0	225	0.84	2.8	1.0	0.83
1.0	C_3H_8	1040	0	1040	39	2.2	0.11	37	446	25	1.3	420	--	--	--	--
1.2	CH_4	0	0	0	--	--	--	--	53	4.8	17	31	1	1	1	1
1.2	C_2H_4	0	0	0	--	--	--	--	12	1.1	2.6	8.6	0.23	0.23	0.15	0.28
1.2	CH_4	199	0	199	175	69	1.1	105	401	158	2.5	240	1	1	1	1
1.2	C_2H_4	208	0	208	87	2.9	1.3	83	194	6.6	2.8	185	0.50	0.042	1.2	0.79
1.2	CH_4	398	0	398	73	17	0.14	56	334	78	0.66	255	1	1	1	1
1.2	C_2H_4	416	0	416	60	0.46	0.91	58	266	2.1	4.1	260	0.82	0.027	6.5	1.0
1.2	CH_4	820	0	820	68	2.0	0.08	66	639	18	0.71	620	1	1	1	1
1.2	C_2H_4	1040	0	1040	56	0.31	0.093	56	629	3.4	1.0	625	0.82	0.16	1.2	0.85
1.4	CH_4	0	0	0	--	--	--	--	42	2.4	6.8	33	1	1	1	1
1.4	C_2H_4	0	0	0	--	--	--	--	38	2.0	2.0	34	0.90	0.83	0.29	1.0
1.4	C_3H_8	0	0	0	--	--	--	--	24	0.94	1.3	22	0.57	0.39	0.19	0.67
1.4	CH_4	199	0	199	94	6.1	0.66	87	211	14	1.5	195	1	1	1	1
1.4	C_2H_4	208	0	208	85	0.49	0.45	84	185	1.1	0.97	183	0.90	0.080	0.68	0.97
1.4	C_3H_8	208	0	208	88	0.46	0.46	87	187	0.99	0.98	185	0.94	0.075	0.70	1.0

(Continued)

Table III-1.15 (Continued)

ϕ	Fuel	Input Fuel N, PPM			Percent of Input FN Out As				Nitrogen Species in Dry Combustion Gas, PPM				Yield Ratio Relative to Methane Fuel			
		NH_3	NO	N_{Total}	TFN	NH_3	HCN	NO	TFN	NH_3	HCN	NO	TFN	NH_3	HCN	NO
1.4	C_2H_4	104	104	208	73	0.56	0.63	71	158	1.2	1.4	155	--	--	--	--
1.4	CH_4	324	0	324	83	2.5	0.51	80	301	9.1	1.9	290	1	1	1	1
1.4	C_2H_4	416	0	416	65	0.22	0.21	64	282	0.94	0.92	280	0.78	0.088	0.41	0.80
1.4	C_3H_8	416	0	416	71	0.72	0.34	70	305	3.1	1.4	300	0.86	0.29	0.67	0.88
1.4	CH_4	170	169	339	206	110	0.66	95	781	418	2.5	360	1	1	1	1
1.4	C_2H_4	208	208	416	63	0.59	0.39	62	274	2.6	1.7	270	0.31	0.0054	0.59	0.65
1.4	C_3H_8	608	0	608	66	0.20	0.17	66	412	1.2	1.1	410	--	--	--	--
1.4	C_2H_4	1040	0	1040	55	0.089	0.088	55	602	0.97	0.96	600	--	--	--	--
1.4	C_2H_4	520	520	1040	60	0.16	0.11	60	653	1.8	1.2	650	--	--	--	--
1.8	CH_4	0	0	0	--	--	--	--	35	2.2	27	5.7	1	1	1	1
1.8	C_3H_8	0	0	0	--	--	--	--	58	1.4	12	45	1.7	0.64	0.44	7.9

III-2. Results from the Jet-Stirred Combustor

In the jet-stirred combustor (JSC) work, five independent variables were investigated. They were fuel species (CH_4, C_2H_4, C_3H_8), equivalence ratio (0.8-1.8), temperature (1800-2000 K), fuel nitrogen species (NH_3 or 1/1 mixture of NH_3 + NO), and fuel nitrogen concentration (0-1000 ppm in reactants). Because of limitations on the time available to this project, a complete set of all combinations of these variables was not run. The conditions that were run are shown in Table III-2.1. These conditions include some that were run to demonstrate consistence with previous work (ref. 4). Those results are discussed in Appendix A. The complete set of results are presented in Table III-2.2.* The results which are of greatest interest to this work, and which will be discussed in this section have been excerpted from this master table and are presented in subsequent tables (a given result may appear in more than one table). These subsequent tables concern the effect of equivalence ratio (ϕ) and fuel type (CH_4, C_2H_4, C_3H_8) on thermal nitrogen fixation at 1900 K (Table III-2.3); the effect of equivalence ratio, temperature, and fuel nitrogen (FN as NH_3) concentration on FN conversion in methane flames (Table III-2.4); the effect of equivalence ratio, FN species (NH_3 or NH_3 + NO), and FN concentration on conversion in methane flames at 1900 K (Table III-2.5); and the effect of equivalence ratio, fuel species (CH_4, C_2H_4, or C_3H_8), and FN (NH_3) concentration on conversion in methane flames at 1900 K (Table III-2.6). In these tables, data extracted from Table III-2.2 has sometimes been rounded off or averaged. This is particularly the case with independent variables such as ϕ, T, or concentration. Such rounding, or grouping, was necessary to render the tables more intelligible. For computational purposes, one may achieve increased accuracy by referring back to Table III-2.2 to ascertain the more exact value.

The results of measurements on thermal nitrogen fixation in CH_4, C_2H_4, and C_3H_8 flames at 1900 K are shown in Table III-2.3. Not all combinations of variables were run and dashes indicate missing data points. In contrast to the multiburner, the JSC does not exhibit large fuel effects in thermal nitrogen fixation. Also in contrast to the multiburner, thermal TFN increases monotonically with ϕ (it had a maximum at $\phi = 1.2$ in the multiburner). These differences could result either from differences in residence times ($\approx$ 3 ms for JSC, $\approx$ 30 ms for MB) or from differences in mixing conditions. This question will be addressed in a subsequent section. It appears as the first question regarding different combustion behavior between the two reactors.

1. Does the larger thermal fixed nitrogen production in the JSC relative to that in the MB stem from the order of magnitude shorter residence time (3 vs. 30 ms) in the JSC or from the strong back-mixing in the JSC relative to the quasi-plug flow in the MB?

While HCN production increases monotonically with ϕ for both CH_4 and C_2H_4 flames, NH_3 production does so for C_2H_4 but not for CH_4 flames. NO production shows a maximum around $\phi = 1.4$ for both fuels.

---

* Starts on page 71 after Table III-2.6.

Table III-2.4 examines the role of temperature in fuel nitrogen (FN) conversion (expressed as percent of FN) in methane flames. The FN was NH_3. The table shows effects of equivalence ratio and FN concentration as well as temperature. In general, TFN conversion increases with ϕ at 1900 K, shows a small maximum at $\phi = 1.2$ at 1800 K, and shows little effect of ϕ at 2000 K. Conversion is not strongly dependent upon temperature. What temperature dependence there is is positive for ϕ less than or equal to 1 and negative for ϕ greater than 1. (As will be shown in the next section, this is consistent with expectations based upon equilibrium considerations.) For all equivalence ratios from 0.8 through 1.4 the major converted species is NO. For $\phi = 1.8$ the major species is HCN. This is true at all temperatures.

Although conversion to TFN appears somewhat higher at the lowest input concentrations, the strength of the concentration effect varies with other conditions. It is never particularly strong, showing a maximum change from 127 to 77 percent going from 208 to 958 ppm input FN at $\phi = 1.2$ and 1800 K.

Some of the conversions shown exceed 100 percent. This can be rationalized through the addition of thermally fixed nitrogen in some, but not all, of the cases. Table III-2.2 also reports percent conversions as "fuel" nitrogen as well as "fuel-plus-thermal" nitrogen. For the results at $\phi = 1.8$ and 1900 K the percentages 145, 116, 139 for TFN (Runs 42, 43, 44) become 80, 84, 121 when converted to "fuel" values. Thus, at an input concentration of 750 ppm the presence of FN as NH_3 has increased the fixation of molecular nitrogen above the purely "thermal" value. This increased fixed nitrogen appears largely as HCN ("fuel" HCN is 108 percent in this case).

These results will be compared with those from the multiburner, and further discussed, in a later section.

Table III-2.5 shows the effect of fuel nitrogen species (NH_3 or NH_3 + NO) on conversion in methane flames at 1900 K. Unlike the MB the JSC shows little effect of replacing NH_3 with NH_3 + NO even at $\phi = 1.4$. For equivalence ratio 1.8, the addition of NO as FN decreases TFN output as contrasted to the increase that it caused in the MB. This decrease results from a decrease in HCN production when NO is added (without any compensating increase in NO production). In the multiburner the addition of NO as FN decreased both NH_3 and HCN production but these decreases were more than compensated by an increase in NO production. These observations pose a second significant question relative to the two combustors:

2. Why do the JSC and MB behave so differently in their response to changing FN species? Does the change result from the large differences in residence times or from the different mixing conditions in the two combustors?

This question will be addressed in a subsequent section.

Table III-2.6 shows the effect of fuel species (CH_4, C_2H_4, C_3H_8) on FN (NH_3) conversion in methane flames at 1900 K. Three FN concentrations were run at each equivalence ratio and concentration effects overlaid on fuel effects and equivalence ratio effects cause the overall picture to be rather complex. These results will be discussed separately for each equivalence ratio.

At equivalence ratios around unity, conversion to TFN appears independent of fuel species (in marked contrast to the MB) at all FN concentrations. However, the distribution of TFN over the three output species shows sensitivity in that with CH_4 as fuel, output NH_3 and HCN are higher relative to NO (at low FN concentrations) than is the case with C_2H_4 or C_3H_8 as fuels. The situation changes at $\phi = 1.4$ where NH_3 and HCN production relative to NO is no longer highest for CH_4 and where HCN production is least with C_2H_4 and greatest with C_3H_8. Conversions to NH_3 and HCN exceed those in the MB while conversions to NO in the MB exceed those in the JSC at this ϕ.

At $\phi = 1.8$ only CH_4 and C_2H_4 were used as fuels. The data viewed over all FN concentrations presents an equivocal picture, but no clear sensitivity of output fixed nitrogen to fuel species is demonstrated except for output NO which is more favored when C_2H_4 rather than CH_4 is the fuel.

The following general observations may be drawn from these data.

17. At 1900 K in the JSC hydrocarbon fuel species does not play an important part in thermal nitrogen fixation either quantitatively or in trend with changing equivalence ratio.

18. At 1900 K thermal TFN produced from methane in the JSC increases monotonically with from 0.8 to 1.8. The change is from 41 to 133 ppm. NO is the dominant species except when $\phi = 1.8$, then HCN is the dominant species.

19. Thermal NO produced at 1900 K maximizes around $\phi = 1.4$ while thermal HCN increases monotonically with ϕ with a large change (15 ppm to 121 ppm) occurring from $\phi = 1.4$ to 1.8 for methane and ethylene. Thermal NH_3 production shows no clear trend in methane flames but increases monotonically with ϕ in ethylene flames. Data are insufficient to establish trends with propane.

20. Conversion of fuel nitrogen (NH_3) to TFN is not temperature sensitive in the range 1800-2000 K. This lack of temperature sensitivity also holds for conversion to NH_3 and NO. Conversion to HCN also demonstrates lack of temperature sensitivity for $\phi \leq 1.2$ but for $\phi = 1.4$ it shows a strong maximum at 1900 K. While NO is the dominant output species for $\phi \leq 1.4$, HCN becomes dominant at $\phi = 1.8$, T = 1900 K (the only temperature run at that equivalence ratio).

21. Conversion of fuel NH_3 to NO shows a maximum at $\phi = 1.2$ with the highest conversions occurring at 1800 K.

22. High ϕ favor conversion of fuel NH_3 to HCN and 1900 K is more favorable to this conversion than are either 1800 or 2000 K. "Fuel" TFN can exceed 100 percent at $\phi = 1.8$ and T = 1900 K for both methane and ethylene (see Table III-2.2).

Table III-2.1

Combinations of Variables Run in Jet-Stirred Combustor Experiments

Report/Table	Fuel	T,K	Equivalence Ratio	Fuel Nitrogen Type and Concentration, PPM		τ, ms
				NH_3, PPM	NO/NH_3	
2/79/I or 4/79/I	CH_4	1916/1915	0.8	0, 1300	0	1.94, 1.94
	CH_4	1994/1983	1.0	0, 1300	0	1.86, 1.87
	CH_4	1956/--	1.1	0, 1300	0	1.97, -
	CH_4	1956/1895	1.1	0, 1300	0	1.87, 1.93
	CH_4	1962/1955	1.1	0, 1213	0	1.86, 1.87
	CH_4	1900/1895	1.2	0, 1300	0	1.89, 1.89
2/79/II or 4/79/II	CH_4	1818/1819	0.8	0, 1303	0	3.08, 3.08
	CH_4	1947/--	0.9	0, 1303	0	2.88, -
	CH_4	1961/1951	1.0	0, 1303	0	2.85, 2.86
	CH_4	1934	1.1	0, 1302	0	2.84, -
	CH_4	1891, 1879	1.2	0, 1300	0	2.85, 2.87
	CH_4	1815	1.4	0, 1289	0	2.85, -
	CH_4	1717	1.41	0, 1302	0	3.03, -
2/79/III or 4/79/III	CH_4	1881-1912	1.0, 1.4, 1.8	0, 111, 210, 400, 750	0, 55/52, 100/100, 200/200	3.39 to 2.63 (range)
1/79/III	CH_4	1695/1706	0.8	0, 1195	0	4.39, 4.36
	CH_4	1901/1901	1.0	0, 1195	0	3.91, 3.91
	CH_4	1988/1992	1.2	0, 1195	0	3.61, 3.60
	CH_4	1717/1709	1.4	0, 1195	0	4.04, 4.06
	CH_4	1695/1691	1.5	0, 1195	0	4.03, 4.04
1/79/IV	CH_4	1881/1891	0.8	0, 1195	0	3.96, 3.94
	CH_4	1976/1985	1.0	0, 1195	0	3.77, 3.75
	CH_4	1977/1946	1.2	0, 1195	0	3.64, 3.70
	CH_4	1935/1930	1.3	0, 1213	0	3.62, 3.63
	CH_4	1855/1849	1.4	0, 1195	0	3.73, 3.75
	CH_4	1840/1825	1.5	0, 1213	0	3.72, 3.75
	CH_4	1777/1772/1778/1691	1.6	0, 1213, 0, 1195	0	3.76, 3.77, 3.76, 3.96

(Continued)

Table III-2.1 (Continued)

Report/Table	Fuel	T,K	Equivalence Ratio	Fuel Nitrogen Type and Concentration, PPM		τ, ms
				NH_3, PPM	NO/NH_3	
10/78/I	CH_4	1813/1899/1998	0.85/0.8/0.8	0	0	2.85, 3.11, 3.31
10/78/II	CH_4	1899/1904/1895/1890/1903/1905	0.8/0.8/0.8/1.2/1.2/1.2	200/400/749/200/400/749	0	3.11, 3.10, 3.12, 3.50, 3.07, 3.14
10/78/III	CH_4	1995/1997/1999/2007/	0.8/0.8/0.83/0.94/	211/421/790/211/	0	3.32, 3.31, 3.34, 3.40
	CH_4	2008/1992/1988/1985/	0.94/0.9/1.2/1.2/	421/790/211/421/	0	3.39, 3.29, 3.40, 3.40
	CH_4	1988/1991/2007/1995	1.21/1.4/1.4/1.4	790/211/421/790	0	3.40, 3.25, 3.22, 3.24
9/78/II	CH_4	1793/1798/1791/	0.85/0.85/0.85/	207/415/827/	0	2.89, 2.88, 2.89
	CH_4	1796/1795/1804/	1.0/1.0/1.0/	208/415/1037/	0	3.63, 3.64, 3.62
	CH_4	1797/1803/1797/	1.2/1.2/1.2/	208/414/958/	0	3.42, 3.41, 3.42
	CH_4	1806/1812/1798	1.4/1.4/1.4	200/393/999/	0	3.82, 3.81, 3.84
1/79/II	C_2H_4	1893/1891/1892/1887/	1.0	0/211/421/811	0	3.39, 3.40, 3.39, 3.40
	C_2H_4	1901/1900/1902/1896/	1.4	0/216/432/811	0	2.76, 2.76, 2.75, 2.76
	C_2H_4	1895/1893/1897/1892	1.8	0/216/432/811	0	2.44, 2.44, 2.44, 2.44
11/78/II	C_3H_8	1894/1894/1905/1905	1.0	0/216/432/811	0	3.39, 3.39, 3.37, 3.37
	C_3H_8	1897/1894/1888/1889	1.4	0/216/432/811	0	2.98, 2.98, 2.99, 2.99

Table III-2.3

Effect of Equivalence Ratio on Fixed Nitrogen Produced in the Jet-Stirred Combustor With Hydrocarbon*/O_2/N_2 Flames at 1900 K Without Fuel Nitrogen

ϕ	TFN in Dry Gas, PPM			NH_3 in Dry Gas, PPM			HCN in Dry Gas, PPM			NO in Dry Gas, PPM			Residence Times, ms		
	CH_4	C_2H_4	C_3H_8	CH_4	C_2H_4	C_3H_8	CH_4	C_2H_4	C_3H_8	CH_4	C_2H_4	C_3H_8	CH_4	C_2H_4	C_3H_8
0.8	41	--	--	1.6	--	--	1.5	--	--	38	--	--	3.1	--	--
1.0	--	52	60	--	1.7	1.2	--	1.4	1.9	--	49	57	--	3.4	3.4
0.97	60	--	--	1.0	--	--	1.0	--	--	58	--	--	3.4	--	--
1.4	80	96	89	3.0	6.2	3.7	15	17	26	62	73	59	2.9	2.8	3.0
1.8	133	117	--	1.4	8.9	--	121	88	--	11	21	--	2.6	2.4	--

* Fuels used (CH_4, C_2H_4, C_3H_8) are subheadings of columns.

Table III-2.4

Effect of Equivalence Ratio, Temperature, and Concentration of Fuel Nitrogen (NH_3) on Conversion of Fuel Nitrogen in $CH_4/O_2/N_2$ Flames in the Jet-Stirred Combustor

ϕ	Input NH_3 PPM	Percent of Fuel Nitrogen as TFN Out			Percent of Fuel Nitrogen as NH_3 Out			Percent of Fuel Nitrogen as HCN Out			Percent of Fuel Nitrogen as NO Out			Residence Time, ms		
		1800 K	1900 K	2000 K	1800 K	1900 K	2000 K	1800 K	1900 K	2000 K	1800 K	1900 K	2000 K	1800 K	1900 K	2000 K
0.8	200		79			0.63			1.0			77			3.1	
	211			100			0.74			0.51			99			3.3
	400		79			0.31			0.17			78			3.1	
	421			85			0.43			0.23			85			3.3
	749		78			0.15			0.089			78			3.1	
	790			82			0.12			0.16			82			3.3
0.85	207	77			0.81			0.16			76			2.9		
	415	72			0.36			0.081			72			2.9		
	827	71			0.19			0.051			71			2.9		
0.92	208	84			0.39			0.20			83			3.6		
	415	86			0.16			0.16			85			3.6		
	1037	73			0.071			0.031			73			3.6		
0.94	211			101			0.50			0.42			100			3.4
	421			80			0.23			0.19			80			3.4
0.90	790			75			0.10			0.11			75			3.3
0.97	210		86			3.1			3.5			80			3.4	
	421		78			1.2			1.2			76			3.4	
	788		75			0.21			0.62			74			3.4	
1.2	200		100			2.1			2.9			95			3.5	
	211			111			0.82			0.55			109			3.4
	208	127			0.64			1.5			125			3.4		
	400		104			1.9			1.6			100			3.1	
	421			95			1.0			0.39			94			3.4
	414	110			1.3			1.0			107			3.4		
	749		75			0.39			0.59			74			3.1	
	790			78			1.4			0.22			76			3.4
	958	77			1.4			0.15			75			3.4		

(Continued)

Table III-2.4 (Continued)

ϕ	Input NH_3 PPM	Percent of Fuel Nitrogen as TFN Out			Percent of Fuel Nitrogen as NH_3 Out			Percent of Fuel Nitrogen as HCN Out			Percent of Fuel Nitrogen as NO Out			Residence Time, ms		
		1800 K	1900 K	2000 K	1800 K	1900 K	2000 K	1800 K	1900 K	2000 K	1800 K	1900 K	2000 K	1800 K	1900 K	2000 K
1.4	200	109	107		1.7	4.9		3.7	29		103	73		3.8	2.9	
	211			113			4.4			7.5			101			3.3
	399		92			4.5			28			60			2.9	
	421			90			3.3			4.8			82			3.2
	393	77			2.6			4.4			70			3.8		
	748		76			2.0			14			60			2.9	
	790			73			1.4			1.2			71			3.2
	999	71			1.3			0.95			69			3.8		
1.8	200		145			4.9			124			16			2.6	
	401		116			9.2			99			8.3			2.6	
	750		139			8.6			124			6.5			2.6	

Table III-2.5

Effect of Equivalence Ratio and Fuel Nitrogen Species (NH_3 or NO + NH_3) on Conversion of Fuel Nitrogen in $CH_4/O_2/N_2$ Flames at 1900 K in the Jet-Stirred Combustor

	Input Fuel N, PPM			Percent of Input FN Out As				τ
ϕ	NH_3	NO	N_{Total}	TFN	NH_3	HCN	NO	ms
0.97	55	52	107	103	0.77	1.5	101	3.4
0.97	210	0	210	86	3.1	3.5	80	3.4
0.97	111	104	215	55	0.76	0.76	53	3.4
0.97	421	0	421	78	1.2	1.2	76	3.4
0.97	207	194	401	80	0.20	0.41	80	3.4
1.4	55	52		139	3.3	40	96	2.9
1.4	200	0	200	107	4.9	29	73	2.9
1.4	111	103	214	109	3.3	29	77	2.9
1.4	399	0	399	92	4.5	28	60	2.9
1.4	207	194	401	81	1.8	23	57	2.9
1.8	55	52	107	111	1.8	86	23	2.6
1.8	200	0	200	145	4.9	124	16	2.6
1.8	110	110	220	119	4.4	100	15	2.6
1.8	401	0	401	116	9.2	99	8.3	2.6
1.8	208	194	402	107	7.0	87	13	2.6

Table III-2.6

Effect of Equivalence Ratio, Concentration, and Fuel Species on Conversion of Fuel Nitrogen in Hydrocarbon/O_2/N_2 Flames at 1900 K

ϕ	Fuel	Input NH_3 PPM	Percent of Input FN Out As				Collected in Dry Exhaust Gas, PPM			
			TFN	NH_3	HCN	NO	TFN	NH_3	HCN	NO
0.97	CH_4	0	--	--	--	--	60	1	1	58
1.0	C_2H_4	0	--	--	--	--	52	1.7	1.4	49
1.0	C_3H_8	0	--	--	--	--	60	1.2	1.9	57
0.97	CH_4	210	86	3.1	3.5	80	221	8	9	204
1.0	C_2H_4	211	101	0.68	0.42	99	238	1.6	1.0	235
1.0	C_3H_8	216	98	0.82	0.45	97	238	2.0	1.1	235
0.97	CH_4	421	78	1.2	1.2	76	402	6	6	390
1.0	C_2H_4	421	89	0.34	0.40	88	419	1.6	1.9	415
1.0	C_3H_8	432	82	0.49	0.25	81	399	2.4	1.2	395
0.97	CH_4	788	75	0.21	0.62	74	723	2.0	6.0	715
1.0	C_2H_4	811	76	0.20	0.12	75	688	1.8	1.1	685
1.0	C_3H_8	811	76	0.19	0.20	76	694	1.7	1.8	690
1.4	CH_4	0	--	--	--	--	80	3	15	62
1.4	C_2H_4	0	--	--	--	--	96	6.2	17	73
1.4	C_3H_8	0	--	--	--	--	89	3.7	26	59
1.4	CH_4	200	107	4.9	29	73	241	11	65	165
1.4	C_2H_4	216	107	4.7	17	85	243	11	39	193
1.4	C_3H_8	216	114	2.0	45	67	255	4.5	100	150
1.4	CH_4	399	92	4.5	28	60	414	20	124	270
1.4	C_2H_4	432	87	3.3	14	70	398	15	63	320
1.4	C_3H_8	432	100	3.6	47	50	446	16	208	222
1.4	CH_4	748	76	2.0	14	60	638	17	116	505
1.4	C_2H_4	811	67	1.9	4.4	60	569	16	38	515
1.4	C_3H_8	811	83	3.2	41	39	699	27	342	330

(Continued)

Table III-2.6 (Continued)

ϕ	Fuel	Input NH_3 PPM	Percent of Input FN Out As				Collected in Dry Exhaust Gas, PPM			
			TFN	NH_3	HCN	NO	TFN	NH_3	HCN	NO
1.8	CH_4	0	--	--	--	--	133	1.4	121	11
1.8	C_2H_4	0	--	--	--	--	117	8.9	88	21
1.8	CH_4	200	145	4.9	124	16	297	10	255	32
1.8	C_2H_4	216	175	11	139	25	362	23	287	52
1.8	CH_4	401	116	9.2	99	8.3	479	38	407	34
1.8	C_2H_4	432	121	8.9	93	19	500	37	384	79
1.8	CH_4	750	139	8.6	124	6.5	1069	66	953	50
1.8	C_2H_4	811	89	7.3	69	12	688	57	535	96

23. Under conditions of highest conversion to HCN (ϕ = 1.8) fixation of N_2 as HCN occurs over and above the purely "thermal" value (Table III-2.2).

24. At all conditions almost all fuel NH_3 is converted to other nitrogenous species.

25. Percentage conversion of fuel NH_3 to TFN has a weak inverse relationship to input NH_3 concentration.

26. Conversion of fuel nitrogen to TFN output is largely insensitive to the substitution of some fuel NO for fuel NH_3.

27. Conversion of FN to NH_3 or HCN shows a slight decrease as some fuel NO is substituted for fuel NH_3. Conversion to NO is insensitive to this substitution.

28. With fuel NH_3, conversion to TFN is independent of fuel species while conversion to NO shows a slight fuel sensitivity at the higher ($\geq$ 1.4) equivalence ratios.

29. An effect of fuel species on conversion of fuel NH_3 to HCN is evident. For ϕ around 1.0 methane is more favorable to conversion to HCN than are ethylene or propane. For ϕ = 1.4 conversion to HCN is favored in the order $C_3H_8 > CH_4 > C_2H_4$. At ϕ = 1.8 conversion is about equal with CH_4 and C_2H_4 (with an apparent exception for the highest--811 ppm--input concentration).

Table III-2.2

Results from All Experiments Run in the Jet-Stirred Combustor

Run No.	Fuel	T K	Set φ	Computed φ	τ ms	Additives, VPPM		Collected, VPPM in Dry Gas				Collected, Percent of N Added				Collected, Percent of N Added				Collected in Dry Exhaust Gas				
						NH_3	NO	NH_3	HCN	$NO(NO_x)$	TFN	NH_3	HCN	$NO(NO_x)$	TFN	Fuel NH_3	Fuel HCN	Fuel NO	Fuel TFN	CO_2 %	CO %	O_2 %	H_2 %	HC VPPM
1	CH_4	1916	0.8	0.800	1.9	0	0	------	-----	20(28)	----	-----	------	-------	---	------	------	----	----	7.9	0.6	5.7	0.13	14
2	CH_4	1915	0.8	0.800	1.9	1300	0	------	-----	1060(1160)	----	-----	------	69(75)	---	------	------	----	----	8.1	0.6	5.4	0.47	15
3	CH_4	1994	1.0	1.00	1.9	0	0	------	-----	60(64)	----	-----	------	-------	---	------	------	----	----	7.4	4.1	2.4	2.0	10
4	CH_4	1983	1.0	1.00	1.9	1300	0	------	-----	950(975)	----	-----	------	60(61)	---	------	------	----	----	7.3	4.0	2.4	2.1	13
5	CH_4	1956	1.1	1.10	1.9	0	0	------	-----	58(61)	----	-----	------	-------	---	------	------	----	----	7.1	4.6	2.3	2.4	26
6	CH_4	----	1.1	1.10	---	1300	0	------	-----	--(950)	----	-----	------	-------	---	------	------	----	----	6.7	4.8	2.3	2.5	------
7	CH_4	1956	1.1	1.10	1.9	0	0	------	-----	54(56)	----	-----	------	-------	---	------	------	----	----	7.0	4.6	2.3	----	26
8	CH_4	1895	1.1	1.10	1.9	1300	0	------	-----	900(910)	----	-----	------	57(58)	---	------	------	----	----	7.4	5.0	2.3	2.5	38
9	CH_4	1962	1.1	1.10	1.9	0	0	------	-----	54(56)	----	-----	------	-------	---	------	------	----	----	7.2	4.9	2.1	2.9	23
10	CH_4	1955	1.1	1.10	1.9	1213	0	------	-----	795(810)	----	-----	------	54(55)	---	------	------	----	----	7.2	4.8	2.0	1.4	6
11	CH_4	1900	1.2	1.20	1.9	0	0	------	-----	53(69)	----	-----	------	-------	---	------	------	----	----	5.4	6.1	2.8	3.6	13
12	CH_4	1895	1.2	1.20	1.9	1300	0	------	-----	740(800)	----	-----	------	54(58)	---	------	------	----	----	5.7	6.0	2.7	3.7	130
13	CH_4	1818	0.8	0.805	3.1	0	0	------	-----	18(27)	----	-----	------	-------	---	------	------	----	----	7.9	0.55	5.6	0.1	9.0
14	CH_4	1819	0.8	0.805	3.1	1303	0	------	-----	1000(1150)	----	-----	------	65(75)	---	------	------	----	----	7.8	0.56	5.4	0.1	11
15	CH_4	1947	0.9	0.915	2.9	0	0	------	-----	41(51)	----	-----	------	-------	---	------	------	----	----	8.4	1.3	3.8	0.4	20
16	CH_4	----	0.9	0.916	---	1303	0	------	-----	960(1000)	----	-----	------	61(64)	---	------	------	----	----	----	------	----	----	------
17	CH_4	1961	1.0	1.01	2.9	0	0	------	-----	60(81)	----	-----	------	-------	---	------	------	----	----	8.0	2.2	3.1	0.78	9.5
18	CH_4	1951	1.0	1.01	2.9	1303	0	------	-----	125(1175)	----	-----	------	7.8(74)	---	------	------	----	----	8.0	2.5	3.0	0.83	10
19	CH_4	1934	1.1	1.11	2.8	0	0	------	-----	57(61)	----	-----	------	-------	---	------	------	----	----	7.8	3.3	2.7	1.4	29
20	CH_4	----	1.1	1.11	---	1302	0	------	-----	900(980)	----	-----	------	57(62)	---	------	------	----	----	----	------	----	----	------
21	CH_4	1891	1.2	1.21	2.9	0	0	------	-----	66(71)	----	-----	------	-------	---	------	------	----	----	6.7	5.0	2.6	2.7	14
22	CH_4	1879	1.2	1.21	2.9	1300	0	------	-----	840(845)	----	-----	------	55(55)	---	------	------	----	----	----	------	----	----	------
23	CH_4	1815	1.4	1.40	2.9	0	0	------	-----	50(54)	----	-----	------	-------	---	------	------	----	----	5.5	6.6	2.6	4.0	575
24	CH_4	----	1.4	1.40	---	1289	0	------	-----	610(610)	----	-----	------	42(42)	---	------	------	----	----	----	------	----	----	------
25	CH_4	1717	1.414	1.42	3.0	0	0	------	-----	4(32)	----	-----	------	-------	---	------	------	----	----	3.1	5.3	7.6	3.3	28
26	CH_4	----	1.414	1.42	---	1302	0	------	-----	60(180)	----	-----	------	4.1(12)	---	------	------	----	----	----	------	----	----	------
27	CH_4	1893	1.0	0.971	3.4	0	0	1	1	58	60	-----	------	-------	---	------	------	----	----	9.2	3.0	1.6	1.4	5

(Continued)

Table III-2.2 (Continued)

Run No.	Fuel	T K	Set ϕ	Computed ϕ	τ ms	Additives, VPPM		Collected, VPPM in Dry Gas				Collected, Percent of N Added				Collected, Percent of N Added				Collected in Dry Exhaust Gas				
						NH_3	NO	NH_3	HCN	$NO(NO_x)$	TFN	NH_3	HCN	$NO(NO_x)$	TFN	Fuel NH_3	Fuel HCN	Fuel NO	Fuel TFN	CO_2 %	CO %	O_2 %	H_2 %	HC VPPM
28	CH_4	1904	1.0	0.971	3.4	210	0	8	9	204	221	3.1	3.5	80	86	2.7	3.1	57	63	9.3	2.0	2.6	0.7	18
29	CH_4	1907	1.0	0.971	3.4	421	0	6	6	390	402	1.2	1.2	76	78	0.97	0.97	65	67	9.4	1.9	2.7	0.6	15
30	CH_4	1906	1.0	0.971	3.4	788	0	2	6	715	723	0.21	0.62	74	75	0.10	0.52	68	69	9.2	2.1	2.6	0.8	10
31	CH_4	1903	1.0	0.971	3.4	55	52	1	2	132	135	0.77	1.5	101	103	0	0.77	57	57	8.6	2.2	3.3	0.9	10
32	CH_4	1912	1.0	0.971	3.4	111	104	2	2	140	144	0.76	0.76	53	55	0.38	0.38	31	32	8.7	1.9	3.0	0.8	10
33	CH_4	1908	1.0	0.971	3.4	207	194	1	2	390	393	0.20	0.41	80	80	0	0.20	68	68	8.7	1.8	3.6	0.7	13
34	CH_4	1898	1.4	1.40	2.9	0	0	3	15	62	80	-----	------	-------	---	------	------	----	----	6.6	9.5	1.2	5.0	1000
35	CH_4	1888	1.4	1.40	2.9	200	0	11	65	165	241	4.9	29	73	107	3.6	22	46	72	6.4	9.3	1.1	5.1	1500
36	CH_4	1890	1.4	1.40	2.9	399	0	20	124	270	414	4.5	28	60	92	3.8	24	46	74	6.4	8.8	1.6	4.9	1250
37	CH_4	1888	1.4	1.40	2.9	748	0	17	116	505	638	2.0	14	60	76	1.7	12	53	66	6.2	9.0	1.0	5.0	400
38	CH_4	1889	1.4	1.40	2.9	55	52	4	48	115	167	3.3	40	96	139	0.83	27	44	72	6.0	8.8	2.1	5.2	1500
39	CH_4	1881	1.4	1.40	2.9	111	103	8	69	185	262	3.3	29	77	109	2.1	22	51	76	6.2	8.7	1.7	5.1	1250
40	CH_4	1887	1.4	1.40	2.9	207	194	8	103	255	366	1.8	23	57	81	1.1	22	43	63	5.5	9.4	2.1	5.5	1200
41	CH_4	1892	1.8	1.81	2.6	0	0	1.4	121	11	133	-----	------	-------	---	------	------	----	----	4.5	>10	1.4	8.2	30K
42	CH_4	1895	1.8	1.81	2.6	200	0	10	255	32	297	4.9	124	16	145	4.2	65	10	80	4.4	>10	2.1	8.4	30K
43	CH_4	1892	1.8	1.81	2.6	401	0	38	407	34	479	9.2	99	8.3	116	8.9	69	5.6	84	4.3	>10	1.9	8.4	25K
44	CH_4	1899	1.8	1.81	2.6	750	0	66	953	50	1069	8.6	124	6.5	139	8.4	108	5.1	121	4.5	>10	1.7	8.6	20K
45	CH_4	1888	1.8	1.81	2.6	55	52	2	95	25	122	1.8	86	23	111	0.55	-24	13	-15	4.2	>10	2.3	8.9	31K
46	CH_4	1889	1.8	1.81	2.6	110	110	10	226	34	270	4.4	100	15	119	3.8	46	10	61	4.2	>10	2.2	8.8	23K
47	CH_4	1890	1.8	1.81	2.6	208	194	29	358	54	441	7.0	87	13	107	6.7	57	10	75	4.2	>10	2.4	8.8	24K
48	CH_4	1695	0.8	0.801	4.4	0	0	------	-----	14	----	-----	-----	-------	---	------	------	----	----	7.6	0.3	7.0	0.059	9.0
49	CH_4	1706	0.8	0.801	4.4	1195	0	------	-----	850	----	-----	-----	60	---	------	------	59	----	7.6	0.3	7.0	0.065	9.5
50	CH_4	1901	1.0	0.999	3.9	0	0	------	-----	64	----	-----	-----	-------	---	------	------	----	----	8.3	1.6	4.0	0.56	8.5
51	CH_4	1901	1.0	0.999	3.9	1195	0	------	-----	1025	----	-----	-----	70	---	------	------	65	----	8.2	1.7	4.0	0.57	10
52	CH_4	1988	1.2	1.20	3.6	0	0	------	-----	60	----	-----	-----	-------	---	------	------	----	----	6.7	5.4	2.6	3.1	7.5
53	CH_4	1992	1.2	1.20	3.6	1195	0	25	4.2	795	824	1.8	0.30	56	58	------	------	52	----	6.7	5.2	2.6	2.9	9.0
54	CH_4	1717	1.4	1.39	4.0	0	0	------	-----	28	----	-----	-----	-------	---	------	------	----	----	4.3	7.4	3.7	4.6	800

(Continued)

Table III-2.2 (Continued)

Run No.	Fuel	T K	Set ϕ	Computed ϕ	τ ms	Additives, VPPM		Collected, VPPM in Dry Gas				Collected, Percent of N Added				Collected, Percent of N Added				Collected in Dry Exhaust Gas				
						NH_3	NO	NH_3	HCN	$NO(NO_x)$	TFN	NH_3	HCN	$NO(NO_x)$	TFN	Fuel NH_3	Fuel HCN	Fuel NO	Fuel TFN	CO_2 %	CO %	O_2 %	H_2 %	HC VPPM
55	CH_4	1709	1.4	1.39	4.1	1195	0	12	286	310	608	0.88	21	23	45	------	------	21	----	3.8	7.0	4.7	4.5	1325
56	CH_4	1695	1.5	1.50	4.0	0	0	------	-----	2.3	---	-----	------	-------	---	------	------	----	----	2.0	4.5	11	3.0	1450
57	CH_4	1691	1.5	1.50	4.0	1195	0	52	576	110	738	3.97	44	8.4	56	------	------	8.2	----	1.8	4.3	11	3.0	2030
58	CH_4	1881	0.8	0.787	4.0	0	0	------	-----	41	---	-----	------	-------	---	------	------	----	----	7.0	0.35	8.6	0.08	18
59	CH_4	1891	0.8	0.787	3.9	1195	0	------	-----	860	---	-----	------	61	---	------	------	58	----	6.8	0.35	8.1	0.08	18
60	CH_4	1976	1.0	0.984	3.8	0	0	------	-----	72	---	-----	------	-------	---	------	------	----	----	7.4	0.70	7.1	0.14	11
61	CH_4	1985	1.0	0.984	3.8	1195	0	------	-----	900	---	-----	------	61	---	------	------	57	----	7.4	0.70	6.9	0.14	16
62	CH_4	1977	1.2	1.19	3.6	0	0	------	-----	84	---	-----	------	-------	---	------	------	----	----	5.6	4.7	5.3	2.6	12
63	CH_4	1946	1.2	1.19	3.7	1195	0	0.6	62	780	843	0.042	4.4	55	59	------	------	49	----	5.6	4.8	5.3	2.6	14
64	CH_4	1935	1.3	1.31	3.6	0	0	------	-----	87	---	-----	------	-------	---	------	------	----	----	4.1	6.2	1.2	3.6	12
65	CH_4	1930	1.3	1.31	3.6	1213	0	13	45	860	918	0.93	3.2	61	66	------	------	55	----	3.9	6.2	1.2	3.7	14
66	CH_4	1855	1.4	1.40	3.7	0	0	------	-----	59	---	-----	------	-------	---	------	------	----	----	4.0	7.2	5.2	4.6	36
67	CH_4	1849	1.4	1.40	3.8	1195	0	9.5	103	510	623	0.70	7.6	38	46	------	------	33	----	4.0	6.9	5.1	4.5	42
68	CH_4	1840	1.5	1.49	3.7	0	0	------	-----	67	---	-----	------	-------	---	------	------	----	----	3.1	9.1	1.2	5.7	14
69	CH_4	1825	1.5	1.49	3.8	1213	0	318	255	470	1043	24	19	35	78	------	------	30	----	2.9	8.8	1.3	5.7	9
70	CH_4	1777	1.6	1.62	3.8	0	0	------	-----	19	---	-----	------	-------	---	------	------	----	----	2.4	9.9	1.7	6.4	9
71	CH_4	1772	1.6	1.62	3.8	1213	0	------	-----	175	---	-----	------	14	---	------	------	12	----	2.4	9.7	1.6	6.4	12
72	CH_4	1778	1.6	1.62	3.8	0	0	------	-----	11	---	-----	------	-------	---	------	------	----	----	2.9	8.1	5.0	5.4	3800
73	CH_4	1691	1.6	1.62	4.0	1195	0	33	2626	115	---	2.6	206	9.0	---	------	------	----	----	2.9	8.0	5.1	5.4	5250
74	CH_4	1813	0.85	0.849	2.9	0	0	1.6	0.5	45	47	-----	------	-------	---	------	------	----	----	9.6	0.95	2.9	0.29	5
75	CH_4	1899	0.8	0.801	3.1	0	0	1.6	1.5	38	41	-----	------	-------	---	------	------	----	----	10	0.78	4.9	0.14	10
76	CH_4	1998	0.8	0.799	3.3	0	0	3.6	2.3	82	88	-----	------	-------	---	------	------	----	----	10	0.9	5.4	0.15	25
77	CH_4	1899	0.8	0.801	3.1	200	0	1.5	2.4	185	189	0.63	1.0	77	79	-0.042	0.38	61	62	9.6	0.7	5.4	0.11	15
78	CH_4	1904	0.8	0.801	3.1	400	0	1.5	0.8	375	377	0.31	0.17	78	79	-0.021	-0.15	70	70	9.8	0.7	5.3	0.11	10
79	CH_4	1895	0.8	0.801	3.1	749	0	1.3	0.8	700	702	0.15	0.089	78	78	-0.033	-0.078	74	74	9.7	0.7	5.0	0.11	13
80	CH_4	1890	1.2	1.20	3.5	200	0	5.0	6.8	225	237	2.1	2.9	95	100	------	------	----	----	7.9	5.6	1.1	3.1	40

(Continued)

Table III-2.2 (Continued)

Run No.	Fuel	T K	Set ϕ	Computed ϕ	τ ms	Additives, VPPM NH_3	Additives, VPPM NO	Collected, VPPM in Dry Gas NH_3	Collected, VPPM in Dry Gas HCN	Collected, VPPM in Dry Gas $NO(NO_x)$	Collected, VPPM in Dry Gas TFN	Collected, Percent of N Added NH_3	Collected, Percent of N Added HCN	Collected, Percent of N Added $NO(NO_x)$	Collected, Percent of N Added TFN	Collected, Percent of N Added Fuel NH_3	Collected, Percent of N Added Fuel HCN	Collected, Percent of N Added Fuel NO	Collected, Percent of N Added Fuel TFN	Collected in Dry Exhaust Gas CO_2 %	Collected in Dry Exhaust Gas CO %	Collected in Dry Exhaust Gas O_2 %	Collected in Dry Exhaust Gas H_2 %	Collected in Dry Exhaust Gas HC VPPM
81	CH_4	1903	1.2	1.20	3.1	400	0	8.9	7.7	475	492	1.9	1.6	100	104	------	------	----	----	8.1	5.1	1.1	2.8	30
82	CH_4	1905	1.2	1.19	3.1	749	0	3.5	5.3	665	674	0.39	0.59	74	75	------	------	----	----	7.9	5.4	1.0	3.0	25
83	CH_4	1995	0.8	0.799	3.3	211	0	1.9	1.3	255	258	0.74	0.51	99	100	-0.66	-0.39	67	66	10	0.72	6.1	0.1	10
84	CH_4	1997	0.8	0.799	3.3	421	0	2.2	1.2	435	438	0.43	0.23	85	85	-0.27	-0.21	69	68	10	0.70	6.2	0.18	13
85	CH_4	1999	0.83	0.830	3.3	790	0	1.2	1.5	790	793	0.12	0.16	82	82	-0.25	-0.083	73	73	11	0.95	4.8	0.16	20
86	CH_4	2007	0.94	0.939	3.4	211	0	1.3	1.1	260	262	0.50	0.42	100	101	------	------	----	----	10	1.5	3.6	0.4	10
87	CH_4	2008	0.94	0.939	3.4	421	0	1.2	1.0	415	417	0.23	0.19	80	80	------	------	----	----	8.7	1.4	5.4	0.4	13
88	CH_4	1992	0.9	0.902	3.3	790	0	1.0	1.1	720	722	0.10	0.11	75	75	------	------	----	----	9.7	1.2	4.3	0.3	12
89	CH_4	1988	1.2	1.19	3.4	211	0	2.1	1.4	280	284	0.82	0.55	109	111	------	------	86	----	8.7	5.7	2.0	3.2	8
90	CH_4	1985	1.2	1.19	3.4	421	0	5.1	2.0	480	487	1.0	0.39	94	95	------	------	82	----	8.8	5.8	1.9	3.2	13
91	CH_4	1988	1.2	1.19	3.4	790	0	13	2.1	730	745	1.4	0.22	76	78	------	------	70	----	8.2	5.8	1.8	3.1	30
92	CH_4	1991	1.4	1.40	3.3	211	0	11	19	250	279	4.4	7.5	101	113	------	------	----	----	6.6	10+	2.0	6.1	1000
93	CH_4	2007	1.4	1.40	3.2	421	0	16	24	405	445	3.3	4.8	82	90	------	------	----	----	6.7	10+	2.1	6.0	1000
94	CH_4	1995	1.4	1.40	3.2	790	0	13	12	655	679	1.4	1.2	71	73	------	------	----	----	6.7	10+	2.1	5.9	40
95	CH_4	1793	0.85	0.849	2.9	207	0	2.0	0.4	188	190	0.81	0.16	76	77	0.16	-0.040	58	58	9.2	1.0	3.5	0.25	10
96	CH_4	1798	0.85	0.849	2.9	415	0	1.8	0.4	355	357	0.36	0.081	72	72	0.040	-0.020	63	63	9.4	1.1	3.5	0.28	11
97	CH_4	1791	0.85	0.849	2.9	827	0	1.9	0.5	700	702	0.19	0.051	71	71	0.030	0.000	66	66	9.2	1.0	3.4	0.25	15
98	CH_4	1796	1.0	0.922	3.6	208	0	1.0	0.5	212	214	0.39	0.20	83	84	------	------	----	----	9.5	1.7	3.4	0.55	9
99	CH_4	1795	1.0	0.922	3.6	415	0	0.8	0.8	435	437	0.16	0.16	85	86	------	------	----	----	9.5	1.7	1.7	0.91	10
100	CH_4	1804	1.0	0.922	3.6	1037	0	0.9	0.4	925	926	0.071	0.031	73	73	------	------	----	----	9.5	1.7	2.2	0.54	12
101	CH_4	1797	1.2	1.20	3.4	208	0	1.6	3.6	310	315	0.64	1.5	125	127	------	------	----	----	8.1	5.6	1.2	3.2	20
102	CH_4	1803	1.2	1.20	3.4	414	0	6.6	5.1	530	542	1.3	1.0	107	110	------	------	----	----	8.2	5.4	1.3	3.1	15
103	CH_4	1797	1.2	1.20	3.4	958	0	16	1.7	860	878	1.4	0.15	75	77	------	------	----	----	8.3	5.8	1.3	2.5	15
104	CH_4	1806	1.4	1.40	3.8	200	0	3.9	8.6	240	253	1.7	3.7	103	109	------	------	----	----	7.5	9.8	1.1	5.2	125
105	CH_4	1812	1.4	1.40	3.8	393	0	12	20	320	352	2.6	4.4	70	77	------	------	----	----	7.6	9.3	1.3	4.9	60
106	CH_4	1798	1.4	1.40	3.8	999	0	15	11	800	826	1.3	0.95	69	71	------	------	----	----	6.9	>10	1.2	5.6	25

(Continued)

Table III-2.2 (Continued)

Run No.	Fuel	T K	Set ϕ	Computed ϕ	τ ms	Additives, VPPM		Collected, VPPM in Dry Gas				Collected, Percent of N Added				Collected, Percent of N Added				Collected in Dry Exhaust Gas				
						NH_3	NO	NH_3	HCN	NO(NO_x)	TFN	NH_3	HCN	NO(NO_x)	TFN	Fuel NH_3	Fuel HCN	Fuel NO	Fuel TFN	CO_2 %	CO %	O_2 %	H_2 %	HC VPPM
107	C_2H_4	1893	1.0	0.998	3.4	0	0	1.7	1.4	49	52	-----	-----	-------	---	------	------	----	----	9.4	2.8	2.8	0.6	15
108	C_2H_4	1891	1.0	0.998	3.4	211	0	1.6	1.0	235	238	0.68	0.42	99	101	-0.042	-0.17	79	79	9.5	2.2	2.9	0.4	10
109	C_2H_4	1892	1.0	0.998	3.4	421	0	1.6	1.9	415	419	0.34	0.40	88	89	-0.021	0.11	78	78	9.7	2.2	2.7	0.4	13
110	C_2H_4	1887	1.0	0.998	3.4	811	0	1.8	1.1	685	688	0.20	0.12	75	76	0.011	-0.034	70	70	9.3	2.4	2.6	0.4	13
111	C_2H_4	1901	1.4	1.40	2.8	0	0	6.2	17	73	96	-----	-----	-------	---	------	------	----	----	5.7	>10	2.2	3.7	625
112	C_2H_4	1900	1.4	1.40	2.8	216	0	11	39	193	243	4.7	17	85	107	2.0	9.7	53	65	5.8	>10	2.1	3.6	500
113	C_2H_4	1902	1.4	1.40	2.8	432	0	15	63	320	398	3.3	14	70	87	2.0	10	54	66	5.9	>10	2.2	3.5	250
114	C_2H_4	1896	1.4	1.40	2.8	811	0	16	38	515	569	1.9	4.4	60	67	1.2	2.5	52	55	5.9	>10	2.0	3.5	70
115	C_2H_4	1895	1.8	1.80	2.4	0	0	8.9	88	21	117	-----	-----	-------	---	------	------	----	----	3.9	10+	2.0	6.4	15000
116	C_2H_4	1893	1.8	1.80	2.4	216	0	23	287	52	362	11	139	25	175	6.8	96	15	118	3.8	10+	2.2	6.0	11000
117	C_2H_4	1897	1.8	1.80	2.4	432	0	37	384	79	500	8.9	93	19	121	6.8	72	14	93	3.8	10+	2.3	6.0	10000
118	C_2H_4	1892	1.8	1.80	2.4	811	0	57	535	96	688	7.3	69	12	89	6.2	58	9.7	74	3.7	10+	2.3	6.0	8800
119	C_3H_8	1894	1.0	1.00	3.4	0	0	1.2	1.9	57	60	-----	-----	-------	---	------	------	----	----	9.4	3.7	2.4	1.2	4
120	C_3H_8	1894	1.0	1.00	3.4	216	0	2.0	1.1	235	238	0.82	0.45	97	98	0.33	-0.33	73	73	9.5	3.5	2.6	1.1	10
121	C_3H_8	1905	1.0	1.00	3.4	432	0	2.4	1.2	395	399	0.49	0.25	81	82	0.25	-0.14	70	70	9.5	3.4	2.6	1.0	10
122	C_3H_8	1905	1.0	1.00	3.4	811	0	1.7	1.8	690	694	0.19	0.20	76	76	0.055	-0.011	69	69	9.8	3.2	2.7	0.9	12
123	C_3H_8	1897	1.4	1.39	3.0	0	0	3.7	26	59	89	-----	-----	-------	---	------	------	----	----	6.3	>10	2.5	5.1	2000
124	C_3H_8	1894	1.4	1.39	3.0	216	0	4.5	100	150	255	2.0	45	67	114	0.36	33	41	74	6.3	>10	2.4	5,1	2500
125	C_3H_8	1888	1.4	1.39	3.0	432	0	16	208	222	446	3.6	47	50	100	2.8	41	37	80	6.0	>10	2.5	5.2	2500
126	C_3H_8	1889	1.4	1.39	3.0	811	0	27	342	330	699	3.2	41	39	83	2.8	38	32	73	5.7	>10	2.4	5.2	2500

III-3. Comparison of Results Obtained in the Multiburner and the Jet-Stirred Combustor

A comparison of results obtained with the MB and the JSC under similar stoichiometric and thermal conditions will be instructive regarding the mechanism of fuel nitrogen conversion. Combustion conditions in these two reactors differ fundamentally. In the MB premixed reactants pass from a cool porous stainless steel plate through an adjacent laminar flat flame. This flame is thin, certainly not more than 1 mm thick. From the flame they pass in laminar flow up the reaction tube to exit as fully developed Poiseuille flow at a Reynold's number of the order of 100. In these experiments the gases were sampled 2 cm above the burner (flame front) face. The residence time from the burner face to the sampling point was approximately 30 ms. Considering that the flame front itself was less than 1 mm thick, the residence time through the flame front was somewhat less than 1.5 ms. The predominant flame reactions occurred on time scales of this order of magnitude. Because of lower reaction rates much of the important nitrogen conversion occurs over a much longer time scale. While important nitrogen mechanisms are initiated in the thin flame front, important conversions occur during post flame reactions on time scales of the order of 100 ms. Thus, as an element of reactant gas exits from the porous plate and passes through the flame front it is gradually warmed and reacted (preflame reactions → intermediate flame reactions → final flame reactions) to final major combustion products on a time scale of the order of 1 ms. Following this combustion process important post flame reactions involving nitrogenous species continue for times of the order of 100 ms.

In the JSC the situation is quite different. Conditions within the hemispherical reactor are highly turbulent and mixing times are short. The premixed reactants are injected as 0.5 mm dia. sonic jets. Such jets can be expected to be largely mixed with their surroundings in approximately 20 jet diameters (1 cm). Sonic velocity (cold jets) is the order of 34000 cm/s. Thus, jet mixing time is of the order of 30 μs. This is of the order of one one hundredth of the time of passage through the laminar flame front in the multiburner. This time scale is short relative to those of many important combustion reactions. As a result, even early combustion reactions occur in the presence of relatively high concentrations of intermediate and final combustion products. Also, although the average residence time in the reactor is approximately 3 ms, there is a broad distribution of residence times for individual fluid elements around this mean value. Thus, even very late reaction products are available to participate in what in the MB were preflame reactions.

An expected consequence of these differences is that for given thermal conditions and atomic ratios, products from the JSC will be less sensitive to reactant molecular structure than will those from the MB. The reasoning is that in the MB, radicals formed during early preflame reactions carry the identity of their parent molecules as they initiate various reaction paths. In the JSC the large pool of late reaction intermediates should predominate in establishing the overall reaction paths and they carry little of the identity of their parent molecular species.

Against these background considerations, the results obtained with the two combustors will now be compared.

Table III-3.1 presents comparative results on thermal nitrogen fixation in the MB and JSC for three fuels at 1900 K. Considering first CH_4 flames, two striking differences are seen in TFN. The first is that the JSC is a more prolific fixer of nitrogen from N_2 than is the MB. The second is that while nitrogen fixation from N_2 is relatively insensitive to equivalence ratio (ϕ) in the MB (rather flat from $\phi = 1$ to 1.4 with perhaps a slight decrease from 1.4 to 1.8), it increases monotonically (and strongly) with in the JSC. This behavior of the JSC over a wider range of ϕ is seen in Table III-2.3 and that of the MB is seen in Table III-1.7 (where the MB appears to have a maximum in TFN at $\phi = 1.2$). Returning to Table III-3.1, it is seen that the behavior of TFN in the MB is dominated by a maximum in NO production at $\phi = 1.4$ which is not compensated by changes in NH_3 or HCN production (this is seen even more clearly in Table III-1.7 where the maximum TFN at $\phi = 1.2$ is a combination of high NO and HCN production at that equivalence ratio). Conversely, while trends in NO production with changing ϕ in the JSC parallel those in the MB they are overriden by strongly increasing HCN production above $\phi = 1.0$. In neither combustor is NH_3 ever the dominant species. However, it is more prolifically produced in the MB than in the JSC at low (0.8, 1.0) equivalence ratios.

The following differences in thermal nitrogen fixation exist between the two combustors with CH_4 at 1900 K:

30. JSC produces more TFN and NO than the MB. At $\phi > 1.0$ it also produces more HCN.

31. Trend of TFN production with ϕ is relatively flat in MB and dominated by NO. In the JSC it steadily increases with ϕ and is influenced by both NO and HCN production.

32. MB produces more NH_3 at low equivalence ratios than does JSC.

Returning to Table III-3.1 it is seen that TFN production is relatively insensitive to fuel type in the JSC but that it is sensitive in the MB (decreasing with increasing carbon number at $\phi = 1.0$, 1.4 and increasing at $\phi = 1.8$). In the JSC individual N-species show little sensitivity to fuel species except at $\phi = 1.8$ where NO and NH_3 increase and HCN decreases with carbon number. In the MB all three species decrease with carbon number at $\phi = 1.0$, 1.4 while NH_3 and HCN decrease and NO increases with carbon number at $\phi = 1.8$. Thus, it is observed that:

33. TFN and individual N-species show much less sensitivity to fuel species in the JSC than in the MB except at $\phi = 1.8$ where their trends (except for NH_3) are similar. (At $\phi = 1.4$ and above large quantities of unburned hydrocarbons appeared in each combustor. These fragments undoubtedly carried substantial identification of their parent molecules with them and under these conditions one might expect JSC performance to start to resemble MB performance.)

34. For all fuels tested the JSC produces more thermal TFN and NO than does the MB.

Now consider the situation when fuel nitrogen is added as NH_3. The data are shown in Table III-3.2. The independent variables are equivalence ratio, fuel ammonia concentration in reactants, combustion temperature, and combustor used. For each set of independent variables the results are presented as a column of three numbers. They are percent of input fuel nitrogen converted to the given species, ppm of the species detected in the dry combustion products, and ratio of species output concentration to the equilibrium value (sometimes dashes are shown for the third value where equilibrium numbers were not available--the equilibrium values were less than 1 x 10^{-3} ppm in those cases).

One observation can be made immediately. Equivalence ratio $\phi = 1.0$ separates the region where TFN and NO are present in subequilibrium amounts ($\phi<1.0$) from that where they are present in superequilibrium amounts ($\phi>1.0$). Ammonia and HCN are always present in greater than equilibrium quantities. The ratio to equilibrium tends to decrease with increasing ϕ for both NH_3 and HCN, but this trend is subject to fluctuations above $\phi = 1.0$.

Below $\phi = 1.0$ increasing temperature increases conversion of fuel nitrogen (FN) to TFN and NO for both combustors (and by implication decreases conversion to N_2) although it decreases the ratio to the equilibrium value in the MB and leaves it about the same in the JSC (the MB point at $\phi = 0.8$, T = 1900 K and input = 400 ppm appears to be an error). In this region the effect of T upon NH_3 and HCN is unclear.

Above $\phi = 1.0$, increasing T increases conversion to NO for the MB as it decreases its ratio to equilibrium for $\phi = 1.0$, 1.2 and raises that ratio for greater ϕ's. It also increases conversion to TFN for the multiburner at $\phi = 1.2$, barely affects it at 1.4 and decreases it for $\phi = 1.8$ (it decreases ratio of TFN to equilibrium at all ϕ save one case at 1.2). For $\phi \geq 1.0$, conversion to NH_3 in the MB increases with T (except for one point at $\phi = 1.4$, T = 1900, C = 1000 ppm which may be an error). For $\phi \geq 1.0$, conversion to HCN is inversely related to T (and strongly so for $\phi>1.0$) in the MB. The situation differs for the JSC. Temperature data for the JSC are not directly comparable around $\phi = 1.0$ because data were not taken at the same equivalence ratios. For $\phi = 1.2$ and 1.4, increasing T has no clear effect upon conversion to NO in the JSC (if anything conversion is slightly less at 1900 than at 1800 or 2000 K). However, increasing T strongly decreases the ratio to equilibrium at these conditions (in marked contrast to the MB at $\phi = 1.4$). Similar remarks (except for the possible minimum at T = 1900 K) hold for TFN in the JSC. The effect of T upon conversion to ammonia is unclear for $\phi = 1.2$, 1.4 in the JSC. However, for $\phi = 1.2$, 1.4 conversion to HCN shows a maximum at T = 1900 K in the JSC and the ratio of HCN to equilibrium shows a very clear maximum at that temperature.

For both burners, percentage conversions appear to be inversely related to input concentrations although the relationship is quite weak at low ϕ.

For all conditions save two ($\phi = 1.2$, 1.4, T = 1900, 1800, C = 200, 400) conversion to TFN in the JSC exceeds that in the MB. Up to $\phi = 1.4$ conversion to NO is greater in the JSC than in the MB (except at $\phi = 1.2$, T = 1900, C = 200) but for $\phi = 1.4$ this result starts to reverse for T = 1900 and for $\phi = 1.8$ this conversion is greater in the MB than in the JSC at both T's.

Conversion to NH_3 shows no clear trend between the two combustors.

For ϕ = 0.8 there is no clear trend of conversion to HCN between the two burners. Comparable data does not exist around ϕ = 1.0. For $\phi \geq 1.2$ and T = 1800, conversion to HCN in the MB considerably exceeds that in the JSC with the excess increasing with equivalence ratio. For T = 1900, the reverse is true; conversion to HCN in the JSC exceeds that in the MB with the excess increasing with ϕ. This reversal occurs because of a reverse temperature sensitivity of conversion to HCN in the two burners. In the MB conversion to HCN decreases going from 1800 to 1900 K while in the JSC it increases. In all cases HCN is present in great excess over its equilibrium value. In the MB increasing the temperature strongly moves HCN towards its equilibrium value while in the JSC it strongly moves HCN away from (above) its equilibrium value.

The observations made from examining this table are that:

35. For both combustors TFN and NO are present in subequilibrium amounts below ϕ = 1 and are present in superequilibrium amounts above ϕ = 1.

36. Below ϕ = 1.0 conversion to TFN and NO increases with T in both combustors while the ratio to equilibrium decreases in the MB and remains relatively constant in the JSC.

37. Above ϕ = 1.0 conversion to NO increases with T in the MB and is little affected by T in the JSC (see Table III-3.3 for averages over all input concentrations).

38. Increasing T in the MB increases conversion to TFN at ϕ = 1.2, does not affect it at ϕ = 1.4, decreases it at ϕ = 1.8, and decreases the TFC ratio to equilibrium at all ϕ. Increasing T has no effect on this conversion in the JSC at ϕ = 1.2 or 1.4 but it strongly decreases the ratio to equilibrium;

39. Increasing T increases conversion to NH_3 in the MB but apparently not in the JSC. It decreases conversion to HCN in the MB for $\phi > 1.0$. Conversion to HCN maximizes at T = 1900 K in the JSC (see Table III-3.5 for averages over all concentrations).

40. Percentage conversions to fixed nitrogen species have at most a small negative dependence upon input FN concentration.

41. Conversion to TFN in the JSC exceeds that in the MB (by implication the converse holds true for conversion to molecular nitrogen).

42. Conversion to NO in the JSC exceeds that in the MB up to ϕ = 1.2 but for higher ϕ the converse is true.

43. For $\phi \geq 1.2$ at 1800 K conversion to HCN in the MB greatly exceeds that in the JSC but at 1900 K the converse is true.

Table III-3.4 compares results of changing FN species (1/1 ratio NO/NH_3 substituted for pure NH_3) on the performance of the two combustors. The following observations may be drawn from Table III-3.4.

44. Conversion to TFN increases greatly in the MB as NO is substituted for some of the NH_3 as FN (also to NH_3 at $\phi = 1.4$). Conversion to NO also increases. The substitution has a weak effect upon conversion in the JSC and it is inverse to that in the MB.

45. Substituting NO for NH_3 as FN increases conversion to HCN in the MB but decreases it in the JSC.

It should be emphasized that while the MB shows a large sensitivity to the substitution of NO for part of the NH_3 as FN when burning methane, this sensitivity disappears when ethylene is the fuel (at 1900 K). Thus, the sensitivity to FN species is peculiar to the combustion of methane under conditions that were obtained in the MB.

The preceding observations (30-44) may be used to decide whether differences in performance between the MB and the JSC stem from differences in residence time or from differences in combustion environment. Observations 30-32 concern thermal fixed nitrogen. Because fixed nitrogen in these cases must come from molecular nitrogen one would expect that the shorter residence time in the JSC would, other things being equal, lead to the opposite of observation 30. Also, since NH_3 is present at far more than its equilibrium value at the lower equivalence ratios one would expect the shorter residence time in the JSC to lead to the opposite of observation 32.

Similarly, observations 33 and 34 argue against a purely residence time effect. Observations 35, 36, 41 and 42 taken together also argue against purely residence time effects. The burden of all of these cited observations is that differences in performance between the two combustors stem from differences in combustion environment more than from differences in residence time.

Table III-3.1

Comparison of Thermally Fixed Nitrogen in the Multiburner and the Jet-Stirred Combustor for Hydrocarbon/O_2/N_2 Flames at 1900 K

ϕ	Device	TFN in Dry Products, PPM			NH_3 in Dry Products, PPM			HCN in Dry Products, PPM			NO in Dry Products, PPM		
		CH_4	C_2H_4	C_3H_8	CH_4	C_2H_4	C_3H_8	CH_4	C_2H_4	C_3H_8	CH_4	C_2H_4	C_3H_8
1.0	MB	39	--	4.6	14	--	0.98	2.4	--	1.4	23	--	2.2
1.0	JSC	--	52	60	--	1.7	1.2	--	1.4	1.9	--	49	57
0.97	JSC	60	--	--	1.0	--	--	1.0	--	--	58	--	--
1.4	MB	42	38	24	2.4	2.0	0.94	6.8	2.0	1.3	33	34	22
1.4	JSC	80	96	89	3.0	6.2	3.7	15	17	26	62	73	59
1.8	MB	35	--	58	2.2	--	1.4	27	--	12	5.7	--	45
1.8	JSC	133	117	--	1.4	8.9	--	121	88	--	11	21	--

Table III-3.2

Comparison of the Effects of Temperature and Fuel Nitrogen (NH_3) Concentration on Fuel Nitrogen Conversion in Methane Flames in the Multiburner and the Jet-Stirred Combustor

ϕ	Nominal NH_3 Input PPM	Device	TFN Output*			NH_3 Output*			HCN Output*			NO Output*		
			1800	1900	2000 K	1800	1900	2000 K	1800	1900	2000 K	1800	1900	2000 K
0.8	200	MB	53 128 0.060	55 128 0.044	62 145 0.038	0.55 1.3 --	0.80 1.9 --	3.3 7.7 1.1E5	0.49 1.2 --	0.57 1.3 --	1.1 2.7 1.3E8	52 125 0.059	54 125 0.043	58 135 0.035
0.8	200	JSC		79 189 0.065	100 258 0.067		0.63 1.5 --	0.74 1.9 2.7E4		1.0 2.4 --	0.51 1.3 6.3E7		77 185 0.064	99 255 0.066
0.8	400	MB	54 262 0.12	0.83 3.5 1.2E-3	56 253 0.066	0.21 1.0 --	0.23 1.1 --	0.23 1.0 1.4E4	0.25 1.2 --	0.45 1.7 --	0.38 1.7 8.3E7	54 260 0.12	0.15 0.65 2.2E-4	56 250 0.065
	400	JSC		79 377 0.13	85 438 0.11		0.31 1.5 --	0.43 2.2 3.1E4		0.17 0.8 --	0.23 1.2 5.8E7		78 375 0.13	85 435 0.11
0.8	800	MB	56 512 0.24		62 611 0.16	0.11 1.0 --		1.0 10 1.4E5	0.14 1.3 --		0.14 1.4 6.8E7	56 510 0.24		60 600 0.16
		JSC		78 702 0.24	82 793 0.21		0.15 1.3 --	0.12 1.2 1.7E4		0.089 0.8 --	0.16 1.5 7.3E7		78 700 0.24	82 790 0.21

* Columns of three numbers for each condition read from the top: Percent of Input Fixed Nitrogen, PPM Out in Dry Gas, Ratio to Equilibrium Value.

(Continued)

Table III-3.2 (Continued)

ϕ	Nominal NH_3 Input PPM	Device	TFN Output*			NH_3 Output*			HCN Output*			NO Output*		
			1800	1900	2000 K	1800	1900	2000 K	1800	1900	2000 K	1800	1900	2000 K
1.0	200	MB	52 125 0.49	66 152 0.32	64 156 0.19	0.38 0.91 3.1E3	0.43 1.2 --	1.9 4.7 4.5E3	0.61 1.5 1.9E7	0.43 1.2 --	0.56 1.4 1.0E6	51 123 0.49	65 150 0.32	61 150 0.18
0.97	200	JSC		86 221 0.19			3.1 8 --			3.5 9 --			80 204 0.18	
1.0	400	MB	50 238 0.94	61 282 0.60	59 287 0.35	0.18 0.87 2.9E3	0.22 1.0 --	1.2 5.7 5.5E3	0.39 1.9 2.4E7	0.22 1.1 --	0.26 1.3 9.3E5	49 235 0.93	60 280 0.59	57 280 0.34
0.97	400	JSC		78 402 0.35			1.2 6 --			1.2 6 --			76 390 0.34	
1.0	1000	MB	29 354 1.4		51 567 0.68	0.11 1.3 4.4E3		0.48 5.3 5.1E3	0.19 2.2 2.8E7		0.19 2.1 1.5E6	29 350 1.4		51 560 0.67
0.97	800	JSC		75 723 0.63			0.21 2 --			0.62 6 --			74 715 0.62	

* Columns of three numbers for each condition read from the top: Percent of Input Fixed Nitrogen, PPM Out in Dry Gas, Ratio to Equilibrium Value.

(Continued)

Table III-3.2 (Continued)

ϕ	Nominal NH_3 Input PPM	Device	TFN Output* 1800	1900	2000 K	NH_3 Output* 1800	1900	2000 K	HCN Output* 1800	1900	2000 K	NO Output* 1800	1900	2000 K
1.2	200	MB	43 103 28	175 401 32		0.52 1.2 7.6	69 158 1.3E3		4.9 12 5.8E3	1.1 2.5 1.3E3		38 90 25	105 240 19	
	200	JSC	127 315 84	100 237 19	111 284 7.4	0.64 1.6 10	2.1 5 41	0.82 2.1 22	1.5 3.6 1.7E3	2.9 6.8 3.4E3	0.55 1.4 734	125 310 87	95 225 18	109 280 7.3
	400	MB	42 200 54	73 334 26		0.22 1.1 7.0	17 78 641		5.0 24 1.2E4	0.14 0.66 332		37 175 49	56 255 20	
	400	JSC	110 542 145	104 492 39	95 487 13	1.3 6.6 42	1.9 8.9 73	1.0 5.1 53	1.0 5.1 2.5E3	1.6 7.7 3.9E3	0.39 2.0 1.0E3	107 530 148	100 475 38	94 480 12
	900	MB	33 384 103	68 639 51		0.41 1.0 6.4	2.0 18 148		5.3 63 3.0E4	0.08 0.71 357		27 320 90	66 620 50	
	800	JSC	77 878 235	75 674 53	78 745 19	1.4 16 102	0.39 3.5 29	1.4 13 135	0.15 1.7 8.2E2	0.59 5.3 2.7E3	0.22 2.1 1.1E3	75 860 241	74 665 53	76 730 19

* Columns of three numbers for each condition read from the top: Percent of Input Fixed Nitrogen, PPM Out in Dry Gas, Ratio to Equilibrium Value.

(Continued)

Table III-3.2 (Continued)

φ	Nominal NH_3 Input PPM	Device	TFN Output*			NH_3 Output*			HCN Output*			NO Output*		
			1800	1900	2000 K	1800	1900	2000 K	1800	1900	2000 K	1800	1900	2000 K
1.4	200	MB	96	94		0.38	6.1		79	0.66		17	87	
			221	211		0.88	14		182	1.5		38	195	
			112	38		1.8	37		1.6E4	134		26	38	
	200	JSC	109	107	113	1.7	4.9	4.4	3.7	29	7.5	103	73	101
			253	241	279	3.9	11	11	8.6	65	19	240	165	250
			128	44	17	8.1	29	36	743	5.8E3	1.7E3	162	32	16
	400	MB	85	83		0.23	2.5		75	0.51		10	80	
			394	301		1.0	9.1		345	1.9		48	290	
			200	55		2.1	24		3.0E4	169		32	57	
	400	JSC	77	92	90	2.6	4.5	3.3	4.4	28	4.8	70	60	82
			352	414	445	12	20	16	20	124	24	320	270	405
			178	75	28	25	53	52	1.7E3	1.1E4	2.2E3	216	53	26
	800	MB	58			0.18			48			10		
			478			1.5			394			82		
			242			3.1			3.4E4			55		
	800	JSC	71	76	73	1.3	2.0	1.4	0.95	14	1.2	69	60	71
			826	638	679	15	17	13	11	116	12	800	505	655
			419	116	43	31	45	42	951	1.0E4	1.1E3	540	99	42

* Columns of three numbers for each condition read from the top: Percent of Input Fixed Nitrogen, PPM Out in Dry Gas, Ratio to Equilibrium Value.

(Continued)

Table III-3.2 (Continued)

φ	Nominal NH_3 Input PPM	Device	TFN Output*			NH_3 Output*			HCN Output*			NO Output*		
			1800	1900	2000 K	1800	1900	2000 K	1800	1900	2000 K	1800	1900	2000 K
1.8	200	MB	103	77		4.0	5.0		96	3.4		3.3	69	
			221	157		8.5	10		205	6.9		7.0	140	
			115	44		6.4	14		3.3E3	229		13	49	
	200	JSC		145			4.9			124			16	
				297			10			255			32	
				83			14			8.5E3			11	
	400	MB	125	54		0.25	4.2		121	1.2		3.3	49	
			529	222		1.1	17		514	5.0		14	200	
			276	62		0.83	24		8.4E3	166		26	70	
	400	JSC		116			9.2			99			8.3	
				479			38			407			34	
				133			53			1.4E4			12	
	1000	MB	111	32		1.8	0.50		107	12		1.8	19	
			1171	327		19	5.1		1132	127		20	195	
			611	91		14	7.2		1.8E4	4.2E3		38	68	
	750	JSC		139			8.6			124			6.5	
				1069			66			953			50	
				297			93			3.2E4			18	

* Columns of three numbers for each condition read from the top: Percent of Input Fixed Nitrogen, PPM Out in Dry Gas, Ratio to Equilibrium Value.

Table III-3.3

Fuel Nitrogen (NH_3) Conversions Averaged Over All Input Concentrations in the Two Combustors

ϕ	TFN, % of FN			NH_3, % of FN			HCN, % of FN			NO, % of FN		
	1800	1900	2000 K	1800	1900	2000 K	1800	1900	2000 K	1800	1900	2000 K
						THE MULTIBURNER						
0.8	54	55	60	0.29	0.52	1.5	0.29	0.51	0.54	54	54	58
1.0	44	64	58	0.22	0.33	1.2	0.40	0.33	0.34	43	63	56
1.2	39	105	--	0.38	29	--	5.1	0.44	--	34	76	--
1.4	80	89	--	0.26	4.3	--	67	0.59	--	12	84	--
1.8	113	54	--	2.0	3.2	--	108	5.5	--	2.8	46	--
						THE JET-STIRRED COMBUSTOR						
0.8	--	79	89	--	0.36	0.43	--	0.42	0.30	--	78	89
0.97	--	80	--	--	1.5	--	--	1.8	--	--	77	--
1.2	105	93	95	1.1	1.5	1.1	0.88	1.7	0.39	102	90	93
1.4	86	92	92	1.9	3.8	3.0	3.0	24	4.5	81	64	85
1.8	--	133	--	--	7.6	--	--	116	--	--	10	--

Table III-3.4

Effects of Equivalence Ratio, Fuel Nitrogen Concentration, and Fuel Nitrogen Species on Fuel Nitrogen Conversion Compared for the Multiburner and the Jet Stirred Reactor at Nominal 1900 K for the $CH_4/O_2/N_2$ System

ϕ	Input Fuel Nitrogen, PPM						Percent of Input FN Out As								Collected in Dry Exhaust Gas, PPM								Residence Time, ms		Ratio MB Conversion to JSR Conversion			
	NH_3		NO		N		TFN		NH_3		HCN		NO		TFN		NH_3		HCN		NO		MB	JSR	TFN	NH_3	HCN	NO
	MB	JSR	MB	JSR	MB	JSR	MB	JSR	MB	JSR	MB	JSR	MB	JSR	MB	JSR	MB	JSR	MB	JSR	MB	JSR						
1.4	0	0	0	0	0	0	--	--	--	--	--	--	--	--	42	80	2.4	3	6.8	15	33	62	29	2.9	0.53	0.80	0.45	0.53
1.4	324	399	0	0	324	399	83	92	2.5	4.5	0.51	28	80	60	301	414	9.1	20	1.9	124	290	270	29	2.9	0.90	0.56	0.018	1.3
1.4	170	207	169	194	339	401	206	81	110	1.8	0.66	23	95	57	781	366	418	8	2.5	103	360	255	29	2.9	2.5	61	0.029	1.7
1.8	0	0	0	0	0	0	--	--	--	--	--	--	--	--	35	133	2.2	1.4	27	121	5.7	11	26	2.6	0.26	1.6	0.22	0.52
1.8	199	200	0	0	199	200	77	145	5.0	4.9	3.4	124	69	16	157	297	10	10	6.9	255	140	32	26	2.6	0.53	1.0	0.027	4.3
1.8	398	401	0	0	398	401	54	116	4.2	9.2	1.2	99	49	8.3	222	479	17	38	5.0	407	200	34	26	2.6	0.47	0.46	0.012	5.9
1.8	994	750	0	0	994	750	32	139	0.50	8.6	12	124	19	6.5	327	1069	5.1	66	127	953	195	50	26	2.6	0.23	0.058	0.097	2.9
1.8	104	110	104	110	208	220	97	119	0.95	4.4	9.2	100	87	15	207	270	2.0	10	20	226	185	34	26	2.6	0.82	0.22	0.092	5.8
1.8	208	208	208	194	416	402	62	107	1.8	7.0	6.0	87	54	13	264	441	7.8	29	26	358	230	54	26	2.6	0.58	0.26	0.069	4.2

3. In choosing a laboratory combustor as a prototype for a given model combustor, attention must be given to comparing reaction environment between the two if useful results are to be obtained. While the strongly backmixed JSC produces conditions akin to more commercial combustors than does the MB, that need not always be the case, and every case should be examined in detail before setting out on an experimental program.

4. The results produced in this project cover very wide ranges of independent variables, but rather thinly. While they provide benchmarks in the performance map, more dense coverage is advisable with new benchmarks provided by a randomly selected pattern of multiply determined points to give a measure of experimental error over the entire map.

5. The full value of these data may only be realized as they are quantitatively modeled with detailed mechanisms. Not only can they both guide and test such modeling but the modeling work can suggest additional critical experiments to perform.

6. One aspect of the data that should be carefully considered by modelers arises in the case of combustion without fuel nitrogen present, i.e., in the purely "thermal" nitrogen case. That is the occurrence of substantial quantities of product NH_3 and HCN for $\phi \leq 1.0$ especially in the MB (Tables III-1.7, 1.8) but also to a lesser extent in the JSC (Table III-2.3). This occurrence appears to be fuel-specific to CH_4 and to be enhanced by increasing temperature. It cannot, of course, be explained by Zeldovich kinetics and it is probably related to the "prompt NO_x" mechanism.

7. At high ϕ, large quantities of fixed nitrogen can be produced as HCN either thermally or by conversion of fuel nitrogen. At these high values of ϕ the addition of fuel nitrogen can cause the fixation of molecular nitrogen from the combustion air in excess of the purely "thermal" value (i.e., "Fuel" TFN can exceed 100 percent).

IV. CONCLUSIONS

To reiterate, a primary purpose of this project was to provide reliable data on fuel nitrogen conversion over a wide range of combustion conditions for subsequent use in computer modeling. These data have been provided, although considerable supplemental work is needed both to further substantiate some of the data and to extend it to additional regions that are of great interest. However, the data that have been obtained and presented in this report provide a broad scope for quantitative analysis. Only such analysis can draw forth the details of the message that they contain. However, certain conclusions can be drawn directly from the data as they are presented in this report and without further analysis.

Of the several independent variables that were investigated in this work, one of the most important was that of the reactor used, i.e., the laminar flow MB or the strongly backmixed JSC. In discussing differing results between these reactors, the assumption will be made that the differences lie in gas-phase chemistry and not in surface reactions. While surface reactions were demonstrably not present in the MB results, such a fact is much more difficult to establish in the JSC. While attempts have been made to demonstrate the absence of surface effects in the JSC, the situation there cannot be considered totally established and it deserves further effort in the future. However, comparisons that appear below between the reactors are interpreted in terms of gas phase chemistry. With this preamble, the following conclusions may be drawn from this work.

1. The kinetic conditions differ substantially between the MB and the JSC. These differences find their origin in differing reaction environments between the two combustors much more than in differing residence times. Fuel-specific effects are more important in the MB where initial fuel breakdown provides radicals which dominate the initiation of kinetic mechanisms. In the JSC this initial fuel breakdown occurs in the presence of a rich pool of radicals that were formed in all stages of the reaction processes; these radicals initiate paths differing from those in the MB and they predominate. Furthermore, because of sequential conditions experienced by reactants in the MB as opposed to near homogeneous conditions in the JSC, some critical reaction times in the MB may actually be less than in the JSC. For instance, for $\phi > 1$ almost all free oxygen in the MB is used up within the flame zone. Passage through the flame zone occurs in about 1 ms. In the JSC free oxygen is present during the entire 3 ms residence time of an average reactant element. Reactant conditions differ substantially between the two reactors and an adequate reaction model must agree with both.

2. For equivalence ratios up through 1.4 the MB is sensitive to changes in fuel nitrogen species while the JSC is not. These differences lie in the differing reaction conditions discussed above.

V. SUGGESTED WORK

This area of experimentation can be judged far from complete. Much more needs to be done to achieve its full potential. In addition to more densely populating the present range of variables with experimental points and with multiple rerun points, the range of variables should be extended as follows.

1. The data on the effect of substituting fuel NH_3 with fuel NO should be extended to cover all three fuels in each burner over the full range of ϕ and T.
2. Other types of fuel nitrogen (e.g., pyridine) should be substituted for NH_3 and NO over the full range of independent variables.
3. In examining the effect of carbon number the C2 species was ethylene while methane and propane were the C1, C3 species. Experiments should be run with ethane to eliminate single/double bond effects from obscuring carbon number effects in this series of experiments.
4. Other hydrocarbon fuels should be tested, particularly aromatic and cyclic compounds.
5. The work should be extended to higher temperatures (up to 2500 K).
6. An extensive effort should be devoted to investigating the influence of surface effects in JSC's. This is particularly important in that JSC's are very useful and versatile research tools and their veracity should be unequivocally established.
7. Pending the results of 6, larger JSC's should be built to permit the study of residence time effects under similar mixing conditions.
8. Finally, data now being available for modeling, experimental and theoretical work should progress together, each responding to the stimulus of the other.

VI. ACKNOWLEDGMENTS

Especial thanks are due Mr. R. W. Schroeder and Mr. R. J. Kuriskin who were technicians in charge of the JSC experiments and to Mr. A. Petuskey, Jr. who was technician in charge of the MB experiments. Their enthusiastic and competent efforts were essential to the success of this project.

It is almost presumptuous to list my colleague, Dr. Albert Myerson, under acknowledgments (and so see page 18, the introduction). This was Dr. Myerson's project until he left ER&E Co. towards its very end. His contributions included planning of the experiments, overseeing all of the work on the jet-stirred combustor, and the initial work on the multiburner. More importantly, he set the tone of the work and made it into an interesting and exciting project. It was he who insisted that the experiments be carried out over ranges of isothermal adiabatic flame temperatures as opposed to the more normal practice of allowing the adiabatic flame temperature to vary with the equivalence ratio. This vastly uncomplicates the analysis of the results.

Working with Al was always instructive as well as pleasurable and both virtues lingered on in this work after he left. They made the job a pleasure to complete. I hope that sometime I may again enjoy scientific collaboration (and intellectual combat) with Dr. Myerson. Until then, Al, may you enjoy reading this report.

VII. REFERENCES

1. Gordon, S. and McBride, B. J., "Computer Program for Calculation of Complex Chemical Equilibrium Compositions, Rocket Performance, Incident and Reflected Shocks, and Chapman-Jouguet Detonations," NASA SP-273, 1971.

2. Modification 1 to Subcontract EER-8318-3, Energy and Environmental Research Corporation, February 28, 1978, and Exxon Research and Engineering Company, March 16, 1978.

3. Longwell, J. P. and Weiss, M. A., "High Temperature Reaction Rates in Hydrocarbon Combustion," Industrial and Engineering Chemistry, Vol. 47, No. 8, August 1955.

4. Bartok, W., Engleman, V. S., Goldstein, R., and del Valle, E. G., AIChE Symposium Series, Vol. 68, No. 126, 1972.

5. Myerson, A. L., "An Investigation of the Formation and Destruction of Nitrogenous Species During Hydrocarbon-Air Combustion," Monthly Technical Progress Report prepared for Energy and Environmental Research Corporation, Subcontract No. EER-8318-3, January, 1979.

6. Myerson, A. L., loc cit, April, 1978.

7. Engleman, V. S. and Bartok, W., "Mechanism and Kinetics of the Formation of NO_x and Other Combustion Pollutants, Phase 1. Unmodified Combustion," EPA-600/7-76-009a.

8. Engleman, V. S., Siminski, V. J., and Bartok, W., "Mechanism and Kinetics of the Formation of NO_x and Other Combustion Pollutants, Phase II. Modified Combustion," EPA-600/7-76-009b.

9. Blazowski, W., Edleman, R. B., and Harsha, P. T., "Fundamental Characterization of Alternate Fuel Effects in Continuous Combustion Systems," Summary Technical Progress Report, DOE Contract No. EC-77-C-03-1543, ER&E Report No. Exxon COO/1543-12.

APPENDIX A

COMPARISON OF RESULTS FROM THE PRESENT JET-STIRRED COMBUSTOR WITH THOSE FROM PREVIOUS JSC's

During the course of this work it was deemed desirable to check results with the present apparatus against those obtained with previous JSC's to evaluate their consistency. This was done and reported in a monthly progress report on this project (ref. 5). This appendix contains the sections of that report that are pertinent to those consistency checks.

DETAILED TECHNICAL FINDINGS AND DISCUSSIONS

The findings of the past reporting period, all of which involve the JSC, fall into two categories:

(a) the data which are relevant to the original "Work Plan" and comprise the concluding CH_4, C_2H_4 and C_3H_8 combustion data with and without fuel-NH_3 and with fuel-(NH_3 + NO). These latter data will be tabulated in our next progress report.

(b) the most recent results (BM) obtained cooperatively with W. S. Blazowski, in conjunction with his DOE program (1). This experimental work is critical to the DOE program and was funded by that contract.

These data are the result of an effort to reproduce the JSC data taken by Bartok, Engleman, Goldstein and del Valle (BEGD) (2) seven years ago in a somewhat differently designed JSC, and with stoichiometric air, only. Our present work (BM) was done with stoichiometric air, as was Reference 2, for the purpose of ascertaining whether there is a reasonably close general mechanistic relationship between the JSC data taken by BEGD, and modeled by EER at that time, and the constant temperature JSC data we obtained under this contract.

Thus, if we now show reasonable equivalence between the two sets of results (i.e., BEGD and BM), previous EER analytical models should be expected to predict the new data obtained at constant temperature.

While we shall present the data tables for all remaining JSC results, except for the fuel [NO + NH_3] combination, we shall leave the graphical and chemical interpretation for our next report and concentrate herein on the stoichiometric air experiments (BM).

For the findings in category (a) above, Table I and IA present the results of CH_4 combustion at a constant temperature of 1800 K for three different ϕs, viz., 1.0, 1.4 and 1.8 ($\phi = 1.8$ was not previously available in our tables, although it was graphed). There is an obvious but gentle minimum in TFN at $\phi = 1.6$, but NO shows only the pronounced effect of being reduced by the HCs to produce HCN at high equivalence ratios.

Tables II and IIA present similar data for C_2H_4. There is still a TFN minimum but the final value at 1.8 is much less than with CH_4, indicating a superior path to N_2 via

$$CH + NO = CHO + N$$

$$N + O_2 = NO + O$$

$$N + NO = N_2 + O$$

possibly as a result of the greater ability of $CH_2{=}CH_2$ over CH_4 to provide CH and CH_2 radicals.

Turning to category (b) above, all the relevant data obtained are presented in Figures 3 through 7. Complete tables (III, IIIA, IV and IVA) are shown herein for the most important data which form a basis for our comparison. The remaining tables will be provided in our next report.

Vital to the concept of comparing data for the old experiment (BEGD) and the new (BM) are differences in the physical structure of the two JSCs, which are the result of many system improvements accomplished during the intervening years. First, the i.d. of our hemisphere is 2" while that of BEGD was 1-1/2". This influences the heat loss characteristics and internal surface area. Second, the o.d. of our refractory sphere is 6" while that of BEGD was only 5". Last, the shell material is different, the old one being constructed of fire brick while the new one uses a super-castable refractory with superior temperature resistance. This results in less ablation which may involve some differences in mechanism if any surface effects are involved.

In comparing the present data with that of BEGD, it is most important to introduce temperature comparisons. Since, with stoichiometric air, one must accept whatever JSC temperature results (after stabilization), the differences may be significant. Therefore, in Figure 3 we present a curve from the BEGD data which provides the temperature of any BEGD data point as a function of ϕ, the equivalence ratio. On Figure 4, our first graph of $[NO_x]$ as f (ϕ), the temperature corresponding to any given point on the BEGD curve is given on the upper X-axis. Three sets of data are shown on this graph: the old BEGD results with stoichiometric air (SA) and pre-heating shown as a curve (no points); the present (BM) SA measurements (⊖), also with pre-heating; and the present constant temperature data obtained at 1900 K (⊡). As can be seen, the old and new SA data are in fairly good agreement considering the normal JSC data scatter and the differences involved in reactor construction and operating temperature.

Equally significant is the difference in the region of the curve's NO_x maximum, where NO_x is much higher for the BEGD conditions than our constant temperature 1900 K data. This is as it should be since the formation of NO is a high activation energy step ($O + N_2$) (favored by higher temperatures) and its loss a low one ($CH + NO$). At very rich ϕs, coincidence is probably better, since N-fixation also becomes a low activation (Ea) step via $CH + N_2$, aut al. It will be noted that we used $\tau_{res} = 4$ ms rather than the BEGD of 3 ms in order to attain higher ϕs. As will be seen on succeeding figures, the data are not particularly sensitive to τ_{res}.

Figure 5 presents NO_x as a f (ϕ) for the other τ_{res}'s studied. Because these experiments were conducted with no pre-heat, much lower reaction temperatures were obtained (for given conditions, of course). As can be noted, agreement is good on the lean side, but on the rich side, where we did not attain the higher temperatures associated with pre-heat (used by BEGD), the trend is lower, again in line with the thesis expounded in the previous paragraph.

The studies with fuel nitrogen, in the form of NH_3, produced the results shown in Figures 6 and 7. Figure 6 illustrates two possible interpretations (curves) for the BEGD SA data for fractional conversion of NH_3 as f (ϕ). Our present SA data (BM), shown via ▽, closely parallel the BEGD curve but are somewhat higher on the richest portion of the curve. Here, for the most part, the temperature of BEGD is higher, but, with fuel-NH_3, this should favor less NO since the formation of most of the NO is through a low activation energy process, namely the oxidation of NH_3. This latter step's Ea is probably low even with respect to the loss mechanism (via CH + NO) previously mentioned. In addition, if one makes a comparison with our constant T data taken at 1900 K (⊡), it is seen that these 1900 K points also are higher for lower temperatures. The 1900°K data point at $\phi = 1.8$ seems inconsistent with the BEGD data as drawn, but the percent conversion can't be much lower, and there is no real basis for comparison because the BEGD experiments have reached the blow-out.

Finally, Figure 7 presents the rest of the new data involving various residence times with no pre-heat. As can be seen, τ_{res} does not influence the results to any great extent.

In summation, one can conclude that the new and old SA data are in reasonably good agreement, especially in view of the differences between the two reactors and the natural scatter of JSC data. The differences that exist between the stoichiometric air and constant temperature data can be expected and explained in terms of the mechanistic arguments presented herein.

REFERENCES

1. W. S. Blazowski, DOE Contract on Fundamental Characterization of Alternate Fuel Effects in Continuous Combustion Systems, Contract EC-77-C-03-1543.

2. W. Bartok, V. S. Engleman, R. Goldstein, and E. G. del Valle, AIChE Symposium Series, V, 68, No. 126, 1972.

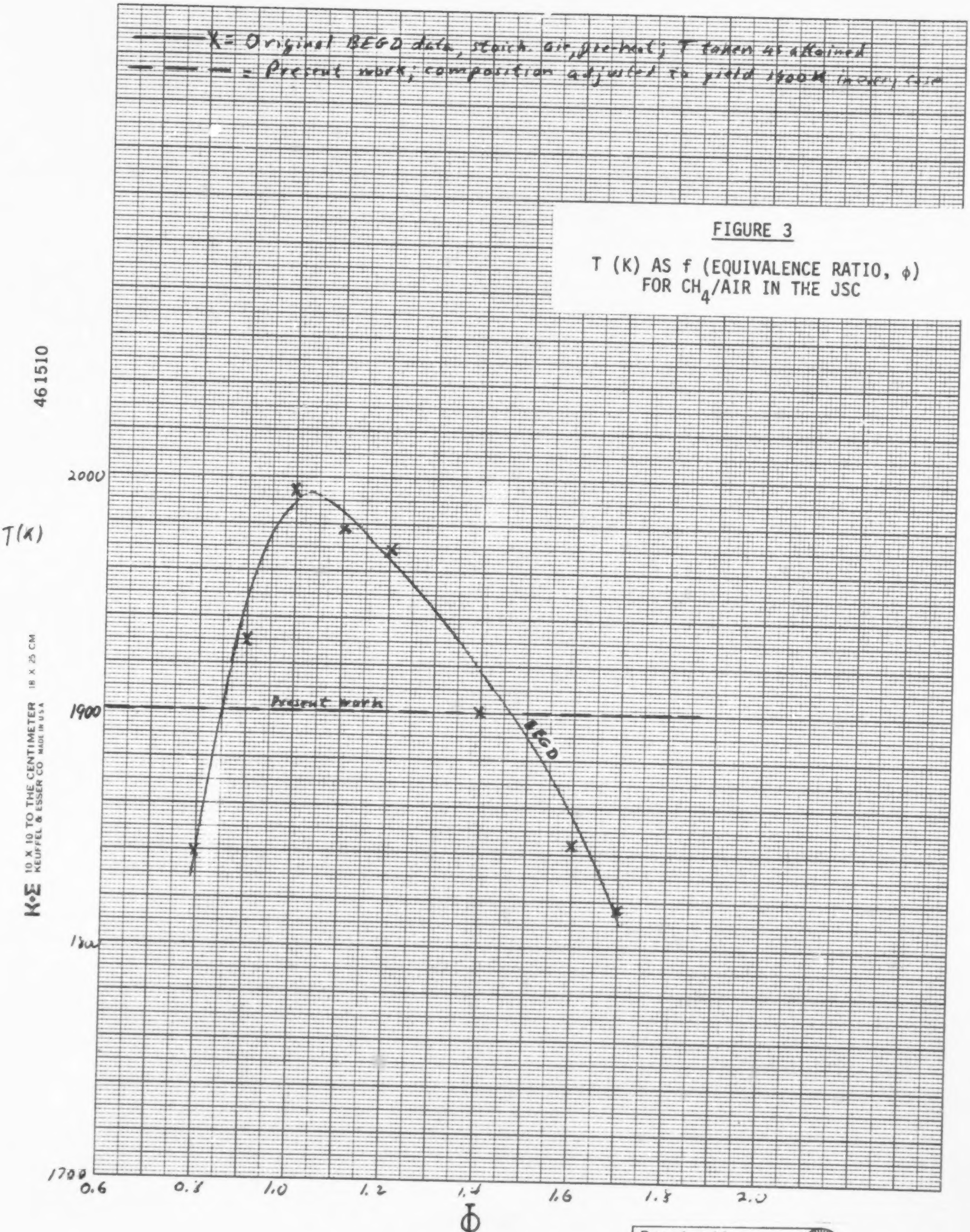

FIGURE 3

T (K) AS f (EQUIVALENCE RATIO, ϕ)
FOR CH_4/AIR IN THE JSC

Reproduced from
best available copy.

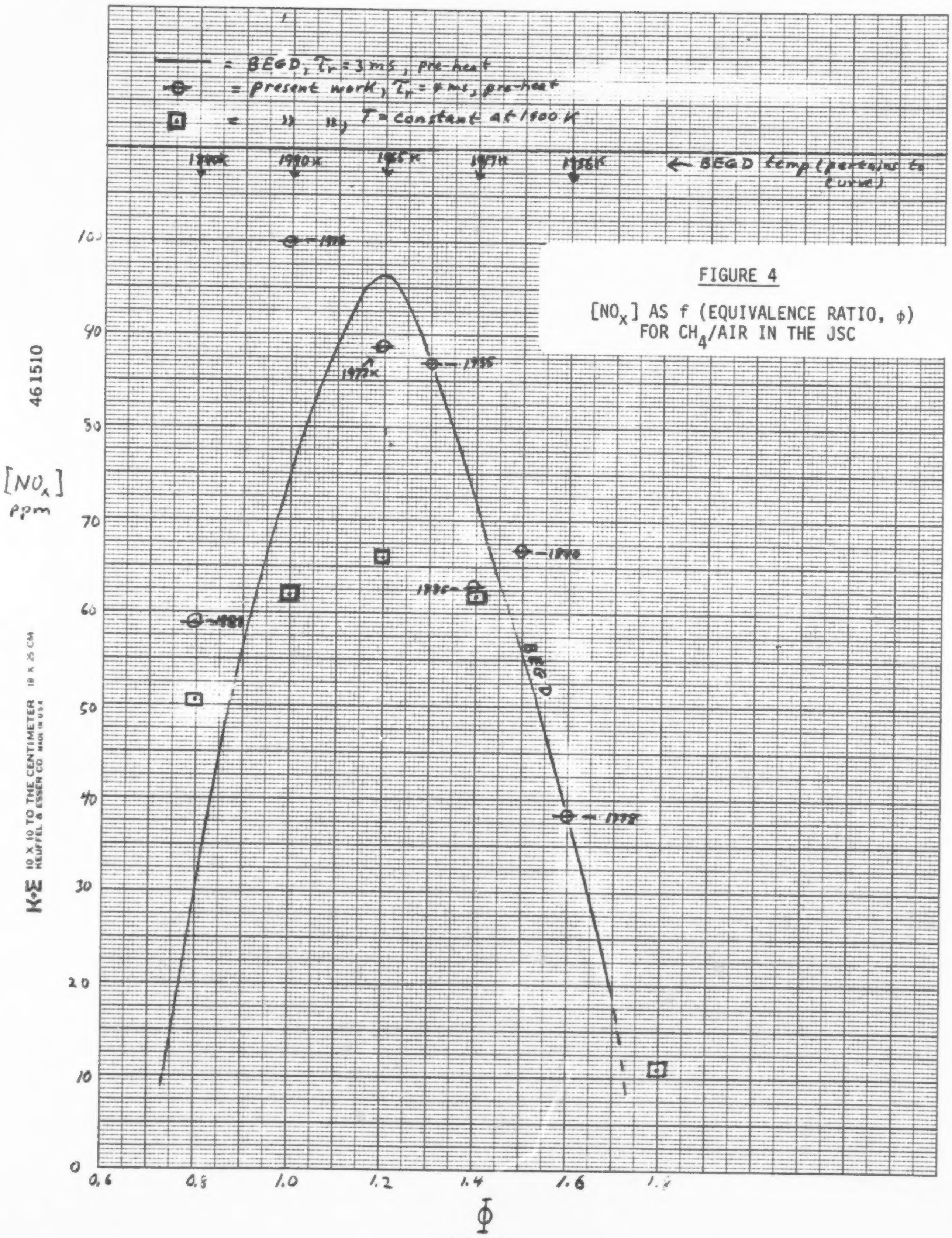

FIGURE 4

[NO$_X$] AS f (EQUIVALENCE RATIO, ϕ)
FOR CH$_4$/AIR IN THE JSC

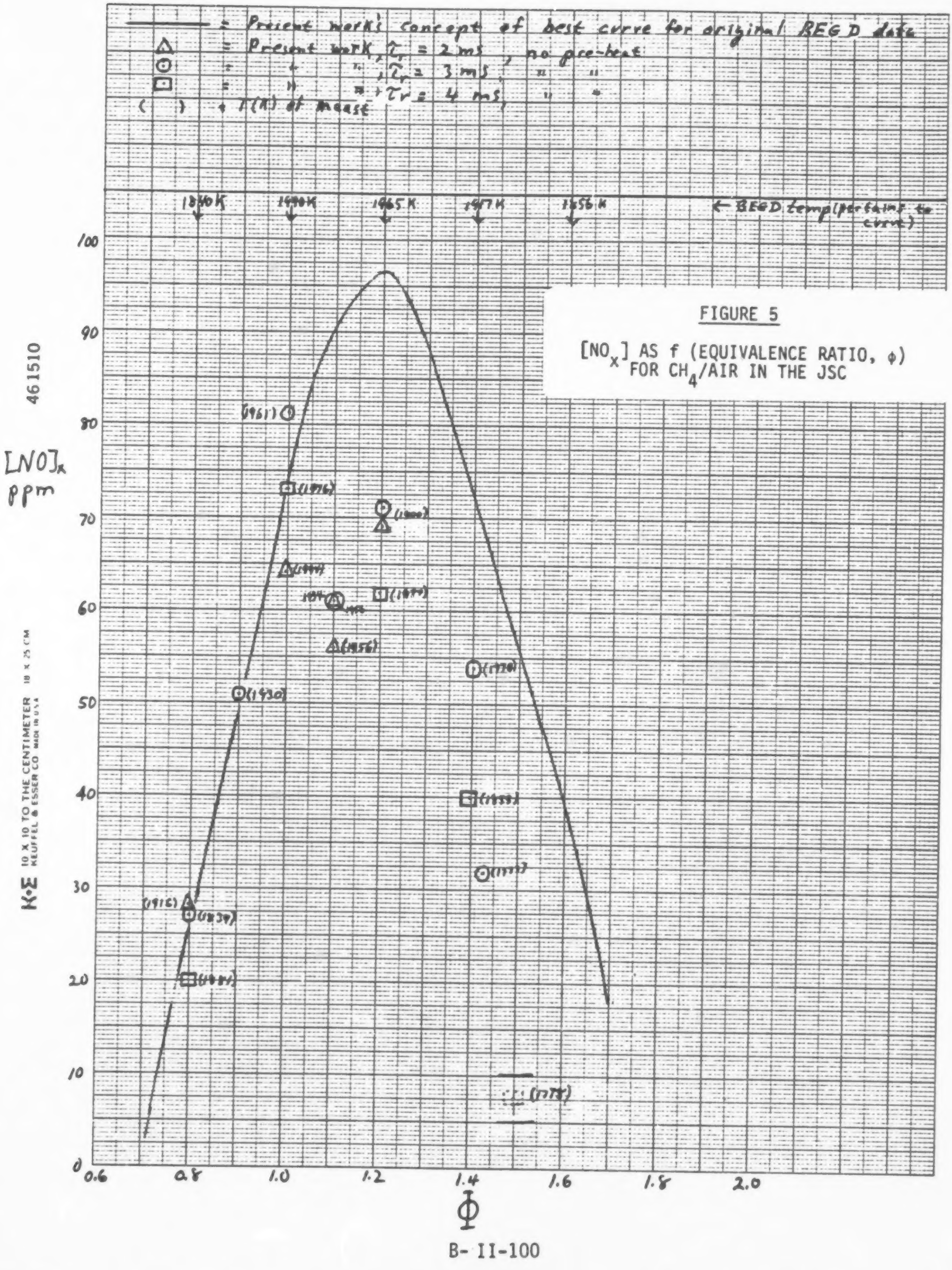

FIGURE 5

[NO$_x$] AS f (EQUIVALENCE RATIO, φ) FOR CH$_4$/AIR IN THE JSC

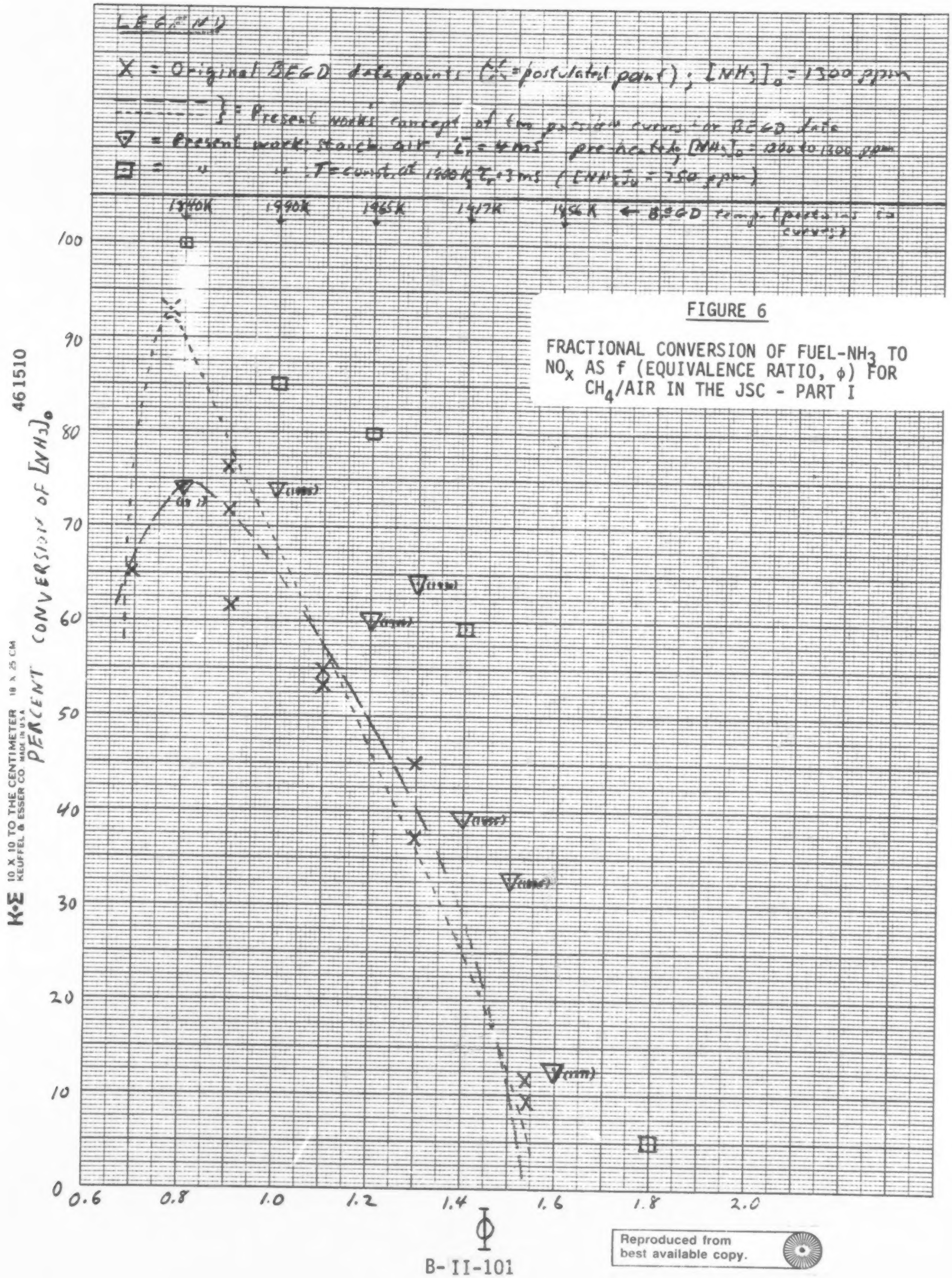

FIGURE 6

FRACTIONAL CONVERSION OF FUEL-NH_3 TO NO_x AS f (EQUIVALENCE RATIO, ϕ) FOR CH_4/AIR IN THE JSC - PART I

Reproduced from best available copy.

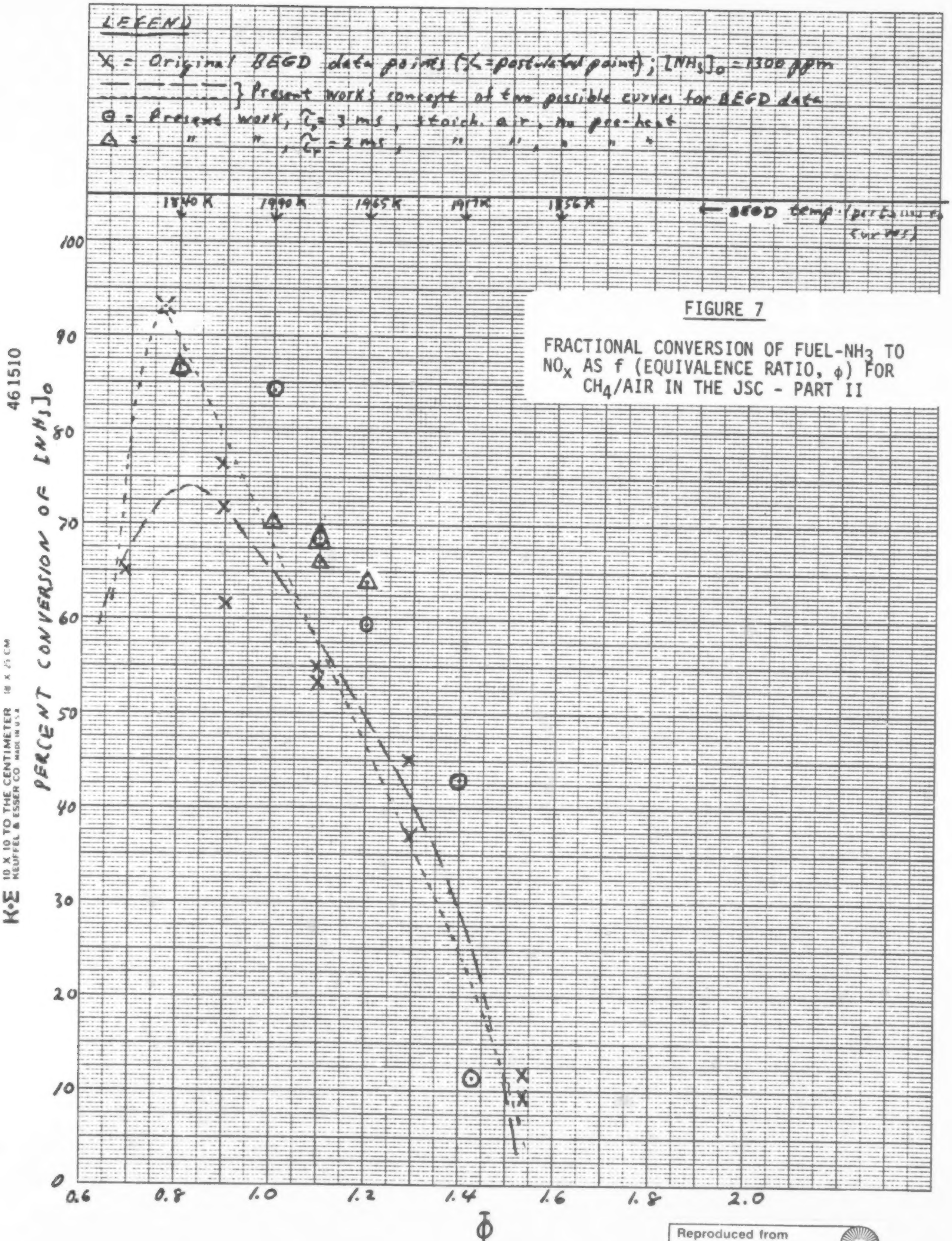

FIGURE 7

FRACTIONAL CONVERSION OF FUEL-NH_3 TO NO_X AS f (EQUIVALENCE RATIO, ϕ) FOR CH_4/AIR IN THE JSC - PART II

Reproduced from best available copy.

APPENDIX B

RADIAL UNIFORMITY IN THE MULTIBURNER

At the outset of work with the multiburner it was deemed necessary to investigate the radial distribution of species within it as a check on the expectation of radial uniformity. This was done and reported in reference 6. This appendix contains the sections of that report that deal with radial uniformity.

DETAILED TECHNICAL FINDINGS AND DISCUSSIONS

As mentioned previously, the multiburner and most of its auxiliary apparatus have been brought to the point where furnace-flame experiments can begin. Barring any further mechanical breakdowns, this should begin during the early part of May. A large water leak in the cooling system of the furnace's main electrical cable has caused some delay and a failure of a component in the CO_2 NDIR analyzer is in the process of repair. Installation and check-out of the GC for H_2 is not yet complete.

It was indicated previously that a stumbling block had been reached with the computerized IR analysis of NH_3, HCN, etc. mixtures because of dispersion limitations with respect to NH_3. Another possibility was mentioned at that time which consists of a completely automated colorimetric method for HCN and NH_3. The aqueous coloring due to steady-state concentrations of NH_3 plus reagents (or HCN in a separate instrument) are read photometrically and automatically and produce a digital output. The only disadvantage would seem to be making up solutions periodically, since the method is extremely sensitive. The basic range is 0 to 1 ppm for HCN, with $\sim \pm 1\%$ accuracy, with extensions to higher levels (100s of ppm) via gas-phase dilution of the original sample. The basic range for NH_3 is higher with similar accuracy. Before considering purchase of these instruments, it is planned to make test runs with them at a later date, with samples taken directly from an actual multiburner experiment.

- - - - - - - - - - -

In a previous discussion here at ER&E, among those involved in this research program, a number of characteristics of the multiburner were considered. Among them was the construction of the MB and its effect on the concentration profiles inside the flow-tube. To this end, we are presenting drawings of the MB in Figures 3 and 4 and some radial profile data$^{(1)}$ for O_2, CO and NO in Figures 5 through 10. As can be seen from these plots, the profiles are really pleasingly flat (the mean deviations from horizontal range, for the most part, from near zero to 10 or 20%). In only one case, with NO (Figure 8), is there a serious deviation from this, but this is one out of so many series of profiles taken (the ones shown represent only a small fraction of the total), that we can accept this as a specific problem of analysis at that time. Thus, while one should explore such characteristics further during our program, the prognosis for meaningful data from the multiburner appears to be excellent.

---

(1) V. Engleman, V. J. Siminski and W. Bartok, "Mechanism and Kinetics of NO_x and Other Combustion Pollutants," Ph. I. EPA-600/7-76-009b, August 1976.

Figure 3

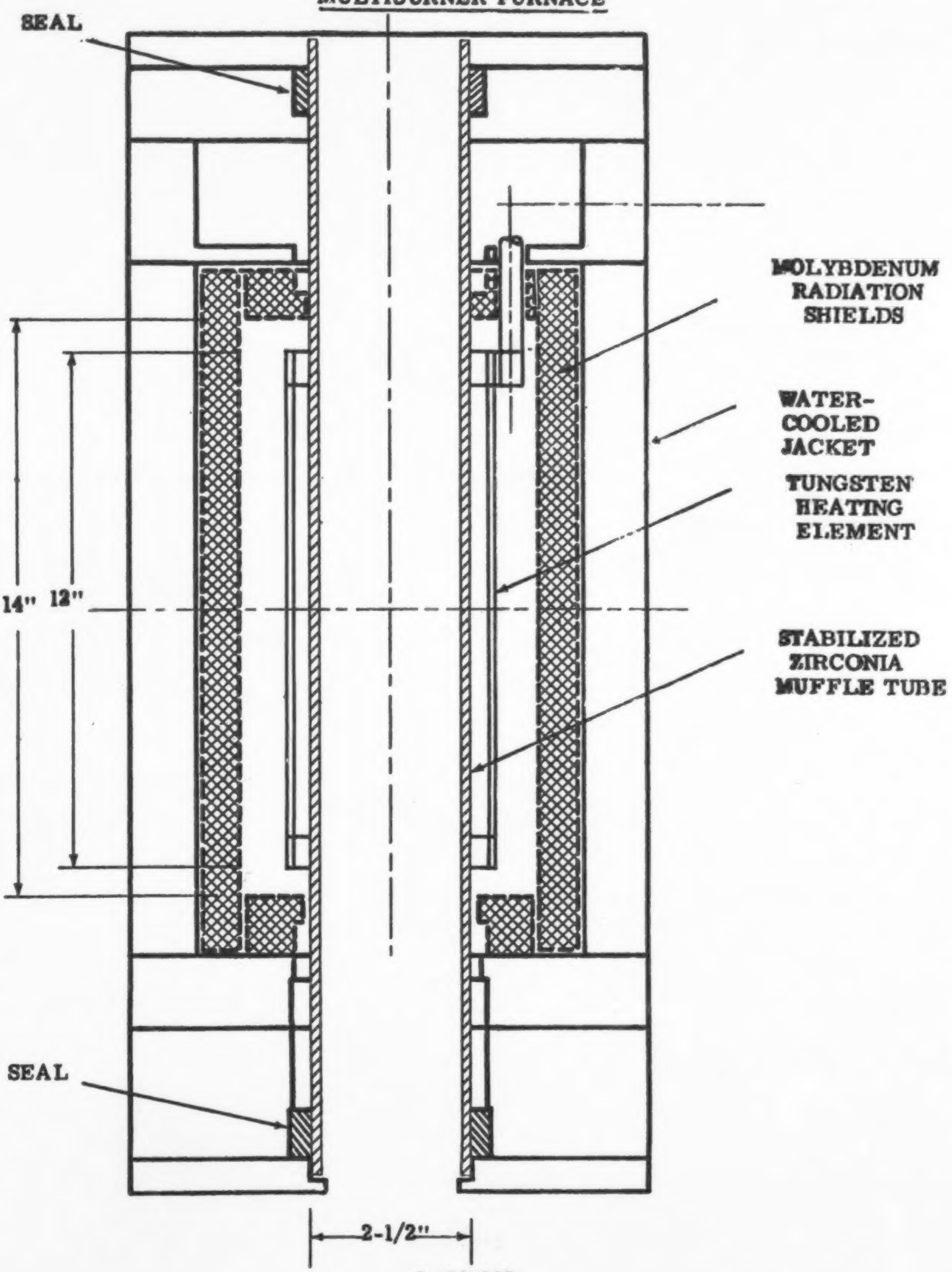
MULTIBURNER FURNACE
SEAL
MOLYBDENUM RADIATION SHIELDS
WATER-COOLED JACKET
TUNGSTEN HEATING ELEMENT
14"
12"
STABILIZED ZIRCONIA MUFFLE TUBE
SEAL
2-1/2"

Figure 4

FLAT FLAME BURNER

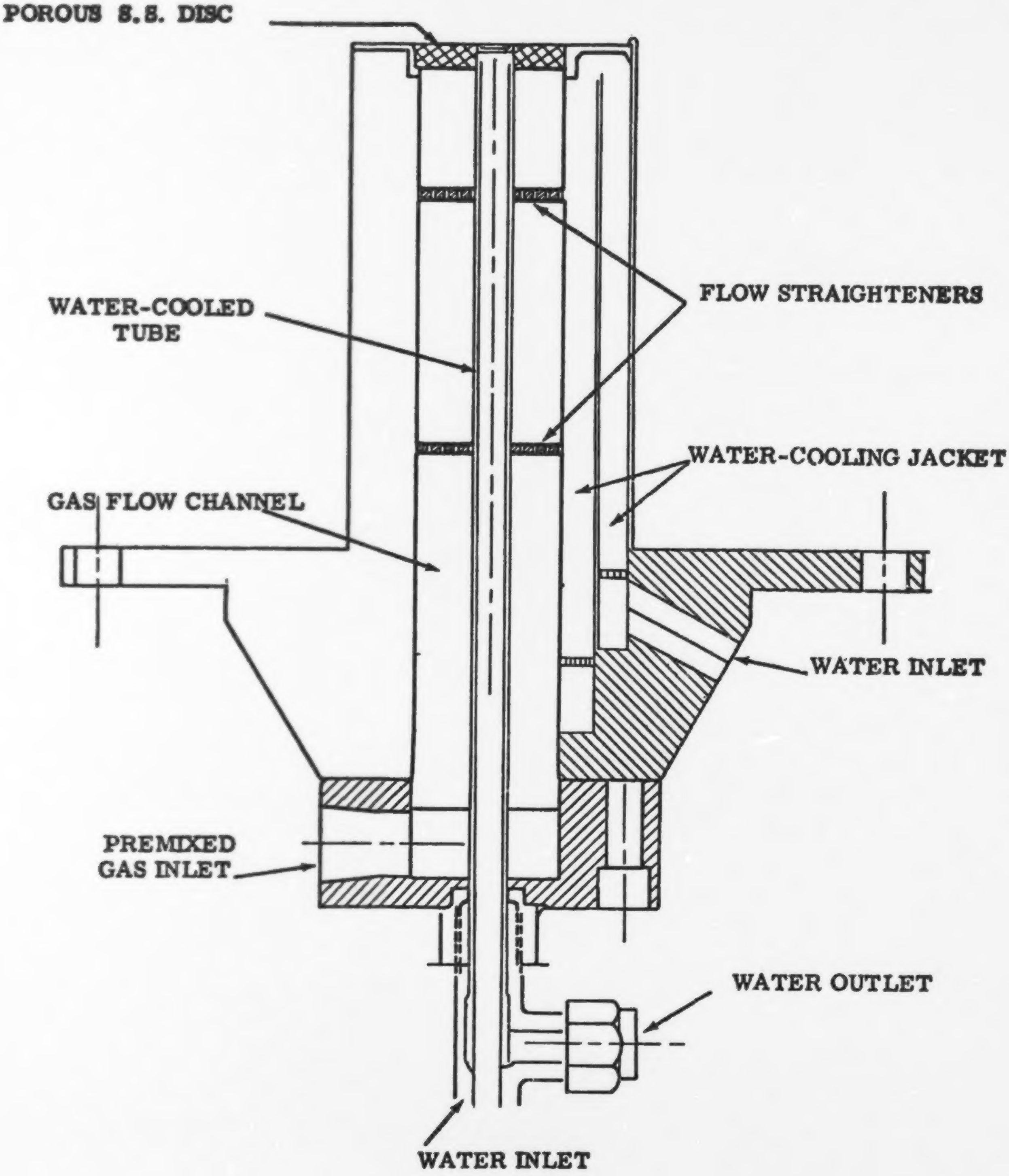
POROUS S.S. DISC
FLOW STRAIGHTENERS
WATER-COOLED TUBE
WATER-COOLING JACKET
GAS FLOW CHANNEL
WATER INLET
PREMIXED GAS INLET
WATER OUTLET
WATER INLET

Figure 5

Multiburner Radial Profile

Fuel - Methane
Twall - 1703°K

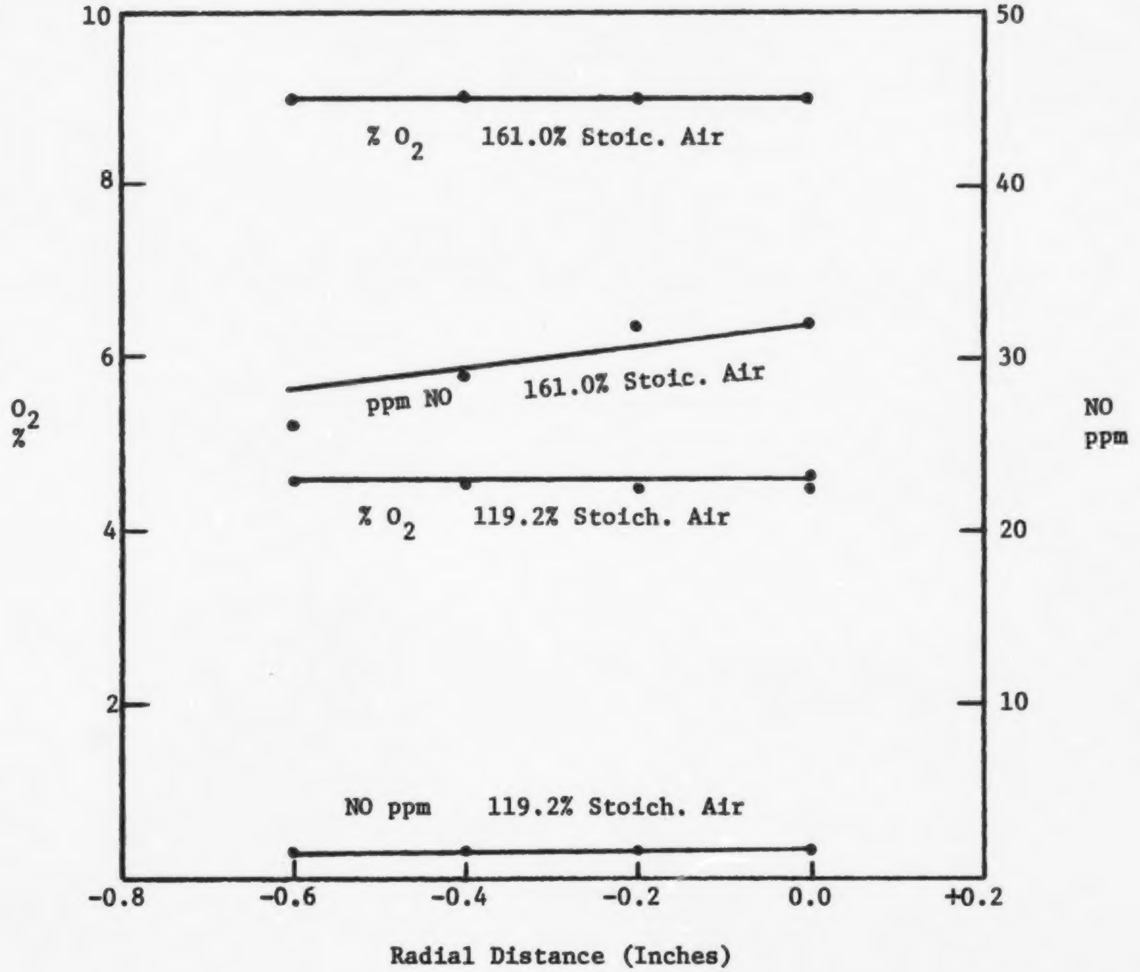

Figure 6

Multiburner Radial Profile

Fuel - Methane
Twall - 2053°K
Stoic. Air - 119.2%

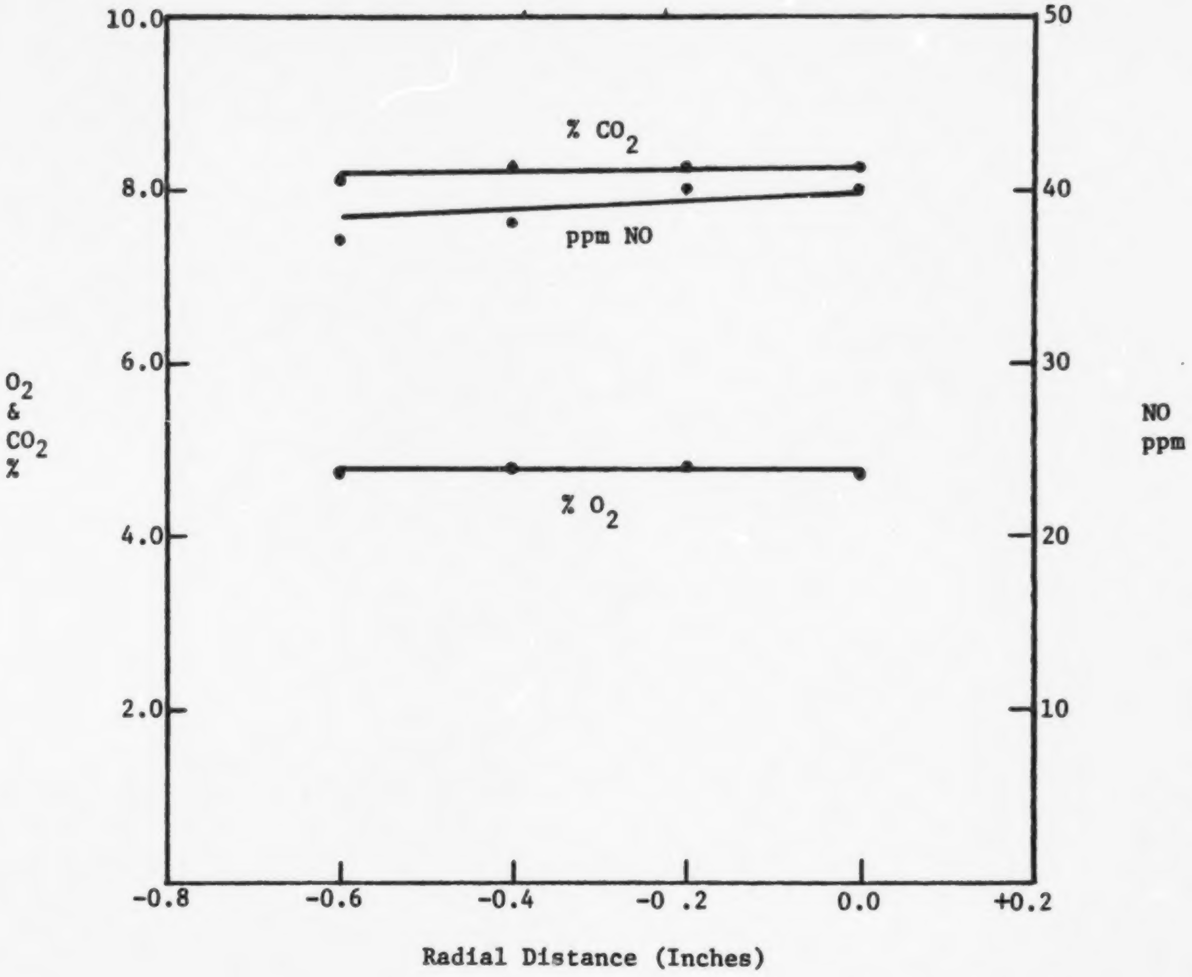

Figure 7

Multiburner Radial Profile

Fuel - Propane
Twall - 1768°K
Stoic. Air - 155.5%

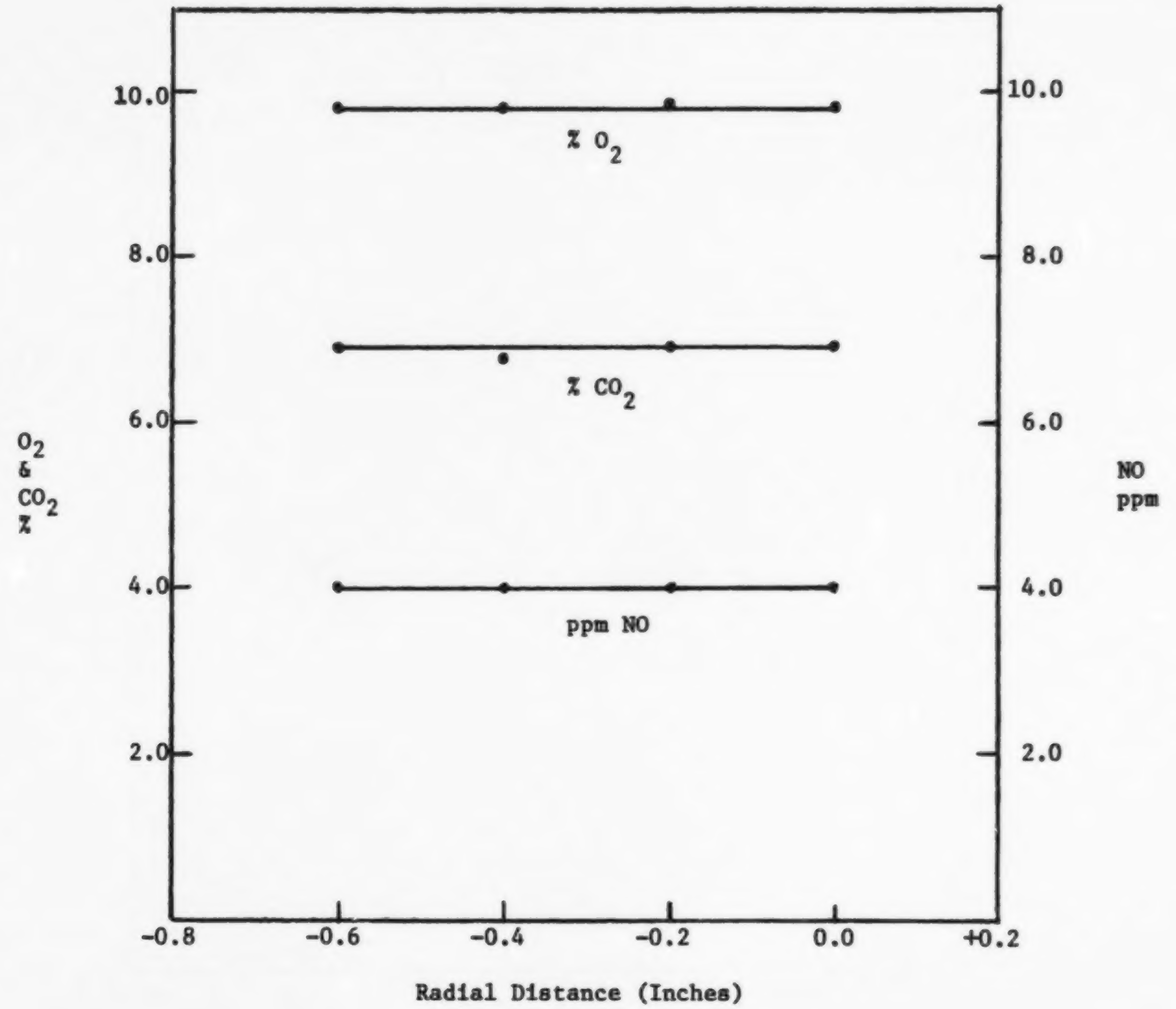

Figure 8

Multiburner Radial Profile

Fuel - Propane
Twall - 2068°K
Stoic. Air - 124.9%

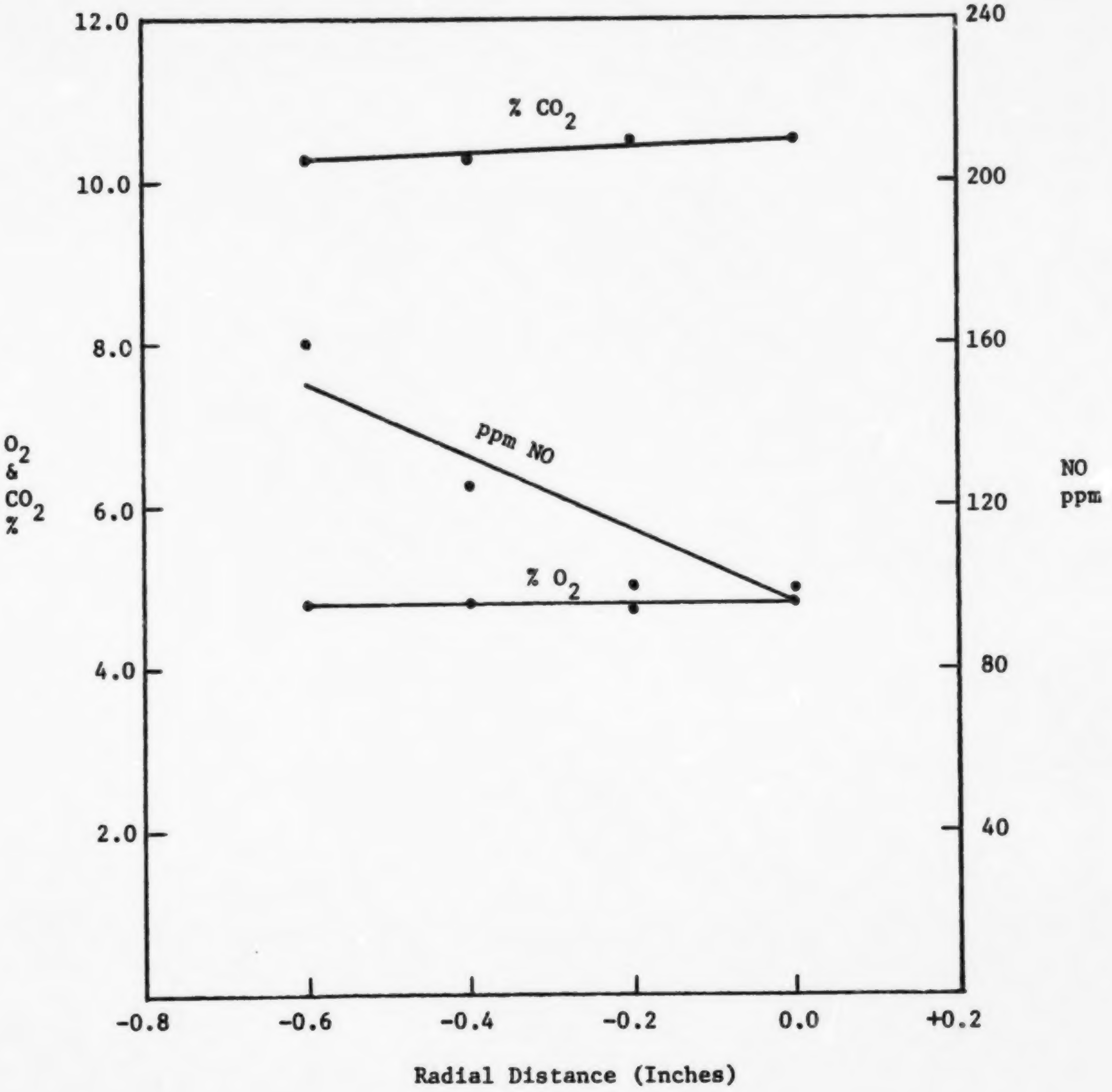

Figure 9

Multiburner Radial Profile

Fuel - Methane
Twall - 1858°K
Stoic. Air - 140.4%

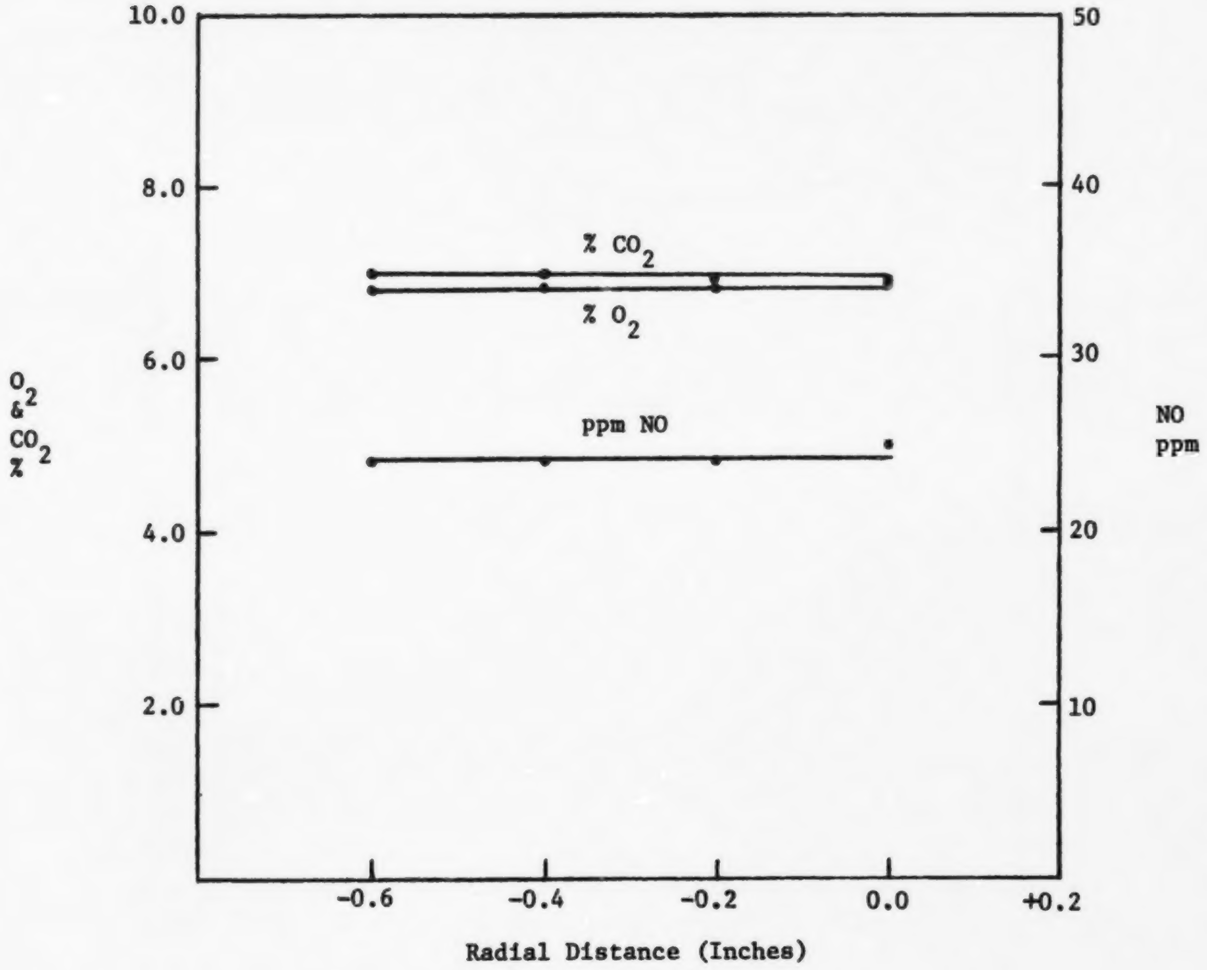

Figure 10

Multiburner Radial Profile

Fuel - Methane
Twall - 2043°K
Stoic. Air - 120.1%